A short presentation was given at the start of the viva voce. The examiners have recommended that reproductions of the slides be added to this thesis, forming an executive summary.

EARTH IMAGING WITH MICROSATELLITES

Marc Fouquet
PhD Viva Voce
15 March 1996

Objectives

The Investigation, Design, Implementation and In-Orbit Demonstration of Electronic Imaging Systems for Earth Observation On-Board Low-Cost Microsatellites.

Research overview

Format of presentation

- Characterisation of microsatellite platform
- Review of imaging payload architectures
- Evolving system & circuit design
- On-board image processing
- Assessment of applicability
- Conclusions

Comparing platforms

	Ratio	Conventional	Microsatellite
cost	30	US$100	US$3
timescale	10	10 yr.	1 yr.
mission def^n		NO	YES
payload mass	50	500 kg	10 kg
payload volume	60	1000 l	15 l
payload power	30	550 W	20 W
attitude control	50	0.1°	5°
control of orbit		YES	NO
comms	550	5500 kbps	9.6 kbps

Assessing microsatellites

Microsatellites present numerous constraints

- Attitude control
- Communications data rates
- Volume

Conventional approach :
suggests microsatellites are useless

Research goal :
innovate to demonstrate feasibility

Suitability of imaging techniques

Whiskbroom systems (using a scanning mirror) (NOAA, Landsat)

– Mass, volume, power, ADCS

Pushbroom systems (using a linear sensor array) (SPOT, IRS, MOS)

– ADCS

Solid-state camera (using a 2D array)

– Immune to attitude instability
– Only currently viable option
– Not popular due to low pixel density

Cameras for Earth observation

- Application not addressed by photonics industry
- Capture still-image
  (like scientific applications)
- Accommodate high scene dynamics
  (high speed like motion video)
- Image product is sensitive to noise

Designing the camera

- Select CCD sensor
  - Pixel density
  - Spectral response
  - Charge transfer architecture (interline tx, frame tx)
  - Special features (integration control, anti-blooming)
- Balance CCD with surrounding circuits
- Trade-off custom vs. off-the-shelf solutions
  - adapt manufacturer's products
- Do not overlook interfacing

(Optics, fault tolerance, radiation damage, calibration, manufacturability, up-gradability)

Overcoming narrow communications channels

- Daily throughput limited by downlink
- Turn-around limited by OBDH
- Real-time service limited by both
- Exploit computational sophistication of microsatellites
- Use on-board image processing to
  - reduce volume of data
  - improve the quality of information retrieved

Overcoming narrow communications channels

- 400% gains demonstrated on PoSAT-1
- Layering of techniques
  - Automatic exposure control
  - Cloud editing (autonomous image analysis)
  - Thumb-nail previews
  - Image compression
- Routines must be tailored for application

trade off compression ratio
vs. degradation
vs. overheads

Implementation

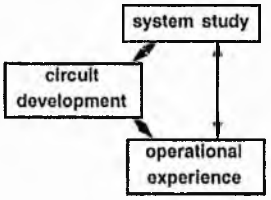

- 8 years
- 11 iterations of camera (prototype, engineering, flight)
- 7 iterations of transputer image processor (prototype, engineering, flight)

= 5 generations of flight imaging systems

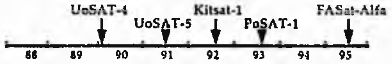

Evaluation of data

Despite modest specifications
(low pixel count, spatial resolution, monospectral)

this imagery can fulfil many applications :

- Meteorology
- Snow cover
- Oil slicks
- Deforestation
- Agriculture, etc.

These cameras have operated routinely, reliably and predictably (PoSAT-1 > 7000 images)

Conclusions
Unique work

- Constrained study
  - Driven by platform
  - Microsatellites are incompatible with conventional payloads
  - Cameras for microsatellites
  - Rapidly moving scenery
- Demonstration
  - In-orbit operation
  - Applications of the imagery
  - Benefits of on-board data processing
- Document
  - Designer's guide

Milestones

First microsatellite to demonstrate:
- *meteorological* scale Earth imaging
- *200 metre* Earth imaging

First satellite to demonstrate:
- *solid-state cameras* for Earth imaging
- *non-governmental* Earth imaging
- *cloud editing* (autonomous image quality analysis)
- *selective downloading* (thumb-nail previews)
- *compression* (software-based unmanned)

Sustained operations

EARTH IMAGING WITH MICROSATELLITES:

An Investigation, Design, Implementation and In-Orbit Demonstration of Electronic Imaging Systems for Earth Observation On-Board Low-Cost Microsatellites.

Thesis submitted to The University of Surrey
for the degree of Doctor of Philosophy.

by

Marc Fouquet

Centre for Spacecraft Engineering Research,
University of Surrey,
Guildford, Surrey, UK.

December 1995

ABSTRACT.

This research programme has studied the possibilities and difficulties of using 50 kg microsatellites to perform remote imaging of the Earth. The design constraints of these missions are quite different to those encountered in larger, conventional spacecraft. While the main attractions of microsatellites are low cost and fast response times, they present the following key limitations:

- Payload mass under 5 kg,
- Continuous payload power under 5 Watts, peak power up to 15 Watts,
- Narrow communications bandwidths (9.6 / 38.4 kbps),
- Attitude control to within 5°,
- No moving mechanics.

The most significant factor is the limited attitude stability. Without sub-degree attitude control, conventional scanning imaging systems cannot preserve scene geometry, and are therefore poorly suited to current microsatellite capabilities.

The foremost conclusion of this thesis is that electronic cameras, which capture entire scenes in a single operation, must be used to overcome the effects of the satellite's motion. The potential applications of electronic cameras, including microsatellite remote sensing, have erupted with the recent availability of high sensitivity field-array CCD (charge-coupled device) image sensors.

The research programme has established suitable techniques and architectures necessary for CCD sensors, cameras and entire imaging systems to fulfil scientific/commercial remote sensing despite the difficult conditions on microsatellites. The author has refined these theories by designing, building and exploiting in-orbit five generations of electronic cameras.

The major objective of meteorological scale imaging was conclusively demonstrated by the Earth imaging camera flown on the UoSAT-5 spacecraft in 1991. Improved cameras have since been carried by the KITSAT-1 (1992) and PoSAT-1 (1993) microsatellites. PoSAT-1 also flies a medium resolution camera (200 metres) which (despite complete success) has highlighted certain limitations of microsatellites for high resolution remote sensing. A reworked, and extensively modularised, design has been developed for the four camera systems deployed on the FASat-Alfa mission (1995). Based on the success of these missions, this thesis presents many recommendations for the design of microsatellite imaging systems.

The novelty of this research programme has been the principle of designing practical camera systems to fit on an existing, highly restrictive, satellite platform, rather than conceiving a fictitious small satellite to support a high performance scanning imager. This pragmatic approach has resulted in the first incontestable demonstrations of the feasibility of remote sensing of the Earth from inexpensive microsatellites.

Images Taken by the PoSAT-1 Microsatellite

Encounter Bay (Australia)

Long Island (USA)

Cape Cod (USA)

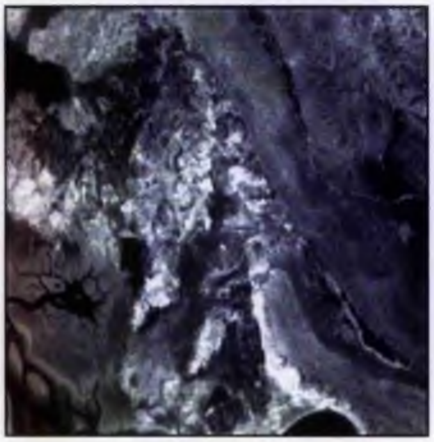

Hendijan (Iran)

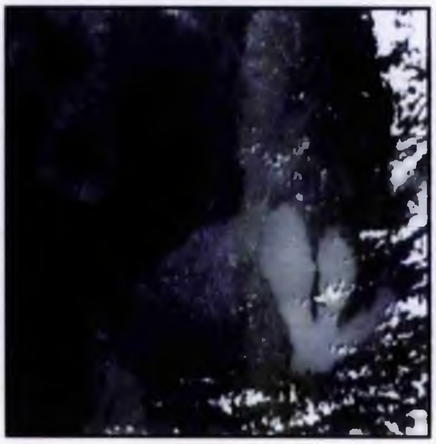

Manila (Philippines)

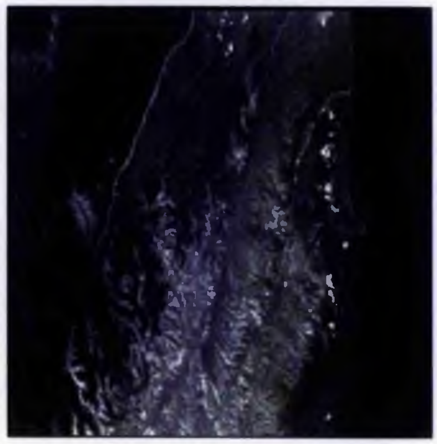

Richmond Range (New Zealand)

Vladivostok (Russia)

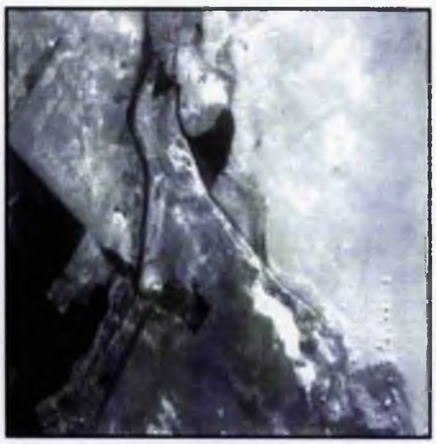

Basrah (Iraq)

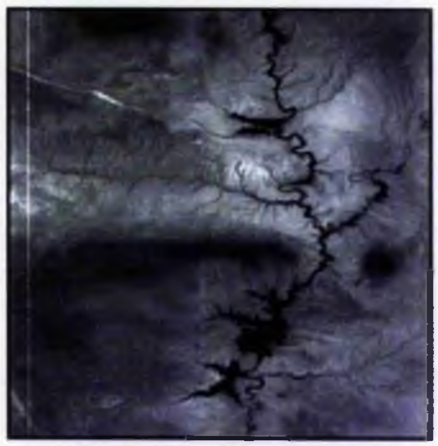

Lakes Powell & Glenn (Utah-USA)

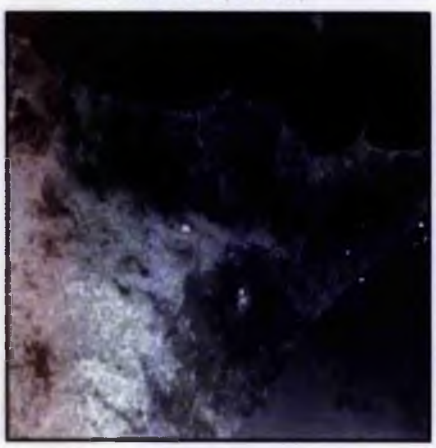

Mount Etna (Sicily)

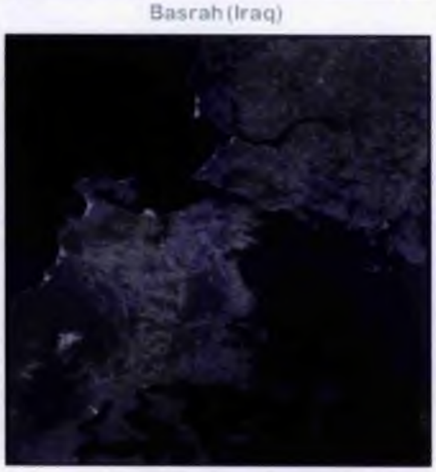

Canal de Chacao (Chile)

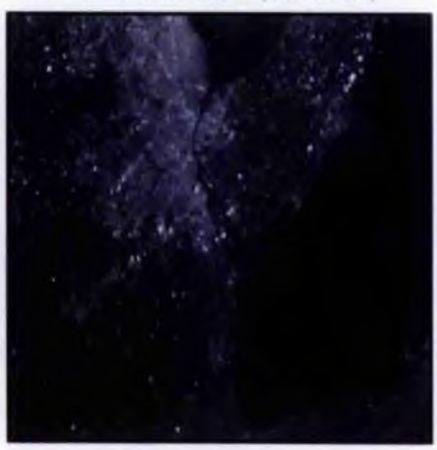

Detroit (USA)

ACKNOWLEDGEMENTS.

Acknowledgements and thanks are due :

- To Surrey Satellite Technology Ltd. for funding this research programme, and allowing me to divert from my commercial responsibilities long enough to write and edit this thesis;
- To Professor Martin Sweeting for fostering a lively and stimulating environment for me to work in, and for supervising this research programme;
- To my friends and colleagues (past and present) at Surrey Satellite Technology Ltd. and the UoSAT Spacecraft Engineering Research Unit who have shared the excitement and occasional disappointment over the years, and who have provided encouragement and suggestions (some useful, some crazy) along the way;
- To my parents, family and friends;
- To Maggie. Thank you. I've got time now.

TABLE OF CONTENTS.

2. BACKGROUND AND CONTEXT.

3. FACTORS GOVERNING THE DESIGN OF REMOTE SENSING INSTRUMENTS FOR MICROSATELLITES.

4. OVERVIEW OF HARDWARE DEVELOPED DURING THIS RESEARCH PROGRAMME.

5. DESIGNING SOLID-STATE CAMERAS FOR EARTH IMAGING FROM MICROSATELLITES.

6. DATA HANDLING FOR THE IMAGING SYSTEM.

7. DEMONSTRATION OF ON-BOARD IMAGE PROCESSING AND COMPRESSION TO IMPROVE DATA THROUGHPUT AND VALUE.

8. IN-ORBIT RESULTS AND PRESENTATION OF IMAGERY.

9. CONCLUSIONS AND TOPICS FOR FUTURE RESEARCH.

APPENDIX 1. REFERENCES.

APPENDIX 2. AUTHOR'S PUBLICATIONS DURING THIS RESEARCH PROGRAMME.

LIST OF FIGURES.

LIST OF TABLES.

CHAPTER I

INTRODUCTION.

1. INTRODUCTION.

Remote sensing of the Earth has long been recognised as one of the major benefits which has resulted from the conquest of space. Orbiting satellites offer unique possibilities for monitoring the Earth's surface and atmosphere, and many programmes have been established to exploit the data from remote sensing spacecraft. The sophistication of the orbiting hardware and the interpretation of the data gathered has been increasing at a steady rate since the astronauts of the Gemini programme brought back the first photographs of the Earth using hand-held cameras. In the mid-1990s, the importance of remote sensing is being increasingly emphasised with proposals for many new missions. Innumerable books, articles and papers have been written discussing the merits of Earth observation and the various applications fulfilled by remote sensing spacecraft. In the author's opinion, the key advantages of using spacecraft, as opposed to aircraft, balloons or sounding rockets, to provide imagery of the Earth are:

- The very high vantage point offers an unrivalled opportunity to obtain panoramic views, allowing conditions at different parts of the Earth to be recorded simultaneously.
- The ability to image regions which are otherwise inaccessible (geographically or politically). This includes land masses, but of equal importance, the oceans and atmosphere.
- The regularity and predictability of the data coming from an orbiting satellite.
- Despite the high initial expenditure, the overall running costs of remote sensing spacecraft are lower than other forms of image gathering.

The purpose of this research programme has been to address this last point to determine whether is it possible to reduce the cost of remote sensing programmes by using low-cost 50 kg microsatellites.

1.1 THE ROLE OF MICROSATELLITES FOR REMOTE SENSING.

While the scientific, economic, environmental and life-saving merits of remote sensing by satellite are universally acknowledged, the funding for the latest, high performance systems is becoming increasingly scarce. There is consequently a need to reduce the cost of remote sensing in order to maintain the services offered by these spacecraft within tightening budgetary constraints.

As a reaction to the huge costs and long development periods of conventional satellites, and following the trend of all modern electronic design towards miniaturisation, smaller spacecraft are gaining favour in a number of application areas, including remote sensing. In theory, by minimising overheads, smaller teams can rapidly develop compact spacecraft for launch on cheaper rockets, improving the cost-effectiveness of remote sensing missions. There have been many study papers devoted to the feasibility of developing and launching smaller satellites for a range of remote sensing applications. The systems presented in these papers have generally fallen into the small satellite (500 to 1000 kg) and occasionally minisatellite (100 to 500 kg) categories. Because the majority of these proposals adopt much of the philosophy of their larger precursors, reductions in mass (and consequently cost) are limited. To achieve significantly smaller remote sensing missions, the designs will need to be more innovative than mimicking the features of large satellites.

Instead of the usual approach of trying to see how far a traditional remote sensing design can be shrunk, the rationale behind this research has been to see what, if any, Earth observation is possible using a 50 kg microsatellite platform. However, it is immediately obvious to anyone possessing any familiarity with the technology of remote sensing spacecraft that such small vehicles present a number of extremely limiting engineering constraints. Therefore, this research has assessed the techniques traditionally used for large remote sensing missions, appraising their suitability for these smaller missions. Where the conventional solution is inappropriate, alternative strategies have been investigated and implemented.

Overall, the traditional imaging systems which use the satellite's orbital velocity to scan the scene do not perform well within the constraints of 50 kg spacecraft. Consequently, the research programme has concentrated on the development of electronic cameras using modern CCD (charge-coupled device) technology, which possess attributes compatible with the conditions on board microsatellites. The various theories presented in this thesis have been developed and refined as a direct consequence of the experiences and in-orbit results obtained from the five generations of Earth imaging experiments specified, designed, built and tested by the author.

The practical implementation of these imaging systems continues in the vein of microsatellite research pioneered by Surrey Satellite Technology Ltd. (SSTL), a technology transfer company wholly owned by the University of Surrey. SSTL is a world leader in the design and construction of microsatellites, and has launched eleven such spacecraft to date. Since joining SSTL in late 1987, the author's role has been to study and design Earth observation systems for deployment on the company's satellites in direct response to the increasingly important issue of mission costs facing the remote sensing community.

The unique aspect of the author's work has been to provide the first successful in-orbit demonstration to date of the feasibility of using microsatellites for scientific and commercial remote sensing. This was accomplished with the system flown on UoSAT-5 (1991), the world's first sub-100 kg satellite to routinely capture high quality imagery from space, and confirmed with the enhanced imagers carried on the KITSAT-1 (1992) and PoSAT-1 (1993) microsatellites.

1.2 CONTEXT OF THIS RESEARCH PROJECT.

This thesis summarises the author's investigation into the design of Earth imaging systems on 50 kg microsatellites. Clearly, producing cameras for remote sensing from space is not new. There have been numerous image sensors mounted on high altitude aeroplanes, sounding rockets and spacecraft since the middle of this century. However, there are many additional engineering constraints on microsatellites that do not exist on large conventional spacecraft. These are imposed principally by the limited resources of the scaled-down housekeeping systems. It is the study of these specific restrictions on the imaging system and the proposal of germane solutions which constitutes the novel aspect of this research.

The constraints of microsatellites are so severe that, for many years, few people in the space industry establishment accepted that systems as compact as Surrey's satellites could be made to fulfil commercially viable or high-precision scientific remote sensing tasks. While probably correct according to the mind-set and design criteria of conventional satellites, this attitude fails to acknowledge the innate strengths of microsatellites, namely that the reduced financial risk of these spacecraft (due to short lead times, small development teams and modest launch fees) allows newer, unproven technology to be used to achieve the mission objectives in unconventional ways.

There are two major conceptual pitfalls that observers from the conventional space business tend to accidentally fall into when considering the possibilities of microsatellites for all applications, and not just remote sensing. Firstly, traditional designers and users of Earth observation satellites have come to expect a certain number of factors as indispensable for mission success. They find it difficult to commit to new systems (i.e. small satellites) which do not live up to, or preferably surpass, existing expectations of quality and resolution, regardless of the potential for significant financial savings. Although there are many complaints about the high cost and limited availability of satellite imagery, there has been, rather oddly, a reluctance to promote remote sensing from small satellites because of the associated reduction of data quality, even though the current technology is more than adequate for many applications. This tendency towards ever improving specifications, coupled with the knowledge that a given design has been successful in the past, has limited the amount of attention devoted to devising cheaper alternative remote imaging systems.

Secondly, whenever small satellites are considered, the designers of large platforms tend to view these missions as trivialised versions of conventional spacecraft. They reason that since a small satellite has fewer components and reduced mission objectives to the spacecraft they are used to, the conceptual design will be easy for them to master, overlooking the fact that many traditional systems designs simply cannot be reproduced within the reduced capacities and margins of small satellites. This argument is analogous to the designer of super-computers dismissing personal computers because they have lower performance specifications, missing the numerous attractions of the smaller system. Furthermore, the smaller systems often make use of equally ingenious design and advanced technology which should not be overlooked.

The purpose of the preceding comments is not to criticise the system design and development philosophies of the traditional spacecraft builders, who have been managing billions of dollars and millions of man-hours in technically challenging space projects for more than three decades. They are merely attempting to point out that the strategies which have evolved to manage and design large missions are not necessarily appropriate when considering the enormous reductions in spacecraft size and budget of microsatellites. It is also necessary to situate the relevance and novelty of this research relative to the on-going body of work in the field of Earth observation.

Due to these factors, the detailed study of imaging systems exclusively for microsatellites has received little, or no, attention to date. The design environment of a microsatellite is very different to that of previous remote sensing satellites, with extremely limited mass, volume, power, attitude stability and communications bandwidths. Even the widely touted missions of the US's recent 'smaller, cheaper, faster' programme are large (hundreds of kg) and expensive (around $60 million each) compared to SSTL microsatellites (with budgets of $2 to 4 million per mission).

Thus, this thesis presents the conclusions of eight years and five successive missions of theoretical work and unique practical experimentation into imaging on microsatellites. In studying a previously overlooked aspect of spacecraft engineering, this research covers new ground, which can be difficult in applied engineering subjects. It addresses both the system-level and circuit-level characteristics necessary for the design of successful microsatellite imaging missions, and makes many recommendations towards the design of future remote sensing systems. Furthermore, the arguments presented have been concretely demonstrated with the systems in orbit. Despite having significantly different designs from the payloads flown on other Earth observation satellites, the cameras developed during this programme have been a considerable success.

In the last two years, there has been a noticeable shift in the design choices made for certain imaging systems, incorporating some of the elements discussed in this thesis. The author is confident that the successful in-orbit demonstration of Earth imaging from microsatellites such as UoSAT-5, KITSAT-1 and PoSAT-1 have played a part in this change of direction. Furthermore, the rate of progress in terrestrial electronic imaging technology is phenomenal, meaning that in a couple of years small spacecraft will be capable of capturing imagery similar to that of SPOT and LANDSAT. The short cycle times of Surrey's microsatellite missions provides an ideal opportunity to capitalise on these technological developments, ensuring a future for this line of research.

1.3 OBJECTIVES OF THIS RESEARCH PROGRAMME.

Through this research programme, the author has investigated the theoretical and practical design of Earth imaging systems for use on microsatellites. The most convincing manner of validating these principles is to demonstrate them successfully in orbit. Therefore, the development, production and launch of suitable electronic imaging hardware has always been the main objective of this research programme.

Achieving the objective of in-orbit demonstration has involved an in-depth study of available sensing technologies to understand the relative benefits and drawbacks of the various scanning and staring imaging techniques. However, while good design of the imaging payload is critical for the success of any remote sensing mission, a clear grasp of the role of supporting systems is equally important. Unless the spacecraft's housekeeping systems are compatible with the particular demands of the imaging instrument, the success of the mission is likely to be compromised. Although this matching of capabilities and needs occurs for all space missions, the options available on a microsatellite platform are especially restrictive. In addition to the obvious mass, volume and power limitations, the performance the attitude control, on-board data handling, RF communications, power conditioning, command and telemetry systems are equally vital in defining the payload's design.

Early in the research programme, it transpired that the key constraint of current microsatellite technology on imaging payloads is the coarseness of attitude control. This factor, more than any other, defines the imaging system's architecture. Scanning image systems cannot preserve image geometry if the satellite's attitude drifts, and solid-state cameras must be used instead.

Therefore, the only imaging systems considered in any depth are all-electronic CCD cameras. Furthermore, the scope of this research, and the cameras produced, has been limited to capturing monospectral, meteorological scale imagery. Considering a wider range of remote sensing applications, such as high-resolution or multispectral capabilities, has been deliberately excluded to avoid failure through over-ambition. Having said this, PoSAT-1 has nonetheless made significant progress towards producing higher resolution imagery.

Having established that electronic still-image cameras are the most suitable remote sensing tool for microsatellites, a circuit level study was conducted. Much of this thesis addresses the choice of CCD sensor and the design of each sub-system within an electronic camera. The recommendations of this design study have evolved as the author improved the performance and reliability of the successive cameras on the UoSAT-4, UoSAT-5, KITSAT-1, PoSAT-1 and FASat-Alfa microsatellites.

Another major limitation of current microsatellite technology for fulfilling commercial remote sensing is the slow data rates experienced on the various on-board and downlink communication channels. In response, the author has considered some of the measures that need to be taken in future missions to overcome these restrictions. This includes a number of useful image analysis, processing and compression techniques demonstrated in orbit by the microprocessor systems on PoSAT-1.

Finally, possible developments for future microsatellite imagers with performances approaching that of existing governmental systems are discussed briefly. Based on the success of the imaging system on PoSAT-1, SSTL has medium-term objectives of providing sub-100 metre, multispectral images rivalling the data from the LANDSAT multispectral scanner (MSS) instrument.

The objectives of this research can therefore be summarised as:

- Understand the conditions on microsatellites and the corresponding effects on different imaging architectures.
- Develop meteorological scale, monochromatic cameras for use on microsatellites.
- Demonstrate convincingly that these cameras can perform reliably and predictably over a lifetime in space.
- Investigate the block-diagram and circuit level design for flexible operation, testing and expansion.
- Make recommendations for the design of future microsatellite imaging cameras.

1.4 SCOPE OF THIS RESEARCH PROGRAMME.

This research has focused on electronic and systems aspects of designing remote sensing instruments for microsatellites, and it has been necessary to limit the scope of this thesis to the specific study of implementing imaging systems. For example, while the author has acquired a considerable understanding of the microsatellite housekeeping functions, only those aspects directly effecting the imaging capabilities are considered here. Similarly, topics such as optical design, calibration and radiation studies, though vital for the successful design of remote sensing payloads, have received less attention. In particular, although the use of advanced on-board image processing techniques enhances the yield of remote sensing microsatellites, this project is not about image processing theory. Any discussions of image processing and compression will be purely pragmatic, concerned solely with their role in supporting the imaging hardware. Despite these reservations, the range of topics covered in this thesis is very broad, reflecting the numerous facets that must be addressed when developing Earth observation systems.

The goals of this research programme have been to establish the feasibility of using electronic cameras on microsatellites for Earth observation, by implementing these capabilities in orbit. Accordingly, there has been a deliberate bias towards illustrating and demonstrating numerous different aspects and roles of these imaging systems, with significantly less emphasis on ensuring that the systems are highly calibrated. For this reason, this document contains more discussion topics than many theses, and correspondingly less numerical characterisation of the instruments developed. This choice has been made to exploit the valuable launch opportunities available during programme to their greatest potential.

1.5 STRUCTURE OF THIS THESIS.

This thesis is the result of eight years of intensive research into the development of operational remote sensing systems for use on microsatellites, and its style reflects the highly pragmatic nature of the investigation. In the programme's course, the author has developed and implemented five revisions of imaging system, acquiring a greater understanding of the subject with each of these projects. However, the repetitive design cycle and the gradual development the theories presented do not lend naturally to the traditional 'background-theory-implementation-results' structure of thesis writing.

After due consideration, it was decided that the most logical, and the most useful, style to adopt for the thesis was to present the arguments in the form of a 'designer's guide'. In this way, the author attempts to distil the experience gained through the hands-on development of electronic camera systems for engineers needing to design or work with remote sensing systems on microsatellites. The conclusions derived, and the advice offered, have matured by observing the relative success and failure of the various strategies adopted over the course of five iterations of system design. The in-orbit demonstration of the principles expounded in this thesis adds considerable credibility to the author's arguments.

This thesis encompasses nine chapters, covering the following subjects:

CHAPTER I INTRODUCTION.

CHAPTER II BACKGROUND AND CONTEXT.

Chapter 2 reviews many of the background issues of this research programme. First, the three basic techniques of generating remotely sensed imagery are described: the whiskbroom scanner, the pushbroom scanner, and the frame camera, and considers their relative merits and historical evolution. Next, the typical characteristics of conventional remote sensing spacecraft are profiled, assessing the power, mass, attitude control and communications services required to support the imaging payload. These requirements are contrasted with the conditions on 50 kg microsatellites. Finally, this chapter reviews the various existing and on-going programmes from around the World attempting to fulfil Earth observation from microsatellites.

CHAPTER III FACTORS GOVERNING THE DESIGN OF REMOTE SENSING INSTRUMENTS FOR MICROSATELLITES.

As noted in Chapter 2, the engineering constraints of implementing Earth observation systems on 50 kg microsatellites are very different to the conditions found on most conventional remote sensing spacecraft. Chapter 3 reviews which parameters are of importance when specifying a remote sensing mission. Next, it considers how a microsatellite's limitations in terms of mass, volume, power, orbits and most importantly, attitude control and data handling effect the design and operation of an imaging system. The main conclusion is that until the attitude stability of microsatellites approaches the 0.1° of traditional spacecraft, it will not be feasible to use scanning imagers, and electronic cameras must be employed instead.

CHAPTER IV OVERVIEW OF HARDWARE DEVELOPED DURING THIS RESEARCH PROGRAMME.

The theories argued in this thesis have been developed in a very practical programme of implementing numerous imaging systems on-board SSTL microsatellites. The author's understanding of the subtle engineering trade-offs associated with implementing remote sensing on microsatellites has grown with each successive generation of the electronic imaging systems. This has permitted a gradual improvement in the performance of these electronic cameras and microprocessor units from the rudimentary circuits flown on UoSAT-4, to the highly integrated and modular systems prepared for FASat-Alfa. Since it is the in-orbit successes of these cameras, particularly on PoSAT-1, which give credibility to the arguments of this thesis, chapter 4 reviews the hardware of the imaging systems developed by the author during this research programme.

CHAPTER V DESIGNING SOLID-STATE CAMERAS FOR EARTH IMAGING FROM MICROSATELLITES.

Based on the experience acquired in the development of the imaging systems described in chapter 4, this chapter provides practical advice on the issues facing the design of electronic camera systems for microsatellites. Chapter 5 discusses the criteria for selecting a CCD sensor depending on the instrument objectives. The various options for implementing the digital, analogue and power conditioning support circuits, and the optical systems, are discussed and appropriate solutions offered. Broader issues such as the calibration of the imager, fault tolerance and resilience to ionising radiation are also considered.

CHAPTER VI DATA HANDLING FOR THE IMAGING SYSTEM.

Having addressed the issues facing the implementation of the sensing units for microsatellite remote imaging in chapter 5, chapter 6 looks at the computer systems necessary for manipulation and transmitting the data collected.

CHAPTER VII DEMONSTRATION OF ON-BOARD IMAGE PROCESSING AND COMPRESSION TO IMPROVE DATA THROUGHPUT AND VALUE.

The small capacities of microsatellite communications systems limit the volume of payload data which can be collected, hampering the development of commercial remote sensing from these spacecraft. In addition to the obvious measures of upgrading the communications hardware, there are a number of software data reduction techniques that can help improve the imaging yield of microsatellites. Chapter 7 explores how various autonomous and interactive image analysis, processing and compression techniques have conferred a four-fold increase in the daily throughput of the camera systems on PoSAT-1. These methods, while of particular benefit to microsatellites, are equally applicable to all remote sensing missions.

CHAPTER VIII IN-ORBIT RESULTS - PRESENTATION OF IMAGERY.

The usefulness of the imagery collected from orbit determines the success of a satellite remote sensing system. Although not of the same class as SPOT or LANDSAT data, the images collected by the author's cameras nevertheless contain a great deal of information. Chapter 8 presents some of this data to demonstrate to the reader that quality Earth observation is possible from microsatellites, and briefly considers a number of applications for this data

CHAPTER IX CONCLUSIONS AND FUTURE WORK.

Chapter 9 summarises the main topics covered and the key conclusions derived in the course of the thesis. Recommendations for the choice of sensors and systems suitable for low, medium and high resolution applications are made. Finally, thoughts on the future direction and opportunities for microsatellite Earth observation are presented.

Therefore Chapter 2 covers general background material regarding imaging instrument topology, and conventional and microsatellite platforms. Chapter 3 represents an analysis of the conditions experienced on microsatellites and their consequences on the imaging payload. Chapter 4 presents a synopsis of the hardware systems developed by the author during the research programme. Whereas chapter 4 is essentially descriptive, chapters 5 and 6 represent a generalised and more abstracted discussion of designing microsatellite imaging systems, reflecting the author's current understanding of these issues. Chapter 7 is a self-contained section discussing the demonstration of on-board image analysis and compression used to overcome the low data rate of the communications channels on microsatellites, and Chapter 8 reviews some of the applications amenable to using microsatellite imagery. References are provided for each chapter, and also grouped in a compendium in Appendix 1.

1.6 SUMMARY.

This thesis investigates the feasibility of using microsatellites for remote sensing, despite the difficult engineering constraints imposed by such platforms. Throughout the thesis, the reader should remember the that pivotal theory presented postulates that :

> ***Given the coarse attitude stability of existing microsatellites, electronic cameras based on area-sensing CCD arrays are the only feasible method of implementing remote sensing on these small satellites.***

The bulk of this thesis (chapters 3 to 6) first of all justify this premise, and then discuss the most appropriate solutions for implementing these electronic cameras. A secondary theme of this research is that:

> ***The restricted data rates on the communications channels of current microsatellites limit the scope for developing commercial remote sensing services.***

Chapter 7 covers the author's demonstration of the suitability of certain image processing and compression techniques to help overcome this situation.

Focusing on these two 'sound-bites' has helped the author select which aspects of the work conducted over this research programme should be included in the thesis. Many other issues faced in implementing the imaging systems of this programme have been omitted because they did not directly support these theories. Similarly, the author feels that if the reader should retain anything from this thesis, it is summarised by these two theories.

CHAPTER II

BACKGROUND AND CONTEXT.

Chapter 2 reviews many of the background issues of this research programme. First, the three basic techniques of generating remotely sensed imagery are described: the whiskbroom scanner, the pushbroom scanner, and the frame camera, and considers their relative merits and historical evolution. Next, the typical characteristics of conventional remote sensing spacecraft are profiled, assessing the power, mass, attitude control and communications services required to support the imaging payload. These requirements are contrasted with the conditions on 50 kg microsatellites. Finally, this chapter reviews the various existing and on-going programmes from around the World attempting to fulfil Earth observation from microsatellites.

2. BACKGROUND AND CONTEXT.

2.1 CHARACTERISTICS OF OPTICAL IMAGING SYSTEMS FOR REMOTE SENSING FROM SPACE.

2.1.1 DESCRIPTION OF REMOTE SENSING IMAGER DESIGNS

The purpose of remote sensing from space is to make observations of the Earth beneath the satellite to provide information that is not available or difficult to obtain using ground-based measurements. To record these images, a remote sensing instrument must include an optical system to focus the scene below the spacecraft onto a suitable electronic sensor. The sensor must convert incoming photons into a coherent electronic signal, which can be sampled, stored and transmitted to the ground. Eventually, this electronic data must be displayed as a representative, and radiometrically and geometrically faithful, image of the original scene.

There are three basic techniques used for electronically producing two-dimensional images of the Earth: whiskbroom, pushbroom and full-frame imaging. There are examples of each type throughout the history of space imagery, for both Earth observation and inter-planetary missions. The most favoured technique has changed throughout the history of spaceflight as new technologies evolve, making one approach more attractive than the others. Each of the design approaches has specific strengths and weaknesses in terms of the imagery produced, and places different demands on the host spacecraft. The trade-off in assessing which approach is optimal for a specific set of mission objectives will be very different if the platform is a large conventional satellite or small microsatellite.

2.1.1.1 The whiskbroom scanning technique.

The longest established technique of producing high-quality electronic imagery is the whiskbroom design, which has been used many times, particularly in the sensors of the NOAA meteorological and LANDSAT remote sensing programmes. A typical example of this sort of imager is the LANDSAT Multi-Spectral Scanner (the MSS).

The principle sensor of the MSS is a high-specification photodiode which is collimated to view a very narrow angle (known as the instantaneous field of view - IFOV). To create two-dimensional images using a point detector, such as a photodiode, it is necessary to scan the image in both axes. The motion of the satellite along its orbit provides a regular sweeping in one axis. A mirror rotating perpendicular to the direction of travel provides the scanning in the other axis. This back and forth motion of the scanning mirror resembles someone using a whiskbroom, hence the name.

The rotating mirror sweeps a portion of the scene over the photosensor, producing a continuous output signal, which must be sampled, quantised and stored. By the time the mirror has returned to its starting position, the satellite has moved along its orbital path and a new portion of the Earth is ready for scanning. Thus the MSS takes about 25 seconds to build up a two-dimensional image covering an area of 185 km^2, comprising 2340 scan lines with approximately 3240 pixels per line. This provides a pixel which corresponds to a ground resolution of 56 x 79 metres from LANDSAT's 705 km orbit, but a post-processing routine 'squares' the pixels before printing and distribution.

In reality, because the full angle of view of the MSS is small (around 11°), an oscillating rather than a rotating mirror is employed. Despite the relatively high frequency of oscillation (30 Hz), it is still too slow to scan each line in turn as the satellite moves along its orbit track. Therefore six lines are scanned simultaneously using six photodetectors lying side by side. Since there are a total of 24 sensors (six in each of the four spectral bands) in the MSS focal plane, the physical construction of the scanning mechanism is very complex to ensure calibration and co-registration of all the photosensors.

Whiskbroom designs have been favoured in US-built remote sensing missions for the last two decades. In addition to the LANDSAT MSS, both the Advanced Very High Resolution Radiometer (AVHRR) system used on the NOAA TIROS-N meteorological spacecraft and the Thematic Mapper (TM - the other principle LANDSAT payload) also use the basic whiskbroom scanning technique to build up full images. The concept has been extended to meet the requirements of meteorological imaging satellites in geostationary orbit. Because these satellites have no velocity relative to the ground, the second dimension of scanning must be provided by the satellite; in the GOES spacecraft, the oscillating mirror scans in the east-west axis, and a second stepping mirror is used to scan north-south. The METEOSAT spacecraft is spin stabilised to sweep the imaging payload east-west, and the mirror scans north-south.

The principle design trade-off of the whiskbroom imager is that mechanical complexity is increased, simplifying the electronics to the point where a simple photo-detector becomes the optical sensor. In addition to the precision active mechanics of the scanning mirror (and in the case of the TM, a second scan correcting mirror), the focal plane arrangements are also highly complex. For example, the TM has a total of 100 photosensors (16 simultaneous scan lines in six spectral bands, and 4 simultaneous scan lines in the thermal-IR band) located on two separate substrates (one actively cooled for IR sensing). The individual sensors are themselves quite complex, with some of the bands requiring photomultiplier tubes to amplify the tiny photonic fluxes associated with the very narrow IFOV (instantaneous field of view). Furthermore, the actual positions of the sensors are staggered so that when read sequentially, their samples correspond to the same patch of ground; the subsequent data format conversion to obtain simple raster images is consequently fairly convoluted.

Up until the mid-1980s, the whiskbroom scanning imager was the only viable design solution for producing remotely sensed data, because the techniques for manufacturing highly integrated semiconductor image sensors had not been perfected. The sole means of obtaining high quality electronic images was therefore to use this mechanical scanning technique with arrays of simple solid-state detectors. However, because of this simplicity, a wide range of detectors could be accommodated within a single instrument, providing very high specification multispectral performance and radiometric calibration.

The design lifetime of mechanically active systems is invariably shorter than fully static designs, due to friction wear and loss of lubricant. This situation is exacerbated in space due the impossibility of servicing, and the specific problems of surviving in a vacuum, such as the cold-welding of bare metal surfaces, and the outgassing or creeping of lubricating materials. Even when a mechanical system can be designed with acceptable reliability, the power consumption of these motor driven systems is high compared to equivalent all-electronic systems.

2.1.1.2 The pushbroom scanning technique.

By the mid-1980s, the manufacturing process of highly integrated silicon imaging arrays had matured significantly from the single photodiodes of previous decades. In particular, the development of charge-coupled device (CCD) sensor arrays has revolutionised all aspects of the imaging industry. The quality of these devices has allowed them to be used as the primary detectors of several remote sensing instruments, the best known of which is the family of French satellites, the SPOT series.

The mode of scanning used on SPOT is known as the pushbroom method, and is exactly the same technique used in modern facsimile machines to scan a sheet of paper which is swept past the detector. A pushbroom imaging instrument will use linear CCD arrays with many thousands of pixels to capture an entire scan line as a single operation.

Successive lines are captured as the satellite moves over the Earth, building up an image of a swath of the Earth's surface.

The whiskbroom and pushbroom techniques are similar in that they require the satellite's along track motion to build the scan lines into complete two-dimensional images. However, the staring CCD array of a pushbroom imager eliminates the need for any moving mechanical parts (i.e. rotating mirrors). Although the electronics of the SPOT HRV is consequently more involved than that of the LANDSAT instruments, most designers consider the pushbroom's all-electronic design a distinct advantage over the mechanics of the whiskbroom. In fact, virtually all new designs of remote sensing spacecraft adopt the pushbroom philosophy. This includes the VNIR and MESSR of Japan's JERS-1 and MOS1 spacecraft respectively, the LISS instruments on India's IRS-1A and 1B, the German MOMS instrument which has flown on Shuttle and Mir, and of course SPOT and its derivative, HELIOS.

By eliminating moving mechanics, a pushbroom instrument is assembled as a monolithic unit. In the SPOT HRV, the 6000 pixels of the final image are produced by 4 CCD arrays mounted onto beam-splitter prism, each with 1728 pixels of which 1500 are used. Multispectral capabilities are achieved by carrying several pushbroom sensors, each of which is fitted with a different optical filter. As the manufacturing techniques have improved, much larger arrays have become available. At the time of writing, single arrays with ten and twelve thousand pixels have been available for a couple of years, and single devices achieve three-band colour by incorporating three separate eight thousand pixel CCDs each fitted with an appropriate colour mask. These trends are likely to continue, particularly in response to the market for high resolution flat-bed scanners, but no doubt with applications in space remote sensing.

The main disadvantage of the pushbroom design when compared to whiskbroom systems is the limited range of photodetector materials. Only silicon can be manufactured to the levels of integration and purity required, limiting the spectral response of a pushbroom imager to wavelengths from 0.4 to 1.1 μm. Nevertheless, on-going research is intense to extend this range into the UV as far as 0.2 μm by using suitable coatings, and into the mid- and thermal-IR by depositing more exotic semiconductors, with different spectral sensitivities, onto a silicon CCD substrate. At the time of writing, arrays of 512 pixels are available at wavelengths from 1 to 2, 2.5 to 5 and 8 to 12 μm, and by the end of the decade, much longer mid- and thermal-IR CCD arrays will no doubt be widely available.

The absence of moving parts in the pushbroom design has many advantages including simpler focal plane arrays, greater robustness, and lower power, mass and volume requirements. The pushbroom architecture is now the most favoured approach for new remote sensing programmes requiring visible and near-IR sensitivities. The whiskbroom designs are still maintained in long-standing Earth observation programmes to avoid redevelopment costs and ensure data compatibility. However, as the emerging technologies for mid- and thermal-IR CCD arrays matures, the pushbroom approach will probably supersede many of the more traditional instruments.

2.1.1.3 The area sensing (camera) technique.

Whiskbroom and pushbroom imagers use sequences of line scans to build up complete images. The alternative to these scanning approaches is to capture the entire scene in a single operation by using a sensor which preserves the two-dimensional structure of the scene. The tubes, and subsequently CCD arrays, used in television cameras do just that, producing a complete image without requiring any moving parts at all.

Frame cameras were used extensively in the early phases of space exploration, with systems using vidicon tubes appearing on the earliest US weather satellites (TIROS, ESSA and ITOS) and large format photographic (i.e. using film) cameras deployed on the manned Gemini, Apollo and Skylab missions. In fact, before its launch, the Return Beam Vidicon (RBV) on LANDSAT-1 was considered the primary payload over the MSS.

When implemented on a remote sensing satellite, a full-frame camera has two particular features of key importance when compared to the scanners discussed previously: an integral two-dimensional structure and a very short exposure time. The sensor architecture ensures that pixels in the image faithfully record the geometry of the ground below. Any distortions caused by the optics or the sensor itself (unlikely in CCDs or film), can be determined in advance, and an inverse transformation applied automatically to correct for these deformations during post-processing. Similarly, the fact that a camera only requires a few milliseconds to take a snap-shot of the Earth, as opposed to a scanner which may take tens of seconds, makes it resilient to drifts in the satellite's pointing accuracy. Therefore, if the spacecraft's stability is not guaranteed, a frame-camera is still able to capture geometrically registered imagery, whereas a scanner cannot.

Despite these advantages, frame cameras received little consideration as remote sensing instruments once whiskbroom scanners had been perfected. This was primarily due to limitations of the imaging medium. Although the sensitivity and resolution of photographic film is excellent, it is difficult to handle in the space environment. Moreover, it is a depletable resource, and delays in viewing the imagery are incurred by the retrieval and developing stages. Nevertheless, many ingenious solutions have been implemented to exploit the advantages of film cameras, particularly in the early years of space exploration. Film has primarily been used on manned missions where retrieving the imagery is not a problem, but Soviet (now the ex-Soviet) unmanned programmes continue to use this medium, jettisoning canisters of exposed film by parachutes on a daily basis, to be recovered by aircraft in flight. On tightly-focused and short-duration missions such as the Lunar Orbiters [Colwell, p.213][Rycroft, p.162] where retrieval was not possible, the film was developed on-board, and scanned electronically for transmission.

However, for the majority of applications, a non-depletable (i.e. electronic) detector is required. Until the mid-1980s, this implied using some form of electron tube device, generally a vidicon, inside the camera. However, unlike solid-state detectors or film, vidicon tubes can suffer from internal distortions due to non-uniform charge build-up on the face-plate, causing the scanning-beam to deflect. Although the technology has doubtlessly improved in the meantime, the vidicon cameras on MARINER-6 and 7 (1969) suffered up to 5 pixels of distortion from this source [Slama, p937]. The fiducial marks on early vidicon cameras allowed most of these errors to be removed during post-processing, by comparing them to a reference grid. The geometric distortions, along with factors like the fragility, the lack of spectral selectivity, the pronounced aging characteristics, and the susceptibility to electrical, magnetic and microphonic interference of the vidicon tubes meant that by the launch of LANDSAT-4 they were entirely supplanted by the scanning instruments with solid-state sensors, not to be used again.

However, since the late-1980s, when high sensitivity field-array CCD sensors became available, cameras have been making a come-back in space imaging systems, particularly for astronomical and interplanetary applications, including the Hubble Space Telescope, Galileo (to Jupiter), Giotto (to Halley's Comet) [Keller et al], and the ill-fated Mars Observer mission [Malin et al, 1991][Malin et al, 1992]. In these situations, the spacecraft generally has no velocity with respect to the scene, and scanning is not possible. Furthermore, light levels are generally very low, so the imager must stare at the subject for prolonged periods (sometimes as long as hours) to collect enough photons. For the same reasons, two-dimensional CCDs are also widely used in star imagers for precision attitude determination. Such devices possess all the features associated with solid-state detectors (sensitivity, linearity, solidity, lower power) but offer the guaranteed geometry of a frame-camera.

Until recently, the principal drawback of area-array CCDs was their limited number of sensing elements; primarily designed as television sensors, CCDs with pixel counts higher than around 550 x 550 pixels were uncommon. However, the manufacturing yield has been continually improving, and 2000 x 2000 pixel arrays are now widely available, and announcements for much larger CCD arrays are making news (Dalsa Inc. - 5000 x 5000 pixels; Ford Aerospace, Loral-Fairchild and Eastman-Kodak - 4000 x 4000 pixels). As with pushbroom arrays, the spectral sensitivity of area-array CCDs is limited to that of silicon (i.e. 0.4 to 1.1 μm). However, the techniques being developed for mid- and thermal-IR linear CCDs applies equally to area-array CCDs; video resolution (560 x 560 pixel) devices are leaving the laboratories, and entering production.

The compactness, mechanical simplicity and low-power of CCD cameras make them suitable for deploying on microsatellites. However, the real advantage of this architecture is the guaranteed image geometry, irrespective of attitude control (within reason). This allows imaging applications to be supported by spacecraft with much more modest attitude control specifications than conventional remote sensing satellites, i.e. microsatellites. This theme is pivotal to this thesis and is explored in considerable detail in chapter 3.

2.1.2 COMPARISON, ADVANTAGES AND DISADVANTAGES OF IMAGER ARCHITECTURES FOR METEOROLOGICAL IMAGING.

The previous sections have outlined the concept of the three basic techniques of generating electronic imagery from space. As alluded to, the technique chosen for a given instrument depends largely on suitability and sophistication of the detector technology when the mission is defined. For this reason there have been continually evolving trends in the design of remote sensing instruments, reflecting the state of perfection of contemporary electronic sensors. As the performance of electronic systems has improved, there has been a move away from the whiskbroom scanners. To illustrate this, it is pertinent to quote [Slater p.435] who provides a useful bullet-point summary of the advantages of a multispectral solid-state pushbroom imager over a multispectral scanning system:

1. *It is simpler, more reliable, and cheaper because there are no moving parts.*
2. *Also because there are no moving parts, the imager can have a higher stability, which is an advantage for high resolution purposes.*
3. *The pushbroom configuration provides imagery of higher geometrical fidelity, and the various wavelength bands can be registered more accurately.*
4. *The longer integration time for the solid-state imager provides*
    a) *a system of higher f-number and hence smaller size, and / or*
    b) *a system that provides imagery of higher signal-to-noise ratio.*

He concludes that based on these four advantages, solid-state pushbroom imagers result in a system of higher performance and lower cost, with two reservations:

1. *Pushbroom imagers have many more detectors to calibrate.*
2. *They have no IR capability at present.*

Although, linear CCD arrays with IR sensitivities are now available, these points do highlight the need to consider the payload requirements carefully before selecting an architecture for a imaging instrument. Despite the huge advances in solid-state sensors in the fifteen years since this list was compiled, there are still some applications where a whiskbroom imager may be most suitable in fulfilling the mission goals. Furthermore, the technology of solid-state cameras has developed, offering a third alternative to implementing remote sensing systems. Each of the three techniques for gathering imagery have their strengths and weaknesses, which must be assessed for each instrument based in the mission objectives and the spacecraft specifications and cost. It is again useful to quote authority [Colwell p.336], and present a table assessing the attributes of the various imager designs.

Imager architecture	Frame	Pushbroom (linear array)	Whiskbroom Scanner
Optics required {1}	Wide angle, both dimensions	Wide angle, one dimension	On-axis
Sensitivity	Longest dwell time	Next longest dwell time	Most restricted dwell time
Effect of platform stability	Least susceptible	Less susceptible	Most susceptible
Multispectral use {2}	Poor	Registration restricted by array * accuracy. Restricted space.	Most suitable
IR capability {3}	Very limited *	Cooling load high	Cooling load modest
Radiometric calibration {4}	Very difficult	Difficult *	Least difficult
Geometric accuracy {5}	Poor for electron beam devices. Detector arrays have good potential	Limited by array technology	Very high precision possible (1 μrad) (represents mature technology)
Number of pixels in scene {6}	Limited by array size and optics	Limited by array length and optics	Unlimited

* Improvement is expected with technology advances

Table 2.1.2 **Comparison of imaging gathering techniques for remote sensing.**

The table is reproduced exactly and summarises the principal trade-offs associated with each architecture. However, the author feels that a number of footnotes are needed to reflect technological advances:

1. The development of sophisticated ray-tracing software in the last decade has resulted in significant progress in the design of optics systems. For many applications, it is possible to custom-design or to use superb quality off-the-shelf lenses and telescopes to illuminate the larger target areas of CCD arrays.

2. Although the optical arrangement necessary to implement multispectral imagers are more complex and voluminous with CCDs than with single photo-sensors, it is not as difficult as this text suggests.

3. The UV and IR capabilities of CCD arrays do still lag behind those of single element sensors, although the discrepancy is rapidly being reduced. The mass of the silicon in a CCD array is not much greater than for a photodiode, and so cooling requirements are not significantly increased.

4. The performance of all modern electronic sensors is very good, with excellent linearity and stability. Therefore, the types of calibration required for the earlier LANDSAT sensors are now guaranteed by the manufacturing process. If a definitive characterisation of each pixel in a CCD is nevertheless required, then there is no doubt that this will be a difficult and lengthy process. (Consult section 5.5.2 for a more lengthy discussion).

5. The geometric accuracies achieved on a single wafer to produce a CCD array can be very high (within a few µm over several mm). Even though there may be some manufacturing tolerance within a single device, this can be characterised and will be invariant. Pixels captured by the CCD will always have this same geometric relationship.

6. While whiskbroom scanners can theoretically have an infinite number of samples, this is not in fact practicable. The decreasing IFOV would result in vanishingly small integration times, with a corresponding loss of signal strength. In practice, 6000 pixels is the most that has ever been required from a remote sensing instrument (SPOT HRV, LANDSAT TM). This is easily surpassed by current linear CCDs and is just being attained by area CCDs.

Using 1995 technology, there is relatively little to choose between the three architectures in terms of the quality of the resultant imagery. Radiometric linearity and stability will be very good for all systems. The whiskbroom approach is slightly more flexible in accommodating IR capabilities or large numbers of spectral bands, but the CCDs provide better signal-to-noise capabilities because of the longer integration times. The pixel counts available from the various architectures is now comparable.

Virtually any ground resolution can be obtained - the onus is on the size and performance of the optical systems. To provide the extremely wide coverage required by meteorological satellites in low-Earth orbit with a CCD-based imager (pushbroom or camera), it is necessary to use a lens with a very short focal length (less than 10 mm dependent on the sensor dimensions). Unfortunately, lenses of the type are prone to significant aberrations and barrel distortion, or cylindrical distortion in the case of a pushbroom imager. Conversely, because a whiskbroom scanner's field of view is achieved by the movement of the mirror, it does not suffer these effects.

Of course, there are numerous engineering factors which contribute to the choice of sensor architecture; if the spacecraft has any limitations in accommodating the mass, volume, power or lifetime requirements of the imaging payload, it will be preferable to select a CCD imager. Similarly, pushbroom and whiskbroom scanners demand a very stable platform to ensure geometric registration of the imagery, placing considerable emphasis on the satellite's attitude control. If this is a problem, an electronic frame camera can be used, its geometric fidelity ensured by the structure of the CCD sensor itself.

2.2 SURVEY OF EXISTING REMOTE SENSING SATELLITES.

Before considering the special design constraints and considerations facing the deployment of Earth imaging instruments on microsatellites, it is first necessary to determine what constitutes a 'conventional' remote sensing spacecraft. While every satellite design is different, reflecting a subtle blend of mission requirements, engineering solutions, launcher opportunities and budgetary constraints, it is nevertheless possible to make some generalisation. In 1989, [Deshayes & Mizzi] performed a review of existing and planned Earth observation satellites which still remains accurate; this study includes Indian and Japanese systems but overlooks any Soviet / Russian or Chinese projects. With the exception of some of the Indian satellites (but not the IRS series) which are either experimental (Rohini, Bhaskara) or dual-use (INSAT supports communications and remote sensing), the spacecraft considered possess many similar attributes.

Given widely different orbital conditions and operational requirements, it is not surprising that [Deshayes & Mizzi] treat Earth observation systems destined for geostationary and low-Earth orbit as two distinct groups. Geostationary missions (METEOSAT, GOES, GMS) tend to be smaller and lighter (around 300 kg) than their low-Earth counterparts. These meteorological missions tend to be spin rather than three-axis stabilised, with modest power and data rate requirements, thereby accounting for the relatively small masses. However since the early 1990s, the GOES and METEOSAT platforms have been growing larger to support a wider payload complement and featuring three-axis stabilisation, presumably in response to the larger payloads capabilities of launchers like ARIANE.

However, due to the limited range of orbits available to microsatellites, the focus of this programme has been on systems in low-Earth orbit. (This situation is very paradoxical; although western launches into geostationary-transfer orbit are far more common than into low-Earth orbit, microsatellites cannot exploit these opportunities because of the absence of propulsion systems to stabilise the orbits). Tables 2.2a and b provide a summary of the physical characteristics of significant, recent low-Earth remote sensing systems and families of satellites. In addition to a mass between one and two tons, these satellites typically run power budgets of around a kilowatt and offer three-axis stabilisation to an accuracy of 0.5° or better. These figures tie in with the conclusions of [Deshayes & Mizzi], and those used by [Truss] (492 kg, 540 Watts, 5.5 Mbps) to characterise a range of possible payloads for various applications.

With the exception of the RBV instruments carried by the earlier LANDSAT satellites, the payloads for these missions invariably use scanning techniques to build up their imagery. The on-going US programmes running from the 1970s continue to employ mechanically scanned whiskbroom imagers, whereas the more recent European and Asian programmes are capitalising on technology developments by using linear CCDs in pushbroom scanners. To support these instruments, the downlink capacities of these satellites are equally large, running from the fairly modest 2.6 Mbps of the NOAA family to the continuous 85 Mbps from LANDSAT-4 and -5.

From a historical perspective, there are a number of interesting trends. The earliest satellites, including the first remote sensing ESSA, TOS, ITOS and TIROS mission in the 1960s, were much smaller than their modern counterparts with masses as low as 150 kg. This was no doubt a consequence of simpler mission objectives and limited launcher capacity. As expectations and the ability to launch heavier payloads grew, so did the size, complexity and cost of these remote sensing satellites. The trend appears to have peaked with the massive LANDSAT, NOAA TIROS-N and SPOT satellites. Although, much larger systems like the Polar Platform and the various EOS programmes were proposed in the 1980s, their future now appears uncertain. Although IRS and MOS appear to be reversing the trend, returning to marginally smaller structures, it is not certain whether this is by choice or necessity. Certainly, the design of the IRS series was constrained by limited financing, the state of indigenous technology and the use of a domestic launch vehicle; when reading about IRS, one gets an impression that the Indian designers are a little apologetic that their satellites are not as big and highly specified as SPOT or LANDSAT, despite fine in-orbit performance.

Regardless of the subtle trends and differences between these spacecraft, it is clear that the mass, volume and power requirements of these conventional Earth observation spacecraft are very different to those of 50 kg microsatellites. Generalising, it appears that convention demands that a remote sensing spacecraft must be able to deliver 0.1° pointing accuracy and support several hundred kg of payload consuming up to 300 Watts. This, in turn, dictates a massive platform to accommodate the various housekeeping and payload systems, and to generate the large power budgets. The similarity in the specification of all existing remote sensing satellites is striking, showing more in common than would be found amongst communications, astronomical, scientific or interplanetary spacecraft. Certainly, despite the large amount of talk on the subject, no operational imaging mission flown in low-Earth orbit in the last twenty-five years has had a platform mass of under 500 kg.

Table 2.2a Characteristics of conventional remote sensing spacecraft.

Satellite	NOAA Advanced TIROS-N	LANDSAT 1-3			LANDSAT 4 +
Orbit type	polar, Sun-synch [1]	polar, Sun-synch 09:30 [1]			polar, Sun-synch 09:30 [1]
Orbit altitude	815 km [2]	913 km [1]			705 km [1]
Revisit frequency		18 days [1]			16 days [1]
Spacecraft mass	1700 kg (launch) [1]	953 kg [1]			1966 kg [1]
Spacecraft power	1260 - 1470 W [1]	560 W orbit average, beginning of life, 980 W peak in Sunlight [1]			1497 W peak, end-of-life [1]
Pointing accuracy		±0.7° (pitch); ±1.0° (roll, yaw) [1]			±0.01° [1]
Pointing stability		0.04° / s [1]			$\pm 10^{-6}$ ° / s [1]
Downlink data rate	2.6 Mbps [5]	15 Mbps [1]			85 Mbps [1]
On-board storage		3.4 GBytes (63 scenes) [1]			Uses TDRSS relay station [1]
Imager name	**AVHRR / 3**	**MSS**	**RBV 1, 2**	**RBV 3**	**TM**
Imager architecture	whiskbroom	whiskbroom [1]	triple frame camera, vidicon tube [1]	dual frame camera, vidicon tube [1]	whiskbroom [1]
Imager mass	33 kg [3]	68 kg [1]	92 kg [1]	76 kg [1]	258 kg [1]
Imager volume	80 x 37 x 29 cm [4]	90 x 40 x 35 cm [1]			200 x 70 x 110 cm [1]
Imager power	28.5 W [4]	50 W [1]	174 W [1]	133 W [1]	332 W [1]
Imager data rate	665 kbps [5]	15 Mbps [1]			85 Mbps [1]
Nominal ground resolution	1.1 km [1]	79 m [1]	79 m [1]	24 m [1]	30 m [1]
IFOV	1.3 mrad [4]	86 μrad [1]			42 μrad [1]
Swath width	2400 km [9]	185 km [1]	185 x 185 km [1]	98 x 98 km x 2 [1]	185 km [1]
FOV	± 55.4° [5]	5.8° half-angle [6]	16.2° diagonal [6]		5.8° half-angle [6]
Spectral bands	5 : 0.58-0.68, 0.72-1.00, 1.58-1.64 or 3.55-3.93, 10.3-11.3, 11.5-12.5 [4]	4 : 0.5-0.6, 0.6-0.7, 0.7-0.8, 0.8-1.1. [1] Also 10.4-12.6 on Landsat-3	3: 0.47-0.57, 0.58-0.68, 0.70-0.83 [1]	Panchromatic 0.51-0.75 [1]	7 : 0.45-0.52, 0.52-0.60, 0.63-0.69, 0.76-0.90, 1.55-1.75, 10.4-12.5, 2.08-2.35 [1]
Pixels / line		2300 [1] after resampling	5375 [6]	5375 [6]	6000
Quantisation levels		64 [1]	64 [12]	64 [12]	256 [1]
Optical configuration	20 cm Cassegrain telescope [1]	Ritchey-Chretien telescope: 823 mm EFL, 229 mm aperture, *f*/3.6 [6]	lens: 126 mm focal length *f*/2.8 [6]	Lens: 236 mm focal length [1]	Ritchey-Chretien telescope: 2280 mm EFL, 410 mm aperture, *f*/5.6 [6]
Mission cost	US$ 43.5 M (1984) [9]				US$ 77 M (1978) [9]

Table 2.2b Characteristics of conventional remote sensing spacecraft (cont.).

Satellite	SPOT	IRS-1A, 1B		MOS-1
Orbit type	polar, Sun-synch 10:30 [7]	polar, Sun-synch 10:30 [8]		polar, Sun-synch 10:30 [11]
Orbit altitude	822 km [7]	904 km [8]		909 km [11]
Revisit frequency	26 days [7]	22 days [8]		
Spacecraft mass	1830 kg [7]	975 kg [8]		740 kg [14]
Spacecraft power	1000 W in Sunlight [7]	690 W end-of-life [8]		
Pointing accuracy	±0.15° [7]	±0.4° (pitch); ±0.5° (roll, yaw) [8]		
Pointing stability	$\pm 10^{-3}$ ° / s [7]	$\pm 3 \times 10^{-4}$ ° / s [8]		
Downlink data rate	24 Mbps x 2 [7]	5.4 Mbps, 10.4 Mbps x 2 [8]		
On-board storage	5.3 GBytes [7]			
Imager name	**HRV**	**LISS-I**	**LISS-II**	**MESSR**
Imager architecture	pushbroom [7]	pushbroom [8]	pushbroom [8]	pushbroom [11]
Imager mass	250 kg [7]	38.5 kg [10]	81 kg [10]	70 kg [11]
Imager volume				
Imager power		34 W [10]	34 W [10]	100 W [11]
Imager data rate	24 Mbps [7]	5.4 Mbps [8]	10.4 Mbps x 2 [8]	8 Mbps [11]
Nominal ground resolution	10 m panchromatic, 20 m multispectral [7]	72 m [8]	36.5 m [8]	50 m [12]
IFOV		80 mrad [8]	80 mrad [8]	55 μrad [11]
Swath width	60 km nadir pointing [7]	148 km [8]	74 km x 2 [8]	100 km [11]
FOV	4.13° [7]	9.4° [8]	4.7° x 2 [8]	
Spectral bands	Panchromatic 0.51-0.73 Multispectral: 0.50-0.59, 0.61-0.68, 0.79-0.89 [7]	4 : 0.45-0.52, 0.52-0.59, 0.62-0.68, 0.77-0.86 [8]	4 : 0.45-0.52, 0.52-0.59, 0.62-0.68, 0.77-0.86 [8]	4 : 0.51-0.59, 0.61-0.69, 0.72-0.80, 0.80-1.1 0 [11]
Pixels / line	6000 [7]	2048 [8]	2048 [8]	2048 [11]
Quantisation levels	256 [7]	128 [8]	128 [8]	64 [11]
Optical configuration	Telescope: 1082 mm EFL, 310 mm aperture, *f*/3.5 [6]	Focal length :162 mm [8]	Focal length :324 mm [8]	
Mission cost				

N.B. The list of references used in compiling tables 2.2a and b can be found in section 2.4.1.

2.3 SMALL SATELLITES AND MICROSATELLITES.

In contrast with the large, conventional spacecraft discussed in the previous section, this research programme has been directed at exploring the possibilities of using much smaller microsatellites to support remote sensing activities. Clearly, the mass, volume, power and other services made available to an imaging payload on a microsatellite will be very different to what is expected by the designers of conventional systems. Before considering the engineering differences in these widely contrasting classes of spacecraft, which are covered in some detail in chapter 3, it is worthwhile reviewing the emerging discipline of microsatellite design, concentrating on imaging activities in particular.

2.3.1 DEFINITION OF THE TERM 'MICROSATELLITE'.

The definition of the various classes of satellite is based solely on their launch mass, as this is the only consistent parameter across all missions. Ultimately, the limiting factor governing access to orbit is the availability of launch services based on the satellite's mass. A system for classifying satellites according to their mass has become fairly well accepted in the industry, and is shown in table 2.3.1. Indeed, because these definitions reflect the position of the launch providers, they are not as arbitrary as they might at first appear.

Class	Mass
Large satellite	> 1000 kg
Small satellite	< 1000 kg
Minisatellite	< 500 kg
Microsatellite	< 100 kg
Nanosatellite	< 10 kg

Table 2.3.1 Definition of satellite class according to mass.

Therefore, SSTL's 50 kg spacecraft fall directly in the centre of the microsatellite category. In fact, the distribution of microsatellite masses tends to be clustered around either 50 kg or 12 kg (i.e. virtually nanosatellites). The 50 kg figure is in fact a hard limit set by Arianespace, the major carrier of microsatellites in recent years. Nevertheless, there seems to be a natural coalescence of designs towards these sizes, as they either shed or add system features. Surveying the literature and the [Small Satellites] internet page, the next 'natural mass' (for want of a better term) appears to be about 130 kg, which occurs when the basic features of a microsatellite have been upgraded to support deployable solar arrays and additional attitude control actuators for three-axis stabilisation.

For the purposes of this thesis, any spacecraft smaller than 100 kg is considered to be a microsatellite. As just mentioned, satellites larger than this 100 kg limit will incorporate additional support features that are not typically found on microsatellites. Nevertheless, many points discussed in this thesis will also be applicable to these larger platforms.

2.3.2 GENERAL CHARACTERISTICS OF MICROSATELLITES.

As with conventional remote sensing satellites, there are numerous different solutions to producing a working spacecraft within a 50 or 100 kg mass limit. Nevertheless, there are many common features which can be used to provide a portrait of a typical microsatellite.

Generally, a microsatellite will have fairly squat structure with a maximum dimension of around 600 mm. Cubes or cuboids are the most popular shapes although there are many examples of approximately spherical or cylindrical microsatellites; the cross-sections of these structures will actually be hexagonal or octagonal rather than circular to ease manufacture. Given the small volume of a microsatellite, there are not too many possible structural configurations. The traditional approach is to use a tube or box-shaped core, containing the battery-packs and any other massive components, onto which the remaining module boxes, sensors and solar panels are mounted. A more recent and more efficient configuration uses a stack of module trays which act both as structural elements and as support for the electronic systems. This approach was pioneered by SSTL on the UoSAT-3 and -4 missions, and despite some initial concern about the structural stiffness, has become widespread in the microsatellite field in the last few years. The advantage of this stacked approach is an increased ratio of electronics to structure mass, and a high degree of modularity allowing the satellite to be dismantled and reassembled speedily, as well as providing significant system portability between missions.

Virtually all microsatellites use solar arrays which are body-mounted onto most of the available flat surfaces, although more recently there have been a few examples of deployable, but not Sun-tracking, arrays. The use of body-mounted solar arrays gives a fairly low power output for the total area because most of the cells will not be facing the Sun at any given time. Conversely, this approach dispenses with complex and massive tracking mechanisms, and at least ensures that the satellite receives power even when attitude lock is lost. A typical power budget would have a peak of around 30 Watts with an orbit-average of about 20 Watts in a circular low-Earth orbit. Between half-a-dozen and a dozen NiCd battery cells will provide 6 to 10 Ampere-hours of charge storage to supply the spacecraft systems during eclipse. Figure 2.3.3.3a represents an exploded view of the PoSAT-1 microsatellite showing the stacked structure and the body mounted solar panels.

The attitude determination and control systems available on microsatellites is modest compared to that of a typical remote sensing spacecraft. While many microsatellites do not devote any resources to controlling the satellite's stability, the most common technique for achieving attitude control uses a gravity-gradient boom and magnetic torquing. While such techniques can be used to achieve good pointing accuracy, in practice the resources available on microsatellites has limited the stability of these spacecraft to between 3 and 5°. The consequence of this moderate attitude control on the deployment of remote sensing instruments on microsatellites is considered in detail in section 3.3.

Another area of significant disparity between conventional Earth observation spacecraft and microsatellites is the capacity of the data downlink. Contrasting with the large bandwidths on the conventional platforms, the downlink data rate of a microsatellite is very much lower, typically 1.2, 9.6 or 38.4 kbps. While the power available to the communication modules and particularly the satellite's transmitters is obviously limited, these data rates are not solely restricted by technical factors. In many instances the ground terminals also need to be low cost, making the use of high-gain antennas unattractive. Again, the repercussions of the limited downlink data rates on the design and exploitation of imaging systems is discussed in chapter 3.

One area where microsatellites lead conventional spacecraft is the use of sophisticated, modern microprocessor technology. This is partly due to short lead times permitting newer semiconductors to be incorporated into the design, and also due to the smaller financial risks associated with microsatellites. Certainly, embedded microprocessors occupy a much smaller volume than the discrete hardware systems of conventional spacecraft, whilst operating far more flexibly and intelligently. On many microsatellite missions, there will be multiple processors communicating over a local-area-network, a situation which is virtually inconceivable in traditional satellite design. Similarly, the use of large solid-state memories for on-board storage rather than magnetic tape recorders [Muench] is widespread on microsatellites. As an example, SSTL's most sophisticated mission to date, the FASat-Alfa spacecraft, incorporated 18 microprocessors and microcontrollers and a total of 300 MBytes of semiconductor memory distributed across several modules.

The other electronic systems on microsatellites also tend to be very sophisticated, making use of many recent developments including high performance microprocessors, programmable logic, and solid-state sensors, to name a few. Indeed, there is often a desire to fly new devices as demonstrations to attract funding from the established space industry, which finds much of this technology attractive but difficult to embrace without in-flight experience. The acceptance of new technology is vital for microsatellites to deliver useful services given the limited resources available on these missions.

In many ways, the philosophy driving the current microsatellite community, this research programme included, is similar to that of the early years of spaceflight. The mission objectives are tightly focused, resulting in smaller spacecraft, with the emphasis being on high pay-off given the relatively high risks accepted in promoting continual innovation. This contrasts with the rigid methodology, documentation and extensive hierarchies that have developed in the mainstream space industry. The resurgence of small satellites under NASA's 'smaller, cheaper, faster' slogan is a direct reaction to the long development periods, huge costs and slow acceptance of modern technology of the traditional space industry.

However, whereas the use of small satellites in the 1960s was dictated by launcher constraints, and there were no strict methodologies because they had yet to be invented, modern microsatellites are deliberately breaking the mould in the belief that they can make a valuable contribution to in-orbit services. In particular, the emphasis is on delivering quality service in tightly defined roles but at a vastly reduced cost and on very short development cycles. The cost of a commercial microsatellite is variable, but between £2 and £4 million is fairly typical, and the lead time from conception to launch is generally 12 to 18 months. Although, the missions of the 1960s may have been small and delivered rapidly, they were certainly not cheap, funded by the huge military budgets of the cold war defence programmes. Furthermore, by employing up-to-date technology, modern microsatellites are striving to make space accessible to a wider range of users by increasing system autonomy, and reducing ground segment costs and technical skills needed by the user.

Therefore, the notion of modern microsatellites reflects not only their physical size and limited system resources in terms of mass, volume, power, attitude stability and communications data rates, but also the aggressive approach in the use of technology. The nature of this research programme reflects how the judicious use of modern semiconductors allows microsatellites to achieve goals (i.e. remote sensing) despite the difficult conditions experienced on these platforms, whilst simultaneously reducing costs.

Interestingly, despite the rhetoric from NASA over the last two years, European institutions have been the most innovative in the field of microsatellites for the last decade. While the absence of centralised co-ordinating authorities like NASA or the various US defence bodies has hampered the development of space in Europe, it is presumably this vacuum which has engendered the lateral thinking behind the recent resurgence of small spacecraft. Many institutions and groups have evolved independently to provide novel solutions to pursuing space research on tiny budgets. While a full listing of the various microsatellite activities around the World would be tedious, a mention of some of the groups active in the field is in order. There is considerable enthusiasm in Germany with groups at the Technical University of Berlin's TUBSAT [Renner et al, 1993][Renner et al, 1994], the University of Bremen's BREMSAT [Ginati et al] and the University of Marburg spearheading the AMSAT-DL organisation's Phase-3D minisatellite. The STRV-1A and -1B [Wells] missions were co-ordinated by the UK's Defence Research Agency involving contributions from a number of parties, including SSTL.

Similarly in the US, the long-running microsatellite research programmes have been fostered largely by collaborations between Universities and the amateur radio / amateur satellite communities. The most typical example is the tiny, 12 kg Microsat platforms [King et al] which have been frequent companions to the SSTL missions on the ARIANE ASAP. Recent policy changes of US government agencies (NASA, DARPA, BMDO, etc.), have caused a huge injection of cash into the field of small satellite engineering (at least compared to earlier microsatellite budgets). Orbital Sciences Corp. is a typical example of private enterprise funded to a greater or lesser extent by government contracts. Virtually every large US manufacturer is currently producing paper satellites that are much smaller, and presumably cheaper, than their traditional designs (although certainly not in the same category as SSTL microsatellites).

For an extensive listing of launched and planned microsatellites, nanosatellites and minisatellites, consult the SSTL-sponsored [Small Satellites] home page on the internet.

2.3.3 SSTL MICROSATELLITES.

As part of establishing the context of the author's work, a more detailed review of the family of SSTL microsatellites is appropriate. As these satellites embody many features typical of microsatellites in general, it is reasonable to use these spacecraft as a representative of the whole industry. While SSTL does not have a monopoly on design technique, its reputation for innovation and ability to deliver working systems has made its spacecraft both a yardstick and source of inspiration for much of the microsatellite community. Certainly, the author's work described in this document is heavily influenced by the conditions on these microsatellites. However, in general, it is the approach to systems design, interfacing between modules and deployment of on-board resources that makes microsatellites different from one another rather than outright hardware specifications.

2.3.3.1 UoSAT-1 and UoSAT-2.

The University of Surrey's UoSAT Spacecraft Engineering Research Unit was formed in 1979, with the launch of UoSAT on 6 October 1981 being the culmination of a two year project. The aims of the UoSAT mission were largely educational, involving students and staff to produce a microsatellite as a practical project, following the well established tradition of the amateur radio and amateur satellite communities. While there may have been secret ambitions to develop subsequent missions, in general the UoSAT satellite was considered a one-off project. However, when the opportunity for another launch was offered for 1 March 1984 as an auxiliary payload to LANDSAT-5, following the sudden failure of LANDSAT-4, the UoSAT-2 project was kicked-off, to be completed within a mere six months.

Both UoSAT-1 (renamed from the original UoSAT) and UoSAT-2 were launched on NASA Delta rockets, free of charge. Their structure was based around a central core, as described in the previous section. After initial commissioning difficulties, including the snarling of the mast on UoSAT-1's gravity-gradient boom preventing its deployment, both spacecraft eventually had successful lives producing data from a number of experimental modules, including the first implementation of store-and-forward communications (the Digital Communications Experiment), Geiger counters, an electron spectrometer, a space dust detector, and a digital voice synthesiser which allowed the satellites to 'speak' (a feature popular with younger experimenters). Special issues of the IERE Journal provide detailed descriptions of the [UoSAT-1] and [UoSAT-2] missions and the various sub-systems.

Of particular interest to this research programme, were the experimental CCD cameras flown on these two microsatellites. These cameras were built using developmental frame-transfer CCDs with 385 x 288 pixels from the GEC laboratories (the MA357 on UoSAT-1, and the P8602 on UoSAT-2), which were the precursors of the EEV devices used on the later SSTL missions. Given the primitive state of the sensors (for example, users had to apply their own store-shields to mask half the CCD from incoming light to provide electronic shuttering functions) and that the drive circuitry made from discrete logic, it is not entirely surprising that the results were rudimentary. Nevertheless, UoSAT-1 did produce some recognisable images of the Mediterranean and the limb of the Earth, with one image in particular revealing details of Corsica, Sardinia and the coast of Italy. More information on the UoSAT-1 and -2 cameras is available in [Trayner & Jeans] and [Radbone] respectively.

More important than the results of the individual experiments, the UoSAT-1 and -2 missions provided an invaluable training exercise for the team at Surrey. The focus of the group departed from the traditional forte of British universities in the area of space science, concentrating instead on the overall system design of microsatellites, particularly on the less glamorous power, communications, telemetry, telecommand, attitude control and other housekeeping systems. The overall success of the two missions on a combined budget of around £0.25 million galvanised the University's activities in spacecraft research and projected the notion of cost-effective microsatellites into the space community at large. Certainly, had these missions not been successful, the author would not have had the opportunity to perform the work described in this thesis.

2.3.3.2 Subsequent SSTL microsatellite missions.

Following the success of the first two missions, the University of Surrey established the UoSAT Spacecraft Engineering Research Unit on a permanent basis, and in 1985, formed Surrey Satellite Technology Ltd. to market commercially the cost-effective small satellite techniques developed by UoSAT researchers. [1]

The author joined the growing group in late 1987 to develop new imaging systems for these microsatellites. At the time, work had just commenced on the University of Surrey's next spacecraft, UoSAT-C, to be launched on a Delta in 1989. This was the first microsatellite to use the structure of stacked module trays described in section 2.3.2. Unfortunately, the launch opportunity scheduled for UoSAT-C was cancelled, but at almost the same time, Arianespace took the decision to actively encourage microsatellite research

[1] Although the UoSAT Unit and SSTL are distinct administrative and financial entities, there is in practice little technical distinction in the activities of these two organisations. with the technical staff (the author included) being employed by both simultaneously or alternating between the two. For the sake of this thesis. the symbiotic activities of the two bodies are indistinguishable. Nevertheless, the reader may wish to make note of the subtle differentiation between the commercial missions secured through SSTL and the research projects funded internally by the UoSAT programme.

by developing the ARIANE Structure for Auxiliary Payloads (ASAP). This ring is fitted to the rocket's structure beneath the main mission. The planned 70 kg mass of the UoSAT-C microsatellite was too large to be accommodated by the ASAP, and the payloads of this mission were split between two smaller spacecraft, UoSAT- D and -E, which were developed instead. These became UoSAT-3 and -4 when they were launched alongside SPOT-2 and four nanosatellites (including Webersat - see section 2.3.5.3).

The positive experience of this first launch for all parties convinced Arianespace to continue with the ASAP on subsequent launches. The timing of the ASAP was fortuitous for UoSAT / SSTL, whose success was starting to generate considerable commercial interest from a number of sources. The following half decade has seen a succession of SSTL microsatellite launches, the details of which are presented in Table 2.3.3.2. Although the relationship between SSTL and Arianespace remains strong, a decline in the number of suitable orbits on Arianespace's manifest has forced SSTL to consider using other launch services as well.

Mission	Launch	Status	Primary payloads	Customer
UoSAT-1	1981- Delta 2310	decayed 1989	technology demonstration & research	UoS
UoSAT-2	1984 - Delta 3920	operational	S&F communications & research	UoS
UoSAT-3	1990 - Ariane V35	operational	S&F communications (HealthNet)	SatelLife
UoSAT-4	1990 - Ariane V35	non-operational	technology demonstration	DRA, ESA
UoSAT-5	1991 - Ariane V44	operational	S&F comms, remote sensing, science	UoS, DRA
KITSAT-1	1992 - Ariane V52	operational	S&F comms, remote sensing, science	S. Korea
S80/T	1992 - Ariane V52	operational	LEO communications research	CNES
PoSAT-1	1993 - Ariane V59	operational	S&F comms, remote sensing, science	Portugal
HealthSat-2	1993 - Ariane V59	operational	S&F comms (Healthnet)	SatelLife
KITSAT-2	1993 - Ariane V59	operational	S&F comms, remote sensing, science	S. Korea
CERISE	1995 - Ariane V75	operational	military (classified)	MoD France
FASat-Alfa	1995 - Tsyklon	launcher failure	remote sensing, S&F data collection	Chile

Table 2.3.3.2 Summary of SSTL microsatellite missions.

The UoSAT-4, UoSAT-5, KITSAT-1, PoSAT-1 and FASat-Alfa missions carry Earth imaging cameras developed by the author. The details of these systems is provided in chapter 4 of this thesis. The range of activities supported by all of the SSTL microsatellites is wide with store-and-forward communications, in-orbit technology demonstration, radiation studies, and, of course, remote sensing being the most common themes. Many of the missions, including PoSAT-1 and FASat-Alfa, carry up to a dozen different experiments, not considering the various new technologies deployed around the spacecraft. Conversely, the S80/T and CERISE missions were commissioned to carry specific payloads developed by SSTL's customers. The KITSAT-1 and -2, PoSAT-1 and FASat-Alfa missions have been conducted as part of technology transfer packages for institutions in South Korea, Portugal and Chile respectively. As part of the on-going technology transfer programme, KITSAT-2 was built under licence in Korea from the SSTL designs for KITSAT-1. For more details of the mission profiles and of SSTL's activities in microsatellite engineering and R&D, consult [Sweeting, 1992], [Sweeting, 1995] and [Allery et al].

The cost of an SSTL microsatellite purchased commercially is typically £1.5 to £3 million including the launch. The variation in cost depends on the complexity of the systems required to fulfil the customer's requirements.

The design lifetime of the satellites is targeted as three years for low-Earth orbits, although the UoSAT-1, -2 and -3 missions have survived considerably longer; UoSAT-2 is still operational after eleven years in orbit. All the missions continue to operate successfully at the time of writing with the exception of UoSAT-1, which burned up in the atmosphere at the end of its orbital life in 1989, and UoSAT-4 and FASat-Alfa. UoSAT-4 was launched successfully, and operated for around 30 hours before ceasing transmissions. Following complex diagnostics involving tracking the satellite with a 30 m dish, six months after launch the stray emissions of receivers' local oscillators (at -190 dBW !) were found to be working, indicating that the power system was still functional. Eventually, the most probable cause of failure was determined to be coronal discharge in a partially out-gassed transmit filter. Although very disappointing at the time, the review following the failure of UoSAT-4 highlighted numerous possibilities for improvement for the design and preparation of subsequent missions. Many unnecessary risks were eliminated, and systems that 'had worked before' were extensively redesigned. With hindsight, the failure of UoSAT-4 turned out to be one of the most important learning experiences for the SSTL team.

Most recently, in September 1995, the FASat-Alfa mission was launched into orbit by a Ukrainian Tsyklon rocket from the Plesetsk cosmodrome, which deployed the main mission successfully. In a rather unconventional configuration, FASat-Alfa was mounted to the main payload, SICH-1, instead of the launch vehicle. Unfortunately, the systems on SICH-1 to release FASat-Alfa have failed to respond, leaving the microsatellite stranded, attached to the side of the main payload, which otherwise is operating nominally.

Although the failure review board has yet to submit its conclusions, there is little hope of resolving the situation favourably. The Chilean customers have made an insurance claim, and intend to use this sum to finance a repeat mission, FASat-Bravo, to re-fly the same experiments as soon as possible.

Without wishing to overstate the significance of two failures in twelve missions, the author feels it is nevertheless important within the context of this thesis to be honest about the relative successes and failures of the missions described. Overall, one operational and one launcher / deployment failure in twelve missions remains somewhat better than the space industry as a whole, and decidedly better than the record for microsatellite missions. Certainly, the many aspects of system redesign implemented for FASat-Alfa, including the significant reworking of the imaging modules, are not lost and will definitely be featuring on many of SSTL's future microsatellites.

2.3.3.3 The SSTL microsatellite bus.

Figure 2.3.3.3a shows an exploded view of the PoSAT-1 spacecraft, which uses the structure typical of all SSTL microsatellites apart from UoSAT-1 and -2. Figure 2.3.3.3b shows the satellite when integrated, ready for launch with the gravity-gradient boom stowed. As already mentioned, these spacecraft are built up of a stack of individual trays without any traditional structure. Because of this unconventional approach, there was some concern regarding the satellites' stiffness and ability to survive a launch. Repeated launches and qualification vibration tests have validated the suitability of the approach; indeed significant mass has subsequently been removed from the structural components to improve the payload capability of these microsatellites without any compromise to its mechanical integrity.

Each tray in an SSTL microsatellite is 260 by 260 mm; the depth varies from module to module depending on the height of the electronics to be accommodated but is approximately 30 mm deep for all trays except for the battery box which is 80 mm deep. One edge of the tray is recessed by about 300 mm to accommodate the thickness of the connector plugs and sockets. The satellite's wiring harness is essentially 2-dimensional, running along one side of the module stack. When integrated, the eleven modules are about 450 mm tall, leaving a 150 mm compartment at the top of the stack to accommodate the gravity-gradient boom.

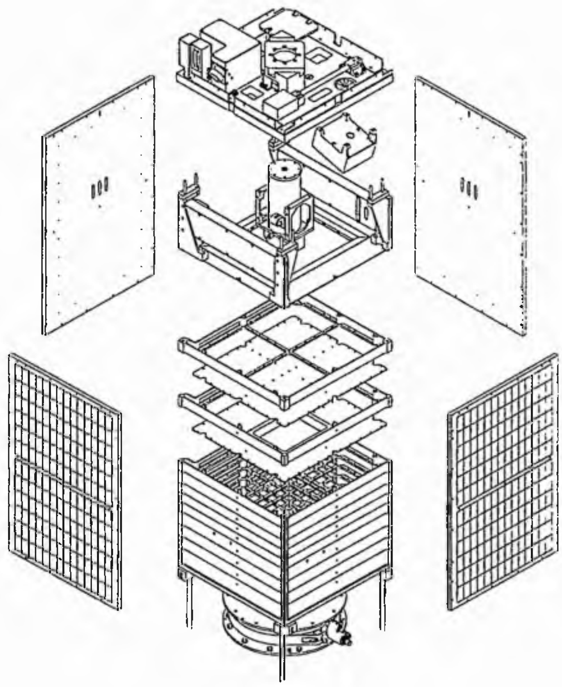

Figure 2.3.3.3a. An exploded view of the PoSAT-1 microsatellite.

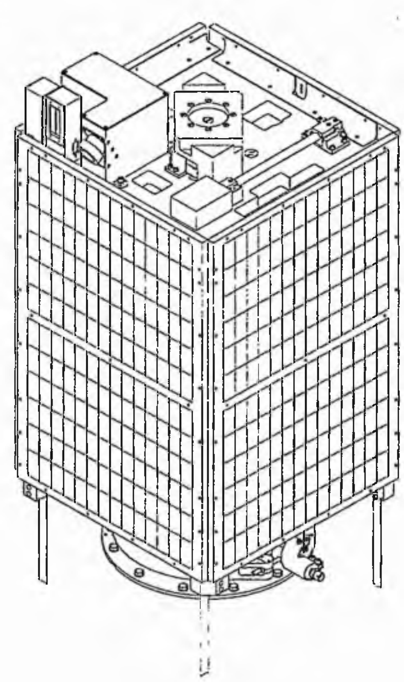

Figure 2.3.3.3b. The PoSAT-1 microsatellite when integrated.

The notion of this modular, stacked structure is that each electronic sub-system occupies its own tray, which can be inserted and removed from the structure with ease, requiring only a few minutes to perform this operation. Although seeing modules being extracted from the satellite on a regular basis can be disconcerting to the unaccustomed viewer, it lets the engineering team make best use of short development time by allowing the various systems to be assembled, tested on the bench and tested in the integrated stack in parallel. When the satellite is fully integrated, only one sub-system can be tested at a time, effectively wasting this time for the other systems. The modular structure provides a great deal of flexibility in this respect.

This modular approach also gives the individual systems a certain amount of independence to either be carried over from mission to mission with minimal change, or conversely to be completely redesigned, with little disruption to the other systems. Although to the outside world the various sub-systems may appear to be unchanging between missions, there is in fact considerable emphasis in redeveloping the electronics to accommodate improvements in performance or technology. SSTL promotes a philosophy of gradual, but continual, product development whenever justifiable.

The breakdown of the modular stack is very similar for all SSTL microsatellites. Only brief details are presented here, emphasising the arrangement of the modules on

PoSAT-1 and FASat-Alfa, showing at the same time both the similarity and yet the diversity of the spacecraft. Compared to the rushed tempo of previous missions when the launch rate was two spacecraft per year, the two year period leading up to FASat-Alfa launch has given the technical team a relatively long gap in which to implement various changes. The characteristics of the spacecraft systems directly effecting the performance of the imaging payloads (i.e. the attitude determination and control, communications, and power systems) is discussed in much greater depth in chapter 3.

Starting from the bottom of the spacecraft:

1. *Battery box.* The base of this module is very much thicker than the rest of the trays to provide enough mechanical stiffness to support the large mass of the battery packs. The attach-fitting to mount the satellite onto the launcher is bolted to the underside of this module. In addition to the batteries and some power conditioning electronics, this box contains parts of numerous other systems which need to have access to the Earth-facing surface of the spacecraft, including various receive and transmit antennas, filters and co-axial cabling, and of course the Earth imaging cameras.

2. *Receiver box.* The satellites employ three separate receiver chains to accept commands and uploaded data. Two of the receivers can be switched between two fixed frequency settings, while the command receiver is fixed, giving the satellite five separate uplink channels in the VHF region. This module also contains hardware demodulators and demultiplexers to fan the uplink signals out to the telecommand system, the various computers and any other modules that may require this data stream. Future microsatellites may well replace the fixed hardware receivers and demodulators with synthesised frequency generators and digital signal processors. The uplink data rate is currently 9.6 kbps.

3. *Transmitter box.* Two modulator and transmitter chains provide downlink capabilities. The modulated baseband signal is mixed onto a synthesised UHF carrier [Da Silva Curiel et al]. Various mixer, pre-amplifier, amplifier and power amplifiers are used to generate nominal power levels of either 4 or 10 Watts of RF power at around 50 % efficiency, although other (lower) power settings can be obtained at a small loss of efficiency. Experimental DSP modulators have been implemented on PoSAT-1 and FASat-Alfa [Sun et al, 1994][Sun et al, 1995], and will doubtlessly be featured as standard on future missions. The main downlink data rate on PoSAT-1 is 9.6 kbps, with an experimental 38.4 kbps modulator which has operated successfully. The default speeds of the FASat-Alfa downlinks were to be 38.4 and 76.8 kbps.

4. *Power system.* This module contains the remaining elements of the power system not located in the battery box. The Battery Charge Regulator converts the raw power from the solar panels into voltages suitable for charging the batteries; on missions where the power budget is marginal (e.g. S80/T), the solar arrays' maximum power point can be tracked under software control from the main on-board computer. The other elements of the power system includes the Power Conditioning Module which produces regulated +5V and ±10V rails using switching regulators, and the Power Distribution Module which feeds the various systems via fused lines or via semiconductor switches featuring presettable over-current protection.

5. *Telemetry and Telecommand (TTC).* The telecommand system is composed of four identical microcontrollers listening to the uplinks, the main on-board computer and the spacecraft's serial data buses for coded command instructions. When a valid command is received, the microcontroller will drive a CMOS latch into the correct state, setting or resetting the command line. The telemetry system can be operated either in an automatic hardware mode which generates telemetry frames to be sent onto the downlink, or more routinely, is interrogated by the on-board computer which generates software telemetry packets for the downlink, merged with the various other data streams. The advantage of the software approach over the more conventional fixed hardware sequence is the ability to concentrate on key parameters more intently and to format the data more conveniently. This is particularly useful when executing difficult or potentially dangerous sequences when the update rate of the hardware mode is too slow to provide adequate time resolution.

   The main limitation of the current telecommand system is the limited number of commands (around 128) that can be supported. Similarly, the telemetry channels are limited, and can only be polled by one system at a time (i.e. the on-board computer). To remedy such problems, these centralised facilities are being replaced with a distributed system, with each module containing an appropriate microcontroller and interface, allowing random access to an unlimited number of command and status channels. Furthermore, the notion of TTC is also extended from its traditional role to encompass communication and interactions between software processes on different computers. FASat-Alfa carried numerous experimental and semi-operational implementations of this distributed network. Although disappointed with the absence of feedback on its in-orbit performance, SSTL will certainly use this technology more prominently on all forthcoming missions.

6. *Telecommand expansion and second on-board computer.* Like several others, this module is split into two halves, each containing a separate sub-system. The 'expansion' module contains several additional telecommand lines that cannot be handled by the main telecommand module. (The limitation is generally the number of pins available on the TTC module connectors, rather than another technical reason). The expansion box is also available for any miscellaneous circuitry such as extra power switches, communications return lines, and temperature and current sensors that cannot be accommodated elsewhere. Another advantage of adopting a distributed TTC system is the reclaiming of this one and a half module trays for payloads.

   The other half of this module is devoted to the spacecraft's secondary on-board computer. Unlike the main OBC which preserves a high degree of pedigree from mission to mission, this secondary computer provides scope for a certain amount of experimentation: on PoSAT-1 and Healthsat-2, an Intel 80C188 (known as the OBC188) fulfilled this function, whereas a more powerful Intel 80C386 (OBC386) was developed for FASat-Alfa, potentially replacing the established main OBC in orbit. In either case, this redundant computer can take over all of the main OBC's functions if necessary.

7. *Main on-board computer (OBC).* The main on-board computer for all of SSTL's recent microsatellites has been an Intel 80C186 (OBC186), although significant performance upgrades to enhance speed, compactness and features have been implemented over the missions. The SSTL philosophy is to develop hardware-based power, communications, attitude, or TTC systems that can survive quite happily without any OBC control, for example during commissioning or a software crash. However, the next layer of functionality and performance is provided by the OBC's programmes. This allows more flexibility, efficiency and complex operations than with hardware alone, but without compromising mission integrity.

   In addition to these basic aspects of system control typical of all satellite OBCs, including the TTC, attitude control and power management, the SSTL OBCs also act as file servers to both ground stations and other on-board modules. As such, the computer fulfils the role of a central hub in the store-and-forward communications network, typical of SSTL and other microsatellites (refer to section 3.4.2 for a more detailed discussion of these facilities). The OBC has access to a large array of semiconductor memory (currently 16 MBytes) known as the Ramdisk, in which to store communications traffic and on-board data.

8. *Payload.* Three modules are left to accommodate the electronics of the various experiments or payloads. In the case of the S80/T and Cerise missions, the whole of this space was allocated to the customer to fill as required. On the other microsatellites, these trays of electronics are filled with a range of different systems. On UoSAT-3 and -5, tray 8 contained the Ramdisk until it was condensed to fit in with the main OBC186. On KITSAT-1 and PoSAT-1, this module contained the Cosmic Ray Experiment, profiling the energies and prevalence of radioactive particles striking the spacecraft, and an experimental digital signal processing modulator. On FASat-Alfa, a more advanced DSP system, the Data Transfer Experiment, was carried to investigate the possibility of using techniques like frequency hopping and modulation pre-emphasis to combat channel degradations to sustain communications with very low cost ground terminals.

9. *Payload.* On the missions carrying cameras, this module has contained the processing elements of the imaging system, i.e. the transputers. On KITSAT-1 and PoSAT-1, the camera microcontroller was also housed here. Electrical connectivity to the sensing elements of the cameras is over a dedicated sub-harness.

10. *Payload.* On PoSAT-1 and FASat-Alfa, half of this module has contained the GPS receiver, whose antenna is mounted on an external surface. On PoSAT-1, the other half was occupied by the microcontroller portion of the star camera, with the CCD sensor and support electronics mounted to the top of the spacecraft viewing deep space. On FASat-Alfa, the star sensor is replaced with the Solid-State Data Recorder, an experiment to assess the suitability of very high density memories for use in space. This comprised 256 MBytes of dynamic RAM, supported by an Intel 80C386 processor to monitor the contents of the memory and preserve its integrity through software encoding.

11. *Attitude control and safety.* The topmost module of the stack contains an array of attitude determination and control systems, including the latching relays and current drivers for the magnetorquer windings. The electronics for the magnetometers are also contained in this box, although the sensing heads are positioned on an external surface, away from the electrical and magnetic interference of the spacecraft. This module also contains the circuits for safe-arming the satellite and for firing the pyrotechnic bolt-cutters needed to release the gravity-gradient boom.

12. *Boom compartment.* A fairly large compartment, some 150 mm deep, is required to accommodate the deployment mechanism of the gravity-gradient boom. The mast of

the stowed boom passes through a hole in the satellite's top facet, where it is attached to a relatively massive 3 kg tip-mass. The tip-mass is secured to the top facet during transportation and launch; firing the pyrotechnic cutters releases the tip-mass, where upon the spring-loaded mast deploys to a length of around six metres.

The remaining space in the boom compartment and on the top facet is used to house a range of smaller systems such as the magnetometer heads, optical Sun, horizon and / or star sensors, a GPS patch antenna, safe-arm plugs, radiation monitors and other small experiments. Unfortunately, despite the relatively large volume available in this compartment, it is not possible to accommodate especially large instruments because of the imposing presence of the boom mechanism and tip-mass.

The author hopes that this has provided a reasonably good overview of the various systems that make up a typical SSTL microsatellite, offering an insight not only to the hardware but also revealing some of the design philosophy behind the spacecraft. There is a constant effort to shrink the housekeeping systems to improve the spacecrafts' payload capacity, whilst also striving to improve the overall performance. This generally involves further modularising the sub-systems to cope with increasingly diverse requirements. Modules which are notionally experiments such as the GPS receiver, the star sensor or Earth imaging cameras and transputers are in fact becoming fairly standard units which can be added to augment the standard spacecraft facilities.

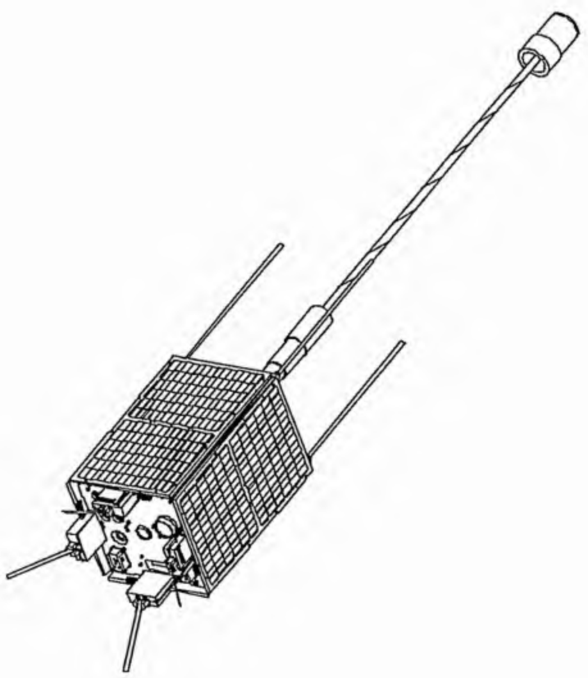

Figure 2.3.3.3c

The FASat-Alfa microsatellite in orbital configuration with boom deployed.

The reader may have noticed that the battery box and boom compartment are relatively full of various sensors and antennas which need to have access to the external surfaces of the satellite, which is made difficult by the dominating presence of the boom and battery packs. (Only the top and bottom of the spacecraft are available for these systems given the body-mounted solar arrays on the four remaining surfaces). Responding to this limitation, the boom has been carefully re-engineered to fit on the underside of the battery box for the Cerise, and subsequent, missions. Figure 2.3.3.3d represents an exploded view of FASat-Alfa, shows how this provides a reasonably large volume for accommodating larger payloads, including imaging systems with larger focal lengths. Although the satellite maintains the same up-and-down orientation with respect to the launch vehicle, once in orbit the battery box now faces to space. To prevent confusion, the enlarged area is explicitly referred to as the Earth Observation Compartment. On FASat-Alfa, this space allowed four cameras to be supported alongside a range of other experiments. Although this newer configuration will almost certainly be used for all future SSTL missions carrying imaging systems, the existing structure will also be retained due to its lower cost.

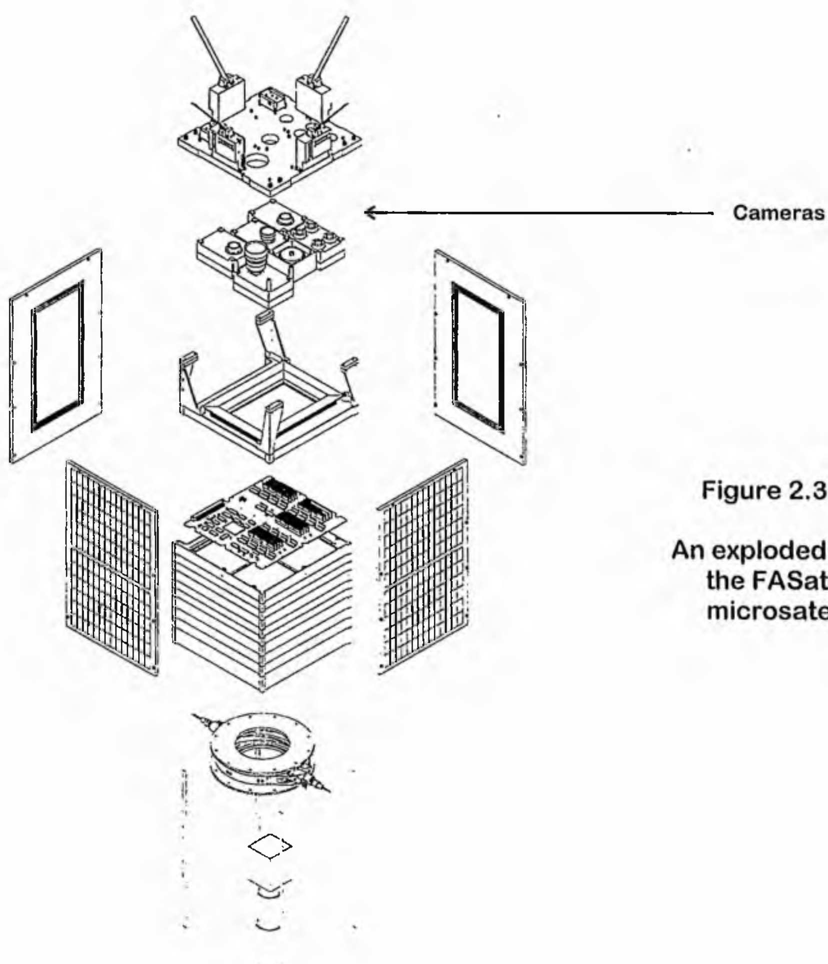

Figure 2.3.3.3d

An exploded view of the FASat-Alfa microsatellite.

2.3.4 KEY DIFFERENCES BETWEEN MICROSATELLITES AND CONVENTIONAL SATELLITES WITH RESPECT TO REMOTE SENSING.

Having painted a portrait of microsatellites in general, and of the SSTL spacecraft in particular, it is worth assessing the key differences between these small satellites and conventional remote sensing platforms. Without pre-empting the detailed examination of the conditions on-board microsatellites presented in chapter 3, it is clear that the capacities of and facilities provided by microsatellites will be inadequate to support the requirements of most or all of the instruments presented in tables 2.2a and b. Very briefly, the principal engineering constraints imposed by a microsatellite platform (dedicated entirely to imaging payloads) can be summarised as:

- Payload mass under 12 kg
- Payload volume no more than 30 cm cube
- Continuous payload power under 10 Watts, peak power up to 40 Watts
- Attitude control to within 3 to 5°
- Reduced communications data rates of 9.6 to 38.4 kbps
- Preferably no moving mechanics

Although microsatellites are clearly very demanding platforms on which to fly Earth observation instruments, there are huge benefits in terms of vastly reduced construction, launch and operational costs, coupled with short development cycles. These factors allow the technology used on such small spacecraft to be more up-to-date than would be possible on a conventional mission. Furthermore, the low cost allows microsatellites to be targeted at specific applications, or even to be stored and deployed in response to specific events (assuming the launch facilities are equally versatile).

These issues will be considered in much greater depth in the next chapter, but it is nevertheless worth drawing these items to the reader's attention at this stage. In particular, the relatively coarse attitude control of current microsatellites presents difficulties in accommodating some of the architectures of imaging instruments described in section 2.1.

2.3.5 MICROSATELLITES CARRYING IMAGING EXPERIMENTS.

To situate the relevance of the work described and defended in this thesis, it is necessary to review other efforts in the field of microsatellite Earth observation. Despite the considerable attention paid to the Earth observation from small satellites, a literature search has revealed relatively few examples of remote sensing microsatellites. In conducting this review, three reasonable criteria have been applied to short-list specific systems :

1. The satellite's mass must be under 100 kg,
2. The microsatellite must be in the civilian arena (i.e. not solely funded from military budgets),
3. The microsatellite must have demonstrated imaging capabilities in orbit.

This thesis considers remote sensing on microsatellites, and the first criterion merely restates the definition of a microsatellite. The second point is largely a caveat; many military projects and technologies are surrounded in secrecy. Even when the missions are not classified, the large budgets available to these programmes can give them an huge instantaneous impetus that is inconceivable in a civilian project, and including them in this review would result in an uneven perspective. The LOSAT-X microsatellite described later is an example of the accelerated progress that is possible when funding is not scarce.

However, the third criterion is to be stressed particularly. There are innumerable papers published in conference proceedings describing various organisations' ambitions to build and launch microsatellites. However, the vast majority of these do not progress much beyond the stage of a preliminary feasibility study. Given that these 'paper studies' never have to address the serious technical and financial design trade-offs of a real mission, the authors are capable of (and often succumb to) making outlandish claims as to the performance of their system. As the only incontestable measure of a system's suitability for an application is its ability to deliver a service or demonstrate a technology in-orbit, the author's search has been limited to systems that have been productive. (The reader should consult the annual proceedings of the *AIAA / USU Conference on Small Satellites* at Utah State University, or the SPIE conference on *Small Satellite Technology and Applications* (various locations) for a broad sample of articles on 'paper satellites').

The quality of the imagery (or total lack of imagery) published in the literature supports the author's contention that the work carried during this research programme is the most convincing demonstration of remote sensing capabilities from a microsatellite to date. Only three other satellites meet the criteria listed above: Rohini-3 (1983), Webersat (1990) and the very recent MicroLab-1 (1995). The author is convinced that the quality of imagery and the consistency of operation of the SSTL imaging microsatellites, in particular PoSAT-1, surpass the performance of these missions.

However, a review featuring only three systems would not give the reader a good impression of the state of endeavour in the area, and a number of other systems have been included, at the author's discretion, to present a wider and more representative perspective of the issues. Thus, a few heavier and failed satellites are also described for completeness.

2.3.5.1 Indian Space Research Organisation's Rohini series.

Rohini was an integral part the Indian Space Research Organisation's (ISRO) starter programme to develop both domestic satellite technology and launcher capabilities. As such it is an interesting programme, with all the systems specified and, as far as the author can tell, developed and built in India, unlike the country's larger 'conventional' remote sensing and communications spacecraft which have had relatively little indigenous technical input. The Rohini family of 40 kg spacecraft were conceived to act as payloads for the first experimental firings of the SLV-3 rockets launched from the Sriharikota base. Rohini-1 was launched and failed to achieve orbit on 10 August 1979. Its successor, the 35 kg Rohini-1B was carried into an eccentric 305 x 905 km, 45° inclination orbit on the SLV-3's first successful launch. Similarly, Rohini-2 (launched 31 May 1981) failed to achieve a stable orbit, re-entering after eight days; confusingly, this microsatellite is also referred to as Rohini-D1. The slightly heavier 42 kg Rohini-3 (Rohini-D2) was successfully launched on 17 April 1983, enjoying a 5 year orbital lifetime. (Details from [Turnill]).

Given that this programme was not only developing the satellite systems, but also experimenting with the rocket technology, the Rohini family did not enjoy a high rate of in-orbit success, limited by launcher failures. Similarly, the somewhat unconventional orbits (nominally 300 x 850 km, 45° inclination) into which these satellites were placed also testifies to the developmental stage of the launch vehicle. These microsatellites delivered 15 Watts of power, had a downlink rate of 32 kbps, and used magnetic torquing to achieve a 6 to 8 RPM spin. The spin axis was perpendicular to the orbit plane, so that the satellite had a characteristic 'barrel-roll', the Thompson equilibrium.

[Alex] and [Alex et al] describe the imaging systems flown on Rohini-2 and -3. The design of these imagers was unconventional, as can be expected from a spinning satellite in low-Earth orbit. A 250-element linear array operated in a pushbroom mode, but relying on the satellite's spin rather that its orbital velocity to scan the scene. The detector was not a CCD, but an array of photodiodes from EG&G Reticon incorporating a self-scanning output device for multiplexing between the sensing elements. As the sensor's optical axis swept though nadir, 80 scan lines were captured, recording the scene through a cone of ±4.5°. On the satellite's next revolution, another 80 x 250 pixel image was captured with a 10 to 15 % overlap of the previous image. The start of each imaging sequence was triggered by a horizon sensor mounted at a suitable angle with respect to the spin geometry.

The system is quoted as having a 80 x 250 km coverage at 1 km resolution from an altitude of 500 km. The sensor had panchromatic sensitivity, and the output signal was quantised to 6-bits. The lens had a 25 mm focal length and an *f*-number of 1.8. The power consumption and mass of the imaging instrument were 3 Watts and 2.5 kg.

This instrument was enhanced for Rohini-3, by adding a second detector array to provide dual-spectral sensitivities in the conventional red (0.6 to 0.7 μm) and near-IR (0.8 to 0.9 μm) bands. Mass and power requirements of this enhanced imager were correspondingly increased to 3.5 kg and 4 Watts. An interesting experiment in on-board image processing was the implementation of a feature identification algorithm. This used a logic circuit to take the ratio of the two bands and classify the pixel as belonging to one of four possible categories: water (low pixel brightness in both bands), vegetation (dark in the red, bright in the near-IR), bare soil (the opposite), and snow or cloud (bright in both bands). The 2-bit identifier was transmitted to the ground, and is estimated to have an accuracy of around 85% [Alex].

The author has never seen any imagery from Rohini-3. (Rohini-2 did not survive long enough to produce any conclusive data). The absence of any image reproductions in the publications describing the Rohini project suggests that the imaging experiment was not entirely conclusive. The imagery would have suffered significant distortions caused by variations in the satellite's spin rate, and the residual attitude nutations and librations that would have occurred. Without a momentum or reaction wheel to damp out this residual energy, it would be virtually impossible [Hashida] to control these two aspects of the attitude behaviour sufficiently to prevent misalignments between the image sweeps. Furthermore, the attitude sensors provided would not have had sufficient accuracy to allow these errors to be removed in an open-loop post-processing algorithm. Similarly, it would have been a painstaking task to paste the successive image swaths together given these misalignments, exacerbated by a difference of up to 9° in viewing angle for the overlapping areas. Finally, the satellite's eccentric orbit would have caused variations in the scaling of the imagery, which while not impossible would have been labour-intensive to compensate for.

At any rate, despite some promising initial success, the Rohini programme was terminated (or at least suspended) without revolutionising the domain of microsatellite remote sensing. Certainly. the nation's ambitions had surpassed the capabilities of such small microsatellites as India developed capabilities to launch larger payloads. Rohini was overshadowed particularly by the on-going Bhaskara and INSAT technology-transfer programmes running under the tutelage of the USSR and USA respectively.

2.3.5.2 Indian Space Research Organisation's SROSS series.

The follow-on programme to Rohini was the SROSS (Stretched Rohini) series. Although at about 130 kg, these spacecraft cannot be considered microsatellites, they are nevertheless worth mentioning here. As with the Rohini missions, the SROSS family was principally targeted at developing India's domestic satellite and launcher capabilities. Similarly, the experimental ASLV rocket failed to deploy many of these minisatellites. After two unsuccessful attempts (24 March 1987 and 13 July 1988), SROSS-C and -C2 were deployed on 20 May 1992 and 4 May 1994. SROSS-C2 is now in a 429 x 628 km, 46° inclination, following orbital manoeuvres which consumed 3.7 kg of the satellite's initial supply of 5 kg of propellant [ISRO].

[Das & Kasturirangan] describe how the SROSS satellites have eight body-mounted solar panels mounted onto an octagonal core (1100 mm tall, 820 mm wide) to deliver 45 Watts of power. The two successful SROSS-C and -C2 missions have been designed to have a spinning attitude similar to those of the Rohini microsatellites. The spin rate can vary from 2 to 5 RPM, and the nutation (coning) angle is specified to be less than 2° (reflecting the observations on Rohini's attitude stability). Attitude sensors include magnetometers and Sun sensors, are magnetic torquers are used for control. Six hydrazine actuators deliver 1 Newton of thrust to provide the forces needed during satellite despinning and orbit raising. A passive 'fluid-in-tube' device assists in nutation damping.

[Alex] stresses the alternative, three-axis stabilised configuration of the SROSS-1 and -2 spacecraft. In these missions, the nutation damper was replaced with a single 10 Nm momentum wheel mounted in the pitch axis. Furthermore, the eight body-mounted solar panels were augmented with further eight deployed panels to give the satellite an increased power output of 150 Watts. The three-axis stabilised version of the SROSS platform had a mass of 150 kg compared to the spinner's 110 kg. In the three-axis configuration, the spacecraft accommodated a fairly modest 15 kg of payload, in a volume 500 mm high by 550 diameter [DFVLR].

Of most interest to this study is the implementation of a sophisticated pushbroom imaging system called MEOSS developed by the German DFVLR labs carried as the payload complement of SROSS-2. Having been scaled down from [DFVLR]'s ambitious proposal incorporating both multispectral and stereoscopic capabilities, the instrument carried three linear CCDs for altitude and terrain mapping. The three CCDs were mounted in parallel behind a common lens. The central sensor was nadir pointing, with the other two angled at 22° to image fore and aft of the nadir point. Thus, the scenes viewed by the three CCDs at any instant would each be separated by 162 km along the satellite's ground track, to give a stereo base of 325 km. In addition to providing height information, the particular attraction of using three CCD sensors was to evaluate the possibility of cross-correlating between the three data sets to compensate for stability and orbital fluctuations without having recourse to external attitude or 'ground-truth' knowledge.

From the spacecraft's nominal 400 km circular orbit, the nadir spatial resolution was to be 70 m, but providing a height resolution of 65 m. [Lanzl, 1988] describes that each linear CCD had 3456 photosensitive elements; the manufacturer is not specified but the author deduces that Fairchild or Texas Instruments are the most likely suppliers. The spectral sensitivity of each CCD was the same, covering the band from 057 to 0.70 μm; this choice of band reflects the interest in terrain rather than surface cover because it is relatively insensitive to the presence of vegetation. The optics used was a standard off-the-shelf Zeiss / Hasselblad Distagon lens with a 60 mm focal length set to *f* / 8. The mass and power consumption of the instrument was 10 kg and 25 Watts. The data rate from the instrument was 10.4 Mbps, to be transmitted on the S-band downlink; it is not specified whether this was a real-time data feed, or whether the imagery could be buffered for later transmission.

As already mentioned, SROSS-2 failed to achieve orbit and the MEOSS experiment has not been re-flown on subsequent missions. Indeed, the SROSS family have not demonstrated their three-axis stabilisation capabilities in orbit. This is unfortunate, as the 0.4° attitude stability specifications of the MEOSS instrument were very demanding, and fulfilling these requirements in-orbit would have been a significant step forward in demonstrating the remote sensing capabilities of small satellites.

2.3.5.3 Weber State University's Webersat.

Webersat is one of four extremely small microsatellites launched on the same ARIANE vehicle as UoSAT-3 and -4. These spacecraft [King et al] are tiny 230 mm cubes, with masses of just 10 kg. Webersat is a slightly enlarged version, weighing 12 kg and with the satellite height elongated to 320 mm to accommodate the extra requirements of the CCD camera. With such a small area for body-mounted solar panels these satellites can only generate a peak of 14 Watts of raw electrical power, with an orbit-average (polar Sun-synchronous) of between 5.8 and 6.5 Watts. The transmitters can deliver a peak of around 4 Watts RF (claimed to be 76% efficient), and the downlink data rate is 1200 bps. These spacecraft implement a store-and-forward messaging system compatible with that of the SSTL spacecraft, with a 2 MByte Ramdisk. These nanosatellites possess no active attitude control (refer to section 3.3.2.1 for further details).

According to [Bonsall et al] and [Jackson & Raetzke], the Webersat CCD imager is a modified Canon CI-10 video camera with an integral 25 mm lens and automatic iris. The CCD has around 780 x 488 photosites, and is fitted with an on-chip mask to provide colour information (refer to section 5.4.4.3.5 for elaborations on this technique). When nadir-pointing, the camera's 25 mm focal length lens provides 272 by 216 km coverage, at a mean spatial resolution of 400 m.

The only rework performed on Webersat's off-the-shelf camera was replacing the various potentiometers and electrolytic capacitors, disabling the adjustable focus mechanism and fixing it, the relubrification of the iris mechanism, and the addition of a digitisation circuit phase-locked to the camera's master clock. The power consumption of this camera is 360 mA at 10 V (3.6 Watts) with a power-up surge of around 3 Amps. The analogue-to-digital converter unit is shared with a number of experiments, and dumps data directly into the Ramdisk.

Captured imagery comprises 645 x 240 pixels (one video field) at 8-bit resolution to make a total file length of 155 kBytes. However the sampling is not synchronised to the pixel rate, but derived from some other reference signal. Running at 10.7 MHz, this clock is about 2.4 times the nominal 4.5 MHz bandwidth of the NTSC composite video signal produced. [Smith] describes some of the techniques used to extract the various DC levels, colour bursts and signals modulated by sub-carriers from this sampled signal stream.

At the time [Bonsall et al] published, a few images had been captured in orbit, but they could not identify any specific land features. The restricted field of view of only 150 km, coupled with an absence of attitude control, made identification of land masses difficult. However land, sea and clouds are recognisable in the imagery. The one picture published by [Jackson & Raetzke] containing land features would not, in the author's opinion, satisfy professional remote sensing applications. Allowing for the poor quality of the reproduction, the quality appears comparable, or inferior, to the imagery from the very early Mariner vidicon cameras flown in the early 1960s.

[Jackson & Raetzke] address some of the experiences faced in trying to obtain successfully exposed images by adjusting the iris aperture under computer control. In general, they report that the camera's built-in automatic iris control loops had trouble accommodating the very bright conditions experienced. Additionally the absence of attitude control has made targeting specific areas impossible. Various strategies for waiting until the camera is Earth-facing and then capturing an image met with variable success; between 1 % and 40 % depending on the scheme used before the on-board computer's watch-dog timers disabled the camera. [Jackson & Raetzke] also report difficulties in accommodating seasonal variations, presumably influenced by Sun illumination angles and the satellite's attitude.

Overall, the difficulties faced in exploiting the Webersat imaging system, both in terms of technical aspects such as the absence of attitude control and setting the exposure, as well as the rapid turn-over of the technical staff, have limited the perceived success of the mission in the professional arena. From the author's point of view, the most interesting result is the performance of the mechanically variable iris, which, assuming it was still operational as the time [Jackson & Raetzke] presented their results, had survived 18 months in orbit. This allowed the camera to image (albeit haphazardly) under a wide range of illumination conditions from staring at the Sun to detecting individual stars or planets.

The Webersat project was conceived largely as a one-off, and many of the lessons learnt will no doubt have been lost. The absence of continuity caused by relying on students to such a large degree has meant that Weber State University have not been able to capitalise on their acquired experience. However at the time, given that the performance of the Webersat camera was equivalent (and probably better) than the author's first attempt on UoSAT-4, SSTL considered this imaging system to be a serious competitor.

2.3.5.4 Ball Aerospace's LOSAT-X / QuickStar.

The LOSAT-X mission was launched on 3 July 1991, funded by the US's Strategic Defence Initiative Office (SDIO). Although, it was neither a civilian mission nor carried an Earth imaging camera, one of its payloads was an experimental CCD star camera. Therefore, despite being outside the criteria for comparing imaging microsatellites used in this thesis, it is nevertheless an interesting subject for brief study. The requirements and technology for implementing Earth and star cameras are largely the same, and therefore worthy of review here. Certainly, it is informative to place the author's work in this field in context with the programmes funded through the huge budgets of the US defence programmes. Incidentally, Ball Aerospace is trying to commercialise the platform developed for the LOSAT-X mission as a multi-mission microsatellite system called QuickStar [Garrison & Schrock].

LOSAT-X was a flat spacecraft 1250 mm long by 900 mm wide, but only 300 mm high. This squat configuration was chosen to allow several of these microsatellites to be stacked as auxiliary payloads within the fairing of the Delta II launch vehicle. The mass of a LOSAT-X / QuickStar microsatellite is 70 kg of which a third is available for carrying payloads. The top surface of the satellite is covered with GaAs solar cells to deliver a peak of 214 Watts and an orbit average of 130 Watts (no stated orbit, although it was probably a low-Earth 'parking' orbit from which the primary payload, GPS-11, would have raised itself to 20,000 km). It should be noted that while this deployment of the microsatellite's solar panels is very efficient, it does have a number of fatal configurations whereby no Sunlight is collected. The large power budget available on LOSAT-X allowed it to sustain a very high data rate (for a microsatellite) of 1 Mbps on the S-band downlink.

The LOSAT-X missions appears to have been primarily an in-orbit demonstration of attitude determination and control. Consequently, these systems on the QuickStar spacecraft are uncharacteristically sophisticated for a microsatellite, reflecting the SDIO's interest in complex pointing and tracking requirements. The author has little doubt that LOSAT-X was a prototype for many of the systems that would have been deployed in the Brilliant Eyes / Brilliant Pebbles programmes. The ADCS includes three reaction wheel assemblies, magnetic torquers, two Sun sensors, magnetometers, a star camera and a three-axis gyro package to ensure a fully stabilised platform with a reported pointing accuracy of 0.1°, with the ability to execute very rapid slewing (up to 5° per second). An Intel 80C386 microprocessor, augmented with an 80C387 co-processor, provides the computing power to analyse the star imagery and other attitude sensor data.

Certainly, the LOSAT-X spacecraft presents highly sophisticated attitude control and communications systems, displaying substantially more technology than other contemporary microsatellites. Nevertheless, it is difficult to compare the state of civilian microsatellite projects to those funded by the effectively unlimited budgets of the SDIO. No doubt that the tightly focused goals emphasising the technology demonstration of the mission as part of a larger military programme has resulted in these impressive specifications.

As will be reviewed in chapter 3, the LOSAT-X / QuickStar satellite's specifications are highly suited to supporting Earth observation tasks. With perhaps the exception of the payload volume (1.7 cubic feet - 360 mm cube) and mass, the power budget, platform stability and downlink data rate would support a range of remote sensing payloads, including pushbroom and small whiskbroom scanners.

Given the apparent suitability of the QuickStar platform for applications like high resolution remote sensing, it is surprising to find that it has not been used again since the initial LOSAT-X prototype. Ball Aerospace are not renowned for their timid marketing, and should have been able to generate suitable interest in the programme, so there is presumably some reason why there have been no follow-on missions in the civilian market. It may be that some of the technology used is classified and cannot be employed on commercial missions, or perhaps that the cost of the satellite was so high as to make it uncompetitive in the open market. Alternatively, one can speculate that the in-orbit operation of LOSAT-X was disappointing; [Garrison & Schrock] only devote a couple of paragraphs to the in-orbit performance of the system, preferring to discuss the specification of the QuickStar platform at length. They indicate that the satellite did stabilise quickly after the launch and managed to capture several hundred images with the star camera. However, the reader is left with an impression that the mission did not survive for very long. Nevertheless, despite these reservations, the specification of the QuickStar platform is very impressive. Future microsatellites will need to strive to emulate these capabilities if commercial remote sensing using scanning instruments is to be performed.

2.3.5.5 Orbital Sciences Corporation's MicroLab-1.

MicroLab-1 [Meurer] is a recent addition to the family of imaging microsatellites. Launched on 3 April 1995, MicroLab-1 is a demonstration version of a new microsatellite platform developed by Orbital Sciences Corp. to exploit the facilities of their Pegasus launcher. The satellite is made up of two stacked disks (1040 mm in diameter, but only 165 mm high), one containing the housekeeping systems and the other available for payload. As with the Ball Aerospace LOSAT-X / QuickStar microsatellite, the unusual dimensions of these disks are conceived to make optimum use of the space available in the Pegasus fairing allowing multiple missions to be launched at the same time. With a housekeeping module (dry) mass of 40 kg and a stated payload capacity of 50 kg (including the structure), this vehicle is at the large end of the microsatellite class.

The performance of MicroLab-1 is very similar to that achieved by the smaller SSTL microsatellites, in terms of attitude control (gravity gradient and magnetic stabilisation to within 4°), downlink (57.6 kbps, 10 Watts RF, UHF), passive thermal control, electrical distribution (14V unregulated bus) and processing power of the on-board computer (using a Motorola MC68302 instead of SSTL's Intel 80C186). The communications philosophy is also packet-based, using the X.25 protocol (see section 3.4.2).

In addition to the larger payload mass, the other major performance enhancement of the MicroLab over the SSTL microsatellites appears to be the larger deliverable power of up to 250 Watts peak and 55 Watts orbit-average (740 km polar orbit). This is achieved by placing the solar arrays on the satellite's two flat circular areas, which are deployed out to 90° in orbit. However, by deploying the panels in this way, the ratio between peak and orbit-average power is highly asymmetric, with the power output falling off as a function of the cosine of the illumination angle. The orbit-average is maintained by the provision of the reasonably large capacity of the 10 Ampere-hour battery pack.

Similarly MicroLab-1 carries a cold-gas thruster mechanism for minor orbit adjustments. However, the small reservoir of only 0.8 kg of propellant indicates that this is a technology demonstration rather than an operational system.

[Meurer] describes a plethora of possible upgrades for future MicroLab-1 spacecraft including increased power, three-axis attitude stabilisation to 0.5°, S- and L-band downlinks at 1 to 2 Mbps, hydrazine propulsion, etc. although these additional modules will certainly take the satellite mass to near 150 kg, outside of the microsatellite class in the strict sense. Some early thoughts on an alternative 12.5 kg nanosatellite are also presented.

Unfortunately, neither [Meurer] nor [Optical Transient Detector] provide any significant details on the imaging system carried on MicroLab-1, apart from the fact that its primary objective is lightning detection, and has a field of view of 1300 x 1300 km. Interpreting the information available from [Optical Transient Detector], the author concludes that a CCD camera produces imagery with around 128 x 128 pixels but at a very fast frame rate of 500 Hz. A high performance data processing unit analyses the data to search for bright optical transients (lightning). However, it appears that the system is liable misinterpret radiation-induced events in the CCD (see section 5.6.5.1) as genuine optical transients.

Developed at NASA's Marshall Space Flight Center, the design objectives of the Optical Transient Detector (OTD) on MicroLab-1 are sufficiently different to those of the SSTL Earth imagers to make direct comparison inappropriate. Whereas the author's cameras are striving for high quality still-images of the Earth, the OTD has had to sacrifice a considerable amount of its spatial and radiometric resolution to deliver the very high temporal sampling. In addition to the data on optical transients, the OTD periodically transmits a full visible image, referred to as the 'background', against which to correlate the geographical position of the various lightning flashes. Granted that this imagery is not intended for conventional Earth observation, it is not surprising to find that the SSTL cameras offer superior resolution, sensitivity and definition.

2.3.5.6 Stellenbosch University's Sunsat.

An interesting microsatellite programme that has been under development for a number of years is the Sunsat project at Stellenbosch University in South Africa. Given that a number of exchange students from Stellenbosch participated in the UoSAT-3, -4 and -5 missions, it is not surprising that Sunsat is heavily (and openly) inspired by the SSTL approach to microsatellite design. Structurally, Sunsat is highly reminiscent of the SSTL spacecraft employing a stack of module trays, body mounted solar panels, with a gravity-gradient boom and virtually the same deployment of antennas and attitude sensors. Intended to be launched by ARIANE, the satellite's mass was also 50 kg, but slightly squatter in a 450 mm cube. However, now that a Delta launch has been secured for 1997, the satellite's mass has grown to 60 kg, entirely due to the addition of a GPS receiver. (Details from [Milne et al], [Schoonwinkel et al] and [Sunsat]).

The competence of the engineers who worked at Surrey coupled with the slow, but steady, progress made by the Stellenbosch team lends credibility to their claims, and Sunsat is therefore worthy of inclusion here. The slow pace has been dictated by a fairly small team and the difficulty in securing funds for the project as South Africa changes its political and economic priorities. As with UoSAT-1, the primary motivation of the Sunsat programme appears to be practical training as part of the University's academic programme, combined with amateur radio payloads to encompass a wider educational mission. Of course, the Stellenbosch team were not content to clone the SSTL satellites, and have added a number of additional features. Of particular interest is the imaging payload, which is hoped will generate commercial interest once in orbit.

The Sunsat imaging system will use the pushbroom scanning architecture to achieve 15 metre resolution from a nominal 800 km orbit. (Sunsat's expected orbit will be 400 x 830 km, resulting in significant variations in scaling). Three linear CCDs, with 3456 pixels each, will sense in the green, red and near-IR bands (as SPOT). The CCDs are from Texas Instruments and the 570 mm focal length lens has been developed by the South African Council for Scientific and Industrial Research optics laboratories. The data rate from this three-channel sensor will be 27.5 Mbps, and will be dumped directly to the downlink for collection by a 3.7 m diameter dish at one or two principal control stations. This approach to data handling will limit the coverage to the immediate region of South

Africa. A 64 MByte Ramdisk is also available for storing short bursts of data from other portions of the World.

The imager can be rotated fore and aft to offer stereoscopic capabilities on the same pass. The whole of the sensor assembly is mounted in a cylinder viewing the Earth in a mirror; off-nadir targeting is accomplished by rotating the whole assembly, without changing anything in the optical path.

While the specification of the imaging instrument is impressive, it is the implementation of the attitude determination and control systems that will be most critical for Sunsat's success. The required pointing accuracy is better than 0.1° in pitch and roll, and 0.15° in yaw, with drift rates of less than 5×10^{-3} ° per second. Clearly, accomplishing the same quality of attitude control as achieved by SPOT on a 60 kg microsatellite represents a substantial challenge. Stellenbosch propose a system based on the standard gravity-gradient boom and magnetic torquers, augmented with three small (3.5×10^{-3} Nm) reaction wheels to achieve this level of stability. To reduce power consumption and prolong the lifetime of the wheels, Sunsat will be left in a state with a slow yaw-spin most of the time to equalise thermal gradients. Just prior to imaging activities, the reaction wheels will powered to de-spin the satellite. The sensors used by the attitude system will include magnetometers, CCD horizon and Sun sensors, and a star camera. The intense data processing for this system will be handled by a T800 transputer, supported by 80C51 microcontrollers to drive the reaction wheels.

Unlike many other proposed microsatellite systems, the bold claims of the Sunsat team are coherent, and backed by considerable knowledge and experience (although not in spacecraft design) tempered with realism. The author has little doubt that the imager will behave largely as expected, provided the necessary attitude stability can be delivered. One of the strengths of the Stellenbosch University's Electronic Engineering department is control theory, and this will no doubt assist the Sunsat team in implementing their control algorithms and routines. Nevertheless, the expectations placed on this aspect of the Sunsat microsatellite are very great, particularly for a first mission. It will be extremely interesting to follow the fortunes of this ambitious group over the next few years.

Stellenbosch appears to be collaborating with a number of other small satellites groups, particularly in the provision of their imaging payload. [Kim et al] have recently presented the Korean Advanced Institute Science and Technology's (KAIST - SSTL's partner for the KITSAT-1 and -2 technology transfer missions) plans for the KITSAT-3 spacecraft using the Stellenbosch imager. A throw-away comment by [Ginati] indicates that there may be some collaboration forming between the University of Bremen (ZARM) and Stellenbosch.

2.3.5.7 Israel's TechSAT.

Given its delicate political and defence situation, yet without the finances of a super-power, it is not surprising to find that Israel is involved in developing small satellites and corresponding launcher capabilities. Of particular interest to this thesis is the on-going TechSAT programme, co-ordinated by the Haifa-based Technion University but involving contributions from around a dozen other Israeli companies and research establishments. (Details from [Shaviv], [Shachar & Lapid] and [TechSAT]).

The 50 kg TechSAT-I (also known as Gurwin-1) was launched by a Russian START rocket on 28 March 1995, but the flight was aborted, destroying all three satellites on board. This microsatellite had a mass of 50 kg, and a power budget of 20 Watts split evenly between payload and housekeeping systems. TechSAT-I was intended to be stabilised to within 5°, using magnetic torquers, a single momentum wheel, magnetometers and a horizon sensor. Two replicas of TechSAT are being prepared as follow-on missions for 1995 or 1996.

Very few details have been uncovered on the payloads, but apparently one of the experiments was a CCD camera. Reading between the lines from [TechSAT], the author believes that the camera was adapted from a commercial unit, developed along the lines of the Webersat imager (section 2.3.5.3). The sensor had 380 x 570 pixels and produced a EIA (525-line) video signal. The output signal was digitised and collected by an Intel 80C186 microprocessor equipped with 1 MByte of buffer memory. It appears that the system was equipped with a hardware image compressor implementing the standard JPEG algorithm (see section 7.2.4.1). Other experiments included a GPS receiver and amateur radio communications.

The TechSAT-II mission, targeted for 1998 is rather more ambitious with a launch mass of 70 kg, and carrying a pushbroom imager as its primary payload. Although the design has not been finalised, it appears that 8000-pixel CCDs will be used to sense in three or possibly six spectral bands. While a launcher (and by association, an orbit) has not been identified, the instrument would achieve 12 m resolution from an altitude of 550 km using a 320 mm focal length lens. The mass and power of this imager are estimated to be 10 kg and 30 Watts. A steerable mirror will be used point the optical axis sideways to provide more frequent revisits (emulating a system first implemented on SPOT).

The data handling and attitude control requirements of the TechSAT-II satellite will need to be comparable to those identified for Sunsat. Certainly, the data rate of 40 Mbps per spectral channel (i.e. a total of 240 Mbps for the six band imager) for this type of high resolution system is very much higher than is normally associated with microsatellites. Apparently, the data stream will be sent directly to the ground on a 12 GHz link. To achieve a high gain from the satellite's antenna, a novel phased-array of 156 patch elements will be employed. Although the satellite will have a 48 MByte Ramdisk, this will be inadequate to store any appreciable amount of imagery.

The attitude stability required to support this high resolution instrument is not discussed by [TechSAT] but this microsatellite will be equipped with the same actuators and sensors as TechSAT-I. An 8 kg cold-gas (Nitrogen) thruster will be used for minor attitude and orbital adjustments.

2.3.5.8 BMDO's Clementine and MSTI.

The author is often asked about how SSTL's microsatellites compare to the recent, much-publicised Clementine mission to the Moon which heralded the start of US's 'faster, better, cheaper' programme. Anticipating such questions here, it must be stressed that Clementine was neither cheap nor small by SSTL standards. The dry and wet masses of this spacecraft were 230 kg and 560 kg, and it had a total launch mass of 1700 kg including the orbital kick-motor. Similarly, the direct cost of building the spacecraft was $60 million, not including much of the research and development funded by the Ballistic Missile Defence Organisation (BMDO - the successor to the Strategic Defence Initiative Office). The launch was heavily subsidised, costing the Clementine project only $19 million for the exclusive use of a Titan II rocket (not factored into the cost of the satellite). The vast infrastructure of the NASA Deep Space Network was used to support mission operations. (Details from [Rustan, a], [Rustan, b], [Rustan, c], [Regeon et al], [LLNL] and [Clementine]).

The three MSTI (Miniature Sensor Technology Integration) spacecraft are a similar programme funded by $150 million from the BMDO [Feig et al][Jeffrey et al]. Although slightly smaller than Clementine at 200 kg and 225 Watts, technology demonstration has also been a driver for the MSTI missions. The three missions have carried an increasingly sophisticated array of mid- and thermal-IR sensors, principally for tracking warm objects travelling in the atmosphere. While these are clearly military objectives, these sensors have been demonstrated to have a number of civilian agricultural applications [Jeffrey et al].

Where the Clementine, MSTI and the recently commenced Lewis and Clark programmes [Reichhardt] resemble the SSTL microsatellites is in their short time scales and embrace of advanced technology. Clementine flew many components procured to commercial and industrial levels of screening instead of the traditional space-qualified devices, including 32-bit RISC processors, a 256 MByte solid-state data recorder, area-array CCD imagers, gallium-arsenide solar cells, and nickel-hydrogen batteries.

Clementine employed a number of CCD cameras for both stellar and lunar (as opposed to Earth) observation. Encouragingly for SSTL and the author, much of the technology on Clementine is comparable to that flown on PoSAT-1 and developed for FASat-Alfa. Table 2.3.5.8 provides a quick comparison of some of the technical specifications of the Clementine UV / visible camera and the FASat-Alfa Narrow Angle Camera. The most significant technical difference between the cameras is the presence of a filter wheel on Clementine to provide multispectral facilities (see section 5.4.4.3.3), and the inclusion of a microprocessor interface on the SSTL cameras. Otherwise, despite technical similarity between the Clementine imaging payloads and those produced for the SSTL microsatellites, there is still a huge cost difference.

Satellite	Clementine	FASat-Alfa
Instrument	UV / Visible	Narrow Angle Camera
Mass (excluding optics)	410 g	600 g
Power	4.5 W	5.6 W
Volume	155 x 117 x 104 mm	130 x 80 x 60 mm
Sensor manufacturer	Thomson-CSF	EEV
Pixel density	384 x 288	576 x 560
Output data rate	4 Msamples / s	11 Msamples / s
Digitisation	8 - bits	8 - bits
Optics	90 mm, f / 2	75 mm, f / 8
Spectral	Filter wheel provides six bands (consumes 11 W)	Monospectral
Cost	US $ 500,000	UK £ 15, 000

Table 2.3.5.8 Comparison of the Clementine UV / visible camera and the FASat-Alfa Narrow Angle Camera

Clementine also carries four other experimental cameras (for star, short wave-IR, long wave-IR and intensified imaging). These are all quite similar to the UV / visible camera, using commercially available technology. They have masses of between 500 and 1500 grams depending largely on their optical configurations, and power consumptions of 8 to 30 Watts (mainly due to the cooling requirements of the IR cameras).

2.3.6 CONCLUSIONS.

Having compared the characteristics of conventional remote sensing spacecraft to microsatellites, it is clear that new and different strategies are necessary for implementing imaging systems on these small spacecraft. Chapter 3 will discuss these issues in greater depth. Nevertheless, in spite of the difficult engineering constraints of microsatellites, the reduced costs and fast development cycles make them very attractive for commercial remote sensing. At present, there is a great deal of interest in implementing small satellites to exploit the perceived market for low-cost remote sensing systems and data.

However, although small satellites for Earth observation applications have been receiving considerable attention, with numerous papers written proposing systems or discussing scientific needs and commercial opportunities, there have been remarkably few successful demonstrations of these systems in orbit. Apart from the SSTL missions, the author is aware of only three microsatellites (Rohini, Webersat and MicroLab-1) that have provided any orbital results to date. This situation stresses the gulf between expressing an intention to undertake a microsatellite mission and actually carrying it out.

The ambitions of the Sunsat and TechSAT teams chart the growing expectations and possibilities of using microsatellites for Earth observation. It will be interesting to watch these missions to see if the data handling and attitude control systems of the spacecraft can be mastered sufficiently to support the imaging payloads. Regardless of the success or failure of these specific missions, by the first years of the next millennium, there will no doubt be several small satellites fulfilling the high resolution, multispectral remote sensing capabilities of the type described above. (Of course, SSTL does not intend to be out-done in this area, and has aggressive plans to continuing developing its remote sensing capabilities; this is discussed in chapter 9 of this thesis).

2.4 REFERENCES

Alex T.K. et al: Remote sensing payload for small Indian satellite; Proc of SPIE, Vol.363, p.82-87, 1983.

Alex T.K: Imaging capabilities of small satellites - Indian experience; Proc. of the SPIE Conference on Small Satellite Technology and Applications I, SPIE Vol.1495, Orlando, April 1991.

Allery M.N, Sellers J.J. & Sweeting M.N: Results of University of Surrey on-orbit microsatellite experiments; Proc. of Int. Symposium on Small Satellites Systems and Services; Biarritz, France, 27-30 June, 1994.

Bonsall C et al: Webersat operations and experimental results; Proc. of the 4th Annual AIAA/USU Conference on Small Satellites, Utah State University, 27-30 Aug 1990.

Clementine home page (http://www.nrl.navy.mil/clementine/clementine.html).

Colwell R.N: Manual of Remote Sensing Second Edition; American Society of Photogammetry, The Sheridan Press 1983, ISBN 0-937294-41-1.

Das U.N. & Kasturirangan K: Development of a small satellite series - ISRO experience; Proc. of the 7th Annual AIAA/USU Conference on Small Satellites, Utah State University, 13-16 Sept 1993.

Da Silva Curiel R.A, Sun W. & Sweeting M.N: Design considerations and implementation of the VHF and UHF radio frequency systems on-board the UoSAT LEO store and forward communications network; 3rd International Symposium on Communication Theory and Applications, Lancaster University UK, 10-14 July 1995.

Deshayes J.P. & Mizzi A: Earth observation payloads - user requirements; Proc of the 1st European Workshop on Flight Opportunities for Small Payloads, ESRIN, Frascati, Italy, 8 - 10 Feb 1989; ESA SP-298.

DVFLR: MEOSS, an experimental CCD-camera for remote sensing; NASA Scientific and Technical Aerospace Reports (STAR) reference N83-30469 & N83-30470.

Feig J.R, Matlock R.S. & Yeakel G.S: The Miniature Sensor Technology Integration program - an overview; Proc. of the 7th Annual AIAA/USU Conference on Small Satellites, Utah State University, 13-16 Sept 1993.

Garrison T.P. & Schrock S.R: QuickStar - rapid access to space for small scientific payloads; IAF Conference, 1991.

Ginati A. et al: Bremsat - a small scientific satellite; Proc. of the 4th Annual AIAA/USU Conference on Small Satellites, Utah State University, 27-30 Aug 1990.

Ginati A: Verbal presentation; Conference on Small Satellites for Remote Sensing, The Space Congress, Bremen Germany, 24-25 May 1995.

Hashida Y: Personal communication, 28 Sept 1995;

ISRO: Department of Space - Annual Report; Government of India; Published by ISRO, Bangalore, India, 1995.

Jackson S. & Raetzke J: The Webersat camera - an inexpensive Earth imaging system; Proc. of the 5th Annual AIAA/USU Conference on Small Satellites, Utah State University, 26-29 Aug 1991.

Jeffrey et al: Small satellites (MSTI-3) for remote sensing; Proc. of the SPIE Conference on Small Satellite Technology and Applications IV, SPIE Vol.2317, Rome, Sept 1994.

Keller H.U. et al: Images of the nucleus of Comet Halley obtained by the Halley Multicolour Camera (HMC) on board the Giotto spacecraft; European Space Agency, ESA SP-1127, Vol.1, ISBN 92-9092-080-7.

Kim S. et al: Mission overview of engineering test satellite KITSAT-3; Proc. of the 9th Annual AIAA/USU Conference on Small Satellites, Utah State University, 18-21 Sept 1995.

King J.A. et al: The in-orbit performance of four Microsat spacecraft; Proc. of the 4th Annual AIAA/USU Conference on Small Satellites, Utah State University, 27-30 Aug 1990.

Lanzl G et al: The MEOSS experiment - a test case for future cartographic missions; Proc of IGARSS Symposium, Edinburgh, Scotland, 13-16 Sept. 1988; Ref. ESA SP-284.

LLNL (Lawrence Livermore National Laboratory): Presentation material - Clementine project review; 20 May 1992.

Malin M.C. et al: Design and development of the Mars Observer camera; Int. J. of Imaging Systems and Technology, Vol.3, p.76 - 91, 1991.

Malin M.C. et al: Mars Observer camera; J. of Geophysical Research, Vol.97 No.E5, p.7699 - 7718, May 25 1992.

Milne G.W. et al: SUNSAT, Stellenbosch University and SA-AMSAT's remote sensing and packet communications microsatellite; Proc. of the 7th Annual AIAA/USU Conference on Small Satellites, Utah State University, 13-16 Sept 1993.

Meurer R.H: First class science on a coach class ticket; Proc. of the 9th Annual AIAA/USU Conference on Small Satellites, Utah State University, 18-21 Sept 1995.

Muench G: Advances in spaceborne data recorders; Space Markets, Spring 1988.

Optical Transient Detector home page (http://wwwghcc.msfc.nasa.gov:5678/otd.html).

Radbone J.M: The UoSAT-2 Spacecraft CCD Imaging and Digital Store/Read-out Experiments; The IERE Journal, Vol. 57 N°5, Sept. 1987; ISSN 0267-1689.

Regeon P.A, Chapman R.J. & Baugh R: Clementine - the deep space program science experiment; Acta Astronautica, Vol.35 Suppl. p.307 - 321, 1995.

Reichhardt T: Lewis and Clark, blazing new trails; Aerospace America, V.33 No.7, July 1995.

Renner U, Lübke-Ossenbeck B. & Butz P: TUBSAT - low cost access to space; Proc. of the 7th Annual AIAA/USU Conference on Small Satellites, Utah State University, 13-16 Sept 1993.

Renner U, Lübke-Ossenbeck B. & Butz P: TUBSAT-A,B,C; Proc. of Int. Symposium on Small Satellites Systems and Services; Biarritz, France, 27-30 June, 1994.

Rustan P.L: The Clementine mission; Proc. of the SPIE Conference on Small Satellite Technology and Applications IV, SPIE Vol.2317, Rome, Sept 1994.

Rustan P.L: Personal communication; 29 Sept 1994.

Rustan P.L: Clementine - mining new uses for SDI technology; Aerospace America, p.38 - 41, Jan 1994.

Rycroft M: The Cambridge Encyclopaedia of Space; Cambridge University Press, 1990; ISBN 0-521-36426-4.

Schoonwinkel A, Mostert S & Milne G.W: The Sunsat microsatellite for remote sensing and packet communication; Proc. of Int. Symposium on Small Satellites Systems and Services; Biarritz, France, 27-30 June, 1994.

Shachar M. & Lapid P: The TechSAT programme; J of the British Interplanetary Society, Vol.45 No.12, p.501 - 505, Dec 1992.

Shaviv G: The Gurwin-1 TechSAT project; Proc. of Int. Symposium on Small Satellites Systems and Services; Biarritz, France, 27-30 June, 1994.

Slama C.C: Manual of Photogammetry Fourth Edition; American Society of Photogammetry, 1980, ISBN 0-937294-01-2.

Slater P.N: Remote Sensing - Optics and Optical Systems; Addison-Wesley 1980; ISBN 0-201-07250-5.

Small Satellites home page (http://www.ee.surrey.ac.uk/EE/CSER/UOSAT/SSHP/sshp. html).

Smith J.L: Restoration and enhancement of Earth images from a low cost sampled video system; Proc. of the 6th Annual AIAA/USU Conference on Small Satellites, Utah State University, 21-24 Sept 1992.

Sun W, Sweeting M.N. & Hodgart M.S: A novel implementation of an MSK modem using digital signal processing techniques on-board a low Earth orbit microsatellite; Proc. IEEE Singapore International Conference on Communications Systems, Singapore, p.430-434, 14-18 Nov 1994.

Sun W, Sweeting M.N. & Hodgart M.S: Investigation of MSK and FSK modulation schemes for single channel communications systems using DSP techniques on-board low Earth orbit microsatellites; Proc. 10th IEE International Conference on Digital Communications via Satellites, Vol.1, p.9-16 Brighton UK, 15-19 May 1995.

Sunsat home page (http://esl.ee.sun.ac.za).

Sweeting M.N: UoSAT microsatellite missions; Electronics & Communication Engineering Journal, IEE, June 1992.

Sweeting M.N: Microsatellite & minisatellite programmes at the University of Surrey for effective technology transfer & training in satellite engineering; Proc. of Int. Symp. on Satellite Communications and Remote Sensing, 20-22 Sept 1995, Xi'an China.

UoSAT-1: special issue of the IERE Journal, Vol. 52 N°8/9, Aug. 1982.

UoSAT-2: special issue of the IERE Journal, Vol. 57 N°5, Sept. 1987.

TechSAT home page (http://www.technion.ac.il/pub/projects/techsat/).

Trayner C.P. & Jeans T.G: The Development of a Satellite-Borne Earth Imaging System for UoSAT; The IERE Journal, Vol. 52 N°8/9, Aug. 1982; ISSN 0033-7722.

Truss P: European remote sensing satellite platforms for the 1990s; Proc of IGARSS Symposium, Edinburgh, Scotland, 13-16 Sept. 1988; Ref. ESA SP-284.

Turnill R: Jane's Spaceflight Directory 2nd edition; Jane's Publishing Co. Ltd, London 1986; ISBN 0-7106-0367-3.

Wells N: The Space Technology Research Vehicles STRV-1a and -1B - one year in GTO; Proc. of the 9th Annual AIAA/USU Conference on Small Satellites, Utah State University, 18-21 Sept 1995.

2.4.1 REFERENCES USED IN TABLES 2.2A AND B.

[1] Colwell R.N: Manual of Remote Sensing Second Edition; American Society of Photogammetry, The Sheridan Press 1983, ISBN 0-937294-41-1.

[2] NORAD Keplerian elements sets.

[3] Chen H.S: Space Remote Sensing Systems; Academic Press 1985, ISBN 0-12-170881-0.

[4] ITT Defence & Electronics technical brochure, ITT Aerospace / Communications Division.

[5] Wallach J: The Launch of NOAA-H Weather Satellite: A Mission Profile; The Proceedings of the AMSAT-NA 6th Space Symposium and Annual Meeting; Nov. 11-13 1988; Published by American Radio Relay League.

[6] Slater P.N: Remote Sensing - Optics and Optical Systems; Addison-Wesley 1980; ISBN 0-201-07250-5.

[7] SPOT Press Pack; CNES 1985.

[8] Kasturirangan K: The evolution of satellite-based remote sensing capabilities in India; Remote Sensing Yearbook 1986, edited by Cracknell A. & Hayes L, Taylor & Francis 1986, ISBN 0-85066-313-X.

[9] Harris, Satellite Remote Sensing - an introduction; Routledge & Kegan, 1987, ISBN 0-710203055.

[10] Sudarshana R. et al: Experiments in site selection for coastal aquaculture using Indian Remote Sensing satellite: IRS-1A; Int. J. Remote Sensing, Vol. 14 No. 12, 1993.

[11] Arai K: Preliminary assessment of radiometric accuracies for MOS-1 sensors; Int. J. Remote Sensing, Vol. 9 No. 1, p5-21, 1988.

[12] Dosière P. & Justice C: Spatial and radiometric resolution of the LANDSAT-3 RBV system; Int. J. Remote Sensing, Vol. 4 No. 2, p447-455, 1983.

[13] Pease C.B: Satellite imaging instruments - principles, technologies and operational systems; Ellis Horwood, 1990, ISBN 0-13-638487-0.

[14] Deshayes J.P. & Mizzi A: Earth observation payloads - user requirements; Proc of the 1st European Workshop on Flight Opportunities for Small Payloads, ESRIN, Frascati, Italy, 8 - 10 Feb 1989; ESA SP-298.

CHAPTER III

FACTORS GOVERNING THE DESIGN OF REMOTE SENSING INSTRUMENTS FOR MICROSATELLITES.

As noted in Chapter 2, the engineering constraints of implementing Earth observation systems on 50 kg microsatellites are very different to the conditions found on most conventional remote sensing spacecraft. Chapter 3 reviews which parameters are of importance when specifying a remote sensing mission. Next, it considers how a microsatellite's limitations in terms of mass, volume, power, orbits and most importantly, attitude control and data handling effect the design and operation of an imaging system. The main conclusion is that until the attitude stability of microsatellites approaches the 0.1° of traditional spacecraft, it will not be feasible to use scanning imagers, and electronic cameras must be employed instead.

3. FACTORS GOVERNING THE DESIGN OF REMOTE SENSING INSTRUMENTS FOR MICROSATELLITES.

3.1 DEFINING THE REMOTE SENSING MISSION OBJECTIVES AND IMAGING INSTRUMENT SPECIFICATION.

Before considering the design of a remote sensing instrument, it is vital to define the overall mission objectives. As different applications have different technical requirements of the imagery, it is important to be sure which class of data and which user group is being served by the mission. The key factors to be considered are spatial, spectral and temporal resolution. Each class of application will have it own optimum balance of these attributes.

There are numerous text books describing the factors to be considered when specifying a remote sensing mission. However, designers of remote sensing instruments should take care when consulting these references, as in the author's experience, they invariably consider Earth observation through a theoretical analysis of the physics and end applications rather than as an engineering exercise. One particularly pragmatic, and therefore valuable, presentation on these trade-offs is made in the first chapter of [Colwell, p.19-32].

The system designer must be aware of the technology available to support the objectives of the remote sensing mission, as well as the constraints imposed by the spacecraft platform that could hinder successful implementation. Almost certainly, the initial draft specifications of the imaging instrument will be too demanding to complete within the proposed time, funding or spacecraft platform. Under these circumstances, the systems engineer will need to explain where the problems lie and what trade-offs can be made to obtain satisfactory performance from a practical and affordable system. It will be necessary to discuss with the user group or the mission financiers as to what the real, as opposed to perceived or desired, requirements are for a given mission. [Elliot] reviews a methodology for planning remote sensing missions which emphasise achieving the desired performance without incurring excessive costs.

Even if these negotiations are with experienced designers and users of remote sensing systems, the conditions on-board a 50 kg microsatellite will inevitably be very different to those on conventional Earth observation spacecraft. All traditional expectations and assumptions regarding what can be achieved, and the best means of fulfilling these requirements will need to be reconsidered when designing instruments for small satellites.

3.1.1 SPATIAL RESOLUTION.

The first parameter to be scrutinised when defining a remote sensing instrument is its resolving power. There is a trend for increasingly high resolution to be specified for Earth observation missions, generally to fulfil genuine civilian and military applications, but occasionally to provide a 'muscle-flexing' exercise to show off technical prowess.

At a first glance, it would appear that the specification should strive for the highest spatial resolution attainable, as this would produce a maximum amount of information, thereby fulfilling as wide a range of applications as possible. While in an ideal world this may be true, in a practical system achieving a high spatial resolution has many other implications that may outweigh the benefits of recording the scene in detail.

The most immediate consideration is the optical system necessary to deliver this resolution. For a given satellite orbit, a longer focal length will be needed to achieve a higher level of magnification. To maintain a constant illumination of the image sensor, the optical aperture will need to scale with the focal length (i.e. maintain a constant *f*-number). However, to prevent blurring, the sensor's exposure time will have to decrease with the spatial resolution (discussed in section 3.3.4.2). To compensate for the loss in photons accumulated by the sensor, an even larger optical aperture is needed to ensure adequate illumination, with significant implications on the mass and size of the optics. As focal lengths approach 500 mm, the feasibility of the optical system will become critical on a microsatellite.

Another crucial consideration is maintaining the field of view as the spatial resolution improves. If the sensor has a fixed number of pixels (i.e. it is an array of photo-sensors, as opposed to a mechanically scanned system), it is inevitable that an increase in spatial resolution will result in proportional reduction in the imager's field of view. Given that one of the key advantages of a remote sensing satellite over a photo-reconnaissance aircraft or balloons is the ability to provide wide coverage, any losses in the imaging system's field of view must be carefully justified.

To provide both a high resolution and a wide field of view, it will be necessary to increase the total number of pixels within a scene. To a certain extent (up to about 10,000 pixels per line), this is technically feasible on a conventional satellite but the cost may be prohibitive on a microsatellite. However, to maintain the coverage in a single scene, every doubling of the ground resolution entails a four-times increase in the number of pixels. Therefore, increasing the pixel density has significant repercussions on the imaging instrument's and spacecraft's data handling, storing and downloading capacities.

Finally, but perhaps most importantly, the satellite's attitude control system must be capable of providing adequate stability. As the imager's resolution increases, it will become increasingly sensitive to pointing errors and dynamic drifting of the satellite's orientation. As discussed in some detail in section 3.3, the relationship between the imaging system's architecture and a microsatellite's attitude control system is vital in establishing image quality in terms of blur and registration (misalignment). Ultimately, the errors sustained by the imagery due to these inaccuracies of attitude control will determine the data's usefulness.

Given these restrictions on freely achieving high resolution imaging, it is important to assess the specific applications of a remote sensing mission and pursue the real needs of these applications. While uses like urban planning [Welch], cartography and military intelligence require 1 to 5 metre detail, there are many applications that can be fulfilled with lower spatial resolution. Many aspects of land use management, geology, hydrology, deforestation and erosion, to name but a few, can be served by ground resolutions of the order of 100 metres [Townshend & Justice, Erlich & Estes]. At the other extreme, meteorological applications (including topics like snow and ice cover, measuring ocean currents) have requirements for very large fields of view to provide images on a continental scale. Indeed, for such uses, unnecessarily high ground resolutions (i.e. finer than 1 to 2 km) can make analysis difficult and expensive by inundating the user with surplus data.

Therefore, the application of a remote sensing instrument or mission must be established at an early stage, before considering any technical characteristics. The design team must then determine the most appropriate spatial resolution, amongst other characteristics, for fulfilling the mission objectives. On the whole, the technical challenges facing a remote sensing mission increase proportionally with the spatial resolution.

There are three parameters of importance when specifying the resolution of a remote sensing system: the spatial resolution of the imagery, the resolving power of the instrument, and the distance between the sensor and the target (i.e. the satellite's altitude). While the resolution of a satellite imaging system is generally quoted in terms of metres per pixel, the resolving power of the instrument is expressed by the angle subtended by each pixel, known as the sensor's instantaneous field of view (IFOV). Two imagers with identical IFOVs but placed in orbits of different altitude will produce imagery with different spatial resolution. Although the end user of remotely sensed data is not concerned with the distinction between spatial and angular resolution, it is an important subtlety for the designer to consider.

Figures 3.1.1a and b show the effect of trading-off spatial resolution versus field of view. Both scenes are of the islands along the Dalmatian coast of Croatia, but one is from the KITSAT-1 Narrow Angle Camera and the other is from the PoSAT-1 Narrow Angle Camera. Although both instruments use the same CCD sensors and optics, giving them identical pixels counts (568 x 560) and IFOVs, the spatial resolution of the two images is nevertheless different due to the satellites' altitudes. From KITSAT-1's 1300 km orbit, the field of view is 220 x 160 km at a mean resolution of 350 metres, whereas PoSAT-1 records the scene over 150 x 100 km with 200 metre resolution. Therefore, PoSAT-1's imagery records the scene in greater detail but provides reduced coverage.

For the rest of this thesis, the following definitions of resolution are used when performing calculations:

- low (meteorological applications) defined as 2 km / pixel
- medium (environmental applications) defined as 200 m / pixel,
- high (land resources applications) defined as 20 m / pixel.

Therefore the Wide (2 km resolution) and Narrow (200 m resolution) Angle Cameras flown on PoSAT-1 are examples of low and medium resolution imagers respectively.

3.1.2 SPECTRAL SENSITIVITY AND RESOLUTION.

The use of optical filters to sense in specific portions of the spectrum can enhance the interpretability of remotely sensed data. In monospectral imagers, filters are often used to enhance the contrast of certain features or to reduce atmospheric haze. However, far more significant gains are obtained when sensing simultaneously in several colour or spectral bands to produce multispectral images. The extra dimensions of information provided by multiple spectral bands is often invaluable in differentiating and segmenting types of terrain cover within a recorded scene.

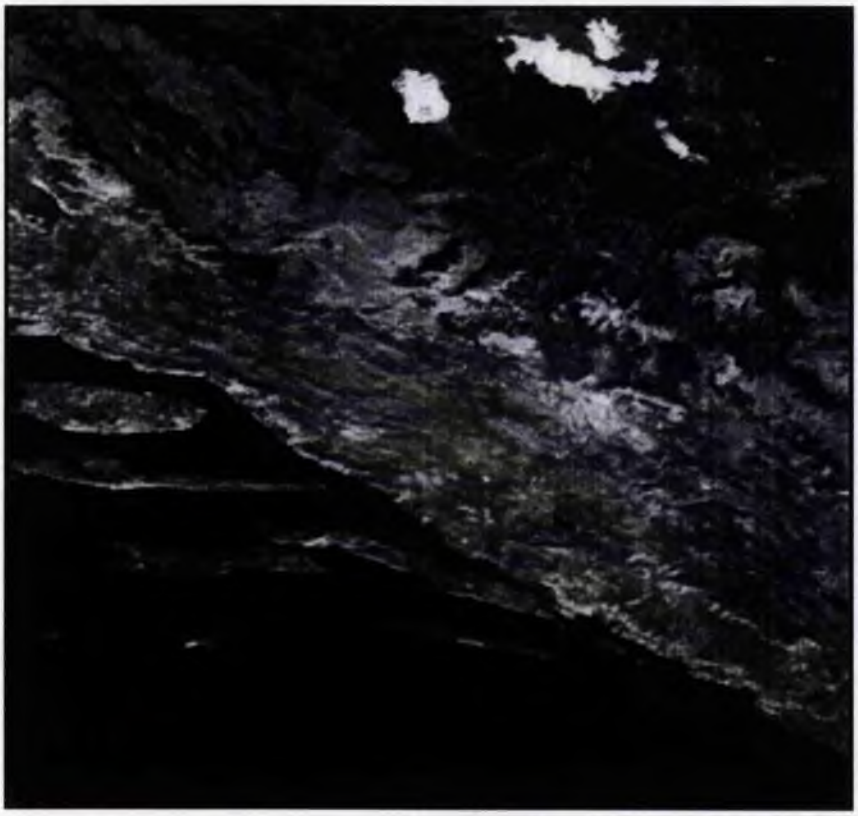

Figure 3.1.1a

KITSAT-1
Narrow Angle
Image of
Croatia.

Figure 3.1.1b

PoSAT-1
Narrow Angle
Image of
Croatia.

A great deal has been written on the subject of selecting spectral bands for remote sensing systems, and there is little point in reiterating this material here. [Lillesand and Kiefer] and [Swain and Davis] provide detailed discussions of many possible options. A few general observations extracted from the literature are that:

- The spectral signatures of different materials become increasingly unique as wider portions of the electromagnetic spectrum are considered. Similarly, closely spaced bands will contain redundant information. This is particularly true of the blue and green spectra of the human visual system's red-green-blue colour structure.
- Chlorophyll has a very distinctive spectral signature with a very strong near-IR reflectance, a strong red absorption and a moderate green reflectance. This rapid variation makes vegetation highly distinguishable from other types of terrain. The red (600 to 700 nm) and the near-IR (800 to 900 nm) bands are therefore the most crucial for most remote sensing applications. A green-yellow band (520 to 600 nm) or blue-green band (420 to 520 nm), or both, are often used to supplement the red and near-IR bands.
- Other bands in the UV, near- mid- and thermal-IR are useful for specific applications such as ice and snow cover monitoring, and various specific forms of atmospheric and oceanic analysis.
- The spectral bands used on the LANDSAT imaging systems were selected following a lengthy study of numerous applications, and are considered the standards for general purpose remote sensing. If in any doubt as to which spectral bands should be used for an application, consult the LANDSAT study reports. A summary of these details are made in [Slater, p.481-484, p.498-499].

When selecting the spectral bands for a specific application, the design team should consult the expert literature for advice. However, a critical eye will be needed to extrapolate the design parameters for a practical imaging system from these theoretical studies.

Particular attention should be paid to the spectral sensitivities of the electro-optical sensors being considered. Certainly, no sensors currently exist that cover the spectrum from UV to thermal-IR. Fortunately silicon has a wide response ranging from the near-UV to the near-IR, including the essential 'vegetation index' bands (red and the near-IR). While alternative semiconductor materials possess sensitivities in other portions of the spectrum, their manufacturing techniques are not as mature as those for silicon. Therefore, if sensor arrays are preferred in a particular design, the choice of spectral bands may be limited. Furthermore, if IR wavelengths longer than about 2 μm are required, the sensors will need to be cooled (sometimes to cryogenic temperatures of 77°K, -200°C) to prevent the noise floor of thermally excited electrons swamping the signal.

Because a SPOT or LANDSAT mission costs in the region of a quarter of a billion dollars, it is imperative for these missions to fulfil as many requirements as possible. Therefore, the spectral bands on conventional spacecraft are chosen to provide good general-purpose imagery, suitable for a wide range of applications. By being general-purpose, these spacecraft cannot fulfil specific applications as effectively. Conversely, microsatellites are sufficiently inexpensive to be affordable by individual government agencies or companies for their specific remote sensing tasks. Thus the spectral bands of a dedicated imaging microsatellite can be fine-tuned to the specialist requirements of oil exploration, biomass surveys, fish stock estimation or forest fire detection, to give a few examples. These attributes of affordability and custom imaging characteristics for dedicated missions are, in the author's opinion, the key features that makes microsatellite remote sensing a viable concept despite the competition of existing conventional Earth imaging system.

Having said this, designing and constructing multispectral imagers is significantly more complex and expensive than a comparable monospectral system. The additional difficulty lies in achieving and maintaining the optical and mechanical co-alignment of the multiple sensors to within the dimensions of a pixel (i.e. to a few μm). Furthermore, the communications systems of current microsatellites do not have adequate downlink capacity to support the additional volumes of data produced by multiple image sensors. Therefore, no attempts at implementing multispectral systems have been attempted during this research programme. However, multispectral capability is a vital characteristic for future remote sensing microsatellites, and is an essential ingredient of SSTL's next generation of electronic camera.

3.1.3 THE SATELLITE ORBIT.

Although the choice of orbits for remote sensing missions is an extensive subject in its own right, by far the most popular orbit is the circular, polar orbit. The principal attraction of this orbit is its Sun-synchronicity, ensuring a constant Sun-angle. This is important because it enables imagery of the same scene, but captured at different times, to be compared directly without having to compensate for the effects of widely varying illumination strengths and directions. By passing over the poles, the satellite can provide global coverage, particularly of high latitudes which are hidden from sensors in geostationary orbit.

The orbital altitude is selected to provide the optimum characteristics for sensor resolution, ground track overlap, revisit period, orbital lifetime and radiation environment. For most remote sensing applications, an altitude of around 800 km provides the optimum trade-off of these and other factors. If the mission requires particularly high spatial resolution, a lower orbit may be preferable because smaller optics will be required. Conversely, if the primary objective is a large field of view, a higher orbit would be more suitable, reducing the distortions caused by the Earth's curvature. Selecting a circular orbit keeps the distance from the scene constant, ensuring that all captured imagery has the same resolution (within the tolerance of orbital and satellite attitude perturbations).

As with the choice of spectral bands, the choice of orbits on a conventional remote sensing mission is very much a compromise between the ideal parameters of the various potential applications. [Colwell, p.517-519] provides a clear discussion of the trade-offs of the initial LANDSAT study, showing that even within the standard Sun-synchronous orbit, the most favourable local Sun-time for imaging will depend on the mission objectives. Eventually most missions choose a mid-morning (09:30 to 10:30) as an optimum solution between the needs of the various applications and favourable cloud build-up patterns. Constellations of meteorological satellites (NOAA, Meteor) will be staggered throughout the day to provide regular (hourly) updates [Price]. Another consideration in specifying the orbit parameters is the frequency of revisit over a specific target regions [Rees].

One of the key roles for microsatellites in the field of remote sensing is to fill niche markets not well served by the large conventional spacecraft. Consequently, the designers of these missions should consider alternative orbits, or phasing within an orbit, to those already used widely. Merely by varying the Sun-angle within the Sun-synchronous polar orbit (i.e. the local time of day when the satellite passes), it would be possible to address the needs of alternative user groups: early morning for geologists, noon for agriculturists, mid afternoon for forest fire detection, late afternoon for ice and snow monitoring, etc. In particular, the long shadows cast by early morning or late afternoon Sunlight would complement existing imagery in producing terrain and elevation contour maps.

Another particularly interesting option for an imaging microsatellite is to use an equatorial LEO to concentrate on the tropical regions. Although a satellite in this orbit would not provide a global perspective, it would have an excellent re-visit capability (every 100 minutes) for equatorial regions. This would provide a unique capability for monitoring daily variations in cloud development, moisture and humidity concentration, tidal effects, and providing up-to-the-hour data for law enforcement (forestry and narcotics). Many equatorial regions have very regular daily build-up of clouds and haze, or burn-off of morning mist; if an area of interest is obscured at the time of day when LANDSAT or SPOT passes overhead, it may be impossible to ever obtain good imagery [Santana]. A satellite in an equatorial LEO orbit would over come this, allowing deforestation and erosion of remote regions to be monitored more effectively.

There is not adequate scope within this thesis to explore further the possible novel orbit configurations for microsatellite imaging missions. Needless to say there are numerous applications that are not ideally served by the traditional Earth observation services. In theory, microsatellites are sufficiently inexpensive to make them affordable to specific-interest organisations; consequently, highly specialised missions dedicated to particular applications are feasible.

N.B. Unless stated otherwise, all calculations in this thesis will use a truly-circular, 800 km, Sun-synchronous, polar orbit as the default.

3.1.3 TIMELINESS AND DELIVERY OF IMAGERY.

Although the designer of imaging instruments is primarily concerned with generating and collecting imagery, it is nevertheless important to consider how this data will be delivered to the end user. It is necessary to define the volume of data and / or the number of scenes to be delivered daily, and ensure that the communications systems are adequate. Section 3.4 considers the impact of a microsatellite's communications systems on the productivity of a dedicated remote sensing mission.

The issue of delivering image data is particularly important in weather forecasting and emergency relief (earthquake, flood, hurricane, fire fighting, etc.), where any delays in dispatching imagery could be costly or even fatal. In these instances, it is necessary for the end user (meteorologists or relief co-ordinators) to be in possession of the imagery as soon as possible, generally within an hour of capture. The standard solution of using a central control station to receive and distribute the satellite data involves far too many delays to meet these requirements, especially when the master station may not see the satellite for several hours after it collects its data of the stricken region. To permit extremely rapid turn-around, it is generally necessary to equip the users with ground terminals, wherever they may be, so that they can gather the data directly. This approach has an immediate implication on the downlink strategy, as the satellite will need to communicate with low-gain 'field terminals' in addition to the principal control stations.

On the other hand, many applications of satellite imagery do not require such rapid turn-around of data. Apart from the previously mentioned cases of disaster warning and relief, a few days delay in the delivery of data will not have a significant impact on its value to the user. In some applications, such as geology or site planning, imagery can often be years old without any particular loss in worth. The relaxation of delivery times gives the spacecraft designers more flexibility in implementing their communications systems. In most cases, it will be cheaper and simpler logistically to employ a single (or a network) of sophisticated ground control stations to collect the data. These stations are essentially one-offs and can therefore be optimised for high data rates without undue concern for cost. With this type of ground segment configuration, the volume of data retrieved from a remote sensing mission is likely to be higher than by going directly to the user.

Another benefit of using a centralised downloading network is that it provides a point of focus for data archiving, and image processing and interpretation expertise. By passing data through a distribution centre, it is possible to provide various levels of standard image correction as routine before it reaches the user, avoiding much duplication of effort and expense on the user's part. It is also possible to exert censorship on imagery of a sensitive nature (military, economic, environmental); whether this is a good or bad thing depends very much on one's point of view, but is generally desired by the organisation funding the mission.

Thus, it is clear that a poorly conceived strategy of data downloading and distribution could ruin a remote sensing mission, particularly if very fast data turn-around is anticipated. Therefore the system design must consider both ground segment and satellite downlink bandwidth when defining the mission specifications, even though this has very little to do with the imaging instrument itself. It will be interesting to watch the impact that on-line data services via the internet will have on the dissemination of satellite imagery, by being much faster at distribution than existing centralised systems but cheaper than a network of ground terminals.

N.B. The timeliness of delivering remotely sensed imagery must not be confused with the temporal resolution which is the length of time between two imaging opportunities of the same scene. A system's temporal resolution is defined by the satellite's orbit and the imager's field of view. Nevertheless, the need for high temporal resolution is often complementary with fast turn-around for the meteorological and emergency services where situations can develop and evolve within hours.

3.2 IMPACT OF THE PRINCIPLE SPACECRAFT HOUSEKEEPING SYSTEMS ON THE DESIGN OF THE IMAGING INSTRUMENT.

Although the imaging system may be a satellite's primary payload, it cannot function without the support of the housekeeping systems. Of particular importance is the performance of the communications, power, telemetry and telecommand (TTC), attitude determination and control (ADCS), and, if necessary, orbit control systems upon which the imager will depend during its lifetime in orbit. If the expectations of the imaging system exceed the actual capabilities of any of these housekeeping services, the mission may well be compromised.

Accordingly, an essential ingredient in the success of any spacecraft payload is a coherent approach to systems engineering. In many ways, ensuring a good system implementation can be more challenging than designing the imaging payload itself, involving many subtle trade-offs, the implications of which are not always immediately obvious. In this respect, the design of microsatellites is no different to any large and complex engineering project.

What is different in the specification of a microsatellite, as opposed to a larger conventional spacecraft, is establishing what constitutes 'acceptable' performances from the housekeeping systems. Given the inherent limitations on mass, size and power faced on microsatellites, it is inevitable that many of the features of large spacecraft will not be available. Correspondingly, many of the design solutions popular for imaging systems on large spacecraft simply will not work on a microsatellite. The designer of the imaging system must understand the repercussions of these constraints, and develop the payload accordingly.

The rest of this chapter reviews what can be expected from a microsatellite bus in terms of the mass, volume, power, communications and attitude control offered to the payload. Significant effects on the design of imaging systems are highlighted. The scope of this analysis is primarily limited to microsatellite technology in-orbit at the time of writing. However, in certain key areas where substantial progress is imminent (attitude control, and especially communications), a short discussion of these important developments is appropriate.

3.2.1 MASS BUDGET.

By definition, the mass of a microsatellite is between 50 to 100 kg, presenting the most obvious restriction of this class of space vehicle. Using the mass breakdown of the SSTL family of 50 kg microsatellites, which are representative for the industry as a whole, about 70 to 80% of the total mass is made up of the structure and essential bus housekeeping systems. This leaves 20 to 30 % (10 to 15 kg) of the total mass budget to accommodate all the various payloads.

While a payload-to-platform ratio of 30 % may appear low, it is in fact unusually high for a microsatellite. This was achieved on the Cerise microsatellite, where SSTL engineers reduced the platform mass sufficiently to allow the customer's 15 kg payload to be carried, yet remain within the total spacecraft mass limit of 50 kg. In comparison, the mass of the UoSAT-3 and -4 spacecraft platforms were 41 kg, able to accommodate up to 9 kg of payload or 18% of the total mass. Most of SSTL's other spacecraft split the mass approximately 75:25 (platform : payload).

The largest contributing factor to a microsatellite's overall mass is the structure itself. While this may appear paradoxical, a strong structure is essential if the spacecraft is to withstand the rigours of launch, and ground handling and transport (which is possibly more stressful than the launch itself). Over the successive microsatellite missions, SSTL has devoted considerable effort to strategically reducing the mass of the structure, liberating more for the various payloads, with Cerise representing the most lightweight version to date. However, striving for lower structural mass involves a delicate trade-off because of the diverse penalties incurred: reduced structural rigidity, increased risk of metal fatigue, increased complexity of manufacture due to reduced machining tolerances, reduced thermal conductivity, reduced radiation screening, etc.

The choice of materials and material thickness in a microsatellite's structure is carefully considered. To achieve an efficient use of the mass, it is important to have each component fulfil as many requirements as possible. It will certainly be lighter for a single element (i.e. a suitably machined metal box) to provide, for example, structural rigidity, support of electronic circuits, thermal relief and shielding from both ionising and non-ionising radiation, than to accomplish these goals with individual components. It would also be possible to use carbon-fibre structures instead of the traditional milled aluminium, but the advantage in terms of mass savings must be balanced with the increased cost and lead times, as well as the impossibility of accommodating late-breaking design modifications.

Typically, the larger the spacecraft, the higher the percentage of payload that can be flown. On SSTL's forthcoming minisatellite (200 - 300 kg), it will be possible to attain payload-to-platform ratios as high as 50 %. Conversely, on 10 kg 'nanosatellites', there is generally no dedicated payload - the on-board computer fulfils a dual-role supporting both housekeeping and a communications payload. Moreover, the payload's requirements from the bus systems also effects the mass of the platform. If particularly high performance is demanded from the power, communications, attitude control, thermal or any other system, there is an inevitable knock-on effect resulting in an increase of this system's mass.

Ultimately, only a small percentage of the spacecraft's overall mass is attributable to the electronics. Indeed, the potential for mass saving in this area is fairly limited given that the module boxes / structure, printed circuit boards, connectors and wire inter-connects are all far more significant contributors to the mass budget. Nevertheless, there is some scope for mass savings by taking advantage of recent progress in the high-density integration of solid-state electronic devices and reduction in the packaging size (e.g. surface-mount technology). However, the general trend in exploiting this new technology is to embed greater performance onto the same board area, without obtaining many returns in terms of mass. Mass savings can only really occur by miniaturising circuits to the point that two systems can share a single module box, thereby reducing the amount of mechanical support required.

While there may be a small amount of lee-way in figures presented here, imaging instruments larger than about 20 kg simply cannot be accommodated on a 50 kg microsatellite, and are at the limit of the capabilities of 100 kg spacecraft. Looking at the specifications of the various instruments in tables 2.2a and b, it appears that mechanically active (whiskbroom) imagers are invariably too massive for this type of spacecraft. The least massive example is the NOAA AVHRR instrument, which at 33 kg is already considerably over-weight. Flying the LANDSAT (MSS: 68 kg, TM: 258 kg) or GOES (imager and sounder: 77 kg each) systems on a microsatellite is completely unfeasible.

Despite the large masses of the SPOT HRV and IRS LISS instruments, it is possible to implement very much smaller all-electronic (i.e. mechanically passive) imaging systems, which are therefore more suited for microsatellite applications. The dominant mass contributor to these imaging systems is generally the optics, which will need to be kept compact and lightweight to fly on these small missions. This immediately limits the scope for deploying very high resolution (long focal length) or low-light (large aperture) systems on a microsatellite.

Incidentally, the 50 kg mass used for a typical microsatellite is not an arbitrary number chosen for the sake of this discussion. It is imposed by Arianespace, the leading agency offering microsatellite launches. Other rockets can provide more lifting capacity, but rarely much more than around 70 kg.

3.2.2 STRUCTURE AND VOLUME.

As the name suggests, microsatellites are small in addition to being low mass. Given the emphasis on keeping the structural mass down, microsatellites tend to be fairly compact and squat (close to cubic or spherical) to withstand the launch conditions. Furthermore, launch agencies rarely offer a large volume for microsatellites launched as auxiliary payloads, as most of the rocket's fairing envelope is employed by the primary customer. These factors dictate that the imaging payload must be compact.

Obviously, the imaging systems will need to have access to the outside of the spacecraft body and to be facing the Earth. However, the external surfaces are at a premium on a microsatellite, being mainly covered with body-mounted solar panels. Given the number of other sensing systems (mainly ADCS, but also other payloads) and communication antennas that need to occupy the remaining space, not much room is left for the imaging system and its optics.

On SSTL microsatellites prior to and including PoSAT-1, the largest volume made available for the camera optics and electronics at the Earth-facing end of the satellite was about 260 x 60 x 40 mm. Similarly, the maximum aperture that could be cut into the bottom of the spacecraft to accommodate a lens was less than 5 cm diameter. An additional 300 x 300 x 30 cm module tray was provided in the middle of the spacecraft stack for the imaging system's remaining (digital processing) electronics. Granted that none of these spacecraft were dedicated imaging missions, these are nevertheless tiny volumes in which to develop remote sensing capabilities, and represent a much greater limitation than the mass or other constraints.

Once again, the Cerise mission is the microsatellite offering the most generous payload conditions. Following significant mechanical redesign and a careful re-deployment of the essential housekeeping systems, an Earth facing payload compartment has been provided, which can hold payloads occupying up to about 250 x 250 x 200 mm. Even though this volume represents a huge improvement compared to the space available on PoSAT-1, it is still a tight constraint on the design of imaging instruments. Certainly, none of the imaging payloads presented in tables 2.2.a and b could exist in this volume.

This configuration was retained for the FASat-Alfa mission, which supported four cameras amongst the numerous payloads, sensors and antennas on the Earth-facing facet. Although the individual cameras are still very compact (130 x 90 x 60 mm excluding optics - see figure 4.6.2a; the largest lens flown takes the dimensions to 130 x 90 x 180 mm), the provision of a less cramped compartment has allowed the camera electronics to take a more natural configuration (see figure 2.3.3.3d), easing their manufacture and testing. On future dedicated Earth observation missions, the entirety of this payload compartment will no doubt be occupied by imaging systems.

Therefore, to be suitable for consideration on a microsatellite mission, the mass and volume of an imaging instrument must be kept extremely low. Given the packing density of contemporary electronic circuits and sensors, this is not a particular problem. The mass and volume restrictions will present greater limitation on the design of the optics. It will be necessary to employ folded optics for focal lengths greater than 200 - 300 mm. Physical apertures greater than 15 to 20 cm will be very difficult to accommodate.

3.2.3 POWER CONDITIONING AND DISTRIBUTION MODULES.

Looking at the specifications of the conventional imaging instruments presented in tables 2.2a and b, the power consumption of the main payload rarely consumes more than about 10 % of the spacecraft's total power budget, except for the massive LANDSAT TM which draws about 22 %. Given the overheads of the housekeeping systems (presumably the attitude control, transmitters, active thermal control and active mechanical systems use the lion's share of the power), there is only moderate emphasis on reducing the power consumption of the imaging payloads. Any savings made by the payloads would only be of minor benefit, and may entail some loss of performance. This situation is unfortunately at odds with the constraints of flying these instruments on microsatellites.

With the mass and volume restrictions of microsatellites, it is not possible for these spacecraft to carry large solar arrays or battery packs for generating and storing electrical power. Mechanical Sun-tracking arrays are too complex and massive to implement on this size of spacecraft, so the solar panels are generally body-mounted. This provides only small areas over which to collect Sunlight. Furthermore, the incident light will rarely be orthogonal to the illuminated panel, reducing the efficiency. Therefore, the power produced from a microsatellite's solar panels will be limited.

The peak power available from a panel on SSTL's most recent spacecraft (Healthsat-2, PoSAT-1 and FASat-Alfa) is about 35 Watts in Sunlight. These satellites are equipped with gallium-arsenide solar arrays with an average efficiency of 19 %, significantly better than can be achieved from silicon cells (typically 14 % efficient). However, these spacecraft spend about a third of their orbit in eclipse, reducing the orbit-averaged power to around 25 Watts (taking battery and conversion losses into consideration).

The typical power consumption of housekeeping modules on an SSTL microsatellite is about 4 Watts. This includes the base-loads of the receivers, modems, telemetry, telecommand, primary on-board computer, attitude determination sensors, attitude control actuators (magnetorquers) and the power system itself, but not the transmitters. The transmitters on SSTL spacecraft are by far the most power-hungry systems drawing up to 20 Watts (for about 8 Watts RF), although 6 Watts (2.5 Watts RF) is more typical if payloads need to be operated as well. The need for this relatively high power from the transmitters is a function of the store-and-forward communications services that these microsatellites provide to low-cost, and correspondingly low-gain, ground terminals (see section 3.4.2 for more details).

In future, it would be logical to use ground stations with high-gain antennas to communicate with dedicated remote sensing microsatellites, liberating the power currently drawn by the transmitters for the imaging systems, whilst maintaining or improving the downlink data rates. Greater savings will be achieved by operating the transmitter in bursts, with very high output powers and data rates when in range of a master ground station, but turned off otherwise.

Therefore, assuming that the transmitter of a dedicated microsatellite draws the equivalent of a continuous 2 Watts, the total housekeeping load will be around 6 Watts. This leaves around 20 Watts for all the payloads. Fortunately, in practice, the imaging systems are generally only required for half an orbit, when the scenes below are in Sunlight. This is advantageous because when operating in Sunlight, energy is drawn straight from the solar panels without incurring any of the losses associated with the batteries. Under these circumstances, the spacecraft should be able to sustain somewhat higher payload powers, approaching 25 to 30 Watts. A 100 kg microsatellite equipped with deployed (but not Sun-tracking) solar panels, should be able to support higher payload powers, around 50 to 70 Watts.

If the payload is not operated continuously, higher peak powers can be sustained briefly. This is the case for the communications payload on the S80-T microsatellite, which draws about 60 Watts for an average of 15 minutes per orbit. If these operations are in eclipse, then it takes longer for the batteries to recover to their fully charged state. In theory, the peak power than can be supported is limited by the maximum discharge current from the batteries, about 10 Amperes or 120 Watts (including the housekeeping systems).

Nevertheless, this is a very small amount of power on which to run an conventional imaging payload. Of the instruments presented in tables 2.2a and b, only the NOAA AVHRR and IRS LISS instruments are close to this figure. Certainly none of the other whiskbroom scanning systems could operate for long periods on this power regime. If there are specific reasons why a whiskbroom imager, particularly its scanning mirror, must be left on continuously and operated in eclipse (e.g. to prevent cold-welding, causing attitude shocks due to change in angular momentum, to maintain constant temperature and rotation rate, etc.), then it will not be feasible to use this type of scanning architecture on a microsatellite. Even if the instrument only operates intermittently, it is marginal whether the payload could be activated sufficiently to justify the mission.

Fortunately, it is possible to implement all-electronic imagers with much more modest power requirements (despite the large consumption of the instruments shown in tables 2.2a and b). Consequently, although the power budget of a microsatellite is very small compared to that of a conventional remote sensing satellite, it does not appear to present as much of a constraint as the mass and volume limitations. From this very quick review, a 20 Watt payload could be sustained continuously, and higher powers for shorter periods. Of course, the final power budget of a mission is highly dependent on the orbital parameters, the configuration of the solar arrays and batteries, the duty cycle of the payload and the need to perform operations in eclipse.

The power regulation and distribution strategy on a microsatellite is fairly flexible and could be tailored to meet the requirements of a specific imaging payload. On SSTL spacecraft the primary power supply is an unregulated +14 V rail (12 to 15 V). It is difficult for a microsatellite to provide the unregulated +28 V supply typical of many spacecraft systems, because of the mass of batteries required. If a +28 V supply was specifically required to be compatible with an existing payload, it would probably be necessary to include a step-up converter to generate this rail, sustaining the additional losses of this converter.

SSTL microsatellites use a Power Conditioning Module to produce regulated +5 V, +10 V and -10 V rails. This arrangement could be modified without undue difficulty if required by the payload. However, the exact regulation scheme is not particularly crucial, as in most instances the imaging system will generate and regulate its own rails locally, to ensure suitable conditioning and noise characteristics (see section 5.3.1). However, the availability of a standard +5 V rail can be useful to drive any logic or computer modules.

3.2.4 THERMAL.

One advantage of a microsatellite's small and compact structure is that thermal variations and gradients are minimised. Although the external surfaces can be subject to fairly rigourous thermal cycling (circa 100°C per orbit), the interior of the spacecraft will remain at a constant temperature, seeing variations of less than 10°C over an orbit. This is less than would be expected on a large spacecraft or even during lab testing on the ground. In addition to minimising the stress of the components, this reduces the likelihood of thermal expansion and contraction disrupting the alignment of the imager's optics.

The traditional polar, Sun-synchronous orbit favoured for remote sensing applications provides a very regular and predictable thermal cycling of the spacecraft, as it passes from Sunlight to eclipse every orbit. Because these periods are invariant, it is possible to balance the satellite's thermal budget accurately. By being located near the large thermal mass of the battery packs, the cameras on PoSAT-1 see a swing of only 3 to 5°C every orbit. Their mean temperature of 12°C will change by a degree or two as the Earth approaches and recedes from perihelion.

Other low-Earth orbits, which are not Sun-synchronous, have 'seasons' as the orbit plane precesses, taking the satellite from the conditions of the regular '10:30 AM / 10:30 PM' orbit to periods of uninterrupted Sunlight (6 AM / 6 PM orbit). Under these conditions, it is more difficult to control the spacecraft's thermal balance, which experiences extremes of heat (in perpetual Sunlight) and cold (in eclipse). Although the S80-T and KITSAT-1 microsatellites (1300 km, 66° orbit) do not experience much greater daily cycling than PoSAT-1, there can be up to 30°C of seasonal variation.

Nevertheless, these are not particularly demanding conditions for the spacecraft electronics, most of which will be rated to operate over the range of -45 to +85°C, as a minimum. In the absence of other considerations, it is preferable to run the imaging systems at cooler temperatures because of the associated reductions in the background noise of the solid-state sensors (dark current generated by thermally excited electrons - see section 5.1.3.2).

However, the thermal design will need to accommodate the most sensitive components in a satellite, which are the batteries and the propulsion fuel (if present) which must never be allowed to freeze. Due to these considerations, it will be difficult to get the imaging payload much colder than (-10 to -20°C). Although it is possible to use passive heat pipes radiating to deep space to cool specific parts of the spacecraft (i.e. the sensor), these will need to be massive to overcome the energy received from facing the Earth.

If the mission must support medium or short-wave infra-red sensors, which need to operate in the vicinity of 77°K (-200°C), then an active cooling system must be employed. This will require the use of a mechanically active heat exchanger, such as a sterling-cycle cooler. However, these devices are large (circa 10 kg) and power hungry (a continuous 15 to 50 Watts depending on the thermal load) in the context of microsatellites, and miniaturising these coolers, whilst retaining their space-worthiness, is the subject of intensive international research. If more moderate (up to 100°C of differential) cooling is acceptable, thermoelectric devices using the peltier effect are a viable alternative.

3.2.5 ORBIT DETERMINATION, ORBIT CONTROL AND STATION KEEPING.

Section 3.1.3 provides an introduction to the orbits suitable for remote sensing spacecraft and some of the novel opportunities available for imaging microsatellites. Unfortunately, microsatellite missions are rarely in a position to dictate the choice of orbital parameters. Riding as secondary payloads, microsatellites must accept the launch conditions and orbital requirements of the principal payload. Fortunately, because it requires significantly less energy to reach low-Earth orbit (LEO) than geostationary transfer orbit (GTO), many dual-purpose rockets (e.g. ARIANE) launching remote sensing spacecraft have spare lifting capacity, and therefore often offer to carry microsatellites. The search for a suitable launch for an imaging microsatellite should not therefore be too difficult. As the new breed of launch vehicles dedicated to small missions becomes available, both the frequency of microsatellite launches and the choice of orbits should increase significantly.

Shortly after launch, a conventional remote sensing spacecraft will use its on-board propulsion system to provide fine corrections to its initial orbit provided by the rocket. The orbital parameters of the satellite are chosen for optimum performance and the satellite must maintain its circularity carefully (for constant image resolution), revisit cycle and orbit phasing (if part of a constellation). Another reason for raising the orbit is to escape from debris associated with the launch vehicle (including any secondary payloads).

Due to the mass and volume requirements of gas thrusters, most microsatellites are deprived of these systems, and have no possibility for orbit control. These spacecraft will be confined to whatever orbit the launch vehicle provides, which will never be optimal but can, on occasion, be quite inaccurate (LANDSAT-4, [Colwell, p.565]). Even if the rocket provides a perfect injection orbit, the various perturbations and aerodynamic drags will cause the orbit to drift. To quantify the extent of these errors and the benefits of orbital control, table 3.2.5 compares the orbits (in August 1995) of the SPOT-3 and PoSAT-1, and the LANDSAT-5 and UoSAT-2 spacecraft which were launched into essentially the same orbits.

Satellite	LANDSAT-5	UoSAT-2	SPOT-3	PoSAT-1
Date of launch	1 March 1984		26 September 1993	
Years since launch	11		2	
Apogee height (km)	706	672	826	805
Perigee height (km)	699	655	824	792
Eccentricity	5×10^{-4}	10^{-3}	10^{-4}	10^{-3}
Orbits /day	14.57	14.51	14.20	14.28
Local time of equator crossing	09:30	05:40	10:30	10:40

Table 3.2.5 Comparison of orbital drift suffered by microsatellites versus conventional remote sensing satellites.

From this table, the most obvious difference in orbital characteristics is the improved circularity of the conventional spacecraft (especially SPOT-3), represented by the smaller eccentricity and the small difference between the apogee and perigee altitudes. Moreover, although the discrepancies in number of orbits per day (the mean motion) may appear small, these have a considerable effect of the satellite's revisit capabilities. Whereas SPOT-3 has a regular repetition of its ground tracks every 26 days, PoSAT-1 does not. In fact, the microsatellite repeats its ground track every eleven days, but without actually covering all parts of the globe. Over the years, UoSAT-2's altitude as fallen, and as a consequence the orbital plane is slowly precessing away from the nominal 09:30 orbit. (N.B. On a month-by-month basis, the satellite's departure from true Sun-synchronicity will be barely appreciable).

Unfortunately, as there is no means of correcting these parameters, the operators and users of microsatellites will simply have to put up with the orbital fluctuations and inaccuracies. Provided the orbital perturbations can be recorded and / or modelled, they can be compensated for during the image post processing stages. Accurate measurements of these parameters is possible on a microsatellite, by using a the transmissions of the

Global Positioning System (GPS) navigational satellite constellation. PoSAT-1 and FASat-Alfa carry GPS receivers to provide autonomous orbit tracking capabilities [Unwin, 1993] [Unwin, 1995]. Otherwise, it is possible to design the imaging instrument with off-axis viewing to provide coverage when the satellite's repeat cycle is incorrect.

3.2.6 CONCLUSIONS WITH RESPECT TO IMAGER ARCHITECTURE.

The mass, volume and power restrictions of a microsatellite platform represent significant constraints in the implementation of remote sensing from these very small spacecraft. Certainly none of the imaging payloads currently in orbit on conventional Earth observation missions are sufficiently compact to be flown on a microsatellite.

The compactness, robustness, mechanical simplicity and low-power of solid-state sensors make them highly suitable for deployment on a microsatellite. With special attention to reducing the mass and volume, it is possible to implement all-electronic systems similar to those currently in-orbit. While the electronics of a microsatellite imaging instrument will be comparable to existing designs, special attention must be paid to keep the mass of the optical and structural support elements within the mission margins. Because of this, missions requiring long focal lengths or large optical apertures may not be feasible on a microsatellite.

Unlike solid-state imaging technology, there is little prospect for achieving adequate miniaturisation of whiskbroom scanners to support them on microsatellites. The mass, volume, and power demands of their rotating mirrors in particular cannot be met by existing, or indeed future, microsatellite technology. Although the conflict of requirements is especially marked on small spacecraft, these characteristics of mechanically-scanned imagers are making them increasingly unattractive. Consequently, whiskbroom imagers have become obsolete in most new spacecraft designs.

While solid-state sensors are the most suitable technology for implementing remote sensing on a microsatellite, the factors considered so far are not the principal drivers in the design of the imaging instrument. Of far more consequence are the performance of the attitude control, and to a lesser extent, the spacecraft's communication systems.

3.3 IMPACT OF SPACECRAFT STABILITY ON THE DESIGN OF THE IMAGING INSTRUMENT.

As with conventional film photography, the physical relationship between the sensor and the scene is crucial in determining the quality of remotely sensed imagery. It is the task of the attitude determination and control system (ADCS) on a remote sensing satellite to keep the imaging platform pointed towards the correct part of the Earth with adequate stabilisation to ensure that the recorded images are useful.

In theory, it is desirable for the satellite's pointing accuracy to be finer than the ground resolution of the imager, so that the images can be aligned to maps automatically (open loop). However, the ADCS meeting such specifications will be large, complex and expensive, especially on high-resolution missions. By relaxing the pointing requirements, there are often significant savings in the design and implementation of the ADCS. Similarly, imaging can be supported on smaller sized spacecraft with fewer resources to devote to attitude control.

Given that the ADCS provided by any satellite, particularly a microsatellite, will be imperfect, the consequences of the various drifts on the performance of the imaging payload must be evaluated. Key aspects considered here include targeting accuracy, registration errors and blur.

3.3.1 ATTITUDE DETERMINATION AND CONTROL OF CONVENTIONAL REMOTE SENSING SATELLITES.

Conventional remote sensing spacecraft invest heavily (in terms of cost, power, mass) in their attitude determination and control system (ADCS) to guarantee the necessary pointing accuracy and stability. Table 3.3.1 shows the stabilisation characteristics for a number of existing remote sensing satellites. All these platforms need complex implementations to maintain this stability, relying on numerous attitude sensors and actuators, including momentum / reaction wheels and mono-propellant gas thrusters.

From table 3.3.1, one can draw the conclusion that recent remote sensing missions demand very high stability from their ADCS, maintaining pointing accuracies around 0.1°. For a typical meteorological imaging mission, this is better than one pixel and the imagery can therefore be treated as perfectly aligned with maps. For a high resolution land resources instrument, these levels of stability will cause several tens of pixels error. However, as the attitude determination of these satellites is always several orders of magnitude better than their control, it is possible to compensate for these small misalignments during the processing stages.

Spacecraft	Pitch control	Roll control	Yaw control	Max. drift rate
LANDSAT 1-3	±0.7 °	±1.0 °	± 1.0 °	4×10^{-2} °/s
LANDSAT 4+	±0.01 °	±0.01 °	±0.01 °	< 10^{-6} °/s
SPOT	±0.15 °	±0.15 °	±0.15 °	< 10^{-3} °/s
IRS-1A, 1B	±0.4 °	±0.5 °	±0.5 °	3×10^{-4} °/s

Table 3.3.1 Attitude control requirements of conventional remote sensing satellites.

3.3.2 ATTITUDE DETERMINATION AND CONTROL CURRENTLY AVAILABLE ON MICROSATELLITES.

Unfortunately, the restricted power and mass budget of existing microsatellites cannot provide the high precision ADCS demanded by conventional remote sensing satellites. This may limit the type of missions objectives and imaging payload design that can be supported by these small satellites. Before considering the restrictions imposed by their coarse attitude control, the techniques available for stabilising microsatellites should be reviewed.

3.3.2.1 Minimal or no ADCS.

Many microsatellites employ no active ADCS, and tumble through space uncontrolled. This is especially prevalent among very small spacecraft, with masses of less than 20 kg. These satellites are mainly used for VHF / UHF communications with omni-directional antennas and can operate satisfactorily despite the absence of all pointing control. Occasionally, primitive passive control techniques are used with limited success, such as adding a permanent bar magnet to align with the Earth's magnetic field. Sometimes, the satellite is encouraged to spin by adding small metal sheets, painted black on one side and reflective on the other, which react to solar illumination pressure. This is done to even out temperature gradients, but is of little use for remote sensing as the effects are quite uncontrollable.

Without any ADCS, it is not possible to control which direction an imaging instrument will be facing, or even if it will ever point at the Earth. Because of this, satellites without active attitude control are very poorly suited to remote sensing. Although unstabilised spacecraft can conceivably be used for technology demonstration, their unpredictability would make experimentation frustrating. Certainly, it would not be feasible to base a commercial / scientific imaging mission on a satellite without any ADCS, as predictability and repeatability would be non-existent.

Two microsatellites without effective attitude control have carried electronic cameras: Webersat (see section 2.3.5.3) does not include any active ADCS by design, and UoSAT-1 (see section 2.3.3.1) whose gravity-gradient boom failed to deploy. The results of these two mission have been correspondingly haphazard.

3.3.2.2 Gravity-gradient booms & magnetorquing.

A well-established and simple technique of controlling a spacecraft's attitude is known as gravity-gradient stabilisation [Hodgart & Wright][Hodgart & Ong][Wertz]. Once in orbit, a long boom fitted with a relatively heavy tip-mass is deployed. This configuration of two connected bodies will naturally align itself with the Earth's gravitational field, so that one of the bodies is facing towards the Earth.

Once the boom has been deployed, it provides a continuous stabilising effect, which is both mechanically passive and consumes no power or fuel. As such it is particularly attractive to microsatellites. On SSTL microsatellites, the mass of the gravity-gradient stabilisation system is 7 kg (3.5 kg for the tip mass, 1.7 for the telescopic boom, 1 kg of supporting structure, and 0.8 kg of electronics and pyrotechnics) representing 14 % of the spacecraft's 50 kg total mass, providing a simple and relatively compact solution.

Although the gravity-gradient effect is significant, it is not adequate to ensure complete spacecraft attitude control. Boom-assisted gravity-gradient stabilisation will keep a typical microsatellite Earth-pointing within a cone of about 45° from nadir for a number of days. Additional ADCS, typically in the form of magnetic torquing systems, is necessary to damp the residual oscillations and provide complete attitude control.

Magnetic torquing, or magnetorquing as it is often known, involves passing a current through large coils mounted on the spacecraft. The EMF generated interacts with the geomagnetic field to generate small torques on the satellite structure. By firing the magnetorquers at judicious moments, it is possible to dump much of the satellite's energy into the geomagnetic field, thereby establishing attitude control.

The combination of gravity gradient stabilisation and magnetorquing has been in use since the 1960's, and although has largely been superseded by momentum / reaction wheels and thrusters for large spacecraft, remains attractive for small satellites where mass and power are at a premium. The principal limitation of these techniques is the small torques generated, so that the system's response time is quite slow. Furthermore, they are primarily suited for use in low Earth orbit, where the gravitational and magnetic fields are quite strong. It is also difficult to operate magnetorquers in the polar regions, because of the rapid convergence of magnetic flux lines.

3.3.2.3 The ADCS of the SSTL microsatellite bus.

In theory, there is no limit to how accurately a satellite's attitude can be controlled using gravity gradient stabilisation and magnetorquing. In practice, the control algorithms and attitude sensors used by microsatellites result in appreciable residual errors. On the SSTL microsatellites, the attitude pointing is routinely kept to within 5°. (From an 800 km orbit, this corresponds to a maximum off-pointing of 70 km, projected on to the ground). The error is largely due to the reliance on magnetometer readings for attitude information and the simplicity of the on-board computer's attitude model. As optical sensors and more sophisticated algorithms are developed and exploited, it should be feasible to improve the attitude control to within 1° or better.

The pointing control of microsatellites is clearly very different from that of conventional remote sensing satellites. However, as we shall see in the following sections the absolute pointing accuracy is not the sole consideration when designing the ADCS for an imaging satellite. The drift rates of the satellite's stability are of greater importance.

Fortunately, the perturbations on the pitch and roll caused by gravitational effects are of low frequency. The oscillations vary over a long time (about 3000 seconds - roll period = T/2, pitch = $T/\sqrt{3}$ [Hodgart 1982]). This corresponds to pitch and roll displacements of 7×10^{-3} ° per second, or 100 metres per second when projected onto the Earth's surface. Similarly, the small torques associated with magnetorquing result in slow changes in attitude, with virtually no transient effects. Thus, gravity gradient stabilisation and magnetorquing are not as poorly suited to remote sensing platforms as may first appear.

However, many microsatellites, including all SSTL spacecraft currently in orbit, employ a slow yaw spin to even out thermal gradients. Even though this spin is slow, at about 1 revolution every 10 minutes (i.e. spinning at 0.6° per second), it has highly detrimental consequences on the imaging payloads as shall be seen in sections 3.3.4.1 and 3.3.4.2. Recognising the inherent unsuitability of a spinning satellite for most imaging and other scientific missions, the ill-fated FASat-Alfa mission was designed to operate with a fixed yaw (i.e. no spin). This non-spinning configuration will no doubt become a standard feature of future imaging microsatellites.

Thus to summarise, almost all microsatellites benefiting from active attitude control use gravity gradient booms and magnetorquers, to keep the satellite's pitch and roll axes librating very slowly within a 5° cone. A moderate yaw spin is often used to provide temperature balancing, but this is being phased out as imaging missions become more prevalent.

3.3.3 ERRORS IN MAINTAINING ATTITUDE POINTING.

Virtually all Earth imaging instruments are aligned to be nadir-pointing, i.e. by definition, with their optical axis parallel to the yaw axis.[1] Failure to maintain perfect attitude in any of the satellite's axes will cause the image to either miss the intended target or to have distorted geometry. It is therefore important to assess the consequences of such inevitable departures from perfect attitude, and establish limits for attitude errors based on the various degradations effecting the imagery.

Although, deliberate off-pointing is occasionally required to provide oblique look-angles or more frequent revisits, only the most common configuration of nadir-pointing is considered here. Alternative alignments of the optical axis are subject to similar analysis, but the trigonometry is a bit more complex.

3.3.3.1 Accuracy of targeting.

Errors in the pitch and roll vectors cause the imager's optical axis to point away from the sub-satellite point. The resultant incorrect pointing does not degrade image quality, but reduces the ability to capture specific target areas on the ground. The imagery will still have the same optical (i.e. angular) resolution and detail, but will not contain the desired features and regions. While it is clearly important to be able to image specific areas reliably, some error may be tolerable, depending on the mission specifications.

Figures 3.3.3.1a and b show the effect of these pitch and roll errors on image alignment. The solid boxes represent the target on the Earth's surface, viewed from the satellite, under perfect attitude conditions. The dashed boxes depict the target actually imaged, under the various conditions of attitude error. Therefore, pitch errors cause the imager to point forward or backwards, roll errors will cause the imager to point to one side of the ground track.

---

[1] The conventional definitions of pitch, roll and yaw are used: the pitch axis is in the orbit normal, with a forward and backwards motion contained in the orbital plane; the yaw axis points towards the Earth's centre in a circular orbit, with a motion in the plane tangential to the orbit; and the roll axis forms the third mutually-orthogonal axis parallel to the satellite's orbital velocity vector, with a side to side motion.

Direction of travel.

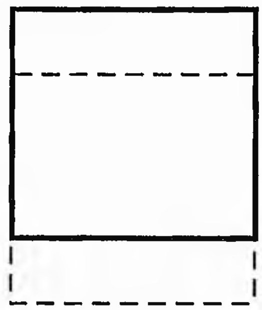

Figure 3.3.3.1a Effect of pitch error on image targeting.

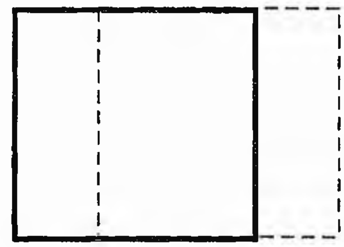

Figure 3.3.3.1b Effect of roll error on image targeting.

A secondary effect of non-nadir pointing, whether deliberate or accidental, is the change in viewing geometry, which distorts the system's ground resolution. Correcting for this is a relatively simple operation during post-processing however, provided the look-angle is actually known.

Variations in the satellite's yaw angle create a rotation between the sensor and the scene. For area imagers, the whole picture is rotated (figure 3.3.3.1c). Conversely, with scanning systems, this situation results in crabbing - a horizontal misalignment between successive scan lines (figure 3.3.3.1d). If the yaw angles are small (and known), the crabbing can be accommodated during processing or display.

Direction of travel.

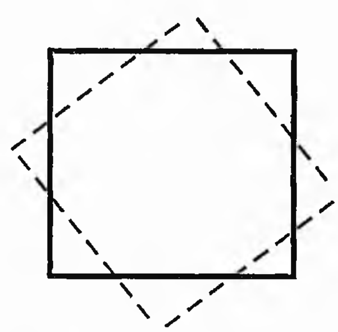

Figure 3.3.3.1c Effect of yaw error on area imager.

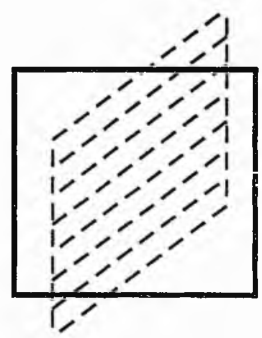

Figure 3.3.3.1d Effect of yaw error on pushbroom imager.

3.3.3.2 Pointing requirements for different imaging missions.

Referring back to section 3.3.1, recent conventional remote sensing missions maintain 'perfect' attitude pointing accuracy (around 0.1°). As we have seen in section 3.3.2, existing microsatellites cannot currently support attitude control of this precision, their ADCS generally being only accurate to a few degrees. Given this, it will not (or rarely) be possible to align microsatellite imagery directly to other data, and additional post-processing (using ground-truth points) will be necessary to accomplish registration to standard maps. The emphasis in specifying the ADCS for microsatellites must therefore be to ensure that imaging activities can be targeted with good probability.

As coarse pointing control is not normally encountered on remote sensing satellites, the literature is sparse regarding what represents acceptable limits. However, the early LANDSAT spacecraft, which had comparatively poor pointing accuracy, can be used as a guide. From their 910 km orbits, a 1° pointing error corresponds to 16 km on the ground, or about 10% of the Multi-Spectral Scanner's (MSS) field of view of 180 km. The author's practical experience also suggests that this is a tolerable value of misalignment for most applications. This may be the case in instances where the characteristics of large areas, rather than specific points, are of interest. Furthermore, the edges of an image tend to be subject to greater geometric and radiometric distortions than the centre, and thus are sometimes of less use, minimising the consequences of inaccurate pointing.

Therefore, a microsatellite's ADCS should be able to provide a pointing accuracy (the combined pitch and roll angles) to within 10% of the imager's field of view. This limit could be extended to 20%, if the mission objectives allow. Of course, these figures are guidelines; if the ADCS can provide better pointing, the results will be more predictable. Note that the maximum extent off-pointing is dependent on the field of view, and not the pixel resolution. Regardless of the actual field of view, the ADCS should keep the image to within 10 to 20 km of its nominal target, or else significant image features could be lost. This corresponds to a pointing accuracy of about 1° from an 800 km orbit.

As discussed in the previous section, departure from the nominal yaw angle (i.e. normal to the orbit velocity) causes crabbing on scanning imagers. As with pitch and roll, yaw errors introduce distortions by scaling the pixel dimensions. While these corruptions are relatively easy to correct, yaw also causes a blurring of detail which is more difficult to remove. The imager's swath width (field of view) will decrease with the cosine of the yaw angle, reducing the spacing between pixel centres (see figure 3.3.3.1d). However, the size of the individual pixels will not be shrunk accordingly. Indeed, the actual width of each pixel will in fact increase slightly because it is scanning askew. Thus, the ground tracks of neighbouring pixels start to overlap, resulting in a loss of contrast and resolution. As this degradation in definition occurs quite quickly, fairly tight bounds must be placed on the maximum tolerable yaw error. An upper limit would have to be at 3°, when the pixel width has increased by 5%. (N.B. This error must be factored into the blur budget described in section 3.3.4.2).

Conversely, the effect of yaw on area sensors is merely a rotation of the entire image. While it is convenient to have images oriented the same way (e.g. with respect to North or the ground track) for easy reference, it is not essential. Rotating the whole image is a simple operation during processing. Because the pixels in an area sensor are all physically bonded, there is no loss of detail, although various scaling terms for non-nadir viewing may need to be applied.

To summarise, to ensure the targeting accuracy and image geometry, the ADCS of a typical remote sensing satellite should control the pitch and roll to within 1° of nadir, and the yaw to within 3° of nominal (relative to the velocity vector). If the imaging system uses area sensors exclusively, the restriction on yaw control can be removed. If deliberate off-pointing is required, the pitch (fore and aft viewing) and roll (sideways viewing) angles can be increased, provided the resultant scaling errors are noted.

3.3.4 IMAGE DEGRADATION DUE TO MOTION.

In addition to keeping the imaging system pointing in the correct direction, it is vital that the ADCS also maintains good stability during image capture. Out-of-focus pictures due to camera-shake is a common problem with film photography, and similar effects can degrade the imagery from Earth observation satellites. To ensure high quality data, the dynamics between the scene and the imaging systems must be limited.

Excessive motion during capture gives rise to two forms of defects: registration errors effecting the geometry of the entire image, and blurring which effects the individual pixels. The different imaging architectures suffer these problems to differing extents.

3.3.4.1 Geometric registration errors.

Registration is the term given to the geometric alignment of pixels, either between two digital images (e.g. two sources of satellite imagery, or map and image data, etc.) or within a single image. Inter-image registration misalignments are caused by factors like lens distortions, a curved Earth, different look-angles, pixel resolution, North-South orientation, and so on. These are not necessarily defects in the imaging systems, but are often the result of different capture conditions. These sources of mis-registration must be catered for during image post processing, either by a-priori corrections based on knowledge of the various systems or by subsequent numerical relaxation techniques.

Registration errors can occur within a single image if the scene / sensor geometry is altered during image capture, resulting in distance and angle distortions between scene features. Unlike targeting error which can often be tolerated, poor registration vastly reduces the value of remotely sensed imagery, particularly for applications like cartography which depend on accurate data. The ADCS must ensure that the drifts in the satellite's attitude remain suitably small during image capture to prevent registration from becoming a problem.

3.3.4.1.1 Susceptibility of imager architectures to registration errors.

Two features of an imaging system make it susceptible to registration errors: an absence of physical structure between the pixels and long collection times.

In an image from a CCD area-array sensor, there is a unique photodetector corresponding to each pixel. These photodetectors are bonded together and cannot change position relative to each other. If the sensor moves during capture, all the detectors will move together ensuring registration (even though the image may be badly blurred). Because of this, CCD area sensors simply cannot have registration errors. (N.B. Although it is theoretically possible for thermal flexing of a CCD to change the photodetectors lattice, it would probably destroy the sensor before having a measurable effect on the pixel structure).

Similarly, within a single scan line of a pushbroom imager, the pixels have a guaranteed registration, assured by the CCD's structure. However, should the satellite drift at all, there will be slight misalignments between the scan lines. Although successive lines may be acceptably aligned, errors accumulate and there may be significant top-to-bottom slip. While the main sources of registration inaccuracies are due to changes in the satellite's attitude, there may also be other contributing factors, such as changes in velocity and height due to orbital perturbation or eccentricity. Figures 3.3.4.1.1a, b, c and d illustrate the effects of drifts in pitch, roll, yaw and altitude during capture on the image registration obtained from a pushbroom scanner.

Direction of travel.

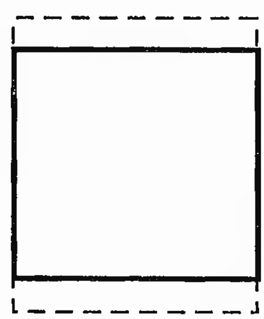

Figure 3.3.4.1.1a Effect of pitch drift on scanned image.

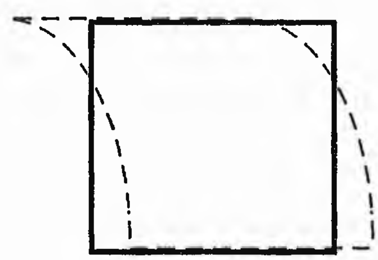

Figure 3.3.4.1.1b Effect of roll drift on scanned image.

Direction of travel.

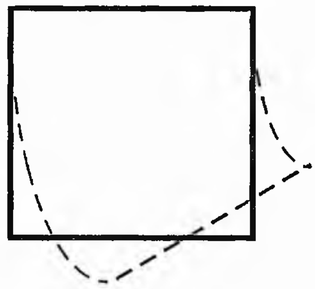

Figure 3.3.4.1.1c Effect of yaw drift on scanned image.

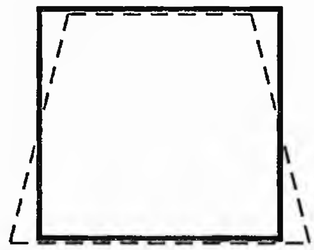

Figure 3.3.4.1.1d Effect of altitude drift on scanned image.

Any drifting in the orientation of the pitch axis will combine with the satellite's orbital velocity, causing the imager to scan the scene either too rapidly or too slowly. The effect of drift in the roll axis results in cross-track slipping; in fact, almost all scanning imagers suffer for a similar type of line-slip because of the Earth's rotation below the satellite, although this will be at a constant rate. The yaw drift causes the scan lines to have differing angles with respect to the velocity vector, causing significant errors in angular geometry. Finally, changes in altitude results in varying scaling (resolution). In practice, a real system would suffer a combination of all of these disturbances.

Thus, because there is no physical structure between the pixels in different scan lines, a pushbroom scanning imager will suffer registration errors if the satellite's attitude is not highly stable. The situation is even worse for a whiskbroom scanner because any drifts will also cause pixel misalignments within a single scan line. Furthermore, any changes in the scanner's mirror velocity will have similar results.

Obviously, systems that require long periods to scan images have a greater susceptibility to attitude-related registration errors. For a given drift rate and image resolution, allowing a longer capture period merely increases the total misalignment suffered.

3.3.4.1.2 Attitude requirements to prevent registration errors.

If a remote sensing satellite carries scanning imagers, the ADCS must ensure that the imagery collected has good registration. Ideally, drift will be kept sufficiently small (i.e. a fraction of a pixel) to ensure alignment across a whole image. There are two way of accomplishing this, and the approach used tends to depend on the mission characteristics.

Most weather satellites produce continuous imagery from pole to pole, or even around the Globe if equipped with infra-red sensors. For these missions, the total pointing error is never allowed to be greater than one pixel from perfect attitude, ensuring that registration does not become an issue. Fortunately, the imaging systems on these missions are of low resolution and effective ADCS is feasible, although large and complex. For example, the angle subtended by a pixel (the instantaneous field of view - IFOV) of the NOAA AVHRR instrument is 0.1°, about the same as the ADCS specification of most remote sensing spacecraft.

On the contrary, providing continuous 'perfect' alignment of this sort for a high resolution mission is not practicable. Despite their large size and budgets, it is not feasible to provide ADCS stable to within the very small IFOV of the SPOT HRV or the LANDSAT TM instruments (circa 10^{-3} °). A certain amount of registration error must therefore be tolerated.[2]

Since perfect attitude is not realistic for high resolution remote sensing missions, acceptable limits for registration error must be established. Although the imager scans a continuous swath, the data tends to be cut into squares, distributed as individual scenes. Therefore, the objective should be to minimise misalignment within each scene by ensuring that the satellite's attitude drift rates remain sufficiently small. In general, maintaining a low drift rate represents a less stringent specification for the ADCS than guaranteeing absolute pointing accuracy.

To be free of registration errors, the satellite's attitude would drift by no more than a pixel whilst capturing a given scene. The maximum allowable drift rate is given by the following expression:

drift rate = IFOV / scan period

= IFOV x [sub-sat velocity / (number of lines in scene x pixel resolution)]

Note that for images with the same number of pixels, the value of drift will be virtually constant, regardless of the resolution. This is because the IFOV and the time to scan the scene vary proportionately (at least within the same orbit). For example, the scene size of the LANDSAT TM and SPOT HRV instruments are both about 6000 scan lines. Even though their pixel resolution and coverage areas are quite different, the attitude of these

---

[2] Attitude stabilisation of this precision is technically possible; the Hubble Space Telescope, and presumably the US KH-11 reconnaissance satellites, maintain pointing to within a few arc seconds (circa 10^{-4} °) for hours on end. However, the mass (> 10 tons) and cost ($2000M for the satellite, plus over $100 million in annual running costs) of these missions is completely outside the realms of Earth observation programmes, let alone low-cost microsatellites

two satellites must drift at a rate of less than 8×10^{-5} ° / s in all axes to ensure each scene is free of registration errors.

Maintaining attitude drift to within these limits is a difficult task, and is not always met. This is the case for the SPOT satellite where, despite a very sophisticated ADCS, about ten pixels top-to-bottom misalignment is present in the imagery. These errors are typically corrected during image processing. Conversely, the ADCS of the LANDSAT-4 spacecraft fulfils the drift specifications.

Clearly, the attitude pointing and drift specifications necessary to ensure registration of images from scanning systems are very severe, and are unfortunately far beyond the capabilities of existing microsatellites. From section 3.3.2.2, typical drift rates in pitch and roll are of the order of 0.01° / s, and the yaw spin is about 0.5° / s. Even if the yaw rate was similar to that of pitch and roll (which is unlikely because yaw motion is not stiffened by the presence of the gravity gradient boom), a pushbroom scanner mounted on a microsatellite would suffer registration errors well in excess of 200 pixels per scene.

Because of their inability to provide exceedingly high stability, very small spacecraft cannot support remote sensing instruments using whiskbroom and pushbroom architectures. Only electronic cameras based on CCD area sensors, and therefore immune to registration effects, can produce quality imagery despite the drift rates and yaw-angle errors. [3]

Regardless of all other factors, it is the intrinsic immunity to registration errors, ensured by their physical geometry, that make CCD area sensors the only currently viable technology for use on satellites with limited ADCS capabilities.

3.3.4.2 Pixel blur.

In a CCD, an array of photodetectors is used to sense the scene illumination, thereby recording an image. Theoretically, a sensing element will only capture photons corresponding to its associated patch of the scene. In static situations, the principal sources of error in recording the scene will be due to factors such as optical dispersion, distortion

---

[3] Other forms of area sensors, including vacuum tubes and solid-state sensors (CID, CMD - charge injection / modulation devices - see section 5.1.2.4) can be subject to small amounts of mis-registration. This is because the pixels are not captured simultaneously, but read sequentially, allowing the scene - sensor geometry to change within a single image. Nevertheless, these devices are much less susceptible to registration errors than scanning instruments, because their read-out times are much shorter (tens of milliseconds versus tens of seconds).

and aberration, light leakage or cross-talk within the imager electronics, or in the case of astronomy, a turbulent atmosphere.

Conversely, if the scene and sensor are moving with respect to each other, the photodetectors will record photons from several scene patches and the resultant image will be blurred. (The term 'smear' is sometimes used for this phenomenon; however in the context of this document, smear refers to a similar effect which can occur within the CCD due to its architecture - see chapter 5.1.2.2). 'Blurring' limits the imager's ability to record fine details in the scene, reducing the system's resolution and contrast (or sharpness, in photographic terms).

Whereas registration errors can be introduced by the length of time to collect the entire image, blur is dependent on the time taken to capture the individual pixels. For constant drift rates, an imager which records each pixel quickly will be subject to less blur than a system which records slowly.

3.3.4.2.1 The effect of motion blur on image sharpness.

The effect of blur is a convolution of neighbouring pixels in the direction of travel. A one dimensional example of this convolution is shown in figure 3.3.4.2.1. In the three cases, the vertical axis shows the contribution of each scene point to the total pixel brightness (assuming even illumination). The horizontal axis shows a one dimensional cross-section of a pixel. In figure 3.3.4.2.1a, the scene is static: all points within the scene patch contribute photons equally to the pixel, and no photons are captured from other scene patches.

In figure 3.3.4.2.1b, the pixel has been moving along the x axis (with respect to the scene) whilst collecting photons. As it travels, points to the left of the scene patch move outside of the pixel's field of view and cease to contribute to the overall brightness. At the same time, new points from neighbouring scene patches come into view, and start contributing. Although the total area under the curve (i.e. the number of photons collected) remains the same in both instances, the case shown in figure 3.3.4.2.1b suffers from motion blur. Thus, if a pixel contains photons collected from an area greater than its nominal ground footprint, it will be blurred.

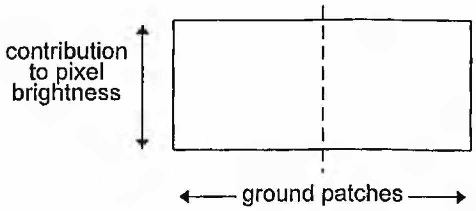

Figure 3.3.4.2.1a
CCD pixels.

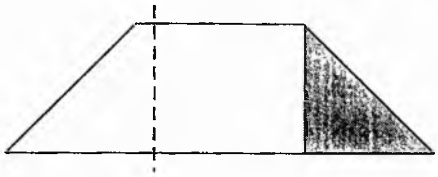

Figure 3.3.4.2.1b
⇒ Direction of travel.

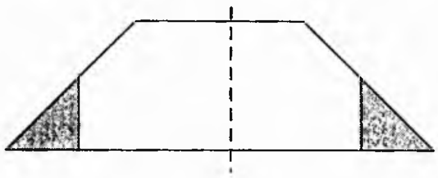

Figure 3.3.4.2.1c
⇒ Direction of travel.

Figure 3.3.4.2.1 Convolutional blurring due to image motion.

The amount of blur suffered by a pixel is determined by the percentage of the pixel's total brightness resulting from scene points outside the nominal scene patch (i.e. the ratio of 'error' photons to 'valid' photons). In this example, the pixel has been moving at a constant rate, and is displaced by a fraction of the pixel dimension. By summing the areas under the curve, the contributions to the pixel's brightness are therefore:

valid contribution = (1 - displacement) + (displacement / 2)

= 1 - (displacement / 2)

error contribution = (displacement / 2)

(N.B. the displacement must be normalised to the pixel dimensions)

Thus, there exists a simple relationship for error contributions of half the displacement. This relationship holds until the displacement is greater than one pixel (i.e. a displacement of greater than unity). Images suffering greater blur will be excessively degraded, and these cases are therefore not considered.

For most remotely sensed imagery, this analysis is overly pessimistic. It assumes that the pixel centre (the vertical dashed line in figure 3.3.4.2.1a and b) is accurately positioned (registered) against the scene. However, this will not be the case for virtually all sensing systems. Due to attitude pointing misalignments, it is not possible to determine in advance which pixel will image a given scene feature. The images preserve the geometry between objects in the image, but their exact locations on the Earth's surface cannot be determined a priori.

The expression for blur can be re-evaluated to take advantage of this fact. The displacement shown in figure 3.3.4.2.1b and c are the same in both cases, but the centre of the pixel has been redefined in figure 3.3.4.2.1c. Although the pixel dimensions and the number of photons collected are the same, the effect of the blurring is reduced. The contribution of blur-induced 'error' photons is a quarter of the displacement. Thus, if a pixel moves by 0.4 of its size during image capture, 10 % of its signal will be blur coming from outside the nominal pixel footprint.

Therefore, in figure 3.3.4.2.1b, the nominal pixel footprint is defined at the point when integration starts, and blur comes only from ground patches encountered subsequently. In figure 3.3.4.2.1c, the nominal footprint is defined to be half-way along the pixel's displacement path, and photons contributing to blurring are received from ground patches both fore and aft. However, in so doing, the pixel's total blur has been halved.

3.3.4.2.2 Establishing acceptable limits of blur.

When defining an imaging system, care must be taken to establish an error budget which accommodates all potential sources of degradation that can reduce image quality. Fortunately, with due attention to the design of the electronics and optics, it is fairly easy to reduce most of the imager's intrinsic impairments such that they become insignificant. Thus, for satellite remote sensing, motion blur is by far the greatest source of image error.

Establishing a design limit for the maximum tolerable motion blur within an image is rather arbitrary, but 10 % is a conventionally accepted value for remotely sensed imagery [Arai] [Kumar] [Goel et al]. The cumulative effect of all forms of motion blur must therefore not exceed 10 % of each pixel's brightness. Of course, an image suffering a smaller percentage of degradations will be a more faithful reproduction of the scene, and vice versa. This value of 10 % is therefore a target rather than a hard limit.

A remote sensing satellite experiences numerous perturbing effects resulting in various translations and rotations within the image plane. To ensure that the overall blur budget is preserved, it is necessary to balance the blur resulting from the satellite's orbital motion and other transient torques (i.e. its attitude dynamics). It is necessary to compare these sources of blur to determine which are the most significant effects. This is done by relating the change in sensor orientation (an angle) during image capture caused by a disturbing torque with the angular resolution of each pixel (the instantaneous field of view - IFOV). Not only does this characterise the imaging system intrinsically (i.e. independent of its orbital viewing geometry), it is directly compatible with the terms of reference used to describe a satellite's attitude control system. Thus, it is possible to generalise and say that imaging systems with long focal length optics (with correspondingly small IFOVs) are more susceptible to blur than similar systems with short focal lengths.

However, for a given mission scenario, it is generally more convenient to project these angles onto the ground (measuring in metres) and compare them with the pixel resolution. Of course, if the satellite's orbit changes then the blur budget must be re-calculated. For the examples provided in the next few sections, the errors will be converted to metres for comparison. The effects of these are considered for low, medium and high resolution imaging systems (2 km, 200 m and 20 m spatial resolution respectively) from an altitude of 800 km. Similarly, time will be counted in milliseconds rather than seconds, because it is closer to the integration times used in electronic image sensors

3.3.4.2.3 Blur due to orbital velocity.

One of the principal sources of motion between a satellite remote sensing instrument and the Earth below is the spacecraft's orbital velocity. In an 800 km orbit, the satellite moves at 7.2 km / s. Of more importance to the imaging payload, the relative velocity between the Earth's surface and the satellite (i.e. the velocity of the sub-satellite point) is 6.6 km / s, or put another way 6.6 m / ms.

Assuming for the moment that orbital motion is the only source of blur, the satellite (and imaging system) can be allowed to travel no more than 40% of the pixel resolution whilst collecting photons. Table 3.3.4.2.2 gives the maximum allowable displacements and integration times for different resolution imaging systems.

Resolution		Max. displacement	Max. integration time
Low	2000 m	800 m	120 ms
Medium	200 m	80 m	12 ms
High	20 m	8 m	1.2 ms

Table 3.3.4.2.2 Maximum integration time allowable to prevent blurring versus ground resolution.

Thus, high resolution systems are more susceptible to the effects of orbital velocity, and care must be taken to cope with this inevitable and constant source of blur. In practice, the only way to ensure that the satellite's orbital velocity does not cause excessive blur is to keep the integration adequately short. [4] Fortunately, all of the integration times listed in table 3.3.4.2.2 are still sufficiently long to be within the capabilities of most modern CCD sensors. Indeed, scanning imagers make use of the satellite's velocity to provide the second dimension of the image. Nevertheless, the pixels of a pushbroom scanner can still be subject to blur along the velocity vector. Area sensing cameras typically require longer integration times (tens of ms) and are therefore more susceptible to motion blur. Conversely, whiskbroom imagers do not blur in either axis because the pixels are sampled rather than integrated, but the scan sweeps are at an angle to the orbit plane due to this velocity.

However, when the integration time must be kept very short, around 1 ms or less, there are relatively few photons striking the sensor and the optics will need to be brighter (and correspondingly more massive) to expose the sensor adequately (refer to section 5.4.1.1.2 for more on this matter). Furthermore, some area sensors can start adding significant degradations when operating under short integration times, particularly frame transfer CCDs which may have appreciable transfer smear (refer to section 5.1.2.2). Thus, the need to have short integration times to combat blur has repercussions on the rest of the system, which must be addressed in the overall system design.

Another inescapable factor in the blurring of imagery, which is often over-looked, is the Earth's rotation. This is equal to 460 m / s at the equator, 325 m / s at 45° of latitude, and 232 m / s at 60°. Although small compared to a satellite's orbital velocity, this source of blur is nonetheless of significance. For polar-orbiting satellites, this movement will be almost perpendicular to the satellite's velocity vector.

Of course, the velocities due to orbital mechanics are only one of the sources of blur to be considered and must balanced against other potential sources.

---

[4] One can envisage complex gimballed platforms to compensate for the orbital velocity, keeping the image steady for short durations, but this is far beyond the capabilities current microsatellites. Certainly no civilian remote sensing spacecraft possess these features, although they may be present on US spy satellites.

3.3.4.2.4 Blur due to drifting attitude.

The various drifts of the satellite's attitude will combine with the orbital motion to increase the blur experienced by the sensor. As with image registration, it is not the value of the pitch, roll and yaw angles which is of importance when determining the blur, but the drift experienced in these three axes.

The effect of drift in the pitch and roll axes are very similar, resulting in a re-orientation of the imager's optical axis. The blur can be assessed by comparing the pitch and roll drift rates and the imager's IFOV, as follows:

Change in pitch angle :

$$\Delta\Theta_{pitch} = \text{rate of change in pitch} \times \text{integration time;}$$

Change in roll angle :

$$\Delta\Theta_{roll} = \text{rate of change in roll} \times \text{integration time.}$$

To appreciate the importance of the pitch and roll drifts to the blur budget, they must be compared to the motion due to orbital velocity. To do so requires projecting the resulting drift angles onto the Earth's surface and obtaining a value in metres. This is a matter of simple trigonometry:

Image displacement (in metres) due to pitch drift :

$$D_{pitch} = \text{satellite altitude} \times \sin(\Delta\Theta_{pitch});$$

Image displacement (in metres) due to roll drift :

$$D_{roll} = \text{satellite altitude} \times \sin(\Delta\Theta_{roll}).$$

By definition, drifts in the satellite's pitch are parallel to the ground track, and directly add to or subtract from the orbital velocity vector. If the exact pitch vector is not known at the time of image capture, one must assume the worst case where the pitch drift and orbital velocity add together. Also by definition, the roll vector is perpendicular to the pitch and velocity vectors, and the total displacement is the root-mean-square of these vectors.

The drifts in pitch and roll are perpendicular to the scene, resulting in a translation of the image across the sensor. Their detrimental effect on image quality is relative to the sensor's IFOV. Conversely, drifts in yaw result in a rotation within the image plane, about the imaging system's optical axis which passes through the centre of the sensor. For CCD arrays, which have many detecting elements, the displacement will be greatest at the edge of the image where the pixels are subjected to the greatest angular velocity. Therefore, the blur resulting from the spacecraft's yaw drift is not dependent on the imager's resolution, but on its dimensions. (This effect is very visible on the PoSAT-1 star sensor which uses a long integration time of 150 ms to collect photons from faint stars. Stars in the centre of the image are blurred points, but those at the edge of the image are recorded as short arcs). The maximum displacement experienced by any pixel within a CCD array is described by the following expression:

Change in yaw angle :

$$\Delta\Theta_{yaw} = \text{rate of change in yaw} \times \text{integration time.}$$

Image displacement (in metres) due to yaw drift :

$$D_{yaw} = 0.5\,(\text{array size} \,/\, \text{pixel size}) \times \sin(\Delta\Theta_{yaw}) \times \text{ground resolution}$$

The displacement caused by the yaw drift has dimensions of one pixel, i.e. is effectively dimensionless. To allow for comparison with the other sources of blur, it must be scaled by the ground resolution of a pixel (in metres). The factor of 0.5 in the expression for D_{yaw} reflects that the rotation axis is in the centre of the CCD array and not at one end. [5]

Note that the pixels in the image will not all blur in the same direction. In a pushbroom sensor, half the pixels will find their yaw-induced displacement is in the same direction as the velocity vector, and the other half will oppose the velocity vector. The situation is more complex in an area sensor, where each pixel will be subject to a different displacement. For the purposes of calculating the blur budget, the worst blur will be experienced by those pixel which have a yaw displacement in the same direction as the velocity vector.

3.3.4.2.5 Typical attitude drift rates.

Fortunately, the perturbing torques acting on a remote sensing satellite's attitude stability are small. Nevertheless, they will accumulate, eventually causing significant disturbance if not damped. There are many sources of attitude disturbance, such as gravitational variations (Earth, Sun and Moon), solar pressure, atmospheric drag or harmonic oscillations linked with the orbit period. In many instances, modelling and calibration errors of the satellite's ADCS will produce the most significant of these effects.

---

[5] A spacecraft's yaw axis passes through its centre of mass. Although the imaging system's optical axis may not be exactly the same as the yaw axis, there will be negligible error in assuming they are the same, provided the two are parallel, i.e. a nadir-pointing imager. This assumption will only need to be revised if the ground resolution approaches the distance between the optical axis and the true yaw axis, i.e. for ultra-high resolution systems imaging features of a metre or less.

The actual disturbances experienced by a satellite will depend on the implementation of its ADCS. Exact figures of the drift rates for different classes of satellite and ADCS are difficult to obtain, but most will be well below 0.01° per second, assuming that attitude control is exercised. As discussed in section 3.3.2.3, this is the case for SSTL microsatellites.

For all satellites in low-Earth orbit which have even moderate attitude stability, the blur caused by the orbital velocity will be far greater than that from the pitch and roll drifts. To equal the sensor-to-scene displacement caused by orbital motion, the pitch or roll would need to be changing at 0.5° per second. This is equivalent to the satellite tumbling once every 13 minutes, effectively out of control.

Of course, the drift rates will be significantly higher if the stability is deliberately disturbed. This is often in the form of a yaw-spin, either used to relieve thermal stresses (circa 0.5°/s) or for spin stabilisation (50 to 1000 °/s). Under these conditions the yaw component of drift will have a considerable impact of the blur budget

3.3.4.3 Attitude jitter.

The sources of blur considered this far (orbital velocity and attitude drift) tend to be fairly constant. Although they can, and do, vary with time, they can certainly be considered invariant over the duration of typical integration times (milliseconds). In addition to these steady-state effects, the satellite may suffer higher frequency attitude perturbations, known as attitude jitter. Although the fluctuations caused by jitter may have a tiny impact on the spacecraft's long term stability, the instantaneous rates of change can be quite high, having considerable repercussions on the registration and blur quality of the imaging system.

Attitude jitter is invariably caused by torques generated by the satellite itself. The principal sources of these forces are attitude control actuators and active mechanical systems. While attitude control actuators are clearly crucial in maintaining the pointing stability of a remote sensing platform, care must be taken to ensure that their operation does not cause transient effects that might degrade imagery. [Goel et al] and [Arai] discuss some of the causes and consequences of attitude jitter on the quality of remote sensing data.

To ascertain whether firing a specific attitude actuator will result in a significant attitude disturbance, it is necessary to compare the torque generated with the satellite's inertia, as defined by the following equation:

Inertia $\times$ angular acceleration = Torque

$$I \times \omega.\text{dot} = N$$

The spacecraft's inertia in a given axis depends on its mass distribution and surface area in that axis. An SSTL microsatellite has an inertia of about 1 $kg.m^2$ about the yaw axis and 100 $kg.m^2$ about the pitch and roll axes (with the gravity-gradient boom deployed). Table 3.3.4.3 shows the torques of several typical attitude actuators and the relative angular acceleration they would cause to a microsatellite. [6]

	Torque	ω.dot	
		Pitch & Roll	Yaw
natural disturbances	10^{-7}	10^{-9}	10^{-7}
SSTL magnetorquer	10^{-4}	10^{-6}	10^{-4}
lightweight reaction wheel	5×10^{-3}	5×10^{-5}	5×10^{-3}
cold - gas thruster	5×10^{-2}	5×10^{-4}	5×10^{-2}

Table 3.3.4.3 Torque generated by various microsatellite attitude control actuators.

Looking at table 3.3.4.3, the magnetic torquing used by many satellites to fine trim their attitude will be unable to generate transients that would disturb an imaging payload. Similarly, changes in the rotation speed of momentum / reaction wheels will result in torques of negligible consequence. However, on spacecraft with thrusters or rocket motors, it is possible that the instantaneous disturbances caused by firings will be of significance to imaging. Fortunately, such firings are relatively uncommon operations, around which the imaging activities can be scheduled (or vice versa). Moreover, it is probable that the imaging systems will need to be made safe during major firings to protect them from the sudden acceleration or from potentially damaging combustion by-products, so such events are unlikely to upset image capture.

Although, the acceleration caused by a given attitude actuator can be determined, the disturbances resulting from its operation will appear random to the imaging system. Therefore, a term for the maximum possible transient attitude disturbance must be included in the blur budget. This evaluation of the satellite's attitude jitter must also include estimates for all other unpredictable attitude perturbations, such as noise from any active

6 The effect of a given class of actuator (magnetic torquer, momentum / reaction wheel, thruster, etc.) on the stability of a remote sensing satellite will tend to be similar, because the ADCS systems will be scaled according to the size of the platform.

mechanics (motor torques, wheel bearing rumble, latches, solenoids, etc.) and thermal flexing of the spacecraft's structure, which caused significant disturbances on the Hubble Space Telescope as the solar arrays entered and left eclipse. [Neeck et al] provide a very detailed analysis of these effects for a high resolution, stereoscopic, pushbroom imaging instrument, which can be used as a template for calculating the effect of attitude jitter on the imagery collected.

3.3.4.4 The blur budget.

The contribution of all the various sources of blur just discussed must be compared and assessed when developing a remote sensing payload. Thus the equation for the total blur experienced by an imaging payload is :

$$D_{total} = \sqrt{[(D_{velocity} + D_{pitch} + D_{yaw})^2 \; x \; (D_{roll} + D_{earth\,spin})^2]} + D_{jitter}$$

Without going into the details of various attitude control systems, a number of general observations can be made.

- Image sensors which use short integration times suffer less blur than similar instruments with long integration times.
- Because of their small IFOV, high resolution systems are more susceptible to blur than low resolution imagers.
- On a conventional, highly-stabilised remote sensing spacecraft, the orbital velocity will be by far the most significant source of blur.
- On typical microsatellites, the attitude stability will not be as great and the contributions to the total blur due to pitch, roll and yaw will be more significant.
- In high resolution imaging systems, the orbital velocity will be the greatest source of blur. The pitch and roll contributions will have a greater effect than the yaw.
- In low resolution imaging systems, yaw drift will be a much more prominent source of blur. On a microsatellite, it is possible for the yaw and the orbital velocity to be of comparable significance.

The designer of the imaging payload must ensure that acceptable imagery will be produced despite the numerous possible sources of blur. If there appear to be problems with the amount of blur suffered, there are basically two courses of action: reduce the integration times of the imager, or remedy some of the satellite's ADCS shortcomings. In virtually all cases, it is far simpler for the payload designer to implement the former than to insist on the latter.

3.3.4.4.1 Case study - the PoSAT-1 Wide Angle Camera.

The PoSAT-1 Wide Angle Camera has the following characteristics:

- sub-satellite velocity of 6618 m / s (800 km orbit)
- 4.8 mm focal length lens,
- CCD array of 568 x 560 pixels
- pixel dimensions : 15 μm x 11.25 μm pixel
- IFOV of 0.18° x 0.13°
- pixel resolution of 2500 m x 1900 m
- a nominal integration time of 25 ms

Because PoSAT-1 has a yaw-spin, it is not possible to know a priori how the sensor will be aligned with respect to the satellite's velocity vector. Therefore, the blur budget must be calculated for the worst case, which occurs when the smallest pixel dimension aligns with the velocity vector. Therefore, the displacement caused by orbital velocity during image capture is:

$D_{velocity}$ = 165 metres = 0.09 pixel

$D_{earth\ spin}$ = 11 metres = 0.006 pixel

Based on the ADCS specifications given for a typical SSTL microsatellite in section 3.3.2.3 ($\delta\Theta_{pitch}$ = 0.01°/s, $\delta\Theta_{roll}$ =0.01°/s, $\delta\Theta_{yaw}$ =0.5°/s), the displacements caused by attitude drifts are:

D_{pitch} = 3.5 metres = 0.002 pixel ($\Delta\Theta_{pitch} = 2.5\text{x}10^{-4}$ °)

D_{roll} = 3.5 metres = 0.002 pixel ($\Delta\Theta_{roll} = 2.5\text{x}10^{-4}$ °)

D_{yaw} = 0.06 pixel = 118 metres ($\Delta\Theta_{yaw} = 0.0125°$)

Ignoring the possible effects of attitude jitter, the total displacement is:

D_{total} = 287 metres = 0.15 pixel

The corresponding blur is under 4 % which is acceptable. The orbital velocity and the yaw-spin contribute significantly to the blur budget, with the other factors having negligible effect.

3.3.4.4.2 Case study - the FASat-Alfa Narrow Angle Camera.

The FASat-Alfa Narrow Angle Camera had the following characteristics:

- sub-satellite velocity of 6850 m / s (650 km orbit)
- 75 mm focal length lens,
- CCD array of 568 x 560 pixels
- pixel dimensions : 15 μm x 11.25 μm pixel
- IFOV of 0.011° x 0.086°
- pixel resolution of 130 m x 98 m
- nominal integration time of 20 ms

Unlike previous SSTL microsatellites, FASat-Alfa was designed not to spin, and yaw-control would have been exercised to ensure that the CCD's larger dimension remained aligned with the velocity vector. Therefore, the displacement caused by orbital velocity during image capture would have been:

$D_{velocity}$ = 137 metres = 1.05 pixel

Without proceeding with the rest of the analysis, it is clear that the 20 ms integration time initially selected for this camera would have resulted in badly smeared imagery. The contribution from the orbital velocity alone causes a blur of over 25 % (i.e. over 25 % of the photons captured by a given pixel will be from different ground patches). A revised integration time of 4 ms was selected. Therefore:

$D_{velocity}$ = 27 metres = 0.21 pixel

$D_{earth\ spin}$ = 2 metres = 0.018 pixel

The pitch and roll drift rates were likely to have been the same as previous SSTL spacecraft. However, because FASat-Alfa would have had no spin, the yaw rate would have been significantly reduced; a very pessimistic estimate of $\delta\Theta_{yaw} = 0.1° / s$ is used for the purpose of this calculation. Therefore, the displacements caused by attitude drifts would have been:

D_{pitch}	= 0.5 metres	= 0.004 pixel	($\Delta\Theta_{pitch} = 4x10^{-5}$ °)
D_{roll}	= 0.5 metres	= 0.006 pixel	($\Delta\Theta_{roll} = 4x10^{-5}$ °)
D_{yaw}	= 0.002 pixel	= 0.2 metres	($\Delta\Theta_{yaw} = 4x10^{-4}$ °)

In this instance the blur budget is dominated by the orbital velocity, and to a lesser extent the Earth's rotation. The contributions from to the satellite's attitude drift are insignificant. It is worth noting that, as expected, the yaw contribution is less than that from pitch and roll, despite the considerably higher drift rate.

Ignoring the possible effects of attitude jitter, the total displacement would have been:

D_{total} = 28 metres = 0.22 pixel

The corresponding blur is about 7 % which is acceptable. A nominal integration time of 4 ms was chosen because it left some margin in the blur budget. Thus, there was still some latitude in selecting the actual integration time, so that scenes of differing brightness could have been accommodated.

3.3.5 CONCLUSIONS

3.3.5.1 Summary.

Unlike conventional remote sensing satellites which provide highly stable platforms for the imaging instruments, the attitude determination and control systems of microsatellites cannot completely remove all of the spacecraft's drift. Existing microsatellites use gravity-gradient booms and magnetic torquing to achieve pointing control to within 5°. This level of attitude control is acceptable for low and medium resolution imaging missions, although not ideal. The coarse pointing accuracy of microsatellites makes it difficult to target images of specific areas on the ground with certainty. However, it is not the off-pointing but the residual drifts of the platform that have the greatest impact on the design of a Earth observation payloads.

Without the guarantee of a highly stable platform, conventional scanning imagers cannot provide imagery free of registration error. For this reason, only imaging systems based on area-sensors can be operated successfully on the current generation of microsatellites. Of the various imaging technologies, CCD sensors (discussed in chapter 5) provide the most attractive solution to implementing electronic cameras for Earth observation from microsatellites.

Area-array CCDs use relatively long integration times (tens of milliseconds) to collect their imagery, making them more susceptible to blur than scanning instruments. A blur budget must be calculated for each instrument to ensure that the resultant data will not be degraded. Fortunately, the attitude control systems of microsatellites use low-torque actuators such as gravity-gradient booms and magnetic torquers, and the drift rates experienced are quite small, keeping blur within acceptable bounds. However, the yaw spin imparted to many small spacecraft presents a significant inconvenience in designing imaging missions. This spin results in blurring at the image edges if short integration times are not used. Future microsatellites designed to carry remote sensing instruments should implement fixed yaw control, thereby enhancing the performance of their payloads.

3.3.5.2 Future developments in microsatellite ADCS.

It is widely accepted that the ADCS available on microsatellites severely limits the range and scope of imaging and scientific payloads that can be carried. As a response, research is on-going to improve the accuracy of the ADCS both by implementing more sophisticated control algorithms and introducing higher resolution attitude sensors and control actuators.

In direct response to the needs of the imaging experiments, the FASat-Alfa microsatellite was designed to operate without a yaw spin, with corresponding modifications to the thermal management, deployment of attitude sensors and the power-point tracking of the power modules (to accommodate the widely varying temperatures of the solar panels).

At the time of writing, SSTL engineers have implemented a new algorithm for the attitude control of the UoSAT-5 microsatellite. Preliminary results indicate that the attitude uncertainty is constrained to within $\pm 1°$. (There remains a 1° bias in the roll axis, due to cross-coupling of the yaw spin. Reducing this spin on UoSAT-5 from 0.1 rpm to 0.05 rpm has immediately halved the 'roll bias'). Simulations have indicated that this algorithm can be extended to provide control of the yaw angle, achieving three-axis stabilisation to within 1° in all axes, principally limited by the accuracy of the satellite's magnetometers. In-orbit evaluation of this capability will take place in January 1996, and if successful, will be used on PoSAT-1 and future imaging microsatellites to enhance the Earth observation payloads. The initial results have been promising, and better than anticipated (i.e. 2° in pitch and roll and 5° in yaw [Hodgart 1989, p7-74] [Hashida]). While these are significant improvements in the ADCS of SSTL microsatellites, the levels of stability remain inadequate to support scanning imagers.

To provide greater stability for future imaging microsatellites, it will be necessary to evolve more sophisticated ADCS. Initially it will be necessary to derive more accurate knowledge of the spacecraft's attitude than is currently provided by magnetometers (as outlined in section 3.3.2.3). The primary emphasis is in developing optical (Sun, horizon, star) sensors to provide additional high accuracy measurements of the satellite's pointing. Star sensors appear to be the most promising option because of the very high resolution of both pointing and drift rate measurements, even though significant computational power is required to analyse the data. Experimental versions of these sensors have been carried on PoSAT-1 and other microsatellites with some success but this data has yet to be integrated to the on-board attitude determination models. Other more exotic attitude sensors such as GPS interferometers and ring-laser gyroscopes are also receiving attention.

To provide sub-degree pointing accuracy, it is almost inevitable that microsatellites will need to emulate larger spacecraft and use momentum and / or reaction wheels. Unlike magnetorquers which can only be fired when the geomagnetic field is suitably aligned, these wheels can be operated continuously (or as required), providing greater opportunities for controlling the satellite's attitude. As a consequence, a number of recent microsatellite missions (FASat-Alfa, TUBsat, Sunsat) have carried (will carry) small experimental wheels.

As with most aspects of satellite ADCS, mastering the control algorithms may prove more challenging than implementing the hardware itself. Nevertheless, wheel-based systems have been used routinely on larger spacecraft for over two decades, and these capabilities will doubtlessly soon (i.e. by the end of the decade) be available on 50 kg microsatellites. Given the sophisticated on-board processing capabilities of most microsatellites, there is no particular reason why this should not happen. Indeed, it may be feasible to fly pushbroom imagers on microsatellites. Assuming that the (3000 second) periods of oscillation remained the same for all three axes (which is not at all certain), the pitch and roll displacements would need to be 46 μrads/s (0.0025° / s, or 40 m/s when projected onto the ground), and the yaw displacement would be 120 μrads / s (0.007°/s, or 0.06 pixels motion / s for a 1000 element sensor, i.e. 1 pixel in 16 seconds). Under these circumstances high resolution (sub-20 metres) imaging using pushbroom arrays with 4000 pixels could be supported.

While implementing improved ADCS on microsatellites will no doubt enhance the scope and performance of imaging and scientific payloads that can be flown, there are some possible drawbacks. Firstly, the active mechanics of a momentum / reaction wheel's bearings presents reliability, lifetime, mass and cost constraints. Furthermore, the rumble of wheel bearings, particularly as they wear with age, will introduce attitude jitter to otherwise mechanically passive microsatellites. Most importantly, tighter and more aggressive control loops will be necessary to ensure continuous pointing accuracy. This will involve actuators with higher torques and more frequent actuator firings, both of which are likely to degrade the drift rate specifications of the ADCS. This will make the drift rates discussed in the previous paragraph rather more difficult to achieve than might at first be thought.

3.3.5.3 Conclusions.

Perhaps surprisingly, it is the limited attitude stability of a microsatellite that is the most crucial factor in determining the imaging system's architecture. From the conventional view-point, a microsatellite is a useless platform for remote sensing because it cannot provide the pointing accuracy and, most importantly, the very low attitude drift rates demanded by scanning imagers. Therefore, without drastic improvement in the performance of their ADCS, the only viable option for remote sensing with these small spacecraft is to use area-sensing cameras, which are immune to registration errors. This factor is the most crucial factor in shaping the content of this research programme.

Considerable effort is being deployed within the microsatellite community to improve the performance of the ADCS, principally by developing optical sensors and small momentum / reaction wheels. Despite these improvements, it is not clear that the stability of microsatellites will ever be adequate to support scanning systems. A new design review trading off image quality, cost, reliability and feasibility of implementing pushbroom scanners on microsatellites will need to be performed when these ADCS technologies have been mastered.

Even when the ADCS capabilities of microsatellites have improved sufficiently to carry pushbroom scanners, it is not obvious that these imagers will become the automatic choice. The features offered by camera systems (i.e. independence from ADCS, and guaranteed registration) will always be attractive to designers and users of satellite remote sensing systems. As the performance (sensitivity, linearity, number of pixels, spectral range) of area sensors continues to improve, the trade-off between pushbroom and area-array imagers will become increasingly subtle.

3.4 IMPACT OF THE ON-BOARD DATA HANDLING AND COMMUNICATIONS SYSTEMS ON THE PERFORMANCE OF THE IMAGING INSTRUMENT.

The data captured by a remote sensing satellite must be returned to Earth for analysis. However, a satellite in low-Earth orbit will only be in range of its master ground station for a small percentage of the time, limiting the opportunities to download the imagery. Therefore, it is necessary for the communications channels to have enough capacity to retrieve from the satellite, day-by-day, a volume of data compatible with the mission objectives.

Although it does not directly effect the design of the imaging hardware or the quality of the imagery, the performance of the communication links is therefore of paramount importance as it determines the productivity of the satellite. If the downlink limits either the quantity of scenes obtained or the speed in despatching the data, the overall worth of the mission may be compromised. Given that much of the value of remotely sensed imagery is derived from its use as a forecasting tool, it is vital to ensure that the data throughput is compatible with the mission objectives.

Ultimately, there will need to be some compromise between the volume of data desired from an imaging payload and what can actually be delivered. Imaging systems are renowned for the volume of data they produce, and it is inevitable that the communications bandwidths represents a bottleneck. Realistic targets must therefore be set, and the communications channels must be designed to deliver the imagery as effectively as feasible. When assessing the data handling performance of a remote sensing spacecraft, there are two important factors to be considered:

- Throughput. (How many images / scenes can be retrieved daily?)
- Turn-around. (How long does it from capturing an image to its becoming available to users?)

Because of the limited transmitter power and antenna gain on a microsatellite, the disparity between the data rates of the imaging payload and the downlink are particularly marked, and therefore problematic. This section examines the consequences of a microsatellite's narrow downlink capacities on the imaging system.

3.4.1 OBDH / DOWNLINK CONFIGURATION FOR CONVENTIONAL REMOTE SENSING MISSIONS.

By the standards of current terrestrial digital communications networks, all satellites appear unsophisticated in their communications techniques. For large telecommunication satellites the complexity (switching, routing, modulation, etc.) is entirely ground-based. The satellites are conveniently placed 'bent-pipe' repeaters, acting with little or no intelligence (including modern on-board regenerative transponders). This is preferable because of the huge investment in the satellite and the small number of ground stations. Placing sophistication on the ground makes economic sense because it reduces the cost and complexity of the most critical and irreplaceable element: the satellite.

Conventional remote sensing satellites adopt this approach by minimising the intelligence and versatility of the space segment. A remote sensing satellite is by definition a data source, producing large amounts of data which need to be transmitted to the ground. Wide downlink bandwidths are needed to achieve the desired hourly / daily throughput of imagery. In keeping with the simple approach to communications, these satellites operate in a fixed transmission mode, either:

- Real-time broadcast to one or more users (weather satellites), or
- Point-to-point (satellite to ground) data dumps.

Meteorological satellites (NOAA, Meteor, METEOSAT, GOES, GMS, etc.) generally send their image data directly to the downlink. The downlink must be matched to the imager data rate, and (relatively) moderate downlink bandwidths are required. For example, the real-time data rate for NOAA is 665 kbps (N.B. the popular Automatic Picture Transmission is a very low resolution derivative using a 2 kHz analogue signal [Wallach]), and the METEOSAT downlink is 166 or 333 kbps [Pfeiffer & Bonnefoy]. In general, meteorological imaging satellites have no on-board storage capabilities, and a network of ground stations must be available to build a global perspective. If no ground station is in view of the satellite, the current data is lost. This is not an issue for geostationary satellites, which are always in view of at least one ground station.

For an imaging satellite in low-Earth orbit to provide global coverage, on-board storage is necessary. The imagery is stored as it is produced and then played back when in range of a ground station. The storage medium is almost always a tape recorder. Because of the large backlog of data that must be transmitted in a short pass, the downlink rates of these playback bands are much higher than for the real-time broadcasts. The stored NOAA data (the same imagery as on the real-time broadcast, but dumped to a master control station) is transmitted at 2.6 Mbps [Wallach], and the downlink of SPOT is at 50 Mbps.

[Colwell] gives a very good overview of the communications systems employed by the LANDSAT series. The MSS instrument flown on LANDSAT-1,-2 and -3 (before the end of 1980) produced about 15 Mbps of raw data (of which less than 50% was valid data - 3300 pixels x 6 sensors x 4 bands x 13.6 sweeps /s @ 6 bits / pixel = 6.4 Mbps). An individual scene consisted of 2340 scan lines or a total of 54 MBytes (430 Mbits). Each tape recorder could store up to 30 minutes worth of data at 15 Mbps, or a total of 3.4 GBytes (27 Gbits) or 63 scenes. Overall, using a world-wide network of ground stations, an average of 100 scenes were retrieved daily per satellite, equivalent to a total of 5.5 GBytes per satellite per day. Given the higher spatial resolution and increased number of spectral bands of the TM instrument carried from LANDSAT-4 onwards, the data rates are even higher at 85 Mbps. Although the newer LANDSAT spacecraft are equipped with tape recorders, these are no longer used routinely because continuous contact with mission control is assured by the US's network of TDRSS data relay satellites. The dual downlinks for the MSS are in the S-band allowing simultaneous real-time and playback transmissions, and the downlink for the TM is in the X-band with a data rate close to 100 Mbps.

On all of these conventional remote sensing spacecraft, the image data (either direct or via the tape recorder) uses a dedicated link to the ground. Telemetry and any other traffic uses a separate channel; on NOAA the playback and real-time data streams have their dedicated bands. Since the downlinks are not shared between data sources, the format used does not need to be complicated, at least at the satellite end. In most instances, a raw data dump from the imaging system or tape recorder is sufficient. The transmissions will either use a continuous fixed data format for real-time broadcasts, or operate in a simple command-and-response mode. In either case, the imaging and transmitter hardware need not be flexible. If more than one mode of operation is possible (e.g. switching between real-time and playback on SPOT), the on-board communications systems will be configured by the ground or under on-board computer (OBC) control.

To preserve the simplicity of the communications protocols, the downlink link budget is conceived with good margins by endowing the satellite and ground station with high-power transmitters, high gain antennas, and expensive and sophisticated ground-based signal recovery systems. This 'brute force' approach ensures that these links require no, or minimal, data coding for error protection. This is the case for METEOSAT, NOAA, LANDSAT. When there is a burst error or a signal fade, the data is generally lost with no means of recovery. This is a relatively common occurrence on LANDSAT, for example. If the transmission error occurs during play-back, it may be possible to rewind the tape and repeat the entire image, but this probably does not happen due to the logistical difficulties of modifying the satellite's operational schedule and splicing the image streams together.

Thus, high data rates on the downlinks of conventional remote sensing satellites are essential to keep the volume throughput and turn-around of data within the mission specifications. These spacecraft use high power, high gain communications systems to support such wide bandwidths with good link margins and error performance. This unsophisticated, hardware-based approach keeps the on-board communications simple and (relatively) inexpensive. However, this offers little flexibility, and when transmission errors occur the data is generally lost without any scope for recovery. Telemetry and the principal payload data will use separate downlinks. In many cases, each payload will use a dedicated channel, and the communications protocols will be little more than raw data dumps. Otherwise, the data streams from the various payloads and storage devices will be switched onto the common downlink by ground or OBC control. The data formats of these systems will only be marginally more complex. On the whole there are few or no requirements for sophisticated on-board data handling (OBDH).

3.4.2 TYPICAL COMMUNICATIONS CONFIGURATION ON MICROSATELLITES.

In contrast with conventional spacecraft, a microsatellite's downlink and OBDH networks are characterised by narrow bandwidths and software-based communications. In particular, microsatellites cannot sustain the high downlink data rates of the large satellites, principally due to limited transmitter power. Furthermore, small spacecraft will generally only have enough power (and space for antennas) to support one downlink. Correspondingly, it is necessary for all communications between the satellite and the ground to share this common resource. The downlink will therefore be time-division multiplexed between command acknowledgement, telemetry, health / status messages and payload data. The primary, or a dedicated, OBC must be responsible for managing the bursts of traffic and ensuring that adequate performance is preserved for all of these tasks.

3.4.2.1 Store-and-forward communications.

There are many possible strategies for implementing the downlink management on a microsatellite. Most microsatellites, and certainly all of SSTL's spacecraft, use a packetised, error-protected scheme. This approach has been adopted to satisfy the requirements of the first commercial application of microsatellites: store-and-forward communications [Ward, 1991][Ward, 1993][Da Silva Curiel & Ward][Allery et al].

In a store-and-forward (S&F) system, the microsatellite's OBC acts as a flying computer bulletin-board, collecting and despatching messages and data files as it comes into range of various ground stations. The principal rationale (and market) of S&F is in providing non-real-time data relay services to users deprived of conventional telecommunications. The emphasis has been to provide a rudimentary communications service to geographically remote users (including medical aid, technical aid, relief workers, polar exploration, and unmanned data-gathering terminals), using very low cost ground equipment.

The requirements of S&F have defined the communications systems of many microsatellites, especially SSTL's family of spacecraft. The satellite must interact with a large number of ground stations simultaneously, with multiple concurrent communications sessions. This dictates the use of relatively sophisticated multiple access protocols implemented in software. To keep the cost of the numerous ground stations down, much of the system's complexity has been centralised within the satellite's OBC.

The ground stations accessing the S&F microsatellite will be geographically distributed. This dictates that a constant transmitter power must be used over the whole orbit to ensure consistent and predictable link conditions to any given user who may potentially be accessing the OBC's file system. Due to the microsatellite's low transmitted power and the use of wide-angle, low-gain antennas, the data rates are correspondingly low.

Because of the satellite's low EIRP, the communications links are subject to significant error rates. To overcome this, and to implement time-division access, a packetised downlink scheme is used. The file being transmitted is sent as a sequence of short packets (typically around 256 bytes). Each packet is coded to protect against errors. If a packet is corrupted and fails its error-check, the ground station will reject it. The ground station collects these packets, building up an image of the original file. By keeping a 'hole-map', the ground station can request any outstanding packets which have been lost, corrupted or simply not yet sent. This will happen repeatedly until the ground station has an identical copy of the original file in the OBC's memory, guaranteed to be error-free.

The philosophy behind the communications of the current generation of SSTL and other microsatellites is clearly very different to the data dumps of most conventional remote sensing spacecraft. The central OBC is the nucleus of a communications system, where multiple ground stations load and retrieve data freely, simultaneously and randomly.

3.4.2.2 The SSTL OBC (and Ramdisk).

The principal on-board computer (OBC) for the SSTL, and many other microsatellites, is based on the general purpose Intel 80C186 microprocessor. Although the 80C186 is pedestrian by terrestrial standards, it is nevertheless quite advanced compared to the processors typically used in space (RCA1802, 1750) on larger missions. This extra margin in performance allows the OBC to take on roles in addition to the standard housekeeping tasks (ADCS, power management, payload activation). This principally involves supporting the store-and-forward digital communication.

The OBC is equipped with a large solid-state memory bank, known as the Ramdisk, to support its S&F activities. For recent microsatellites this is typically around 16 MBytes, although on FASat-Alfa the OBC also had access to the 256 MByte Solid-State Data Recorder Experiment (SSDRE). The Ramdisk contains all the messages and traffic of the S&F network.

3.4.2.3 Collection of experimental data.

The software administering the S&F activities of the OBC and Ramdisk of SSTL microsatellites has been extended to accept data from other spacecraft modules. These modules behave in a similar mode to ground stations, reading and writing data files to the Ramdisk, but using the satellite's local-area-network (LAN) instead of the uplink and downlink. Once a file of in-orbit data has been stored on the Ramdisk and closed, it is conceptually no different to the other files on the Ramdisk, and can be read by ground stations. In particular, this is used to store experimental data (images) as they are captured, buffering them on the Ramdisk until a ground station is ready to retrieve them.

Thus, a microsatellite OBC behaves as a communications hub between all of the spacecraft modules and the various ground stations. By using the Ramdisk as a flexible storage area for the spacecraft payloads generating data, including the cameras, it has been possible to extend the S&F concept to support scientific experiments. This has made it possible for these small spacecraft to support a wide range of other mission profiles without significant deviation from the standard design. Keeping the housekeeping systems (including communications) common across missions is one of the key factors in ensuring that microsatellites remain low-cost and fast-response. This computationally intensive, multiple-role design of the OBC is typical of microsatellites and is, once again, very different to the approach of most conventional satellites.

To assess the communications conditions experienced on existing microsatellites with respect to remote sensing, it is interesting to study the OBDH and downlink systems of one of the most sophisticated microsatellites in orbit, PoSAT-1. Before considering this in any detail, it is worth noting that the data rates for current microsatellites are radically lower than those of larger satellites and inadequate for supporting commercial remote sensing. However, as imaging, and other data-intensive applications become more popular on microsatellites, the OBDH bus and downlink of these spacecraft are being revised to increase bandwidth capacity (discussed in section 3.4.5). Therefore, the systems implemented on PoSAT-1 cannot be treated as a definitive statement on the optimum design for communications on remote sensing microsatellites, but as a reflection on the current state of the industry.

3.4.3 IMAGE THROUGHPUT ON THE POSAT-1 MICROSATELLITE.

The total volume of images obtainable from PoSAT-1 is dictated by the rate at which this data is extracted from the OBC. The daily throughput is therefore determined by the downlink, and is essentially independent of the performance of the imager, the OBDH bus or any other sub-system.

N.B. The length of an image captured by the PoSAT-1 cameras is 323 kBytes. This corresponds to a single frame (two fields) of 625-line television. Whenever 'an image' is mentioned in the following discussion, it will have this size. It must be remembered that this is very much smaller than a full multispectral image from SPOT (circa 64 MBytes for 4 bands) or LANDSAT (circa 300 MBytes for 7 bands).

3.4.3.1 The PoSAT-1 downlink.

The PoSAT-1 microsatellite has a single downlink operating at a hardware data rate of 9600 bps. This downlink is serviced by the OBC in the manner described in section 3.4.2. Provided the OBC is running a normal housekeeping load, it is able to sustain this bit rate continuously, whilst implementing all of the protocol overheads: responding to requests from the uplink, collecting data from the Ramdisk, packetising it and sending it to the transmitter.

About 15% of the downlink capacity is consumed by housekeeping data. This is mainly the overheads of the communications protocol (headers, tailers, checksums) but also includes other vital information like telemetry and housekeeping status messages. Thus, on average, the downlink supports an effective rate of about 8160 bps (750 bytes/s) of useful traffic (S&F, images, experimental data). If the OBC is heavily loaded with other activities (system control, local communications), then it is not able to sustain this rate continuously, and the throughput can drop as far as 5000 bps (450 bytes/s). Of course, this represents the total downlink capacity. If there are multiple ground stations using the S&F facilities, the rate to each user may be significantly less.

On the hardware side, PoSAT-1 maintains a continuous transmitted RF power on the downlink of around 3 Watts RF in Sunlight. This will drop in eclipse as the battery voltage falls, with about 1.5 Watts RF at the very end of eclipse. The DC consumption is about 6 Watts for these values. (The transmitters are less efficient at low supply voltage, so the DC power drawn remains fairly constant despite the large decrease in radiated power). The downlink frequencies for the SSTL family of microsatellites are in the UHF bands (400 - 440 MHz). The uplink is in the VHF band (130-145 MHz).

3.4.3.2 Ground support.

A standard SSTL fixed control ground station[7] uses tracking antennas to follow the satellite across the sky. Using moderate gain UHF antennas (16 dBi), it is possible to receive the satellite downlink from horizon to horizon, in the absence of any large obstructions and strong sources of interference. Certainly, a strong signal should be available whenever the satellite is higher than 5°.

On average, from a ground station at 51° of latitude (Guildford), a satellite in an 800 km polar orbit is visible above 5° for 3300 seconds (55 minutes) per day. This compares with 5000 seconds (83 minutes) per day for horizon to horizon coverage. (Average pass elevation 24.95°, average pass duration 700 seconds, average communications time 465 seconds, 7.2 passes per day). The total daily visibility is highly dependent on the latitude of the ground station: stations at lower latitudes will see less of the satellite, and those at very high latitudes will see the satellite every pass as it travels over the pole.

[7] This section deals only with the performance of the larger, fixed-location ground control stations, including the master ground station for the SSTL microsatellites located in Guildford, and the similar control stations at the sites of SSTL's various customers (e.g. in Portugal for PoSAT-1, in South Korea for KITSAT-1 & -2, in France for S80-T, in Chile for FASat-Alfa, etc.). The many personal stations and very compact field ground terminals employing the store-and-forward facilities will have a lower throughput.

Theoretically, the Guildford station could hope to receive around 2.5 MBytes of data per day (3300 seconds x 8160 bps @ 11 bits / byte), assuming a continuous stream on the downlink. If the coverage was horizon-to-horizon this would be around 3.7 MBytes per day. In reality, the total volume of data retrieved will be less than this due to breaks in the transmission caused by interference, packets in error, breaks in the transmitted stream, pauses for uploads and commands (about 5 minutes daily), and ground station or satellite non-nominality, etc. As a reference, if the spacecraft was continually in range of a ground station, it would theoretically be possible to dump a total of 65 MBytes every 24 hours, assuming no breaks in transmission, errors, etc.

In practice, the Guildford master station receives around 2.1 MBytes daily from PoSAT-1 (averaged over 16-25 July 94). This corresponds to 84% and 57% of the theoretical value for above-5° and horizon-to-horizon coverage respectively. Of the 2.1 MBytes collected, 1.8 MBytes is imagery, 150 kBytes is telemetry and housekeeping data, and 150 kBytes is other experimental science data.

3.4.3.3 Consequences of the store-and-forward communications system on the image throughput of PoSAT-1

The fact that the amount of data downloaded from PoSAT-1 is so close to the theoretical maximum (discussed in the previous section) bears witness to the good link performance at low elevations and the strength of the packetised, error-protected protocol used on the downlink. Despite the satellite spending much of the time very low on the horizon, where the signal is degraded by blocking (buildings, hills, mountains), increased path loss and interference, useful communication is nevertheless possible. Occasionally, communication to about half a degree over the horizon is possible due to refraction of the UHF signal - such occurrences generally happen when the satellite is over the ocean and not suffering from interference. As such the downlink systems of PoSAT-1 are well suited to the requirements of store-and-forward communications.

The organisations using microsatellite-based S&F communications networks are well served by the existing technology. Given the large number (hundreds to thousands) of ground terminals, a small increase in the cost per terminal has a major impact on the overall expense of the network. As there is no specific need for increased bandwidths, the extra cost to ground terminals of implementing higher data rates cannot be justified. Indeed, there is some discussion of further reducing the spacecraft data rates to make it accessible by even simpler ground terminals (very low power uplinks, onmi-directional antennas, etc.). This trend will be accompanied with increasingly sophisticated computing support; the cost of the lap-top PC driving the ground terminals are only a percentage of the overall cost, yet are continually dropping in price and improving in performance (certainly when compared to the rate of development of the other hardware).

Unlike S&F, where the emphasis is on servicing numerous small messages from multiple low-cost ground stations, the design focus of a dedicated remote sensing microsatellite must be towards achieving the maximum downlink data rates when in range of the master control station(s). Therefore the roles of both the space and ground segments will need to be re-evaluated - many of the performance restrictions imposed by the cost drivers of the S&F terminals will no longer be significant, because of the small number of control stations.

To support commercial remote sensing, the downlink requirements of future microsatellites will be much closer to those of conventional spacecraft. Although the storage of data for subsequent transmission remains a vital service, the sophistication of the S&F multiple-access downlink protocol is somewhat wasted when the objective is to dump large volumes of image data to a single master ground station. Moreover, the overheads of an S&F system, as well as the deployment of spacecraft resources (such as transmit power and antenna gain) are not best suited to imaging applications.

In practice, the Guildford control station can capture around 5.5 images (1.8 MBytes) per day from the PoSAT-1 satellite when running a continuous downlink. Each image requires about six minutes to download on a good downlink. While this throughput has been adequate to capture many thousands of images and demonstrate the principles of the electronic camera, it falls far short of supporting a full-time imaging mission. The daily volume of data from PoSAT-1, one of the World's most sophisticated microsatellites, is equivalent to about 10 seconds of NOAA transmissions and a few hundred milliseconds from SPOT or LANDSAT. There is clearly an enormous difference in the data rates from these two classes of spacecraft.

3.4.3.4 Desired throughput for a dedicated imaging microsatellite.

Unfortunately, the low data rates of current microsatellite downlinks impose a considerable bottleneck on the volume of images that can be retrieved from the Earth observation payload, and therefore appear fundamentally unsuitable for commercial exploitation. As with the limitations of current attitude control techniques (discussed in section 3.3), this is understood and accepted by the key players in the microsatellite business. The development of enhanced platforms geared towards small scientific (including imaging) payloads is receiving considerable attention, with associated performance gains from the power, attitude control, communications, etc. systems.

However, it is unreasonable to expect a 50 kg spacecraft with a total power budget of some 25 Watts to provide the type of coverage provided by a NOAA, SPOT or LANDSAT. This section offers suggestions for what may realistically be expected from future dedicated imaging microsatellite missions. The figures ventured are based on the author's experience of microsatellite operations and on indications from prospective customers for such missions.

Although the criteria for improvement in downlink capacity are not so clear, and any answer provided is necessarily arbitrary, it is estimated that the communications of a dedicated remote sensing microsatellite should support at least a ten times increase in the number of images captured (from five to fifty images every day). Thus the imaging system could capture an average of three or four images per orbit (14 orbits per day), without overloading the system. In all likelihood, these images would not be spread evenly over the orbital cycle, but would be clustered together as the satellite passes over regions of particular interest.

The baseline size of each image will also need to increase from the current 323 kBytes to around 4 MBytes; this corresponds to either a panchromatic images with 2000 x 2000 pixels, or a 4-band multispectral image at 1000 x 1000 pixels. Therefore, the total daily spacecraft-to-ground capacity will need to be at least 200 MBytes, effectively a 100 times increase on current microsatellite capabilities.

With a single control station located at Guildford (using the same statistics and downlink efficiency as detailed in section 3.4.3.2), the downlink data rate would need to be in the region of 1 Mbps. Under these conditions, it would take about a minute to download a single 'big' image.

These are clearly large increases in performance of the communications of microsatellites systems. While the spacecraft itself will doubtlessly be enhanced, most of the modifications will be to the ground segment, particularly in the antenna gain. Therefore, the 1 Mbps downlink suggested here is not as unattainable as might first appear. A more detailed discussion of ongoing development in microsatellite RF systems is presented in section 3.4.5.2.

3.4.4 IMAGE TURN-AROUND ON POSAT-1.

On a typical microsatellite, the OBC manages the downlink. Therefore, to queue images for transmission, the imaging systems needs to transfer its data to the OBC. The turn-around of an image is therefore determined by how long it takes to get from the imager to the OBC and then from the OBC to the ground. This length of time is governed by the data rates on the spacecraft's OBDH bus and downlink.

3.4.4.1 Gathering the image.

The output data rates produced from CCD imagers are typically in the region of 3 to 30 MBytes per second and greater. In this respect, the imaging systems carried by microsatellites will be not be significantly different from conventional spacecraft. Unlike conventional remote sensing satellites which have suitable hardware (direct downlinks or tape recorders) capable of handling these data rates, a microsatellite will certainly not. These rates are too fast to be handled directly by a general purpose processor (including most high-end digital signal processing engines), let alone be transferred across the general purpose OBDH network in real-time.

Therefore, the output of the microsatellite's imaging payload must be captured and stored by appropriate hardware, and re-transmitted at a slower data rate compatible with the speed of the OBDH bus. This buffer bridges the analogue and digital hardware of the imager, and the processors and software-oriented communications environment of the spacecraft OBDH network. The implementation of such buffers is a significant extra consideration for the designer of microsatellite imagers, and discussed in some detail in chapters 5 and 6.

Without going into too much detail at this stage, there are a few observations worth making to highlight the crucial role of the image buffer in establishing the productivity of an imaging microsatellite. If the imager fills these buffers at a faster rate than the OBDH network can empty them, the system will fail to achieve global coverage. Furthermore, the size of this buffer dictates how much imagery can be captured in a burst over a specific target region, before needing to be read out. In most cases, if the buffer can only hold one image, it will not be possible to capture another until the first one has been entirely read out to the OBC.

3.4.4.2 Transferring image data across the microsatellite data network.

In the unlikely event of there being a dedicated link between the imager and the microsatellite OBC, it may be possible to use a raw format (as used by conventional satellites) between these modules. However, in most microsatellite designs, the OBC and OBDH network will be standardised with well-defined on-board protocols. All other spacecraft systems, including the imaging payloads, will need to comply with these standards. In most cases, these interfaces will have been defined to be general purpose to support a wide range of potential activities, and have not been conceived to meet the particular demands of imaging systems.

The SSTL microsatellites in orbit, including PoSAT-1, use a serial bus for inter-module communications (the DASH bus) which links all of the intelligent spacecraft nodes (primary and secondary OBCs, payloads). The access protocol for this OBDH network uses a form of collision-detecting, carrier-sensing multiple access. Communications are in the form of data packets protected from errors by checksums. Each packet received must be acknowledged (handshaking) before the communication resumes.

Unfortunately, no standard hardware exists for this protocol, which must be implemented in software at each node. If a module needs to access the OBDH bus, it will need to include some form of processor programmed to adhere to the full specification of the protocol. The implicit need for an embedded processor within the imaging module is another consideration facing the designer of microsatellite systems but not encountered on conventional spacecraft.

This processor will need to recover the stored data in the image buffer, without interfering with the activities of camera hardware. The captured imagery will need to be cut into appropriately sized packets for transmission across the OBDH network. Given that the bandwidth between the processor and the image store is likely to greater than that of the OBDH network, equipping the local processor with additional memory will allow further images to be buffered within the imaging system. This processor can also be used to format the image from the raw data stream, reducing the size of the data set by removing the many spurious samples that invariably accompany the valid image samples.

3.4.4.3 Image turn-around on PoSAT-1.

On the SSTL DASH network, all transmissions are at a standard 9600 bps (873 bytes / sec). However, with all of the protocol overheads (such as waiting for acknowledgements, OBC response, etc.), the effective throughput is in fact much slower, being closer to 450 bytes / sec (3600 bps) during image transfer on PoSAT-1 (322800 bytes in 12 minutes). It is therefore rather surprising that under good conditions and with a single station accessing the spacecraft (as is often the case for PoSAT-1), the speed of the downlink is rather faster than the DASH network, even though their nominal data rates (bits per second on the physical layer) are the same. This is because the DASH acknowledges each packet in turn, whereas the downlink protocol acknowledges (indirectly) in batches. Clearly, the DASH specification and hardware were not designed for the efficient transfer of large volumes of data, but were conceived to produce a simple, compact and low-cost means of allowing different modules to communicate.

The slow speed of the DASH network has two repercussions on the operation of the imaging system. Firstly, by relying solely on the OBC to buffer images, the capture rate is limited by the speed at which the OBC can collect the images. Given the overheads on PoSAT-1, it takes over 30 minutes to completely transfer and process an image pair (captured from the Wide and Narrow Angle Cameras simultaneously), effectively limiting the system to only one scene (pair) in Sunlight per orbit. This is unacceptable in a dedicated imaging mission. It will be necessary to capture and store several images of a region in quick succession (perhaps in response to a particular interest in local features, or to optimise infrequent imaging opportunities).

The second aspect of a slow OBDH network is the loss of timeliness. Because the DASH is so slow, it is not possible to capture an image and download it within the same pass (average total duration 12 minutes). Only on the following pass will the image be available. This is at best an hour and a half later, but may in fact be several hours later. If the delay in the delivery of the data is important (e.g. in a meteorological service), it is absolutely essential that images can be captured and downloaded within a single pass.

3.4.4.4 Desired turn-around for a dedicated imaging microsatellite.

Ideally, the imagery from an Earth observation satellite is made available on its downlink in real-time so that local users can have instantaneous access to data. As already discussed, this is not feasible on current microsatellites because of the restricted bandwidths of both the OBDH network and the downlink. The objective must therefore be to deliver image products to local users within the same pass.

To image a particular part of the Earth, the satellite must be at a fairly high elevation in the sky (above 60°) on a daytime pass. There are about seven minutes (for the standard 800 km orbit) between this point-of-closest-approach and the satellite passing out of range as it travels over the horizon. Therefore, to meet the criteria for 'real-time' imagery, it will be necessary to capture the image, transfer it to the OBC and download it within this time. In fact, given that the link to the satellite may be marginal at low elevation angles, it will be necessary to complete the whole process rather sooner, say within three minutes. This faster rate will allow some margin when conditions are poor, whilst permitting other downlink activity when the situation is nominal.

In section 3.4.3.4, it was calculated that a 1 Mbps downlink would allow a 'big' image (4 MBytes) to be downloaded in a minute. If the transfer of this data from the imaging payload to the OBC also took a minute, the system could deliver timely data, with at least one minute of margin for various on-board delays (image processing, manipulation, queuing, etc.). This requires an effective data rate of 0.5 Mbps across the OBDH network. The actual physical speed of the network will probably need to be 5 to 10 Mbps in order to sustain this transfer rate. These rates are imminently feasible with current LAN-controller integrated circuits, provided the processors within the OBC and imaging payload able to service the network effectively.

Given the data rates used in this example, it appears quite feasible for future microsatellites to capture and deliver imagery within the same pass. In fact, it should be possible for the spacecraft to capture and transmit images continuously, separated by about 90 seconds. If the master control station needed to recover stored data, this schedule would need to be interrupted.

3.4.5 CURRENT DEVELOPMENTS IN MICROSATELLITE COMMUNICATIONS SYSTEMS.

The discussions of the previous sections make it clear that the communications systems developed to support store-and-forward traffic on microsatellites are poorly suited to the needs of dedicated remote sensing missions. This situation is recognised and significant development effort is being devoted within SSTL, and elsewhere, to improve the data rates achieved on both the OBDH network and downlink of microsatellites.

The first steps towards these higher data rates were implemented for the FASat-Alfa mission. As imaging was one of the prime objectives of FASat-Alfa, these upgrades would have represented a significant benefit. Further into the future, the Clementine microsatellite (currently in the definition stages - not to be confused with the BMDO mission to the moon of the same name - section 2.3.5.8) will feature a new downlink system for supporting a data-intensive experimental communications payload. Although unnecessary conjecture has been avoided throughout this thesis by limiting the scope to hardware in orbit, these developments are imminent and therefore worthy of a brief discussion.

3.4.5.1 Maximising image throughput on the satellite downlink.

Different missions produce different solutions to the issue of data flow management. The designers of SPOT and the early LANDSATs accepted that it would not be possible to provide continuous global coverage (i.e. to record and retrieve every scene that passes below the satellite). Even with the high downlink data rates, there is simply not enough time in range of ground stations to dump all the data that the satellite could gather. A compromise was struck to establish what percentage of global coverage was acceptable to justify the cost of the mission.

There are three basic solutions to improving the ratio of scenes captured to scenes lost for a remote sensing mission:

1. Increase the capacity of the downlink, so that more stored data can be dumped.
2. Increase the number of ground stations, to increase that total daily visibility. For polar orbits, ground stations at very high latitudes (e.g. Kiruna in Sweden, Trømso in Norway, Fairbanks in Alaska, and various others inside the Arctic and Antarctic circles) can greatly increase the total daily pass time because they see the satellite every orbit. Going to even greater lengths, the LANDSAT

programme maintains a near-continuous link with the satellite(s) by employing the TDRSS data relay stations in geostationary orbit.

3. Reduce the volume of data collected. Conceptually, by 'reducing' the spatial resolution of their imagers, the NOAA satellites have reduced their data rates to the point were the entire tape recorder contents can be dumped to the master ground station every day, ensuring global coverage. The fact that other ground stations are collecting local real-time data as well is largely irrelevant to the master control station.

It would be naive to expect microsatellites to ever provide coverage similar to that of the large Earth observation spacecraft. Nevertheless, it is important to remember these factors when assessing the viability of a commercial application for imaging microsatellites. All of these approaches should be considered when up-rating the data retrieval systems of a spacecraft.

3.4.5.2 Upgrades to the downlink bandwidth.

3.4.5.2.1 Modems on PoSAT-1 and FASat-Alfa.

The first item to examine when upgrading the throughput of a satellite's digital communications system is the speed of the downlink modulators and demodulators. To this end, PoSAT-1 carries an experimental modem which has a bit rate of 38k4 bps, four times faster than the standard 9600 bps modem. This enhanced modem has been operated successfully in orbit, demonstrating that there is adequate link budget margin to sustain these data rates on the downlink. Unfortunately however, due to its experimental nature, the modem is incompatible with a number of the ground station systems, and is not used for routine operations. The high speed modems (38k4 and 76k8) carried on FASat-Alfa would have been fully operational.

The store-and-forward protocols were retained for FASat-Alfa. Assuming that the effective bit rate on the downlink scales linearly with the speed of the modem, it would have been possible for the Guildford control station to retrieve about 16 MBytes from FASat-Alfa's 78k4 bps downlink daily, about eight times more than with PoSAT-1. (This is a simple extrapolation of PoSAT-1's performance, and does not consider factors like FASat-Alfa's lower orbit, which offers less ground station visibility, or the absence of competition for the downlink). The Guildford and Santiago (Chile) control stations should have been able to retrieve a combined volume of data in the region of 20-25 MBytes per day. In any case, a 323 kByte image would have taken less than a minute to download at these rates.

3.4.5.2.2 FASat-Alfa downlink.

To preserve the link budget at these increased data rates (and bandwidths), the transmit power used on FASat-Alfa would have been increased to around 7 to 10 Watts RF (15 to 25 Watts DC). However, the satellite's power budget would not have been able to support this continuously, especially given the high number of sophisticated, and power consuming, payloads. A credible scenario for downlink operations for this mission was to use the standard (low power, 9600 bps) downlink continuously as on previous missions. The higher power and bit rate service would only have been activated as necessary (either manually or automatically) when required by a major ground control station.

This trend will have to be adopted by future microsatellites needing to sustain high data rates with only a few control stations. To support these higher data rate downlinks, the transmitter will operate in bursts, delivering high speed communications in range of the principal ground stations, at the expense of having a continuous downlink. Rather than spreading the drain on the spacecraft's electrical power over the whole orbit, it should be conserved and, as far as possible, be concentrated on the few passes in range of the control stations.

3.4.5.2.3 UoSAT-12 minisatellite, Clementine and future microsatellite missions.

To obtain higher data rates than these, it is necessary to leave the UHF bands and go to higher frequencies, where it is possible to obtain licences for wider bandwidth transmissions. SSTL is currently developing communications hardware to operate in the S-band portion of the spectrum, in the bands specifically allocated to spacecraft telemetry and scientific traffic.

The first mission to benefit from the new modulator and S-band transmitter hardware will be SSTL's first minisatellite, the 200 kg UoSAT-12 spacecraft scheduled for launch in late 1996. The downlink bit rate will be 1 Mbps, representing a quantum leap in downlink capacity. This will require about 4 Watts of RF power, drawing 20 to 25 Watts of DC power (20 % efficiency is considered good are these frequencies). A low-gain antenna, with a hemi-spherical radiation pattern, will be used to give total coverage within the satellite's footprint, permitting horizon-to-horizon communications with the control stations. On the UoSAT-12 minisatellite, this will be a quadrilfilar antenna, but it may well be replaced with an S-band patch antenna in the future.

Rather surprisingly, these spacecraft systems are not so different from those on the existing microsatellites, yet the link can sustain a dramatically increased data rate. This is achieved by upgrading the ground segment; the ground antenna for this system will need to be a 2.4 metre parabolic dish antenna, offering a gain of 31 dBi, compared to the current antennas which have about 16 dBi. Another essential factor is the vastly reduced noise floor (less terrestrial interference) in S-band compared to UHF.

The first SSTL microsatellite to incorporate this new communications system will be the Clementine spacecraft, due for launch in late 1997 or early 1998 and currently in the advanced definition stages. The mission specifications call for 60 MBytes per day to be downloaded to a single ground station in Toulouse (south-western France). This will be accomplished with a single 0.5 Mbps downlink operating when the satellite is above 5° elevation. The transmitter will produce 2 Watts RF, consuming a little over 10 Watts DC. To conserve power, the transmitter will always be off except when in range of this master control station.

The S-band downlink systems being implemented for SSTL's forthcoming micro- and minisatellites will be versatile and upgradable. It will be possible to operate the system at data rates up to 4 Mbps (at an RF transmit power of 16 Watts - 80 Watts DC - really only feasible on a minisatellite). Due to bandwidth allocations and legal restrictions on power flux density, but not for technical reasons, it is not possible to attain higher rates than this without going to even higher frequency bands (most probably L-band).

To sustain the hardware data rates, it will be necessary to develop new downlink protocols, whilst retaining the OBC's role in collecting and despatching data. A solution is for the OBC to use the periods out-of-range to prepare and format the entire transmitted sequence in advance (including synchronisation bytes, headers, tailers, error-protection or correction checksums and of course the data itself). When the transmissions start, the OBC will activate hardware (a DMA controller) to stuff the contents of the Ramdisk into the modulator input. Following the bulk data transfer, a software sequence will be launched to re-transmit any data missed by the ground station.

The payload on Clementine is scientific and not an imaging system but the requirements for bulk data transfer are clearly very similar. The communications systems developed for Clementine and the UoSAT-12 minisatellite are highly suited to the demands of future Earth observation missions. Given the long time-scale for Clementine (at least by SSTL's standards), it is very possible than a dedicated imaging microsatellite will be in orbit before then.

3.4.5.3 Upgrades to the OBDH network.

Even more than the downlink, the DASH network on PoSAT-1 presents a serious handicap to developing commercial Earth observations from SSTL microsatellites. Even though 9600 bps was an acceptable (although not particularly fast) data rate when the DASH was specified in 1988, it is painfully slow by the standards of current terrestrial computer local-area-network technology. There is a wide range of highly integrated solutions for implementing LAN controllers within microsatellite modules, operating at data rates well in excess of 1 Mbps.

On FASat-Alfa, the DASH has been superseded as the principal OBDH network by the industry-standard CAN-bus (ISO 11898 and 11519-1), developed for use in automotive, aerospace and industrial control applications. The principal role of the CAN-bus (Controller Area Network) will continue to be in providing a distributed telemetry and telecommand network for future SSTL spacecraft, but it will still represent a marked improvement over the DASH for bulk data-transfers. (N.B. The DASH hardware was still included in the design of most FASat-Alfa modules, providing a tried-and-tested back-up had the CAN-bus failed to operate as expected. In future missions, it is likely that the DASH will be removed altogether).

Designed principally for telemetry and telecommand applications, the CAN-bus has a number of features suitable for spacecraft use. The CAN-adaptor hardware fully implements extensive error checking, packet acknowledgement, and address and message-type recognition functions (i.e. the data link layer), relieving the individual computer nodes of these tasks. These result in considerable speed improvements by eliminating many of the software overheads of the DASH, where each processor is interrupted for every byte on the bus, regardless of the actual destination. The data rate of the CAN-bus's physical layer is 1 Mbps, as opposed to the 9600 bps of the DASH, although the effective transfer rate will be significantly less because of factors like protocol overheads (57%), collisions, and the latency of servicing at both ends.

The CAN-bus protocol is message-based, with 8-byte data packets. Although this short data field is not ideal for image transfer, it is still an improvement over the DASH, where the CPU is interrupted for each byte. Even though the CPU activity will probably be much higher in bursts to support the high data rates, overall the CAN-bus hardware will free significant amounts of CPU resource, particularly at the OBC end.

An additional SSTL-defined protocol has been defined to permit data transfers (i.e. images) longer than the eight-byte maximum. Two high-grade personal computers (486) implementing this protocol can transfer a whole image (322800 bytes) in 20 seconds. This corresponds to an effective data rate of approximately 130 kbps (16 kBytes / s). Even though the on-board systems are likely to be slower than this by a factor of two or three, the CAN-bus offers a dramatic improvement over the DASH.

Despite the significant gains in bandwidth offered by the CAN-bus on FASat-Alfa, this is still not a long-term solution as an OBDH bus for an imaging microsatellite. A slightly inappropriate addressing architecture and especially the small size of the data packets make the CAN-bus unsuitable for transferring large volumes of data at high speed. On-going studies into the suitability of a more appropriate on-board data highway (e.g. Ethernet, HDLC, ArcNet, etc.) promise even greater advances in the turn-around of images.

3.4.5.4 Using software to reduce the bandwidth requirements.

As outlined in section 3.4.4.2, the need to interface to a standardised OBDH network dictates that an imaging payload on a microsatellite must incorporate an integrated microprocessor or microcontroller. Although increasing the overall complexity of any given module, endowing it with this processing power can be very beneficial in improving its versatility, flexibility, performance and reliability. Within the specific context of imaging systems, this processing intelligence should be used to enhance the image quality and throughput, potentially offsetting some of the limitations of the communications hardware.

Although the improvements in the communications systems hardware will vastly improve the suitability of microsatellites for dedicated remote sensing missions, there is considerable scope for using on-board analysis and processing to make best use of this resource. Numerous well-researched image processing and compression techniques are available to reduce the size of image files by mathematically transforming the data to remove redundancies. These techniques are as valuable as, and much more flexible than, advanced hardware in improving the useful throughput over the spacecraft downlink. Although the channel bandwidth is not altered, the number of useful images transmitted though it is increased.

Therefore, with the judicious use of on-board processing and compression, the imaging system can play its own part in enhancing the performance of the communications systems. These techniques are discussed in some detail in chapter 7.

3.4.6 CONCLUSIONS.

All remote sensing instruments generate large volumes of data that need to be collected by the spacecraft systems and relayed to the users. The communications path between the imaging payload and the ground involves several stages, with the system throughput and turn-around determined by the slowest link. Given that visibility is limited for satellites in low-Earth orbit, the downlink becomes the limiting factor in retrieving large volumes of imagery from a remote sensing mission. Conversely, all parts of the communications chain effect the ability to provide a rapid turn-around of data. Therefore, the design effort must be balanced between each of the communicating elements to ensure that no one stage degrades the overall performance . Accordingly, the characteristics of the data handling systems on traditional remote sensing spacecraft are simplicity and speed.

Conversely, the communications systems of current microsatellites, including the SSTL family, were conceived to support store-and-forward message transfer. As these systems include numerous ground stations, there has been considerable emphasis on keeping the ground segment extremely low-cost. This has involved keeping the hardware extremely low-power and simple, resulting low communications data rates, but making use of sophisticated software to provide the necessary multiple access protocols. The concept of the centralised file-server on the main on-board computer has been extended to accommodate scientific experimentation by accepting data from other spacecraft modules, emulating ground terminals.

Unfortunately, the 9600 bps data rates typical of current microsatellite downlinks and on-board data handling networks are simply far too slow to support commercial imaging missions, and need to be improved significantly. At the physical layer, this involves developing hardware (and the software drivers) to achieve and sustain higher data rate transfers. On the FASat-Alfa microsatellite, the software-based DASH network was superseded by the higher bandwidth CAN-bus (effective data rates circa 100 kbps), and the downlink was designed to support 38k4 and 76k8 bps.

For commercial Earth observation using microsatellites, it will also be necessary to change the philosophy of the downlink from 'endurance' to 'sprinting'. This means abandoning the existing systems which provide continuous, low-power, low-data-rate transmissions, in favour of newer S-band hardware capable of delivering much higher bandwidths and output powers for the short bursts when the satellite is in range of a master ground station. The data rates of the communications systems will need to be increased significantly beyond current capabilities, with the downlink operating at about 1 Mbps and the OBDH network at 5 to 10 Mbps. The downlink will be used to dump the maximum amount of data to the ground, relying on 'brute force' communications techniques reminiscent of conventional remote sensing missions, rather than the software-based approach generally associated with microsatellites. These issues are currently being addressed in the design of the Clementine microsatellite and the UoSAT-12 minisatellite.

In addition to these hardware improvements in speed, software techniques should be used to improve the quality of the imagery to increase the usefulness of the data received. Judicious use of on-board image analysis, processing and compression must be used to further improve the satellite's image yield. This is discussed in chapter 7.

A tangential issue, but nevertheless worth mentioning, is that the increased downlink capacities anticipated for future remote sensing microsatellites will place a significant extra burden on a ground segment designed for supporting existing store-and-forward messaging. Of particular concern are the capacities of existing facilities for processing, archiving, retrieving and distributing the large volumes of imagery.

3.5 SUMMARY OF CONCLUSIONS.

For designers used to the facilities of large, conventional spacecraft, microsatellites present many restrictions in terms of mass, volume and power. In turn, these factors limit the attitude stability and the communications bandwidths available on a microsatellite. For numerous reasons, the bulky and power hungry designs of whiskbroom imagers (using scanning mirrors) are not suitable for small satellites and mechanically passive CCD imagers need to be used instead. With contemporary technology, it is possible to design solid-state imagers that are compact, robust, draw moderate power and have very good imaging properties.

Imagers which scan the scene using linear CCDs are very sensitive to drifts in attitude stability, which cause in a loss of image registration. Conversely, electronic cameras using area-array CCDs to capture whole scenes in a single operation are effected much less. The current generation of microsatellites are equipped with modest attitude determination and control systems, and are unable to support scanning imaging systems. Therefore, using electronic cameras makes imaging possible on these small platforms.

Although area-array CCD sensors are immune to registration errors, they are susceptible to blur caused by the satellite's motion. A blur budget must be provided for each instrument and satellite platform to ensure that the imagery's resolution and contrast will not be degraded.

Whereas the satellite's attitude stability defines architecture of the imaging instrument, the communications channels define how effectively it can be exploited. The low communications data rates of existing microsatellites limits the effectiveness of Earth imaging payloads. Although improved communications hardware will improve the data throughput and turn-around, software data reduction techniques should also be used to reduce the bandwidth demands of the imaging system.

Although microsatellites may appear unsuited to remote sensing applications because of these various physical constraints, it is nevertheless possible to implement Earth observation systems provided the designer understands these constraining factors and is prepared to be flexible in overcoming them. In so doing, it is possible to exploit a key strength of microsatellites: their short lead times. The time scales allow designers to respond to the continuous developments in modern semiconductor technology and to use many advanced techniques to solve their problems. Conversely, the long development periods and high financial risk of conventional missions do not allow such innovation.

3.6 REFERENCES

Allery M.N. et al: Low Earth orbit microsatellites for data communications using small terminals; 10th IEE International Conference on Digital Communications via Satellites, Proc. IEE Digital Satellite Communications 403, Vol. 2 p.457-465, Brighton UK, 15 May 1995.

Arai K: Requirements for ADEOS orbit, orbit and attitude control, and rate jitter; Proc of IGARSS Symposium, Edinburgh, Scotland, 13-16 Sept. 1988; Ref. ESA SP-284.

Colwell R.N: Manual of Remote Sensing Second Edition; American Society of Photogammetry, The Sheridan Press 1983, ISBN 0-937294-41-1.

Da Silva Curiel R.A. & Ward J.W: Operational store and forward payload for low Earth orbit microsatellite data - collection and file transfer communications; Proc. of International Symposium on Satellite Communication and Remote Sensing, p.294-297, Xi'an China, 20-22 Sept 1995.

Elliot C: Cost-effective environmental monitoring; Earth Space Review, Vol.1 No.2, p.7-10, Apr-June 1992; ISSN 1060-1848.

Erlich D. & Estes J.E: Applications of NOAA AVHRR 1 km data for environmental monitoring; Int. J. Remote Sensing, Vol.15 No.1, p145-161, 1994.

Goel P.S, Venkat Rao M. & Chandra K.S: Attitude control system specifications for a remote sensing satellite; Int. J. Remote Sensing, Vol.10 No.9, p1531-1537, 1989.

Hashida Y: SSTL Internal Technical Note, Document FASAD013, 2 June 1995.

Hodgart M.S: Attitude control and dynamics of UoSAT angular motion; The IERE Journal, Vol. 52 No.8/9, Aug/Sept. 1982; ISSN 0033-7722.

Hodgart M.S. & Wright P.S: Attitude determination, control and stabilisation of UoSAT-2; The IERE Journal, Vol. 57 No.5, Sept. 1987; ISSN 0267-1689.

Hodgart M.S: Gravity gradient and magnetorquing attitude control for low-cost low Earth orbit satellites - the UoSAT experience; PhD Thesis, University of Surrey, 1989.

Hodgart M.S. & Ong W.T: Gravity gradient and magnetorquing attitude control for low Earth orbit satellites; 2nd ESA Int. Conf. on Spacecraft Guidance, Navigation & Control Systems, The Netherlands, April 1994.

Kumar K: Orbital and attitude prediction accuracy requirements for satellites engaged in remote sensing and scientific missions; IEEE Trans. on Aerospace and Electronic Systems, Vol.AES-18 No.2, p188-191, 1982.

Lillesand T.M. & Kiefer R.W: Remote Sensing and Image Interpretation; Wiley 1987; ISBN 0-471-84517-5.

Neeck S.P, Venator T.J. & Bolek J.T: Jitter and stability calculation for the ASTER instrument; Proc. of the SPIE Conference on Sensor Systems for Mission to Planet Earth Platforms, SPIE Vol.2317, Rome, Sept 1994.

Pfeiffer B. & Bonnefoy R.F: The Earth observation preparatory programme, The ESA bulletin, No.51.

Price J.C: Timing of NOAA afternoon passes; Int. J. Remote Sensing, Vol.12 No.1, p193-198, 1991.

Rees W.G: Orbital sub-cycles for Earth remote sensing satellites; Int. J. Remote Sensing, Vol.13 No.5, p825-833, 1992.

Santana C.E: Environmental monitoring of the Amazon region with smallsats; Conference on Small Satellites for Remote Sensing, The Space Congress, 24-25 May 1995, Bremen Germany.

Slater P.N: Remote Sensing - Optics and Optical Systems; Addison-Wesley 1980; ISBN 0-201-07250-5.

Swain P.H. & Davis S.M: Remote sensing - the quantitative approach; McGraw-Hill, 1978.

Townshend J.R.G. & Justice C.O: Selecting the spatial resolution of satellite sensors required for global monitoring of land transformations; Int. J. Remote Sensing, Vol.9 No.2, p187-236, 1988.

Unwin M.J: The PoSAT microsatellite GPS experiment; ION GPS-93 Conference, Salt Lake City, USA; Vol.1, p.811-817, Sept 1993.

Unwin M.J: A practical demonstration of low-cost autonomous orbit determination using GPS; ION GPS-95 Conference, Palm Springs, USA; 13-15 Sept 1995.

Wallach J: The Launch of NOAA-H Weather Satellite: A Mission Profile; The Proceedings of the AMSAT-NA 6th Space Symposium and Annual Meeting; Nov. 11-13 1988; Published by American Radio Relay League.

Ward J.W: Microsatellites for global electronic mail networks; Electronics & Communication Engineering Journal, Vol.3 No.6, p.267-272, Dec 1991.

Ward J.W: Design, implementation and in-orbit demonstration of a store-and-forward digital communication system for low Earth orbit microsatellites; PhD thesis, University of Surrey, 1993.

Welch R: Spatial resolution for urban studies; Int. J. Remote Sensing, Vol.3 No.2, p139-141, 1982.

Wertz J.R: Spacecraft attitude determination and control; D.Reidel Publishing, 1978; ISBN 90-277-1204-2.

CHAPTER IV

OVERVIEW OF HARDWARE DEVELOPED DURING THIS RESEARCH PROGRAMME.

The theories argued in this thesis have been developed in a very practical programme of implementing numerous imaging systems on-board SSTL microsatellites. The author's understanding of the subtle engineering trade-offs associated with implementing remote sensing on microsatellites has grown with each successive generation of the electronic imaging systems. This has permitted a gradual improvement in the performance of these electronic cameras and microprocessor units from the rudimentary circuits flown on UoSAT-4, to the highly integrated and modular systems prepared for FASat-Alfa. Since it is the in-orbit successes of these cameras, particularly on PoSAT-1, which give credibility to the arguments of this thesis, chapter 4 reviews the hardware of the imaging systems developed by the author during this research programme.

4. OVERVIEW OF HARDWARE DEVELOPED DURING THIS RESEARCH PROGRAMME.

The conclusions of the previous chapter indicate that remote sensing is possible from 50 kg microsatellites provided the imaging system can adhere to the mass, volume and power constraints. More importantly, the imaging instruments must be able to cope with the microsatellite's imperfect attitude control and still operate successfully. These restrictions indicate that electronic cameras based on modern area-array CCD sensors represent the most suitable technology for Earth observation under these conditions. Although the limited data rates of the various communications channels may represent bottlenecks in the operational exploitation of the system, this factor does not really influence the design of the sensing instrument as long as adequate local buffering is provided to store a nominal volume of imagery.

The main emphasis of this research programme has been to demonstrate the feasibility of using CCD cameras for commercial and / or scientific remote sensing from microsatellites. The novelty of this research is the practical implementation of these imaging systems, and discussing the observed effects and results, rather than conducting yet another 'paper study'. Therefore, the design, development, construction, integration, testing, in-orbit commissioning and exploitation of these cameras have been the most significant and time consuming aspects of the programme.

During this research programme, the author has designed and implemented five generations of the SSTL imaging system from UoSAT-4 in 1990 to FASat-Alfa in 1995. The development of these systems has played an important role in forming the arguments presented in this thesis. This hands-on experience has provided extensive insight into a range of problems which theory alone could not have yielded. Before proceeding to the general discussion of the design issues faced in developing remote sensing cameras for microsatellites covered in chapters 5 and 6, it is appropriate to review the characteristics and performance of the imaging systems produced by the author. General trends, such as reduced power consumption, decreasing volume, improved image sensitivity, reduced noise, and increased modularity and fault-tolerance that have driven many of the design changes are highlighted.

4.1 CONTEXT AND CONSTRAINTS PLACED UPON THE IMAGING SYSTEM.

The discussions of chapters 2 and 3 will have given the reader an impression of the engineering environment encountered on microsatellites, and of the difficulties faced by the designer of remote sensing instruments. However, these observations have deliberately been kept general, and assume that Earth imaging is the primary, if not sole, objective of the mission. This has not been the case for the systems developed within the SSTL programme, resulting in further constraints and compromise. In addition to these technical aspects there have inevitably been many other financial, scheduling and managerial pressures on the development of these cameras. Of course, accommodating these diverse and often unrelated factors forms an integral part of engineering, and marks the difference between 'talking about it' and actually 'doing it', as discussed in section 2.3.5.

4.1.1 TECHNICAL CONSTRAINTS.

The constraining factors of microsatellite platforms discussed in chapter 3 have effected the design of the cameras. Aspects like the attitude control and communications data rates are exactly as described. However the mass, volume, power and access to the Earth-facing surface of the spacecraft have been very limited compared to the scenarios of chapter 3 which consider dedicated imaging missions. This is because the electronic camera systems described in this thesis form only one aspect of SSTL's research strategy, and each one of the microsatellite missions has needed to fulfil a range of diverse applications and experiments.

In practice, the scarcest commodity in the development of these cameras has been volume, which has been limited to one standard module tray in the middle of the satellite stack and a volume of about 260 x 60 x 40 mm in the Earth-facing battery box (refer to section 2.3.3.3). Given the common design of the successive missions, this basic configuration remained unchanged until the structural redesign of FASat-Alfa, which is far more accommodating towards Earth-facing imaging and scientific payloads (again refer to section 2.3.3.3).

The module tray has housed the digital sub-systems associated with the imaging system, with only the analogue sensor electronics in the battery box. The restricted volume has limited the type of circuits that could be used, and much of the development time has had to be devoted to miniaturising the systems, with some repercussions on performance. This was particularly the case prior to the PoSAT-1 mission in 1993, when surface-mount packaging was not widely available for integrated circuits and passive components.

Given the volume constraints, there was little possibility of consuming excessive mass. The system mass has been between 2 and 3 kg across the missions (except FASat-Alfa). The distribution of mass is approximately a third each for the module tray mechanics, the digital circuitry in the tray, and the camera head in the battery box (including optics). The limitations on power consumption have not been overly restrictive, allowing around 1 Watt of quiescent power to be drawn by the microprocessor units, with peaks of up to 6 Watts during image capture.

Thus, the volume, mass and power allocated to the imaging modules on the SSTL microsatellites are even smaller than those identified in chapters 2 and 3. While the constraints of a dedicated mission are challenging to design with, the resources made available to these cameras have been even more restricted.

4.1.2 NON-TECHNICAL CONSTRAINTS.

In addition to the technical constraints of microsatellites discussed so far, there are factors such as the time scales, budgets, available manpower and the mission objectives which also play a crucial role in defining the imaging payload.

One of the key advantages of microsatellites is their short development cycles, rarely longer than 12 months from concept to launch. However, such short time scales can leave little room for evaluating engineering options, design and research, with only two or three months available for these tasks before the production phases commence. Moreover, in this twelve month period, two working revisions of the systems must be delivered: a prototype / engineering model and the flight model (except for PoSAT-1 where only the flight model was built).

In addition to the short time-scales of the individual missions, the microsatellites discussed in the thesis have been launched at yearly intervals, a pace dictated by the availability of launch opportunities. At this rate, there is very little 'recovery time' between missions. In some instances (e.g. UoSAT-5 to KITSAT-1, and KITSAT-1 to PoSAT-1) the design of the next spacecraft had started before the previous one had been launched. Similarly, the fact that the author was essentially working alone in producing the imaging systems for these projects, further limited the scope of for redesign and innovation between missions.

Accordingly, an approach of implementing small incremental changes has been adopted in developing the capabilities of the imaging systems. The repetitive cycle of designing, developing, and exploiting a system, and feeding the results into the next generation of camera has been extremely valuable in developing the author's engineering skills and in ensuring a rapid development of SSTL's imaging capabilities. Overall, the author feels that developing the cameras in a succession of small steps has been more productive, and successful, that a one-off project. It is recognised that this approach could only have been conducted in an organisation as prolific as SSTL / UoSAT. Nevertheless, the results are hold valid for all microsatellite imaging applications.

4.2 THE UOSAT-4 CAMERA.

The author's first effort at developing an electronic camera was deployed on the UoSAT-4 mission. In addition to all the constraints listed above, the funding available for the UoSAT-C mission was extremely limited. This was exacerbated when this mission was transformed into UoSAT-D and -E (UoSAT-3 and -4), resulting in doubled expenditure on the housekeeping systems. This had a direct repercussion on the selection process of the CCD sensor and remaining components of the circuit. The choice of Fairchild CCD222 device used for this mission was based solely on its being donated to the UoSAT Research Unit, thereby saving this money for other systems. The drawback of using this sensor was an absence of dedicated support chipsets as well as minimal documentation and technical support (including no circuit diagrams). This situation meant that the author had to develop the circuits to drive the CCD from first principles using discrete components. Fortunately, there was a fairly long period of two years for these circuits to be designed and tested, so that eventually they exhibited fairly stable performance.

4.2.1 DESCRIPTION OF THE UOSAT-4 CAMERA.

The detector used for the UoSAT-4 camera was a Fairchild CCD222. This device used the interline transfer architecture (see section 5.1.2.3), and produced imagery with two interlaced fields of 384 x 244 pixels [1] compatible with the EIA (525-line) television standard. To simplify the circuitry only one of the two fields was generated and captured.

Although built up entirely of discrete components, the block diagram of the UoSAT-4 imager was similar to that of any other CCD camera. The basic topology of a CCD camera and digital still camera are shown in figures 4.2.1a and b (these are identical to the figures in section 5.2.1 where the building blocks of a typical electronic camera are discussed in detail). The UoSAT-4 camera's sequencing logic was composed of discrete CMOS (4000 and HC families) and TTL gates occupying half of the module tray in the stack. The DC-DC converters required for voltage conversion were also in the main tray.

The high-speed sequencing clocks were sent to the camera head in the battery-box, via the main wiring harness. The clock buffers were also built out of discrete components, especially the drivers for the vertical clocks which were made of transistors and passive

[1] While this resolution is modest by today's standards, most personal computers at the time were unable to display this imagery, equipped as they were with EGA display capabilities. Computers with VGA displays (640 x 480 pixels by 16 grey levels) became available mid-way through the project in 1989.

components. As with all parts of the camera, a lot of testing was required to develop this circuitry. The absence of technical support was critically felt in developing the clock driver circuitry, with several months of delay caused by a typographical error in the data sheets, resulting in incorrect biasing of one signal to the CCD.

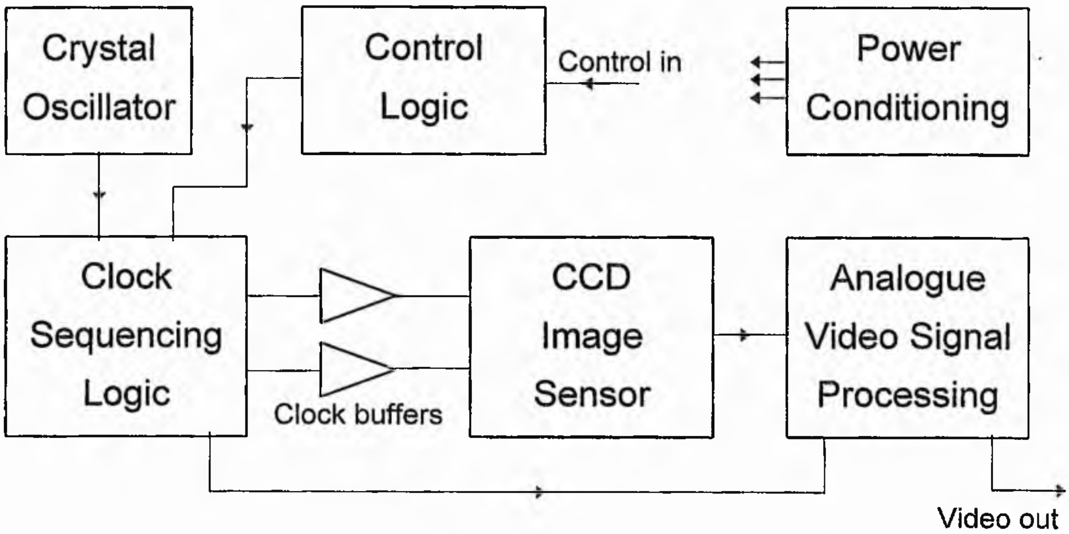

Figure 4.2.1a **Typical CCD camera block diagram.**

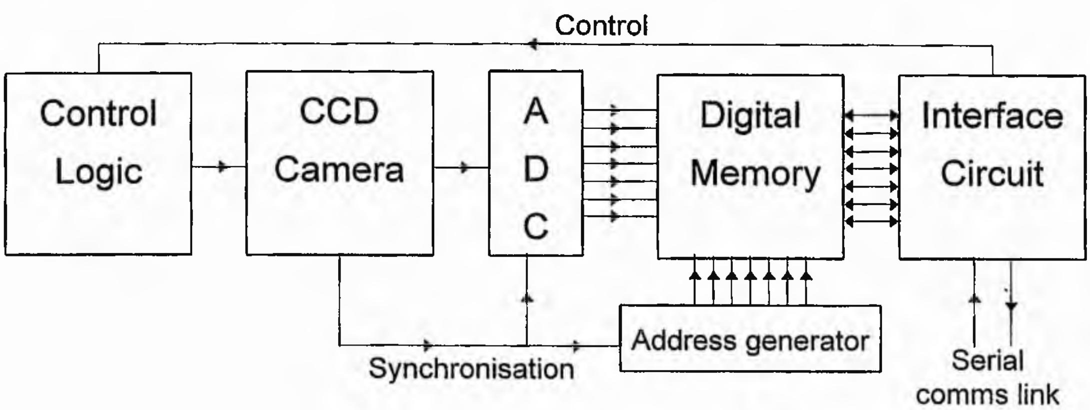

Figure 4.2.1b **Typical block diagram of a digital still camera.**

The video processing was simple, consisting of two high speed op-amps, amplifying and level-shifting the signal so that it could be accepted by the analogue-to-digital converter. No separate sampling was implemented apart from the implicit action of the ADC itself. This resulted in a relatively noisy signal without sharp contrast between pixels. The output of the CCD was DC-coupled to the op-amps, making the camera very susceptible to the temperature drifts of the CCD's output FET amplifier (see section 5.3.4). During development, the camera had remained essentially at room temperature and these drifts had not been apparent, only becoming obvious during thermal testing late in the programme. At this stage there was little time and no room on the board to implement AC-coupling and black-level restoration. Eventually, a compromise solution was achieved by biasing the circuit to operate nominally at its expected orbital temperature of 5°C, allowing the camera to produce images between -10°C and 20°C without drifting out of the ADC's range. This temperature drift represented the greatest potential problem to retrieving images from the camera in orbit.

The optics were something of an after-thought given the author's natural emphasis on electronics. The lens was designed in-house using a pair of catalogue-ordered aspherical elements, resulting in poor definition and significant spherical aberration, causing the edges of the image to be out of focus. Off-the-shelf optics have been used for all subsequent missions.

The digitised signal from the camera was clocked into a buffer memory which was located in the module tray. The separation between the two halves of the circuit caused a loss of signal quality, particularly to the crucial CCD clocks which would pick up noise and cross-talk along their long signal path through the wiring harness. This physical division of the sensor circuitry and the digital logic was soon realised to be a major flaw in the implementation of the UoSAT-4 imager.

Once the data was stored in the image memory, it needed to be transferred to the transputer unit. As will be discussed in section 6.1.2.1, the camera communicated with these processors over a high speed serial link (an Inmos link). The camera logic hardware interpreted the bytes sent by the transputers to activate a number of operational modes (standby, capture image, dump image memory, load test pattern), working reliably although inflexibly.

Apart from the problem of temperature drift, the overall performance of the UoSAT-4 camera was reasonably good given the use of discrete technology and the author's inexperience. Certainly, it provided a valuable learning experience, directly contributing to the enhanced capabilities of the following generations of camera. Many of the techniques employed in the later imaging systems were used for this mission, or were developed in direct response to problems encountered. The fact that virtually none of the circuitry used on UoSAT-4 was carried over to UoSAT-5 attests to the rudimentary performance of the camera and to the rapid learning curve that the author was subjected to during this period. Indeed, the need for this rework was so evident at the time that it would have taken place regardless of whether UoSAT-4 had operated in orbit or not. Therefore, the experience of this campaign was valuable even though the instrument never produced any data in orbit.

Figures 4.2.1c through f show some representative imagery collected by the UoSAT-4 engineering and flight model cameras. Figure 4.2.1c displays one of the first images recorded by the engineering model camera. The poor contrast and very pronounced striping (caused by noise injected via the power supplies) testifies to the very rudimentary performance of this system. These factors were addressed and improved for the flight model camera (figures 4.2.1d to f). Nevertheless, the image quality and specifications are modest compared to those of the author's subsequent cameras.

Figure 4.2.1c

Picture from the UoSAT-4 engineering model camera.

Figure 4.2.1d

Picture from the UoSAT-4 camera of UoSAT-3 in SSTL clean room.

Figure 4.2.1e

Picture from the UoSAT-4 camera in the lab.

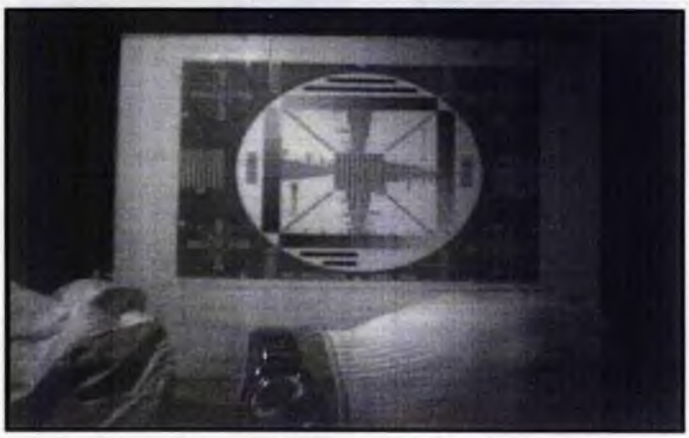

Figure 4.2.1f

Picture from the UoSAT-4 camera.

4.3 THE UOSAT-5 CAMERA AND TRANSPUTERS.

The failure of the UoSAT-4 spacecraft shortly after launch in January 1990 was very disappointing at the time. Following the UoSAT-4 failure review, extensive redesign took place for most of the UoSAT-5 housekeeping and payload systems, but the imaging modules probably received the most attention. A new CCD sensor was chosen, virtually none of the circuitry was retained from the UoSAT-4 camera, and the scope of the system was expanded to include microprocessor control.

Fortunately, the simultaneous UoSAT-3 mission was very successful, carrying the first commercial version of the store-and-forward communication system, and generated sufficient commercial and scientific interest to support the UoSAT-5 mission. The original intention of UoSAT-5, launched in July 1991, was to re-fly the experiments carried by UoSAT-4, but it soon evolved into a far more substantial and coherent mission.

4.3.1 THE UOSAT-5 CAMERA.

The Fairchild sensor used on UoSAT-4 was replaced with the CCD04-06 from EEV Ltd.; the selection process of this device is reviewed in section 5.2.2.3. This device produces an output signal compatible with the CCIR 625-line television standard. The sensor uses the frame-transfer technique, and has a 2/3" format imaging area with 578 x 576 pixels arranged as two interlaced fields of 578 x 288 pixels. However, the format of a digitised image is 611 x 576 due the sampling of dummy pixels at the start and end of each image line. Only 568 x 560 pixels of this contain genuine image data. Because of the rectangular dimensions of each pixel, the final image has an aspect ratio of 4:3, and not 1:1 as the numbers of pixels might suggest. The sensor incorporates anti-blooming (to prevent sensor saturation) and electronic integration control (i.e. exposure control) as integral features, improving overall image quality and flexibility of operation compared to sensors used on missions before UoSAT-5.

Apart from the sensor's physical attributes, the availability of support chips to fulfil the various building blocks, and EEV's willingness to provide technical support made it an attractive choice. In addition to the CCD, four dedicated chips obtained from EEV fulfil the circuit functions of the camera identified in figure 4.2.1a: a sequencing logic chip, a clock driver for the high capacitance vertical clocks, another clock driver for the high speed horizontal register clocks, and a video processing chip. Using the CCD's chipset vastly reduces the size of the camera, allowing all the camera electronics to be accommodated within the satellite's battery box.

The cumbersome logic circuit of UoSAT-4 (counting some 25 integrated circuits) is replaced by a semi-custom gate-array supplied by EEV which produces all of the waveforms needed to drive the camera. In addition to the clocks for the CCD, there are a number of other reference signals available which are used to synchronise the ADC and the image buffer memory with the pixel flow from the CCD. The timing of all of these signals adhere to the CCIR 625-line standard and are derived from a specific crystal reference.

The clocks to the CCD are buffered by two current amplifiers to isolate the logic chip from the large capacitance of the CCD. The output from the CCD is sampled, amplified, clamped, DC restored, and blanked by the video-processing hybrid to produce a composite video signal that can drive a 75 Ω monitor input directly. Although not specifically required for a satellite remote sensing camera, the ability to drive a monitor can be useful in bench-testing and calibration. The gain and black level of the composite output are adjustable by trimming resistors.

From the continuous stream of analogue video, a single frame (comprising two fields) is digitised by an analogue-to-digital converter. This ADC is a Sony CXD1175 two-step flash converter specifically designed for sampling video signals. Although higher performance ADCs are available, the low power consumption of approximately 90 mWatts (full flash ADCs can consume anything from 300 mWatts to 5 Watts) and low cost of the CXD1175 makes it ideal for use in a microsatellite system.

The pipeline of components described above (excluding the ADC) is identical to that used in EEV's range of commercial CCD cameras. These cameras include a fifth support chip to perform various additional signal processing functions like gamma correction and automatic gain control, but which are not of any specific benefit in the context of a remote sensing camera.

In addition to the basic building blocks provided by the EEV chipset, the board in the battery box also accommodates the switching and linear regulators providing local power conditioning, and various interfaces accepting control parameters. The most important control parameter is the CCD's integration time. A counter circuit, driven by the camera's clocks, produces a pulse delayed from the start of each frame by a time proportional to the value of the 8-bit command word. Varying the delay of this pulse alters the CCD's integration time. The pulse's rising edge is presented to the logic chip, which drives the CCD in the appropriate manner. Two 4-bit commands drive simple digital-to-analogue converters to adjust the high (white) and low (black) reference voltages on the

ADC. The main purpose of this is to trim out any biasing uncertainties or residual temperature drift not removed (or introduced) by the video processing circuitry.[2]

Based on the experience of UoSAT-4, commercial optics is used for the UoSAT-5 camera. This is a 4.8 mm focal length lens from Pentax-Cosmicar, which has low mass, and is compact and inexpensive. Despite the inevitable barrel distortion associated such an extremely wide angle lens, it was chosen to give the widest coverage possible, giving a mean ground resolution of 2 km across 1500 x 1050 km. The camera is fitted with a yellow filter to provide strong contrast between cloud, water and arid terrain. This choice maximises the chance of obtaining interpretable imagery over cloud-free desert regions, despite sacrificing contrast in more temperate (vegetated) regions. The 605 to 615 nm optical filter is perhaps narrower than strictly necessary, but serves its purpose.

4.3.2 THE IMAGE BUFFER MEMORY.

As the pixel rate from the camera is very high, it is not possible for a computer to capture the digitised data directly, so the image is dumped into a buffer memory instead. This memory is multi-ported (triple-ported in the case of UoSAT-5) with a microprocessor, which retrieves the data once captured.

Thus to record an image, the appropriate command powers the camera (issued by the controlling microprocessor). The camera free-runs for around a second to allow the system to stabilise and to clear the CCD of any spurious charge present at power-up. After this, a single frame of the video signal is sampled by the camera's ADC and stored in the image memory. Additional signals derived from the sequencing logic drive the memory control strobes (chip select, write enable) and increment the address counter in step with the arrival of each digitised pixel on the bus.

Once an image has been successfully captured, the camera will turn itself off, to save power (see section 5.3.1), and control of the buffer memory is handed back to one of the transputers, which can then retrieve the contents of the image buffer memory at a more suitable rate. This form of multi-ported memory is the simplest way to convert between the fast pixel rate of the camera and a slower rates suitable for handling by the processor. Arbitration logic, based on the status of various commands, determines which of the camera or the transputers has access to this memory at any given moment. When not

[2] By altering the dynamic range of the ADC with these trim controls, it is possible to effect the gain of the video signal; for this reason these commands are sometimes referred as 'gain control' although this does not reflect their true purpose.

available to the camera, the image memory appears to be in the memory space of one or other of the transputers. This configuration is shown in figure 4.3.2.

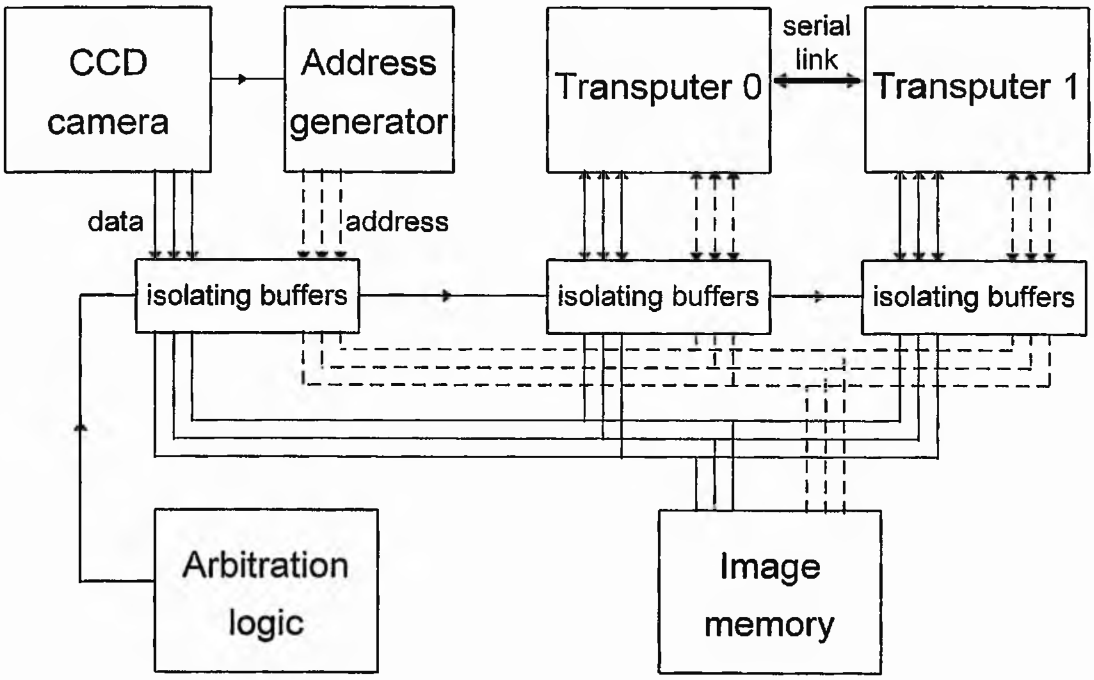

Figure 4.3.2 **Block diagram of UoSAT-5 image memory connectivity.**

The image memory and the camera's address-generating counter are located in the main module tray, and not in the battery box, to minimise the amount of wiring between the two parts of the imaging system. By keeping the image memory in the same box as the microprocessors, it is easy to connect their address and data busses to this buffer.

4.3.3 THE IMAGE PROCESSING TRANSPUTERS.

Although the circuitry is entirely different between the UoSAT-4 and UoSAT -5 cameras, they both have the same basic block diagrams of all digital still CCD cameras, reflecting the configurations shown in figures 4.2.1a and b (5.2.1a and b). Conversely, the hardware interface of the UoSAT-4 camera was quickly abandoned, and it was logical to place the camera's image memory directly in the memory space of a microprocessor. For this reason, the author developed the transputer circuits for the UoSAT-5 imaging system.

The role of these processing elements is discussed in some detail in chapter 6. Briefly, placing the camera circuitry under direct microprocessor control gives the imaging instrument added versatility and flexibility to operate in different, and sometime unforeseen, modes. Furthermore, a dedicated image processing unit can be used to support the primary on-board computers, relieving them of the data-intensive tasks associated with image manipulation. Certainly, from the time of UoSAT-5, there has been a desire to implement on-board image compression to overcome some of the limitations of the microsatellite's restricted communications channels. The close coupling of image sensors and high performance microprocessors has therefore been a feature of SSTL's imaging systems since this time. Chapter 7 covers the application of in-orbit image processing and compression implemented during this research programme.

The primary processing element of the UoSAT-5 imaging system is the transputer 1 (T1) module. Transputers are 32-bit microprocessors, allowing them to manipulate the large arrays of image data with ease. In addition to having access to the camera's image buffer memory, T1 has 2 MBytes of its own static memory for programme code, variables and imagery. This memory is fully protected by hardware error-detection-and-correction circuitry to protect the processor's integrity despite the incidence of radiation-induced memory upsets. (The design of the transputers for the UoSAT-5 and subsequent missions is described in much greater depth in chapter 6).

Therefore transputer 1 fulfils all of the processing tasks associated with image collection: scheduling the events in response to time-tagged commands from the ground (via the main OBC), supervision of camera operations, collection, processing, packing and transmission of captured data to the OBC. In addition to activating the camera and collecting the image data, the transputer must also set parameters to control the camera's exposure settings (the integration time, and the white and black thresholds of the ADC) prior to capture.

A second transputer (T0) is also used included in the module tray. This processor is equipped with less memory (only 16 kBytes of radiation-hardened silicon-on-sapphire SRAM) and fewer features, making it less versatile but also more reliable. T0's role is therefore to act either as a co-processor to T1 for parallel processing, or as a back-up to support basic image capture in the event of T1 failing.

Therefore, the main module tray contains a number of different sub-systems. Transputer 1 requires half of the available space; Transputer 0 occupies a quarter of the board; the image memory, camera's address counters and the various isolating buffers take up the remaining quarter of the module.

4.3.4 RESULTS OF THE UOSAT-5 IMAGING SYSTEM.

By the time the UoSAT-5 mission was launched, the UoSAT project had been attempting to demonstrate imaging for over a decade, and there was considerable internal pressure to succeed. Fortunately, ten days after launch, the team's perseverance was rewarded by imagery with detail and quality that surpassed all reasonable hopes and expectations. After one featureless over-exposed image, the first scene successfully recorded by the UoSAT-5 camera was of Italy, Sicily and Sardinia shown in figure 4.3.4a. After the murky shapes of the UoSAT-1 and -2 images, the scenery recorded in this single UoSAT-5 image was indisputable. [3]

The quality of this first image was confirmed by hundreds of others of scenes around the World, becoming the first convincing demonstration of the feasibility of using microsatellites for Earth observation. A practical application of this imagery for environmental monitoring was revealed almost at once in the summer of 1991, when UoSAT-5 images recorded the pollution from the aftermath of the Gulf War. Figure 4.3.4b is one of a sequence of images showing the smoke plumes from the Kuwaiti oil fires extending more than 700 km across the Arabian peninsula towards Qatar. The progress made in extinguishing the well-fires from the launch of UoSAT-5 in July 1991 to the end of the year was recorded by the cameras. On a weekly basis, the range of the smoke was visibly reduced as control of the situation was regained. Furthermore, variations in the prevailing winds on each occasion can be determined by the direction of the plumes relative to their source. In this particular image, the altitude shear of the wind is marked by the sudden change in the plume's heading. Another image in September of that year, figure 4.3.4c, is centred on Iraq showing the fertile valleys of the Tigris and Euphrates rivers. Kuwait is partially obscured by the satellite's antenna in the lower-right of the image, but the smoke plumes clearly have a different coverage pattern.

Figure 4.3.4d shows an image of the English channel recorded in May 1992. The alluvial basins around London and particularly Paris are very distinct, as are the Ardennes mountains in southern Belgium. It is interesting to contrast the features resolved by the UoSAT-5 camera's yellow filter (605 to 615 nm) as opposed to PoSAT-1's red filter (610 to 690 nm) shown in figure 4.5.2b.

---

[3] The two protruding objects in the image are the satellite's antennas which encroach on the camera's field of view - another difficulty of operating within the small confines of a microsatellite.

These are just a few examples of the imagery captured by the UoSAT-5 camera. While the imagery contains certain defects, such as a higher than desirable noise floor and marginal pixel-to-pixel definition (perhaps loss of focus), the data from this instrument provided the first irrefutable demonstration of microsatellite remote sensing capabilities. Several hundred images have been collected by UoSAT-5, all of which have demonstrated a consistency of operation and image quality necessary for commercial usage.

For the satellite's first year in orbit, imagery was scheduled and collected on a daily basis, with minimal disruption to routine service. Since then, the UoSAT-5 camera has been operated less and less frequently for a number of reasons. Firstly, the downlink is completely saturated with amateur store-and-forward traffic, limiting the effective retrieval rate to only one image a week. Secondly, for the last year, the spacecraft has been used as a test-bed for new in-orbit attitude control routines (see section 3.3.5.2), occupying many of the on-board computer's resources required to support imaging. Nevertheless, efforts are made to exercise the camera at sporadic intervals simply to verify that all the circuitry continues to function. On each occasion, the performance is consistent.

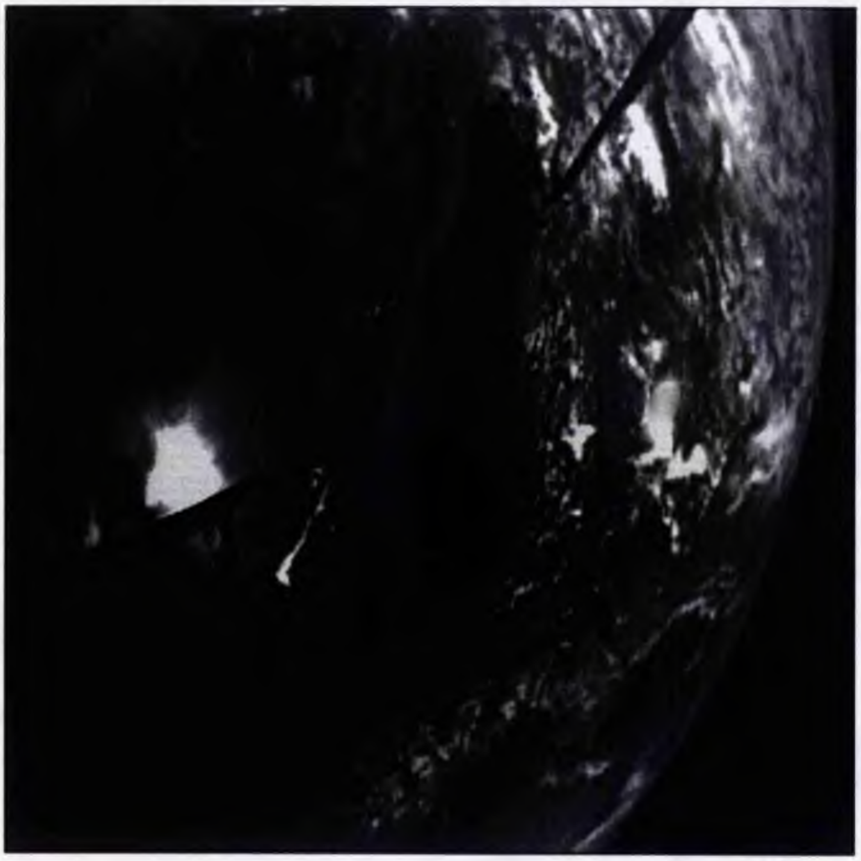

Figure 4.3.4a

UoSAT-5's first image - Italy.

Figure 4.3.4b

UoSAT-5 image of smoke over the Persian Gulf.

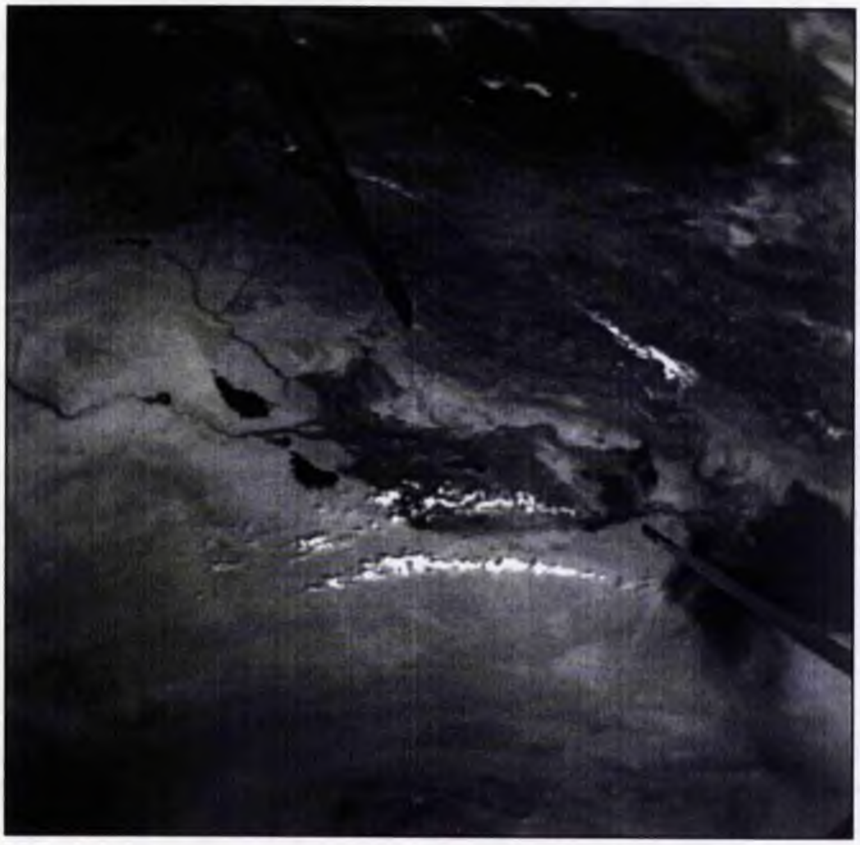

Figure 4.3.4c

UoSAT-5 image of Iraq and smoke over the Persian Gulf.

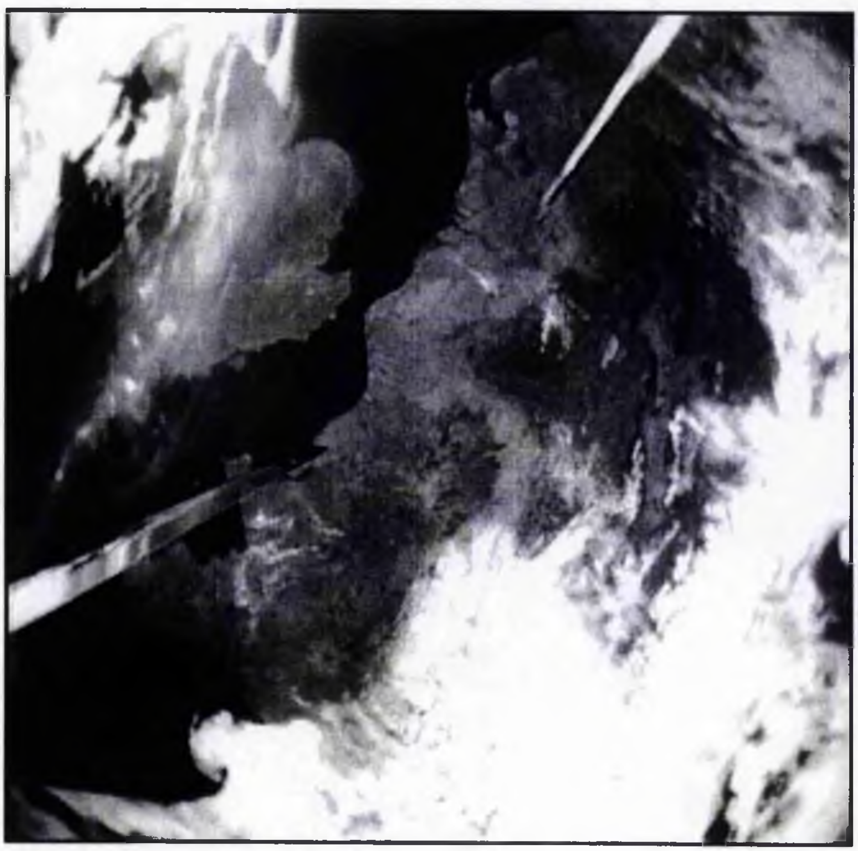

Figure 4.3.4d

UoSAT-5 image of England, the Benelux, and northern France.

4.4 THE KITSAT-1 CAMERA AND TRANSPUTERS.

Following the success of the camera on UoSAT-5, the imaging system has become one of the most popular payloads on SSTL's technology transfer missions. In addition to having an interest in developing low-cost remote sensing, these customers also find the cameras attractive because of the immediate impact and interpretability of images from space by a wide public in their home audiences. In many ways, this has been fortunate for the development of SSTL's imaging capabilities, as continuing funding has been secured easily. Furthermore, the technology transfer customers are often encouraging in the use of new technology following the author's suggestions, provided it endows the imagers with visibly enhanced characteristics (i.e. generally possessing higher spatial resolution).

Since the massive redesign of the UoSAT-5 imaging system, there has been a hesitation to modify the circuitry too much, due in part to minimising the risk associated with untried design, and also to fit within the very short time scales discussed in section 4.1.2. Therefore, there have been three drivers for change from mission to mission: firstly, to deliver the customer with apparently enhanced image specifications, dictating changes of varying impact. Secondly, configurational changes to improve modularity and production, preparing for SSTL's future imaging requirements. Thirdly, minor alterations and up-grades to improve the camera's performance in some engineering aspect like image noise, power consumption, fault-tolerance or operational flexibility. In the development of successive imaging systems, the author has learned that the effort in reworking the imaging system should be expended in the order of this list, as this provides the best return on investments. Certainly, there have been instances where the author has pursued technical improvements (particularly in noise and power performance) which have gone entirely unnoticed by the rest of the World. It also follows that the most obvious changes are not necessarily the most difficult to achieve.

4.4.1 THE KITSAT-1 CAMERA.

The most noticeable enhancement for the KITSAT-1 mission (launched August 1992) was the introduction of a second EEV CCD04-06 sensor to the existing camera. This was accomplished by modifying the basic CCD camera architecture used for UoSAT-5 (shown in figure 4.2.1a) to that shown in figure 4.4.1. The same clock signals from the sequencing logic drive both CCDs in synchronism, although separate buffers are used. A video speed analogue multiplexer switches the input of the video processing hybrid between the output signal of the two sensors. When the camera is activated, a predetermined hardware sequence captures one field from both sensors and stores them in an appropriately partitioned buffer memory. Although the images are recorded some 100 ms apart, they can be considered simultaneous for most applications.

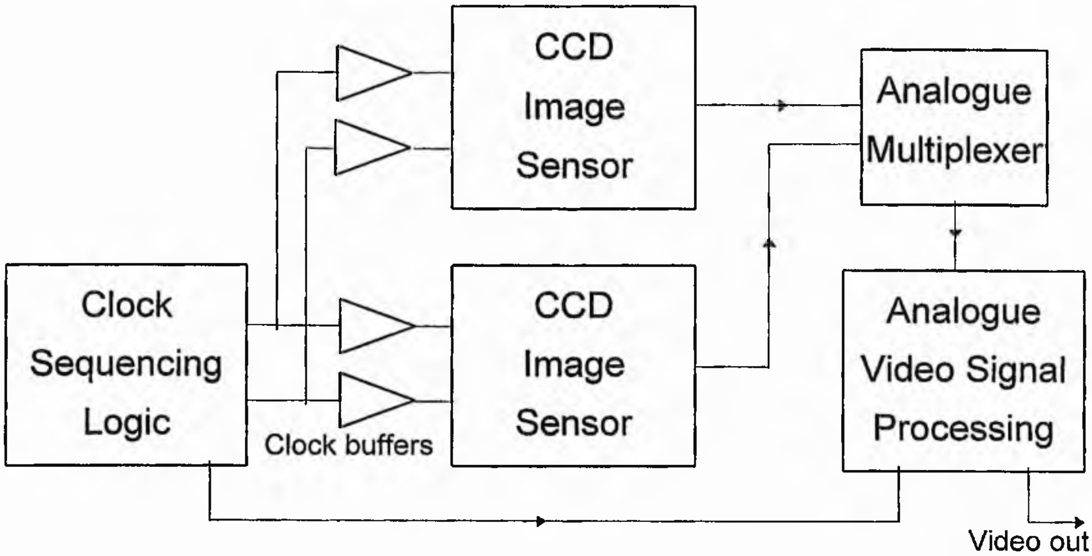

Figure 4.4.1 **Block diagram of KITSAT-1 camera.**

The topology of this imager is clearly a single circuit, equipped with twin sensors. In practice it means that the two sensors cannot be operated independently, and must always use the same exposure settings. A failure will almost certainly disable both sensors. Conversely, this approach was the only way to accommodate another imager within the cramped confines of the spacecraft's battery box.

On KITSAT-1, the two sensors were fitted with different lenses and presented as the Wide and Narrow Angle Cameras (WAC and NAC), although they obviously share a lot of circuitry. The WAC uses the same wide angle 4.8 mm lens as carried on UoSAT-5, but the NAC is fitted with 50 mm focal length optics to achieve a higher ground resolution but over a narrower swath width. Given the volume restrictions, it was not feasible to use an authentic 50 mm lens for the NAC, because this would interfere with the spacecraft's clamp-band (which must deploy to separate the satellite from the launcher). Instead, a 25 mm lens with a 2x focal length extender was employed to provide a more compact solution, despite some loss of optical quality; fortunately the Earth is sufficiently bright to illuminate the CCD adequately despite the reduced of sensitivity caused by the range extender.

From KITSAT-1's 1300 km orbit, the WAC and NAC have 3.5 km and 350 m resolution respectively, with coverage areas of 2550 x 1800 km and 220 x 160 km. The WAC is fitted with a near-IR optical filter to provide maximum contrast between land and sea, but with less sensitivity to terrain variations. Conversely, the NAC's red filter highlights these differences.

With this dual-sensor topology it would be possible to fit the CCDs with identical lenses but with different optical filters to give a limited multispectral capability. (The red and near-IR bands would be the most natural choice, providing 'vegetation index' data). However, the system's resolution would need to be kept fairly coarse to minimise the effect of the delay in capturing the images from the two sensors. This dual-spectral option was offered to the Korean customers of KITSAT-1, who chose the Wide and Narrow configuration instead.

4.4.2 THE IMAGE BUFFER MEMORY.

The most significant rework to the imaging system implemented for the KITSAT-1 imager went virtually unnoticed by most onlookers, yet was very important in the development of SSTL's remote sensing capabilities. Rather than use the UoSAT-5 technique of dumping the imagery directly into the transputers' address space, it is gathered by a microcontroller which interfaces with the transputers over serial links. The rationale behind this architectural change, and the subsequent evolution of the image memory and microcontroller configuration are detailed in some depth in section 6.1.1, so there is no point in pre-empting this discussion here.

The advantage of introducing the microcontroller was to increase the system's modularity, separating the transputers and the electronic camera into distinct units. The benefits of this modularised approach were limited on KITSAT-1, but the advantage of clean and simple interfaces was identified as necessary for future expansion of the imaging system. In particular, the parallel interface between the image memory and transputer would make the inclusion of additional sensing units extremely difficult. Conversely, by using serial links for all interfacing, this expansion has become straight forward. Similarly, the system is far more fault-tolerant, isolating failure to within a given sub-system. This isolation is highlighted by the block diagram, shown in figure 4.4.2.

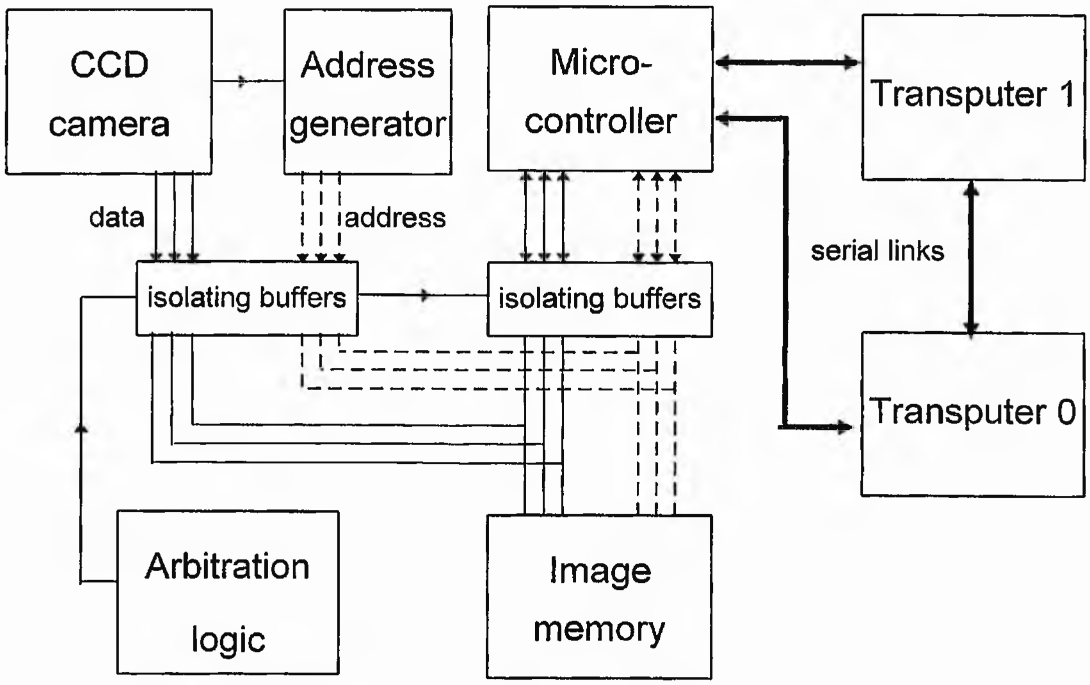

Figure 4.4.2 Block diagram of KITSAT-1 imaging system connectivity.

4.4.3 THE IMAGE PROCESSING TRANSPUTERS.

Despite numerous small changes to improve the reliability and operational flexibility of the transputer modules, the casual observer would notice no substantial systems changes between UoSAT-5 and KITSAT-1. The principal changes involved the redesign of Transputer 1's error-detection-and-correction system, and various modifications reducing the quiescent current consumption by around 0.5 Watts.

4.4.4 RESULTS OF THE KITSAT-1 IMAGING SYSTEM.

The KITSAT-1 mission has been entirely operated from the control station in South Korea. For this reason, the author has relied on the intermittent efforts of the Korean team for results. Nevertheless, the camera has been operated around 200 times since the satellite's launch, capturing some very impressive images of various parts of the Earth (though most frequently of the Korean peninsula). These few dozen decent images testify to the efforts made to improve the cameras' noise performance, reducing the noise floor to the amplitude of the analogue-to-digital converter's least significant bit.

When the KITSAT-1 imager has been operated successfully, the data recorded has confirmed the results from UoSAT-5 regarding the suitability of microsatellites for meteorological scale imaging. Indeed, the KITSAT-1 system is more suitable for this application, given its higher altitude and correspondingly wider field of view, its near-IR sensitivity and its superior noise performance.

A good example is shown in figure 4.4.4a, captured by KITSAT-1 in October 1992, revealing a virtually cloud-free sky over coastal China and the Korean peninsula. The cloud formation over Japan is particularly interesting with the clouds matching closely the shapes of the islands, including the outline of the peninsula to the north-east of Tokyo. This is presumably caused by a cloud \ mist \ fog build-up at night that has been blown eastwards after the land has warmed again with the new day. Land features such as the Yangzi river and the lakes near Shanghai are clearly discernable.

The distinct land-masses of the Mediterranean Sea are very recognisable and are therefore often used as targets during the commissioning of the SSTL imaging systems. Figure 4.4.4b was the first intelligible image captured by the KITSAT-1 system after the satellite had achieved attitude stabilisation. Although it is slightly over-exposed, the coastlines shown in this image are very distinguishable. This image and the UoSAT-5 image of the same region (figure 4.3.4a) permit a direct comparison of the difference in resolution and field of view between these two imagers.

Whereas the KITSAT-1 Wide Angle Camera (WAC) confirmed the results of UoSAT-5 by further demonstrating the suitability of microsatellites for meteorological scale imaging, the Narrow Angle Camera (NAC) demonstrated the possibilities of achieving higher spatial resolutions. Figures 4.4.4c and d show a pair of images captured simultaneously by the two instruments in March 1993. The WAC image in figure 4.4.4c covers the whole of Central America from Mexico to Panama. The scene viewed by the NAC covers the central 10% of this area. In figure 4.4.4c, it is possible to resolve the thin white line of the Sierra Madre mountains, the dark line of the reservoir at La Concordia (Chiapas State, Mexico) and the black dot of lake Solola (Guatemala). The NAC image of figure 4.4.4d provides much greater detail of this area, revealing terrain patterns not discernible at the WAC's coarser resolution. Note the cumulus clouds forming along the ridge of the coastal mountain range.

Figure 4.4.4a

KITSAT-1 wide angle image of Japan, Korea and coastal China.

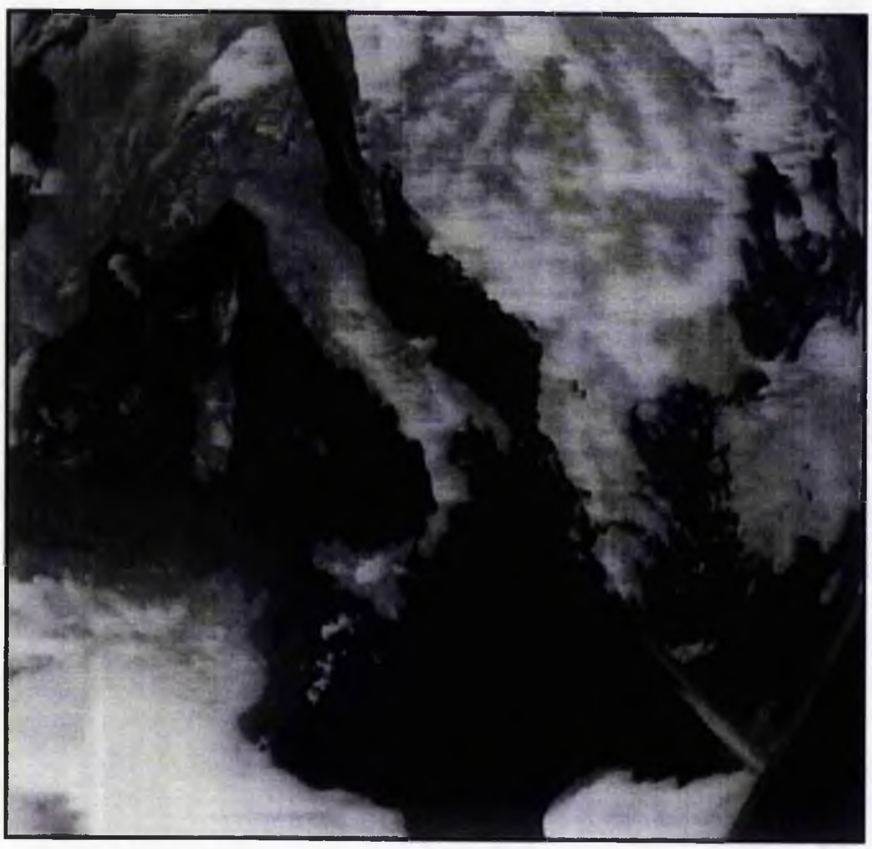

Figure 4.4.4b

KITSAT-1 wide angle image of the Mediterranean.

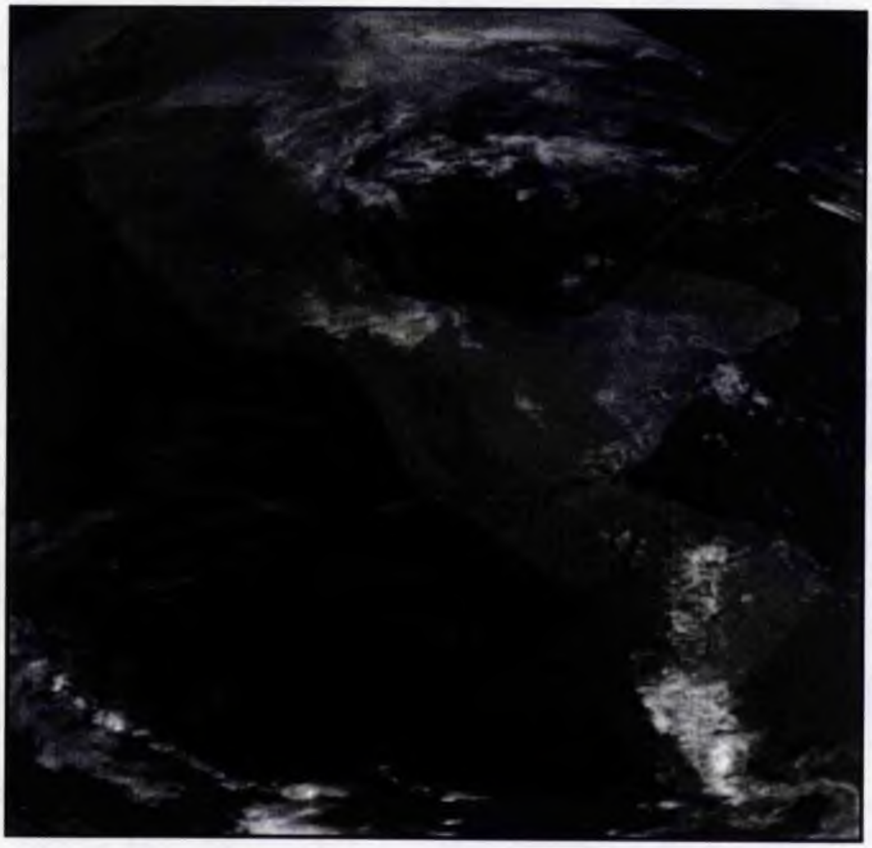

Figure 4.4.4c

KITSAT-1 wide angle image of Central America.

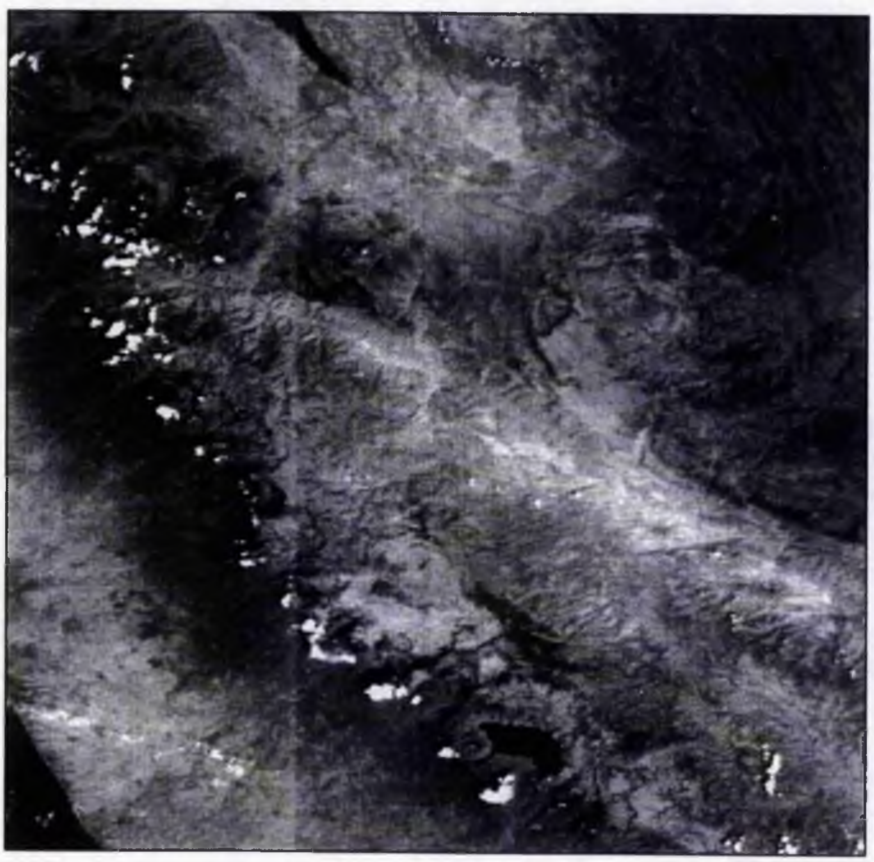

Figure 4.4.4d

KITSAT-1 narrow angle image of Guatemala.

4.4.5 THE KITSAT-2 IMAGING SYSTEM.

The KITSAT-2 microsatellite, launched in September 1993, was built as the final phase of the technology transfer programme between SSTL and its Korean partners, KAIST. Since it was built entirely in Korea, the author was not involved with the project in any practical way, although the satellite was assembled using designs and from kits of parts provided by SSTL.

The Korean team retained the design of the camera based on the EEV CCD04 used for KITSAT-1 to implement the Narrow Angle Camera on KITSAT-2. In theory, this camera should have had very similar performance to that of the PoSAT-1 camera built concurrently at Surrey (described in the next section). However, the results presented in [Yoo et al], and other imagery that the author has seen, shows that quality of the KITSAT-2 data is inferior to that of KITSAT-1 and PoSAT-1, stressing that although the cameras use commercially available building blocks, these are nonetheless sensitive analogue components.

Unbeknownst to each other, both the SSTL and the KAIST teams exploited the increased modularity offered to the KITSAT-1 imaging system resulting from adding the microcontroller unit, by adding an additional electronic camera. In the case of KITSAT-2, this new camera replaced the WAC, with an equivalent camera using a Samsung / Sony sensor. This sensor used a colour mask of the type described in section 5.4.4.3.5. In the author's opinion, the results from this 'colour' camera are about as good as can be expected from this type of CCD.

4.5 THE POSAT-1 CAMERA, STAR SENSOR AND TRANSPUTERS.

Given the very short delay between the KITSAT-1 and PoSAT-1 missions, as well as the very heavy loading on SSTL personnel (three microsatellites were built in parallel that year), it is not surprising to find that the imaging systems on these two missions are very similar. Apart from a few minor alterations to reduce noise, the two transputers and the dual-sensor Earth imaging camera were essentially identical to the KITSAT-1 systems.

In line with the comment made for KITSAT-1, the principal requirement for SSTL's Portuguese customers regarding the Earth imaging cameras was increased resolution from the Narrow Angle Camera. For the reasons already discussed for KITSAT-1, is was not feasible to equip the NAC with a lens with a focal length longer than 50 mm without attempting folded optics, a difficult task given the increasingly cramped conditions in the battery box. Fortunately, PoSAT-1's 800 km orbit is at virtually half the altitude of KITSAT-1, and has provided the necessary magnification.

Although the transputers and the Earth cameras remained largely the same, substantial effort was devoted to adapting the design of the successful cameras into a star imager. Furthermore, the PoSAT-1 transputers also support a GPS (global positioning system) receiver, which provides the satellite with a capability to detect its orbital position autonomously. The author was not involved in the hardware or software of the GPS system, but needed to modify transputer 0 to accommodate the receiver's basic requirements. To this end, T0's memory was increased to 1 MByte; this memory is neither protected by error-correction circuits nor is radiation-hardened silicon-on-sapphire, but uses commercial RAM known to have significantly better-than-average radiation tolerance (demonstrated on previous SSTL missions).

The communications topology of the transputers, Earth imaging cameras, star camera and GPS receiver is shown in figure 4.5. In practice, T1 handles all imaging activities, and T0 supports the GPS receiver; a small software routine on T0 straps the links to the star camera and to T1 together.

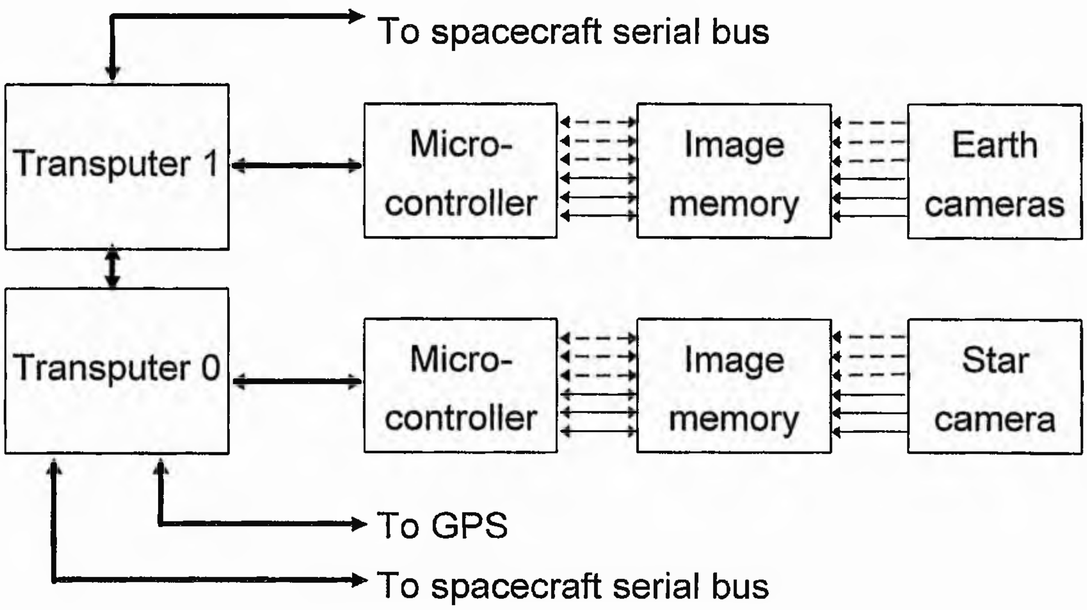

Figure 4.5 **PoSAT-1 transputer and imager connectivity.**

4.5.1 THE POSAT-1 STAR CAMERA.

Although, the development work towards the PoSAT-1 star camera was a side-step from the main thrust of this research programme, it nevertheless demonstrated the adaptability of the systems developed. The modularity and use of serial links made it possible to accommodate this new star sensing module with minimal disruption to the existing systems. The entire camera and microcontroller unit were duplicated schematically, although the physical lay-out was very different. Only a few modifications were required to give the star camera sufficient sensitivity to detect faint stars: the camera's crystal oscillator was slowed to lengthen the integration time to 150 ms, a non-linear transfer function was applied to the video signal to devote more of the ADC's grey levels to the dimmer stars, and a very bright 50 mm *f*/ 1.4 lens was fitted.

Although at a tangent from the main thrust of the author's research programme into low-cost remote sensing of the Earth, the star camera experiment has generated significant interest from the industry at large. In many ways, it epitomises SSTL's approach to low-cost spacecraft engineering; the cost of the PoSAT-1 star camera, which granted is an experiment rather than an operational system, was in the region of £10,000 including labour. This contrasts with other 'low-cost' star cameras from the traditional space industry, which are quoted at around $1 million, despite similar (commercial) components and performance. The author and other members of SSTL receive frequent enquiries regarding this star camera, largely because it offers a direct comparison between the cost of SSTL's technology and traditional systems.

Furthermore, the need to sense faint stars forced the author to analyse the noise performance of the CCD sensor, and the camera as whole. This analysis has provided an insight into the potential problems that may be encountered in low-light and any other sensitive Earth observation measurements that may be required in the future.

Examples of the data from the star camera can be seen in section 5.6.5.1. For further information of the PoSAT-1 star camera, consult [Leitmann et al, 1993] and [Leitmann et al, 1994]. At the time of writing, an upgraded version of the PoSAT-1 star camera is being developed for use as an operational sensor on SSTL's forthcoming UoSAT-12 minisatellite mission. The author will be responsible for the hardware of this sensor, and is participating in the development of fast star identification and pattern matching algorithms for autonomous in-orbit operation.

4.5.2 RESULTS OF THE POSAT-1 IMAGING SYSTEM.

The cameras on PoSAT-1 have again confirmed the suitability of using CCD imagers on microsatellites for meteorological scale imaging. Since the satellite's launch in September 1993, over 8000 images have been collected by the cameras, at a daily average of around 15 to 20 images being scheduled at the time of writing. The low-noise, high contrast and sharp focus of the PoSAT-1 cameras provides a convincing and, in the author's opinion, conclusive demonstration of the feasibility of microsatellite remote sensing.

Figure 4.5.2a is a PoSAT-1 image of Iraq and the Persian Gulf, taken in January 1994, after the Kuwaiti oil fires had been extinguished. Much of the area that was masked by the thick smoke in the UoSAT-5 image of the same area (figure 4.3.4b) is now visible. The only signs of the environmental aftermath of the Gulf War are the occasional dark patches (e.g. the crescent to the south-west of Kuwait city) on the otherwise bright desert terrain. These dark areas lie around the main oil wells and are caused by a combination of the staining of the sand by spilled crude oil and to the continuous thick smoke from the flares of functional wells.

On a more general note, these images from UoSAT-5 (figure 4.3.4b and c) and PoSAT-1 (figure 4.5.2a) clearly show the improvements in camera performance achieved between the two missions. The PoSAT-1 image has sharper definition, better contrast and lower background noise than its predecessor.

Another typical image captured by the PoSAT-1 Wide Angle Camera is shown in figure 4.5.2b, when the microsatellite recorded the North Sea beneath it in October 1993. The image shows (counter-clockwise from top left), Britain and Northern Ireland, northern France, the Benelux countries, northern Germany, Denmark, Sweden and Norway. Water appears dark, land in mid-greys and clouds in bright white. It is very rare for the sky to be this clear over northern Europe, especially at this time of year. Most days, much of the land would be obscured by thick cloud. Bands of cloud are visible over central France and Norway. The spatial resolution of the camera can be ascertained by inspecting the coastlines and identifying features like the Isle of Wight, Jersey and Guernsey, the Thames and Severn estuaries, the Wash, the Humber, the Firth of Forth and Lough Neagh in northern Ireland. On the continent, the Rhine, Schelde and Elbe estuaries or the Ijsselmeer in the Netherlands are distinctive features.

This image reveals the camera's ability to detect differences in the type of land cover. For example, London is slightly darker than the surrounding countryside because there is less vegetation (which is a strong reflector of near-infra red light). Similar effects are visible for Birmingham and Bristol, and more clearly for Brussels, Gent, Namur and Liege in Belgium, and Hamburg in Germany. The camera's sensitivity also detects agricultural variations. The recent polders around the Ijsselmeer are less fertile (and therefore darker) than the surrounding, more established farmlands. Similarly, the Franco-Belgian border is traced quite accurately, indicating more intensive land use in Belgium (which appears slightly lighter).

Figure 4.5.2c shows another wide angle image captured by PoSAT-1 in February 1995, on a particularly clear day over the coast of eastern China. The coast can be traced from Xiamen and Fuzhou in the south to Qingdao in the north, with South Korea just visible to the north east. The great Yangzi river stands out prominently as far as Nanjing and more faintly to Anqing, where it vanishes beneath the thick cloud. The Grand Canal can also be traced past the lakes Gaoyou Hu, Hongze Hu, Weishan Hu and Nanyang Hu just before it reaches the Huang He (Yellow) river. Although the Huangpu river is not discernable, the city of Shanghai stands out as a darker patch, contrasting with the highly reflective vegetation of the surrounding countryside. To the east of the large lake Tai Hu, the towns of Wuxi and Suzhou and a number of smaller lakes are also visible. This image can be compared with the KITSAT-1 image (figure 4.4.4a) of the same area.

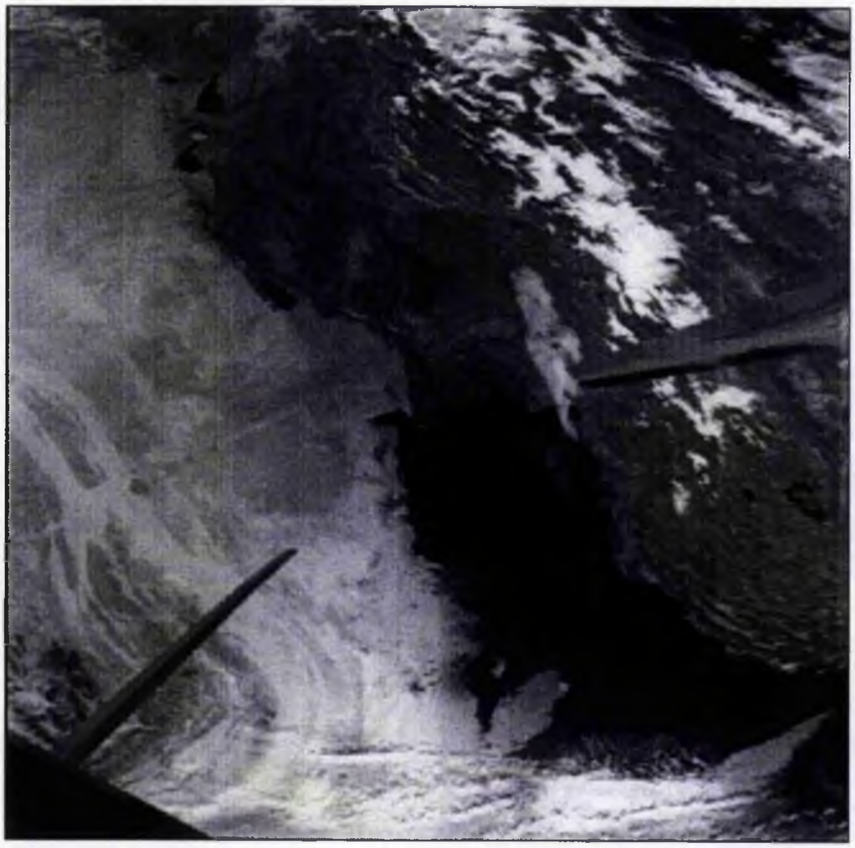

Figure 4.5.2a

PoSAT-1 wide angle image of the Persian Gulf.

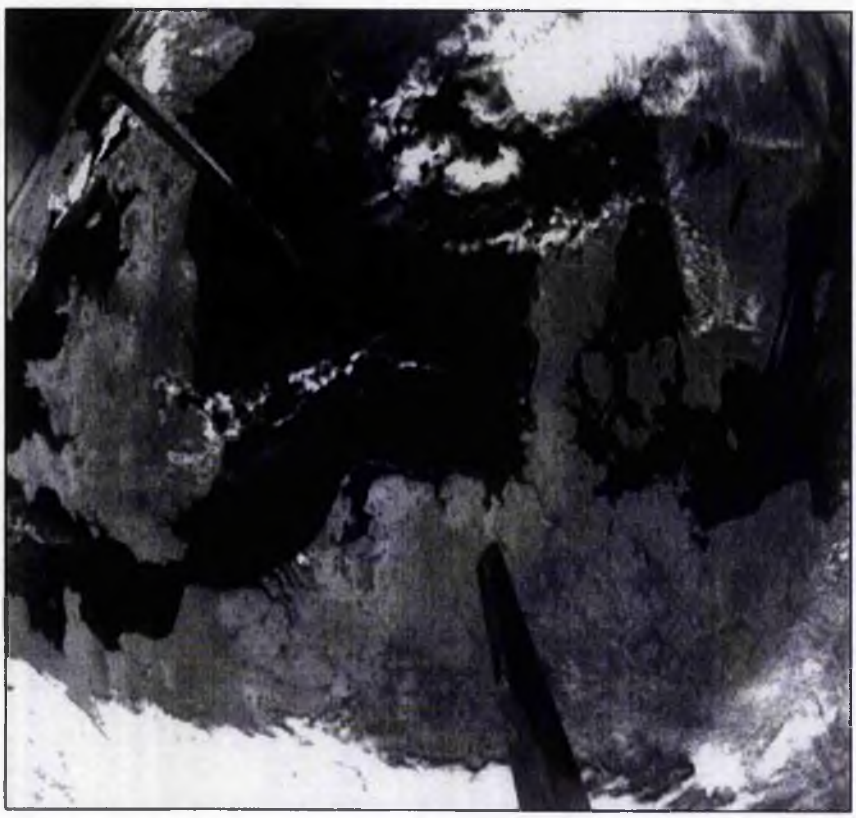

Figure 4.5.2b

PoSAT-1 wide angle image of the North Sea.

Looking at these few representative images, there can be little doubt that the CCD cameras on UoSAT-5, KITSAT-1 and particularly PoSAT-1, have fulfilled their principal task of demonstrating the feasibility of using inexpensive microsatellites for meteorological scale Earth observation. However, it has been the success of the PoSAT-1 Narrow Angle Camera which has generated the most interest to date. Although its resolution is not quite sufficient for some applications (crop monitoring, urban planning, etc.), the NAC has demonstrated that high resolution remote sensing is possible from a low-cost microsatellite, attracting considerable attention from potential customers.

Figure 4.5.2d shows the narrow angle image corresponding to the scene in figure 4.5.2c, effectively serving as an enlargement of the central area of the wide angle image. The complex network of canals around Shanghai stands out clearly, demonstrating the suitability of microsatellite imagery to applications such as hydrology. The Yangzi carries large quantities of sediment, and the swirling patterns either side of Chingming island reveal where the sand is being deposited. Conversely the small lakes to the east of Suzhou appear dark because the water is still and clear, absorbing most of the incident Sunlight. Even though this image was captured in the height of winter, the climate and the fertility of the Yangzi delta is adequate to support extensive crops, principally winter rice, revealed by the low reflectance of the vegetated terrain.

The narrow angle image captured at the same time as the scene in figure 4.5.2a (Persian Gulf), shown in figure 8.2.1a (Kuwait). Unfortunately, when the Wide Angle Camera captured figure 4.5.2b, the Narrow Angle Camera imaged the featureless waters of the North Sea. Many further examples of the imagery from the PoSAT-1 cameras will be displayed in chapter 8 as part of the discussion of some of the applications of this data.

In addition to the hardware demonstrated by this mission, sophisticated image analysis, processing and compression have been implemented in-orbit for the first time. Chapter 7 covers this novel work in full detail.

Overall, the author is very satisfied with the exceedingly high quality of the data and the steady operational performance demonstrated by the PoSAT-1 imaging systems. Beyond all reasonable argument, these images fulfil the 'proof of concept' of the practicality of microsatellite remote sensing systems that forms the main objective of this thesis.

Figure 4.5.2c

PoSAT-1 wide angle Image of coastal China & the Yangzi river.

Figure 4.5.2d

PoSAT-1 narrow angle image of the Yangzi river, Lake Tai Hu, Suzhou & Wuxi (north-west of Shanghai).

4.6 THE FASAT-ALFA CAMERAS AND TRANSPUTERS.

The FASat-Alfa microsatellite represents the most sophisticated system developed to date at Surrey. In contrast to the previous half decade when the production rate was about around two spacecraft per annum, the two years available in which to develop the FASat-Alfa mission appeared luxurious. This interval has allowed the design team to develop and incorporate many new features, systems and concepts into the FASat-Alfa mission. This was done partially to improve the satellite's performance and partially to pave the way for the far more demanding design challenges faced in SSTL's forthcoming minisatellite programme.

From a systems engineering point of view, the key theme in the reworking of the FASat-Alfa sub-systems was modularity, and the imaging units reflect this more than any others; unquestionably, it would have been impracticable to produce a total of eight cameras (four for the engineer model, four for flight) in any other way. Similarly, the first steps were taken towards implementing a fully distributed telecommand and telemetry system on SSTL satellites (see section 2.3.3.3).

Following the success of the imaging experiments on PoSAT-1, it was apparent that Earth observation would place an increasingly large role in stimulating future research and business. To this end, the spacecraft's structure was redesigned (benefiting from the effort deployed in making similar changes to the Cerise microsatellite) as described in section 2.3.3.3. By liberating the whole of FASat-Alfa's Earth-facing surface of large housekeeping systems (i.e. the battery packs and the gravity-gradient boom), this new configuration allows a far more practical deployment of imaging payloads than previously possible. The four separate CCD cameras are discernable on the under side of the satellite in figure 2.3.3.3d.

4.6.1 THE FASAT-ALFA IMAGING PAYLOADS.

Remote sensing was a key objective of the mission statement of the FASat-Alfa microsatellite. Of course, this included the customary Wide and Narrow Angle Cameras, based on the EEV CCD04-06 sensor. As on the previous missions, the WAC is fitted with the same 4.8 mm focal length wide angle lens, although the resolution and field of view are slightly smaller due to FASat-Alfa's 650 km orbit.

The intended spatial resolution of the NAC was further reduced to provide a pixel footprint of 100 x 130 m on the ground. Section 5.1.2.5 describes the measures that needed to be taken to achieve this resolution despite the poorly suited interlaced architecture of the

CCD04-06. The more flexible volume of the FASat-Alfa Earth-facing platform accommodated the 75 mm focal length lens with ease; indeed, there is some scope for mounting even larger lenses within this structure.

Both of the visible cameras were fitted with near-IR filters. The NAC's spectral sensitivity was changed from the red band used previously to provide stronger contrasts for Chilean agriculture and better penetration of atmospheric haze. Furthermore, there was some logic in trying something different; the possibility of merging FASat-Alfa and PoSAT-1 narrow angle imagery to obtain vegetation data was anticipated.

In addition to these regular cameras, FASat-Alfa carried two UV-enhanced systems to investigate the possibilities of using this technology for low-cost sensing of Antarctic ozone concentration and depletion. The UV cameras were fitted with optical filters to provide sensitivity to the 312 to 322 nm (subject to strong ozone absorption) and 375 to 385 nm bands (weak ozone absorption, provides Earth albedo reference). In theory, by subtracting the data of the 380 nm band from that of the 317 nm band it is possible to remove the reflective contributions due to the Earth's surface and atmosphere, leaving only ozone contributions. This is feasible because the albedo reflectance is highly constant over such a small spectral range, whereas ozone has a far more pronounced spectral signature. The near-IR data from the WAC would have supplemented the albedo information.

The author did not make much contribution to the scientific definition of the ozone sensing experiment, which was researched by a Chilean Air Force staff scientist, but was responsible for delivering the finished units. Like the PoSAT-1 star sensor, the FASat-Alfa UV cameras needed increased sensitivity to operate in much lower lighting conditions that the usual visible cameras. Many of the same techniques, such as slower clock speeds to lengthen the integration time and reduce the output signal's noise bandwidth, have been used for the UV cameras. Furthermore, the standard EEV CCD04-06 detectors have been replaced with the pin-for-pin identical CCD02-06 devices; the larger photosite dimensions and the absence of anti-blooming gates, which occupy 40 % of the CCD04's photosensitive surface, doubles the light-collecting capabilities of these cameras. (The CCD02 will be used in future star cameras for the same reason).

The CCDs for the UV cameras needed to be treated with a special organic (lumigen) coating to give the silicon sensors a UV sensitivity. This coating, applied to the photosensitive surface by the manufacturer, fluoresces when illuminated with UV light, re-radiating in the green (i.e. wavelength doubling). Similarly, the optics needed to be made of specialist fused silica materials to overcome the opacity of conventional crown glass at these short wavelengths.

Sadly (as described in section 2.3.3.2), FASat-Alfa has not separated from the main payload and no data has been retrieved from any of the systems. Nevertheless, the rework devoted to the cameras has improved their versatility and manufacture, allowing more ambitious multispectral imaging to be considered on future microsatellite missions. It is therefore appropriate to dwell slightly longer on the hardware of the FASat-Alfa imaging modules. These cameras will be re-flown without any rework on the follow-on FASat-Bravo mission. Of course, the author already has a number of enhancements in mind for the next generation of modular camera.

4.6.2 THE FASAT-ALFA MODULAR CAMERA.

Curiously, by making more room available to the cameras, it has been possible to make them smaller. This has happened by allowing the cameras to take a more natural, and more cubic form, than was previously possible in the satellite's battery box. Each of the cameras is contained in a small milled box with dimensions of 130 x 80 x 60 mm. Effort has been spent on ensuring that the various cameras are as similar as possible, with identical connector pin-outs and mechanical interfaces. While it has been necessary to use quite different lenses for the various cameras, these could all be accommodated by the modular box using a mechanical adapter. With identical mounting points, the only difference to the outside world is the diameter and mass of the lens.

The camera box is made of two mating segments (shown in figure 4.6.2a), each holding a small 120 x 70 mm printed circuit board. The CCD is positioned behind the lens opening, with all the support chips, analogue-to-digital converter, power conditioning and control logic around it. The other board houses the microcontroller, all its memory and other glue logic, the image buffer memory, and the various communication interfaces to the spacecraft systems. Much of the design effort was expended in shrinking the circuits used on PoSAT-1 to fit on these two small boards. The extensive use of surface-mount technology, populated on both sides of six and eight layer printed circuit boards was needed to achieve this miniaturisation.

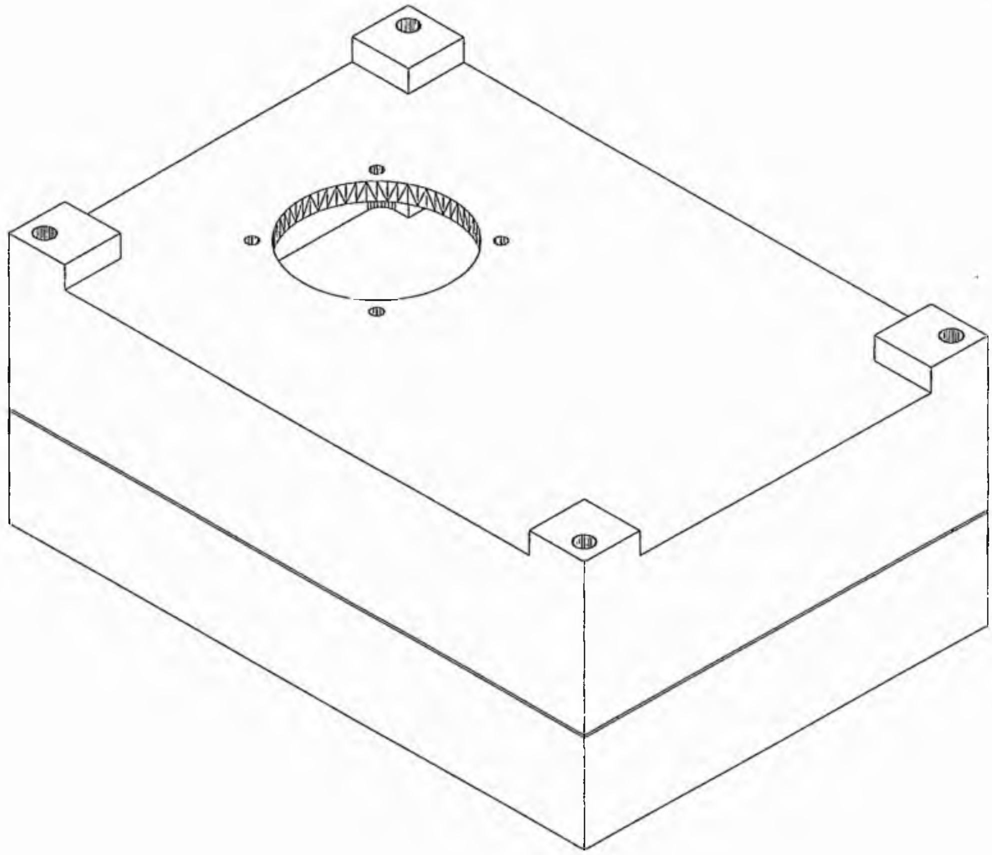

Figure 4.6.2a Mechanics of the FASat-Alfa modular camera.

The attraction of the modular approach is that each camera is a stand-alone unit, which can be assembled, tested, handled and integrated in complete isolation from the other imaging units. In particular, as each camera is fitted with adequate intelligence and communications interfaces, it can be operated without needing the transputer units. This feature was used at great length during development and test, thereby avoiding many of the integration and testing conflicts and bottlenecks faced on the previous missions, when the cameras and transputers always needed to be available together. Although the relationship between the transputers and cameras is very similar once in-orbit, the advantages offered by being able to operate and test the individual units in physical and conceptual isolation are very important. Furthermore, the physical modularity of the FASat-Alfa cameras gives them a fault-tolerance that was impossible in the previous implementations.

The most obvious application of such modularity is the increased, and essentially unlimited, number of cameras that can be supported by the spacecraft, at least with respect to connectivity. The connection strategy and the various communication paths are revealed in figure 4.6.2b. (Note that the WAC and NAC on FASat-Alfa are two distinct cameras,

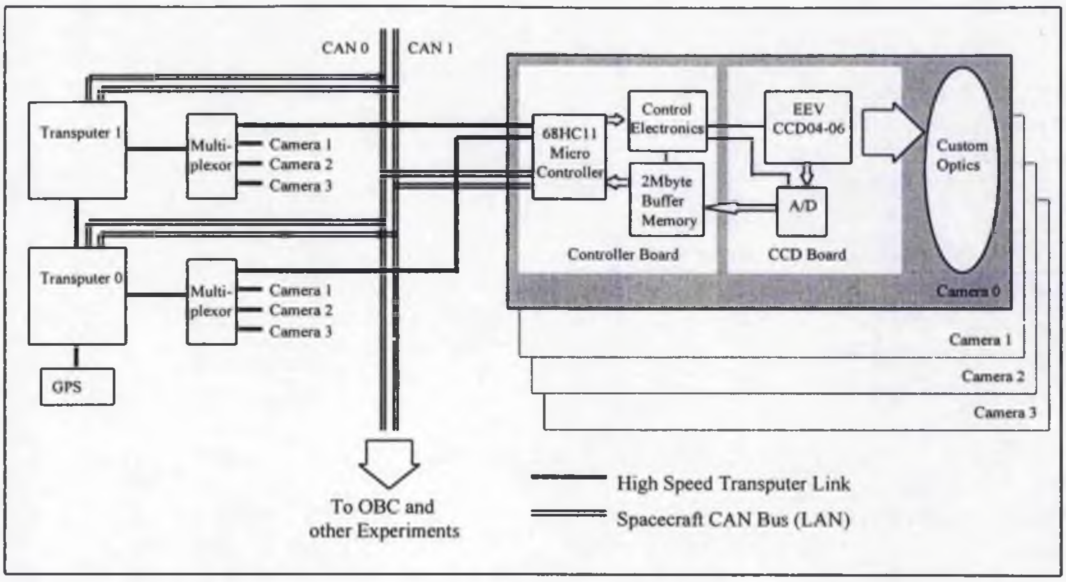

Figure 4.6.2b **Overview of the FASat-Alfa modular camera.**

and share no common circuitry as in previous versions). The microcontroller on each camera can communicate with both the primary and redundant telemetry and telecommand local area networks (CAN0 and CAN1 - based on the industry standard Controller Area Network), accepting instructions and transmitting status and image data. Similarly, each camera is still equipped with a link adaptor to support high speed point-to-point contact with the transputers; the single link from the camera microcontroller passes through a multiplexer, switching this signal's destination between transputer 0 and 1. Although essentially obsolete, the interface to the existing DASH0 network is also preserved, but this may be removed in future implementations in favour of more useful features.

The notion of modularity has also been adopted between the microcontroller and the camera head. All of the command parameters (integration, ADC references, etc.) are sent to the camera head over a simple serial link adhering to the Motorola Serial Peripheral Interface standard (SPI - virtually the same as the Philips I²C interface). In future revisions, this interface will be bi-directional to receive telemetry such as temperature, voltage and current readings; the SPI link is expandable in either direction to accommodate more commands or status lines. In the opposite direction, a fairly standard set of data and control lines have been defined for dumping digitised imagery into the frame-store memory.

The point of pursuing this internal modularisation is that rework can be isolated to the digital or analogue sections of the electronic camera. In particular, to fulfil SSTL's impending ambitions in remote sensing, it will be necessary to abandon the tried-and-tested EEV CCD04 for more advanced sensors. The simple interface between the boards, in addition to reducing the amount of wiring, provides a clean break-point between the two sub-systems. Therefore, provided the total number of pixels to be recorded does not exceed the 2 MByte capacity of the image buffer memory, new sensors can be supported without any rework to the microcontroller.

Each of the modular cameras has a mass of 600 grams when ready for flight, excluding the mass of the optics which was different for each of the four FASat-Alfa units. The largest and heaviest lens was required for the Narrow Angle Camera, adding another 350 grams to its mass. The base-line power consumption of the microcontroller circuit is 225 mWatts (45 mA at 5 V), peaking at 5.6 Watts (400 mA at 14 V) for the few seconds when the analogue circuits are active during image capture.

4.6.3 THE FASAT-ALFA TRANSPUTERS.

As before, the FASat-Alfa transputer module comprises two T805 transputers which can operate either independently or in tandem. However, because the section of the module tray that was previously occupied by the image memory or the camera microcontroller has been vacated, transputer 0 has been upgraded to the same specification as T1. Echoing the modularity of the cameras, the schematics and PCB layout of the two transputers are identical, with a few small differences in the population of the two sub-systems reflecting the different experimental requirements.

Given the mission profile of the FASat-Alfa mission, it had been assumed that the two transputers would operate independently, with T1 supporting the imaging activities and T0 supporting the GPS and attitude experiments. If necessary, T0 could support all of the imaging activities normally associated with T1. Similarly, the two transputers can be used for parallel processing at any time, simply by selecting the appropriate compiler options.

Despite the cameras' potential independence, the normal mode of operation in the FASat-Alfa configuration is the same as on previous missions, with T1 supervising the imaging activities, treating the cameras as slave units and being the sole point of contact for the on-board computer.

Each processor is equipped with error-protected static memory (4 MBytes for T1 and 2 MBytes for T0), EPROM, and various input / output peripherals including an interrupt controller. The two CAN busses and the DASH networks provide communications paths between the transputers and the rest of the spacecraft. Instructions to the cameras are issued over the CAN bus, but the data is retrieved using the high speed Inmos links. To overcome the limited number of link engines on each transputer, one of the links is fitted with a multiplexer, allowing this link to be switched between the various cameras.

4.6.4 RESULTS OF THE FASAT-ALFA IMAGING SYSTEM.

Sadly, there are no images from orbit to support the author's claims of the improved performance of the modular cameras developed for FASat-Alfa. Nevertheless, the results from bench testing indicate that the extremely tight printed circuit layout has had significant benefits in further reducing the cameras' noise characteristics. Both the background noise and the pixel drop-out from the analogue-to-digital converter (refer to section 7.3.1 for a detailed discussion of these effects) have been reduced to imperceptible levels, noticeable only under extreme illumination conditions. Indeed the noise characteristics are so improved that the author commenced searching for other, far more subtle, image imperfections. For example, a faint slew-rate limiting on certain contrast transitions (that is only discernable to the trained eye) was discovered because all the other camera degradations have been tamed. Furthermore, this reduction in the noise levels has been achieved despite the presence of the digital microcontroller circuits only a few millimetres away.

Figure 4.6.4a shows an image captured by the FASat-Alfa Wide Angle Camera during ground testing, showing a clean room at SSTL. (Note the mock-up of SSTL's forthcoming 200 kg minisatellite - see section 9.4, and the barrel distortion caused by the wide angle lens). The large uniform areas in this image would make any noise very noticeable, yet they are free of defects. The 'stair-casing' effect visible on diagonal lines demonstrates that the imagery suffers minimal focusing and smearing errors. These lines would be blurred if any such defects were present. Results from the Narrow Angle Camera were similar.

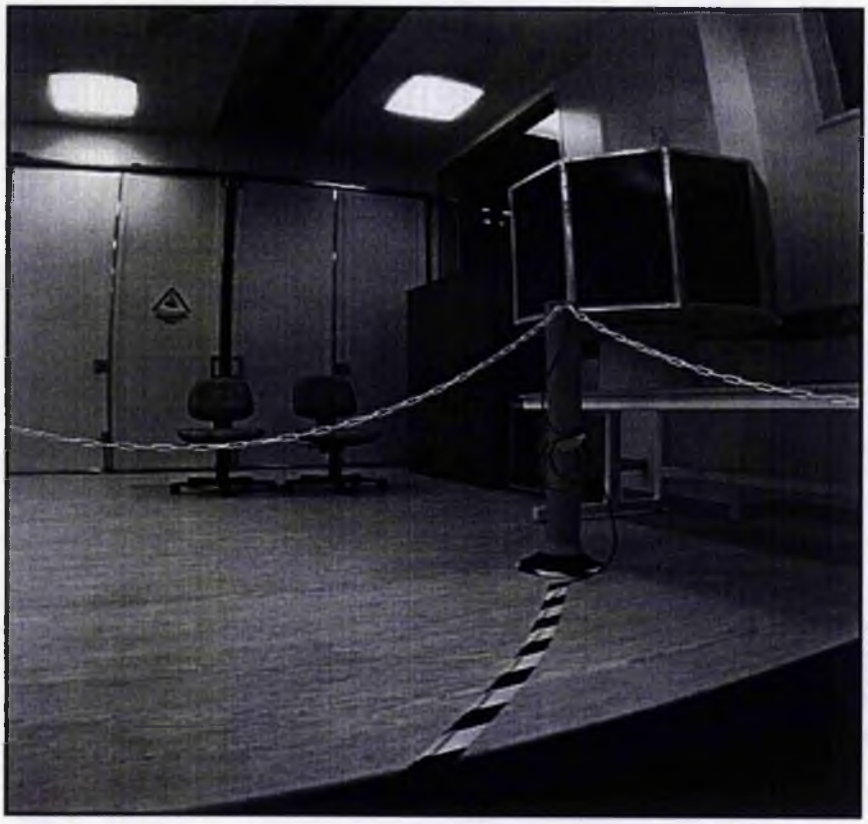

Figure 4.6.4a

FASat-Alfa wide angle image of the SSTL clean room.

Figure 4.6.4a

FASat-Alfa ultra-violet image of an outdoor scene.

Figure 4.6.4b is an image captured of an outdoor scene by one of the ultra-violet (ozone) cameras. Trees and an lamp-post supporting traffic signs are silhouetted against the sky, and a yucca-plant is discernable as a tuft in the foreground. The Sun's radiance in the UV spectrum is around four orders of magnitude less than in the visible. Given that most natural UV is absorbed and scattered by the atmosphere, the illumination conditions for this image are equivalent to that of a Moon-less night when imaging in the visible bands. To achieve adequate brightness, the camera's lens had an f-number of 1.0, which made it sensitive to aberrations and depth of focus errors. Accordingly, the contrast of this imagery is inferior to that of the visible cameras. Nevertheless, the sensitivity of the camera augured well for its role in orbit.

As anticipated, the modularity of the circuits has shown to be a great asset in the integration and testing of the various units. It has been possible to calibrate the cameras, one at a time, without getting caught up in any problems associated with the transputers or other spacecraft systems. This is particularly important when adjusting the optics; the camera is aligned in the laboratory and bolted onto the satellite's Earth-facing platform as a complete unit, unlike previous versions where a certain amount of final adjustment had to be done in situ in the battery box. Overall, the development of all the hardware, firmware and software for the cameras and transputers has been made simpler because of this modularity.

Attention has also been paid to the ease of manufacture of these circuits, reflecting the overall stream-lining within SSTL of this aspect of microsatellite engineering. The components were assembled onto the printed circuits by skilled technical (but non-engineering) staff, ready for verification by the author and his junior colleague. Despite a number of manufacturing faults, including two cases of broken tracks on the printed circuit boards, an average of only a day per camera was required for the complete debugging, testing and calibration of the camera electronics. A further couple of days were needed to match the optics (focus and iris aperture) to the individual cameras. Certainly, for the repeat mission, FASat-Bravo, there should been no need for the author to participate in the procurement of parts and assembly of the camera units, only being required to verify the cameras' correct operation and for alignment and calibration. This level of reproducibility is the result of the numerous iterations of circuit redesign and the successive refinements in performance and stability.

Finally, as indicated in section 4.6.2, it is very feasible to use these modular units as the basis of future cameras employing more sophisticated CCD sensors than currently used. (A few of the options are discussed in chapter 9). Similarly, star sensor units for the UoSAT-12 minisatellite can be made directly from the existing circuit boards; the extra features developed for the PoSAT-1 star camera have been included in the modular camera circuits, but left unpopulated for FASat-Alfa.

4.7 SUMMARY.

This chapter has reviewed the five generations of imaging system developed by the author in the course of this programme, tracing the evolution of the systems across the missions. The conclusions derived from this practical development work and the in-orbit results form the remainder of this thesis.

The UoSAT-4 camera was a very basic system using discrete hardware and a donated sensor, producing tolerable imagery on the bench. The experience of this project lead to a complete redesign and expansion of scope for the UoSAT-5 imager.

The selection of the EEV CCD04-06 for UoSAT-5 was based not only on its sensing attributes, but also on the basis of a chipset fulfilling most circuit functions, and good technical support. This choice was auspicious as Surrey's UoSAT-5 microsatellite, launched in July 1991, became the first sub-100 kg satellite to demonstrate reliable, predictable and repeatable Earth observation. Its status as a milestone in the development of low-cost remote sensing from space was enhanced by also being the first successful imaging mission independent of governmental control.

Since then, the electronic cameras and transputers first implemented on UoSAT-5 have been reworked and enhanced for flight on SSTL's collaborative microsatellite missions, KITSAT-1, PoSAT-1 and FASat-Alfa, confirming this innovative remote sensing capability. The quality of the imagery from these cameras is very high, and the data from the PoSAT-1 cameras in particular is quite spectacular when one considers their low cost relative to existing imaging systems. Most recently, the demonstrated circuitry of the camera and microcontroller unit have been re-packaged to implement a very modular system allowing simple replication, as well as providing a clear up-grade path. Table 4.7 provides a summary of the specifications of these imaging payloads.

Satellite	Camera	Spectral Band	Orbit	Mean Resolution	Area of Image
UoSAT-4	Single	580 - 640 nm	800 km	2 km	760 x 570 km
UoSAT-5	Single	600 - 615 nm	800 km	2 km	1500 x 1050 km
KITSAT-1	Wide	810 - 890 nm	1300 km	3.5 km	2550 x 1800 km
	Narrow	810 - 890 nm	1300 km	350 m	220 x 160 km
PoSAT-1	Wide	810 - 890 nm	800 km	2 km	1500 x 1050 km
	Narrow	610 - 690 nm	800 km	200 m	150 x 100 km
	Star Sensor	400 -1000 nm	800 km	0.01°	10° x 7°
FASat-Alfa	Wide	810 - 890 nm	650 km	1.7 km	1150 x 850 km
	Narrow	610 - 690 nm	650 km	115 m	75 x 55 km
	UV 0	308 - 318 nm	650 km	900 m	450 x 330 km
	UV 1	375 - 385 nm	650 km	900 m	450 x 330 km

Table 4.7 Summary of camera specifications.

4.8 WORK BREAKDOWN OF THE SSTL IMAGING SYSTEMS.

While the flight models of the various imaging systems have been the culmination of the project efforts, there have also been many prototype and engineering models built in the development of these Earth observation systems. Table 4.8 shows a break-down of the time spent on the various projects over the years of this research programme.

Year	Project	System	Model
1988	UoSAT-4	camera	prototype
1989	UoSAT-4	camera	engineering, flight
1990	UoSAT-5	camera, transputers	engineering
1991	UoSAT-5	camera, transputers	flight
1991	KITSAT-1	camera, transputers	engineering
1992	KITSAT-1	camera, transputers	flight
1993	PoSAT-1	camera, star sensor, transputers	flight
1994	FASat-Alfa	visible & UV cameras, transputers	prototype, engineering
1995	FASat-Alfa	visible & UV cameras, transputers	flight

Table 4.8 Time break-down of projects during this research programme.

The author has been solely responsible for all of these deliverables, for the most part working alone. A number of students and junior engineers have supported the development of the necessary software and firmware. The greatest contribution was the test and operations software produced for the UoSAT-5 transputer systems by [Laker] as part of an M.Sc. project. This software has served as the basis for the subsequent missions, with the author developing, upgrading and occasionally debugging as necessary to reflect the evolving hardware. The microcontroller firmware was first implemented by a Korean junior engineer for KITSAT-1, but completely rewritten and debugged by the author for PoSAT-1. The extra facilities of the FASat-Alfa modular cameras has required a full redevelopment of the microcontroller firmware, undertaken by two SSTL junior engineers. The image compression software described in chapter 7 was undertaken by a junior engineer [Brewer] as part of a six month contract. The image processing routines (chapter 7) to filter the images of noise were developed and written by the author.

Therefore, the author has performed the virtual entirety of the hardware development, systems level design and implementation of the imaging systems over these missions; of course, this has been in the context of an engineering team where open discussion is encouraged. Some assistance with the assembly and test of the cameras has been available on the KITSAT-1 and FASat-Alfa missions, and for the development of software and firmware. However, all of this work was under the direct supervision of the author, and none of these contributors participated for more than a year.

4.9 REFERENCES.

Brewer A.W: On-board image compression using adaptive MPBTC algorithm; Internal document SSAB001B, Surrey Satellite Technology Ltd, 1994.

Fouquet M: The UoSAT-5 Earth imaging system - in-orbit performance; Proc. of the SPIE Conference on Small Satellite Technology and Applications II, SPIE Vol.1691, Orlando Florida, 21-22 April 1992.

Laker C: Software environment for the UoSAT-5 Earth imaging system; M.Sc. dissertation; University of Surrey, 1991.

Leitmann M.G, Fouquet M. et al: Attitude and position determination using a star mapper on the small satellite PoSAT-1; Proc. of the SPIE Conference on Small Satellite Technology and Applications III, SPIE Vol.1940, Orlando Florida, 14-15 April 1993.

Leitmann M.G, Fouquet M. et al: PoSAT-1 star imaging system- in-orbit performance; Proc. of the SPIE Conference on Small Satellite Technology and Applications IV, SPIE Vol.2317, Rome, Sept 1994.

Yoo S.K. et al: The KITSAT-2 Earth Imaging System Experiment; Proc. of the SPIE Conference on Small Satellite Technology and Applications IV, SPIE Vol.2317, Rome, Sept 1994.

Images Taken by SSTL Microsatellites in LEO

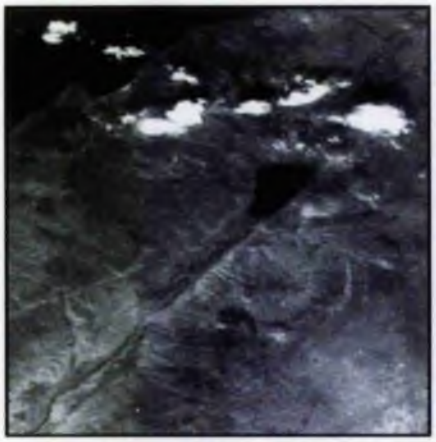

Sea of Galilee (Israel)

Baltimore & Chesapeake Bay (USA)

Cascaval (Brazil)

Plains near Katmandu (Nepal)

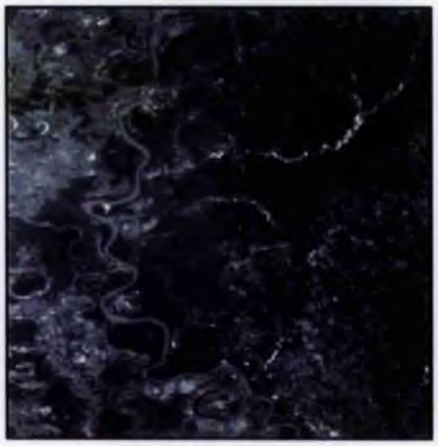

Mississippi Valley (USA)

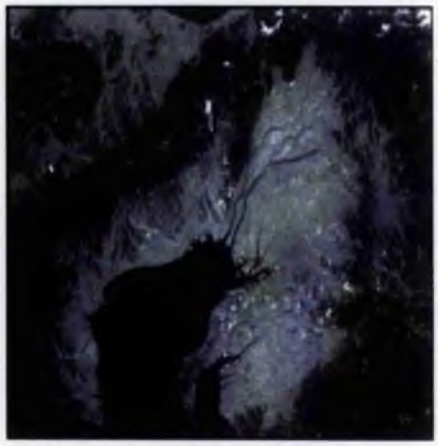

Nagoya (Japan)

Lisbon (Portugal)

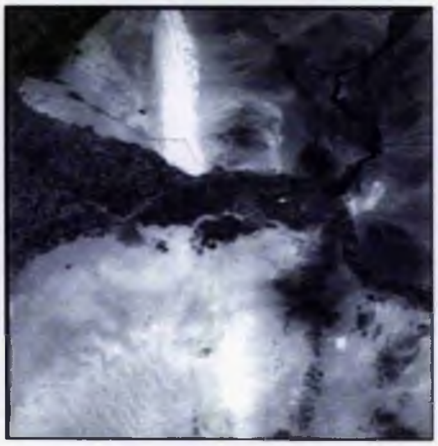

Yuma, Arizona (USA)

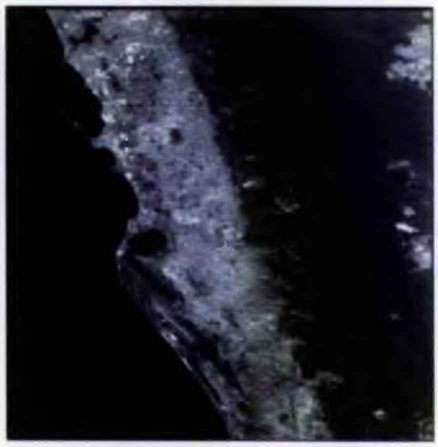

Perth & Fremantle (Australia)

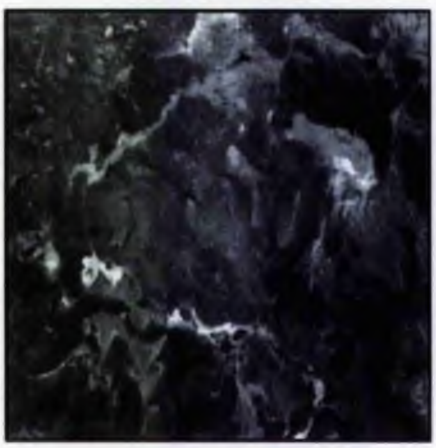

Cape Province (South Africa)

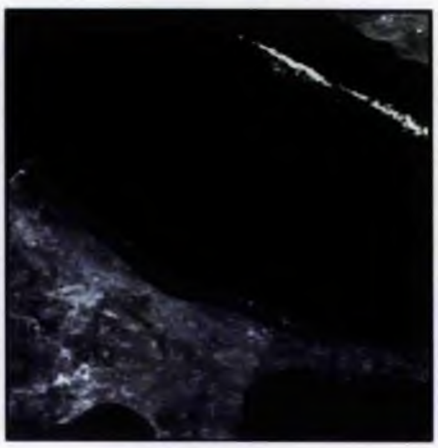

Eastern Cyprus

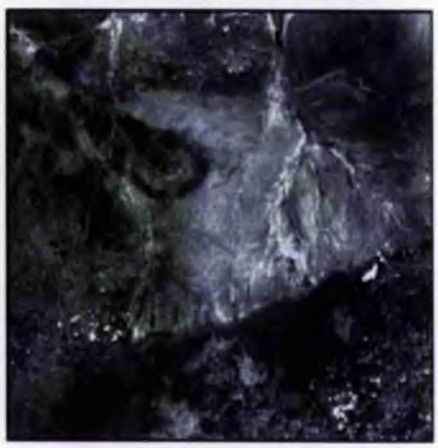

Mashonaland Central (Zimbabwe)

CHAPTER V

DESIGNING SOLID-STATE CAMERAS FOR EARTH IMAGING FROM MICROSATELLITES.

Based on the experience acquired in the development of the imaging systems described in chapter 4, this chapter provides practical advice on the issues facing the design of electronic camera systems for microsatellites. Chapter 5 discusses the criteria for selecting a CCD sensor depending on the instrument objectives. The various options for implementing the digital, analogue and power conditioning support circuits, and the optical systems, are discussed and appropriate solutions offered. Broader issues such as the calibration of the imager, fault tolerance and resilience to ionising radiation are also considered.

5. DESIGNING SOLID-STATE CAMERAS FOR EARTH IMAGING FROM MICROSATELLITES.

5.1 CHOICE OF CCD SENSOR.

The discussion of chapter 2 has highlighted the growing trend of replacing the traditional mirror-scanned imagers with solid-state arrays for most satellite remote sensing applications. Given the resilience to attitude instabilities offered by frame cameras, area-sensing CCDs, rather than linear arrays, are needed for use on microsatellites.

There are several types of area CCDs, each with distinct features and characteristics, resulting from both the device's physical structure and the manufacturer's perception of the device's main application. Unfortunately, the specific needs of microsatellite Earth observation missions (high pixel count, but with high speed readout and all-electronic operation) are distinct from most other applications. Furthermore, it is not possible to specify a generic architecture for a remote sensing camera, as different missions will place differing demands on the sensor. It is therefore crucial to consider the consequences of numerous factors when selecting a sensor for a given imaging mission.

N.B. The following terminology is used for the rest of the chapter. A 'photosite' refers to the physical detector on a CCD array. A 'pixel' corresponds to the digitised output from a photosite, either as a binary word or a notional element of the image to be manipulated or displayed. There is no particular industry-standard, and the literature tends to use the term 'pixel' indiscriminately for these, and other, concepts. The choice here is merely to ensure consistent wording and to avoid possible confusion.

5.1.1 OVERVIEW OF CCD SENSORS.

5.1.1.1 Brief description of area-array CCD architectures.

There are numerous texts dealing with the general theory of operation of charge-coupled devices [Howes & Morgan][Beynon & Lamb][Hobson], and it is unnecessary to reiterate these here in any detail. In particular, [Janesick & Elliot] provide an excellent review of the physical properties of modern CCD sensors. Nevertheless, a brief description of certain aspects of area-array CCDs is necessary because these factors are highly relevant in the design of remote sensing systems.

The principal of image-sensing CCDs is the combination of the photosensitive nature of a semiconductor with their behaviour as analogue shift registers. As photons strike the surface of a semiconductor, they split into electron - hole pairs, generating an electronic current. In this respect, CCDs are similar to other silicon photo-detectors. However, instead of producing a DC current, each photosite within the CCD traps these electrons into a charge packet. By integrating the electrons over a period of time, the array of charge packets records the spatial variations in luminous intensity of the image focused onto the sensor.

The majority of area-array CCDs have their photosensitive area arranged as a series of electrically isolated columns (the sensing registers) of photosites with a single row (the readout register) across the bottom of the sensor. To read the charge packets collected by the sensor, all the columns will be shifted down by one place, with the contents of the bottom-most photosite of each column falling into the horizontal readout register. The readout register is then driven rapidly to move the charge packets towards the output amplifier. When one line has been completely read out, the columns are again driven to load the next row into the readout register. This cycle is repeated until all the charge packets associated with the photosites have been transferred to the output. In designing the two-dimensional lattice of photosites in an area-array CCD, and implementing the sequential readout of the charge packets, it is possible to generate an electronic signal representative of the scene viewed. This topology and sequence of operation delivers signals compatible with the existing television standards.

As charge packets are transferred within the CCD, they are physically moved across the surface of the silicon lattice towards the output amplifier. Because the entire surface of a CCD is photosensitive silicon, these charge packets will continue collect any incident photons as they are being moved. Unfortunately, these extra photons will have no correlation to those originally captured by the photosites, resulting in noise. Given the column architecture of the CCD, these spurious photons cause a vertical smearing of the recorded image.

To remain radiometrically faithful to the scene, it is therefore important that each charge packet contains a large majority of electrons recorded by the original photosite, with as few additional spurious electrons as possible. To eliminate the smearing effect, it is necessary to use a shutter to prevent any additional photons from striking the CCD once integration has terminated. In many instances this shuttering is accomplished with an external mechanical shutter, identical to those used in film photography or cinematography.

Alternatively, many CCDs implement a form 'electronic shuttering' internally, without having recourse to mechanical systems. This is performed by storing the charge packets in optically shielded buffers located on the surface of the CCD. Once a charge packet is safely in a shielded buffer, it will not collect any further photons, and can be read out without being subject to any further smearing (with some limitations). While most CCDs are similar in the way they record incoming photons as charge packets, it is the storage (or lack thereof) and read-out processes which makes them different, and determines their suitability for various applications, including satellite remote sensing.

5.1.1.2 Features of commercial and scientific CCDs.

Area-array CCDs can be separated into two broad categories: commercial video and scientific applications. Commercial devices, by definition, are designed to produce a signal directly compatible with one of the existing television standards (CCIR / PAL, EIA / NTSC, HDTV). The market for these commercial devices is dominated by the large Japanese manufacturers of electronics and television equipment (Sony, Panasonic, JVC, Hitachi, Sharp) providing sensors for both high-grade broadcast television as well as domestic video cameras. Although several European and US manufacturers (Philips, EEV, Thomson, Texas) were prominent in the early development of the commercial CCD market, intense competition from the Japanese companies has reduced their influence. Nevertheless, most of these western manufacturers still maintain limited product lines in this area. Because of the high volume market, and the maturity of the fabrication technology, these CCDs are comparatively inexpensive (a few hundred pounds per device, depending on the exact specifications).

To adhere to the television standards, the number of lines (the vertical resolution) in an image from a commercial CCD is predetermined: 625 lines (576 active) for CCIR / PAL, 525 lines (488 active) for EIA / NTSC, around 1100 active lines for HDTV. The horizontal resolution (pixels per line) is generally the about the same as the vertical resolution. However, higher horizontal resolution is now easily available as the technology can support it. A ratio of 4:3 is most common, although pixel counts as high as 1000 per line are available.

To remain compatible with the television standards, all commercial CCDs must use interlacing (see section 5.1.2.5) of two image fields to attain full vertical resolution. Furthermore, all commercial sensors feature on-chip buffers to implement electronic shuttering, thereby avoiding the extra complexity, maintenance requirements and noise of mechanical shutters. Most also include electronic exposure (integration) control as a standard feature.

Conversely, the loose term of 'scientific' sensors is appellation used to group all non-compatible CCDs. In many scientific applications, the television standards can place unnecessary restrictions on the imaging conditions, and numerous other CCDs are designed and produced to meet the various requirements of medical imaging, astronomy and spectroscopy to name a few. There is no Japanese participation in this sector, and these devices are made by European and north American companies, with smaller sales volumes, and correspondingly at a higher cost. [Lake] reviews some of the driving factors in establishing the costs of CCDs. However the market is still competitive, and the extra cost reflects improved quality, specification, performance and pixel counts.

Other than not being compliant with a television standard, there are few generic features to scientific sensors. Most of these CCDs are designed for a specific imaging application (e.g. large format, spectroscopy, slow scan, high speed, low noise) with correspondingly distinct features. One general characteristic however, is that these devices often do not incorporate electronic shuttering (i.e. they use full-frame imaging). This is particularly the case for devices with very high pixel counts.

The developing field of sensors for computer or robotic vision and commercial digital cameras is bridging the gap between the two categories of CCDs, both in terms of features and cost. Nevertheless, they are still considered a sub-class of scientific sensors. In general, these 'machine vision' devices feature the all-electronic operation of commercial devices, but with higher photosite counts, no interlacing, and with pixel formats suitable for computer manipulation (256^2, 512^2, 1024^2).

Before reviewing the characteristics of the different classes of area-array CCDs, it is worth mentioning that none of the categories fits the application of microsatellite remote sensing perfectly, although the machine vision sensors combine most of the desired characteristics.

5.1.2 ARCHITECTURES FOR AREA-ARRAY CCD SENSORS.

5.1.2.1 Full-frame CCDs.

As the name suggests, the entire surface of a 'full-frame' device is devoted to imaging photosites, with no buffer area for electronic shuttering. Therefore, an external shutter must be employed to shield the CCD from light during read-out. Using strobed illumination can have the same effect in certain situations. Without electronic shuttering, full-frame CCDs are poorly suited for commercial TV. Although some of the earliest CCDs, in the early 1980s, could only achieve the pixel density necessary for TV compatibility by going full-frame, such devices have been obsolete for many years. Therefore, almost by definition, full-frame devices are for scientific applications (although not all scientific sensors need to be full-frame). The major manufacturers of full-frame CCDs are EEV, Thomson, Eastman-Kodak, Tektronix, Texas Instruments, Loral-Fairchild, Ford Aerospace, Sarnoff, Dalsa and EG&G Reticon.

Given that an external shutter is a prerequisite for most cameras using full-frame CCDs, many of the control features found in commercial sensors (i.e. electronic shuttering, integration control, antiblooming) are not included as they are provided by the shutter. By eliminating such features from full-frame devices, the fabrication involves fewer stages and a more efficient use is made of the sensor's photosensitive areas, resulting in a significantly better radiometric performance than is available with all-electronic sensors. Full-frame CCDs are able to offer improved spectral sensitivity, quantum efficiency, dynamic range, linearity, optical fill factor and uniformity between photosites, largely by excluding the extra complexity of electronic shuttering from within the photosite structure. The extra sensitivity and accuracy offered by a full-frame sensor meets the important requirements for many scientific applications. Furthermore, the simplified manufacturing means that the pixel-for-pixel cost of full-frame devices is generally less than for all-electronic CCDs (assuming comparable sales volumes).

Furthermore, many applications require pixel formats different from those of the TV standards. In particular, without the electronic shuttering mechanisms, it is feasible to implement imaging arrays with much higher photosite counts, whilst preserving acceptable production yields. As a result, full-frame CCDs are currently available in sizes up to 4000 x 4000 (Ford Aerospace, Eastman-Kodak, Loral-Fairchild) and 5000 x 5000 (Dalsa). Conversely, it is rare for an all-electronic sensor to have more than 1 million photosites (1000 x 1000). Therefore, if very large imaging arrays are imperative for a specific application, then it is almost certain that a full-frame device will be required.

However, CCDs with large photosite arrays are much more expensive than a commercial sensor (circa US$ 10,000 for a 2000 x 2000 device; much more for larger CCDs). While the budgets of scientific users can be extended to meet the extra cost of these large sensors, customers rarely want to sacrifice half of the imaging photosites to serve as a shuttering buffer. Compared to the cost of the sensor and the complexity of the whole camera, implementing a shutter is trivial in most cases. Moreover, the controlled conditions of scientific applications often makes shuttering unnecessary. Therefore, even if it was technologically possible, there is very little demand for all-electronic sensors with very large photosite counts.

Therefore, to implement a remote sensing camera with a full-frame CCD, it will be necessary to select a high-speed device and equip it with an external shutter to prevent smearing and motion blurring. Although using a shutter on the ground is simple, it represents a liability in the space environment, and has limited the deployment of full-frame sensors in remote sensing instruments.

5.1.2.2 Frame transfer CCDs.

The most common form of implementing electronic shuttering on a CCD uses the frame transfer architecture, shown in figure 5.1.2.2. In this design, the bottom of the CCD is covered with an opaque mask, shielding the lower part of each column and the horizontal readout register from incident light. The photosites in the exposed region collect photons in the normal manner. At the end of the integration period, the columns are rapidly strobed to move all of the image charge packets from the exposed area into the storage area. Once inside the storage area, the charge packets are shielded from incoming photons, and can be read out in relative leisure without the recorded image being disturbed. In practice, the activities of the imaging and storage areas are clocked independently. While one image is being read out of the storage buffer, the next image is being integrated in the exposed photosites. The two regions only synchronise when the first field has been completely read, and the next image is transferred into the storage region.

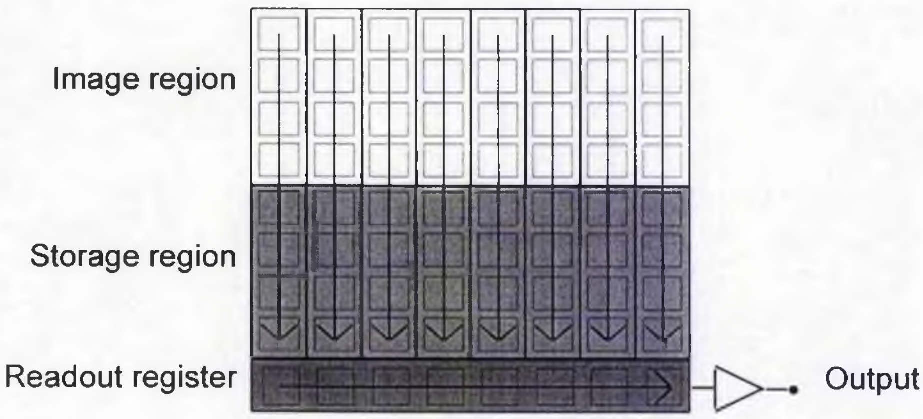

Figure 5.1.2.2 Schematic architecture of a frame-transfer CCD.

The fabrication process of a frame transfer CCD is not much different to that of an equivalent full-frame device, except for the deposition of the optical mask. Not surprisingly, the frame transfer approach tends to be the favoured method of achieving electronic shuttering from manufacturers normally associated with the manufacture of scientific sensors. Indeed, many devices can be obtained either with the optical shield for all-electronic operation or in full-frame mode for increased pixel counts.

As a consequence, frame transfer CCDs can possess many of the desirable radiometric properties normally associated with full-frame sensors: good optical fill factor, spectral response and dynamic range. Of course, if numerous features like integration control or antiblooming are included in a frame transfer CCD, then these radiometric factors will be degraded. Similarly, larger CCD arrays with electronic shuttering tend to be frame transfer, because much of the technology can be adapted from existing full-frame sensors. Frame transfer CCDs aimed at the high definition television (HDTV) market are now available with photosite counts of around 2000 x 1152 lines (interlaced, 576 lines non-interlaced).

When the transfer from the imaging to the storage regions takes place, the charge packets are still vulnerable to smearing. On the whole, this effect is minimised by ensuring that the duration of the transfer is small compared to the total integration time, so that the percentage of 'smearing' pixels remains small. For example, in most commercial TV sensors, the vertical registers will be driven at about 2 MHz, taking about 100 μs to transfer the image. This transfer time is an adequately small fraction (0.5 %) of the nominal 20 ms field rate, and smearing is rarely a problem.

However, if very short integration times are used, the finite transfer time represents the principal drawback of the frame transfer architecture. For example, if the total integration time is around 1 or 2 ms, then a 100 μs transfer time becomes significant, and smearing is inevitable. For high resolution remote sensing, short integration times are essential to prevent the satellite's motion blurring the image (see section 3.3.4.2.1), conflicting with the conditions for low smear. The only way to prevent this is to drive the column registers faster during transfer, incurring a significant penalty in the camera's power consumption (essentially doubling the power consumption for every doubling of the vertical clock speed). In large arrays or in devices designed for very high frame rates, the CCD is sometimes split into 2 or 4 sectors, stored and read individually, to accelerate the capture and read-out process.

5.1.2.3 Interline transfer CCDs.

An alternative design of the electronic shuttering facility is to provide each of the imaging photosites with a shielded partner to perform storage and transport. In this architecture, shown in figure 5.1.2.3, each of imaging columns is separated by a storage column.

Because of the interleaving of the imaging and storage sections, the manufacture of an interline transfer CCD is more complex than an equivalent frame transfer device. The shielding masks must be applied with great precision or else the imaging photosites will be obscured, and the storage areas will be exposed and susceptible to smear. Problems of light leaking under or through the extremely fine masks were reported with the earliest interline transfer CCDs. Although this would appear to be an inherent flaw of this architecture, the fact that interline transfer devices are widely used in commercial TV sensors without any noticeable degradation of quality implies that the manufacturers have mastered the technique for depositing the masks.

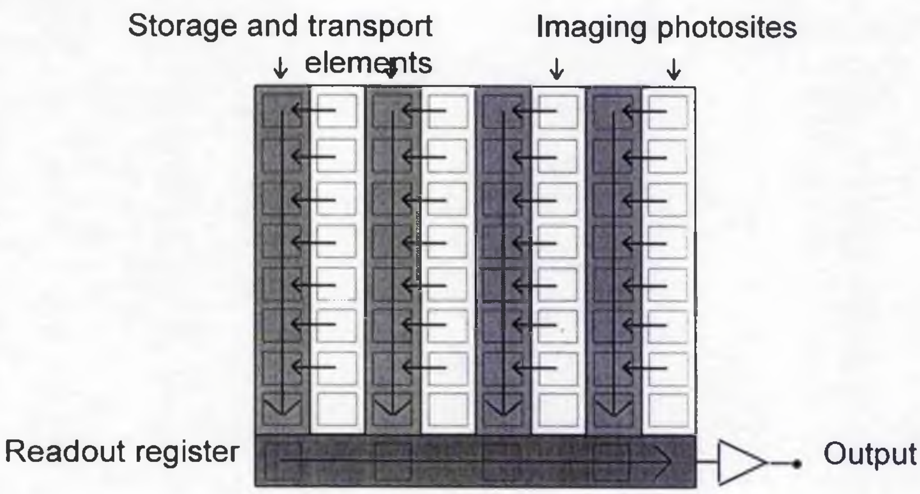

Figure 5.1.2.3 Schematic architecture of an interline-transfer CCD.

The main advantage of the interline transfer architecture is the instantaneous (hundreds of picoseconds) transfer from the active photosite to the storage bins, thereby eliminating the problem of smearing. This allows much shorter integration times to be accommodated than is feasible with a frame transfer CCD. From a remote sensing perspective, this allows higher resolution imaging to be performed without suffering from either blurring or smearing. For most other imaging applications, it gives the CCD a much greater range of possible integration times, allowing it to operate under more widely varying illumination conditions, without requiring an external iris or shutter.

However, the overall loss of photosensitive area on the CCD's surface degrades many of its optical properties, including reduced spectral response and fill-factor. While these losses are not particularly problematic for commercial TV, they are of significance to remote sensing applications. The increased level of semiconductor integration on an interline transfer CCD effects the natural spectral sensitivity of the underlying silicon, effectively curtailing operation to the visible regions (0.45 to 0.75 μm). Although not encroaching upon the red, green or blue spectra of the human visual response, there is a significant loss of UV and, most importantly, of near-IR sensitivity. The low fill-factor caused by masking off alternate columns of photosites can cause aliasing of high frequency patterns. Fortunately, the recent innovation of placing micro-lenses over every photosite on the CCD to fill in the blind areas has reduced the problem of aliasing as well as increasing the overall sensitivity of these devices.

While interline transfer CCDs are the predominant type of sensor used in current television applications, it would appear that the manufacturers are having difficulty in producing these devices with higher pixel counts. Even the Japanese companies, who largely favour the interline transfer architecture, are employing the frame transfer approach for their HDTV sensors. The largest device structure using the interline transfer method is made by Eastman-Kodak with 1024 x 1024 photosites (non-interlaced).

5.1.2.4 Charge injection devices (CIDs).

Another form of solid-state imaging technology is the charge injection device (CID, or charge modulation device - CMD - as they are sometimes referred to). Although they are area-array image sensors, CIDs have a number of distinct properties to CCDs. The principal difference is the CID's addressable structure, making it possible to have random access to the individual photosites. This is particularly useful for forms of industrial process control, target tracking or surveillance, where a small object of interest can be monitored continuously without having to read out the entire image. Under more normal operation, an entire image is captured by rapidly selecting each photosite in sequence. Furthermore, the reading process is non-destructive, and it is possible to continue integrating a charge packet in a given photosite after reading. According to the manufacturers, CIDs also offer better sensitivity and radiation tolerance than CCDs.

A conventional CCD reads its data by physically transferring charge packets from photosite to photosite across the surface of the sensor towards the output amplifier. Unless these charge packets are shielded from incoming light (by a storage region or a mechanical shutter), they will suffer smearing. However, CIDs read the charge packet from a photosite by connecting it directly to the final amplification stage. This is accomplished by activating a semiconductor switch to gate a particular photosite onto a buried channel in the substrate. By multiplexing the charge packet straight onto the output, no smearing can occur, and a CID does not require any form of shielding. This means that the CID can use the whole of its surface for imaging without having to sacrifice large photosensitive areas for storage.

Despite these advantages, the CID's architecture presents has a number of serious deficiencies for capturing the rapidly moving scenes viewed by a remote sensing satellite. In a CCD, the shuttering ensures that all the pixels are collected simultaneously and then transferred to the storage for read-out. It is this simultaneous collection that guarantees that the image geometry is preserved. Conversely, the CID's sequential scanning and clearing of the photosites produces a phase difference across the sensor. Although this delay is negligible between neighbouring photosite, it will be significant between the top and bottom lines, resulting in serious distortion and mis-registration in the captured image.

Moreover, because all the pixels in a CCD collect light in phase, a simple reset can be used to shorten the integration time, or to minimise blur. Conversely, the reset rate of a CID is determined by the period between successive readings of each photosite, and it is not possible to implement integration time control electronically, making a mechanically-variable iris necessary. Alternatively, if all the photosites are reset simultaneously, those read first will have integrated for a much shorter time than those read last, resulting radiometric non-uniformity across the image.

The characteristics of a CID are primarily suited to producing moving images of low-dynamic scenery or object-tracking in high-dynamic scenery. While this may be of use in many applications, these attributes are a serious disadvantage in the context of satellite remote sensing. In particular, the sequential, as opposed to simultaneous, collection of the charge packets are susceptible to very bad distortion. The freeze-frame operation of a CCD is much more appropriate for this application.

5.1.2.5 Interlaced vs. progressive scanning.

The television standards use the trick of interlacing to double the perceived image resolution, whilst retaining the same signal bandwidth. A full-resolution video frame is made up of two fields, one containing all the even lines and one with all the odd lines. The odd and even fields are transmitted alternately, relying on the averaging effect of the human eye to create an impression of continuous motion at the higher resolution. This effect provides a useful gain when transmitting a continuous moving sequence of images.

Conversely, using a sensor with interlacing to gather a snap-shot (i.e. remote sensing by satellite) can generate significant artefacts in the image. This is caused by a displacement in the scene between the moments the two fields are captured. For example, most interlaced CCDs are for video applications, where a new field is produced every 20 ms (or 16 ms for EIA / NTSC). (N.B. Even though the individual fields may use shorter integration times, they will always be captured 20 ms apart). During this time, the sub-satellite point of a spacecraft in an 800 km orbit will have moved by 130 metres. If the pixel resolution is comparable to this displacement (i.e. less than 400 metres), there will be some loss of alignment between the two fields. If the ground resolution is 100 metres or less, the displacement will be greater than one pixel, the lines of the two fields will not be correlated, and interlacing will not produce valid results. [Hofmeister] echoes these points.

Therefore, although low resolution systems can use interlacing to increase the image resolution beyond the sensor's natural limits, this will not be possible for medium or high resolution applications. 'Progressive-scanning' is the term used for sensors which capture all pixels simultaneously, i.e. which do not use interlacing. Regardless of the remote sensing application, progressive scan devices are always preferable, because they are designed for capturing still images, rather than interlaced sensors which are conceived for motion pictures. The geometry and resolution of a progressively-scanned CCD is certain. Full-frame CCDs virtually always use progressive-scan.

In the specific case of the FASat-Alfa Narrow Angle Camera, the mission called for 100 metre resolution but there was inadequate time to develop a new camera to replace the interlaced sensor used on previous SSTL missions. Despite the interlacing, it is nevertheless possible to capture correctly registered imagery at this resolution, provided the imaging conditions are carefully controlled. To understand this, consider the following argument. Figure 5.2.1.5a shows an object as it would be imaged by an interlaced camera under static conditions. The edges of the object are well aligned. One field is shown shaded.

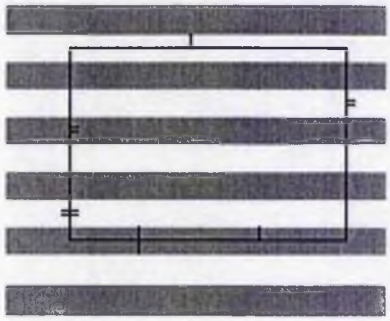

Figure 5.2.1.5a

Static camera.

Figures 5.2.1.5b and 5.2.1.5c show the effect of a moving camera when imaging the same object. In the cases shown, the shift in the image corresponds exactly to the pixel resolution. Note that the edges are no longer co-registered between the two fields.

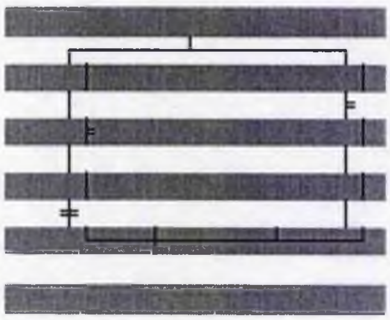

Figure 5.2.1.5b

⇒ Direction of travel.

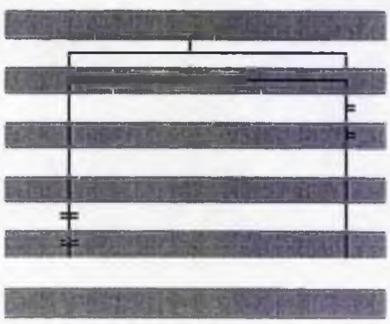

Figure 5.2.1.5c

⇓ Direction of travel.

Figure 5.2.1.5 Effect of motion on imagery from an interlaced CCD.

Clearly, recording a dynamic scene with an interlaced sensor can introduce distortions. As the diagrams suggest, the sampling errors are greatest, and most difficult to remove during post-processing, when the motion is perpendicular to the image lines. Note that because of PoSAT-1's yaw spin, the motion can be in any direction with respect to the sensor. However, it is possible to eliminate this effect in the final image, provided two criteria are met:

1. the satellite's motion is always parallel to the CCD lines as shown in figure 5.1.2.5b (i.e. the satellite's yaw spin is eliminated and a fixed yaw angle maintained),

2. the scene moves by exactly one pixel between the capture of the two fields.

Under these conditions, it will be possible to re-sample the second field so that it registers exactly with the first field. Because the displacement will be constant for all images, this can easily be done on the satellite by the one of the on-board computers, prior to any other processing or compression.

If an interlaced device is used for remote sensing, there are a few additional factors to be considered. Some interlacing CCDs (e.g. EEV, Thomson), do not actually have separate photosites for the two fields but use a pseudo-interlace to simulate the odd and even photosites by offsetting the photosite centre. Thus the pixels in the odd and even field overlap, and the true vertical resolution is less than the pixel count suggests. Devices using pseudo-interlace will sometimes have a slightly different response between the two fields, resulting in one field being marginally brighter than the other.

5.1.2.6 Brief comparison between field-array CCDs and other sensor technology.

In virtually all areas of electronic imaging, solid-state CCDs have replaced vacuum tubes. In particular, solid-state systems are more robust, have a lower power consumption, do not require high voltage supplies, and are immune to magnetic fields and microphonics. Scientific-grade CCDs can provide greater photosite density, and all CCDs offer greater sensitivity, signal-to-noise and spectral range than tubes in almost all applications. Table 5.1.2.6 was compiled by Thomson-CSF as part of their marketing material for CCDs; although it overstated the case of CCDs at the time of printing (1987), it is now an accurate reflection of the relative advantages of solid-state imagers over tubes.

There remain a few specialist areas where tubes still prevail such as streak cameras or intensified imagers. As discussed in sections 2.1 and 3.1.2, silicon photodetector do not possess an adequate spectral range to meet every remote sensing requirement. In particular, there are a number of technologies, including tubes and other solid-state technologies (FLIR, pyroelectric, photodiode) which have better thermal imaging characteristics than silicon CCDs. Nevertheless, for most optical imaging that would be considered suitable for a microsatellite, a CCD or other semiconductor array would be more appropriate than a vacuum tube.

	Image Tubes	CCDs
Material	Glass/metal	Ceramic / silicon no deformation with time
Shape	Tube	Integrated circuit
Size	diam = 30 mm (50 mm with yoke), l = 200 mm	l = 30 mm, w = 15 mm, h = 7 mm
Weight	Tube = 100g, Yoke = 200g	A few grams
Mechanical Resistance	Relatively rugged	Totally rugged
Dynamic Range @ 25°C	1000:1	2500:1 for area sensors, 6000:1 for linear sensors
Gamma	< 1	Equal to 1. No deformation of the output signal
Operating Temperature	-40°C to +70°C	-100°C to +70°C
Signal Form	Analogue	Analogue and sampled
Signal Available	tens of nA (into 100kΩ)	300 to 1000 mV (into 1kΩ)
Centre-to-Edge Non-Uniformity of Resolution	20%	None
Lag	Some (?)	None
Damage by Over-Lighting	Possible	No risk
Antiblooming	Good	Good
MTBF	10,000 hours	Unlimited. No maintenance
Magnetic Sensitivity	Affected	Insensitive
Geometrical Distortion	Dependent on associated circuitry	None
Maximum Supply Voltage	500V	24V
Operating Power	A few Watts	A few milliWatts.

Table 5.1.2.6 **Comparison of CCD and vidicon tube imaging technology.**

5.1.3 CONSIDERING CCD CHARACTERISTICS FOR EARTH IMAGING.

Having reviewed the characteristics of different area-array CCDs (and other imaging technologies), it is worth recapping the desirable features of these architectures with respect to Earth imaging from microsatellites. High pixel count and adequate spectral sensitivity are clearly of importance when choosing a sensor. To minimise the trade-off between resolution and coverage area, future microsatellite camera systems will need to produce imagery with at least 2000 x 2000 pixels. The CCD will need to cover the visible and near-IR range up to 1.0 to 1.1 µm, and UV-enhancement may be necessary for certain applications. Fortunately, these characteristics are easily determined from a quick glance at the device's data sheets.

More subtly, but of equal importance, is the sensor's ability to capture images without smearing. Currently this rules out the use of full-frame CCDs on microsatellites until adequately reliable shutters can be identified and / or developed. Until then, electronic shuttering is essential.

Imaging from a satellite in low-Earth orbit always involves a moving scene; the dynamics more significant for higher resolution systems (see section 3.3.4.2.3). The camera's integration time must therefore be kept sufficiently short to prevent motion blurring. Similarly, the transfer of charge packets from the imaging photosite to the storage region must be a small fraction (less than 1%) of the integration time, to keep image smearing down. If the integration time must be very short, smearing will be a problem for CCDs using the frame transfer approach.

To summarise, until full-frame CCDs can be supported, frame transfer devices will be the sensor of choice for most microsatellite imaging missions, because of their improved optical and radiometric specifications. However, if very short integration times are required for high resolution imaging, then interline transfer devices must be used to avoid transfer smearing.

Regardless of the exact architecture chosen, there are a number of general points that apply when considering a CCD for microsatellite remote sensing. These are discussed in the following sections.

5.1.3.1 CCD data and signal formats.

When implementing an electronic still-image camera, there is no specific reason to comply directly with an existing TV standard. Obviously, the operational modes of many scientific sensors make this impossible. In particular, sensors requiring interlacing to achieve full resolution should be avoided if at all possible.

However, if a commercial CCD is used, there may be some particular advantage in speeding the clock rate up or down. Faster speeds may be necessary to shorten the integration or read-out time. Alternatively, slower operation will reduce power consumption and can improve the noise performance of the whole circuit by reducing switching transients and eliminating timing glitches.

Of course, if total or part compliance to the TV standard is useful, there is no particular reason to deviate. By the same token, there is no point in arbitrarily lengthening the integration times beyond the 20 ms of video systems, unless absolutely necessary to increase the system's sensitivity for low-light (star, night-time, UV, etc.) imaging. If a video compatible sensor is used, retaining the ability to drive a video monitor can be extremely useful during test and calibration, even if the final flight configuration is different.

5.1.3.2 Dark current.

Thermal excitation causes electron-hole pairs to be generated randomly within the silicon lattice of a CCD. These liberated electrons are trapped by the photosites and are indistinguishable from electrons generated by photonic activity. Although another electron and hole will eventually recombine from the lattice to neutralise the thermal effects, this will not be spatially or temporally correlated to the original event, and therefore results in noise. This dark current noise (so called because it is the current generated by the CCD even when it is in the dark) obeys the diode law, and therefore decreases as the CCD is cooled. At room temperature, it will take about three seconds for a typical CCD to saturate with dark current, and a reduction in temperature of about 8°K will halve the noise floor.

A CCD camera's susceptibility to dark current noise is therefore dependent on its operating temperature and the length of time the charge packets are exposed to dark current (i.e. the combined integration and read-out times). Fortunately, the total integration and read-out period will be kept to around 100 ms or less for satellite remote sensing, and provided the CCD's temperature is kept reasonably cool, the dark current will be sufficiently low for all but the most sensitive applications.

In most cases, passive cooling will be adequate to keep the sensor at 20°C or less. At these temperatures and integration times, the camera's noise performance will generally be dominated by reset errors in the charge amplifier at the CCD's output and noise in the subsequent signal processing circuits (10 times greater than the dark current in the SSTL cameras). If these stages are extremely accurate and noise-free, and dark current dominates the noise budget, the signal-to-noise ratio can be improved by reducing the operating temperature, although it is not recommended to take a normal CCD device below -30°C as mechanical failure may result. Conversely, if the operating temperature of the camera is likely to exceed 60°C, then it will probably be necessary to consider using a thermo-electric (peltier effect) cooler.

Therefore, for most Earth observation applications, dark current noise will not be an issue, because the integration and read-out times will need to be kept short. If high sensitivity is required, cooling may improve the camera's noise performance, provided dark current is the major noise source. If some other aspect of the camera's electronics dominates the noise budget, then cooling will have little effect. In most cases, the most effective way to improve the system's signal-to-noise characteristics is to boost the signal (by using brighter optics) rather than attempting to reduce the noise floor.

5.1.3.3 High-speed versus low-noise CCDs.

Many scientific CCDs are often optimised for either low-noise or high-speed applications. Low-noise CCDs rely on being cryogenically cooled to dramatically reduce the dark current noise floor. Accordingly, they are designed with suitable semiconductor processes to ensure that the carrier mobility is not effected by operating at such low temperature. Indeed the term low-temperature devices is probably more apt than low-noise.

These sensors are intended for applications requiring long integration times (seconds, minutes or even hours - known as slow-scan operation) to build up images in very faint illumination, and need cooling to prevent the noise from accumulating and swamping the useful signal. At cryogenic temperatures, dark current rates can be reduced to around one electron per minute or less. (In astronomical imaging, periods of up to several hours are used to collect photons from faint sources; in these slow-scan applications, the smearing suffered during the tens of milliseconds of the readout are insignificant, and shuttering is not required, even with full-frame CCDs). Similarly, the CCD's analogue stages are designed for low-noise rather than high bandwidth.

Conversely, the high-speed version of a CCD will be designed for room-temperature operation, with relatively short integration times (less than a second) and fast read-outs, and shuttering is necessary. For any form of remote sensing application, the integration time will need to be kept very short (tens of milliseconds) to prevent blurring, and will need to use the high-speed version of a CCD. Although the exposure times for satellite imaging will be very short, brightness of illumination is rarely a problem. The Sun provides plenty of light when imaging the Earth's surface and / or atmosphere in the visible and near-IR bands, and normal high-speed devices will be sufficiently sensitive. (Other applications such as UV, night time, or auroral imaging require extra consideration however).

5.1.3.4 Photosite and array sizes.

The dimensions of the individual photosites and the whole CCD array are important in determining the characteristics and resolution of the imagery. Although the other criteria already discussed are more likely to decide the actual sensor used in a given instrument or application, it is nevertheless important to consider the impact of the photosite dimensions.

With identical optics, a CCD with smaller photosites will produce higher resolution imagery and one with a larger photosensitive surface will provide wider coverage (see section 5.4.1.1). As the size of a CCD's photosites can vary from as small as 7 μm up to over 30 μm, this can mean up to a four-times change in the focal length of the optics for a given application. If the optics are likely to be overweight, or the lens's brightness is marginal, choosing a CCD with differently sized photosites may provide an improvement in overall design.

If the signal strength is likely to be inadequate, either because the scene is dimly illuminated or because a short integration time is necessary, a photosite with a larger surface will gather more photons. However, it is important to consider the actual photosensitive area of the photosite and not assume that the spacing between photosites reveals this parameter. The spacing, or pixel pitch, is often quoted in the CCD data sheets; however, it is a photosite's fill-factor which indicates how much of this area is taken up by non-imaging structures (inter-column guard bands, antiblooming gates, storage areas for interline transfer, etc.). This information on the percentage of photosensitive area on the CCD will often not be provided as routine, and the manufacturer must be asked specifically for details of the photosite structure. Furthermore, any significant reduction in fill-factor will increase the risks of optical aliasing.

Finally, most remotely sensed imagery will be displayed on a computer terminal, the majority of which will only be able to handle square pixels. Therefore, selecting a CCD with square, rather than rectangular, photosites will ensure that the images are displayed with the correct aspect ratio. Similarly, having square photosites provides equal resolution along both axes, and simplifies many post-processing tasks, such as pixel resampling, because the same algorithms can be used in both dimensions.

5.1.4 CONCLUSIONS WITH RESPECT TO EARTH IMAGING FROM MICROSATELLITES.

5.1.4.1 Low resolution (meteorological) imaging.

The wide IFOV of a low resolution imaging system makes it fairly insensitive to the various motions (orbital velocity, pitch and roll, but not yaw) experienced on a microsatellite which can result in degraded imagery. Because of this, integration times compatible with standard video (20 ms) and longer can be used without any noticeable blurring of the image. With such long integration times, the transfer time of frame transfer devices is sufficiently fast to ensure adequately low smearing of the image. For the same reason, it is feasible to use interlaced CCDs in low resolution applications, as long as the satellite's displacement between the capture of the two fields remains small.

Fortunately, the insensitivity of a low resolution imager to the various motions places fewer restrictions on the choice of sensor. All of the architectures used for area-array CCDs are suitable for use in these systems. For meteorology, where the emphasis is on the macroscopic scale of the imagery, the aliasing effects of interline transfer CCDs are unlikely to be problematic.

However, interline CCDs generally have a poor spectral response in the near-IR. As this is a crucial remote sensing band, the suitability of many of these devices is limited. Although full frame CCDs have excellent optical characteristics, they require some form of external shutter which represents an additional overhead and liability in the context of microsatellite remote sensing. Therefore, the frame transfer design can be considered the most suitable CCD architecture by a process of elimination. These devices will have an all-electronic operation, variable integration mode, good fill factor and good spectral sensitivity. The frame transfer video sensors used in the various SSTL cameras have worked well over a range of ground resolutions and spectral bands. The only possible criticism of their performance for this application is the low photosite count.

5.1.4.2 Medium resolution (environmental) imaging.

In medium resolution imaging applications, the effect of motion blur is more pronounced, and the CCD's integration times must be kept suitably short, around 10 ms. Nevertheless, these timings can be handled by conventional video sensors without suffering undue blurring or smearing of the image. Therefore, all of the arguments presented for selecting a sensor for low resolution imagers are equally valid, and frame transfer CCDs are also the most attractive option for this application.

However, if an video sensor with interlacing is used, the delay between the two fields will start to become noticeable at these resolutions. The slip between the fields is apparent in the images from the PoSAT-1 Narrow Angle Camera. By enlarging part of an image (captured over Tibet in May 1994), figure 5.1.4.2a reveals this effect prominently; figure 5.1.4.2b shows the same sub-image after re-sampling one of the fields during processing to remove this misalignment.

Although the choice of CCD architecture is fairly open for medium resolution imaging application, the use of progressively-scanned sensors is therefore recommended. If the imaging conditions can be carefully controlled, as they would have been on FASat-Alfa (see section 5.1.2.5), it is possible to side-step the effect of the delay between the two fields.

5.1.4.3 High resolution (land resources) imaging.

The effect of the satellite's motion is very pronounced when performing high resolution imaging, imposing an integration time of about 2 ms or less for 20 metre resolution. Under these conditions, the transfer time of a frame transfer CCD will be a significant percentage of the integration time, resulting in bad smearing of the image. It may be possible to drive the field transfer clocks at a much higher rate to reduce the effect of this smearing, but custom electronics are needed to support this. Even so, there will be a dramatic increase in power consumption, system noise, and ultimately the transfer smear will still be present (albeit at a reduced level).

Therefore, for high resolution remote sensing cameras requiring fully electronic operation, the interline transfer architecture is the most suitable type of CCD. Despite the other limitations of these sensors, the instantaneous transfer eliminates the problem of smear. If the full specifications of the imaging system (principally spectral response) cannot be met by an interline device, the only remaining option is to use a full-frame CCD with a shutter.

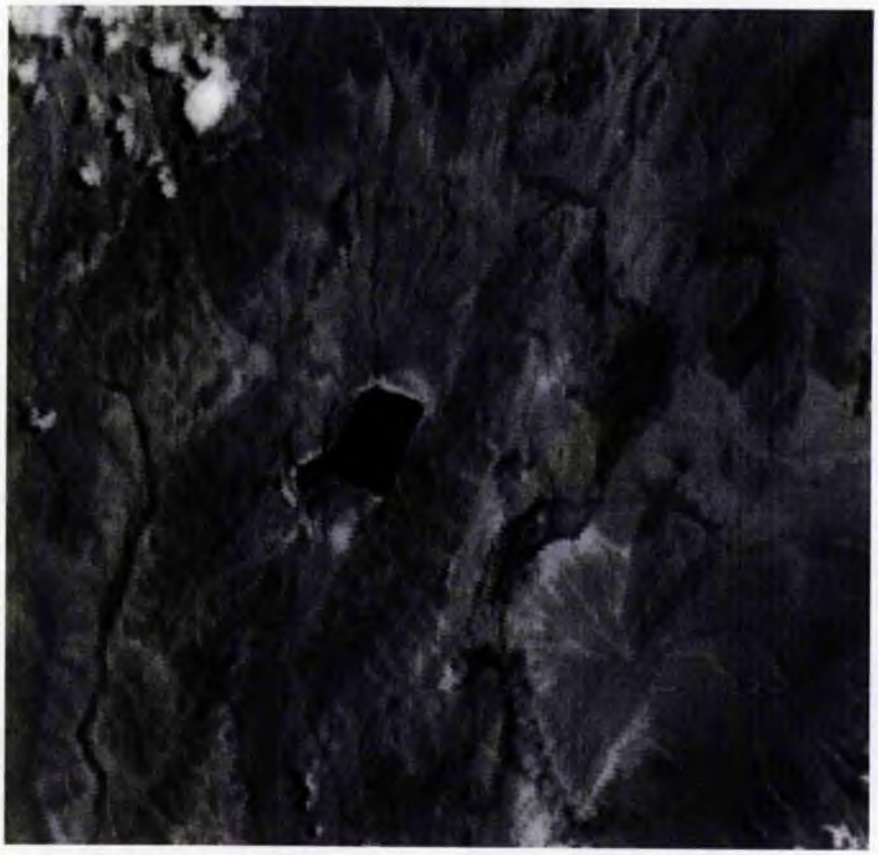

Figure 5.1.4.2a

PoSAT-1 narrow angle image suffering inter-field offset due to interlaced CCD.

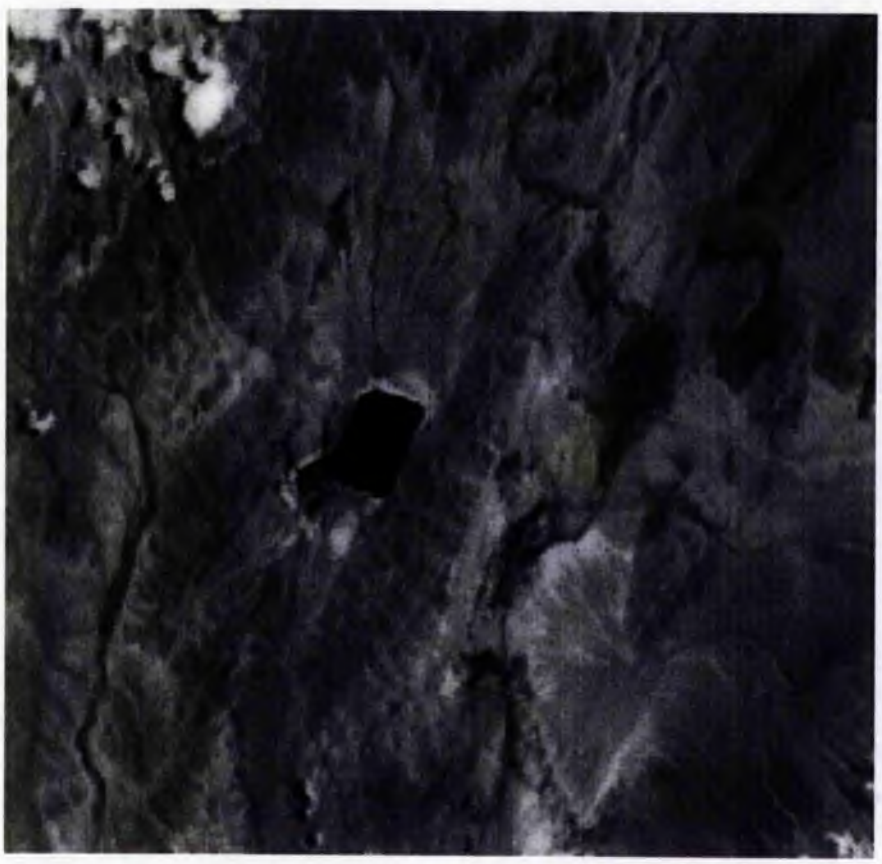

Figure 5.1.4.2b

Same image following correction by resampling odd field.

5.1.5 CHOICE OF SENSOR FOR THE EARTH IMAGING SYSTEM.

The CCD sensor used in SSTL's Earth imaging cameras on the UoSAT-5, KITSAT-1 PoSAT-1 and FASat-Alfa microsatellites is the CCD04-06, manufactured by EEV Ltd of Chelmsford, UK. It uses the frame transfer architecture and has a 578 x 576 pixel format, of which 568 x 560 pixels are active. This device is designed to produce television compatible signals and, as a consequence, uses interlacing. Useful features of this device are antiblooming and electronic integration control.

From the previous discussions, the CCD04-06 is an acceptable choice for a low resolution imaging system. Although the photosite count is not particularly impressive by today's standards, it was competitive for a CCD with electronic shuttering when the UoSAT-5 camera was designed in 1990. The larger HDTV and computer vision sensors now available did not exist then.

Two other commercial devices with similar characteristics were also considered: the Thomson-CSF TH7864 (550 x 576 photosites - frame transfer), and the Sony ICX024AL (756 x 581 photosites - interline transfer). The characteristics of these three CCDs are very similar and the deciding factor for the EEV device ultimately had little to do with its imaging properties; it was based on the level of technical support offered by EEV. As we shall see in section 5.2, it is not the CCDs characteristics alone that are important when designing electronic cameras.

5.1.6 CONCLUSIONS.

In keeping with the tradition of using simple designs on microsatellites, an all-electronic approach must be favoured for implementing remote sensing cameras. Unfortunately, this rules out the use of full-frame CCDs until a compact yet reliable shutter technology can be developed or demonstrated.

The two main techniques of implementing electronic shuttering are frame transfer and interline transfer. Although their properties are largely similar, the frame transfer architecture generally offers better performance in the near-IR and slightly better fill-factors. If the total photosite count is important, then frame transfer devices conceived for HDTV have the edge. Therefore frame transfer CCDs are the preferred choice for microsatellite imaging systems for ground resolution coarser than 100 m.

For finer ground resolution, the integration time used will need to be kept very short to reduce the motion blur suffered. Unfortunately, with short integration times, the transfer time of a frame transfer device becomes significant, resulting in image smear.

Therefore, it is necessary to select an inter-line transfer to avoid this smearing. Table 5.1.6 summarises the most suitable area-array sensor for a given resolution.

Class of resolution	Nominal ground resolution	Most appropriate CCD architecture
Low	2000 m	Frame transfer
Medium	200 m	Frame transfer
High	20 m	Inter-line transfer

Table 5.1.6 Most suitable area-array CCD versus ground resolution.

5.2 SPECIFYING A CAMERA AROUND A CCD SENSOR.

5.2.1 BASIC CAMERA ARCHITECTURE.

Although the CCD sensor is the most important component of an electronic camera, it cannot produce images by itself. Having identified a number of suitable sensors for a given application, the surrounding circuit elements must be considered. The basic architecture of a CCD camera is virtually the same for all area-array CCDs, regardless of the device's exact specifications. Dedicated logic circuitry generates the complex clock timing and phasing needed to drive the CCD's integration, transfer and readout processes. These signals must be buffered to isolate the sequencing logic from the CCD's capacitive load, driving the CCD's inputs within the tightly defined specifications. Sophisticated analogue signal processing stages are required to extract and amplify the weak signal from the CCD's output, and convert this into a useful signal (generally to drive a 75Ω input on a video monitor). Local power conversion and conditioning is also necessary to supply both the high current digital rails for the logic and buffers, and the low current analogue bias rails for the CCD and the video processing. Figure 5.2.1a shows a block diagram of a typical CCD camera.

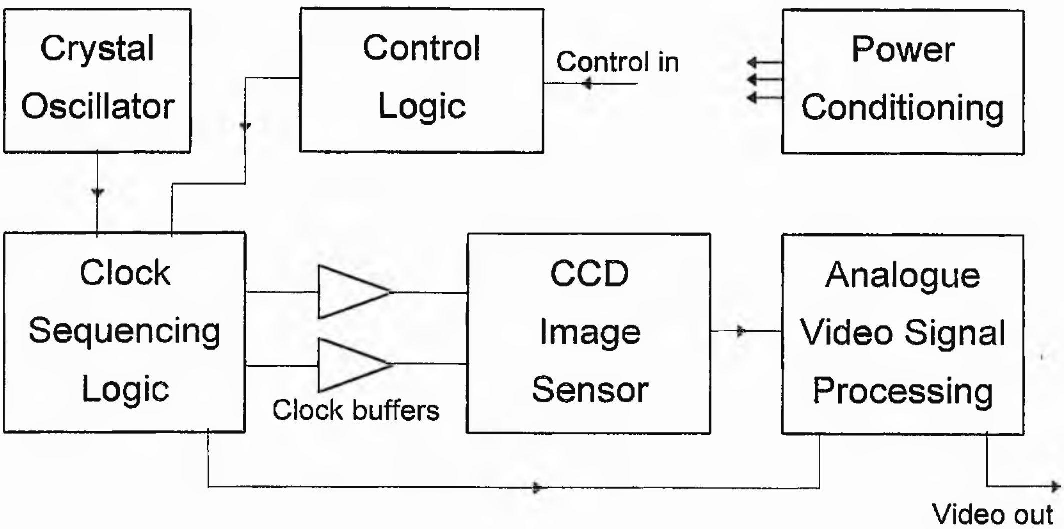

Figure 5.2.1a Typical CCD camera block diagram.

In the case of an electronic still camera, various additional digital interfaces are needed to link this basic camera circuit to a host microprocessor. These include a number of digital command lines to exercise control over the camera's operation (e.g. to set integration, gain, bias offsets; to activate the circuit: on / off, capture now, etc.). Also required are a video speed analogue-to-digital converter to sample the pixel stream in the video signal and a frame store to buffer the digitised image. The extended block diagram of the digital cameras developed for this programme is shown in figure 5.2.1b (except UoSAT-5 which uses a parallel interface).

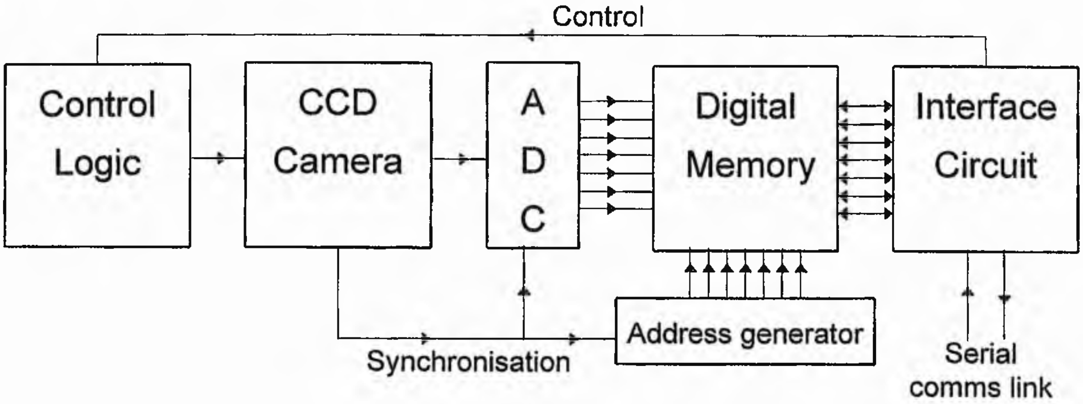

Figure 5.2.1b **Typical block diagram of a digital still camera.**

To produce high quality images from an electronic camera, it is vital that the support electronics draw the best from the CCD sensor. The design of the support circuitry and judicious choice of components is as vital as the CCD in producing high quality images. Although the functionality of the items within the camera's circuit is quite clear, fine-tuning them to provide optimum performance can be a difficult job. While the choice of the CCD is made based on the science of the application and the sensor characteristics, the design of the surrounding circuitry requires a proficiency in high speed electronics. For example, these circuits need to provide the correct phasing of the digital clock signals, including their attack, decay and cross-over characteristics and the DC biasing, which are all crucial in ensuring that the CCD captures and transfers the charge-packets optimally. The high-speed digital and analogue techniques for amplifying and sampling the CCD's output signal are also subtle and complex.

Furthermore, because of the manufacturers' proprietary design and production techniques, every CCD requires different inputs (frequency, phasing, voltage levels, bias) and produces different outputs. Even CCDs from a given manufacturer may differ significantly in their operational requirements. This makes designing electronic cameras even more difficult, because there are few standard circuits which can be ported from design to design. While previous experience is useful, knowledge of a specific sensor's characteristics will not instantly permit the use of a camera design based on another CCD. Therefore, as with any complex electronic circuit, it is necessary to visualise the operation of the full camera circuit in detail before making any significant investments of cash or time.

It is important to assess the difficulty faced in implementing all aspects of a camera before making the final selection of the CCD. The designer must feel confident that all of the major design issues have been addressed early on, including the specific peripheral components that will be used, as well as any potential problem areas.

5.2.2 USING OFF-THE-SHELF TECHNOLOGY TO DESIGN THE IMAGING SYSTEM.

Fortunately, manufacturers realise the difficulties of extracting images from their CCDs, and most go to considerable lengths to offer assistance to the user. Clearly, if it was necessary to be a skilled video engineer to use their products, their sales would be extremely limited. Certainly, the manufacturers will have already invested significant time and money into developing circuits to evaluate and test their sensors, and most will make this knowledge available to customers. As with all forms of electronic design, the designer of a remote sensing camera should make use of existing expertise to promote the chances of success, and any advice proffered by the CCD manufacturer should be heeded.

This assistance can come in several forms ranging from extensive data sheets, technical notes, applications notes, and circuit diagrams covering aspects of driving the CCD and processing the signal, to the availability of existing support hardware either as dedicated chipsets or complete cameras. However, because the requirement of an Earth observation camera are somewhat different to most applications, the designer must assess the suitability, and availability, of any such support circuits before committing to them.

Equally indispensable is the willingness of the supplier to give on-line technical support. This must be ensured early in the project as the order quantities from a microsatellite mission are small, and the manufacturer may not necessarily be forthcoming in providing this expensive resource.

Although the products offered by the manufacturers are designed to support the major applications of their devices, which may or may not be compatible with the requirements of satellite remote sensing, the designer should nevertheless seek as much advice as possible and use what is relevant. Borrowing from literature and the manufacturer's knowledge pool should not be viewed as poor design practice, provided the choices are well understood. Indeed, it is sufficiently difficult to design a successful camera, even with this help. The sole objective of the designer must be to produce a system which captures images of acceptable quality. Consequently, if accepting help improves the camera, then it is a good thing.

5.2.2.1 Using complete cameras.

By far the most common source of user support from the manufacturers of CCDs, and almost too obvious to mention, is the development of complete camera systems. As the majority of users do not care what is happening inside the camera, and are only interested in the pictures produced, this meets the requirements in most cases. Certainly for all TV compatible sensors now available, the manufacturers produce complete cameras. Finished products for a range of television applications (professional broadcast, news gathering, closed-circuit, production monitoring, etc.), rather than components, will represent the bulk of their sales volume.

The TV standards have fulfilled the vast majority of imaging applications for the last three decades. Conversely, because of the diverse range of applications and disparate requirements, fewer manufacturers of scientific CCDs produce complete cameras, although some do exist. Regardless of the final application, if an off-the-shelf camera exists that fulfils all of the mission requirements, it must be considered carefully. It will be virtually impossible to improve on the cost or speed of delivery of a finished camera by attempting to design and build an equivalent imaging system in-house.

However, it is unlikely that these off-the-shelf items will be acceptable as sold for the application of microsatellite remote sensing. Most cameras do not possess all the necessary operational attributes for satellite imaging: variable frame / field rate, clock rate (i.e. transfer speed), and integration control. Even when these features are available, there may be difficulties in interfacing the analogue camera to the digital systems on the satellite. Any controls on a camera to set parameters like the integration time will generally be manual switches or dials and not digital interfaces. Moreover, the digital sampling of the output signal is of crucial importance in ensuring image quality. Without access to the camera's internal signals, pixel clock recovery (in both frequency and phase) will be very difficult, if not impossible, and certainly sub-optimal.

Unfortunately, no standard camera will use the temperature and vacuum rated (let alone mil-spec or space-qualified) components generally considered necessary for use on a spacecraft. These commercial cameras will include many inappropriate components such as integrated circuits specified to 0°C, wet electrolytic capacitors, PVC wiring, PCB solder resist, nylon connectors, washers and spacers, to mention but a few. Furthermore, even though many CCD cameras are very compact, the dimensions may not suit the available volume within the microsatellite. Other mechanical considerations include the build quality of the housing and the fixings of the printed circuits and / or lens mounts, which will rarely be sufficient to restrain the camera during launch. Similarly, large components may be unsuitably mounted or assembled to survive these vibrations. Finally, the handling of the components, the assembly, the soldering and the cleaning of a commercial camera will not have been performed to a level commensurate with (even moderate) reliability standards. Components and labour will not be traceable to provide adequate quality assurance.

Unfortunately, for these reasons, it is very unlikely that any existing off-the-shelf camera will meet all the requirements of a microsatellite imaging mission. If the camera unit meets all of the operational and interfacing aspects of the mission, it may be feasible to remove and upgrade any components and materials which are out of specification. Similarly, it may to possible to cut and re-route PCB tracks to inject and pick off signals on the camera to provide the necessary level of interfacing control. However, this sort of rework is undesirable because of the scope for stress and damage on either the PCB or the components. Heavily reworked wires and tracks will inevitably be of limited reliability. Accordingly, the author cannot recommend the use of off-the-shelf commercial cameras, either for TV applications or the recently introduced digital still cameras, for space remote sensing systems.

Nevertheless, this approach has been adopted before, and a reworked commercial video camera was flown on the Webersat microsatellite in 1990 (see section 2.3.5.3). The success of the experiment is not well documented, and the images published are inconclusive. Certainly the imagery is not of the same quality as produced by its contemporary UoSAT-5, let alone the subsequent SSTL cameras. Furthermore, extracting and reconstructing the imagery from the digitised data stream has proven to be difficult.

This said, complete camera systems from the manufacturer can serve as an invaluable reference or guide from which to build the flight model. The timing and signal conditioning of an operational system can be compared to the data sheets specifications to assess the margins and temperament of the CCD. Also, by performing various PCB modifications, one can obtain very quick and low cost prototypes. Given that in most instances, a complete camera costs the same (and often less) than purchasing the semiconductors individually, this will be the cheapest and quickest solution for proof-of-concept implementations. (Further savings will be made by avoiding the layout and production of the PCB, and labour for assembly, test and debugging).

5.2.2.2 Using dedicated support chips.

When it is not feasible to use an off-the-shelf CCD camera design produced by the manufacturers (and occasionally by third parties in the scientific field) directly on the satellite, the designer should attempt to pick out as much of use as possible from these tried-and-tested circuits. Of particular interest are the dedicated chips used to support the CCD, including the clock sequencing logic, the clock drivers, and any analogue signal processing.

In the mid-1980s, there was a heavy emphasis on developing and launching new CCD products. All the support circuits were made entirely from discrete components and logic. This allowed some flexibility in adapting to frequent design revisions of the sensors, or in overcoming widely varying tolerances of the CCD's characteristics. Accordingly, the manufacturers did not devote much effort into producing highly integrated chips to fulfil these support functions. However, at the end of the decade, when the fabrication techniques for the CCDs had largely been mastered, dedicated chipsets started to become common. Today, they are considered virtually indispensable for all commercial TV sensors.

The main purpose of these dedicated support devices is for use by the manufacturer inside its cameras, but they are generally available for purchase as individual components. By integrating complex logic and signal processing functions onto single chips, the finished cameras clearly benefit in reduced mass, volume and power consumption, and improved portability. Furthermore, they are also more reliable, simpler to test, and generally offer better performance by minimising parasitic effects and noise cross-coupling. Certainly, for imaging applications where the standard video formats (or slight deviations from them) are acceptable, these chipsets will provide very good service in a compact volume.

Fortunately, in many instances, a chipset will incorporate additional features (integration control, clock speed / transfer speed adjustments, non-standard operating modes, etc.) that are not available externally on the finished camera. Although not considered useful or necessary for the general user, these features give the CCD and chipset enough flexibility for designers (both in-house and customers) to use the same basic hardware in a range of applications. These features are sometimes included to allow peripheral chips to be used across a family several sensors (EEV, Thomson) or to accommodate future circuit or packaging modifications. For all three of the CCDs short-listed during the UoSAT-5 development campaign, gaining access to these extra functions made an otherwise unacceptable camera fit the specifications.

Of course, it is by no means essential to use a manufacturer's chipset to design an electronic camera. Indeed many scientific cameras are built without these tools. Furthermore, for very high specification imaging systems, the chipset will probably not be able to deliver the necessary performance and discrete circuits will need to be implemented, using a range of components. Similarly, not all the features offered by a chipset will really be of use for the given application, and some analysis and intuition will be needed to determine the whether a particular task is best fulfilled by the dedicated device or by custom circuitry. Unfortunately, most of the time, the support chips will not be available to any superior standard of screening, temperature performance or radiation resilience, which may be an issue for certain missions.

On balance, in most instances, building a camera around the chipset provides the best compromise between a discrete design (allowing full flexibility, control and choice of components, but presenting a wide scope for design error) and using a complete camera (simple to produce but failing to meet the imaging or material specifications). By using and adapting a suitable chipset, a designer can operate the CCD in the desired fashion but without having to delve too deeply into the implementation of the control logic and, especially, the video signal processing, effectively getting the best of both worlds.

Regardless of some potential loss of flexibility and component specification, using the manufacturer's dedicated support chips will jump-start a design. By simplifying the designer's task, the camera will stand a better chance of being ready on time and having a predictable behaviour once in orbit. Inexperienced camera designers are recommended to make use of this springboard, although experienced designers will be in a better position to dispense with these support devices and design their own circuits to more demanding specifications.

However, the chipset from a manufacturer will rarely implement a complete remote sensing instrument. In particular, all of the digital interfaces and analogue-to-digital conversion stages will need to be developed. (Due to commercial sensitivity, the circuits for new digital still cameras are not made available by the manufacturers). Therefore, the designer will need to augment a basic chipset with discrete components and ICs to produce the final system. The schematic diagram of the final system will be similar to the manufacturer's, but surrounded by the additional circuits provided by the camera designer. Apart from the half a dozen support chips themselves, all remaining passive and discrete components can be procured to the relevant specifications, and the PCBs can be made to fit the available volume and area.

Thus, the designer of any microsatellite imaging system should consider the support available for the short-listed sensors very carefully before finally deciding which device to use. Choosing the right CCD and chipset will dramatically improve the chance of success. This is demonstrated by comparing the cameras on UoSAT-4 (built using discrete components) and Webersat (used a reworked camera module) to the UoSAT-5 system (built around a CCD and chipset). Despite being designed a year later, in less than half the time, the UoSAT-5 system shows vast improvements in the image quality, circuit stability and operational flexibility over both of its predecessors.

5.2.2.3 Final selection of camera components.

The final decision on the key camera components must be based on the likelihood of their producing quality images in-orbit. This may appear to be a truism, but this point can sometimes be overlooked when a system is being developed. The success of the instrument will be judged solely on its ability to produce quality imagery, and the contents of the camera's 'black box' will not be a primary concern.

The search for camera components must start with the CCD sensor itself. Obvious factors such as the CCD's photosite count, spectral sensitivity, electronic shuttering and integration control can be assessed quickly, eliminating many unsuitable devices early on. Equally crucial is the sensor's physical architecture, and its characteristics for smearing or blooming (the runaway condition where a single severely over exposed photosite leaks into neighbouring photosites, causing gross image degradation).

Once a set of suitable CCD sensors have been selected, the availability of dedicated support chips should be the next consideration. The existence of these devices to drive the CCD and process the output signal will greatly improve the probability of retrieving images in orbit, as well as contributing to their overall quality. The three CCDs (EEV, Thomson, Sony) short-listed for the UoSAT-5 camera all had these features; suitable imaging and architectural characteristics, and chipset available. Many other devices were considered and rejected on one or more of these criteria; typically it was the absence of integration control and / or no chipset, which were not as common then as they are now.

Prior to purchasing a CCD, it is also vital to establish the availability of plentiful and detailed data sheets, application notes and circuit diagrams. In addition to detailed descriptions of the CCD and chipset during normal operation, examples of non-standard implementations are also essential. It is worthwhile to make a wider survey of data sheets and application notes for other devices and manufacturers, as this is useful in identifying potential problems and picking up design ideas.

Securing adequate technical support can be a hidden obstacle in preparing complex electronic camera systems. Sony's corporate policy, like many Japanese companies, is geared towards volume sales, and was unprepared to devote technical support resources to a project as small as SSTL's microsatellites. Similarly, although Thomson made vast quantities of detailed literature available, the response was not as forthcoming as EEV, whose engineers and sales staff were very enthusiastic and helpful, despite the small sales forecast. Although, interpreting a corporate attitude is not strictly relevant to electronic design, it was nevertheless crucial in the success of the UoSAT-5 imaging experiment. EEV's attitude to a small, 'off-beat' project like the UoSAT-5 camera reflects the relatively small size of the company and their background in scientific R&D.

As mentioned previously, the EEV CCD04-06 is a video-compatible sensor, with a number of desirable features for microsatellite Earth observation. EEV's forte is large full-frame scientific sensors, and this focus consequently makes their limited range of video sensors more sensitive and linear than most commercial sensors. (Thomson-CSF also covers both sectors, and has a similar reputation). Nevertheless despite many attractive technical features, the EEV sensor was ultimately chosen for the camera based on the characteristics of the chipset and the technical support offered by the company. After four generations of cameras on microsatellite missions, the wisdom of the rationale governing this choice has yet to be put in doubt. Although this image sensor is being phased out of future SSTL designs because of the dramatic advances in the performance of CCD technology, the selection of alternative CCDs is being conducted by assessing the same criteria, moderated to a small extent by the increased experience in the design of cameras for microsatellite remote sensing applications.

Thus the CCD selected for a microsatellite electronic camera must meet all of the following criteria: imaging and architectural characteristics, adequate documentation, guaranteed technical support, and (ideally) the availability of dedicated support chips.

5.3 DESIGNING THE CAMERA ELECTRONICS.

When the CCD has been selected, the detailed design of the surrounding circuit can start. If a sensor with support chips has been chosen, this task will be simplified considerably. Even if this chipset is not available, the manufacturer's schematic diagram of an electronic camera using their device is a good starting point. This circuit diagram should be used as a template for the new design, adapted as necessary.

The majority of complete chipsets are designed to produce continuous video signals for TV, and the literature emphasises various aspects this application. However, the requirements of electronic still-image cameras are somewhat different. The most obvious difference is that instead of free-running continuously, still cameras operate in a 'snap-shot' mode. Various set-up parameters to control the time of capture and exposure need to be introduced to the camera prior to capturing the single frame of imagery. Furthermore, the analogue video signal needs to be digitised so that it can be stored, ready for transmission or display. In particular, the effect of noise is much more disturbing in a still-image than in a continuous stream, because the eye has time to linger on any image defects. It is important to take extra precautions against supply-borne and cross-coupled noise that is not normally necessary for applications using continuous video.

Overall, implementing an electronic camera is similar to other video circuits, and conventional high speed analogue and digital design techniques must be used to ensure good performance. This includes factors such as the use of ground planes, the separation of analogue and digital components and signals, careful PCB layout, generous supply rail decoupling, and a general care with timing glitches and propagation delays. As with other video frequency designs, it is important to keep the physical distances between components as small as possible to avoid degradation of the signals, especially between the CCD and signal buffers, and CCD and video pre-amp.

Unlike other spacecraft systems which may have different design objectives, the quality of the captured image must be the key motivating factor at all stages in the development of an electronic camera. Although a camera's success will be judged by its performance in fulfilling the imaging goals, the electronics will nevertheless need to respect the usual design criteria for small spacecraft: low mass and volume, physical robustness, reliability and hopefully, some radiation tolerance. While the camera's power consumption is also of importance, the design considerations will differ from usual practice because of its distinctive mode of operation. Section 5.3.1 discusses this in further detail.

5.3.1 DESIGN OF POWER CONDITIONING.

5.3.1.1 The SSTL bus power system.

The standard Power Conditioning Module (PCM) of an SSTL microsatellite bus provides regulated +5V, +10V, -10V rails and a raw battery rail which varies between +12.5V and 14.5V (+14.5V in Sunlight). Clearly, the details of the regulated voltage rails supplied by the power system on any given microsatellite platform vary, but the SSTL power system is fairly representative. In general, standard +5V (to power digital systems) and +28V rail (adopted from the aeronautics industry) are popular.

Most modules fed by the power system will have their supply lines interrupted by a switch. It is imperative that the power to all non-vital spacecraft systems (i.e. everything but the telemetry, telecommand, power and receiver modules) can be switched off to isolate and protect the rest of the spacecraft in the event of a module failure or a short circuit. Furthermore the ability to activate power-hungry modules selectively is often necessary to maintain a positive power budget.

Therefore, the power to all of a microsatellite's imaging systems must be switchable. Power switches are a limited resource on a microsatellite, and it eases the power system design if modules can use as few rails as possible. On the whole, the power demands of cameras (peak power drawn, duty cycle, range of supply voltages, need for clean rails) will be incompatible with the regulated supplies offered by the microsatellite bus. Therefore, in most cases, it is appropriate for the camera to be supplied by the raw battery supply and to regulate its own rails locally. Furthermore, using a single rail for a module minimises the probability of a circuit being partially powered (with one rail on and another off), which can be very damaging to the circuitry.

The control of the camera's supply can be driven by a spacecraft telecommand. However if control is kept local to the imaging system, for example by a dedicated microcontroller, significant benefits can be obtained in the timing of image capture and flexibility of operation.

5.3.1.2 Supplying the camera's power rails.

Most CCD sensors and their chipsets require a range of voltage rails. The EEV CCD04 camera is a typical example, requiring four separate voltage rails: +12V for the clock drivers, +5V for the logic, +24V to bias the CCD substrate, -5V to bias the analogue ICs. The +12V and +5V rails carry the bulk of the current. The -5V rail carries some 10 to 20 mA and the +24V rail carries under 1 mA. Although the exact voltages will vary, most CCD circuits require a similar range of voltage and current supplies.

Apart from the +5V rail, these requirements do not match the spacecraft's regulated supplies and it is necessary to implement local power conditioning within the camera to provide these rails. The satellite's +10V and -10V rails are designed as bias rails for low-power applications (under 50 mA for the whole spacecraft). Clearly, they cannot support the high current demands (pulses of over 1 Ampere) of the camera.

The spacecraft's raw battery supply will be a fairly constant (but unregulated) +14.5V during Sunlight. Fortunately, simple linear regulators can be used to provide any lower voltage rails (+5V, +10V, +12V) needed. Switching regulators will be needed to generate any negative or higher voltage supplies. If the camera calls for a +15V rail, then it may be feasible to add another cell to the battery packs to increase the nominal voltage by 1.4V to around +16V. This was performed on the S80-T microsatellite to comply with the requirements of the customer's payload.

Nevertheless, even if suitable voltage rails were available from the PCM, it would be unwise to use them. These communal spacecraft supplies are generated using switching converters to maintain good efficiency, and are consequently quite noisy, suffering appreciable high frequency ripple and droop. This supply-borne noise will have a detrimental effect on image quality, particularly at the CCD output amplifier which inevitably has a poor power supply rejection because of its simple structure. Furthermore, the noise on the output of a switching regulator increases in amplitude as the loading increases. Therefore, on an imaging microsatellite, the rail's condition will always be at its worst when the cameras are powered. Clearly, using the main spacecraft regulated rails to supply the camera's sensitive analogue circuitry is incompatible with obtaining high quality images.

Fortunately, the spacecraft's +14V rail is significantly cleaner than the regulated rails because it is isolated from the main noise sources (computers and other digital systems) by the PCM, and because it is smoothed by the large capacity of the batteries.

Similarly, substantial current drawn by the camera(s) from the raw rail will cause minimal impact on the other systems.

Finally, using the raw battery supply rail is more efficient than using a regulated line because the PCM's efficiency factor is not sustained. Similarly, as imaging virtually always takes place in Sunlit phase of the orbit, the power comes straight from the panels and not the battery, slightly improving the satellite's overall power efficiency. If the microsatellite's power budget appears marginal, then these slight gains in power usage will be beneficial, offsetting some of the losses incurred by the camera's local conditioning.

5.3.1.3 Power utilisation of an electronic camera.

Although there is clearly a need for electronic cameras on microsatellites to be thrifty with their power requirements, the design philosophy of the local power conditioning is rather different to that of most other housekeeping or payload systems. Typically, electronic CCD cameras consume 3 to 7 Watts. If a dedicated imaging microsatellite carried only two or three cameras, it might be feasible to leave them on all the time. However, if there are multiple cameras (as in a multispectral camera) or other necessary sub-systems (high performance computers, attitude sensors or actuators, or high power downlink transmitters), this payload power consumption is too high to leave the camera(s) on continuously, and they must therefore be turned off whenever not actually capturing images.

The imaging system will still need to have some circuits which are on continuously (probably the controller unit scheduling the up-coming activities), and these must have modest power demands. Typically, this will be a microprocessor and digital logic, running from a +5V power switch. If the processing stages are modularised, they may require a switch each. Conversely, the image capture circuitry (i.e. the camera itself) will be switched on only as required.

Perhaps incongruously, this strategy of frequently turning the camera off, developed to minimise the camera's power consumption, leads to a scenario where its actual power consumption becomes immaterial. Consider that the actual capture time of an image with an area-array CCD will take a few hundred milliseconds, at most. Allowing for a certain amount of time either side of this event to allow the camera system to stabilise, the camera should not need to be on for more than 10 seconds at a time, but probably as little as 2 or 3 seconds. Even if the camera operations are extremely active capturing a couple dozen scenes per orbit, the overall on-time is very small (no more than about five minutes per orbit).

Therefore, provided the camera's duty cycle remains very short, it can have a large peak power without significant impact on the spacecraft's power budget. Under these conditions, the camera circuitry should be optimised for imaging performance even if this is at the expense of instantaneous power consumption.

5.3.1.4 Conditioning the camera's supply rails.

As just mentioned, the presence of any noise on an electronic camera's supply rails is likely to have a direct impact on the quality of the imagery produced. Therefore, linear regulators should be used on all camera rails to reduce the amount of ripple, even on the rails supplying digital circuits. If a local switching regulator is used to produce a negative or higher voltage bias rail, this should always be followed by a linear regulator to smooth out the converter ripple. (A filter of passive components would be physically larger and would not provide the same level of noise rejection). Furthermore, analogue and digital circuits should be regulated separately wherever possible to minimise the effects of cross-talk.

Some care must be taken in ensuring that these linear regulators have adequate heat-sinking if they are going to be dissipating appreciable amounts of power. This is most likely to be an issue if the rail consumption is high (e.g. greater than 250 mA) or if large voltage drops are experienced (e.g. generating a +5V rail directly from a +28V supply). It may be more appropriate to use a switching converter to provide an intermediate rail at 2V above the required rail voltage, and use a linear regulator for the final conditioning.

Any DC-DC converters used should be run at as high a frequency as possible to minimise the amplitude of the ripple placed on the supply rails and ground. The UoSAT-4 camera used a DC-DC converter running at close to the line rate, resulting an unpleasant horizontal striping in the captured image. Successive generations of the SSTL camera have used converter chips with increasingly fast clocks, and the impact of ripple has been steadily decreasing, although some noise is still present in the last couple of bits of the digitised image.

Fortunately, there are now many families of switching regulator circuit available either as discrete converter ICs or complete hybrid units. Many of these use extensive filtering to provide very good noise specifications. Nevertheless, it is worth designing or selecting a switching converter to provide a couple volts more than is actually required, and then using a series linear regulator. This provides the best compromise between the efficiency of switching regulators (only the last two volts are dropped by the linear stage) with the low-noise characteristics of linear regulators.

If small amounts of current (under 20 mA) are required on a bias rail, the most suitable solution is to employ simple diode - capacitor charge-pumps for local DC-DC conversion. Although they are less efficient than many other converter circuits, charge-pumps inject far less noise onto the ground rail because no inductors are used to store charge.

To designers accustomed to traditional practice of reduced power consumption in space electronics, especially for microsatellites, the liberal use of linear regulators may appear wasteful. However, the power dissipated as heat within these regulators will probably only represent an extra few percent on top of the camera's nominal consumption. Furthermore, provided the camera has a low duty-cycle, as discussed in section 5.3.1.3, its actual power consumption is unlikely to have any impact on the satellite's power budget. Nevertheless, the positive effect that linear regulators have on image quality is so great that their use would be justifiable, even if the power budget was degraded by the camera's drain.

5.3.1.5 Assessing the supply noise on the image quality of SSTL cameras.

Noise carried by a camera's power supplies can significantly degrade the instrument's performance. Given that some parts of the analogue circuitry will have poor supply rejection performance (especially the CCD's on-chip charge amplifier), it is important to ensure that the camera is presented with clean supplies. Indeed, this has been the dominating source of noise in the SSTL cameras built during this research programme. (For this reason, the discussion of the cameras' noise characteristics is included at this point).

To assess the noise performance of an imaging instrument, it is necessary to capture data without any incoming light. All other parameters must be representative of normal operating conditions when collecting these 'dark images'. Table 5.3.1.5a shows samples of this reference imagery for the various systems developed, allowing the progress in this area to be assessed comparatively. [1]

---

[1] These samples correspond to 100 x 100 pixel sub-images from representative 'dark images'. The grey-scale contrast of these sub-images has been stretched to accentuate the noise characteristics. In each case, the linear portion of the histogram stretch corresponds to 16 grey levels. Therefore a noise signal filling the full dynamic range of a sub-images is inserting 4 bits of noise into the imagery recorded. Only noise is of significance, and any variations in mean value, making one image brighter or darker than another, are irrelevant. Where appropriate, both wide and narrow angle, and single-field and interlaced imagery is provided.

The design of the power conditioning circuits of the SSTL cameras has evolved over the missions. On UoSAT-4, the spacecraft's +5V, +10V and -10V rails were used and a low-frequency (4 kHz) DC-DC converter generated a +18V rail. The camera consumed about three times as much as the rest of the spacecraft combined on the ±10V rails (120 mA versus 40 mA), resulting in poor regulation on the lines when the camera was operating. Figures 5.3.1.5a and b show examples of 'dark' imagery captured by the UoSAT-4 camera during ground testing. The horizontal striping is very pronounced, principally caused by the DC-DC converter's ripple. Virtually every pixel is subjected to a full 4 bits of supply-borne noise.

On UoSAT-5, the camera was redesigned to run from the battery's +14V supply, which is capable of delivering the necessary current. Linear regulators provide the +12V and +5V rails, and charge-pump DC-DC converters running at about 10 kHz are used to provide the -5V and +24V rails (no series linear regulation). Examples of UoSAT-5 imagery is provided in figures 5.3.1.5c to f. Although there is still some striping, it does not effect every pixel, resulting in diagonal artefacts. When the CCD's two fields are interlaced, this noise generates a herringbone pattern on the image, which is most noticeable in uniform dark areas (sea). Pixels captured directly on the DC-DC converters' transients are subject to 4 bits of noise, and the remaining pixels to about 3 bits of noise.

On PoSAT-1, the same approach was adopted as on UoSAT-5 but with linear regulator stages following the two switching converters. The use of two ground planes on a multi-layer PCB has also contributed to reducing the noise floor of the camera. Figures 5.3.1.5g to j show reference data for the PoSAT-1 system. Virtually all of the striping effects present in the previous cameras has been eliminated by using linear regulation on all supply lines and by providing separate analogue and digital supplies. A diagonal pattern remains, effecting the occasional pixel, but which in practice is indistinguishable from other sources of noise. Overall, the PoSAT-1 camera noise possesses a more conventional Gaussian distribution, providing 2.5 bits of degradation.

Although the additional linear regulation on PoSAT-1 has reduced the camera's noise floor, it has increased the camera's overall consumption. The UoSAT-5 camera draws 260 mA from the raw +14V rail. Conversely, the PoSAT-1 camera draws close to 320 mA (when populated with only one of the two CCDs). However, this also includes an number of extra analogue integrated circuits used to support the dual sensor design (about 15 mA).

Finally on FASat-Alfa, the DC-DC converters are running at almost 30 kHz and separate regulation is provided for the analogue and digital rails. The physical lay-out of the cameras has also been improved by using surface-mount technology, with the printed circuit board area occupying two thirds less space than in previous cameras. The PCB uses six layers, including two ground planes and one power plane. Again, this results in

Spacecraft	Sample 1 (WAC)		Sample 2 (NAC)	
	Single field	Interlaced	Single field	Interlaced
UoSAT-4	 Figure 5.3.1.5a		 Figure 5.3.1.5b	
UoSAT-5	 Figure 5.3.1.5c	 Figure 5.3.1.5d	 Figure 5.3.1.5e	 Figure 5.3.1.5f
PoSAT-1	 Figure 5.3.1.5g	 Figure 5.3.1.5h	 Figure 5.3.1.5i	 Figure 5.3.1.5j
FASat-Alfa	 Figure 5.3.1.5k	 Figure 5.3.1.5l	 Figure 5.3.1.5m	 Figure 5.3.1.5n
FASat-Alfa (UV camera)	 Figure 5.3.1.5o	 Figure 5.3.1.5p	 Figure 5.3.1.5q	 Figure 5.3.1.5r

Table 5.3.1.5a Samples of background noise from test images.

noise performance, with power supply noise effecting only the least significant of 8 bits (figures 5.3.1.5k to n). Another 1 bit of noise is generated by the CCD's intrinsic properties (dark current non-uniformity and output amplifier reset error) and by the video signal processing support chip.

As a comparison, samples from one of the ultra-violet (ozone) cameras on FASat-Alfa are shown in figures 5.3.1.5o to r. These cameras ran at a much slower speed to give them greater sensitivity to faint UV illumination. By reducing the cameras' master clock from the usual 33 MHz to only 2 MHz, the effect of noise has been further diminished to a maximum of 1 bit per pixel. Under these conditions, the CCD's output amplifier and other analogue components have significantly more settling time, leaving only the power supply as a significant noise source.

Table 5.3.1.5b summarises the noise suffered by the imagery in terms of bits per pixel. Given that all of these cameras produce 8-bit data, an estimate of their signal to noise performance is also made. This is a very crude calculation which does not consider many effects, but is nevertheless indicative of the improvements achieved with each generation of the SSTL imaging systems.

Spacecraft	Noise (bits per pixel)	Estimated SNR
UoSAT-4	4	16
UoSAT-5	3	32
PoSAT-1	2.5	45
FASat-Alfa	2	64
FASat-Alfa (UV camera)	1	128

Table 5.3.1.5b Estimate of signal to noise performance for SSTL cameras.

Despite the progress between missions, there is still room for improvement. Future cameras will need to use switching regulators running at speeds above 100 kHz, and care will be required to ensure an improved grounding strategy. The digital and analogue components will be further isolated both electrically and physically to prevent cross-contamination. As the level of supply noise is reduced, it will no longer mask the other sources of noise, which will need to be addressed more attentively.

5.3.1.6 Summary.

The regulated rails provided by an SSTL microsatellite's Power Conditioning Module are poorly suited to the conditioning requirements of an electronic camera. It is therefore more appropriate to use the spacecraft's unregulated supply straight from the batteries and provide local power conditioning.. This allows the camera designer to implement the power regulation that the camera needs rather than what the spacecraft provides. This, in turn, simplifies the design of both the camera and the power module.

As the cameras on microsatellite will have a very short duty cycle, it is possible to use linear regulators and other inefficient techniques to ensure clean power supplies. Conversely, it is not feasible to implement these measures within a centralised power system feeding the entire spacecraft. The analogue stages of a CCD camera are very sensitive to noise on the supply rails, and any improvement in rail cleanliness and regulation will be of direct benefit to the quality of the imagery.

5.3.2 DESIGN OF THE DIGITAL SEQUENCING ELECTRONICS.

5.3.2.1 The role the digital sequencing electronics.

A CCD image sensor is primarily an analogue shift register endowed with photosensitive properties. To read an image captured by an area-array CCD, it is necessary to transfer the charge packets towards the output amplifier. The camera's sequencing logic must generate the clocking waveforms prescribed by the CCD's specifications to ensure correct operation. This logic circuit must therefore provide suitable pulse trains to operate the various phases of photon capture, transfer to the storage region (if present), transfer to output registers, and readout of the charge packets one-by-one, as well as driving the video processing stages in synchronism with the arrival of each pixel.

To comply with commercial video standards, the camera produces a continuous stream of images, one every 20 ms. The CCD's output signal is compelled to respect the field rates and line rates of the TV standards, which in turn dictate the speeds of the CCD clocks. (N.B. All timings are for the 625-line CCIR / PAL standards; the 525-line EIA / NTSC timings are slightly different but follow a similar process).

According to the CCIR standard, a new video line must be produced every 64 μs, and all the pixels must be read in 60 μs (allowing 4 μs for beam fly-back). To transfer all of the charge packets in the readout register to the output amplifier, the clocks must be driven at around 10 MHz; this is typical for a device with 600 horizontal pixels, devices with higher resolutions will need to run faster.

The vertical clocks will be driven in synchronism to load a new image line into the read-out register at a rate of 15625 kHz, so that exactly 312.5 lines are processed in 20 ms (625 lines in 40 ms). The vertical shift takes place during the 4 μs when the horizontal readout register is idle during beam fly-back. If the readout register is not static during this shift, there is a significant possibility of corrupting the charge packets. This cycle repeats until all 288 lines of an active video field have been shifted into the horizontal register and read.

Whilst an image field is being read from the storage buffer in this manner, the next field is being captured by the imaging photosites. When an entire field has been read, the new image is transferred to the storage region and the process repeats. Thus the imaging region, the storage region and the readout register operate independently but synchronise at the end of a line or field to transfer charge packets, line-by-line.

Although the exact timings will vary, this procedure holds for most CCDs with electronic shuttering (interline transfer or field transfer, TV compatible, computer vision, etc.). If a full-frame imager is used, there is no storage area and the photosites alternate between collecting photons, and shifting data towards the readout register (when the shutter is closed). Nevertheless, the general principal of operating the CCD is the same.

It is the task of the sequencing logic to drive the CCD in the correct fashion to ensure that these capture, transfer and readout processes occur in synchronism without degrading the quality of the image. If integration control is implemented, the sequencing logic will also need to drive the imaging photosites independently from the storage and read-out registers, dumping and collecting photons as dictated by the external commands, without disrupting the on-going image transfer and readout.

5.3.2.2 Implementing the digital sequencing electronics.

The most natural way of implementing a CCD sequencing logic circuit is to use nested counters with the horizontal pixel counter running fastest, then the vertical line counter, and finally the field counter. The video standards are respected by ensuring that the counters are driven at precisely the right frequency. While the role of the logic blocks within this circuit is fairly easy to conceptualise, implementing them can be rather more difficult given that the camera's master clock runs very fast (30 to 50 MHz depending on the number of pixels). The speed of this master clock will be several times faster than the pixel clock frequency, so that there are enough edges from which to derive the multiple phases of the output register clocks using combinational logic.

In addition to sustaining these high rates, the logic circuit must also ensure that the clock edges are well conditioned and free from jitter by minimising propagation delays and race conditions. CCDs are very sensitive to frequency and phase instability on their output register clocks, and the image will be degraded if these are not consistent. Of particular importance is the cross-over characteristic between successive clock phases; the charge packets are transferred on the clock edges, and any noise or delay at this critical point will result in charge loss (smearing). For these reasons, microprocessors cannot be used to generate the CCD clocks directly because their time-keeping and phase accuracy are too poor.

Ideally, the CCD chosen for the microsatellite camera will be accompanied by a support chip to perform these functions. This chip will be optimised to operate with a specific CCD (or set of CCDs), ensuring that all of the timing and phasing requirements are met. If this support device is available, there will be relatively little for the designer to worry about provided all the necessary signals and modes of operation are provided.

Conversely, if no dedicated sequencer chip exists, or it fails to provide all the required features, it will be necessary to design a controller circuit from scratch. During the 1980's, the logic circuit would have been mainly out of discrete TTL or high speed CMOS logic, even when developed by the manufacturer. As a consequence, the circuitry was large, power hungry, and prone to propagation delays and glitches between the gates. Fortunately, the developments in the late 1980's, first ASIC and hybrid technologies, and then programmable logic (PALs, EPLDs, FPGAs, etc.) allowed the manufacturers to produce highly integrated logic controller chips. The new availability of these high-density programmable logic devices over the last few years has simplified the job of developing the camera's logic circuits. The simple logic elements needed to implement the sequencing circuit (counters, flip-flop, logic gates) are ideal for embedding into these programmable devices.

Many camera producers (e.g. EEV, Eastman-Kodak) now prefer to use FPGAs rather than develop dedicated chips for implementing their sequencing logic. FPGAs offer great flexibility for reprogramming a camera's sequencing to accommodate new sensors or applications. Devices using an EPROM for configuration are especially attractive; a standard ROM exists for video compatibility, but alternative ROMs can be programmed to generate non-standard timings. Programmable logic is primarily used by the manufacturers who supply scientific CCDs, as the non-recurring costs are low. Conversely, in the mass market for commercial sensors targeted by the Japanese companies, it is cheaper to develop custom sequencing chips, rather than use relatively expensive programmable devices.

Similarly, the features of programmable logic can be used by the camera designer to produce the logic circuits in-house for otherwise unsupported CCDs or to implement features omitted from the manufacturer's chipset. The availability of these products has greatly simplified the task of designing the CCD's sequencing logic. Nevertheless, working from a manufacturer's design is still of benefit, especially if the designer is not highly experienced.

5.3.3 DESIGN OF CCD CLOCK BUFFERS.

Although the sequencing logic generates the phased signals to operate the CCD, it is not able to drive the CCD directly. Due to the distributed grid structure of the electrodes on an area-array CCD, these clock inputs have very high capacitance. For a typical TV-compatible sensor, each of the vertical clocks will have a capacitance of about 7,000 pF (EEV CCD04: 9,000 pF; Thomson 7864: 5500 pF; Sony ICX024: 5000 pF) which will need to be driven at 16 kHz during readout, and at up to 3 MHz during frame transfer (if appropriate). Although the horizontal readout register clocks are not as capacitive, typically 200 pF (EEV CCD04: 240 pF; Thomson 7864: 250 pF; Sony ICX024: 180 pF), they have to be driven at much higher rates, around 10 MHz. The loading of large 2000 x 2000 pixel scientific sensors is even higher (e.g. EG&G RA2000J: 35,000 pF, 600 pF; Loral-Fairchild CCD442: 60,000 pF, 400 pF).

These capacitive loads are too high for most conventional logic devices, causing their outputs either to oscillate or to be completely slew-rate limited. In either case, the sequencing logic will not be able to drive the CCD, and permanent damage is a likely result if this is attempted. Special buffers are therefore required to isolate the logic from the CCD. However, it is necessary to use different designs for the vertical and horizontal buffers. The vertical registers have very large capacitance (tens of nanofarads) and need to be driven at about 20 kHz, while the horizontal registers have lower capacitances (hundreds of picofarads) but need to be driven in excess of 10 MHz. These buffers must remain stable with such large capacitive loads, and have adequate bandwidth and sufficiently short propagation delays to handle the high speed clocks.

Not only do the buffers provide current and voltage amplification, they must also perform wave-shaping to give the clock edges the right characteristics for driving the CCD. Numerous parameters will be specified to ensure good charge transfer, such as monotonic edge slopes, absence of ringing, asymmetric attack and decay slewing characteristics, and correct phase overlap. Therefore, although their function is essentially digital in providing current amplification, the design of the buffers must adhere to many analogue specifications, providing the correct waveforms to the CCD inputs.

Once again, dedicated chips provided by the manufacturers for this purpose will have been optimised for the specific timing and pulse-shaping requirements of the camera, and generally represent the best option for bridging between the logic circuit and the CCD. Even if the manufacturing company does not make any custom devices, it will certainly be able to recommend general-purpose drivers, or provide circuits for discrete transistor buffers.

Failing this, a number of ICs for developed for driving distributed system-clock lines on computer boards are suitable for CCD horizontal clock buffers. In particular, the DS0026 (originally produced by National Semiconductor, but now supplied by many others as well) and the TSC430 (Teledyne Semiconductor) are suitable dual-buffers available in small 8-pin packages (DIL and surface-mount). In some instances, it may be possible to use high-speed TTL devices (F-family), with their high output current handling able to drive the horizontal clocks.

If no buffer drivers are immediately obvious, the designer should also consider using devices made by other CCD manufacturers (in particular the large Japanese CCD and camera companies). Although the exact voltages, frequencies, waveforms, clock phases etc. of these buffers will be tailored for a specific CCD, their general characteristics are nevertheless quite similar. Therefore, it may be possible to press a buffer chip originally intended for another CCD into service for the current design. However, extensive bench testing (with dummy loads and in-camera) are absolutely necessary to verify this option. Under no circumstances should a device be operated at, or near, its absolute limits; although it may appear to operate nominally, this is likely to stress the device in the long term, dramatically shortening its lifetime.

As with the logic for the sequencing circuit, on-going developments in semiconductor technology has made custom design of the buffers more feasible than just five years ago. In particular, there has been a dramatic increase in the range of not only high speed digital drivers but also video speed, and faster, analogue components. Many of these video op-amps and analogue line-drivers are stable when driving capacitive loads of a few hundred picofarads, as encountered in long lengths of coaxial cable, and can therefore be used directly to buffer the horizontal registers. Furthermore, because of their analogue nature, they can be used to provide very accurate and flexible wave-shaping of the digital clocks from the logic circuit, in addition to the necessary voltage and current amplification. There is a growing number of manufacturers of this type of product including Analog Devices, National Semiconductor, Harris, Maxim, Linear Technology, Raytheon Semiconductor and Comlinear Corp., but the most notable supplier of suitable video products is Elantec.

Although the frequency of operation is much lower, the vertical clocks are more difficult to design for because their high capacitance exceed most conventional IC's stability ratings. It may be necessary to use power audio transistors (TO220 packaging) a in totem-pole booster circuit to isolate the logic or the analogue signal conditioning from the CCD. Although they are sold as audio components, most of these transistors will have a cut-off frequency of around 200 MHz, amply suitable for these applications. However, unlike specialist RF components, these devices will have a large DC current handling capability.

To summarise, the design of the clock buffers is important in isolating the sequencing logic from the capacitance of the CCD inputs and to provide suitable pulse-shaping and level-shifting of the clock signals. While most manufacturers offer suitable buffers for their CCDs, there is a wide range of alternative components and parallel technologies that can be employed if the manufacturer's solution is not practicable. In general, the function of the buffer circuitry is quite simple, and the behaviour of a custom circuit can be successfully characterised using analysis software and test circuits (without risking the CCD). Thus the camera designer can depart from the manufacturer's standard circuit when needed, with a fair chance of success.

The majority of a CCD camera's power is consumed by the buffers. High transient currents are required to charge and discharge the capacitive CCD inputs at megahertz frequencies. For hand-held applications which require the camera to be battery-operated, adjusting the operation of the clock buffers is the most effective way of saving power. Some designs implement special schemes to reduce the buffers' power drain by reducing the full voltage swings, gating the clocks, etc. However, reduced image quality is a price often paid for the power savings of these implementations. If so, they should be disabled for a remote sensing camera. As described in section 5.3.1, small power savings do not justify compromising the image quality. For example, the EEV CCD04 chipset incorporates a feature to reduce the vertical clock amplitude during less critical phases of the capture cycle. Given that activating this feature reduces the CCD's resilience to anti-blooming, it has been bypassed on UoSAT-5 and all subsequent missions.

5.3.4 DESIGN OF ANALOGUE SIGNAL PROCESSING CIRCUITS.

Of all the sub-circuits identified by the block diagram of a standard CCD camera, implementing the analogue signal processing is the most technically challenging area. The design of high speed analogue electronics requires a certain amount of experience to penetrate the 'black magic' associated with video engineering. It follows that these elements of the circuit are those where manufacturer's support chips are the most valuable.

All CCDs have a charge amplifier at the end of the horizontal register which converts the charge packets recorded by the photosites into a small voltage (occasionally current) swing. However, the output of this amplifier is not directly usable as the amplitude of the valid image information is very small, generally only a couple hundred millivolts in amplitude. Furthermore, only certain phases of the output signal are of interest, and the rest is dominated by noise and reset-clock breakthrough, generally of much greater amplitude than the useful signal. It is therefore important to extract the image information and amplify it selectively against a background of noise.

The first stage of the analogue signal processing must therefore be a low noise pre-amplifier to boost the signal levels, and isolate the CCD's charge amplifier from any loading which may distort the signal. Often the CCD provides a complementary output signal, driven in the same way as the principal output but without the video information. If available, this facility should be used at the pre-amp stage, subtracting the dummy signal from the real signal to remove common-mode noise.

Following the pre-amp, a sample-and-hold circuit is needed to pick out the useful constituents of the output signal. Two stages are often required to reject all the meaningless components of signal. The best design of the sample-and-hold uses a technique known as correlated double sampling (CDS). This involves using one polarity of a dual-slope integrator to sample the output signal immediately prior to each pixel, thereby establishing the noise floor. The valid pixel information is then integrated using the opposite slope, effectively subtracting the noise from the valid data. Correlated double sampling is especially effective at compensating for many forms of noise, both inherent to the CCD (clock breakthrough, dark current non-uniformity, DC drift, etc.) and induced by the surrounding circuit (supply borne noise and cross-talk). Unfortunately, the dual-slope integrator must be operated at slow rates (below 100 kHz) to allow adequate settling time, and is not really suitable for video speed signals (1 to 10 MHz). At these higher video rates, a more conventional sample-and-hold circuit will have to be used.

The signal from the CCD is subject to significant temperature drifts caused by changes in the dark current build-up and the output amplifier characteristics. In most instances, the CCD outputs are AC-coupled to eliminate these drifts, making it necessary to perform subsequent black-level clamping to restore the true DC level. A conventional video circuit carries this out at the start of every line using the dark-reference pixels which precede the valid signal. Conversely, correlated double sampling performs DC restoration for every pixel, thereby achieving its improved noise-rejection.

Finally, if the signal is being conditioned to adhere to a composite video standard, it may need to be level shifted, have its gain trimmed, and be mixed onto various synchronisation pulses. The useful amplitude of the a composite video signal is about 700 mV peak-to-peak. Fortunately, this is a suitable input for most analogue-to-digital converters. However, there is no particular reason to comply with a video standard within a remote sensing camera, and if it is available, a 2 to 3V signal (often produced prior to sync mixing and the output 75Ω buffer) provides a better signal-to-noise ratio for the ADC circuits.

If the manufacturer provides a dedicated chipset, it is likely that all of the stages just described (except the correlated double sampling) are incorporated within a single IC package. There is often a subsequent signal processing chip that adjusts the camera based on the composite video signal, performing functions like automatic gain control, iris control, gamma correction, and pixel correction using a look-up ROM. Under most circumstances, these features will not be of significant benefit to a digital still camera, and this auxiliary chip should probably not be included. If required, these tasks are often better fulfilled by image processing on the digitised image.

As the performance of the video processing and conditioning circuits are crucial in defining the final image quality, it is advisable to use the manufacturer's devices as far as possible. The amplification and sample-and-hold stages will be tailored specifically to that device, avoiding much of the scope for confusion and wasted time. Nevertheless, the camera designer will need to be prepared to experiment with the timing and gain adjustments provided by the various video processing stages to optimise them for the particular application.

Unlike commercial video cameras where the criteria for the signal processing are determined by the television standards, the signal conditioning requirements of scientific systems are not defined. Because of widely differing user requirements, the signal processing is often left to the camera designer to implement according to the specific needs of the application at hand. Fortunately, this task is somewhat simpler than a decade ago, thanks to the rapid developments made to the stability and ease-of-use of the current generation of video speed op-amps and other devices. Nevertheless, the design the video processing stages is still a challenging task and is rather more difficult than for the logic circuit and the signal buffers, whose behaviour is more predictable.

If no recommended circuit exists for processing the CCD's output signal, then it is worthwhile surveying other manufacturer's solutions and components for ideas. Many of these will be transposable from one CCD to another with minor adjustments. However, the data sheets alone will rarely be adequate to determine the exact composition of the CCD output signal and the best way to process it. The designer must be prepared to perform extensive testing and bread-boarding to determine the most suitable video processing topology and to evaluate its performance. While general principles of video speed analogue design can be established in advance (a discussion of which is outside the scope of this thesis), the characteristics of the circuit used will be determined not only by the sensor, but also on the physical layout of the board and an interaction between components.

5.3.5 DESIGN OF DIGITISATION CIRCUITS.

Assuming that it has been designed properly, the video processing circuit provides a clean output signal, free of most of the noise and spurious impulses that were present on the CCD's output. For most applications, ensuring that this signal complies with a video standard is all that is required. However, in an electronic still camera used for satellite remote sensing, extra stages are required to digitise the analogue video stream. It is very rare for the manufacturer to have considered the digitisation, and it will need to be developed by the camera designer.

Fortunately, there are many suitable high-speed ADCs available. As with all aspects of video technology, the choice and performance of these devices has increased dramatically in the last decade. Most of these components are quite straight forward to use, provided the instructions and advice offered in the data sheets and application notes are respected. All video ADCs are optimised to work with the standard video amplitude of 1V peak-to-peak, but most can operate over a wider range of input voltages, up to about 4V.

To operate at frequencies above 1 or 2 MHz, the ADC will almost certainly use the flash (or half-flash) architecture. A number of semiconductor technologies are used to implement video ADCs: CMOS, bipolar, ECL, hybrid. ECL devices are required if the frequency of operation is approaching the gigahertz range, but for most applications are unnecessarily fast, power hungry and difficult to interface with. Any of the others technologies are suitable for implementing a remote sensing camera. Although CMOS ADCs tend not to be as accurate (linearity, drift) as the other technologies, they are generally good enough for all but the most demanding digital camera applications. CMOS and bipolar ADCs are now available in 10 and 12-bit resolutions with a linearity of better than two times the least significant bit.

Traditionally, remote sensing instruments have digitised their analogue data stream to 8 bits, although some systems, such as the LANDSAT MSS and RBV only use 6 bits. This has been adequate to record the video signal given the instruments' noise floor and radiometric accuracy (see section 5.5.3.1). Any increase in the quantiser's resolution would increase the volume of data to be handled, without improving its information content. Furthermore, given that most digital hardware is byte-oriented (8 bits), using other quantisation schemes will make the data format of the imagery incompatible with the satellite's data handling systems, requiring cumbersome and time-consuming data packing to overcome this.

Nevertheless, as the performance of instruments improve, 10 and 12-bit resolution will become more prevalent. Higher resolution can increase the radiometric detail recorded, provided the combined noise from all sources within the camera (CCD output amplifier, dark current, video processing, power supply, quantisation) are kept to less than half the amplitude of the least significant bit on the most sensitive ADC setting. Conversely, lower grey-level resolution will result in 'grainy' images, especially if poorly exposed.

In practice, achieving 8-bit resolution and 1-bit linearity is not so difficult when using a CMOS ADC by carefully specifying and routing all of the analogue components (including the ADC). The combined linearity and noise of all the components in the signal path must have adequate performance. A frequently overlooked aspect of using video ADCs is the low impedance and moderately high capacitance of their input, which can result in distortion if the signal is not suitably buffered by a high slew-rate stage.

As important as the specification of the components in the digitisation circuit, the timing of the ADC's sampling is crucial in ensuring image quality. Even with the sample-and-hold stages in the video processing, there is always an optimum moment to trigger the digitisation. The best approach is to use a derivative of one of the horizontal read-out register clocks from the sequencing logic to drive the ADC in phase with the arrival of each new pixel. Often, however, none of these clocks will be directly suitable to provide the sampling edge, and combinational logic must be used to derive additional edges, phases and pulse widths from the various read-out clocks and the system's master-clock. As there will be no guidelines from the manufacturer, it is essential that the camera designer experiments with this part of the camera to ensure that precise and optimal sampling of the video signal is obtained.

It is possible to digitise video signals without having access to the camera's reference clocks. There is an entire industry developing around the sampling of remote video imagery. These frame-grabber units either use over-sampling to ensure that minimal information is lost or implement complex clock recovery circuits to synchronise the sampling with the individual pixels within each video line and field. Although the results are acceptable for many applications, the sampled imagery does not possess the quality of a truly synchronised ADC. In addition to producing sharper and more accurate sampling than a frame grabber, it is far simpler to use the master clock from the logic circuit than attempt clock recovery.

Finally, although the sampling nature of flash ADCs can be used to simplify the sample-hold circuits of the video processing circuit, it will not replace full correlated double sampling.

5.3.6 DESIGN OF THE IMAGE MEMORY.

Once the camera's video signal has been digitised, the data must be collected. The very high output speed from the ADC makes it impossible for a microprocessor to handle the imagery directly, and this byte-stream must therefore be stored as it arrives, and later retrieved at a rate that the processing unit can manage. In conventional remote sensing satellites, one or more magnetic tape recorders are used to store and playback the large volumes of image data. However, this approach is unsuitable for a microsatellite because of the very large mass, volume and power requirements of these recorders. Furthermore, these instruments are notoriously unreliable.

Solid-state storage is much more appropriate for microsatellites, especially as the density of semiconductor memory devices continues to increase. The Solid-State Data Recorder Experiment carried on the FASat-Alfa mission was a pioneering in-orbit prototype of this technology carrying 256 MBytes of memory. Larger versions of similar solid-state recorders are likely to replace tape recorders on many future Earth observation spacecraft.

In the specific case of a microsatellite imaging experiment, the best solution for buffering the incoming digitised data is to use a dual-ported memory bank. The camera writes to the memory during image capture using one port and the processing unit collects this data via the other port at a convenient later time. The simplest form of arbitrating the access to this shared resource is a simple logic lock-out which prevents the microprocessor from addressing the memory when the camera is operating. There are numerous alternative approaches to this, such as using direct memory access (DMA) whereby the camera seizes control of the processor bus for the duration of the image capture process. Although DMA has the benefit of minimising the number of extra components, it is impossible for the processor to access its own program memory, and is therefore unable to execute code, for these relatively long periods. Another possibility it to use specialist video RAM (VRAM) which is inherently dual-access, although these devices are quite power hungry and difficult to interface to.

As the camera will only be operated for a few seconds to capture the imagery, it is necessary to power the image buffer memory from a separate supply. This will enable the digitised imagery to be preserved for an indefinite period after the camera has been switched off. If static memory (SRAM) is used, the quiescent current consumption of this memory will be negligible. However, precautions need to be taken to ensure that the inactive camera does not interfere with the operation of the memory, or accidentally get power from it.

Compared with the camera or ADC circuits, the image memory is a conventional piece of digital design and therefore relatively free of complications. Care must be taken to avoid any possible conflict between the memory, the camera and the microprocessor, and to minimise propagation delays through the control logic which could interfere with the smooth capture of the images. Conventional low-power static RAM, as used microprocessors, is more suitable than other types of memory. This SRAM must be sufficiently fast (probably between 45 and 75 ns access cycle time) to be able run in synchronism with the arrival of each new pixel. Even if the camera runs at higher speeds, very fast SRAM (up to 10 or 12 ns) is available, although unnecessarily fast devices should be avoided because of the dramatic power consumption penalties incurred for memories faster than 55 ns. The density of these SRAM chips is increasing constantly, with 4 Mbit (512 kBytes by 8) devices flown on the FASat-Alfa mission. (In comparison, UoSAT-5, launched only four years earlier, used state of the art 128 kbit memories). The density of solid-state memory should continue to grow at a faster rate than the pixel densities of the area-array image sensors.

The camera must generate addresses for the image memory as it is writing its data. This is most easily accomplished by incrementing a counter in synchronism with each new pixel. In operation, the address counter will be reset at the beginning of each new image or field. Thus, the first digitised pixel will be stored in location zero. At the end of the first write cycle the counter will be incremented in preparation for the next pixel, and so on, until the entire image has been recorded. The counters need to be cascaded to have a wide enough addressing range; for example, an 18-bit counter is required to generate all the addresses in a field (half the image frame) for the EEV CCD04 sensor. Similarly, a progressively scanned 2000 x 2000 pixel area-array device will require 22-bit counters. Because of the frequency of operation and the large number of bits, it is vital to employ a fully synchronous (not ripple) counter design to avoid propagation delay through all these stages.

In addition to generating valid addresses, the camera must also provide the chip select and write enable strobes to drive the memory. As with the sampling of the ADC, these signals are best derived from the horizontal readout register clocks in compliance with the timing of both the pixel stream from the ADC and the memory's write cycle. Fortunately, since the camera will never need to read the memory, this line on the memory devices can be disabled (tied high) during image capture.

Although the image is actually a two-dimensional entity, it is stored as a one-dimensional array in memory. To reconstruct the 2-D image, it is necessary to extract the individual image lines from the stored data. Short of trial and error, the only way to do this is to have prior knowledge of the number of pixels in each video line, and to read the data in appropriately sized blocks. It is therefore very important that exactly the same number of pixels are recorded for every image line, otherwise there will be slips in alignment between the image lines (registration errors). Consequently, any variations in the sampling procedure from image to image, but especially from line to line, result in seriously degraded quality of the image. This flaw also makes automatic image processing impossible until the image has been manually corrected for any slippage.

Thus, it is crucial that the signals from the sequencing logic used to generate the various memory and counter strobes are inspected for consistency. A continuous analogue video signal used to drive a TV screen will suffer no ill-effect if a line occasionally has a few more pixels than the rest, provided the standard timings are observed. Conversely, such variations cause significant trouble in a digitised image. If the signals from the logic circuit exhibits any such instabilities, it will be necessary to mark the beginning of each line in some way; for example, by using a predetermined fixed address for the start of each new line, by adding extra gating to the clocks from the logic circuit to disable spurious pulses, or using a distinctive code inserted in the data stream between lines. While these solutions can be used to save an otherwise unusable digitisation circuit, it is far better to address these issues early and make sure that no slippage can occur.

In most instances, hardware error protection will not be needed for this storage memory. As the data will not be stored in this memory for long, it is at very little risk from being corrupted by radiation-induced single-event-upsets (see section 6.2.3.1). (If the data is left unprotected in memory, a typical error rate for standard SRAM is about one SEU per Mbit per day). Provided the images are retrieved fairly rapidly from the memory and transferred to a more suitable storage medium, the number of errors encountered should be acceptably small. On the odd occasion, this type of error will no doubt occur, but it will be contained to a single pixel. If this exposure to radiation errors is still unacceptable, software coding or hardware error protection on the memory must be implemented, adding considerable complexity to the design.

Overall, the implementation of the image buffer memory is quite straight forward. A key factor to consider is the stability and repeatability of the signals incrementing the address-counter. Any inconsistencies in this stage will ruin the framing of the data, making all subsequent stages requiring automatic image manipulation ineffective. Clearly, the memory must be large enough to hold an entire image. If more memory can be accommodated then it becomes possible to have several buffers, so that new images can be captured without writing over previous images that still need to be read. Furthermore, the camera is always able to fill this buffer memory far faster than the processing stages can empty it. If the data retrieval rates are too slow or the buffering is inadequately sized, this image memory may inadvertently become a bottleneck, limiting the imaging system's turnaround.

5.3.7 DESIGN OF SYSTEM INTERFACING.

Unfortunately, CCD cameras are not particularly compatible with the highly computerised environment of a microsatellite. Some form of interface circuit is needed to bridge between the standard digital connections of the spacecraft bus and the free-running analogue camera. This interface must accept commands to capture images and change the imaging parameters, and also to manage the transfer of the stored image data to an on-board computer. Going into the camera, it is necessary to provide triggering pulses to activate the capture sequence and to control the integration modes, for example. In the opposite direction, the image buffer memory is a major transition point in the imager design. The camera front-end is automated hardware producing high-speed bursts of sequential data, but beyond this, intelligent processors dominate, implying slower speeds dictated by random-access software routines.

For consistency, the discussion of the camera's digital circuits, including the interfacing and communications systems, are discussed in section 6.1. However, it is important to note at this stage that due to the widely differing requirements placed on this part of the camera, its design is one of the most complex issues in developing remote sensing instruments for microsatellites.

5.3.8 SYNCHRONISING MULTIPLE SENSORS.

Although it has not been faced in the systems developed during this research programme, there is often a need to synchronise multiple CCD sensors. This is particularly the case if the imaging system provides multi-spectral data using an individual sensor for each colour band (see section 5.4.4.3). Under these circumstances it will be necessary to synchronise the sequences of all the CCD sensors so they capture their imagery simultaneously, failing which the pixel co-registration these images will be compromised.

The simplest and most accurate method of achieving synchronism is to use a single sequencing logic circuit to drive all of the sensors. This will ensure pixel correlation to within a few nanoseconds. Of course individual current buffers, video processing, digitisation and storage stages will be needed for each sensor.

However, a centralised logic circuit represents a single-point-failure. An alternative would be to use a centralised sequencer but with a redundant logic circuit which can be enabled in the event of failure. It would be necessary to ensure that the signals from the two logic circuits can be multiplexed or bussed to each of the sensor units in such a way that the inactive or inoperative unit does not interfere with the performance of the rest of the cameras. Unfortunately, this configuration transfers the single-point-failure from the sequencing logic to the switching system. Furthermore, it is likely that the logic and CCDs will be physically separated, degrading the quality of the clock signals.

A better approach is to use a technique known as genlocking. This is used in commercial TV to synchronise remote cameras to a master signal. By synchronising all the field and line scans, it is possible to switch between cameras without having the image jump. The dedicated logic chips for all TV compatible cameras will incorporate the circuitry to genlock to a master signal. This is often implemented by using a voltage controlled oscillator which speeds up or slows down to match the master signal. Alternatively, the incoming signals simply reset the pixel and line counters, forcing the camera into synchronism with the master. In the absence of a master signal, the cameras free-run, deriving the timing from their own internal clock.

The loose coupling between cameras involved in genlocking is very advantageous for a satellite remote sensing system. Each camera operates independently, sharing no common hardware, and is thus immune to failures on other cameras. When the genlocking is functional, or enabled, the cameras will run in synchronism; if the genlocking fails, the cameras will free-run, and although they will not be fully synchronised, will nonetheless be producing imagery which can be registered manually during post-processing.

An approach to providing even more fault-tolerance is to connect the synchronising signals from one camera to the genlock inputs of the next camera in a daisy chain, as shown in figure 5.3.8. Each of the cameras will have control over the inputs to its own genlocking circuit, either accepting or isolating itself from the output of the previous camera. It will be necessary to break the chain at one point with a switch to prevent the whole system from oscillating or locking up. The first camera in the chain will therefore act as a master, with the others synchronising to it. If any one camera or genlocking stage fails, for example camera 0 as shown in the diagram, then the daisy chain will need to be reconfigured to make camera 1 the master. Thus all the remaining cameras will remain genlocked. Moreover, it is also possible to synchronise to an external standard for even higher accuracy by injecting a reference signal into the chain, although this will probably not be necessary for most microsatellite applications.

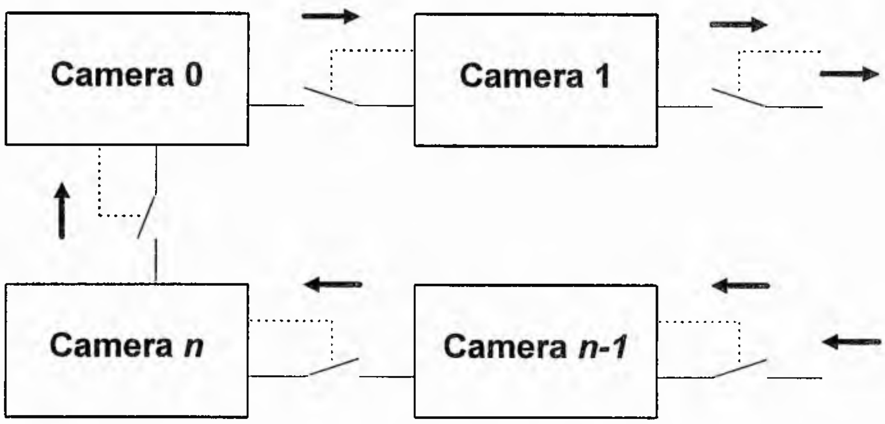

Figure 5.3.8 Daisy-chain architecture for implementing inter-camera synchronisation.

N.B. This architecture has not been used in-orbit yet, but has been conceived in response to SSTL's forthcoming imaging requirements.

5.4 THE CAMERA OPTICS.

Having selected a CCD sensor and reviewed the options for implementing the circuitry for the remote sensing camera, it is necessary to consider the optical system required to focus an image onto the detector. The optics for an electronic imaging system on a microsatellite consist of the lens(es) or telescope, and the colour filter(s).

The quality of the optics is of equal importance to the electronics in establishing the imaging system's performance. Clearly if the optics deliver a badly focused and distorted image to the sensor, the electronic systems will be able to overcome this. (The deformations of the Hubble Space Telescope's primary mirror are a convincing demonstration of this).

5.4.1 SPECIFYING THE LENS.

The lens projects photons arriving from the scene into a focused image on the CCD sensor. For photographic applications, the performance of the camera and film is sufficiently good to make the lens the most important factor in determining image quality. Any imperfections in the lens will have an immediate impact of the ability to record the scene faithfully. Particularly crucial is the flatness of the image (spherical aberration) and chromatic aberration, but internal reflections (ghosting) and geometric distortions also present problems.

The principal constraint placed on the choice of optics by the microsatellite platform will relate to mass and volume. While lens manufacturers strive to keep their systems lightweight, they are nevertheless likely to be considerably more massive than the camera electronics. If several cameras need to be carried, the combined mass of the optics may become critical. With the exception of a few, very large full-frame devices, most CCDs (typically 12 x 8 mm) are much smaller than 35 mm film (36 x 24 mm). Therefore, if a standard 35 mm lens is used it will be much larger than is strictly necessary. The mass of the lenses will become particularly problematic if very long focal lengths or wide apertures are required for high resolution or low light imaging respectively. Although not of the same quality, closed-circuit TV (CCTV) lenses are designed for smaller CCD sensors and are consequently much lighter and more compact. Fortunately, it is often possible to remove many parts of the lens housings which are not necessary in flight to save mass. In particular, the mechanisms for manually adjusting the focus and aperture are superfluous on a satellite. Indeed, an average of approximately 50 % of the mass of the commercial lenses used so far on the SSTL cameras has been removed without altering the optical performance.

However, it is the lens parameters, and not its mass, that will determine the characteristics of the resultant imagery.

5.4.1.1 Focal length.

The focal length of lens determines the magnification of the image, and thereby dictates the spatial resolution in an electronic camera using a CCD area-array sensor. Figure 5.4.1.1 shows how the focal length of the lens (f ') and the satellite's altitude above the ground (H), combined with the CCD sensor's dimensions, determine the coverage area and pixel resolution of the final image. By substituting the CCD's photosite spacing or the CCD's total imaging surface into **r** in this equation will provide the system's pixel resolution or field of view, respectively.

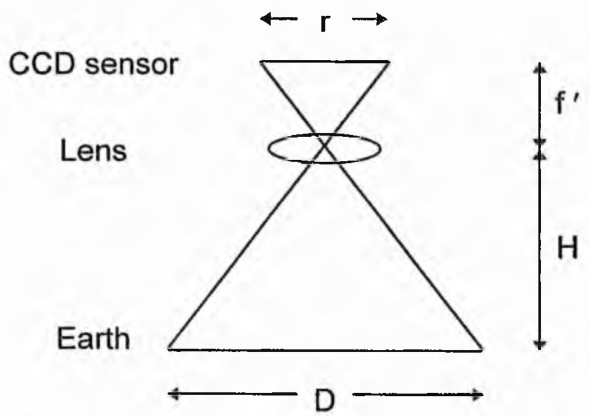

$$\frac{f'}{r} = \frac{H}{D}$$

Figure 5.4.1.1 Relationship between camera characteristics and spatial resolution.

Because it is simple to calculate, this is the widely used definition of spatial resolution for remote sensing cameras. As highlighted in [Slater, p.333] the term 'scale' is in fact more accurate than the more commonly used 'ground resolution', because this assumes a perfect lens and detector. In reality, the true resolution of a camera is rather more difficult to establish. Each element in the optical system, including the sensor, will introduce point spreading losses (described by the modulation transfer function - see section 5.4.2.1) which reduce the actual ground resolution from this theoretical value. [Forshaw et al] discuss the numerous factors that determine the true resolution of satellite imagery, including the modulation transfer function of the optics and the sensor, noise, mis-registration and motion blurring. Fortunately, with careful selection of the optics and imaging parameters, these losses should be small compared to the coarseness of the CCD photosite structure. Conversely, it is also possible to detect objects smaller than the nominal ground resolution, provided they are of sufficiently high contrast.

Despite these qualifying comments, the simple relationship between the CCD dimensions, the focal length and the orbital altitude define the imaging system's resolution and field of view. Given that the orbit of a microsatellite will be beyond the control of the camera designer, and the dimensions of the selected CCD are fixed, the only real variable in the system is the lens. Therefore, the choice of lens focal length effectively determines the imager's resolution.

For a typical CCD with 15 μm photosites situated at 800 km above the Earth, lenses with focal lengths of 6 mm, 60 mm and 600 mm will provide a nominal ground resolution of 2 km, 200 m and 20 m respectively. Of course, for a sensor with a fixed number of photosites, the field of view will scale in accordance with the ground resolution.

For lenses with a simple design, there is a close relationship between the focal length of lens and its physical length. For this reason, very high resolution imaging payloads will be difficult to accommodate on a microsatellite platform. If very long focal lengths are required (i.e. 400 mm and longer) it may be advantageous to use mirrors to bend the light path to fit within the cramped conditions on a microsatellite. Conversely, wide angle (short focal length) lenses will not be as small as their focal length suggests. Given that simple lens systems are poorly corrected for spherical and chromatic aberrations, further elements are added (up to around eight elements is common in photographic lenses) to deliver higher quality images. Under these circumstances, the lens dimensions can often grow significantly larger than their simple equivalent. Furthermore, to make camera lenses interchangeable, they are often referenced to a mounting flange at a fixed distance from the focal plane. In such cases, the size of the lens may bear little relationship to the focal length. Therefore, it is worthwhile assessing the optical and mechanical properties of several lenses early in the project to ensure that they will not be too large to be supported by the microsatellite.

5.4.1.2 Lens aperture and exposure

5.4.1.2.1 Using the lens aperture to control exposure.

It is important that the image captured by the camera is correctly exposed. A perfectly exposed image would use all of the sensor's dynamic range without saturating. In reality, for most remote sensing systems, 'well exposed' means that about 50 % of the dynamic range is used for any given image, allowing some latitude to accommodate fluctuations in scene brightness, particularly prominent in higher resolution imagery.

There are two means of controlling exposure within an electronic camera: varying the length of time that photons are collected, and varying the lens aperture. To make an image brighter, one can either collect photons for longer or increase the size of the lens aperture. The rule of reciprocity holds for all linear sensors (including film and silicon sensors) which states that doubling the collection time is equivalent to increasing the aperture area by two (its diameter will increase by $\sqrt{2}$). Combining these two controls allows a camera to be used over a very wide range of illumination conditions.

In film photography, the collection time is governed by the shutter speed, which will be adjustable from a few seconds to as short as a few hundred microseconds (1/5000 th of a second). For CCD cameras, controlling the integration time is equivalent to altering the shutter speed. However, for most electronic cameras, the integration will be adjustable by a factor of 100 (6.5 stops) at the most. In reality, it will probably only be adjustable from 1 to 20 ms (4 stops). This range will be sufficient to accommodate natural variations in scene brightness across the Earth, but not enough to handle gross over or under exposure. It is therefore important to ensure that the aperture is correctly sized to give a good average exposure for the expected imaging conditions, using the integration control for fine trim.

A lens acts like in an analogous fashion to a parabolic dish antenna - the larger the aperture, the more signal will be collected. The ratio of the focal length to the optical aperture, known as the *f*-number, defines the brightness of an optical system and how much light it collects. Smaller *f*-number indicates a larger aperture and a brighter image (i.e. it captures more photons). Lenses with the same *f*-number will provide equivalent illumination, even if they have very different focal lengths.

However, unlike a CCD camera's integration control adjustment, changing the aperture size requires moving mechanics to physically open or close the iris. Electrically driven auto-irises are available on many lenses, which although simple, are moving mechanical items whose presence on a microsatellite constitute a limit to reliability. A mechanical iris was flown as an integral part of the reworked commercial camera used on the Webersat microsatellite, but the performance of the iris is not documented (see comments in section 2.3.5.3). Irrespective of the success or failure of this camera, a moving iris should be avoided wherever possible.

Therefore, on a microsatellite the iris should be fixed prior to launch. In fact, the range of illumination conditions experienced by a Earth observation mission in low-Earth orbit is sufficiently constant to not require a variable iris, provided electronic integration control is available. However, it is crucial that the diameter of the aperture is set correctly, or else the entire imaging mission could be ruined, consistently over or under exposing the imagery. Fortunately for cameras imaging in the visible spectrum, the Sun provides very strong illumination and there will be no special requirements for very bright optics.

5.4.1.2.2 Determining the aperture size.

Unfortunately, relating the photometric parameters of the scene and the optics to the electrical units of the sensor is a complex process [Slater, p.539]. While it is possible to analyse the physical phenomena of the Earth's albedo and atmospheric propagation and scattering of light rays, this is a very intricate procedure, subject to numerous uncertainties in the values attributable to certain effects. The author has preferred to use the more pragmatic approach of referring to existing systems to determine the correct exposure for the electronic cameras flown on SSTL missions. By comparing the sensitivity of a new system to a successful orbiting instrument, one can obtain the crucial information on lens parameters very quickly. Indeed, unless some significant deviation in performance is anticipated, there is really little point in repeating the theoretical exercises performed as part of the mission-definition stages of conventional space missions.

For silicon CCDs, the best reference is the HRV system on the SPOT satellite. In panchromatic mode (i.e. with no optical filters to attenuate the incoming signal), the integration time is 1.5 ms. The optics are $f/3.5$ but the light is attenuated by 8 due to the presence of three semi-reflecting beamsplitters in the optical path. Thus a baseline for silicon CCDs with 13 x 13 μm photosites and 100 % fill-factor can be established: $f/8$ for a 1 ms integration time (no filters). From this reference, it is possible to moderate the f-number of the design in hand by allowing for factors like the photosite's dimensions and the fill-factor, the average integration time, and the CCD's spectral characteristics and quantum efficiency. If optical filters are employed, their attenuation relative to a panchromatic (unfiltered) system is assessed by integrating the Sun's power spectrum, the CCD's frequency response and the filter's pass band. Although there are many items influencing the final brightness of a camera, evaluating these is far simpler than performing the calculations from first principles. This comparative approach has been used with success for the UoSAT-5, KITSAT-1 and PoSAT-1 cameras, and will continue to be used for future SSTL imaging missions.

Having determined a suitable for *f*-number for the camera configuration, it is necessary to fix the iris size in the lens. It is important to remember that it is not the physical diameter of the iris which is used to calculate the *f*-number, but the projection of the iris onto the lens's entrance pupil. Therefore, given that in most lenses the iris is located part way between the entrance pupil and the focal plane, the actual aperture is smaller than the effective aperture.

Given the brightness of the scenery viewed by a remote sensing satellite, most Earth observing CCD cameras will have small apertures, unless very narrow optical filters and / or short integrations are used. Using large *f*-numbers is advantageous, because is ensures a good depth of focus, making the optics relatively insensitive to errors in focusing, which may occur during the intense vibration of launch. If in any doubt as to the precise aperture that must be set, it is better to err on the side of under exposure by using a smaller aperture; to a certain extent, under exposed images can be 'stretched' during digital image processing to increase their contrast. Conversely, there is no corrective action that can be taken to compensate for a saturated image.

Due to the need to set the iris aperture for each camera as a function of its own characteristics and those of any optical filters that may be used, it is important to select an optical system which allows this. In particular, the catodioptric (mirror) lenses sometimes used to provide compact implementations of long focal lengths usually have a fixed *f*-number (often *f* / 8). While the compact mechanics of these telescopes is attractive for high resolution imagers on microsatellites, the inability to alter the aperture setting is likely to be a problem.

5.4.1.2.3 The Rayleigh criterion.

Having calculated an aperture size to give suitable exposure, it is important that these dimensions obey the Rayleigh criterion for angular resolution [Slater, p.322]. In the same analogy with a parabolic dish antenna, where the diameter of the dish dictates the beamwidth, the effective aperture diameter of a lens determines the smallest angular separations that can be resolved. Given that the *f*-number selected for a remote sensing camera lens is likely to be quite large, there may be a potential problem in meeting the Rayleigh criterion as a consequence of the small apertures.

The Rayleigh resolution is defined by the expression:

$$\sin\theta = 1.22\,\lambda / d$$

where θ is the smallest angular separation resolvable, λ is the wavelength of operation, and d is the effective diameter of the lens aperture. (Note that this expression is independent of the focal length). In the case of an Earth observation camera, it is necessary to make the aperture diameter sufficiently large to ensure that the angle θ is smaller than the instantaneous field of view (IFOV) of a single pixel. On the whole, it is unlikely that a lens designed for these applications will violate this condition, but it is nevertheless important to verify, especially for high resolution systems. If the lens design is inferior to the Rayleigh criterion, it is necessary to enlarge the aperture and use an optical filter to compensate for the increase in brightness.

5.4.1.3 Spectral characteristics.

Crown glass is the principal material used for the manufacture of lens elements. This type of glass has a very good transmissivity of over 90 %, with a flat response, covering the whole of the visible region (silicon's spectral band). In most instances, special coatings are applied to the surfaces of the assembled lenses elements to improve the transmissivity to around 98 to 99 %, thereby reducing the number of internal (ghost) reflections. For the majority of remote sensing applications operating in the visible portion of the spectrum, no additional measures will be necessary.

Although most photographic lenses are designed to operate in the visible, they generally have an acceptable behaviour in the near-IR as well. If the application is critical, then it may be necessary to have such a lens characterised for transmissivity and chromatic aberrations in the additional spectral bands. This is only really significant for multispectral systems, where co-registration of the image planes may be compromised by chromatic discrepancies.

However, if the instrument needs to image in the ultra-violet (using a UV-enhanced CCDs), crown glass becomes opaque and fused silica or quartz needs to be used for the optical surfaces. These materials have about 40 % transmissivity in the UV bands, and excellent properties in the visible, but are less widely available and significantly more expensive than conventional glass. Similarly, for wavelengths longer than 2μm, specialist materials such as germanium, sapphire, zinc selenide or calcium floride are needed.

5.4.1.4 Geometric distortion.

All lenses suffer from a certain amount of geometric distortion. In general, the problem is worse for wide angle lenses (short focal lengths) because of the increased sphericity of the scene which must be projected onto a flat focal plane. Eliminating the distortions from a lens requires complex design and manufacturing processes, which is reflected in the cost of the lens. As a general rule, lenses with more optical elements (sometimes in excess of eight or ten) are better corrected than those using simpler designs.

As the design of distortion-free optics is a challenging task, it is largely a matter of selecting a lens with good characteristics for the remote sensing camera. Most lens manufacturers will provide charts and statistics describing the various distortions and degradations on request. If necessary, this data can be used to correct images for distortion during post processing using 'rubber sheet' transformations. Similarly, it is worth taking a series of reference images of test patterns with grid structures before launch. Provided a careful note of the imaging geometry is made (viewing distances, angles), these will provide a useful source of feedback in assessing the effectiveness of the correction algorithms.

While post processing for image artefacts like geometric distortion can enhance the usefulness of the data, these steps should be used sparingly. There is an inevitable loss of resolution incurred during the resampling stages of image processing algorithms, and should therefore be avoided as far as possible. It is definitely best to specify a lens with sufficiently low distortion to not require any corrective post processing.

5.4.2 USING OFF-THE-SHELF SYSTEMS.

Much of keeping the total cost of a remote sensing camera low is to use off-the-shelf systems as far as possible. However, unlike the camera electronics for which it is difficult to find implementations appropriate for remote sensing, there are huge ranges of lenses available that may be suitable. The search for lenses should not be restricted to those designed for applications such as television where a CCD is the intended sensor. The lenses considered should obviously include the wide range for 35 mm and larger format film photography, as well as alternatives such as enlargement or projection lenses. There should be few problems in identifying optics with the focal lengths and *f*-numbers required for a given Earth observation application.

Certainly, if the lens chosen is intended for professional photography and designed by one of the established manufacturers of quality optics (Zeiss, Leitz, Nikon, Canon, etc.), it will have outstanding optical properties. These lenses will have excellent characteristics for distortion, spherical and chromatic aberration, and spectral purity, as well as being built to very high standards. Although lenses of this grade are expensive for individuals (thousands of pounds), they are affordable within the context of an Earth observation microsatellite mission. Care should taken when evaluating cheaper lenses, as their optical performance is almost always inferior.

Given the large research and development investment made by the major manufacturers of photographic equipment, it is unlikely that the designer of a microsatellite imager will be able to do a better job. Identifying off-the-shelf elements to meet the remote sensing camera's requirements is a crucial ingredient in keeping the system low-cost. If custom optics are absolutely necessary to meet the mission objectives, the designer (who will presumably be an electronics specialist) should seek an expert optical consultancy to undertake the design work; this will almost certainly be cheaper, faster, less troublesome and deliver better optics than by doing it in-house.

5.4.2.1 The Modulation Transfer Function.

The only aspect of a high specification photographic lens that may be inadequate when illuminating a CCD sensor is its resolving power. Whereas the Rayleigh criterion (discussed in section 5.4.1.2.3) establishes the theoretical limit of resolution based on the aperture size (i.e. for diffraction-limited optics), a lens's resolving power defines its true ability to record fine detail. In effect, the resolving power quantifies the point spreading characteristics of the lens.

This potential problem arises from the relatively small photosites of a CCD, typically 10 to 20 μm. To ascertain whether a specific lens has sufficient definition to suit a CCD sensor, it is necessary to compare the modulation transfer function (MTF) of the two components. (A description of the process for characterising a system's modulation transfer function and optical resolving power are beyond the scope of this thesis, but a good introduction is provided in [Slater, Ch.11 and Appx.1]). Without going into any depth, the MTF describes how faithfully the optical device records fine detail in the scene, and is expressed in units of line pairs per millimetre.

The characteristic MTF of a CCD is shown in figure 5.4.2.1. The units of spatial frequency are normalised to the photosite pitch, so that 1.0 on the abscissa equals to the number of photosites per millimetre. (For CCDs with 10 and 20 μm photosite spacing, this corresponds to 100 and 50 lines per millimetre respectively). The MTF response rolls off from unity as a sinc function ($\sin(x) / x$) until it reaches the value of 0.64 at twice the photosite spacing. This cut-off point corresponds to the Nyquist condition for sampled signals, after which aliasing becomes apparent.

The MTF of a lens will not be as generic as that of a CCD, and will depend heavily of the materials and design used. To avoid any loss of resolving power to the overall system, it will be necessary for the lens's MTF to be significantly better (about a factor of ten) than that of the CCD. In practice, a lens from a quality manufacturer like Zeiss (supplier to Hassleblad) or Leitz (Leica) will have an MTF figure of about 90 % at 30 or 40 line pairs per millimetre, and will make virtually no contribution to the limitations of the system's overall performance. [2]

As some indication of the effective grain size relative to photosite size, standard 35 mm images (36 x 24 mm) are digitised at about 750 x 500 pixels, giving an effective photosite size of 50 μm (see footnote). Similarly, medium format film images (70 x 60 mm) have about the same effective resolution as a 1500 x 1500 CCD.

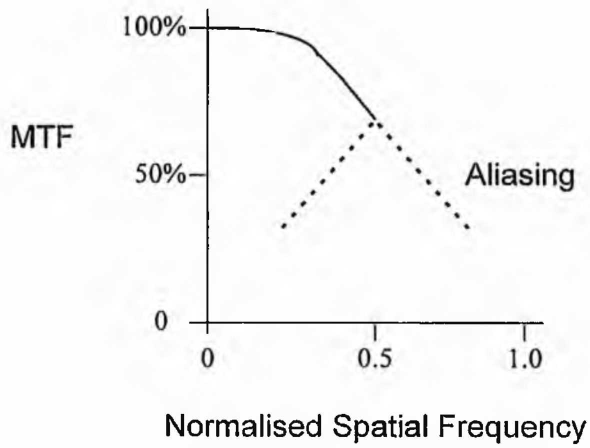

Figure 5.4.2.1 Modulation transfer function of a CCD.

There is inadequate scope within this document to deal fully with establishing and comparing the modulation transfer function of CCDs and other optical components.

---

[2] When evaluating the performance of a photographic lens, it is not adequate to assume that a CCD will have a coarser resolving power than a fine-grain film. Despite the availability of MTF charts, direct comparison of the 'photosite size' of film and a solid-state sensor is not straight forward. The film is made of photosensitive halide crystals, each of which is about 1 μm [Slater] in diameter. However the non-uniform distribution of these crystals in the emulsion results in clusters of particles, which can reduce the film's ability to record light intensities faithfully by altering the film's density when developed. The average size of these clusters for a low grain film is about 50 μm (derived from the specifications for diffuse RMS granularity provided by [Slater] and [Kodak]). Although the cluster dimensions will limit the performance of a film, it is inappropriate to compare this to the photosite size of a CCD because these clusters comprise many smaller photosensitive elements. Although the cluster will limit the radiometric resolution of the image, finer structural detail will be discernible. The film's MTF will reflect the combination of these effects.

Needless to say, further reading of texts (e.g. [EEV, p.12] and [EG&G, p365]) dealing with this matter in greater depth will be necessary for the camera designer to appreciate the theoretical and practical implications of a CCD's MTF. [Burt] provides a detailed theoretical analysis of the MTF of CCDs, including wavelength dependent effects. Nevertheless, it is safe to say that high quality lenses produced by reputable manufacturers will have adequately good MTFs to ensure that the remote sensing camera suffers no appreciable degradations to the imagery.

5.4.3 ACCEPTABLE MATERIALS FOR USE IN SPACE.

A requirement for satellite remote sensing systems rarely encountered in terrestrial applications is the need for materials compliance. It is important that none of the materials used in a manufactured lens degrades or out-gasses in the hard vacuum of space. In effect, this requirement limits the lens housing to be made of metal, and the optical elements to be of glass. The principal offending materials will be plastics in the housing, rubber seals or hand-grips, and liquid or fluid lubricants for adjustable focus and / or iris systems.

As vacuum-rating is an uncommon requirement for most photographic systems, the technical support staff for these components will generally be unaware of the specifications of their products. Notable exceptions are Hasselblad / Zeiss and Leica / Leitz who use their products' space-rating as a marketing ploy. Indeed, these camera systems are used off-the-shelf for the US's manned space programme (the only modifications are enlarged knobs and controls so that they can be operated despite the astronauts' thick gloves), and are therefore directly suitable for use on microsatellite remote sensing missions. According to these companies' technical support teams, the reworking required (hermetic seals, stable materials, dry lubricants, etc.) to meet the vacuum specifications of the Gemini and Apollo missions in the 1960s, resulted the cameras performing better under adverse terrestrial conditions (humidity, temperature extremes, dust and sand, salt spray, etc.) and the modifications were made standard to all models.

If there is any doubt as to the material specification of an off-the-shelf lens, it will be necessary to dismantle a representative sample and investigate. Any housing or optical elements which may be outside the vacuum out-gassing specifications (which are generally issued by the rocket's launch agency or principal payload) will need to have their materials identified by the manufacturers. In general, asking the manufacturer for the specific characteristics of an individual component is far more likely to receive a reply than a vague request for the lens's bill of materials. In practice, the suitability of most components in the lens is pretty obvious, either being glass or metal, or some form of plastic or rubber. The most ambiguous elements are often thin polymer gaskets or shims, and the glues and other bonding agents.

Therefore, it will often be necessary to disassemble the lens to identify any potential problems in materials specifications. Any offending components will need to be removed and, if necessary, replaced by a suitable alternative. This is also a convenient time to determine whether any superfluous mechanical components, normally associated with variable focus or aperture, can be removed to reduce the lens mass. This stage of inspection is particularly important with many modern (Japanese) lenses which make extensive use of plastics, not only in the lens housing but also in the optical surfaces, and are clearly unsuitable for use in a vacuum. Fortunately, there are still many traditional lens designers who use glass and metal exclusively in their construction.

It is unlikely that the coatings applied to the optical surfaces to reduce reflections will be effected by exposure to vacuum. These coatings are generally applied in a vacuum sputter chamber and therefore need to be inert under vacuum to survive the deposition process. Similarly, although ionising radiation is known to cause a darkening of standard crown glass, this is unlikely to be an issue because the external surfaces of a satellite in low-Earth orbit receives doses of tens of kilorads per year, whereas total doses of the order of megarads are required to cause these optical changes. Finally, there may be some components, such as polymers, adhesives or optical coatings, which may degrade when exposed to the increased levels of ultra-violet radiation of deep space.

5.4.4 OPTICAL FILTERS.

5.4.4.1 Choice of spectral bands / optical filters.

The choice of spectral bands for use in an Earth observation camera are important (as mentioned in section 3.1.2). Optical band pass filters are used to separate the colour (or spectral) bands. When choosing filters for remote sensing imaging systems, only laser-grade filters should be used for these applications, obtained from distributors of research-quality optical components. These will be made out of carefully selected metal, glass and ceramic materials, with well defined optical and mechanical properties. In most instances these filters will be individually characterised by the manufacturer, and their spectral response curves will be provided as standard. Conversely, although significantly cheaper, the glass, plastic or gel filters used in the photographic industry are supplied for their artistic merits, and will never be qualified to the levels needed for satellite remote sensing. In addition to often being made of plastic or resin and therefore prone to out-gassing in a vacuum, these photographic filters do not have defined cut-off characteristics and vary unpredictably from batch to batch.

5.4.4.2 Lens / filter interactions.

If used, optical filters should ideally be placed in front of the lens where the incoming light waves are parallel and effected equally by the changes in refractive index introduced by the filter. If the filter is placed between the lens and the sensor, or inside the lens, it can introduce optical path length variations on the converging light rays, resulting in spherical aberrations (such that the image is no longer focused in a plane but on a curved surface, throwing the edges out of focus). Of course, in certain types of multispectral imager (see section 5.4.4.3.2), it is necessary to place the filters behind the lens and care must be taken to prevent aberrations.

As the optical filters are resonant structures made of successive layers of metal, ceramics and cavities, light rays arriving at oblique angles of incidence will see slightly larger distances between the various plates in the filter. Consequently, the resonant wavelength (pass band) will be slightly longer (up to tens of nanometres at 45°) for non-perpendicular rays. This is only a significant issue if very precise and narrow spectral bands are required, for example, to differentiate molecular resonance bands of atmospheric aerosols (e.g. ozone, carbon dioxide or water vapour) from the background scene. For most remote sensing applications, the spectral bands are quite wide and this effect is unlikely to be problematic, except for extremely wide angle lenses.

An important consideration is that filters attenuate the total amount of light reaching the sensors. This attenuation must be evaluated and compensated for by enlarging the iris used by the lens. In a multispectral system, it may be necessary to use precision neutral density filters to balance the light received by the various detectors. The effect of the filter's attenuation combines with the changes in the CCDs sensitivity and the Sun's output power over wavelength.

Despite using high quality components, there are often some slight variations in the characteristics of each filter (peak transmissivity, centre wavelength, 3 dB and 10 dB cut-off wavelength). Although these individual errors do not effect the spectral discrimination of a camera adversely, there can be 5 to 10 % variations in total transmissivity. Therefore, each individual filter must be characterised when calculating the lens aperture or neutral density filter adjustments.

5.4.4.3 Multispectral imaging.

Although, implementing multispectral systems has not been addressed as part of this research programme, future SSTL imaging systems must incorporate these features. It is therefore appropriate to address briefly some of the key issues facing the development of these capabilities. A number of solutions are discussed, mentioning their various benefits and disadvantages, but no definitive conclusions are reached because a full development review has not been conducted as part of this programme.

Fortunately, most CCD silicon photosensors recommended earlier in this thesis are sensitive to the most important remote sensing bands located in the visible and near-IR wavelengths. If an Earth observation camera is to fulfil general purpose applications it should sense in the near-IR, red and green, which are considered to be the most relevant bands. However, one of the main attractions of microsatellites is that their low cost makes them suitable for dedicated specialist missions, providing scope for using alternative spectral bands, optimised for these specific applications.

The traditional solution achieving multispectral capabilities, or colour for broadcast quality television, is to use several identical CCD sensors driven in synchronism. Each CCD has a different optical filter, and the output from the three devices is combined to produce a colour image with the full resolution. Of course, the mechanical and optical alignment of the three sensors is crucial so that the imagery from each sensor is co-registered, with pixels viewing exactly the same part of the scene in each case.

Although the red, green, blue colour scheme is used for television applications, these can be replaced with any desired combination of visible and near-infrared bands for remote sensing. Furthermore, more than three spectral bands can be accommodated, although more than four or five in the visible / near-IR is probably superfluous.

5.4.4.3.1 Multispectral imaging using multiple cameras.

There are several methods for implementing multispectral camera systems. Conceptually, the simplest approach is to use several identical cameras, each fitted with a different filter. The advantage of this is modularity, with each imager being a fairly standard and completely independent unit. It is relatively simple to add, remove, test or upgrade individual cameras without disturbing the rest of the imaging system. This approach has been used for the LANDSAT RBV instruments, and many of the US's lunar and interplanetary missions including the Apollo [Slater, p.444], Skylab [Slater, p.447] and Mariner [Slama, p.936] missions, and more recently in the Indian IRS family's LISS sensors [Pease].

The main drawback of this implementation is that a separate lens is required for each spectral band, resulting in slightly different imaging conditions for each camera. Even if the lenses are nominally identical, there are nevertheless some differences in distortion, magnification, chromatic balance, boresight alignment, etc. that make registration of the multiple image planes difficult. Lengthy pre-flight calibration is needed to characterise these effects and intensive image post-processing to compensate for them. Furthermore, as the lenses are generally the largest components in a camera, replicating the optics greatly increases the overall system mass, potentially exceeding the mass budget for a microsatellite. Finally, since each camera is fairly massive, say 3 kg, it can be difficult to achieve and then maintain the sensors' alignment to within a photosite through the spacecraft's handling, transportation and launch.

5.4.4.3.2 Multispectral imaging using beamsplitters.

Another popular approach for achieving multispectral capacities is to use optical beamsplitters to project identical images onto several CCD sensors, with a distinct filter placed in front of each detector. Because a single shared lens illuminates all the CCDs, the overall system mass is reduced. Moreover, any optical distortions or pointing errors will be suffered equally by each image, providing well registered, although not necessarily corrected, images. This configuration is often preferred for solid-state imagers, including the SPOT HRV instruments, as well as most other pushbroom systems.

The beamsplitter implementation results in a compact optical unit suitable for use on microsatellites, but can make assembly, test and adjustment rather intricate and difficult. It is possible to include additional spectral bands to an existing design without too much difficulty, and the choice of filters can be altered at any time. One drawback is that each beamsplitter in the light path will attenuate to signal by two, resulting in considerable losses if numerous (i.e. more than four) images need to be cast.

The beamsplitters can be made either from thin semi-reflective mirrors or by bonding two coated prisms to make a optical cube. For microsatellite applications, the beamsplitter cubes are more appropriate because several can be glued together to make an integrated unit. This is advantageous because an accidental displacement of a single splitting element can have a disastrous effect on image registration; if all the beamsplitters are bonded together, any positional shifts will effect all images equally. Thin-film 'pellicle' beamsplitters are not suitable for space use because they are unlikely to withstand launch and are generally made with organic membranes which will out-gas.

In general, each CCD is positioned and bonded into a fixed position relative to the other sensors to an accuracy of less than a photosite (i.e. a few microns). This alignment is a very demanding mechanical task, but is made easier because only the CCDs themselves need to be positioned. As they only weigh a few grams, the load-bearing requirements of the precision alignment mechanics will be much smaller than for entire cameras (as discussed in the previous section). Care must be taken to design the system so that a damaged or soiled element can be removed without destroying the entire camera.

5.4.4.3.3 Multispectral imaging using filter wheels.

An alternative approach for collecting multispectral imagery is to use a single camera carrying a carousel fitted with several optical filters. The filter wheel is rotated in synchronism with the frame rate so that an image is collected through each filter in turn. The great advantage of this approach is that a single camera is used, reducing volume, mass and cost, and eliminating the delicate mechanical alignment of multiple sensors. Many deep-space missions including Viking, Voyager, Gallileo, Mariner [all from Rycroft] and the recent Clementine mission (see section 2.3.5.8, not to be confused with the forthcoming SSTL mission of the same name) have employed filter wheels successfully.

Another great benefit of this solution is that any number of spectral bands can be accommodated merely by adding extra filters. Although most carousels will hold a maximum of around a dozen filters, it is possible to cascade multiple wheels, each fitted with at least one clear slot. By aligning a filter on one wheel and the empty slots on the other wheels, any given filter can be chosen. Other combinations, such as mixing spectral (colour) filters with polarising, neutral density or graduated filters, are supported far more easily than with the alternative approaches to generating multispectral imagery.

The real drawback of this approach for microsatellite remote sensing is that the imager losses its independence from the spacecraft's attitude stability because of the time delay between the images. If the attitude pointing, and most particularly the satellite's alignment with respect to the orbital velocity vector (i.e. the yaw) is very well controlled, it is a simple matter to register the multiple images during post-processing. However, if the satellite attitude is allowed to drift, then the images will not be aligned. Unlike a pushbroom sensor which can suffer from registration errors within a single image, each of the images from a filter wheel camera will be correctly registered, but the successive images will need to be translated and rotated to register with each other. Fortunately, these errors are small because the capture process will only require a few hundred milliseconds for a full multispectral set - one image frame per filter, plus a few dummy frames to allow a new filter to moved into position.

Although moving mechanics are generally undesirable on microsatellites, a simple stepper motor can be used to turn the filter wheel without incurring an excessive reliability risk. The control electronics must be able to drive the motor in both directions, as this can often be used to overcome a sticking motor. Additionally, redundant motors can be fitted to drive the wheel.

The torques generated when starting this filter wheel, and its angular momentum once running, will result in significant attitude disturbances. The filter wheel's inertia (e.g. 10 cm diameter, 300 gram mass, 3 Hz rotation rate) will be comparable to that of a typical microsatellite reaction or momentum wheel (smaller but faster). However, by ensuring that the angular momentum of the filter wheel is matched by a counter-rotating mass, this system can have a net momentum of zero. Given that the slow rotation of the filter wheel will probably need to be geared down from a faster motor speed, the counter-rotating object already exists. To achieve zero net momentum, it will be necessary to make the ratio of the two moments of inertia ($\frac{1}{2}$ mass $\times$ radius^2) equal to the value of the gear ratio.

5.4.4.3.4 Multispectral imaging using focal plane arrays.

A frequently used solution for increasing the photosite density of an imager is to mount several CCD sensors in the focal plane of a single lens to view adjacent portions of the scene. This can be adapted to fulfil multispectral applications, by using filters and relying on the satellite's orbital velocity to move the target scene across each sensor in turn.

This is effectively a synthesis of the beamsplitter and filter wheel approaches, unfortunately embodying most of the worst features of both. While the imager is small and compact, as with the beamsplitter configuration, the accurate alignment of the sensors is also needed. Similarly, because the spectral images are time-delayed there is the risk of registration errors.

This solution will only be attractive for microsatellites missions where mass restrictions and a need for entirely passive mechanics make the multiple camera and filter wheel approaches impracticable, and for low-light applications where the signal attenuation of beamsplitters cannot be tolerated.

5.4.4.3.5 Single-chip, colour CCD cameras.

A recent development in colour imaging is the use of single-chip, colour CCD sensors developed for hand-held video cameras. Because they are inexpensive and mechanically robust, these sensors appear attractive for use on microsatellite remote sensing missions. These devices obtain their colour information by having a mask applied to the photosensitive surface of the CCD in groups of four pixels: one pixel each of red, green, blue and clear (or alternatively cyan, magenta, yellow, or some other increasingly complex colour scheme). The video processing circuitry combines the output of this group of pixels to produce a colour signal.

However, since the pixels have been clustered in this fashion, there is a corresponding loss in spatial resolution, which is why the picture from consumer video cameras often appear ill-defined or 'soft'. This loss of resolving power, as well as the poor definition of features that are recorded, makes the image quality from single chip colour cameras inadequate to meet the demands of broadcast-quality television applications, and the same argument applies to satellite remote sensing. A colour sensor of this type was flown on the KITSAT-2 microsatellite (discussed briefly in section 4.4.5), and the results confirm the author's opinion that this technology is inappropriate for serious Earth observation.

Furthermore, if a single colour CCD is employed there is no control over the spectral bands sensed because the filter mask is fixed at the factory. With the multiple sensor system, however, the combination of optical filters can be chosen to highlight whichever features the design team wishes to view. Therefore, multispectral cameras should have a dedicated sensor for each spectral band or use a filter wheel approach.

5.5 TESTING AND CALIBRATING THE IMAGING INSTRUMENT.

Once an imaging system has been developed and built for a remote sensing satellite, it is necessary to test and calibrate the instrument to ensure its performance. Since it is impossible to record the scene free of all distortions or errors, these degradations must be quantified to determine the accuracy of the data. Regardless of the intended application of the imagery, the user will want to know what the strengths and limitations the data are.

The goals of this research programme have been to confirm the feasibility of using electronic cameras on microsatellites for Earth observation. The objective has therefore been to deliver working systems in-orbit, and once demonstrated, subsequent effort has been devoted to improving the cameras' operational capabilities. Correspondingly, there has been relatively little emphasis on ensuring that the systems are highly calibrated. This has been a deliberate strategy, emphasising (qualitatively) the operational versatility and the range of applications suitable for microsatellite remote sensing, rather than a quantitative study of the performance of the instruments developed.

However, future systems will need to be more accurate, or at least better characterised. Therefore, a brief overview of some of the more important measurements is appropriate. In addition to the items mentioned here, the author recommends a few other sources. Once again, [Colwell, p.364-367, p.873-897] offers a useful introduction to these issues. Although [Karara] is concerned with non-topographic photogammetry (i.e. deliberately avoiding the topics of aerial and satellite remote sensing), there are a number of interesting passages, notably [Fryer] and [El-Hakim], and to a lesser extent [McGlone] and [Wester-Ebinghaus]. Finally, [Slama, p.233-274] includes a detailed summary of the techniques used to calibrate aerial photographic cameras, which although not entirely appropriate to solid-state imagers, provides such extensive recommendations and references to be of considerable use.

5.5.1 ESTABLISHING THE REQUIREMENT FOR CALIBRATION.

While the principle of calibrating conventional remote sensing systems is similar to that required for microsatellite cameras, it is important to remember that neither the budgets nor the time scales of these small missions will permit large expenditure of time and money on elaborate calibration programmes. Traditionally, much of the justification for the great expense of Earth observation instruments leans heavily on the premise of delivering highly accurate and calibrated data. This is at odds with the philosophy of fast response and cost-effectiveness intrinsic to microsatellites.

Fortunately, many applications do not depend on absolute calibration. This is succinctly supported by no less an authority than [EOSAT] which states that "very few analysis techniques require the use of actual radiance values. Thus, generally it is not critical to know the relationship between the digital number and the radiance. However, it is extremely critical that all detectors within a given band for any optical sensor use the same scale within a given scene; that any given digital number means the same radiance, regardless of which detector made the measurement." Therefore, low noise and consistency in the output from the photosites of a CCD camera is vital, but stringent linearity and absolute calibration is not. Only if the imagery is to be compared or merged with data from another instrument, is it necessary to know the absolute calibrations. This position is echoed by [Price], who states that "the need for quantitative radiometry has been absent from most research work and applications".

Therefore, as mentioned in section 3.1, the exact requirements of the mission's principal customers must be established clearly. There is little point in using some arbitrary level of calibration as a criterion (e.g. the same level as achieved from SPOT, or ten percent radiometric accuracy), as this will either fail to meet the real user requirements or else be an overkill, wasting money in unnecessary calibration stages. The emphasis for microsatellite remote sensing must be to implement a calibration regime commensurate with the mission requirements, only fulfilling those tasks strictly necessary, achieving a suitable balance between cost and accuracy. In practice, the short time-scales of microsatellite programmes will often preclude extensive ground-based testing, relying entirely on in-orbit calibration techniques (to be discussed in section 5.5.3.2).

5.5.2 CALIBRATING THE OPTICS.

With the exception of very wide angle lenses for meteorological imaging, it should be possible to use virtually distortion-free optics in a remote sensing instrument. To this end, the additional cost of a high quality lens from a manufacturer like Leitz, Zeiss or Angenieux will generally be justified because of the extra performance they deliver. With these systems, it should be possible to obtain optical image quality superior to the resolving power of the CCD sensor, minimising, or even eliminating, the need for extensive calibration of the camera. Therefore, as discussed in section 5.4, paying for quality optics generally saves money in the long run. Although it is possible to use digital image processing to correct for numerous defects, these manipulations invariably entail some loss of definition, and should therefore be avoided by making the camera as perfect as possible.

5.5.2.1 Adjusting the focus.

Regardless of the quality of image delivered by the optics, it will always be necessary to position the lens and the CCD sensor with accuracy to ensure that the focusing is sharp. Unfortunately the mounting of the CCD's photosensitive surface within the package, and all the mechanical supports, will have cumulative tolerances which can be as large as a couple millimetres. Because these tolerances are too great to permit guaranteed focusing, this must be done explicitly for each camera once it has been fully assembled.

Irrespective of the type of lens selected, its focus must be fixed at infinity to image the very distant Earth. There is no point in selecting the lens's hyperfocal point (as may be done in film photography) instead of true infinity, because there will no foreground to record. Focusing at infinity but using a small aperture will provide a greater depth of focus, giving the lens more resilience to focusing errors (potentially caused by the vibration of launch).

If the lens has an adjustable iris, it will be best to fix the aperture (see section 5.4.1.2) after the focusing. Firstly, opening the aperture to the brightest *f*-number will reduce the lens's depth of focus, thereby making the lens more sensitive to focusing error; when the aperture is reduced for flight, the regained depth of focus will provide increased tolerance to this error. [3] Secondly, when the lens is prepared for orbit with optical filters and a small aperture, the images cast are too dim to be useful when illuminated under laboratory conditions. Although it will be necessary to verify the focus with the final assembled optics, this approach ensures that the optics are in their most favourable configuration for focusing. Provided the iris can subsequently be fixed without completely dismantling the lens, and a suitable mount is used, it should be possible to remove the lens for minor adjustment and replace it without introducing appreciable positioning error.

The recommended method for focusing the camera is to present it with collimated light, projecting a test image at infinity. The lens should then be focused to present a sharp rendition of the test image, viewing the CCD's signal on a monitor. This will occur when point sources of light fall within a single photosite. An alternative is to look for the 'stair-casing' effect on diagonal lines caused by the sampled nature of the CCD's output;

---

[3] This approach is used in virtually all single-lens-reflex photographic cameras to assist with focusing. The iris remains open until just before the shutter fires, when it is changed to the selected aperture.

continuous, slightly fuzzy projections of these lines are indicative of poor focusing. The targets used should have low-contrast; if highly differentiated black and white patterns are used, it is possible to set the lens for the highest contrast of a specific feature rather than the sharpest focus.

There will be a small range of positions which will appear to provide equally sharp focus; this 'circle of confusion' is a result of the lens's inability to produce perfect images (or the sensor's inability to record them). The extent of this range should be noted and the mid-point used for the final focusing. It is important to verify the focus at several points of the image plane, and to not rely solely on measurements made along the optical axis, which can be misleading. Similarly, if the system is used for a wide range of spectral bands, appropriate tests at all the relevant wavelengths are necessary. Furthermore, the focusing can change if any additional optical materials, such as filters or beamsplitters, are introduced between the lens and the sensor, altering in the medium's refractive index and increasing the optical path length.

When setting the focus of a camera, it is important to make use of all the tools available. In particular, although rarely advocated by the scientists who work with these instruments, the human visual system has a great sensitivity to poor focusing, and this should be used to complement these 'objective' measurements. While it is impossible to quantify these factors, it is nevertheless important to recognise that even moderately experienced amateur photographers intuitively 'know' when an image is in or out of focus.

Certainly, any laboratory settings must be confirmed by imaging real-world scenes (always sufficiently distant from the camera to be at optical infinity), relying on the appreciation of trained operators to assess the overall performance. Under laboratory conditions, it is very easy to concentrate on a few specific features when focusing a lens, neglecting the overall effect. The author has been surprised on several occasions during this programme when lenses focused using geometric shapes and patterns in the labs subsequently have proven to be poorly set when more conventional scenery is viewed. Indeed, given that, short of using interferometric techniques, the final alignment will require a trained operator to determine the best focus by eye, there are some arguments for relying on visual judgement for these optical adjustments, if the operator feels more confident in the results produced.

If the lens has adjustable focus, this may be of use when setting up a remote sensing camera. In a modular photographic camera with interchangeable lenses, the film plane and the optics assembly will both be referenced to the flange on the lens mount, ensuring that the mated units will always have the correct positioning. Although referencing to the lens mount may be useful in a remote sensing camera, it is not strictly necessary. It is possible to deliberately position the lens too close to the sensor, so that the image is out of focus (or focused beyond infinity). By using the adjustment mechanism, the lens's focusing can be brought forward to be sharp at infinity, or any other convenient point. Of course, there will be no relationship between the final focusing distance and the markings on the lens barrel. When the focus adjustment is finalised, the lens's setting must be fixed (perhaps by gluing the lens barrel) to prevent it shifting during the vibrations of launch or transportation. If the lens has a fixed focus, it is necessary to use shims or precision spacers to alter the distance between the lens and the sensor.

5.5.2.2 Characterising lens distortions.

The characteristic distortion curves for a lens should be obtained from the manufacturer. While this provides an excellent generalisation of the main distortions suffered, additional errors are introduced by mechanical misalignment of the sensor to the lens's optical axis, or between the sensor surface and the image plane. While ensuring that the positioning of the various mechanical elements is optimised to reduce these effects, it is only possible to quantify optical distortions and aberrations through measurement.

The need to confirm the lens distortion characterised by the manufacturer's generic information with recorded imagery is supported by the results obtained by [Owens]. While the correction routines developed during this project removed the majority of the lens distortion suffered by the UoSAT-5 and KITSAT-1 Wide Angle Cameras, the processed imagery visibly contained residual errors. These are attributable to incorrect mathematical characterisation of the manufacturer's graphical data and / or physical differences between these cameras and the reference system.

The issues and procedures for calibrating geometric distortions are covered by the references listed at the start of section 5.5. In general, this task involves capturing images of test cards containing geometric patterns (grids of lines or points, and concentric circles). By making careful note of the imaging conditions (distance and angles between the camera and the scene), it is possible to characterise the distortions by comparing what the camera should have seen and what it actually recorded. The geometric patterns of the reference images provide numerous control points from which to develop mathematical transformations which warp the captured imagery back to its 'true' perspective. Fortunately, these distortions do not change, and once corrective transformations have been defined, they will remain constant for the duration of a camera's lifetime. Furthermore, the physical rigidity of an area-array CCD does not contribute its own set of distortions, as would a vacuum-tube image sensor.

A practical means of obtaining these reference patterns is to image the sides of buildings. A building will be sufficiently large to fill the camera's field of view whilst remaining at optical infinity, and brickwork provides a suitably regular grid pattern. Perhaps most importantly, the target's configuration is not likely to change during the test campaign (although the lighting conditions will). Assuming the camera's position and orientation can be well defined (perhaps on the roof or window ledge of another building), it is possible to make identical measurements at a later date with the same or other cameras. Furthermore, if additional control points in the test images are required, it is a simple matter to measure the building's dimensions.

A similar approach is to use the stars as a convenient geometric target [Slama, p.257]. Given that they are truly at infinity, eliminating parallax, the actual position and orientation of the camera need not be recorded with great accuracy. Provided the approximate latitude, longitude and time of the measurements is known, it is possible to compute the correct position of the camera relative to the stars. It is of course necessary for the camera's integration time to be extended to expose the faint stars adequately. If integration times of longer than a few seconds are required, it will be necessary to cool the CCD sensor to reduce dark current, although this can be done by careful refrigeration of the entire camera. Unfortunately, the software infrastructure for this method of geometric referencing is high, requiring sophisticated algorithms for identifying and matching the stars to the patterns of dots recorded by the camera.

Finally, if a representative engineering model or flight spare camera is produced along with the flight instrument, it should undergo the same calibration regime. Hopefully, the performance of the two versions of the camera will be similar, and the unit left on the ground remains available for further measurements, should the first set prove to be inadequate. Indeed, if time constraints are too tight at the end of the microsatellite's development cycle to perform a full set of calibration tests, it may be acceptable to generate a quick sequence of reference images from both cameras under the same conditions. When time permits, a set of absolute measurements can be performed on the engineering model, allowing the characteristics of the flight camera to be inferred by comparing the results of the preliminary test campaign.

5.5.2.3 Aligning multiple sensors.

Multispectral imagers will suffer the same distortion, aberrations and focusing errors experienced by single cameras. However, as mentioned in section 5.4.4.3, the sensors will need to be carefully aligned to ensure that the multiple image planes are co-registered.

The procedure for aligning CCD sensors involves focusing the first sensor and then fixing it and all other optical components (lenses, filters, beamsplitters, etc.) firmly in place. Precision mechanics alone will probably not be adequate to keep all the components in place to within one or two microns during vibration, and a strong glue is needed as well. The position of remaining detectors will need to be adjusted, one at a time, to align accurately with the first CCD. Micropositioning instruments are required to offer the CCDs up to mounting brackets, and then moving them into exact alignment with the reference sensor. A test card consisting of a grid of points is useful to ensure that the imagery from the various sensors can be aligned to with in a single pixel. Although each subsequent sensor is referenced to the first CCD, checks must be made between the detectors to ensure that errors do not accumulate.

The sensors must also be focused during the alignment process. Subsequently, the usual procedures for calibration and measuring distortion will need to be performed. It is also necessary to ensure that the brightness of the image presented to each of the CCDs in their various spectral bands is matched to avoid introducing radiometric inaccuracies. The need to perform the additional alignment and calibration stages will dramatically increase the assembly time and cost of a multispectral imager compared to a monochromatic instrument.

5.5.2.4 Verifying image brightness.

Even though the calculations for determining the *f*-number of a CCD camera from reference values are straight forward (see section 5.1.2.2), it is always worthwhile to perform empirical tests to confirm that the finished system is correctly defined. This involves using the camera under representative illumination conditions is verify its performance. To eliminate additional sources of error that may be introduced by using an artificial illumination source, it is most logical to use a brightly Sunlit scene.

To recreate the orbital conditions most effectively, the camera should be facing north (in the northern hemisphere) to view the test scene, so that the Sun is behind the camera illuminating the target. It is necessary to perform the test on a bright summer day, without any overcastting which attenuate the Sun's rays considerably. The scene should comprise a mixture of materials, both natural and man-made, and must not be viewed through a window, which attenuates the illumination and distorts the spectral balance. In particular, large white-washed buildings are representative of the reflectance of clouds. The camera should be able to accommodate small direct reflections of the Sun, for example from car windows, without degrading the overall image although individual pixels may be saturated. Under these conditions, the imagery should only use the lower quarter to third of the camera's dynamic range (except for the direct reflections). This allows for the fact that the Earth viewed from space is twice as bright as on the surface due to the scattering of the atmosphere, plus a little additional margin.

5.5.3 CALIBRATING THE CAMERA.

In addition to the optical systems, there are also numerous electronic parameters to be measured and calibrated in a CCD camera. While the characterisation of the lens pertains to the geometric fidelity of the remotely sensed imagery, the sensor and surrounding electronics determines the radiometric accuracy of the data. Calibration is necessary to establish the relationship between the radiance of the scene and of output of the camera. A more feasible measurement is the relationship between the number of photons striking a CCD photosite and the corresponding digitised count produced for it.

In a traditional whiskbroom scanning imager, such as those used on the LANDSAT spacecraft, the sensors are single element photodetectors. As such, they are relatively simple to characterise in isolation, separate from the rest of the circuitry, and their input-output relationship is determined for a wide range of illumination and temperature conditions. Nevertheless, despite the careful selection of these detectors, there are often significant differences in the behaviour of the sensors serving specific spectral planes (see section 2.1.1.1), which result in substantial striping effects in the raw imagery. Although well characterised at launch to compensate for these effects, their performances tend to diverge as the detectors age, especially when fitted with photo-multiplier tubes [Curran, p. 144]. The need to counteract the drifts and errors encountered in whiskbroom scanners and preserve the usefulness of this imagery, has defined much of the traditional approach to the calibration of remote sensing imagers.

Conversely, CCD arrays are composed of many thousands of photosites, making the characterisations of the type performed on the LANDSAT sensors difficult and time consuming. In theory, it is necessary to test for illumination and temperature response on every single photosite, as well as a number of additional investigations for properties unique to CCDs (cross-talk, smearing, blooming, dark current, etc.). Fortunately, the advances in solid-state sensor technology has eliminated many of the sources of errors encountered in the older detectors, making much of the traditional measurements redundant. The manufacturing processes of most contemporary CCDs guarantee photosite-to-photosite uniformity, linearity and dark current to within 2 %. If the application is critical, CCDs that have been screened are available with radiometric tolerances to within 1 % and better. If further characterisation is required, the manufacturer can generally subject the devices to additional levels of testing, at a cost.

Furthermore, as all of the detectors in a CCD are mounted on a common silicon substrate, any drifts through temperature or aging tend to be experienced by all the photosites, preserving the relative calibration within a given image. Moreover, because all the circuitry for reading the charge packets is common, from the CCD's output amplifier through the various processing stages to the analogue-to-digital converter, each pixel in the image will be subject to the same degradations. Therefore, it is not really necessary to treat each photosite as an individual sensor requiring full characterisation; it is the performance of the whole camera which is important. Thankfully for the designer of remote sensing cameras, the CCD manufacturers now address many of the issues which previously needed to be resolved by testing.

5.5.3.1 Characterising the camera electronics.

[Slater, p.404-408] introduces some of the key parameters in calibrating and characterising a camera's radiometric performance. The first stage in ensuring the accuracy of an imaging system is to address these issues early in the camera's development, and to design systems with adequate noise, linearity and stability to minimise the need for extensive and frequent measurements. If the system is designed with sufficiently high performance, then the calibration stages will only involve assessing the maximum errors rather than trying to develop corrective transfer functions to be applied in post processing.

Inaccuracies in the camera's output come from two sources: noise from the sensor and peripheral electronics, and errors in the characterisation of the system's transfer function. To establish the camera's noise performance, it is necessary to calculate the contributions from the sensor itself and also from the surrounding electronics. The CCD will introduce noise through dark current and errors in resetting the output charge amplifier, the characteristics of which can be obtained from the manufacturer. In practice, dark current builds up quite evenly, and its noise can be treated as two distinct components: firstly, a uniform offset which effects all photosites equally, causing an artificial lightening of the scene, and secondly, the dark current non-uniformity (DCNU) which accounts for photosite-to-photosite variations in dark current. For a typical CCD, the DCNU will have a peak to peak amplitude of about 10 % of the dark current offset. As discussed in section 5.1.3.2, the dark current accumulated will depend on the operating temperature of the sensor and the duration of the integration time.

The CCD's output amplifies the current from the charge packets into a useful signal. Before each new charge packet, the gate of this amplifier is reset to a nominal voltage by a clock pulse. However, there is generally a small residual charge left on the amplifier, resulting in an equivalent error in the output signal. For a typical commercial CCD sensor running at video speeds, the DCNU and amplifier reset error both contribute about 300 to 500 electrons of noise per charge packet, or about 0.5 % of the photosite's saturation charge. While it increases the dark current, running the CCD at a slower rate conversely reduces the noise from the output amplifier by increasing the duration that the reset pulse is applied to the gate. While the designer has some control of the noise performance of the CCD by altering the clocking speeds and operating temperature, its overall performance is really defined by the device's manufacture.

There are numerous other sources of noise in the camera, most of which have already been discussed in some detail in section 5.3. Noise can be introduced via the supply rails, the video signal processing stage, the analogue-to-digital converter or cross-coupled from the digital clocks. It is the job of the camera designer to ensure that these stages do not inject unacceptable amounts of noise. The designer's target should be to keep the overall system noise amplitude to less than that produced by the CCD itself, or half of the analogue-to-digital converter's least significant bit, whichever is greater.

In practice, this is a difficult goal to reach, especially as the performance of the CCD and analogue-to-digital converters improve, and signal-to-noise ratios (SNR) of around 100 : 1 will probably be good enough for many applications. Indeed, the SNR of the LANDSAT MSS ranges from 72 : 1 to 123 : 1 depending the spectral band [Colwell, p.526], the LANDSAT TM from 102 : 1 to 250 : 1 [Slater, p.507], and the SPOT HRV instruments are about 200 : 1 [Begni].

Fortunately, the linearity of modern CCD detectors, including their output amplifier, is very good, generally better than 1 % until the device is driven into saturation. [Photometrics] and [Djorgovsky] provide very detailed discussions of the excellent radiometric performance, stability and consistency of certain scientific CCDs; the procedures described can be used to assess the radiometric quality of prospective sensors.

The performance of the rest of the circuit can be verified by injecting test signals instead of the authentic CCD output. To assess the radiometric accuracy of the instrument, it is necessary to image calibrated light sources through a diffuser. These sources are generally lamps that are well characterised to laboratory standards. Alternatively the Sun can be used for this, attenuating its light with precision neutral density filters. By making enough of these measurements, it is possible to establish the absolute radiometric calibration of the imager.

5.5.3.2 In-orbit radiometric calibration.

5.5.3.2.1 Hardware calibration systems.

Once the satellite is in orbit, there is a need to perform new calibration measurements to assess the imager's on-going aging and drifting. [Price] presents a balanced discussion of these issues. For dark current and noise measurements, it is often sufficient to run the imager with no incoming illumination by closing the optical aperture, revealing the noise amplitude and patterns. An alternative is to activate the imager during the satellite's eclipse period. However, anomalous readings can be obtained by air-glow, aurora or other atmospheric effects [Eather] and this approach is certainly not suitable for mid- or thermal-IR wavelengths where the Earth has a significant radiance. Furthermore, a single reference point is of limited use for calibration, especially when it is free of illumination and therefore does cover the imager's operational dynamic range.

In many conventional spacecraft, one or more calibration lamps are included within the instrument for the purpose of in-flight calibration [Jones et al]. In a mirror-scanned whiskbroom imager, the detectors are swept past these reference sources at the end of every scan-line. In other instrument designs, it is necessary to interrupt the imager's normal operation to point it at the lamps, either by opening a shutter or rotating a mirror. By illuminating the sensors with a uniform source of known output radiance and spectral characteristics, it is possible to check the noise and sensitivity of all the detecting elements of the instrument, updating the system's calibration.

Unfortunately, the lamps themselves are subject to drifts and aging which can make absolute calibration difficult, although still permitting relative calibration between detectors in the same spectral band. For this reason, constant targets like the Sun are also used as calibration sources. However, direct solar illumination will generally saturate the sensor, and various filters need to be positioned in front of the imager to attenuate this illumination.

These systems require power-hungry lamps or moving mechanics to enable solar calibration, making them incompatible with the capabilities of microsatellites. A similar, but more modern, solution is to use light emitting diodes (LEDs) to illuminate to CCD sensor(s). The advantage of using LEDs is that they are small and low power, allowing them to be accommodated within a CCD camera. Accordingly, they can be placed near the sensor, directly illuminating it when necessary, without disturbing the operating temperature of the sensor or needing complex moving mechanics to alter the viewing axis of the optics. Compared to filament lamps, LEDs have very stable long-term performance although their radiation-tolerance will need to be evaluated. Furthermore, they can be pulsed on and off very quickly to provide different illumination levels with minimal additional circuitry. This arrangement is used to provide in-orbit calibration of the LISS instruments on the IRS spacecraft [Pease, p324], and will probably be used increasingly in future.

5.5.3.2.2 Comparative approaches to in-orbit calibration.

If no calibration source can be accommodated in a microsatellite imaging system, the only remaining option is to compare the imagery captured with data from another source, which is calibrated [Ahern et al]. Indeed, this is a technique which is used for many remote sensing spacecraft to augment the other forms of calibration. Post-facto calibration generally involves imaging parts of the Earth that possess very uniform and predictable reflectances. Frequently used targets include ice and snow fields in Greenland and Antarctica [Begni], cloud-free regions of the north Atlantic [Fraser & Kaufman], Sun-glint off the ocean [Holben et al], and most commonly large expanses of deserts [Holben et al]. [Wirth & Peeters] address some of the issues facing the use of simultaneous satellite and aircraft measurements for data validation.

Of particular significance for calibrating remote sensing instruments is the expanse known as White Sands, around Alamogordo, New Mexico. This area is routinely used for calibrating LANDSAT [Castle et al], SPOT [Begni], NOAA and other Earth observation satellites. As such, the reflectances of the region are highly characterised from frequent ground based and aerial measurements, providing an excellent target against which to calibrate the satellite imagery. Figure 5.5.2.2 is a PoSAT-1 Narrow Angle image showing the very high reflectance of the White Sands test range. [4] The dark area to the north of White Sands (partially out of this scene) is not a lake, but a bed of black lava, known as the

---

[4] This area has been deliberately saturated during processing to ensure the other features in the image have acceptable contrast.

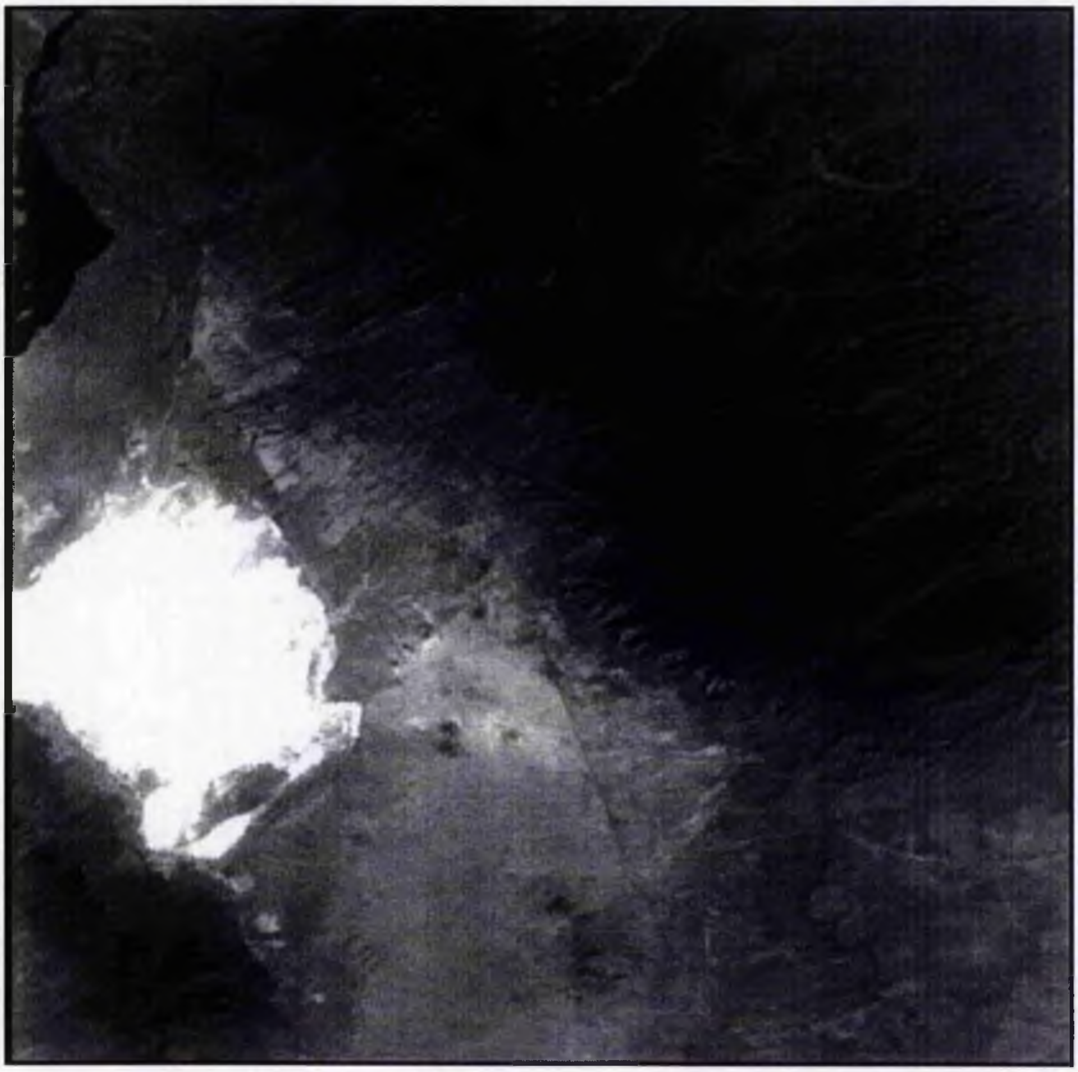

Figure 5.5.2.2 PoSAT-1 narrow angle image of White Sands, New Mexico.

Malpais ('bad lands'), which serves as a suitable dark reference. (Refer to [Sheffield, 1983 p.108] for a LANDSAT MSS image and a description of this area). The variety of soil types in this imagery will help establish the camera's transfer function in converting scene reflectance into digitised numbers.

The paper by [Holben et al] is particularly useful for the designer of a microsatellite remote sensing system because it describes the techniques used to calibrate the NOAA-11 AVHRR instrument in-orbit despite the absence of any pre-launch calibration data and no specific on-board facilities. They advocate imaging regions of the Libyan and Egyptian Sahara, which present bright and highly constant targets because of the clear skies, geological stability, minimal interference from human or animal activity, and virtually no vegetation to cause seasonal variations. With these techniques they achieve an estimated ± 3 % accuracy with respect to other AVHRR instruments in orbit, and ± 6 % absolute calibration. [Fraser & Kaufman] advocate a similar procedure for providing in-orbit calibration of the imaging instruments on the geo-stationary GOES satellites, which could be adapted for low-Earth orbits. [Castle et al] conclude that there is up to 10 % of discrepancy between the LANDSAT Thematic Mapper's pre-flight calibrations and the measurements made in orbit, and that periodic calibration campaigns are essential to maintain the radiometric accuracy of the instrument. [Royer et al] report that after suitable post-processing, the LANDSAT MSS and TM instruments are generally quoted as having absolute radiometric accuracies to within 10 % and 5% respectively.

Of course, a conventional remote sensing payload will generally use both internal (lamp) and external (ground truth) referencing techniques to provide radiometric calibration. [Sakuma et al] and [Slater et al] present papers discussing these two aspects of the same instrument. However, it must be remembered that the ASTER instrument is destined for the multi-ton EOS platform, and will experience conditions radically different from those on a microsatellite. Therefore the techniques discussed, though of interest, do not necessarily apply to a microsatellite remote sensing payload.

5.6 RELIABILITY AND REDUNDANCY.

With any spacecraft system, it is necessary address the issues of reliability and redundancy. The reliability of a camera is of importance in assuring that the mission's objectives are fulfilled, but fortunately no other systems are directly dependent on the imaging module as they would be from, say, the power system or the on-board computer.

Quality assurance and reliability analysis are crucial stages in the development of conventional spacecraft programmes. Much additional cost can be incurred by extensive specification, qualification and analysis of a satellite payload or platform without actually contributing to its success. Just how much quality assurance is commensurate with retaining cost-effectiveness within a microsatellite mission is a debate raging in the industry, with many, very different views being put forward (often defended with an almost religious fervour). Although many microsatellite missions will not be subjected to the same procedures as a traditional spacecraft, it is important to consider ways of improving the reliability of the imaging payload.

5.6.1 LIMITS OF IMAGER RELIABILITY.

It must be recognised that the natural configuration of a CCD imager is not conducive to fault tolerance within the camera. There is a long chain of electronic sub-circuits running from the clock sequencing logic, through the clock buffers, the CCD itself, the video signal processing, the analogue-to-digital conversion, the storage memory, the controller unit and the controller's interface ports. A failure in any one element of this chain is likely to cripple the entire module.

Because of this chain architecture, there is little point in trying to implement redundancy within a camera. Even if this was possible, the circuitry to switch these sub-blocks in and out of the camera chain would result in a significantly larger and more complicated design. However, this extra complexity can in fact reduce the system's overall reliability by transferring the critical failure-point from the camera electronics to the switch itself. Furthermore, introducing these additional components is likely to degrade the camera's imaging performance, due to the increased noise, cross-talk, propagation delays and clock-edge degradation experienced.

Therefore, given the natural topology of a CCD, it must be accepted that there is not much scope for implementing internal redundancy. This should only be considered if there is one particular sub-circuit which is significantly more vulnerable to failure than the rest of the system. Although this an unlikely situation for all-electronic cameras, this may be the case if active mechanics such as a shutter or a filter wheel are used.

5.6.2 COMPONENT SELECTION AND SCREENING.

Many spacecraft definitions call for electronic components to be manufactured and screened to some higher level of specification (i.e. to an established military, ESA or NASA qualification level). However, most CCD imagers are not available to any widely recognised level of screening. Nevertheless, all CCDs are expensive semiconductor products and correspondingly are manufactured, packaged, handled and screened with appropriate care. Most go through detailed in-factory testing to evaluate their imaging performance, such as sensitivity, output amplifier linearity and saturation levels, and to ensure an absence of defects in the photosite lattice. More expensive scientific devices may also be characterised for factors such as dark current non-uniformities and the linearity of each photosite.

All CCDs are mounted on a ceramic, or occasionally metal, substrate to guarantee the device's structural rigidity. The physical invariance of this substrate is vital in preserving the imaging geometry. Most CCDs are specified to operate over a temperature range of -40 to +85C°. Scientific sensors will generally be more robust than this, especially at colder temperatures because of the prevalence of active cooling. (Note that normal CCDs cannot be run at cryogenic temperatures; they need to be specially designed for this).

Thus, although the CCDs are rarely compliant with military specifications, they are subjected to extensive and representative testing at the factory. Therefore, they can be treated as having received 'superior' screening, by default. Many of the manufacturers of scientific CCDs will also have facilities for further military-compliant screening. In particular, Thomson advertise about offering not only military specification devices, but also ESA-approved space-qualification levels of screening on their CCD products. If this level of screening is absolutely necessary, then these avenues can be pursued. It must be remembered that procuring devices to space-rated levels will be extremely expensive, and contrary to the low-cost design principles intrinsic to microsatellites.

Conversely, the dedicated support chips provided by the manufacturers receive little, if any, of this screening. Japanese manufacturers generally offer these devices in dipped-epoxy (plastic) casing only, with commercial (0 to +70°C) or occasionally industrial (-40 to +85°C) temperature ratings. The European and north American manufacturers of scientific devices generally provide their components in ceramic packaging to industrial temperature specification, although dipped-epoxy packages are becoming increasingly common. Again, Thomson releases many of its support devices to full military specifications.

Therefore, if a manufacturer's chipset is being used to implement the camera, there is little point in procuring the rest of the components to a very high level of specification. If available, components qualified to mil-spec 883 will be more than adequate. However, many of the necessary components within the camera will not be available with any form of screening, especially if they are in modern surface-mount packages. Care should be taken to ensure that all the components are at least rated to industrial temperature specifications, as the spacecraft's operational regime may well require the cameras to run at temperatures below freezing.

Thus, it is difficult to make electronic cameras that comply with the established quality-assurance and / or procurement standards normally associated with space missions. It is therefore necessary to qualify the imaging system by extensive burn-in, temperature cycling and in-orbit demonstration of the integrated unit, rather than by procuring the individual elements to specific standards. Nevertheless, the success of SSTL's imaging microsatellites provides evidence that electronic cameras can work well in space, despite being made up almost entirely of components procured to lower levels of specification.

5.6.3 MODULAR DESIGN TO INCREASE REDUNDANCY.

From the points just mentioned, it is clear that the compact CCD cameras discussed in this thesis do not conform to the conventional notion of high-reliability spacecraft systems. Overall mission reliability can therefore only be achieved through modular redundancy. It is certainly simplest to make duplicate cameras than to consider ways of improving the reliability of individual systems.

It is essential that no electrical components are shared between the various cameras, as this would negate the effects of their modularity. Each camera will need to implement the full imager chain in entirety. Any circuitry needed to synchronise the cameras (section 5.3.8), must not compromise the isolation of the modular units. Similarly, the camera and computer processing units should be modularised as far as possible to isolate faults to a single sub-module. All communications should be via high speed serial links, with alternative communications routes available to all sub-modules. Each of the image capture and data processing sub-modules must run from separate power supplies.

Fortunately, if designed properly, the electronics of individual cameras can be compact and lightweight. If the optics are too massive to be duplicated, it may be feasible to share them between the primary and redundant cameras. Indeed, the optics may be considered a low-risk item, provided they are assembled correctly and well supported mechanically. Therefore, if it is absolutely necessary to introduce a single-point-failure item into the design, it is reasonable to make the optics this critical element.

Once spare cameras are introduced, there are numerous ways these can be used to increase the mission objectives. These additional cameras can either be left off to provide cold-redundancy, or more profitably, be used to complement the main camera(s) operationally. For example, instead of just being nadir pointing, the cameras can be mounted to look off at an angle to provide either a larger coverage area (side looking) or a stereo image pair (fore and aft looking). In a multispectral imager, the redundant camera could be fitted with a colour wheel. The main spectral bands are provided by the primary fixed-colour cameras, and the redundant imager senses through a different, but complimentary, band to increase the system's multispectral capabilities. However, if one of the main cameras fails, the colour wheel is rotated so that the redundant camera now provides coverage in this band. In either of these cases, the principal missions objectives can still be fulfilled when a camera has failed, but are enhanced by the imaginative deployment of the redundant unit.

5.6.5 RADIATION EFFECTS.

Coping with the presence of ionising particles is another aspect of developing systems for space which is rarely encountered in terrestrial applications. There are two basic issues which need to be considered: short-term transient effects caused by particle strikes, and total-dose effects accumulated over a lifetime in space. [Stassinopoulos & Raymond] provides a good review of the space radiation environment, and [ESA] is considered by many to be the standard reference on the effects of ionising radiation on semiconductors and other materials. [Harris] also provides a useful discussion of these effects, although the conclusions drawn are to be viewed with the caution appropriate to any sales brochure.

This section covers the general issues of radiation effects briefly. While the causes of radiation-induced loss of performance are similar in analogue and digital circuits, their effects and the possible counter-measures are very different. The topic of protecting digital memories from single event upsets is addressed in section 6.2.2.3.1.

5.6.5.1 Transient effects of radiation in CCD sensors.

When an energetic particle strikes another material, it can displace electrons or nuclei from the atomic lattice. If the material is a semiconductor in an integrated circuit, this collision results in a small electronic current, which can momentarily upset the operation of the device. These transient, spurious electrons will combine with the charge packets collected by CCD photosites. While this does not result in disrupted operations, as would be the case with corrupted computer memory, it does provoke inaccuracies in the image recorded by the CCD. A particle strike causes a significant brightening of the effected photosites, as the electrons generated by the ionising radiation combine with the electrons from conventional photonic activity.

According to [Lomheim et al], a 17 MeV passing proton can deposit as many as 55,000 electrons in a silicon CCD, although the actual amount depends on the particle's energy and the exact sensor topology. Even more significantly, collisions with cosmic rays will invariably saturate a CCD photosite well [Lomheim et al][Oldfield], thereby generating several hundred thousand electrons although the exact amount cannot be quantified. These estimates of the effects of protons events are compatible with the tests reported by [Ashton & Hopkinson]. Given the fairly large cross section of a CCD sensor (at least in atomic terms), but despite the short integration times, peak occurrences of particle strikes in the standard 800 km orbit is about 60 protons in the South Atlantic Anomaly (3000 particles / cm^2 / sec at 50 to 100 MeV [Janesick et al]) and around 0.3 cosmic rays over the poles (2 to 4 particles / cm^2 / sec [Oldfield]) per image. Furthermore, the device will also be subject to less energetic, but substantially more abundant, particles, causing a general, random, low-amplitude effect on the image.

Regardless of the exact amount of charge generated by a passing nuclear particle, it is clear that these spurious increases in the charge recorded by the CCD produce (sometimes dramatic) radiometric errors in the imagery. If a cosmic ray's direction of travel is perpendicular to the CCD's surface, this charge will be released in a single photosite, causing it to saturate. Grazing collisions will result in charge trails of smaller magnitude but effecting several photosites. Whereas the gross error from a cosmic ray should be readily apparent, the subtle effects of the less energetic particles will be more difficult to detect, and result in a degradation of the imager's signal-to-noise performance. Evidence of such 'erroneous' pixels is fairly common in the KITSAT-1 imagery, which is subject to a ten-times harsher radiation environment than UoSAT-5 or PoSAT-1 due to its higher orbit.

The effects of these particles is graphically demonstrated by figures 5.6.5.1.2a and b showing two sets of (heavily processed) star images captured by the PoSAT-1 Star Imaging System (SIS). Figures 5.6.5.1.2a (STAR002A) is a typical set; the bright objects are (currently unidentified) stars or planets. The faint points are mostly thermally generated noise (dark current non-uniformity) but undoubtedly contain some faint stars as well.

The star camera captures four images in close succession, separated by 500 milliseconds. This serves two purposes: firstly, to identify 'false stars' generated by energetic particle collisions; true stars will be present in all four images, but particle hits will only be present in one. A few false star candidates can be found: e.g. top right image, bottom left corner, immediately to the left of the bright star. Secondly, by analysing the displacement of the stars across the images, the satellite's attitude drift can be deduced, although this is not currently implemented, awaiting the development of the necessary software. The integration time is 150 milliseconds per image.

Figure 5.6.5.1.2b (STAR002C) is a similar star image set captured in the heart of the South Atlantic Anomaly. These two image sets have been processed in a similar fashion, and the star scenes in figure 5.6.5.1.2b are clearly subject to a vast increase in the amount of particle hits on the CCD sensor. Indeed, there are so many radiation-induced objects, including a number of 'radiation trails', that it is virtually impossible to identify the genuine stars. Comparing these images, it is not so surprising that the Hubble Space Telescope, which relies on multiple star trackers for its pointing, often loses attitude lock in the SAA [Harris]. [5]

Although these radiation events will also be present in data from the Earth-facing cameras, the vastly stronger signals and the shorter integration times reduces their impact on the image quality. Nevertheless, they are doubtlessly a source of appreciable radiometric error, especially when imaging targets in Latin America. Unfortunately, there is very little that can be done to prevent errors caused by these single particle events. The

[5] The star imagery presented has been subjected to heavy non-linear stretching to accentuate the presence of the faint stars and noise. The majority of the objects visible represent only 3 % of a saturation signal (the noise floor is around 1 % of saturation). Conversely the large object in the centre of figure 5.6.5.1.2a is of saturation brightness (i.e. about 4 orders of stellar magnitude larger) and the brighter trails in figure 5.6.5.1.2b are about 30 % of the sensor's full dynamic range. Finally, the images are displayed in negative to improve their interpretability: bright stars and radiation events now appear dark against a bright background.

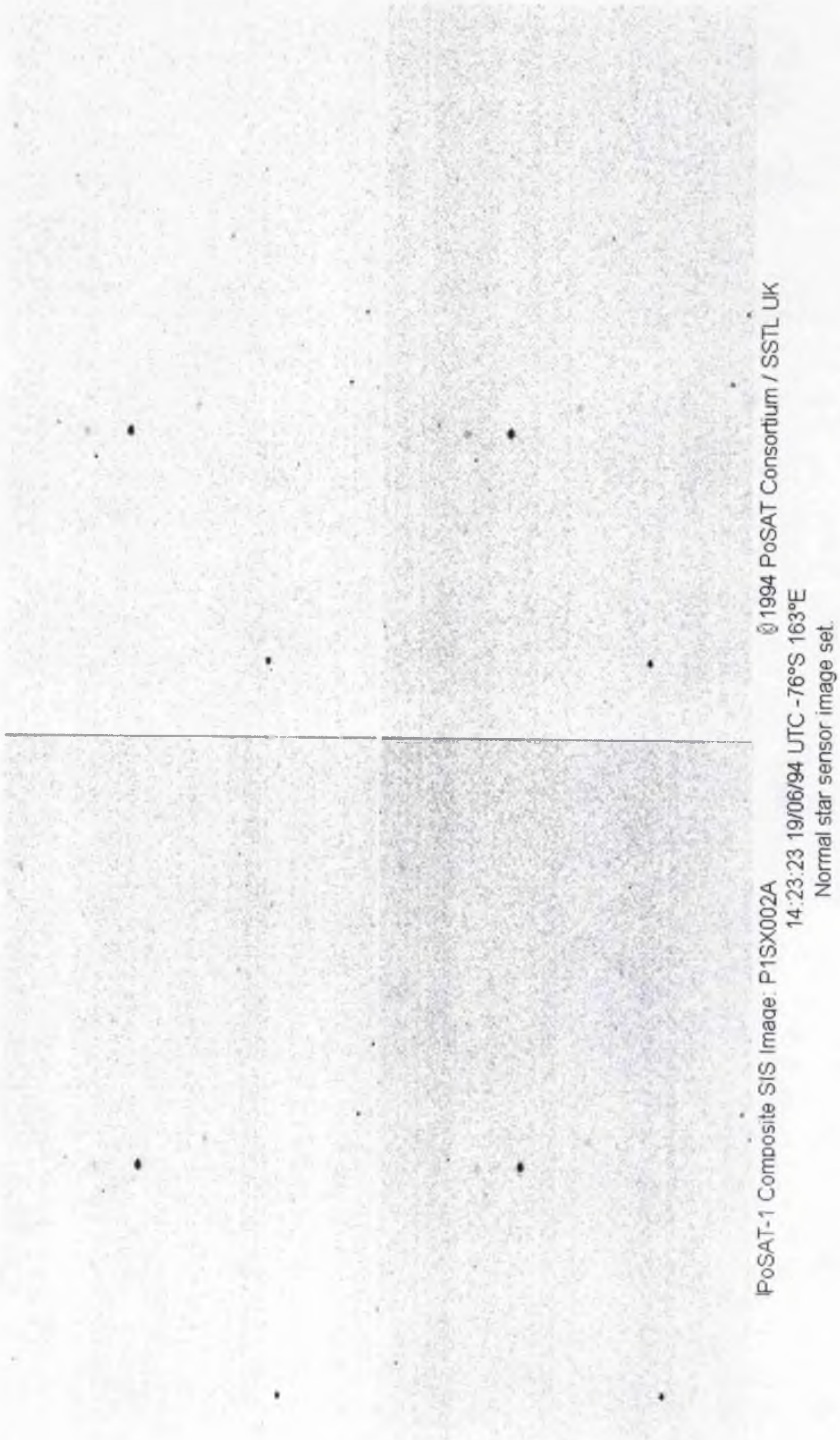

Figure 5.6.5.1.2a

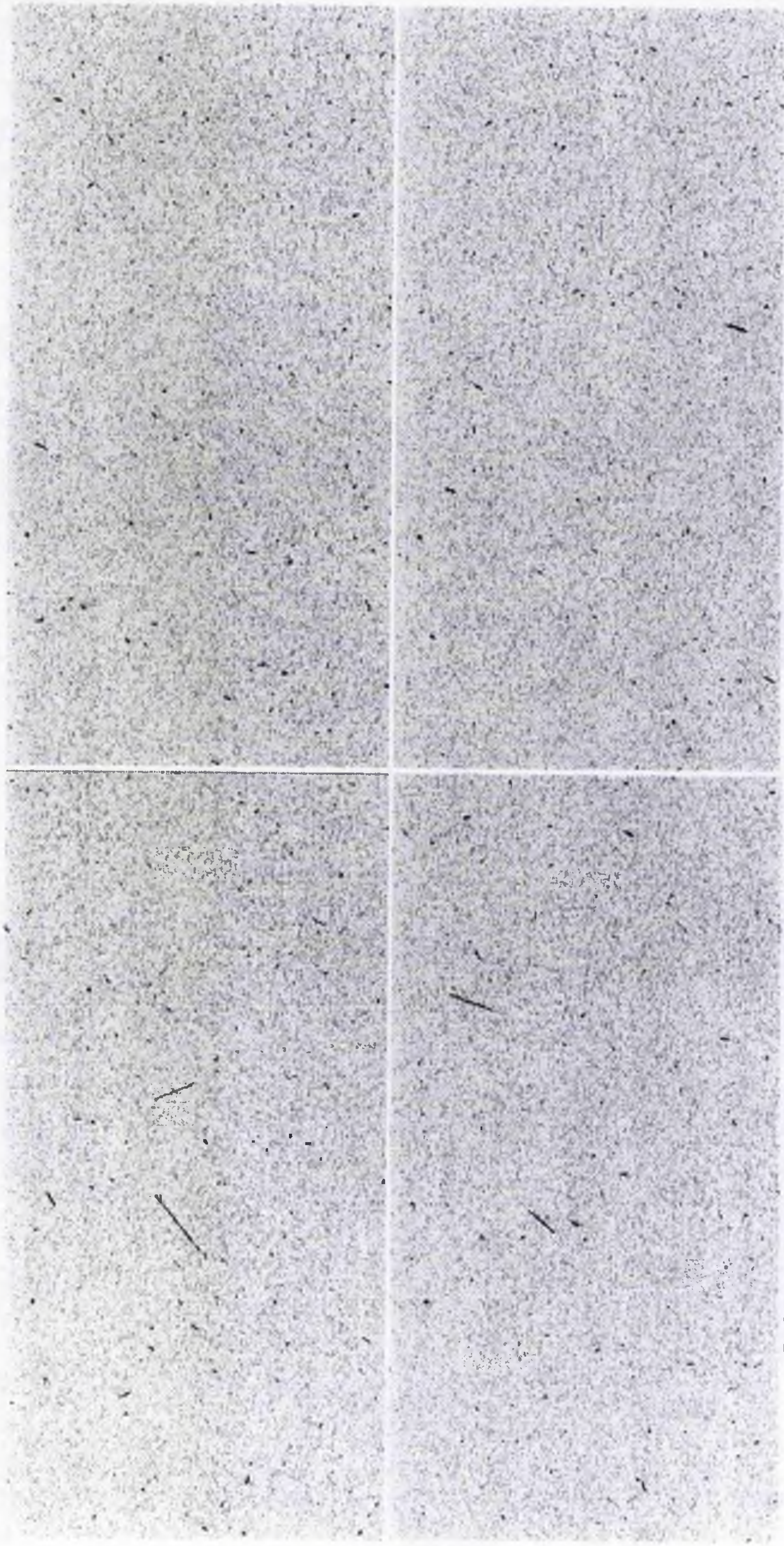

PoSAT-1 Composite SIS Image: P1SX002C ©1994 PoSAT Consortium / SSTL UK
03:00:22 07/07/94 UTC - 32°S 60°W
Energetic particles in the South Atlantic Anomaly striking the CCD sensor.

Figure 5.6.5.1.2b

only real measure that can be taken is to reduce the integration time, thereby reducing the amount of time the image is left exposed to this source of degradation. As just mentioned, the dramatic errors caused by cosmic rays will be apparent, and can be ignored or removed during post processing. The occurrence of these events should be sufficiently infrequent to not cause undue disruption to the users of the imagery, provided they are aware of the possibility of these anomalies.

Given the sensor is surrounded by an appreciable amount of screening from its box and the spacecraft structure (presumably made of aluminium) and the lens, it will be shielded from the majority of low energy particles. Thicker shielding can provide more protection from electrons, but can also result in a increase of secondary radiation effects (known as bremstrahlung). However, shielding is ineffective against the more energetic, but less common, particles which will pass straight through this material to deposit significant charge in the sensor.

5.6.5.2 Long term radiation damage to CCD sensors.

Prolonged exposure to ionising radiation results in long-term damage to semiconductor materials. The various damage and recovery mechanisms in irradiated semiconductors is extremely complex, and the subject of on-going research. Nevertheless, there are some important items worth mentioning.

As discussed in the previous section, a nuclear particle striking a CCD will generate numerous electron - hole pairs in the semiconductor lattice. The principle mechanism for radiation damage appears [Janesick et al] to be the congregation of these liberated carriers around energetically favourable locations, generally near impurities in the silicon structure. This has a number of consequences, the most disruptive of which is the loss of charge transfer efficiency (CTE) [Janesick et al][Holland et al]. (In a perfect CCD, there will be no change in the charge packets as they are moved from photosite to photosite. The CTE measures the number of electrons actually lost per transfer in a real-world CCD). [Janesick et al] reported that tests on CCD sensors from Ford Aerospace have revealed a nominal CTE of 0.9999937 (a very good performance). After 5 kilorads and 20 kilorads of irradiation, this CTE figure had dropped to 0.99991 and 0.9995 respectively. Although this may still sound like an acceptable performance, remember that if there are 2000 transfers along the CCD's vertical and horizontal register, this will result in a cumulative efficiency of 0.367 after 20 kilorads (from 0.987 before radiation). Another effect of the accumulation of carriers around lattice imperfections is the increase of the CCDs dark current, and more particularly the creation of dark current spikes (increasing the dark current non-uniformity - DCNU) [ESA][Hopkinson & Chlebek]. However, the scope for radiation damage is constrained to the CCD photosites and shift registers; according to [Holland at al], the output FET amplifiers are virtually unaffected.

The susceptibility of CCDs appears to be highly dependent on the manufacturing strategy used for the device. On the whole, sensors employing more complex doping structures (so that only one or two phases are required to drive the CCD shift registers) are more sensitive to radiation damage [Janesick et al]. The Texas Instruments and Ford Aerospace CCDs evaluated by [Janesick et al] and the Eastman-Kodak device tested by [Lomheim et al] have total dose survivability of 20 to 30 kilorads, whereas [Ashton & Hopkinson] report that EEV CCDs are tolerant to radiation doses of up to 10 kilorads and functional up to 100 kilorads. (Most of EEV's devices use a three-phase clocking system, and are manufactured in very similar fashions, increasing the photosite density by photographic reproduction of the wafer masks). However, it is very difficult to estimate the effects of radiation on a specific CCD, and testing is required to verify a particular device's tolerance. [Janesick et al] describe how some of the Hubble Space Telescope's CCD sensors have failed to meet expectations because of assumed performance based on testing similar, but obviously slightly different, CCDs.

Unlike the radiation damage in many other semiconductor materials, [Holland at al] report that the degradations suffered by CCDs occur regardless of whether the device is powered or not. To minimise the accumulated deterioration, they recommend that the CCD is continually powered with the electrodes biased in inverted mode (i.e. several volts negative with respect to the substrate). This technique is also used to suppress dark current by repelling electrons away from the depletion region at the surface of the CCD and back into the substrate where they can be absorbed by the prevailing surplus of holes.

Interestingly, temperature also plays a role in the sensor's loss of performance through ionising radiation [Janesick et al][Holland at al]. At low temperatures (below -100°C), the electrons generated by particle strikes have reduced mobility and tend to recombine locally with their original holes. Conversely, at temperatures above +50°C, the holes are sufficiently energetic to be swept away with the 'photonic' charge, leaving few permanent traces of the nuclear event. Therefore, [Holland et al] recommend that the CCD be actively cooled to around -100°C to reduce the rate of CTE degradation, but that it should also occasionally be heated to approximately 120°C (for 100 hours) to help the annealing process. Unfortunately, subjecting the sensor to these temperature extremes is not likely to be easy within the confines of a satellite instrument, especially when flown on a microsatellite.

Given that a CCD for a remote sensing mission will be chosen for its operational imaging properties, it is unlikely that the device's radiation performance will be a major factor in the selection process. Therefore techniques like inverse-biasing, active cooling and annealing can help the CCD survive longer than otherwise possible. Similarly, [Holland at al] suggest closing the imager aperture with a mechanical shutter in the South Atlantic Anomaly to shield the CCD from the peak radiation fluxes experienced in this region, although this will only be effective if the sensor is directly exposed to space. (Most sensors used in Earth observation will be shielded by at least one layer of optical material).

On the whole, the long term radiation effects on integrated circuits are principally studied for the benefit of satellites in geo-stationary or highly elliptic orbits, which suffer much fiercer radiation environments than spacecraft in low-Earth orbit. These high altitude orbits are subject to very harsh radiation conditions, up to 10 kilorads per year or higher Conversely, satellites in 800 km, polar orbits are subjected to a much lighter annual dose, with electronics inside the spacecraft structure receiving some 300 rads per annum [Dyer et al]. Even devices with total dose limits as poor as 3 kilorads should survive for the duration of a five year mission under these regimes, although it would be unwise to use a device this 'soft' unless absolutely unavoidable. Therefore, provided moderate care is taken in avoiding components which are known to have poor radiation tolerance, there are few special precautions or restrictions in employing a range of semiconductor technologies (including CCDs) for remote sensing spacecraft in low-Earth orbit.

If the imaging system will be subjected to very high radiation doses, then alternative sensor technologies to CCDs will need to be employed. [Carta] describes that charge-injection devices (CIDs - see section 5.1.2.4) are substantially harder to radiation than CCDs, reporting continuing functionality at doses up to 14 Megarads. These sensors are routinely used in the refurbishment of nuclear reactors, where the radiation fluxes can be as high as 100 kilorads per hour. Apparently, this resilience also allows CIDs to deliver better image quality than CCDs under high radiation rates. [Carta] states that CID cameras exposed to 450 kilorads per hour produced signal-to-noise ratios a factor of 32 better than equivalent CCD cameras exposed to 'only' 20 kilorads per hour. Nevertheless, this radiation hardness is unlikely to be of much benefit in the conventional low-Earth orbit used for remote sensing. In the context of imaging in space, the author imagines that such radiation-hardness would only be of use in the hostile environments near the Sun and

Jupiter, or possibly in highly elliptic orbits which force the satellite to spend significant amounts of time in the radiation belts.

5.6.5.3 Radiation damage to lens glass.

Radiation damage can also perturb the optical properties of the glass in the imaging system's lens. The effect of large doses of ionising radiation is a gradual darkening of the glass, reducing the lens's transmissivity.

However, as one would expect when comparing lumps of glass to sophisticated integrated circuits, the optical materials in a lens are far less sensitive to radiation than electronics. [ESA] provides a good account of the mechanism of radiation damage in optical materials, which are highly dependent on the wavelength of operation. An experimental ten-element lens system was irradiated rapidly with a dose of 100 kilorads. The combined system suffered 20 % transmission losses at 0.8 μm (near-IR), 50 % at 0.6 μm (red) and 90 % at 0.4 μm (blue), giving the lens a pronounced red or brown colour-bias. However, the lens recovered 50 % of the transmissivity lost at all wavelengths after a few months of annealing. [ESA] also states that optical coatings are too thin to present serious opportunities for radiation losses in the visible region.

Despite these dramatic effects, the optical system will be far more resilient to radiation damage than virtually all electronics, including radiation-hardened silicon-on-sapphire. Even though the front surface of the lens is subjected to a harsher radiation flux of low-energy electrons because it is not screened, the electronics will still be the limiting components; [Dyer et al] estimates that devices on the exterior of a spacecraft in 800 km orbit will receive about 15 kilorad per annum, as opposed to the 0.3 kilorad for electronics screened by two millimetres of aluminium.

Fortunately, the effects of radiation on the optics will not be problematic for missions in low-Earth orbits. If the satellite is intended for a higher orbit, where radiation issues are of greater concern, the crown glass components in the lens will need to be replaced with more resilient materials, particularly for the front-end elements which will experience the greatest accumulated doses. Materials like pure sapphire (surely very expensive) and synthetic fused silica are extremely insensitive to radiation-induced losses.

5.7 CONCLUSIONS REGARDING IMAGING SYSTEMS FOR SMALL SATELLITES AND MICROSATELLITES.

5.7.1 Choice of sensor architecture.

Having opted for the CCD camera as the most suitable type of imager for deployment on microsatellites, it is important to select a sensor architecture compatible with providing image quality. The principal source of image degradation is blur caused by the satellite's motion over the scene, and the sensor must be able to implement shuttering to grab short snap-shots in order to minimise the effect of this blur. As the camera's spatial resolution improves, the sensitivity to this blur increases and alternative measures need to be taken to combat this.

Because full-frame sensors rely on an external mechanical shutter to isolate them from incoming light, they are unsuitable for use on microsatellites until appropriate systems have been demonstrated. Conversely, it is possible to use CCDs that implement internal electronic shuttering, employing either the frame-transfer or interline-transfer architecture. For low and medium resolution applications (coarser than 100 metres / pixel), frame transfer devices offer better imaging performance. However, at higher resolutions, the short integration times needed to minimise blur cause smearing with frame transfer devices. When very short integration times are a necessity, inter-line transfer devices must be used instead, despite a slight degradation of the CCD's other imaging properties.

In all cases, but particularly for high resolution imaging, the CCD should capture the whole image in a single sweep, and not use the interlaced format common in sensors producing TV compatible signals.

5.7.2 Camera architecture.

There are limited variations in the basic structure of a CCD camera. In addition to the sensor itself, all cameras require sequencing logic to drive the various control strobes and clocks, current buffering to isolate this logic from the capacitance of the CCD, video signal processing and power conditioning. While it is possible to develop these circuits from discrete components, it is often more convenient to use dedicated support chips provided by the manufacturers. Discrete designs are generally less attractive in terms of volume, mass, power consumption, reliability and development time, and should only be attempted by experienced designers in order to fulfil specific requirements (very low-noise operation, very long integration times, non-standard read-out formats, etc.).

Conversely, the manufacturers' chipsets relieve the camera designer of having to implement these circuits and generally offer most of the functions required for the remote sensing camera. It is logical to employ these components wherever possible, and careful consideration should be given the availability of support chips to implement these functional blocks before selecting a specific CCD sensor. Using chips and circuits developed by the manufacturer will give the camera designer an appreciable head-start in producing a working camera.

Conversely, ready-made camera units are unlikely to satisfy the design criteria of a remote sensing camera, particularly in terms operational modes, unsuitable dimensions and volume envelope (although the overall volume will be small) and the presence of unsuitable components and materials. Therefore, the design of the camera should be based on a manufacturer's standard circuit, but adapted to meet the specific needs of the remote sensing application and the environmental constraints of the microsatellite.

To capture still images from a CCD camera, additional stages are required including video speed analogue-to-digital conversion, a frame-store memory to buffer the digitised imagery and (in most instances) a microprocessor to control the camera's operations and to interface to the other spacecraft systems. These circuits are rarely provided by the manufacturer, and therefore need to be implemented by the system designer. Although the circuit-level design of these digital systems is unlikely to present as many difficulties as the analogue parts of the camera, there are many more system-level factors to be considered.

5.7.3 Choice of optics.

Unlike the camera's electronics, there are many off-the-shelf optical designs that are suitable for use with CCD image sensors on microsatellites. Once the sensor and the system's field-of-view, spatial resolution and spectral sensitivity have been defined, the optical focal length and aperture will be known and various lenses and filters can be evaluated to ensure they meet the mission requirements (volume, mass, vacuum-rated materials, distortion, etc.). It must be remembered that in most applications, the optics will be significantly larger and heavier than the camera electronics.

If there is a very special requirement, generally for applications demanding UV or thermal-IR sensitivity, it may be necessary to consider a custom lens design. In general, these cases should be referred to an external consultant, unless the camera designer, who is presumably an electronic engineer, has the relevant skills in optical design.

5.7.4 Calibrating the imaging instrument.

Although not a primary concern for the cameras developed during this research programme, future microsatellite remote sensing systems will generally require greater levels of calibration. Optical performance such as focusing and geometric distortion will need to be characterised prior to launch. Conversely, given the complexity of calibrating to establish radiometric accuracy (principally determined by the camera's electronics), it is most appropriate to perform these tests in orbit. Given the success of these approaches, there is an argument for dispensing with lengthy pre-launch calibrations and relying entirely on post-launch measurements, which are cost-effective and offer more conclusive results.

Given the unfeasibility of carrying reference lamps on microsatellites, calibration information will need to be obtained from LED arrays, and more importantly, by comparing this imagery to other data sources. Collaboration with an establishment (CNES, NASA, EOSAT) proficient in this form of image analysis is recommended to ensure that the process is executed without error. Ideally, the calibration of the microsatellite payload would be synchronised to a similar campaign for other spacecraft, maximising the accuracy of the survey.

5.8 REFERENCES

Ahern F.J. et al: Radiometric correction of visible and infra-red remote sensing data at the Canada Centre of Remote Sensing; Int. J. Remote Sensing, Vol. 8 No. 9, p1349-1376, 1987.

Ashton J.E.U & Hopkinson G.R: High performance star trackers using direct contact peltier cooled CCDs; obtained directly from EEV Ltd, Waterhouse Lane, Chelmsford, Essex CM1 2QU.

Begni G: SPOT image quality - Twenty months of experience; Int. J. Remote Sensing, Vol.9 No. 2, p1409-1414, 1988.

Beynon J.D.E. & Lamb D.R: Charge-coupled devices and their applications; McGraw-Hill 1980; ISBN 0-07-084522-0.

Burt D.J: MTF calculations for CCD image sensors; CCD Technical Note 19, EEV Ltd, Waterhouse Lane, Chelmsford, Essex CM1 2QU.

Carta R.A: Camera helps refurbish nuclear reactor; Photonics Spectra, November 1994.

Castle K.R. et al: In-flight absolute radiometric calibration of the Thematic Mapper; IEEE Trans. on Geoscience and Remote Sensing, Vol.22 No.3, p.251 - 255, May 1984.

Colwell R.N: Manual of Remote Sensing Second Edition; American Society of Photogammetry, The Sheridan Press 1983, ISBN 0-937294-41-1.

Curran P.J: Principles of Remote Sensing; Longman 1985; ISBN 0-582- 30097-5.

Djorgovsky S: CCDs - their cause and cure; Proc of the Workshop on Improvements to Photometry, NASA Ames Research Centre, Nov 1984, p.152-176; NASA Science & Technical Abstract Report ref N85-17905.

Dyer C.S. et al: The low-Earth orbit radiation environment and its evolution from measurements using the CREAM and CREDO experiments; IEEE Trans. on Nuclear Science, Vol.40 No.6, p.1471 - 1478, Dec 1993

Eather R.H: DMSP calibration; J. of Geophysical Research, Vol.84 No.A8, p.4134-4144, Aug 1979.

EEV Ltd: CCD Imaging III; EEV Ltd, Waterhouse Lane, Chelmsford, Essex CM1 2QU.

El-Hakim S.F, Burner A.W. & Real R.R: Video technology and real-time photogammetry; p.279 - 304 of [Karara].

EG&G Reticon: Solid State Camera Products Data Book 1993/94; EG&G Reticon, 345 Potrero Avenue, Sunnyvale, CA 94086-4197.

EOSAT Corp: A process of radiometry; EOSAT Notes, Vol.9 No.2, p.10, Summer 1994.

ESA: The radiation design handbook; European Space Agency; Publication No. PSS-01-609 Draft Revision 1; ISSN 0379-4059, Jan 1987.

Forshaw M.R.B et al: Spatial resolution of remotely sensed imagery - a review paper; Int. J. Remote Sensing, Vol.4 No.3, p.497-520, Mar 1983.

Fraser R.S. & Kaufman Y.J: Calibration of satellite sensors after launch; Applied Optics, Vol.25, p1177-1185, 1986.

Fryer J.G: Camera calibration in non-topographic photogammetry; p.59 - 69 of [Karara].

Harris: Integrated circuits for the space environment; Space Product News, Special edition, Military & Aerospace Division, Harris Semiconductor 1993.

Hobson G.S: Charge-transfer devices; Edward Arnold 1978; ISBN 0-7131-3396-1.

Hofmeister R.A: Catching the action with progressive-scan CCDs; Photonics Spectra, July 1995.

Holben B.N, Kaufmann Y.J. & Kandall J.D: NOAA-11 AVHRR visible and near-IR inflight calibration; Int. J. Remote Sensing, Vol.11 No. 8, p1511-1519, 1990.

Holland A. et al: Techniques for minimising space proton damage in scientific charge-coupled devices; IEEE Trans. on Nuclear Science, Vol.38 No.6, p.1663 - 1670, Dec 1991.

Hopkinson G.R. & Chlebek C: Proton damage effects in an EEV CCD imager; IEEE Trans. on Nuclear Science, Vol.36 No.6, p.1865 - 1871, Dec 1989.

Howes M.J. & Morgan D.V: Charge-coupled devices and systems; John Wiley & Sons, 1979; ISBN 0-471-99665-3;

Janesick J, Elliot T. & Pool F: Radiation damage in scientific charge-coupled devices; IEEE Trans. on Nuclear Science, Vol.36 No.1, p.572 - 578, Feb 1989.

Janesick J. & Elliot T: History and advancement of large area array scientific CCD imagers; Astronomical Society of Pacific Conference Series, Tucson Az, USA, 1991.

Jones G.D, Hilleary D.T. & Fridovich B: A diffuse light source for calibrating meteorological satellite television cameras; Applied Optics, Vol.4 No.3, p.307-309, March 1965.

Karara H.M: Non-topographic photogammetry; American Society for Photogammetry and Remote Sensing, 1989, ISBN 0-944426-10-7.

Kodak: Telephone enquiry to professional technical support, quoting the diffuse RMS granularity at a density of unity of Kodak T-MAX ISO100 film to be 8 and T-MAX ISO100 to be 10 when measured with a standard 48 μm microdensitometer; 27 July 1995.

Lake D: Imaging sensors - why do they cost what they cost?; Advanced Imaging, June 1995; ISSN 1042-0711.

Lomheim T.S. et al: Imaging charge coupled device (CCD) transient response to 17 and 50 MeV proton and heavy ion irradiation; IEEE Trans. on Nuclear Science, Vol.37 No.6, p.1876 - 1885, Dec 1990.

McGlone J.C: Analytic data-reduction schemes in non-topographic photogammetry; p.37 - 57 of [Karara].

Oldfield M: Personal communication, 5 Sept 1995.

Owens J.D: Geometric corrections of UoSAT-5 CCD images; M.Sc. dissertation; University of Surrey, 1992.

Photometrics: New generation imager system; Photometrics Inc, Tucson Az, NASA Science & Technical Abstract Report ref N88-18398.

Pease C.B: Satellite imaging instruments - principles, technologies and operational systems; Ellis Horwood, 1990, ISBN 0-13-638487-0.

Price J.C: Radiometric calibration of satellite sensors in the visible and near-IR: history and outlook; Remote Sensing of the Environment, Vol. 22, p3-9, 1987.

Roy T, Watts S.J. & Wight D: Radiation damage effects on imaging charge coupled devices; Nuclear Instrumentation Methods in Physical Research, A275 p.545 - 557, 1989.

Royer A. et al: Radiometric comparison of the LANDSAT-5 TM and MSS sensors; Int. J. Remote Sensing, Vol.9 No.2, p.187-236, 1988.

Rycroft M: The Cambridge Encyclopedia of Space; Cambridge University Press, 1990; ISBN 0-521-36426-4.

Sakuma F, Ono A. Arai K: Radiometric calibration techniques for ASTER; Proc. of the SPIE Conference on Sensor Systems for Mission to Planet Earth Platforms, SPIE Vol.2317, Rome, Sept 1994.

Sheffield C: Man on Earth; Sidgwick & Jackson, 1983; ISBN 0-283-98956-4.

Slama C.C: Manual of Photogammetry Fourth Edition; American Society of Photogammetry, 1980, ISBN 0-937294-01-2.

Slater P.N: Remote Sensing - Optics and Optical Systems; Addison-Wesley 1980; ISBN 0-201-07250-5.

Slater P.N. et al: The in-flight radiometric calibration of ASTER by reference to well-characterised scenes; Proc. of the SPIE Conference on Sensor Systems for Mission to Planet Earth Platforms, SPIE Vol.2317, Rome, Sept 1994.

Stassinopoulos E.G. & Raymond J.P: The space radiation environment for electronics; Proc. of IEEE, Vol.76 No.11, p.1423 - 1442, Nov 1988.

Ward J.W: Personal communication, 23 Aug 1995.

Wester-Ebinghaus W: Trends in non-topographic photogammetry systems; p.377 - 387 of [Karara].

Wirth J. & Peeters M: AVCSR - an airborne radiometer as a tool for satellite data validation; Proc of IGARSS Symposium, Edinburgh, Scotland, 13-16 Sept. 1988; Ref. ESA SP-284.

CHAPTER VI

DATA HANDLING FOR THE IMAGING SYSTEM.

Having addressed the issues facing the implementation of the sensing units for microsatellite remote imaging in chapter 5, chapter 6 looks at the computer systems necessary for manipulation and transmitting the data collected.

6. DATA HANDLING FOR THE IMAGING SYSTEM.

As discussed in sections 3.4, 5.3.6 and 5.3.7 it is probably necessary, or at any rate simpler, to embed microprocessor control within the imaging system's interface in order to comply with the microsatellite's on-board data handling (OBDH) bus protocols. This represents another overhead in the design of a microsatellite camera not faced by a conventional remote sensing system. Fortunately modern microcontrollers are easy to use, and will offer a huge increase in the flexibility of operating the camera. Once the decision to include a processor in the camera circuit is made, there are numerous extra options available for implementing diverse hardware functions and software control features.

There are two groups of tasks to be fulfilled by the processing elements of the imaging system. Firstly, the computing unit must exercise control of the camera and manage all aspects of the image capture process. Associated with this are a number of housekeeping tasks and, of course, interfacing with the spacecraft's OBDH network(s) to receive commands and relay the digitised image data to the on-board computer (OBC) to be queued for the downlink. The second aspect of data handling is a range of autonomous image analysis, processing and compression tasks to improve the performance and productivity of the imaging system.

The need for this processing support for microsatellite imaging systems was recognised early in this programme, and considerable attention has been paid to developing the necessary data handling infrastructure. Although there are many possible options for implementing the processing elements of an imaging system, a two-tier approach has been adopted for the SSTL imaging systems, reflecting the two broad classes of processing jobs to be executed. A microcontroller is used to interface each camera onto the spacecraft's buses, to operate the image capture routines and to distribute the imagery to other modules on the spacecraft. Conversely a high performance transputer unit is employed for the image processing tasks; the transputers also relieves the OBC of a number of scheduling tasks, although this is not strictly necessary. This solution of dual-processing was first implemented on KITSAT-1, and retained and enhanced for subsequent generations of the camera (PoSAT-1 and FASat-Alfa).

By segmenting the processing tasks, it is possible to design the individual computers optimised for their specialised role. The hierarchical pyramid of the on-board processing of SSTL's microsatellites is shown in figure 6. This contrasts with the centralised approach used for most spacecraft, where the main OBC must discharge all processing tasks. Perhaps counter-intuitively, the modularised approach offers greater flexibility and ease of upgrading than the centralised option, largely due to the self-contained nature of the software, which reduces the complexity of software maintenance.

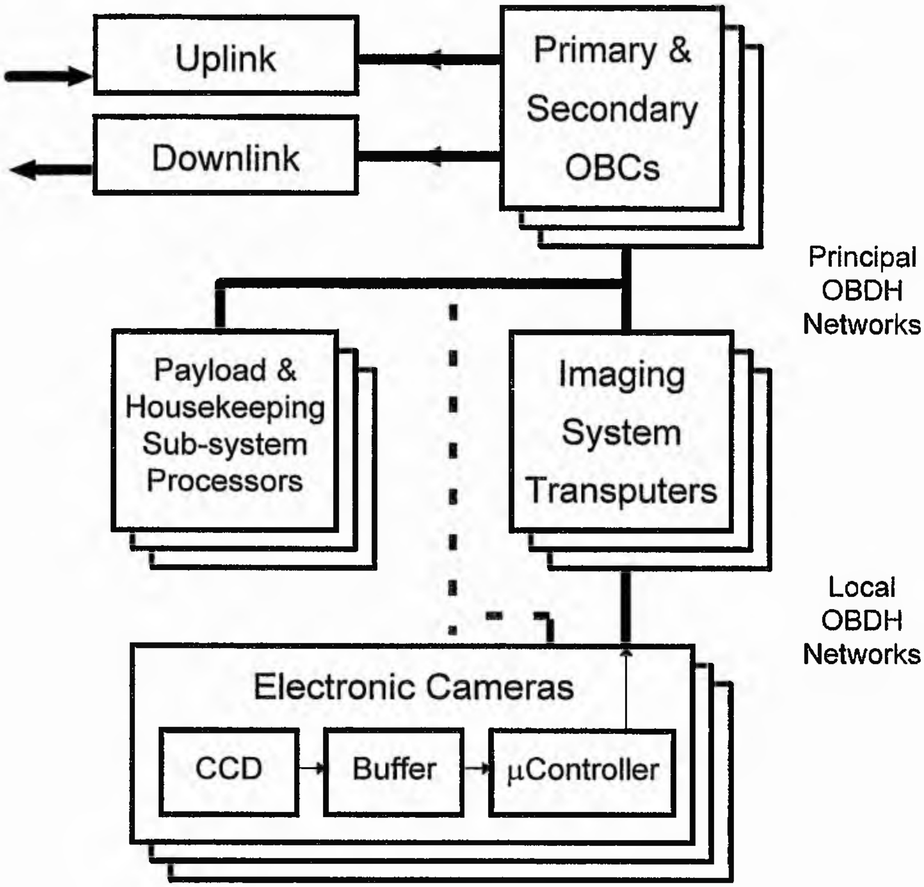

Figure 6 OBDH structure of SSTL imaging systems.

In the two-tier design, the transputer module serves as the principal source of intelligence for the imaging systems. These transputers implement all of the system scheduling, decision making and other high level tasks within the imaging systems. In particular, they collect the raw imagery from the camera(s) and perform various image processing and compression tasks before relaying the data to the OBC for transmission to the ground. The transputer module is the principal point of contact onto the main OBDH network, and hence the primary OBC, and accommodates all of the necessary communications protocols without restricting its performance.

Conversely, a simple microcontroller is used to interact directly with the camera and buffer memory. The processing load for this controller is low, but it must have all of the hardware attributes necessary to operate the camera without needing vast amounts of additional glue logic. In this design, the microcontroller responds in a set fashion to implicit instructions from the transputers, or alternatively from the OBC, leaving all decision making to the higher-level processors. In this respect, the microcontroller behaves more like programmable hardware than as an intelligent microprocessor although, as its firmware evolves over the missions, greater demands are being made of the microcontroller.

As will be discussed in this chapter, implementing the circuitry to bridge the inflexible hardware of the camera onto the OBDH networks represents the largest systems-level challenge of a microsatellite imager's design. Conversely, once the basic specification of these computing units has been defined, the circuit-level design is relatively straight forward, calling on conventional digital techniques. Without wishing to trivialise to task of developing on-board computers for microsatellites, the circuit-level design issues are not as formidable as for the analogue systems of the camera, or indeed the overall systems design of the imaging payload. Certainly, without having to deal directly with the camera, the high performance (transputer) image processing element is a fairly standard satellite computer.

Although much effort has been spent during this programme in perfecting the camera microcontroller and transputer processing units, it is not necessary for this thesis to provide a detailed account of the hardware. Instead the general issues facing these sub-modules are addressed. Many aspects of the hardware implementation reflect the specific constraints and features of the processors used, and are therefore probably of limited use or interest to the designer of a future imaging system. Clearly, a new imager design must reflect the huge range of suitable microcontrollers and microprocessors currently available; no doubt, the components selected will be significantly more advanced than those available to the author in 1990 to 1992.

6.1 DESIGN OF THE CAMERA MICROCONTROLLER AND INTERFACE.

6.1.1 ROLE OF THE CAMERA INTERFACE.

To fulfil all of its tasks, implementation of the camera's buffer memory and interface must not only meet the requirements of image capture, but also be compatible with the subsequent image processing and analysis stages as well. There are numerous, and often contradictory, requirements which must be addressed in the design of the interface circuits, such as the need for high data throughput, low power consumption, flexible operation, fault tolerance, and ease of assembly, integration and test. Perhaps surprisingly, because it must accommodate and trade-off these various factors, the design of this interface unit represents some of the most complex issues in implementing a remote sensing camera for microsatellites. Often overlooked in favour of the more glamorous sensor circuitry, it is actually the performance of the interface unit that defines the overall communications effectiveness of the imaging system. The designer must understand and evaluate these requirements and constraints early to ensure that the systems-level design aspects are satisfactory. In contrast, once the general conceptual outline is in place, the component-level design of the buffer memory and interface is a relatively straight forward piece of digital design.

6.1.2 OPTIONS FOR IMPLEMENTING THE CAMERA INTERFACE.

Although developing the transputer and microcontroller circuits has increased the overall complexity of the cameras, it has allowed many more functions to be incorporated, and most importantly has allowed the performance of the system to grow gradually within a well-established framework. Anticipating the effect of minor circuit modifications on the execution of future applications requires considerable experience, and represents the most intangible aspect of this research programme. It was only during the development of PoSAT-1 and FASat-Alfa missions, whilst attempting to progress beyond the basics of image capture, that the author grasped the full range of consequences stemming from the design of the communications interfaces.

There are numerous solutions to implementing the interfacing and processing stages of an electronic camera. The transputers have been a feature of the SSTL imaging system since UoSAT-4. The circuitry between the transputers and the camera control registers and the dual-ported image storage memory has changed several times, and presenting them briefly gives a perspective on some of the diverse considerations facing this facet of the camera design. (See chapter 4 for complementary discussions on the hardware of the various camera systems).

6.1.2.1 UoSAT-4.

On UoSAT-4, the transputer module was not designed by the author, and it was not able to accommodate any camera-specific hardware. The only available communications path between the transputers and the camera was a serial link using Inmos's proprietary protocol, and all commands and data had to be relayed over this link.

The dedicated interface circuit servicing the link at the camera end was made entirely of discrete logic. A device called a link adaptor, similar to a conventional UART, was used to convert the serial bit stream on the link to parallel and vice versa. The camera logic had to emulate the activities of a microprocessor in order to observe the Inmos serial link protocol. Although this circuit eventually worked predictably, it was large, slow, inflexible and took a very long time to develop and debug. Although appearing simpler than embedding a computer at the start of the project, trying to make hardware logic behave like a microprocessor transpired to be a very difficult and time consuming, ultimately requiring far more effort.

6.1.2.2 UoSAT-5

On UoSAT-5, the author assumed responsibility for implementing the transputers, and they were integrated to the camera circuits. All of the camera control registers (for integration, gain, etc.) and the dual-ported image memory were located within the address space of both transputers. Arbitration logic controlled access to this memory, switching between the two processors (depending on the state of a telecommand) and the camera during image capture. This effectively implemented DMA dumping of the image data into the transputers' memory, eliminating the need for an explicit transfer stage in collecting the imagery.

Although very fast and compact, there were a number of drawbacks. Firstly, the arbitration logic was complex, causing significant propagation delays to the address and data buses, and the control strobes, with race-conditions occasionally corrupting the data read back from the dual-ported memory. To overcome this, software wait-states were inserted into the code, to ensure that the buses remained static when accessing the image memory. This could have been reworked for future missions. However, the overall speed of the transputers was sacrificed to support the camera control, reducing the ability to perform high level image processing tasks. Furthermore, the centralised approach of the image buffer memory introduced many single point failures to the imaging system. If any one of over a dozen components failed, the entire system (both transputers and the camera) would be incapacitated. Finally, the parallel interfaces (address and data buses) between the transputers and the camera, made expansion to include multiple cameras a difficult proposition.

Although the UoSAT-5 system has performed well, and the DMA approach to delivering the imagery makes this camera system the fastest of SSTL's imaging payloads, it was realised that the fully parallel approach would limit the development of the imaging capabilities on SSTL's microsatellites in the medium term.

6.1.2.3 KITSAT-1

The camera controller unit was introduced on the KITSAT-1 mission to overcome the problems of the UoSAT-5 interface, in particular to avoid the single-point failures and the restricted upgrade path. In many ways, it resembles the architecture of the UoSAT-4 interface in as much as the transputers and the camera communicate via an Inmos serial link. However, the new camera controller uses an embedded microcontroller, dispensing with the cumbersome logic of UoSAT-4.

The microcontroller does not have a particularly difficult task to fulfil, relaying commands and data between the camera and the transputers. Nevertheless, having a programmable interface has finally allowed the camera to exist as an autonomous and flexible unit. The Motorola 68HC11 microcontroller was chosen because it fulfilled all of the basic needs of the camera, principally: enough input / output lines to control the camera and enough address lines to access the image space. Under normal circumstances, the microcontroller executes ROM-based firmware, giving it a simple but adequate repertoire of functions for interacting with both transputers (load exposure parameters, capture image, transfer blocks of image data, perform health checks, etc.). Although not used under normal circumstances, the microcontroller unit is also connected to the various OBDH buses, to provide back-up communications paths or bootloading facilities if required.

By separating the various elements of the imaging system (the transputers, the cameras), the threat of single point failure has been removed, containing faults to a single sub-system. The sub-systems use serial links to communicate, again isolating hardware faults. Additional cameras can be supported by simply adding more communications channels. The various sub-modules may change and evolve independently, provided they continue to respect the communication protocols.

6.1.2.4 PoSAT-1 and FASat-Alfa.

The imaging systems on the PoSAT-1 and FASat-Alfa missions continue to use the microcontroller-based topology first explored on KITSAT-1. On these missions, efforts have been made to improve the performance of the various imaging and processing sub-modules within this same architecture. The concept of modularity was stressed particularly within the redesign for FASat-Alfa. The mechanical and electrical interfaces have been standardised allowing multiple cameras (four on FASat-Alfa) to be produced, tested and flown with minimal inconvenience. This modularity has been extended to defining coherent but upgradable interfaces between the microcontroller unit and the camera front-end, in anticipation of forthcoming major revisions to the camera circuit.

The principal drawback of using these serial links is a slower transfer of the image data to the transputer. The microcontroller hardware and firmware have been upgraded on the successive missions (KITSAT-1 to PoSAT-1 to FASat-Alfa) to overcome this. In addition to providing faster communications, the microcontroller now performs certain image analysis tasks, such as generating histogram statistics and automatic exposure assessments. Since these functions are not computationally intensive, but sometimes handle large data volumes, performing them on the microcontroller accelerates the entire image capture process. Similarly, maintaining software control provides more flexibility than implementing functions in hardware.

6.1.3 IMPLEMENTING THE CAMERA'S COMMUNICATIONS INTERFACE.

The greatest influence the interface circuit has on the imaging system's performance is its ability to transfer data away from the camera's buffer memory. The need to provide fast transfers of imagery to the spacecraft's processing units suggests the use of a parallel interface. However, on the whole, serial links are preferred for inter-module communications because of their reliability, modularity and smaller wiring requirements. (A microsatellite's wiring loom represents a considerable mass which can easily be overlooked). For these reasons, the microsatellite's on-board data handling network will generally be a well defined serial bus, the specifications of which the camera must obey. These characteristics are also advantageous when implementing communications interfaces local to the imaging systems. Unfortunately, serial interfaces are inevitably slower than similar parallel interfaces.

In addition to sending the data serially, a microsatellite's OBDH networks also tend to be slow because they are software based, requiring fairly intensive servicing from the host processors. Although important for all of the communications channels, this is a particular issue for the link between the camera microcontroller and the transputers where large volumes of data need to be transferred rapidly. In these situations, it is advantageous to implement a simple communications protocol which requires a minimum of software servicing.

Transputers are equipped with four 10 Mbps serial links integral to the processor chip. Due to the silicon implementation of these communications engines, the latency overheads incurred by the transputer when using the links are extremely good, allow the processor to sustain the full bandwidth on all four links simultaneously with good margins. As long as transputers are used within SSTL's imaging systems, it is logical to use this protocol for image transfer between the camera. (Indeed, much of the transputer's attractiveness is the presence of these links). If an alternative processor replaces the transputers in future imaging systems, a similar 'low overhead' communications engine should be selected.

Although the Inmos link is 'native' to the transputer, it must be accommodated within the camera microcontroller. The most compact way of servicing the link is to use software polling. While this allows relatively sophisticated messages to be passed between the transputer and the microcontroller, it is rather slow. On KITSAT-1, the software implementation of the link protocol could sustain a transfer rate of about 8 kBytes / s. By tightening the assembly language code used for this routine, the speed on the Inmos link on FASat-Alfa camera was improved to over 16 kBytes / s. However, this is still a long way from the performance of UoSAT-4's hardware interface which was able drive the Inmos link at its full rate of about 900 kBytes / s. Clearly, in terms of sheer speed, the hardware solution is most attractive.

To improve the transfer rates, SSTL's next generation of electronic camera will feature a communications interface designed as an amalgam of the previous implementations. Software will be used to interpret the incoming commands and to reply to most requests for status information. However, when a bulk image transfer is requested, the microcontroller will configure and then activate the hardware system to step through the whole of the image memory using the same counters as employed for image capture. This will provide the speed of DMA transfer, without requiring any additional hardware and without suffering the added complexity and power consumption of a dedicated DMA controller.

6.1.4 THE CAMERA MICROCONTROLLER.

As just discussed, the most difficult aspect facing the design of the camera controller is to ensure that it does not restrict the rapid flow of data, which can easily occur due to is low processing capabilities. Once the system topology for data handling has been addressed, the design choices for the camera microcontroller are remarkably straight forward.

The microcontroller's role is really very simple, accepting commands and instructions from the transputer, OBC or other host processor, such as the exposure and other capture parameters. It must monitor the camera hardware for smooth operation, and return digitised imagery and status messages to the transputers. Given its operational simplicity, it is convenient to treat the camera as a peripheral to the transputer module.

Under normal conditions, the OBC will only interact with the transputer, and the camera will be disabled from the principal spacecraft OBDH networks. Nevertheless, there should be a redundant data path for the imagery in the event of the transputer unit failing, or for facilitating ground testing. Although useful, it is not strictly necessary for the camera microcontroller to obey all of the OBDH network protocols provided the image data can be retrieved in some fashion.

Fortunately, the instructions to be implemented will be dictated largely by the camera hardware, so that the range of necessary commands can be fully anticipated before launch. Therefore, it is perfectly feasible to encode the microcontroller's programme code as firmware stored in ROM. Rather than endow the microcontroller with re-programmable software, changes to operations or sequencing can be more easily accommodated by modifying the routines of the host processor.

The range of microcontrollers suitable for this job is vast, the only real practical constraint being the need for (at least) 16-bit external addressing so that the image buffer memory can be accessed. Even so, this will not be sufficient to address the whole memory space, and an additional output port will be needed to provide the highest address bits, thereby accessing this memory as a series of 'pages'.

The microcontroller will require a number of programmable input and output lines (about a dozen of each) to provide all the control and status functions needed to operate the camera. Before selecting a specific device, however, a careful count of every conceivable input / output lines must be made. Inevitably, extra lines are needed at a later stage to add new features or facilities, so it is always wise to select a controller with more capacity than anticipated. Whereas the KITSAT-1 and PoSAT-1 versions of the SSTL camera used an increasing number of parallel i/o lines running between the microcontroller and the camera, the FASat-Alfa revision of the circuit implemented the majority of the camera control functions over a dedicated serial connection. This provides a convenient break-point between the two units, deliberately creating modularity in response to SSTL's future imaging needs with alternative image sensors. Requiring just four wires, this interface is adapted from Motorola's standard SPI (serial peripheral interface - very similar to the Philips I^2C bus or other 'three-wire' interfaces), to implement simple bi-directional communications.

Selecting a microcontroller that has this type of function embedded on-chip can reduce the amount of extra 'glue' circuitry. Similarly, a microcontroller which features a built-in interface to the satellite's OBDH networks will be useful in keeping the camera unit small and low power. Most microcontrollers incorporate a host of other features, such as counters, timers, communications ports and internal analogue-to-digital converters, which may be useful in supporting the camera's operation.

Overall, the selection of a microcontroller to support the Earth imaging camera is routine. The current SSTL design uses the F1 variant of the well-known Motorola 68HC11 microcontroller. It features 16-bit external addressing, enough i/o lines to support the camera, an internal SPI and an internal analogue-to-digital converter to sense various camera voltages, while the interfaces to the communications channels (CAN-bus telemetry and telecommand bus, and the Inmos high speed links to the transputers) must be accommodated externally. However, there are numerous microcontrollers now available, many of which are substantially more integrated than the Motorola HC11.

The main reason for using a microcontroller over a more powerful microprocessor is the reduced power consumption. Given that these devices will need to be powered near-continuously, waiting for an imaging event, it is essential that they remain low powered, especially if multiple cameras are featured. For example, the camera microcontroller flown on the SSTL microsatellites draws only 20 mA at +5 V. (Unfortunately, the high-speed communications interfaces are just as demanding; 20 mA for the Inmos link adaptor, and 20 mA for the pair of CAN peripherals and line drivers. At least one of these three interfaces must remain powered, in practice, to accept commands from a parent processor). In comparison, a typical microprocessor would draw between 100 and 200 mA. Furthermore, the high levels of integration of microcontrollers allow them to be packaged into smaller volumes.

As mentioned in section 5.3.1, it is most appropriate to have the microcontroller activate the power switch to the camera rather than relying on a spacecraft telecommand. This allows the controller unit greater flexibility and speed in operating the camera (i.e. iterative exposure control, or rapid successions of images). Decentralising this particular command line does not put the spacecraft at a greater risk in the event of a permanent short circuit on the camera; removing power to the controller unit will instantly kill the drive signal to the camera's power switch. Special care is required to ensure that lines from the controller unit are suitably protected against accidentally powering the camera; the problem of partially powered circuits is commonly encountered on spacecraft.

6.1.5 SUMMARY.

Hopefully these discussions have illustrated that the camera's communications and control interfaces require significant design effort to achieve the desired performance.

Above all, it is important to remember that the most effective solution for making these interfaces fast, low power and compact is not necessarily obvious. By focusing too closely on the camera's imaging performance, its data handling easily overlooked, which is nevertheless of crucial importance in determining the overall ability to deliver the requisite imagery.

Given the subtlety of some of the trade-offs, several iterations of design will probably be needed before an optimum configuration can be determined. Similarly, as the nature of SSTL's imaging programme evolves from simple technology demonstrations to the development of commercially viable remote sensing cameras, the importance of these interfaces has grown. On the UoSAT-4 and -5 missions, the sole objective was to demonstrate that using microsatellites for Earth observation was feasible, and the interface and communications sub-systems implemented were adequate. However, by FASat-Alfa, and increasingly on future missions, the imaging technology has largely been mastered and the emphasis on effective communications is greater. This change reflects the transition from technology demonstration missions towards developing operational remote sensing systems.

The best implementation of the interface will be highly dependent on the nature of the spacecraft's OBDH networks and downlink, and the camera's processing units. This reflects one of the most important systems-design issues facing SSTL spacecraft: as one part of the OBDH bus, the downlink, the software protocols or the servicing rate of the communications nodes gets upgraded, a previously satisfactory part of the system becomes the new bottleneck. Because of the constant pressure to improve the imaging system's data throughput to the ground, it is difficult to make a definitive statement on the design of the camera interfaces, which will need to evolve to keep up with expectations.

Nevertheless, there is great potential for the camera interface to become a bottleneck in terms of the image turn-around (as it is on PoSAT-1 - see section 3.4). There is some incentive in making sure that the image buffer memory is emptied as quickly as possible, perhaps to another storage device, even if the whole of the spacecraft cannot keep up with this pace. While this approach simply transfers the data bottleneck to some other system, it does have the advantage of recycling the centralised resource of the image buffer memory quickly, making it ready for further image collection.

Experimentation with a number of alternative approaches has shown that a two tier implementation of the imaging system's processing has a number of advantages. A central, high performance processing unit, in this case based on the Inmos transputer, performs most of the system's scheduling, decision making, and sophisticated image processing and compression. This processor will manage the high level operation of one or more camera units, each one fitted with a microcontroller to implement the communications protocol and co-ordinate the low-level operation and sequencing of the camera front-end.

6.2 DESIGN OF THE IMAGE PROCESSING UNIT.

6.2.1 SELECTING THE PROCESSOR.

Whereas the camera controller needs the various hardware interfaces to exert control over the camera circuitry, the main image processing element will need to be endowed with sufficient computing power to manipulate the large image files without difficulty. This immediately dictates a 32-bit microprocessor, with a 24 or 32-bit address space, to be able to cope with the megabyte arrays of image data. Similarly, arbitrary partitions in the address space, such as the 64 kByte (16-bit) pages encountered with the Intel X86 family, hamper the free manipulation of this data and should be avoided because the amount of inelegant software work-around needed to implement the software.

As with the camera controller, the ability to sustain high data rates is important. For a 32-bit processor, it is always feasible to implement fast transfers across the data bus by implementing a DMA (direct memory access) controller, although it is generally more expedient to select a device that has these features built-in. On-chip communications engines invariably minimise the circuit and timing overheads needed to support high speed transfers, as well as simplifying the designer's task. As discussed in the preceding section, fast serial interfaces are preferable to equivalent parallel communications ports. Other factors, such as the microprocessor circuit's quiescent, average and peak powers, and the compactness of its implementation are obviously also of importance on microsatellites, and need to be evaluated.

The image processing and compression tasks are inevitably computationally intensive, and the microprocessor circuit design must be sufficiently fast to execute these within the constraints of the mission objectives. This presents a dilemma: to support the vast processing requirements of real-time image processing implies a high performance processor, which inevitably consumes more power. Correspondingly, the performance of the computer will need to be balanced with the mission objectives and the intensity of the anticipated processing. If mathematically complex compression such as transform or sub-band coding is to be implemented (sections 6.3.2.4.1 and 6.3.2.4.3 respectively), a floating-point co-processor will accelerate the computer's performance. Similarly, graphics features such as block data transfers or bit-masks can sometimes be of use in speeding up the processing stages. Excessively complex processing or compression algorithms and / or inadequately specified hardware will limit the turn-around and throughput of the imaging system, thereby negating the benefits expected from this stage.

There are numerous processors available to fulfil these requirements, and there cannot possibly be a unique solution for this circuit. In most cases, a processor primarily designed for embedded digital signal processing applications will provide the best blend of built-in peripherals, ease of use, processing speed and special functions to accelerate image processing. Nevertheless, provided the basic requirements stipulated above are satisfied, any microprocessor will do, and the decision may often be based on the designer's or programmer's personal preference. Indeed, there will sometimes be a specific reason to use a particular microprocessor even though it does not appear to have all the suitable attributes; if the desire is strong enough, it is always possible to overcome these with various hardware and software. However, stubbornly sticking with a specific processor can often lead to inferior performance and a limited up-grade path.

Having short-listed a number of microprocessors, it is worthwhile reviewing the tasks and applications that the image processing unit is expected to fulfil. As the chore of software development is often more onerous than designing the hardware, it is important to give at least equal emphasis to software issues, such as ease of programming the device or the portability of code, as to the hardware considerations. Even with processors nominally fulfilling the hardware requirements, there can be aspects of using a specific device which are objectionable to the programmers, such as restricted choice of programming languages or insufficient support for compilers and debugging tools. Certainly, if extensive code for a specific processor or family is available, this must be an influencing factor in determining the device that will be used.

Therefore, the most demanding aspect of designing the image processing unit is selecting the microprocessor. This requires making trade-offs regarding the difficulty of implementing the hardware and software functions, and the performance in execution of various solutions without having the finished product to hand to evaluate. In this situation there is a tendency to over-specify the system, to be sure that the mission objectives are met at the expense of mass, volume and power. Once the processor has been selected, the remaining design issues will follow fairly logically.

To fulfil these, and other, requirements, the Inmos transputer has been for the high level management and processing functions of SSTL's imaging systems. Transputers are highly integrated 32-bit microprocessors featuring four 20 Mbps serial links, timers, a programmable external memory interface, an interrupt controller, a DMA controller and even a 64-bit floating-point co-processor all on a single chip. The fact that so many useful facilities are incorporated into a single package makes transputer-based computers more compact and more straight forward to design with than most microprocessors which implement these functions in discrete devices. Rather sensibly, Inmos ensure that most of their processors have identical pin-outs so that existing boards and designs can be upgraded or accelerated without requiring any rework. Consult [Inmos, 1992] for further details of the specific features of transputers.

6.2.1.1 Transputers and parallelism.

However, the main feature of the transputer is its intrinsic suitability to parallel processing. Although the limited resources of microsatellites will force the network of transputers to be small, prohibiting 'massive' parallelism, the concept has still been explored and exploited by the SSTL imaging systems. In addition to running tasks in parallel on separate machines, processes running on a single transputer can also be written in parallel. Although this obviously does not happen physically, the transputer has a built-in hardware scheduler that time-slices between the various processes the emulate parallelism. Even though this is closer to multi-tasking, it appears to the programmer as genuine parallelism since the same code could be executed on multiple transputers if they were they available (subject to recompilation).

This parallelism offers two major benefits to the imaging system's software. Firstly, the development of distinct parallel modules ensures complete isolation between the different processes except where explicitly invoked by the programmer. The sensible use of parallelism promotes modularity, thereby improving the integrity, interpretability and portability of the software. Furthermore, the hardware scheduler assures that each active process has its fair share of the processing time without wasting any of this resource on inactive processes. This relieves the programmer from having to supply a fully-fledged multi-tasking operating system. Moreover, the transputer allows processes to be classified as high priority allowing them to interrupt low priority processes when an important event occurs, possibly requiring urgent servicing.

Given the parallel capabilities of transputers, from the start it appeared mandatory to have at least two of them to allow some limited exploitation of these facilities. In practice, the software for the two transputers has remained fairly isolated, minimising the genuine parallelism of the system. Although, they have been exploited as two distinct microprocessors, one serving the Earth imaging camera and the other controlling the GPS receiver and the star sensor camera., the hardware is in place to implement parallel software whenever required.

Although the transputers have gone through numerous design iterations, the two were identical on FASat-Alfa, one again demonstrating the modularity emphasised as one of the design objectives for this mission. Each processor occupied half of a standard SSTL microsatellite module tray (230 x 110 mm). If further parallelism is required on future missions, the modules can be replicated with ease.

6.2.2 TASKS TO BE EXECUTED BY THE PROCESSING UNIT.

There are numerous tasks to be fulfilled by the imaging system's master processor. The computer receives commands and parameters dictating the sequence of forthcoming imaging events from the OBC, or conceivably directly from the uplink. These commands must be decoded and the appropriate hardware elements, including the camera microcontrollers, activated appropriately.

Once again, there are innumerable different solutions for implementing the image processing software. However, a fairly conventional approach is to have to central software loop waiting for specific events to occur, such as incoming communications or a timer firing. A state-table or the parameters of an incoming command dictates the appropriate action to be taken in response: for example, capture, process, compress or transfer an image, update various housekeeping tasks or return status information. To support the various operational needs, it is necessary for this main loop, or process handler, to be able to launch multiple tasks under a multi-tasking, or parallel, environment.

6.2.2.1 Communications.

The image processing unit needs to communicate with a range of different targets including the cameras, the various spacecraft OBDH buses and possibly even the uplink and downlink. A wise strategy is to use distinct networks for widely different applications, rather than try to force one system into meeting all the spacecraft's requirements. In this scenario, which is being introduced to SSTL satellites, one network is typically used for the satellite's low speed applications such as telemetry, telecommand (perhaps complementing the underlying hardware system) and inter-processor traffic. In the case of FASat-Alfa, this was the CAN and DASH buses. For dedicated imaging missions it will certainly be necessary to provide another network for high speed, bulk data transfers. These will almost certainly use different standards, neither of which is likely to be the same as the local bus between the image processor and the cameras. Therefore, the image processing unit needs to accommodate a wide range of hardware communications devices and software protocols to adhere to the various data channels. Primary and redundant paths must be accommodated.

For general-purpose spacecraft data buses, the format will not be dictated by the specific requirements of the imaging units. This is especially the case on microsatellites, where off-the-shelf solutions are sought to maintain the low costs, and it is necessary for the imaging systems to adhere to the standard used. In general, these protocols will be software-based to be expandable and flexible, and are unlikely be conceived for the huge data transfers associated with remote sensing.

If the mission objectives call for some specific level of remote sensing performance in terms of data volume or turn-around, then it will be necessary for at least one of the OBDH networks to be adequately specified to meet these objectives. Care must be taken to ensure that the effective data transfer rate is considered for this, absorbing protocol overheads and latency of software servicing routines. This level of performance is not guaranteed by the raw bit rate of the physical layer.

The selection and definition of OBDH systems and protocol is complex and subtle. At this point it is sufficient to reiterate the comments of sections 3.4 and draw attention to the significant role communications and data transfer will play in the operation and performance of the image processing unit. The microprocessor chosen must be sufficiently versatile to accommodate whatever standard is dictated by the spacecraft, but be fast enough to avoid degrading the overall system throughput.

6.2.2.2 Scheduling imaging activities.

Given that a microsatellite will probably not provide a continuous, real-time imaging service, some method is required to allow ground operators to instruct the imaging system to collect data when out of range. The on-board computers, including the transputer-based image processing unit, must provide these functions. Overall, giving the computers extensive autonomy to execute routine operations helps minimise ground segment costs, compatible with the principles of low-cost satellite engineering. The sequence employed for imaging activities on PoSAT-1 provides a good example of how SSTL's camera systems are operated on a daily basis.

1. *Target selection* is performed by a ground operator using predictive tracking software to scan when the satellite will be passing over area of interest. For PoSAT-1, ten or twelve such targets are selected daily.

2. *Time-tagged commands* for these targets, including capture parameters, are written into a 'schedule' file which is automatically loaded to the main OBC, which passes the instructions on to the transputer module. Within the schedule file, there is no limit either for the number of commands that can be included or how far in advance the commands can be issued.

3. *On-board scheduling* is handled by the transputer which keeps a list of all the forthcoming imaging events.

4. *Payload activation* occurs fifteen seconds before an image is due, when the transputer activates the camera. This allows time for the camera circuitry to settle after power-up. If the camera's automatic exposure option has been selected by ground control (set for each image in the schedule file), this time is used to assess the scene brightness and adjust the CCD's integration time accordingly.

5. *Image capture.* At the correct time, the transputer issues a 'capture image' command, and within 100 milliseconds the camera will have stored the entire digital image in the microcontroller's buffer memory. Following successful image capture the camera's sensing circuitry is disabled to save power, and the microcontroller transfers the digitised image data over the one of the OBDH networks. On FASat-Alfa, it would have been possible to operate the cameras individually or in parallel, recording simultaneous images on several cameras.

6. *Image analysis, processing and compression* is implemented by the transputer, as described in chapter 7. The compressed image file is sent to the OBC where it is queued for the downlink.

7. *Downloading* occurs automatically with the ground station software retrieving the data files using the satellite's store-and-forward communications protocols. Images are automatically decompressed and archived, ready for viewing.

The implementation of the scheduling software is fairly standard, and can be supported either centrally by the main OBC or locally by the image processing unit. In practice, local implementation is more useful because it gives greater flexibility to the order of execution. If the scheduling task is run on the OBC, it will not be feasible to implement more fanciful sequences without compromising the overall mission integrity. Isolating all imaging software from the OBC allows these tasks to be more ambitious than would otherwise be possible.

Similarly, although time-tagged instructions are generally used to schedule future activities, other possibilities exist. In particular, if navigational software is implemented on board, this could be used to activate the imaging system every time a specific target (latitude and longitude) is surpassed.

As long as time-tagged commands remain the main method of scheduling events in the future, it is vital to maintain the accuracy of the on-board clocks. If the computer clocks are allowed to drift, incorrect targeting will result. To avoid this, the transputer clock is synchronised at least once a day, either to the on-board GPS receiver or to a master ground station.

6.2.2.3 Internal housekeeping tasks.

As with any on-board computer, the image processing unit will need to implement a range of housekeeping tasks to ensure continued smooth running. This covers various miscellaneous aspects from synchronising the software clocks used for scheduling to supervising and managing the communications sessions.

One of the most important aspects of running a microprocessor is booting executable code when it is powered up. In the OBCs of virtually all conventional spacecraft, the entirety of the flight software is hard-coded in a ROM prior to launch. Run-time variables and 'patches' can be loaded to modify the execution to a small extent. However as a rule, for reasons discussed in section 6.2.3.3, SSTL microsatellites provide facilities for completely reloading operational software in orbit. The mechanisms for booting computers over a noisy and intermittent uplink require careful forethought. SSTL has standard protocols for bootloading, either directly from the uplink or via the OBC, to which payloads must adhere. While loading new code in orbit alleviates the need for extensive testing of the main operational software before launch, the bootloading routines need to be fully verified. Nevertheless, unless the operational software is trivial, testing the bootloader is much simpler than the application code. Since transputers are designed for parallel applications, where 'flood-booting' of a network is necessary, they incorporate a suitable bootloader in the chip's micro-code; this facility is exploited in SSTL missions by selecting a special compilation option and having the OBC emulate the 'root transputer' over the spacecraft's serial bus.

Once the processor has booted, from either ROM-based firmware or a file sent by the OBC, there are numerous tasks to be implemented to ensure that the system continues to function. The software clock used to schedule imaging activities must be initialised and resynchronised at regular intervals to prevent clock drift. The various communications channels must be configured; the housekeeping software must also ensure that the communications sessions remain synchronised, and must be able to recover from loss of contact autonomously.

A vital function of the housekeeping software, not encountered in terrestrial applications, is maintaining the integrity of the processor's semiconductor memory. As discussed in section 6.2.3.1, CMOS memory is susceptible to errors caused by transient radiation. Even though the processor may be protected from executing these erroneous bits by hardware error-detection-and-correction (EDAC) circuitry, the memory itself will not be corrected. To prevent the accumulation of these errors, it is necessary to periodically 'wash' the memory; this simply involves reading every memory location, thereby providing the processor with a corrected version of the memory contents, and writing the same value back again. Although this sounds simple in theory, some care is needed to ensure that other tasks running in parallel will not be disrupted by the abnormal memory access. Similarly, any data protected by software coding will need to be periodically processed to eliminate a potential build-up of errors, which would eventually become uncorrectable.

Given that the imaging events on an microsatellite will often be sporadic, with prolonged idle periods, the ability to place the image processing unit into a low power state will significantly reduce its total current consumption. The scheduling software will need to determine whether the forthcoming events are sufficiently far into the future to justify entering the idle condition. When instructed to do so, the housekeeping routines will need to store all important variables that might be lost, and systematically disable the various non-essential functions and peripherals. Of course, the processor (or master if there is more than one) will still need to be able to respond to events, such as incoming communications or impending imaging activities, to wake the system up again. The most appropriate technique for reduced power consumption with contemporary CMOS microprocessors is to slow the system clock, resulting in a proportional reduction of power. If parallel networks or dedicated image processing or compression hardware is employed, many of these elements can be completely powered down without any significant disruptions. The software will need to take account of the changing system clock to ensure accurate time-keeping, and will need to reconfigure all systems back to normal when imaging resumes.

This presents a brief overview of some of the most important tasks to be implemented by the image processing computer. A far more detailed account of the UoSAT-5 transputer scheduling and housekeeping software is provided in [Laker]; although some specifics have evolved to take account of the changing hardware and operational requirements of the subsequent imaging missions, the basic structure remains intact.

6.2.2.4 Image processing and compression.

As mentioned earlier, the primary role of a high performance computer within the imaging system is complex and computationally intensive image processing. For simple image capture and transmission, the scheduling facilities supported by the main OBC will be more than adequate. However, if more substantial image manipulation is required, it is logical to provide a dedicated processing element for this purpose. In general, a satellite's primary OBC will be a well-established system with a known pedigree but with correspondingly modest computational performance, and ill-suited to the demands of sophisticated image processing. The design of a dedicated unit will be optimised for the particular requirements of image processing. Furthermore, on demonstration missions like the SSTL microsatellites to date, having a separate processor allows more novel and experimental software routines to be deployed without risking the overall mission integrity. If implemented on the OBC, incompletely debugged software could cause significant disruptions to the overall mission. Conversely, if the SSTL transputers crash, the error is isolated and rebooting them is straight forward.

Chapter 7 discusses the experiments in on-board image processing and compression conducted as part of this research programme. The results have been encouraging, demonstrating some of the benefits of in-orbit image analysis, processing and compression. The transputer processing elements has proved to be a highly suitable platform of this type of experimentation. It is adequately powerful and flexible to accommodate the various algorithms, but remains simple to programme despite the multi tasking / parallel environment.

6.2.3 OTHER DESIGN CONSIDERATIONS.

6.2.3.1 Radiation-induced single-event-upsets in semiconductor memory.

In the same way that ionising radiation causes degradations to a CCD's performance (discussed in section 5.6.5), semiconductor memories also suffer from transient and long term effects. Perhaps the best-known of these is the phenomenon of single-event-upsets (SEUs) which occur when the current generated by the energetic particle alters the state of the trapped charge in a memory cell, resulting in random 'bit-flips' of the data stored. Because the mechanisms of storing charge, dynamic RAM is significantly more susceptible to SEUs than static RAM; the need to store smaller charges also accounts for DRAM's higher density. Conversely, all forms of ROM are essentially immune to these effects.

A conventional CMOS static memory device in an 800 km, polar low-Earth orbit will have its contents corrupted at a rate around 1 SEU per Mbit per day [Harboe-Sorensen et al][Underwood et al, 1992][Underwood et al, 1993]. If no precautions are taken, this can have significant disruptions on the operations of the imaging system or the data produced. Although SEUs can occur anywhere, they are concentrated primarily in the region known as the South Atlantic Anomaly, where the Earth's radiation belts converge with the satellite's orbit, and over the poles.

If the memory concerned is used as programme memory for one of the spacecraft's microprocessors, it will be necessary to provide hardware coding to protect it from SEUs. Known has error-detection-and-correction (EDAC) systems, these circuits sit between the processor and the memory, and use combinational logic to encode the contents of data bus. When data is written to memory, the EDAC generates additional coding information which must be stored in an auxiliary memory. When the data is read back, it is compared to the appropriate coding data, using the redundant information (contained in the code) to detect errors and correct them if necessary. The advantage of hardware EDAC is that it is transparent to the processor, operating independently to ensure that the processor is never presented executable code corrupted by SEUs. The disadvantages of EDAC are the overheads in terms of increased chip count, circuit complexity, power consumption and reduced speed.

Fortunately, EDAC is only necessary if the programme code is stored in RAM, and is not required to protect ROM, which is immune to SEUs. As the camera microcontroller probably uses ROM-based firmware, it will therefore be spared the extra overheads of implementing EDAC. Conversely, the sophisticated programmes executed by the main processing units (the on-board computers or the SSTL transputers) will be stored in RAM, needing EDAC protection.

On the other hand, if the semiconductor memory is used to contain payload data, as opposed to programme code or variables, it is not always necessary to implement hardware EDAC protection because there is no chance of the processor attempting to execute from this memory. For this data, it is often more appropriate use software codes to protect against SEUs. By employing software techniques it is possible implement much more sophisticated algorithms than would be possible with simple hardware. For example, the cyclic-redundancy-code (CRC) used on the SSTL OBC's Ramdisk requires only four bytes of coding overhead for 252 bytes of data, yet can cope with a number of single or multiple errors [Hodgart][Hodgart et al]. However, since it is necessary to process the entire block every time a single byte is written or read, the speed penalties can be significant.

The strategy adopted to combat SEUs in semiconductor memory must be chosen judiciously according on the role the memory plays in the system. When storing image data for prolonged periods, for example when waiting in the downlink queue in the OBC's Ramdisk or in a solid-state data recorder, software coding is most appropriate. Conversely, when manipulating the imagery intensively, for example during image processing, it is more effective to transfer the data into EDAC protected memory so that random access to the data is possible without suffering the delays associated with block codes.

Alternatively, it is possible to dispense with SEU protection for the short duration of image capture and processing, accepting the risks that this entails. Provided the imagery is only left unprotected for short periods, the statistical chances of being corrupted by SEUs is small. [1] The consequences of having the odd bit in error must be assessed, and traded-off against the additional complexity of implementing hardware EDAC. Certainly, the design of the image buffer memory is rendered vastly more difficult if EDAC must be implemented (software coding is not feasible because of the high data rates). As the data will only be in this memory for a few seconds until it is transferred to another on-board processor, the risk is very small (1 SEU per Mbit per day in an 800 km polar orbit). It may also be appropriate to have unprotected 'scratch-pad' memory available for temporary

---

[1] The compiled code for the PoSAT-1 transputers is about 40 kBytes long. Using conventional CMOS memory, statistics indicate that this code will be corrupted once every 3 days. Ninety percent of errors will occur in the South Atlantic Anomaly. Large arrays of variables are equally susceptible to single-event-upsets.

storage during image processing; the absence of EDAC will speed operations involving this memory.

The final solution to the problems of SEUs in memory is to use a radiation-hardened semiconductors, as advocated intensely by [Harris]. By developing integrated circuits that do not deposit the active circuitry onto bulk silicon, but employ an insulating substrate like sapphire, it is possible make SEU-immune devices. Whereas the charge generated by a particle strike in a conventional silicon device is free to migrate towards the sensitive depletion regions, it is constrained by the low conductivity of an insulator. Therefore, although charge is generated in radiation-hardened devices, it cannot move and is forced to recombine locally. Through this, and various other factors like reduced gate profiles and improved minority carrier mobility, these silicon-on-sapphire (or silicon-on-insulator) devices have a much higher tolerance to SEUs, purportedly four or five orders of magnitude more resilient than conventional memories, making them virtually immune to radiation effects in low-Earth orbit.

However, designing systems around these radiation-hardened devices can be far less attractive than with conventional memories. Their memory density is vastly inferior, at about 64 kbits compared to 4 Mbits. Furthermore, silicon-on-sapphire devices are extremely difficult to obtain, particularly if low volumes are required. On the UoSAT-5, KITSAT-1 and PoSAT-1 missions, a few devices were obtained around nine months after their initial delivery date, critically late in the rapid development cycle of these microsatellites. With the discontinuation of numerous lines of specialist military and space semiconductor products, these devices will become even more difficult to come by. Finally, when they are available, silicon-on-sapphire memories are very expensive at about £1000 per device; standard silicon CMOS memories are about £10 for 64 kbit and £200 for 4 Mbit devices. For these reasons, silicon-on-sapphire memories are no longer used on SSTL missions, as their limitations cannot be justified. Nevertheless, there may be situations where this immunity to SEUs outweighs the other drawbacks of silicon-on-sapphire technology.

There are various approaches to combating radiation-induced SEUs in CMOS memories, and the SSTL imaging systems use many of them, with the method selected as dictated by the circuit's functionality. The microcontroller firmware is hard-coded, stored in a ROM. Small amounts of unprotected RAM are necessary for the temporary storage of run-time variables, but these are only required for a few seconds at a time, minimising the exposure to SEUs. Similarly, the design of the image buffer memory is simplified by the absence of EDAC protection. Conversely, the transputers' memory is fully covered by a hardware EDAC implementation, allowing the programme code, variables and data to be manipulated and stored without risk of corruption. Finally, software block codes are used when the imagery is stored indefinitely on the on-board computer's Ramdisk.

The transputers used in the SSTL imaging systems incorporate 4 kBytes of internal RAM. Because this memory is on-chip, its access time is very much faster than for external memory (50 ns versus 150 ns, or 350 ns for the EDAC-protected memory of the SSTL design). By placing critical code and variables in this internal memory, the speed of execution can be significantly increased, providing many of the benefits associated with on-chip 'cache' memory. Unfortunately, this memory does not posses any of the necessary hardware protection needed to safeguard against SEUs. Moreover, tests by [Thomlinson et al] have shown that the SEU performance of this internal memory is poor, with a modelled error rate of 8.5 SEU per Mbit per day (in a 900 km polar orbit). [2] For these reasons, the transputers' internal memory has been disabled in the SSTL design, relinquishing the speed advantages offers, but providing up to 50 times more SEU resilience [Thomlinson et al].

6.2.3.2 Long term radiation damage to digital semiconductors.

Simplistically, the silicon-dioxide layer isolating the active (doped) regions from the silicon substrate in a conventional CMOS device traps holes generated by ionising radiation. As these holes accumulate, an increasingly negative threshold voltage is needed to switch the FET on or off, resulting in a loss of switching speed. As the radiation damage accrues, it requires greater drive voltages to activate the component, until eventually the device fails on or off because the source cannot provide a large enough voltage swing.

For typical CMOS logic, around 30 kilorads of accumulated dose is required for the device to fail. This is the figure offered by [Thomlinson et al] for the total dose required to cause failure in transputers, although [Barrington Brown et al] show that there can be significant disparity between batches and manufacturing revision of a device. Despite the variation in total dose survivability, [Barrington Brown et al] conclude that all members of the transputer family tested (including the T800 and T805 models used for the SSTL systems) are suitable for use in low-Earth orbit. However, the 'radiation-hardness' of the internal RAM is significantly poorer than the rest of the device, with only 5 kilorads of tolerance [Inmos, 1990]. If this memory is enabled, it will dictate the lifetime of the

[2] Tests performed on the UoSAT-5 transputer indicate an effective SEU rate of around 4.5 SEUs per Mbit per day. Unfortunately, the data sets are not sufficiently complete to confirm this figure.

device in a radiation environment, although fortunately it does not appear to accumulate dosage when disabled.

In general, it is the performance of the oxide layer of field-effect transistors (FETs) that is critical in establishing the radiation hardness of a component. Because of the different manufacturing process, bipolar transistors are more resilient to radiation damage. By eliminating the silicon-dioxide layer, [Harris] reports that their silicon-on-sapphire devices have total dose immunities as high as 1 Megarad, although this needs to be moderated by the biased opinion of this document; a factor of around ten is often required to marry the figures from [Harris] to conventional wisdom, and a total dose immunity for silicon-on-sapphire of 100 kilorads is probably more realistic.

As discussed in section 5.6.5, the total radiation dose received in the standard 800 km orbit is fairly low, around 300 rads per annum. This dosage does not justify a strict regime for selecting the electronic components in microsatellite imaging systems, particularly when the costs of radiation-hardened devices are considered. Nevertheless, some care is required when using new devices with no known pedigree. An appropriate solution is to irradiate samples of interesting components in ground-based tests, to determine their survivability. [Brylow & Soulanille] describe the technique used for this type of screening during the design of the Mars Observer inter-planetary spacecraft, but which is equally suited to small satellites.

6.2.3.3 Incorporating flexibility into the system to overcome unforeseen failures.

Regardless of the actual implementation of the imaging system and its processing units, it is important to design the entire system with enough versatility to overcome failure, and continue to function despite these difficulties. There are a number of obvious measures to be taken, such as the use of modularity to isolate faults and the provision of redundant communications paths to bypass faulty units or networks. These back-up communications paths do not need to be as sophisticated as the primary buses. Reduced functionality, speed and flexibility can be tolerated, provided the essential system operations are still supported. In the case of processing units executing their programme code from ROM-based firmware (such as the camera microcontroller), it must be possible to redirect communications without any additional software.

In addition to these standard measures, there are other steps that can be taken to improve the system's survivability. Perhaps the most beneficial facility, and one which is not widely embraced by the conventional space industry, is the ability to reprogramme on-board computers in orbit [Ward & Price]. This is the approach adopted for all of SSTL's computers (but not necessarily for the microcontrollers), where only basic bootloading, communications and 'safe-mode' routines are committed to ROM before launch. All other (applications) software is loaded to the satellite after launch. This allows the programming team to work on the flight software for the several extra months between the final assembly of the spacecraft prior to environmental testing and when this software is actually needed during in-orbit commissioning. It also allows the satellite's operations and services to progress as new software is developed. This has enabled the SSTL store-and-forward services, for example, to remain consistent across the missions even though the software has been radically upgraded since the launch of UoSAT-3. Another example, is the image compression software written and loaded to the transputers on PoSAT-1 a year after launch (described in chapter 7.2.6).

Despite these clear advantages, the most vital aspect of being able to load modified software is the ability to respond to unforeseen operational situations. Unfortunately, on any spacecraft, there are always a number of systems that do not function entirely as anticipated, and while not necessarily failing altogether, do not provide a complete service. This is particularly the case for microsatellites on short development cycles, where time and budgetary constraints do not allow the traditional, prolonged testing of the spacecraft. When these anomalies do appear, it can be extremely useful to be able to reprogramme the on-board computers to operate and manipulate the hardware systems in alternative manners.

Within the context of the imaging systems, reprogramming the processing units can modify the operation of the cameras to overcome subnormal performance. In the case of UoSAT-5, signal race-conditions experienced in the image buffer memory at cold temperatures corrupted the retrieval of the stored data (see section 6.1.2.2). This was cured by altering the sequence of operations when accessing this memory to ensure that the address and data buses remain static during a read operation. Although this was a trivial modification to the software, it has allowed the data to be gathered without corruption. This temperature-dependent defect was detected before launch, but after the final assembly of the circuit. Compared with the simplicity of changing application software, modification of firmware at this stage would have been difficult and risky, requiring the ROMs to be cut out of the printed circuit board, and replaced with new ones.

A similar software work-around was used on PoSAT-1, when one of the camera's power conditioning circuits deteriorated during launch, causing it to operate intermittently. The transputer software has been modified to drive the camera repetitively to 'pump up' the rails on this locally regulated -5V supply, and to analyse the imagery collected to ensure that the camera is operating correctly at this point. If the entire image capture sequence had been hard-coded in firmware, it is unlikely that the camera would have provided more than a few frames of valid data. Since the software rework was implemented, it has been possible to operate the camera virtually as normal, with a slight uncertainty (± 5 seconds) in the moment of image capture being the only residual effect of the fault.

On the SSTL missions currently in orbit, the only part of the imaging systems that is re-programmable is the transputer modules, with the cameras' operation fixed in hardware and / or firmware. The flexibility comes from varying the sequence of operations dictated to the cameras by the transputers. However, given the near catastrophic failure experienced on PoSAT-1, additional measures have been implemented on the FASat-Alfa cameras to provide better facilities for dealing with any eventual failures. While procedures for routine operations will again be handled by the cameras' firmware, the repertoire of microcontroller functions has been extended to allow numerous alternative commands, many of which drive the camera into unconventional modes which may be useful for debugging. If necessary, the transputers or main on-board computers can assume total control of the camera hardware by using 'peek' and 'poke' instructions to gain access to all of the microcontroller registers, providing great flexibility in the possible emergency sequences that can be attempted. Hopefully these features will never be needed, but implementing them has not been a significant overhead and their existence may prove invaluable in saving imaging modules in the future.

The examples mentioned above show how retaining the ability to modify operational software in orbit has salvaged degraded imaging experiments. Similar modifications have been made to correct or enhance the performance of numerous other spacecraft systems. Moreover, even if the spacecraft hardware discharges its tasks flawlessly, there is an even greater probability of the firmware containing bugs which will not have been detected during ground-based testing. While these flaws can be remedied with ease in up-loadable software, it is impossible to alter firmware. While such firmware fiascos are not widely publicised, the author is aware of one mission, the Orbcomm-X microsatellite (launched at the same time as UoSAT-5), which failed due to an incorrectly programmed ROM in the satellite's power system [Ward].

Given the numerous advantages of being able to reload software in orbit, it is surprising to SSTL engineers why this approach is not used more frequently in other spacecraft. This is a reflection of the compartmentalised approach to spacecraft design adopted in the conventional space industry, where separate groups are responsible for providing hardware, software and post-launch operations. With these arrangements, fluid software is incompatible with the systems of extensive checks, reviews and documentation considered necessary for controlling the mission. Conversely, in the small teams used for microsatellite missions, the same people are involved in all stages of the programme and are able to adapt quickly to continually evolving situations. Indeed, provided the software team can react quickly to urgent situations, it is also far less expensive implement software modifications as necessary. This means that the time otherwise used trying to anticipate and programme firmware for every possible failure mode (which is of course impossible), can be used more profitably by writing applications software instead.

6.3 CONCLUSIONS.

In contrast with the tightly defined block diagram and operating sequence of a CCD camera, there is no fixed way of implementing the digital systems of an imaging instrument. Because of this, there is an unlimited range of solutions for collecting and processing the digitised imagery. This makes it difficult to address the issues of data handling in depth, whilst remaining succinct.

Conceptually, the buffer memory and the processing elements of an imaging system act as a bridge between the free-running camera and the digital systems of the microsatellite's on-board data handling networks. Since the data rates from an imaging payload will inevitably exceed the capacities of the other systems on a microsatellite, it is necessary to buffer the data stream. Likewise, the imaging service will occasionally (or frequently) need to be interrupted to accommodate this disparity in data rates. While the satellite's downlink capacity determines the daily throughput from the imaging system, the rate at which the image buffer can be serviced plays a key role in defining the image turn-around.

The communications and data handling capabilities of the camera interface need careful consideration, because they limit the imaging system's ability to recover from each burst of activity. However, the quest for sheer speed in data handling must be traded-off against a number of other factors, including:

- high speeds invoke a power consumption penalty,
- fast parallel interfaces are less modular (reduced fault-tolerance, expansion more complex) and heavier (more wires) than slower serial interfaces,
- hardware solutions are faster but less flexible than software.

The system definition and specification of the OBDH networks and the camera interface are amongst the most subtle design issues facing the implementation of commercial remote sensing from microsatellites. In some ways, developing the interface represents an opposite challenge to that of the camera's analogue parts. The interface demands carefully planning and specification to ensure that mission requirements will be served; once this has been decided the actual implementation is relatively straight forward. Conversely, the system level design of the camera is generally quite clear, with the difficulty lying in the circuit-level issues.

The author has adopted a two-tier approach for data handling with the SSTL imaging systems. A microcontroller supervises the low-level performance of the camera and collects the data dumped in the image buffer. A more powerful transputer unit provides high level system management and implements the computationally intensive image processing and compression tasks. The modularity of this solution has allowed rapid and flexible expansion. The principal drawback of the current implementation is using the microcontroller to retrieve the imagery. The servicing rate of the controller is far too slow, and this function will be implemented in hardware in future.

6.4 REFERENCES

Barrington Brown A.J, Ward A.K. & Entwistle P.M: Transputers and their use in on-board computers; Symposium on Space Electronics, British Interplanetary Society, April 1995.

Brylow S.M. & Soulanille T.A: Low-cost quick-look radiation testing of electronic components for the Mars Observer Camera; Proc. of the 6th Annual AIAA/USU Conference on Small Satellites, Utah State University, 21-24 Sept 1992.

Inmos: The Military and Space Transputer Data Book, Appendix C - radiation tolerance; Inmos Ltd, 1990.

Inmos: The Transputer Data Book; Inmos Ltd, 1992.

Harboe-Sorensen R. et al: Observations and prediction of SEU in Hitachi SRAMs in low altitude polar orbits; IEEE Trans. on Nuclear Science, Vol.40 No.6, p.1498 - 1504, Dec 1993.

Harris: Integrated circuits for the space environment; Space Product News, Special edition, Military & Aerospace Division, Harris Semiconductor 1993.

Hodgart M.S, Underwood C.I. & Ward J.W: Single event upset error protection for solid state data memory on microsatellites; Proc. of the 5th Annual AIAA/USU Conference on Small Satellites, Utah State University, 26-29 Aug 1991.

Hodgart M.S: Efficient coding and error monitoring for spacecraft digital memory; Int. J. Electronics, Vol.73 No.1, p.1-36, 1992.

Laker C: Software environment for the UoSAT-5 Earth imaging system; M.Sc. dissertation; University of Surrey, 1991.

Thomlinson J, Adams L. & Harboe-Sørensen R: The SEU and total dose response of the Inmos transputer; IEEE Trans. on Nuclear Science, Vol.NS34 No.6, p.1803-1807, Dec 1987.

Underwood C.I et al: Observations of single-event upsets in non-hardened high-density SRAMs in Sun-synchronous orbit; IEEE Trans. on Nuclear Science, Vol.39 No.6, Dec 1992.

Underwood C.I et al: Observations of single-event upset and multiple-event upset in non-hardened high-density SRAMs in the TOPEX/Poseidon orbit; IEEE Trans. on Nuclear Science, Vol.40 No.6, Dec 1993.

Ward J.W. & Price H.E: Re-usable software for microsatellite on-board computers; EUROSPACE Symposium on On-Board Data Management, Rome Italy, 25-27 Jan 1994.

Ward J.W: Personal communication, 24 Aug 1995.

CHAPTER VII

DEMONSTRATION OF ON-BOARD IMAGE PROCESSING AND COMPRESSION TO IMPROVE DATA THROUGHPUT AND VALUE.

The small capacities of microsatellite communications systems limit the volume of payload data which can be collected, hampering the development of commercial remote sensing from these spacecraft. In addition to the obvious measures of upgrading the communications hardware, there are a number of software data reduction techniques that can help improve the imaging yield of microsatellites. Chapter 7 explores how various autonomous and interactive image analysis, processing and compression techniques have conferred a five-fold increase in the daily throughput of the camera systems on PoSAT-1. These methods, while of particular benefit to microsatellites, are equally applicable to all remote sensing missions.

7. DEMONSTRATION OF ON-BOARD IMAGE PROCESSING AND COMPRESSION TO IMPROVE DATA THROUGHPUT AND VALUE.

As discussed at length in section 3.4, the downlink data capacity of current and future microsatellites represents a severe constraint on the development of commercial remote sensing from these small spacecraft. While there certainly is potential for increasing the data rates to the region of 1 Mbps by developing appropriate hardware systems, this still falls short of the data rates experienced on conventional Earth observation missions.

A solution is to use the computational sophistication found on microsatellites to improve the use made of the valuable downlink resource. Realising that on-board image analysis, processing and compression are valuable tools in exploiting remote sensing microsatellites, a demonstration of these techniques has been included as part of this research programme. Although the schemes implemented are relatively simple, they have been highly effective, achieving substantial increases in the volume of image data retrieved from PoSAT-1.

It must be stressed that the emphasis of the programme covered by this thesis has not been to research image processing or compression. It has been to assess the suitability and demonstrate the benefits of using existing techniques to enhance the performance of remote sensing microsatellites.

7.1 IMPROVING THE VALUE OF REMOTELY SENSED DATA.

Generally, efforts to improve the yield of remote sensing satellites emphasise a decrease in the number of bytes required to describe an image, i.e. image compression. An alternative, and frequently overlooked, approach is to be selective in deciding which imagery is transmitted to the ground, thereby improving the value of the data downloaded.

7.1.1 AUTONOMOUS IMAGE EXPOSURE CONTROL.

The reflectance of the Earth's surface and atmosphere can vary widely depending on the incidence angle of Sunlight, which is much brighter at the equator than at the poles. The surface cover has an even greater influence on the scene reflectance. In the visible spectrum for example, clouds, snow and ice are highly reflective, clear water is highly absorptive, and bare soil is more reflective than vegetated terrain. Therefore it is not really possible to specify a consistent exposure for Earth imagers which is optimal for all conditions.

Most conventional Earth observation systems use fixed integration and gain settings which provide enough dynamic range to image successfully under most conditions, perhaps suffering a little saturation in the very brightest conditions over polar ice caps [Dosière & Justice]. However, the scene below the satellite rarely contains both bright and dark regions, and the imager's full dynamic range is therefore seldom employed to record any given image. Since most imagery is quantised to 8 bits on board, only 5 or 6 bits of information will actually be provided for any particular scene.

Transmitting these 'under exposed' images as 8-bit entities is clearly wasteful of a significant percentage of the communications capacity. Nevertheless, this approach is used on virtually all remote sensing satellites, with SPOT being the sole exception; a hardware encoder implements an 8-bit to 6-bit conversion scheme directly on the output data stream to reduce the volume of data [Pease, p.291]. Clearly, imaging payloads on microsatellites must avoid such inefficiency. Although it is feasible to implement this type of simple data reduction on a microsatellite, non-real-time compression software will produce far more effective savings.

The alternative approach to making better use of the 8-bits available from the analogue-to-digital converter is to implement exposure control. By adapting the camera's capture parameters to the current scene conditions, it is possible to get more bits of information per pixel. This can either be accomplished by varying the sensor's integration time or by altering the signal gain in the video processing stages. In addition, careful manipulation of these parameters can be used to concentrate on specific scene features; for example, slight over-exposure will cause marginal saturation in bright clouds but ensures a greater radiometric resolution when imaging darker land features.

On the SSTL missions up to and including PoSAT-1, manual exposure control has been implemented by having a moderately experienced ground operator define the exposure parameters for each image in advance and sending them to the spacecraft as part of the standard command sequence. Although there is significant variation in reflectance across the Earth's surface, the brightness of a specific area is quite predictable by accommodating factors like the terrain cover, latitude and season of the year. Using this type of open-loop approach to setting the image exposure almost always produces data with 6.5 bits of information, but routinely provides 7.5 to 8 bits of imagery.

Alternatively, control of the exposure can be handed to the on-board systems. This can be performed without any additional hardware, by having the camera assess a sequence of images and adjust its exposure controls iteratively until a well exposed image is produced. A simple automatic routine has been implemented on PoSAT-1, whereby the transputers evaluate the brightness distributions (i.e. the histogram of grey scales) of successive images, adjusting the CCD's integration time until it meets an acceptance criteria. A maximum number of iterations is specified to stop the algorithm oscillating in the event of getting confused. Except for a brief experimental trial, this process has not been used in practice because the camera's microcontroller unit is too slow to service the transputer before the target of interest leaves the camera's field of view. (The operational difficulties described in section 6.2.3.3 also preclude the use of this feature). Nevertheless, the concept has been demonstrated, and has been implemented locally within the camera microcontroller in the FASat-Alfa modular cameras. The loop converges within a few hundred milliseconds, effectively performing real-time exposure control.

The advantage of implementing variable exposure control is that the full dynamic range be used for every image, regardless of the actual conditions at the time of capture. In addition to increasing the information (as opposed to data) throughput, correctly exposing the image provides an improved signal-to-noise ratio. By ensuring that the CCD collects as many photons as possible without saturating, the amplitude of the signal is increased with respect to the camera's underlying noise floor. For this reason, it is important to control the exposure by varying the CCD's integration time, as opposed to the video gain which will amplify the CCD noise as well.

The drawback with fully automatic image exposure is that images collected with different settings cannot be compared directly. For this reason, even if an automatic mode is anticipated for general use, it is important than a manual exposure mode is preserved within the camera. Nevertheless, provided the integration and gain control settings are fairly well characterised, it is possible to process images to a common scale (i.e. electrons captured per grey scale) for comparison. Clearly, if a scanning imager is employed, as opposed to a camera, changing the exposure parameters whilst collecting a single scene must be performed with great care.

Therefore, with the perhaps the exception of instruments that have very accurate radiometric calibration, the ability to implement automatic exposure control enhances the value of the imagery by making full use of the camera's dynamic range. This not only makes better the utilisation of the communications channels, but also improves the signal-to-noise characteristic of the imagery. If data reduction is used on the final image, the compression achieved for a correctly exposed image will not be as high, but much more of the scene's fine detail will be recorded. In most instances (except perhaps for real-time services), improving the quality of an image will be more of a driving factor than reducing the bandwidth required to transmit it, making exposure control a desirable asset..

7.1.2 IMAGE PREVIEWS.

In practice, many scenes captured by the imaging systems on any satellite will be of little interest. In particular, images from medium and high resolution systems will often be completely dominated by clouds. If the mission's, or even that particular image's, objectives are to view surface features (land and sea), these cloud-filled images will be of no interest. Expending valuable downlink capacity on these useless images clearly reduces the system's productivity. If it is possible to 'edit out' poorly exposed and / or uninteresting images, more downlink time can be devoted to desirable scenery.

As discussed in section 3.4.1, the operation and data handling of most conventional remote sensing payloads is uncomplicated: an image is scheduled, captured and the data returned to the ground station. If the image is poorly exposed or contains no interesting features, it will be transmitted nonetheless. To reduce wasting the precious resource of the microsatellite's downlink that this entails, a technique of image previews was developed for SSTL cameras in 1992.

In addition to transferring the full image to the OBC, the transputers also generate a highly compressed version of the image. This is a very simple process whereby the image is subdivided into small tiles of a few pixels and only the mean value of each tile is transferred. After some experimentation, tiles of 4 by 4 pixels were determined to achieve the best trade off between compression and retaining enough of the original image features. Although much of the scene detail is lost in these thumb-nail images, the main features are still discernible. Certainly it is possible to assess the quality of the exposure, and to identify the larger features in the image (regions of land, sea and cloud) and determine how useful the image is likely to be for the end user. Figure 7.1.2a shows an image captured over the delta of the Mekong river in southern Vietnam in February 1995, and figure 7.1.2b is the corresponding thumb-nail image.

Figure 7.1.2a

PoSAT-1 narrow angle image of the Mekong delta.

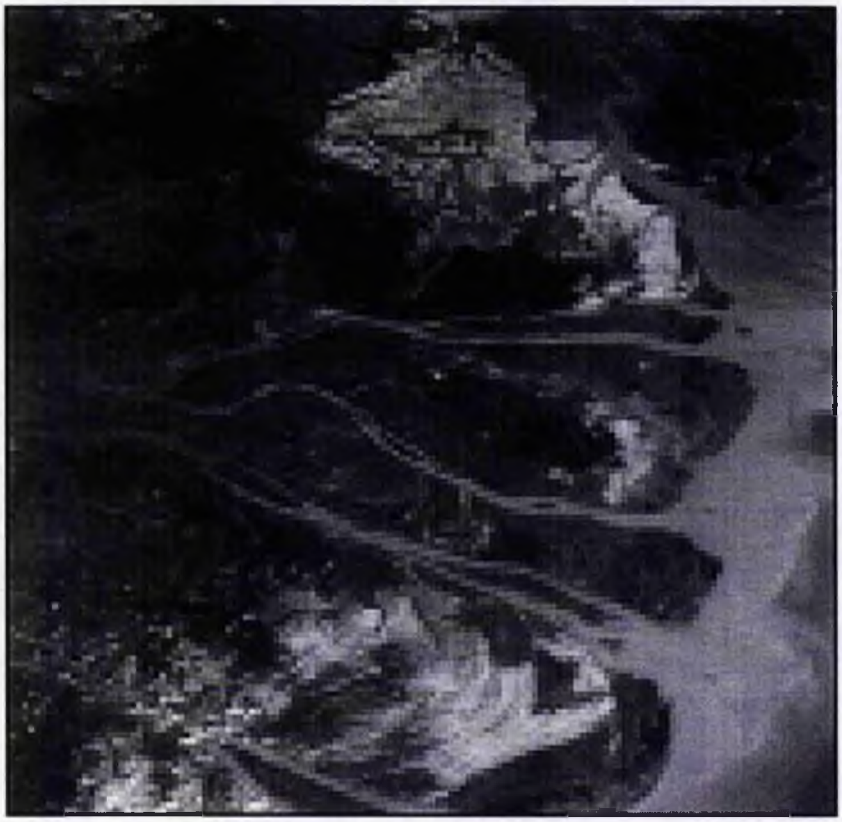

Figure 7.1.2b

Thumb-nail image of the scene in figure 7.1.2a.

Although the files are produced at essentially the same time, the ground station software is automated to always download the thumb-nail images prior to other forms of imagery. This gives ground controllers the opportunity to inspect the thumb-nail files and decide which of the full images should be retrieved and which may be discarded. Once all the high priority files have been retrieved, the ground station's default settings download the remaining full images, so no data gets lost in the absence of a firm decision from ground control.

Although relatively simple to implement, the availability of the thumb-nail images is of great help in practice. During PoSAT-1's first six months in orbit, 22 and 32 % of the wide and narrow angle images respectively were rejected on the basis of these thumb-nail images. (Thereafter, a number of additional techniques have been added, as described in the following sections, but the percentages are similar). The rate of discarded images depends heavily on the prevailing weather conditions of the target regions; very low (tropical) and high latitude (temperate and polar regions), and coastal targets have correspondingly higher cloud cover than arid or continental climates, resulting in a higher rate of abandoned images.

Using tiles of 4 by 4 pixels to generate the thumb-nail image results in a 16 times size reduction, so that this file is only 20 kBytes long. Of course, if a given full image is subsequently downloaded, the thumb-nail file represents an unnecessary overhead. Nevertheless, provided enough images are discarded prior to transmission as a result of the thumb-nails (as has been the case), it is a useful addition to the imaging experiment. Despite the overheads, the use of thumb-nail files alone has increased the number of images captured from PoSAT-1 by 26 %. (If the overhead of the thumb-nail is ignored, the improvement is 36 %). Of course, by using more sophisticated compression routines, it would be possible to obtain even smaller thumb-nail images whilst maintaining better preservation of detail. However, the increased processing requirements (and associated delays) for these 'improved' thumbs-nails would probably offset the small gains in extra compression.

7.1.3 AUTONOMOUS IMAGE ANALYSIS AND SELECTION.

An extension to the concept of using thumb-nail images to discard images of identifiably little interest is to implement the rejection process on board. The principle reason for eliminating images is the predominance of clouds, resulting in either monotonous, or occasionally over exposed, images. (Of course, monotonous scenes cannot be transformed into interesting images by exposure control). Because of the excessive presence of clouds, many of the images rejected by the ground operators have distinctive grey scale distributions (their histogram) reflecting an absence of interesting features. Therefore, by making the on-board processors analyse the distribution of grey levels, poor exposure and image invariance can be deduced autonomously, allowing the computer to assume some of the responsibilities for image assessment.

Since April 1994, the PoSAT-1 transputers have been implementing simple checks to look for grossly over and under exposed images, and images with poor distribution of grey levels corresponding to scenery of little variation caused by uniform clouds or sea. (As alluded to in section 7.1.1, the exposure of the PoSAT-1 cameras is generally biased toward slight over exposure to provide greater contrast of land features at the expense of uninteresting clouds. Therefore, the saturation of cloudy images is not as uncommon as on other missions, and indeed occurs fairly frequently). Images failing to meet the transputers' quality criteria are simply not transmitted to the on-board computer for downloading. The thumb-nail files are still generated as normal to let ground control assess the accuracy of the transputers' decision making.

During the initial testing phase of the experiment into on-board image assessment on PoSAT-1 (i.e. the first six months of operation), the transputers rejected 10 % of wide angle and 22 % of narrow angle images in this way. Thus, the transputers automatically detected that about a fifth of all images are suitable for discarding. Of course, some scenes are subsequently discarded by the operators assessing the thumb-nail images. These generally contain significant amount of broken cloud and, whilst obscuring much of the land features, do not possess the uniformity sought by the transputers' algorithm. For the same six month period, a further 10 % and 14 % of images were deleted by ground operator, raising the combined rejection rate to 20 % for wide images and 35 % for narrow images. This is virtually identical for the period when the decision-making was entirely ground-based.

During the trial phase, there were only two cases where an image was discarded which would have been selected by a human operator. Both cases involved narrow angle images of small islands surrounded by sea; the transputers mistook the uniform darkness of the sea to indicate that the image was under exposed, even though the land masses were correctly exposed. The rejection parameters have been adjusted subsequently and no more incidents of this type have occurred. The two lost images would pass the current criteria. Since then, there have been a few incidents (under a dozen in over four thousand scenes analysed) of images rejected by the computers that might have been retained by a human operator; all of these involve a small patch of interesting land being visible though the otherwise dense cloud.

Although relatively simple, this on-board image analysis offers a significant advantage in relieving the ground operators of having to perform the image assessment tasks so rigourously. This is particularly important in maintaining the low operating cost of microsatellite missions, enabling the ground station to be left unattended at night and at weekends. Under these circumstances, the ground station computers have a number of default settings for the order in which files must be downloaded. As all images are of equal priority, they will be transmitted in order, regardless of the image quality. By having the transputers weed out the worst images, a higher percentage of desirable image will be downloaded during these unsupervised periods, which represent around 70 % of passes.

Of course, if no mechanism for image previews is implemented the benefits of autonomous image assessment are even greater. This process is commonly known as 'cloud editing', and although a popular theme at the moment in the specification for future remote sensing satellites, the author is not aware of any satellites other than SSTL's microsatellites that have actually implemented this in orbit. For example, the NASA SSTI (Small Satellites Technology Initiative) Lewis intends to demonstrate cloud editing as on of its 'key new technologies' [Reichhardt]. The flexibility of the transputer processing unit has allowed valuable image analysis on these small spacecraft much sooner than on conventional spacecraft.

7.2 IMAGE COMPRESSION.

The techniques mentioned in the two previous sections have enabled PoSAT-1, in particular, to enhance the value of the imagery obtained over the narrow communications channel by eliminating uninteresting images prior to downloading. However, around fifty percent of images captured by the cameras are deemed worthy of transmission. For these images, it is appropriate to implement compression to further improve the yield on the remote sensing microsatellite's downlink.

There are numerous books, articles and papers describing many different aspects of image compression. [Jain], [Netravali & Limb] and [Kunt et al] are seminal papers in this field from the early 1980's. While theoretical works abounded on the subject prior to this, the growing availability of reasonably priced computers in this era transformed this theory into a practical discipline. Additionally, the author has found that [Rabbani & Jones] is a very clear and practical introduction to image compression, emphasising many 'real-world' considerations sometimes omitted from more academic publications.

In the course of this research programme, a number of simple, but effective, image compression techniques have been demonstrated in orbit. The approach has been very pragmatic, but has not penetrated deeply into the vast topic of image compression for remotely sensed imagery. Therefore, a brief summary of what the author considers relevant to microsatellite Earth observation is provided to support the in-orbit demonstrations. A number of references are included to provide the start of a 'paper trail', but the author has not performed an exhaustive literature search in this area.

7.2.1 OVERVIEW OF THE PRINCIPLES OF IMAGE COMPRESSION.

In contrast with the heuristic approaches to bandwidth optimisation described earlier in this chapter, image compression is a well developed field of image processing. The basic premise of image compression is that there are significant similarities, or correlations, between neighbouring pixels in any image. Rather than merely transmit the image pixel by pixel, it is possible to reduce the total volume of data necessary to represent the original scene by describing the similarities and / or differences between pixels, and sending this information instead. Therefore, compression uses various mathematical operations to remove some of the redundancy present in images.

There are two broad classes of image compression: lossless and lossy compression. As the name suggests, lossless techniques are fully reversible so that encoded images can be decoded to reproduce identical copies of the original. Conversely, lossy algorithms sacrifice some of the scene details to achieve significantly greater compression with, hopefully, minimal impact to the overall perception of the image.

The two main criteria for assessing the performance of a compression algorithm are the reduction in data obtained versus the fidelity in preserving the features of the original image. An algorithm's efficiency at packing data is expressed simply by the ratio of the file sizes of the original and compressed image it achieves (the compression ratio). To be representative, the size of a compressed image must also include any look-up tables or other coding overheads which need to be transmitted to extract the image. Routines with higher compression ratios manage to reduce the image data further.

As a general rule, algorithms offering higher compression ratios introduce more errors into the imagery. (Obviously, lossless routines cause no such degradations). A procedure's ability to preserve detail is evaluated by compressing and extracting the image and then comparing back to the original. The most common means of expressing the prevalence of errors resulting from the compression process is known as the root-mean-square-error (RMSE), describing the rms error in grey levels per pixel averaged across the entire image. Therefore, an algorithm producing lower RSMEs generates fewer coding errors. While the RMSE is a quantitative evaluation of the compression-induced artefacts, it fails to describe the nature and distribution of these errors. Some algorithms cause small errors uniformly across the image, whereas others can cause localised effects such as blockiness, slew-rate limiting or loss of texture. When selecting an algorithm to compress remotely sensed imagery, evaluating the characteristics of compression errors is as important as the total RMSE value.

A third factor which can be traded off against compression ratio and fidelity with the original image is the computational sophistication of the algorithm. As would be expected, algorithms involving more complex mathematical characterisation of the image, searching for more intricate relationships between the pixels, can achieve greater compression with less degradation for a given data set. Of course, the penalty to be paid is greater costs in software development, power consumption of the on-board computers, and increased delays in delivery whilst the data is being analysed and processed. While the computing resources available on microsatellites are large compared to conventional remote sensing spacecraft, they are not comparable with the VAX and Sun work-stations typically used for image processing on the ground.

7.2.2 COMPRESSION FOR REMOTELY SENSED IMAGERY.

Much of the current research in image compression is geared towards applications such as digital television and 'head and shoulders' video conferencing, where the degradations caused by the compression are assessed in terms of subjective visual impact. In these and many other applications, the trade-off between data reduction and loss of fidelity is based on the intended audience's appreciation of image quality. Excessive degradations may be unpleasant, but will not have any serious repercussions, especially if are only experienced temporarily.

Conversely, the compression techniques used for remotely sensed or, even more importantly, medical imagery must not cause errors that would prejudice the analysis or diagnosis processes which depend on the data. When Earth observation data is used for environmental or military monitoring, the presence of errors in the imagery (of all types, not just compression-induced) can result in faulty interpretation. Therefore, errors introduced by the processing stages must be minimised, or at least constrained to those types of artefacts which can be accommodated by the analysis procedures.

In addition to being used for 'objective' applications, the nature of remotely sensed imagery is different from many other forms of image information. In general, this data is richly textured, containing numerous small details. Given that it is the fine geometric and radiometric structure in satellite images which enables changes on the Earth's surface to be monitored with precision, it is important that any processing or compression applied to the data preserves these features. When looking for subtle changes in vegetation or hydrological patterns, receiving approximations of the scene may destroy all of the vital information needed for the analysis. As just mentioned, if the integrity of the imagery is damaged by the compression process, the value of the data may well be compromised.

The need to preserve this detail makes the task of effectively compressing satellite imagery more challenging. Many types of compression algorithm sacrifice these critical features to achieve greater compression. Apart from expanses of sea, cloud or ice sheets, large areas of uniformity are rare, limiting the opportunity for clustering techniques to be used. Finally, as there are no straight lines in nature (apart from the occasional evidence of human activity), satellite imagery will be mainly composed of fractal shapes and any straight line or blocky artefacts will be highly noticeable. The need to respect the delicate detail in the imagery is a key aspect in selecting an algorithm for remote sensing applications.

Having just stressed the importance of preserving the delicate structure of remotely sensed images, there are many applications for Earth observation data which are more resilient to compression errors. The key to successful deployment of image processing and compression is to assess the user's requirements for any given type of imagery, and use appropriate coding. With flexible on-board microprocessors, it is feasible to support a number of compression routines, selecting them as dictated by the final destination of the data. Indeed, it should be possible to train a computer to analyse the imagery and select the compression scheme accordingly.

If image previews are used on a remote sensing mission, the compression routines should be compatible with this. In particular, if a thumb-nail image has already sent a good representation of the scene to the ground, this data should be re-used as far as possible in the compression proper to minimise overheads. Therefore compression algorithms which decompose the image into low and high (spatial) frequency components, to be processed and transmitted separately, are more amenable to implementing previews. Conversely, routines which handle on the image in blocks, treating them as discrete sub-images, or coding the entire image in a single operation tend to be less suited to image previews. In the brief review of image compression techniques which follows, those algorithms directly compatible with generating quick-view images are identified.

7.2.3 LOSSLESS COMPRESSION.

Lossless image compression can be considered a branch of traditional information theory, whereby the data is coded to allocate 'symbols' to data bytes or sequences. Image coding differs from other forms of text or data reduction principally by accommodating the distinctive characteristics of imagery. [Jain], [Netravali & Limb], [Cappellini], [Jayant & Noll] and [Rabbani & Jones] provide good introductions to a number of lossless image compression algorithms. Similarly, [Börger] presents a detailed study of a number of lossless algorithms, although the reader is warned that many of the 'proprietary' schemes described are in fact minor variants of well established 'public' routines.

Because they guarantee preservation of all image details, and the computational demands of implementing them are relatively modest, fully reversible codes are often favoured for archiving remotely sensed data. However, their compression is modest, especially for well-exposed scenes with lots of detail. In practice, compression ratios of better than 2 : 1 will be rare.

7.2.3.1 Huffman coding.

One of the most common forms of lossless compression is known as Huffman coding, which utilises variable length code-words. By attributing short codes to common grey levels (or indeed pixel sequences) and longer codes to increasingly infrequent grey levels, the entropy (i.e. the information content per bit) can be increased, and the total number of bits to be transmitted can be reduced. However, Huffman coding requires the transmission of a code table along with the image data, relating the code-words to the individual grey levels. This represents an overhead and effectively prohibits real-time transmission because the complete image must be stored and analysed on-board to establish a table of probabilities before transmission.

Unfortunately, the histogram distribution of many remotely sensed scenes are quite uniform, limiting the scope for compression by substituting codes for the original. Huffman coding relies on the image histogram being condensed and peaky to achieve significant compression. The author's preliminary attempts at implementing Huffmann compression on a sample of PoSAT-1 imagery were unsuccessful, with the 'compressed' file being several times larger than the size of the original image due to the presence of significant coding overheads. Although better results would no doubt be obtained by devising a more suitable procedure for generating the coding table, but the compression ratios are still likely to be modest (no better than 1.5 : 1 for well-exposed imagery).

7.2.3.2 Run-length coding.

Run-length coding is a technique which is effective if many sets of neighbouring pixels have exactly the same grey level. Long runs of the same grey level can be coded as a value, followed by the number of pixels in the run [Jayant & Noll]. However, given the richly textured nature of remotely sensed imagery, run-length coding will not compress effectively. If grey levels can be rounded by a few counts, the compression will be higher. In fact, run-length coding is mainly used for imagery that is either very homogeneous or quantised to only a few grey levels (such as the binary images from facsimile machines), and therefore is not well suited to sensitive satellite imaging systems.

7.2.3.3 Differential pulse-code modulation.

Differential pulse-code modulation (DPCM) is a type of reversible image compression more suited to remotely sensed images. Instead of transmitting absolute grey levels for each pixel, only the difference in grey level between a pixel and its predecessor is sent [Cappellini]. As described earlier, most pixels in a region of a satellite image will be closely clustered around a local mean with fairly small variations from pixel to pixel. (This is why the thumb-nail images used on SSTL microsatellites provide a good representation of full imagery even though the fine texture is lost).

Although the histogram of a remotely sensed image will be well distributed, the spread of the differences between neighbouring pixels are generally more tightly clustered. Therefore the output of a DPCM compressor can be Huffmann encoded for further data reduction. [Gonzalez & Wintz, p.244-253] provide an example of using lossless DPCM followed by Huffman coding to compressed two sets of LANDSAT MSS data. [1] Predictive variants of DPCM are often implemented to make further use of the correlations in the image by estimating the next pixel given some function of the previous history of the image. By running identical prediction routines on the satellite and on the ground, the image data is transmitted in terms of an 'error' signal reflecting the divergence of the image from the predictor. A number of predictive schemes are detailed in [Börger] and [Jayant & Noll].

Although, DPCM is essentially a reversible compression technique, the output of the coder is often limited to a specific range (e.g. using 6-bits to cover differences from -32 to +31), losing some of the image information through slew-rate limiting on sharper scene transients. These losses are confined to obvious features in the images (indeed most frequently at the edge of clouds contrasting against the surrounding land or sea), but result in significant compression savings due to the simplified coding processes. Nevertheless, given that the image is based on the differences in pixel value, any single error in the data stream from the decoder will cause the rest of the sequence to also be in error, effectively applying local offsets to the image after each incorrect pixel extraction. It is vital, therefore, that the encoder accommodates any slew-rate errors which occur, applying remedies as soon as possible to prevent gross errors from accumulating.

If a thumb-nail image has already be transmitted, it is possible to use DPCM to encode the differences between the local mean (provided by the thumb-nail) and the actual pixel values. It is likely that the variance of the output data stream will be more tightly clustered than if the conventional pixel-by-pixel approach is used, and therefore provide

---

[1] LANDSAT MSS data is expanded from 6 to 7 bits during ground processing to compensate for the transfer functions of the numerous sensors. [Gonzalez & Wintz] treat this data as a 7-bit entities, even though there is only ever 6 bits of information. Furthermore, the image histograms only use half of the system's dynamic range, reducing the effective information content to 5 bits. The DPCM / Huffman coding describes the data with 3.11 bits per pixel (over the four spectral planes), achieving an effective compression of either 56%, 48% or 38% depending on one's interpretation of the source data's information content.

more compression when subsequently Huffman encoded. Even if this is not true, the algorithm will be simpler as errors will only ever effect single pixels, and cannot propagate through the image.

7.2.4 LOSSY COMPRESSION.

There are numerous forms of non-reversible compression using diverse mathematical operations to describe the characteristics and correlations of the imagery. However, such compression degrades the image in as much as it is not possible to completely reconstruct an exact copy of the original. To achieve higher compression ratios, lossy algorithms make various approximations when describing certain forms of high frequency spatial features and minor radiometric changes. It is these rounding operations that introduce inaccuracies in the reconstructed imagery. However, for most techniques, it is possible to adjust the compression parameters to ensure that the degradations remain within specific limits. The trade-off between compression and fidelity is complex, but in practice for a given algorithm the relationship between the two criteria is fairly linear. Sources like [Rabbani & Jones] provide good reviews of many non-reversible compression techniques, and [Kunt et al] reviews some novel directions for future image coding.

7.2.4.1 Discrete cosine transfer coding.

The discrete cosine transfer (DCT) is one of the most popular approaches to image compression. It involves transforming an image from its conventional format in the spatial domain into the spatial frequency domain. This process is virtually identical to the conventional Fourier transform used with in one-dimensional signal processing (time and frequency domains), but applied in two dimensions across the image (spatial and spatial frequency domains). The DCT transform only uses the real part of a discrete Fourier transfer (DFT), and discarding the imaginary parts (the sine transform).

The transform itself does not result in any compression, merely an alternative representation of the image. However once in the spatial frequency domain, various approximations can be made, resulting in data reductions. Given that low spatial frequency components are the most crucial elements in describing the image, and that higher frequencies contribute less and less to the overall appearance of the scene, it is possible to encode the data with a preference towards the lower frequencies. This can take various forms, either using more bits to quantise the lower frequency components, or simply discarding the higher frequencies. These coefficients are transmitted, and the decoder performs the inverse transform to reconstruct the image as faithfully as possible given the approximations made.

In general, the DCT is preferred to the DFT because it requires real as opposed to complex processing, and has reduced 'blockiness' characteristics by minimising the prevalence of spurious spectral components [Rabbani & Jones, p.110]. Of course, the availability of fast algorithms for the DCT and DFT presents a distinct advantage for implementing these schemes on microprocessors. There are a range of other algorithms similar to the DCT and DFT in as much as they transform the imagery from the spatial to spatial frequency domain, but which offer subtle advantages. The standard literature includes the Karhunen-Loeve transform (which permits optimal coefficient selection to improve image fidelity for a given compression, but is extremely difficult to implement practically), and the Walsh-Hadamard transform (inferior compression but employing integer arithmetic only) [Jayant & Noll]. Numerous other novel derivatives of transform compression are described in the literature including, for example, Reed-Muller coding (similar properties to the Walsh-Hadamard) [Reddy & Pai], and the Scrambled Real DFT (similar performance to DCT but reduced complexity) [Ersoy & Chen].

There are a multitude of variations within the basic principle of the DCT compression, and it is not possible to describe them here. However, it is important to note that specific performance can be defined, either for the compression ratio or the level of errors introduced, by tailoring the quantisation process of the coefficients. Therefore, the degradations experienced by remotely sensed imagery can be tightly defined by selecting an appropriate coding of the transformed data.

However, the computing requirements to implement DCT compression are quite high, involving significant amounts of floating-point, as opposed to integer, arithmetic. For this reason, DCT compression rarely operates on the entire image, but on smaller blocks of data. Unfortunately, by dealing with smaller sub-images, the number of errors experienced increases as the coefficients transmitted no longer reflect the characteristics of the entire scene. As a compromise between computational simplicity and fidelity of reproduction, the image is generally manipulated as blocks of 8 x 8 pixels. However, if substantial compression (i.e. more than around 5 : 1) is demanded using this size of sub-image, there is often a pronounced blockiness to the reconstructed image, caused by discontinuities at the boundaries between blocks. For the same compression ratio, using larger sub-images results in fewer errors, but requires greater amounts of processing.

The main attraction of using a DCT-based compression algorithm is the fact that it has been adopted as a World-wide standard for image compression, endorsed by the CCITT's Joint Photographics Expert Group (JPEG) [Gonzalez & Woods, ch.9]. Because of this, there has been considerable research into the suitability of different coding schemes for different imaging applications, and the designer of a satellite remote sensing system can draw heavily on the existing literature. Furthermore, numerous implementations of the encoder and decoder are available as libraries for virtually every high performance computer system. Potentially, the most attractive aspect of the JPEG variant of DCT compression is the availability of dedicated hardware chips to support conventional microprocessors. Provided these peripheral components retain enough of the flexibility to meet the requirements of a Earth observation mission, they are very attractive because of the high speed of execution, vital for real-time imaging services.

7.2.4.2 Vector quantisation.

Vector quantisation [Gray 1980][Gray 1989 - numerous references][Linde et al] can be viewed as an extension of Pulse Code Modulation, except that instead of representing a scalar value (the brightness of the pixel), the transmitted code represents a block of image data. Conceptually, this is a fairly simple process. A vector quantiser works with a 'code-book', comprised of templates of numerous typical sub-image shapes and patterns, and assigns the most representative code available to describe each block of imagery. Thus, having removed and transmitted the local mean, the encoder describes the residual image as best it can, given the limited vocabulary of its code-book. The range of available code-words determines both the compression ratio of the image and its fidelity of reproduction; more code-words will obviously provide a better description of the original image, but requires a larger number of bits to be identified.

While the principle of vector quantisation (VQ) is really quite simple, approximating image blocks to the nearest available code-word, its implementation is rather more complex. Both the generation of suitable code-books and the decision process when assigning code-words are highly critical and complex tasks. In particular, the development of suitable code-books is vital if the reconstituted imagery is to be similar to the original. There are numerous techniques available, using code-books either predetermined and trained on representative imagery, or else generated on-board for each image, or a hybrid of both. This latter technique requires more on-board processing and will have lower compression due to the overheads of transmitting the code-book, but will provide more faithful representation. A discussion of the various strategies for code-book generation is beyond the scope of this thesis.

The results presented in [Rabbani & Jones] conclude that VQ is a technique suited for very high compression ratios but with correspondingly significant degradations. Similarly, their worked examples confirm this, with substantial loss of subtle detail. It is the author's opinion that VQ is therefore most suited to generating image previews, with subsequent data used to provide the fine detail required for remote sensing applications. This application is alluded to in [Israelson & Harris].

The application of VQ in remote sensing may be more appropriate in the field of compressing multispectral imagery, coding in the spectral rather than in the spatial domain [Gupta & Gersho][Jaggi]. As there is generally greater correlation between co-registered pixels in different spectral planes than between neighbouring pixels within a single colour plane [Memon et al], there is reasonable scope for implementing effective and accurate coding in this dimension. Furthermore, many applications employ computers to 'cluster' and 'classify' pixels based on their spectral characteristics; the output of the classification is often of more use than the absolute radiometric brightnesses of the pixels. Therefore, it would be quite feasible (and useful) to combine the vector quantisation and classification stages.

7.2.4.3 Sub-band coding.

Sub-band coding (SBC) is an image compression algorithm which is becoming more popular with the development of new digital signal processing (DSP) techniques and increasing availability of suitable hardware. The image signal is separated into frequency bands by an array of carefully matched filters [Gharavi & Tabatabai]. The output of these filters are multiple image planes visibly containing various image features. Viewing these planes, the lowest frequency sub-band is a clear representation of the image, but at reduced resolution, similar to the 'thumb-nail' images described in section 7.1.2. The higher planes are busy in heterogeneous regions of the image, and uniform in homogeneous regions. The very highest frequency planes are virtually white noise. Given that the various sub-bands do not possess the full bandwidth of the original scene, they can be sub-sampled without any loss of information.

When the image has been filtered into these frequency sub-bands, different schemes can be used to code the various image planes. In many ways, SBC is reminiscent of the DCT, in as much the encoding extracts the low and high spatial frequencies, allowing them to be manipulated separately. Once again, the filtering stage of a SBC compressor does not provide any data reduction; it is the selective encoding of the various coefficients according their relative contributions to the overall image that provides the compression.

[Rabbani & Jones] discuss a number of possible coding options. Generally, the lowest sub-band is encoded in a lossless DPCM (section 7.2.3.3) to exploit the high correlation between pixels. The higher sub-bands are either coded in lossy PCM, or some more exotic fashion, for example vector quantisation. Subsequent Huffman coding is effective at reducing the data sets of the higher frequency sub-bands because of the reduced correlation between pixels. Indeed, in some instances the highest frequency sub-band(s) can be discarded altogether. The effect of the coding choices will depend on the image statistics and the degree of fidelity demanded. A feature of compressing the sub-bands individually is that the errors introduced are distributed more evenly across the image than with DCT or VQ which produce distinct blockiness. Clearly, depending on the aggression of this coding phase, it is possible to implement either lossy or lossless compression with SBC.

The principle difficulty in implementing SBC is designing the filters to separate the frequency sub-bands without introducing any over-lap or aliasing. As this is not possible in practice, carefully controlled aliasing must be introduced to allow the filters to be implemented. In general, digital filters known as quadrature mirror filters (QMFs) are used [Pei & Jaw][Lhuillier & Nguyen][Vaidyanathan] to provide matched cut-offs and to preserve gain and phase response within the sub-bands. A compensating filtration stage must be applied in the decoder to remove the effects of the aliasing. [Rabbani & Jones] suggest that other filter designs may prove advantageous in certain applications.

Given the similarities between SBC and DCT image compression, it is not surprising to find that the performance of these two algorithms in terms of compression ratio, fidelity to the original image and computational requirements are equivalent. The principal computational requirement is the very large number of addition and multiplication operations needed to implement the digital filter, and the large amount of memory to store the individual sub-bands. In practice, this processing overhead will preclude the use of SBC in software-only systems. However, the availability of programmable hardware implementing 32- and 64-tap filters makes this strategy considerably more feasible; in particular, Inmos Ltd manufactures this type of product, making it highly compatible with the transputers already featured in SSTL microsatellites.

Conversely, decompression is very simple, with the decoded sub-bands simply being added together, after being passed through the anti-aliasing filters. If the encoder's filters had 'brick-wall' cut-offs, then this extra filtration in the decoder would not be necessary.

Despite the similarities between SBC and DCT compression, SBC is probably more attractive to remote sensing applications because of its flexibility and the successive transmission of the sub-bands. By retrieving the lowest sub-band first, this strategy implicitly provides a mechanism for delivering image previews. The ground station downloads sub-bands until the desired level of reconstruction has been achieved. Furthermore, standard SBC can be extended to add an additional file containing the residual errors caused by the compression, to be downloaded only for the most demanding of applications which cannot tolerate any errors. Finally, there is significant scope for adapting the coding strategies used for the various sub-bands, depending either on the image contents or on the user's requirements; these variations can be accommodated more easily within SBC than the other compression algorithms presented.

7.2.4.4 Block-truncation coding.

Block-truncation coding (BTC) is, in some ways, similar to vector quantisation or DCT compression because the image is divided into blocks which are then coded independently from the each other. However, BTC [Mitchell & Delp][Halverson et al] is far less demanding computationally than these two techniques, and provides a high degree of fidelity to the original image. Despite the correspondingly modest compression ratios, these features make this scheme attractive for remote sensing applications.

The block sizes used for BTC are typically 4 by 4 pixels. The encoder extracts the mean of this block, in exactly the same way described for the 'thumb-nail' images in section 7.1.2. The encoder also provides the variance of the pixels about this mean, as well as a bit-map describing whether each pixel is greater or smaller than the mean (i.e. the block is thresholded by the mean). During reconstruction, each pixel is assigned to one of two values (the mean plus or minus the variance) as dictated by the bit-map for that image block. Moment-preserving encoders are often used to skew the variance value to reflect the statistics of the block more accurately.

It is clear that this approach results in significant errors in the radiometric accuracy of the reconstructed imagery. Conversely, it preserves features and small details with greater fidelity than many other compression algorithms. [Rabbani & Jones] suggest a number of augmentations to standard BTC, making it adaptive and allowing it to respond more appropriately to the varying conditions across the image; adding several adaption levels allows the encoder to use fewer bits to describe uniform areas and to devote more bits to image regions containing significant activity, giving a more faithful rendition of the original image.

The adaptive extension to the standard BTC involves selecting a slightly different compression scheme depending on the variance of the sub-block. Following detailed experimentation [Brewer], the following thresholds were established for PoSAT-1 imagery: if the 4 x 4 pixel sub-block has a variance of 0 or 1 grey levels (typical in clouds, sea or other highly uniform areas), the mean value alone will suffice to reconstruct this part of the image. If the variance is between 2 and 9 grey levels, the conventional BTC algorithm is used. Finally, if the variance is greater than 10, indicating significant local image activity, the basic 4 x 4 pixel tile is broken down into four 2 x 2 tiles, which are themselves BTC coded, providing a more detailed description of the sub-block. It would be feasible to accommodate further adaption levels, but the returns would probably be minimal.

Although the bits per pixel is fixed depending on the level of adaption selected (0.5 bits / pixels for low variance, 2 bits / pixels for medium variance, and 5 bits / pixels for high variance), the overall image size will depend on the number of each category of sub-block found in the image. A further two bits per block (0.016 bits / pixel) of overhead is required to support this adaption to inform the decoder which procedure is needed for decompression.

The basic BTC technique of extracting the image blocks' mean and variance is often mixed with other forms of compression to encode the residuals. In particular, vector quantisation [Udpikar & Raina] can be used to describe this bit-map. The compression benefits will be enhanced if the blocks contain larger numbers of pixels (e.g. 6 x 6, 8 x 8).

7.2.4.5 Fractal compression.

Using fractal transforms for image compression has received a great deal of attention in the technical press recently, with claims of dramatic compression ratios in excess of 100 : 1 frequently being made. Unfortunately, the amount of media attention and hyperbole surrounding this procedure, which is patented and marketed commercially, has clouded the perspective on the relative merits of this technique.

The principle of fractal encoding is to decompose the image into a few basic shapes or patterns. The image is then reconstituted by a series of affine transformations (scaling, rotation, translation) of these 'building blocks'. This is based on the principle of 'self-similarity' of many types of signals or imagery, whereby enlargements of small sections of the data carry some resemblance to the whole; for example, a coastline is always 'crinkly' regardless of how closely is it viewed [Fisher].

Unfortunately, due to the commercial secrecy surrounding this algorithm, it is difficult to develop much further on the practical implications of fractal compression for remote sensing applications. However, a review paper [Clarke & Linnett] provides some indications. Their conclusion is that fractal coding produces imagery which is very similar, but undeniably different, from the original image. This is caused by the fact that while images may possess 'self-similarity', they do not posses the 'self-indenticality' of abstract fractals. For example, they site the ubiquitous fractal fern; while the image is clearly recognisable as a fern, it does not form a truthful representation of any actual fern. Correspondingly, they anticipate that fractal compression will be of most use in applications such as computer graphics or animation, where synthetic, but realistic-looking scenes are required. Even the creators of the fractal transform, [Barnsley & Sloan] in a technical report for NASA, concur that their system is most applicable for image sequences where successive images are very similar, and fractal coding would describe these changes very efficiently.

When compressing real-world still imagery, fractal encoding appears to be significantly less efficient than when describing these stylised objects. [Clarke & Linnett] comment that the results published in professional, refereed journals for fractal compression [Jacquin] are not much different from other, more established algorithms such as vector quantisation. Therefore, with the field of remote sensing, it would seem that fractal compression is best suited for generating highly compressed image previews. However, [Barnsley & Sloan] claim that a lossless version of the fractal algorithm exists, but do not provide any details.

Regardless of these considerations, it is certain that the fractal encoding of images is extremely demanding of computing resources, much more so than any of the other algorithms already mentioned. Realistically, it is necessary to employ hardware accelerator cards to perform this compression, which may represent an unacceptable overhead on microsatellite missions. The encoders are highly asymmetric, with the computing requirements for decoding being less than for JPEG [Iterated Systems]. This makes fractal compression most suitable for tasks like archiving where the information will need to be retrieved frequently. Given these traits, it is not surprising to discover that

Microsoft uses a licensed derivative of fractal coding for its CD-ROM encyclopaedias. In these circumstances, the coding asymmetry, the high compression ratios, and subjective and uncritical eye of the users makes this approach to image compression attractive.

However, as discussed in section 7.2.2, users in the field of remote sensing have rather different expectations from compression algorithms. Despite the extremely high compression ratios claimed, the apparently poor image fidelity and difficulty in encoding the data leads the author to believe that fractal image compression is not compatible with the needs of microsatellite remote sensing. The veil of secrecy and hype surrounding fractal image coding has made comparative evaluation of this process very difficult. Nevertheless, the revolutionary approach of this compression strategy is worthy of interest, and future developments may make fractal compression more attractive for encoding remotely sensed imagery.

7.2.5 IMAGE COMPRESSION WITH UOSAT-5 DATA.

In 1992 and 93, the impact and effectiveness of various image compression algorithms was evaluated on a number of UoSAT-5 images. This student project was performed in collaboration between the University of Surrey and Spar Aerospace Ltd (Canada). Although the bulk of the work was implemented by two students in Canada under day-to-day supervision at Spar Aerospace, the author was involved in the selection of compression procedures and in reviewing the results, and enjoys a co-authorship of [Montpetit et al] describing the results of the study.

Sample UoSAT-5 images were coded using a number of different algorithms including two forms of the discrete cosine transform (DCT), block truncation (BTC), vector quantisation (VQ), as well as a couple of lossless methods. Because this microsatellite operates in the amateur frequency bands, any compression routines deployed must be available to the amateur radio community. Therefore, the algorithms tested included standard compression techniques widely described in the literature, and precluded any proprietary strategies developed by Spar Aerospace.

The DCT was implemented using both the conventional 8 x 8 kernel (as used in the JPEG standard) and a smaller 3 x 3 kernel. The BTC used 4 x 4 tiles in a non-adaptive mode, giving a fixed compression ratio of 4 : 1. These two algorithms were implemented using publicly available software. The VQ was written by the students at Spar Aerospace, merging software from other sources. The vectors were 4 x 4 blocks, and used a simple code-book with 16 code-words to achieve a compression of 8 : 1. The code-book was trained on other UoSAT-5 images not used for this survey, and its development proved difficult and time-consuming given the highly irregular nature of the remotely sensed data. The lossless Huffman and GIF [Compuserve] routines were also used to provide a benchmark against which to test the other compression procedures. As expected, the lossless coders achieved only very modest data reduction.

The algorithms were first tested on the standard 'Lena' image to ensure that the results were compatible with the literature, and then evaluated on eight UoSAT-5 images. Figure 7.2.5a shows a typical UoSAT-5 test image from October 1991 of the Karakoram mountains in the western Himalayas and the Tarim Basin. Figures 7.2.5b through f show an enlargement of original image and the same area from the decompressed images, allowing them to be compared side-by-side. Compression ratios and root-mean-square-errors (RMSEs) of the various routines were compared, and the results averaged across the eight images are shown in table 7.2.5. Overall, these statistical characteristics and the visual effects of the algorithms are compatible with the general expectations.

Method	Input Size	Output size	Ratio		RMSE
VQ (4 bits)	361469	45173	88 %	8 : 1	22.9
DCT-3	361469	49244	87 %	7.3 : 1	14.5
DCT-8	361469	38098	91 %	9.2 : 1	14.2
BTC	361469	89744	75 %	4 : 1	15.5
GIF	361469	270000	25 %	1.3 : 1	0
Huffman	361469	227700	37 %	1.6 : 1	0

Table 7.2.5 Performance of compression algorithms on sample UoSAT-5 imagery.

Based on both the compression ratio and the RMSE figures, it appears that the 8 x 8 DCT provides the best results. Similarly, the final chapter of [Rabbani & Jones] (which reviews a dozen different compression algorithms including DPCM, DCT, VQ, SBC and BTC), concludes that DCT-based algorithms provide the best signal-to-noise (i.e. fidelity of reproduction) to compression performance. Presumably, this is a direct result of the routine's computational complexity, and the background of intensive research which no doubt permits programmers to select compression coefficients optimally.

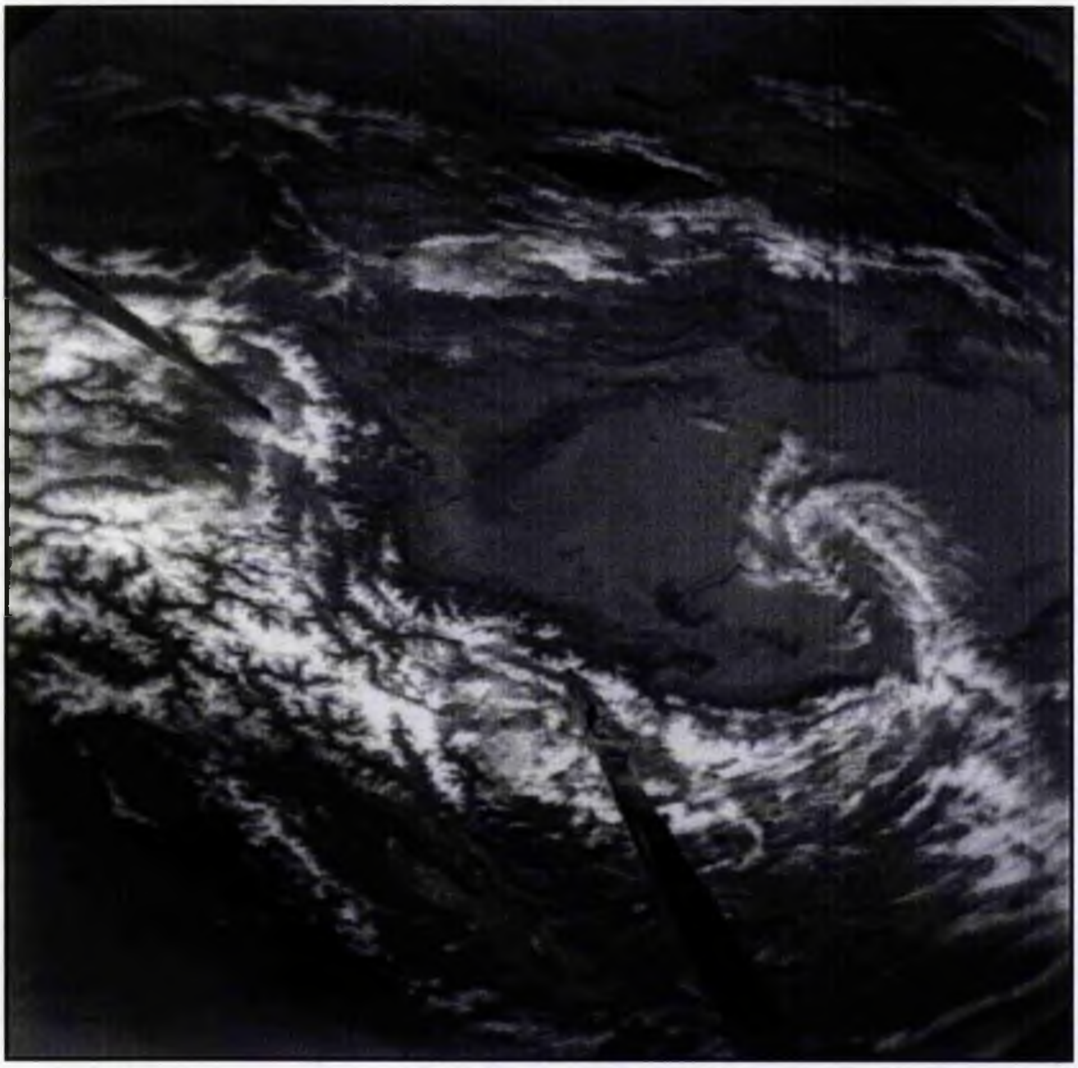

Figure 7.2.5a Original UoSAT-5 'Karakoram' image prior to compression.

However, despite providing 9 : 1 compression and the best RMSE, the DCT-8 (figure 7.2.5d) algorithm undeniably introduces a very objectionable blockiness to the image, destroying many of the original features. Indeed, when viewing these sub-images subjectively, it is hard to believe that the DCT-8 produces the best statistical results, confirming the objections many people, including [Rabbani & Jones] and [Barnsley & Sloan], have to using the RMSE as a measure of fidelity. The DCT-3 (figure 7.2.5c) also features this blockiness but to a much less objectionable degree.

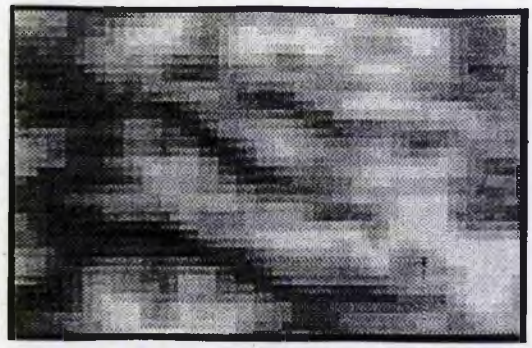

Figure 7.2.5b

Original sub-image.

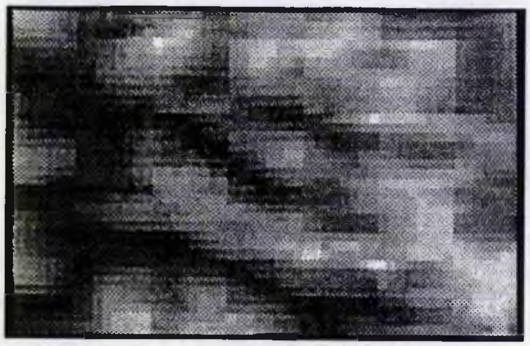

Figure 7.2.5c

Decompressed DCT-3 sub-image.

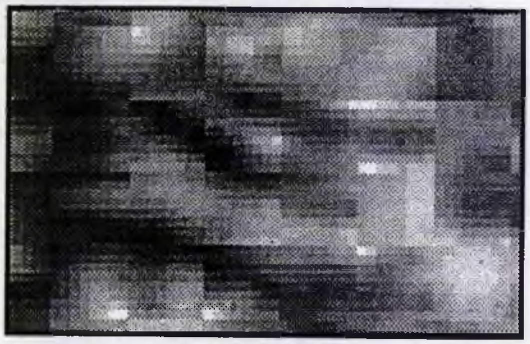

Figure 7.2.5d

Decompressed DCT-8 sub-image.

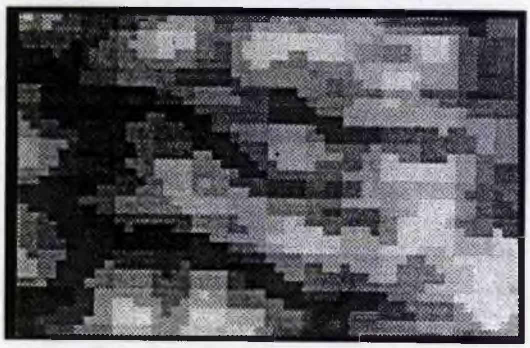

Figure 7.2.5e

Decompressed BTC sub-image.

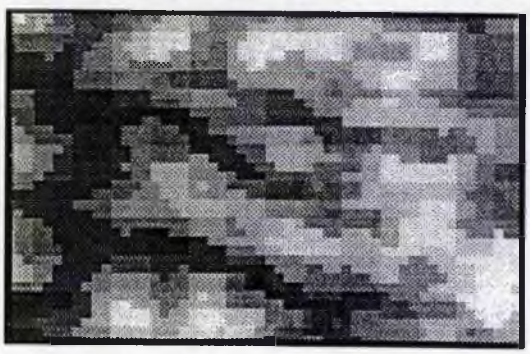

Figure 7.2.5f

Decompressed VQ sub-image.

As expected, the BTC had the shortest computing time but achieved a lower compression ratio. Although the RMSE of the BTC routines is very similar, and slightly inferior, to those of the DCT algorithms, the observable degradations (figure 7.2.5e) are significantly reduced. All of the features are preserved, and even enhanced compared to the original image (figure 7.2.5b). This confirms the BTC's ability to preserve the geometric detail in the imagery, despite appreciable radiometric approximations.

The VQ has resulted in a significant compression, but the imagery (figure 7.2.5f) has suffered substantial reconstruction errors. The blurring of the original features is higher than with the other compression techniques. However, it was felt that with an improved code-book and by generating a table of residual errors, superior results could be expected from VQ coders without significantly compromising the compression performance.

Although the results of this survey were not particularly surprising, confirming many of the general characteristics and expectations for the image compression algorithms, it was useful to compare them side by side with appropriate remotely sensed data, and not have to interpolate their performance when using alternative types of imagery. The conclusions of the study were that the on-board computers should be adaptable to the needs of various users. In particular, scientific or 'value-added' users would benefit most from the feature-preserving aspects of the BTC. Conversely, for general purpose 'operational' users with less demanding requirements, the DCT algorithms provide good compression with acceptable image quality. By adhering to the JPEG standard, the satellite operators are relieved of having to provide user support for the decompression stages, relying on the widespread acceptance of this format by image display packages.

7.2.6 ON-BOARD IMAGE COMPRESSION ON POSAT-1.

Building on the results of the collaborative programme with Spar Aerospace, block truncation coding compression has been implemented on the PoSAT-1 microsatellite. In addition to delivering high quality image compression with modest computational requirements, the BTC algorithm is directly compatible with the strategy of using 'thumb-nail' images to provide 'quick-look' previews. This is accomplished by separating the mean value of each image tile into a separate file which is downloaded in preference to the remaining data. [2]

---

[2] Although the thumb-nail image has proven to be a valuable tool in reducing data volumes in its own right, this volume of data is included when calculating the statistics for image compression presented here (i.e. the thumb-nail is treated as part of the image, as opposed to a separate entity).

Rather than using the fixed-rate version of BTC tested during the first study, the operational software implemented for PoSAT-1 is the fully adaptive version described in section 7.2.4.4. On average, the compressed image files queued for the downlink on PoSAT-1 are around 90 kBytes long, with an additional 20 kBytes of thumb-nail image, corresponding to a compression ratio of approximately 3 : 1.

While the adaptive version of the BTC compression provides inferior compression to that achieved in the Spar Aerospace programme, it results in vastly improved RMSE values at around 1.5 grey levels. Tables in [Brewer] show the distribution of these error amplitudes falling off rapidly, even though the occasional pixel remain with an error as high as 50. Analysis of the error residuals showed that these large discrepancies occur principally at the edges of clouds where dramatic changes in contrast occur. To a lesser extent, this also happens on coastlines where errors can be in the region of 20 grey levels. [3] Away from these boundary regions, no errors of greater than about 6 were encountered in land-only regions of the images. Although it proved too complex (and too subjective) to verify this in practice, the author estimates that the RMSE of the 'interesting' parts of the imagery is probably around 1.0. Certainly, the test image containing numerous small cumulus clouds (Grand Canyon in [Brewer]) had an RMSE of about twice that of a clear scene (Kuwait). Interestingly, despite their lower RMSE, PoSAT-1 images containing only land and sea features will compress further than partially clouded (or snowy) scenes; for example, the Kuwait image is 25 % smaller than the Grand Canyon image.

To a small extent, the compression and RMSE can be traded-off by altering the thresholding characteristics of the adaptive algorithm, although the values finally selected by [Brewer] lie on the knee of the curve, indicating an optimal selection of threshold parameters. In the author's opinion, this should only be altered to improve the RMSE performance; if greater compression is required, an alternative algorithm will probably be more suitable. Although the transputer code uses the default thresholds determined to be optimal during ground-testing, these can be altered at any time, and the ability to download the raw imagery without any compression is also retained.

Figures 7.2.6a to c demonstrate the improved fidelity of reproduction offered by the adaptive variant of BTC over the standard version, showing the same UoSAT-5 sub-

---

[3] There appeared to be an anomalous interpretation of these results as the imagery from the Wide Angle Camera invariably delivered worse RMSE performance than the Narrow Angle Camera. Eventually this was attributed to the additional sharp transitions encountered along the edges of the satellite's antennas visible in the Wide Angle scenes; when these portions of the image are masked off, the RMSE of the two classes of imagery are comparable.

image as displayed in figures 7.2.5b to f. Both the original image (figure 7.2.6a) and [Brewer's] implementation of conventional BTC (figure 7.2.6b) are highly consistent with the imagery published in [Montpetit et al], confirming these results. However, the fidelity of the adaptive moment-preserving BTC (figure 7.2.6c) is visibly superior to that of the standard BTC, being virtually indistinguishable from the original. The compression ratio achieved with this image is 65%.

Figures 7.2.6d and f show enlargements of two original images downloaded from PoSAT-1. Figure 7.2.6d provides detail of the image of Kuwait (figure 8.2.1a), and figure 7.2.6f of the Karakoram mountains (figure 8.2.2a). Figures 7.2.6e and g show the reconstructed images after compression and decompression. With careful scrutiny, it is possible to detect slight variations in pixel brightness between the two versions of the same image. All of the structural detail and texture has been preserved, demonstrating the suitability of this algorithm for coding remotely sensed data (as expected). Although these are both examples from the Narrow Angle Camera, they are representative of all of PoSAT-1's imagery.

The Adaptive Moment-Preserving BTC algorithm was selected for image compression on-board PoSAT-1 because of the superior fidelity of the reconstructed imagery. This recognises that feature retention is generally a more important characteristic for future microsatellite remote sensing missions than raw compression power. Even with its modest compression ratio, the BTC implemented has had a dramatic impact on the volume of imagery retrieved from PoSAT-1 since the software was first executed in November 1994, instantly trebling the number of images collected from the satellite.

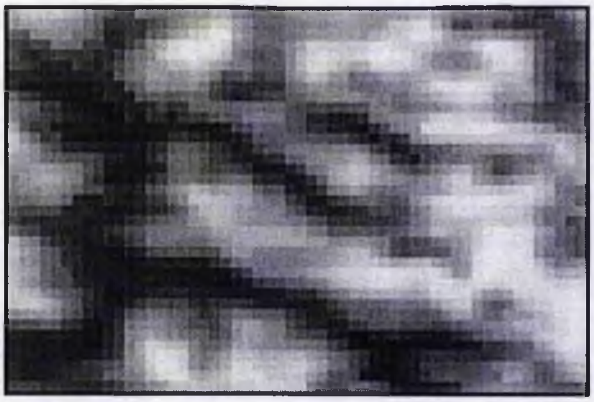

Figure 7.2.6a Original sub-image.

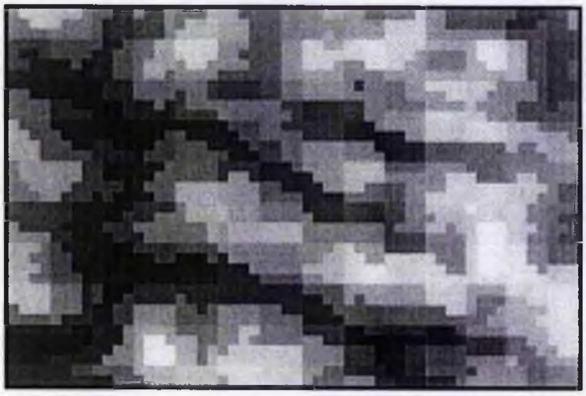

Figure 7.2.6b Sub-image compressed using standard BTC.

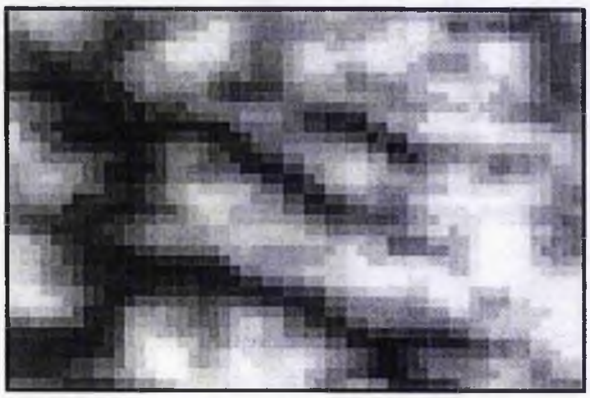

Figure 7.2.6c Sub-image compressed using adaptive moment-preserving BTC.

Original Image

Coded Image

Figure 7.2.6d

Figure 7.2.6e

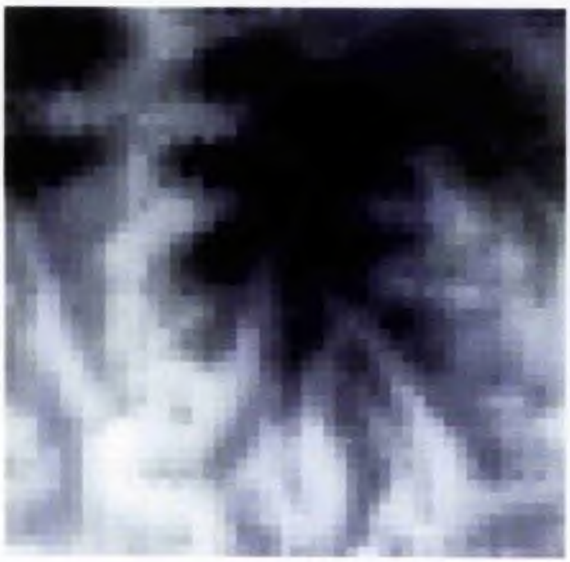

Figure 7.2.6f

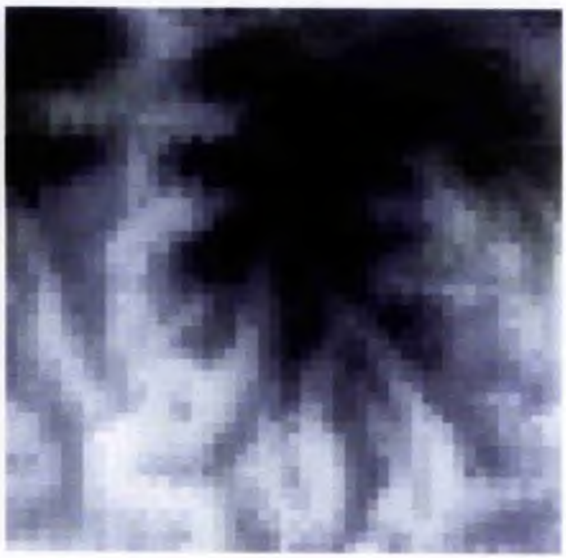

Figure 7.2.6g

7.2.7 SUMMARY.

To the author's knowledge, PoSAT-1 is the first unmanned [4] satellite to implement autonomous on-board image analysis (cloud editing) and image compression. The Adaptive Moment Preserving Block Truncation Coding selected for compressing PoSAT-1 data provides compression of 3 or 4 to 1 (depending on the data) whilst remaining very faithful to the original image. Without these measures, five images could be retrieved daily from PoSAT-1 given the total downlink capacity of 1.8 MBytes (see section 3.4.3). The addition of automatic image analysis, previews and compression has dramatically increased this daily scheduled load to around 20 images (10 wide / narrow image pairs), without any changes to the satellite's communications systems. Of these twenty images, a third are rejected, limited to extremely low interest scenes saturated with clouds. If the ground operators were more ruthless in discarding imagery, the imaging system could easily be run even more effectively.

The successful demonstration of in-orbit image analysis and compression endorses the design philosophy of using embedded processing adopted for the imaging systems flown on SSTL's microsatellites. As discussed in chapter 3, the limited communications capabilities represents the most significant limitation to the deployment of dedicated remote sensing microsatellites, and the implementation of these data reduction techniques represents a big step towards overcoming this hurdle.

The research into the use of image compression to enhance microsatellite imaging payloads only represents a small aspect of this programme. Nevertheless, because of its clear applicability to all remote sensing spacecraft, this activity has generated significant amounts of interest, even amongst sections of the industry not noted for their affinity to small satellites.

7.2.8 POSSIBILITIES FOR FUTURE IMAGE COMPRESSION DEVELOPMENTS

Despite of the compelling success of the demonstration of image compression on PoSAT-1, there are many possibilities for further developing this field of research. However, without identifying a particular usage for the remotely sensed data, and assessing the effects of the compression-induced errors on the post-processing and analysis

[4] Shuttle astronauts have used lap-top personal computers to compress imagery from hand-held digital cameras. prior to transmission to the science teams on the ground.

associated with this application, it is not really possible to make a significant contribution to the field.

Establishing these criteria effectively is a deceptively difficult task, and requires a broad understanding of the remote sensing business, spanning the two distinct groups of image gatherers and image users. It will be necessary to investigate the needs of the end users to appreciate the consequences of the compression on their activities. While it is relatively straight forward for the two groups to concur on the broad characteristics of the imagery (spatial and spectral resolution, etc.), the area of added degradations due to on-board manipulations is a far more contentious issue, and circumspection is required.

Nevertheless, the author has a few thoughts for conducting this programme. Once again, the specification for these algorithms will blend the necessary performance in terms of compression, errors introduced and computational demands. In the author's opinion, the fixed factors for most medium and high resolution (scientific) applications will be the fidelity to the original image and computational overheads, leaving the compression ratio to be the variable term. Conversely, for low resolution (meteorological) applications, the balance will probably be towards higher compression to transfer a large volume through the system, accepting the loss of image quality to achieve greater coverage; this category of users will be more readily satisfied by the types of algorithm (DCT, SBC, VQ) already reviewed.

Within both sides of the remote sensing industry, there is often a refusal to contemplate lossy compression because of the introduction of errors in the reconstructed image. However, this is something of a 'knee-jerk' reaction which fails to recognise that the imagery is imperfect to start with. Firstly, the instrument has a certain signal-to-noise performance. [Roger & Arnold] reviewed various systems, concluding that the presence of noise on the image reduces pixel correlation, and thus the effectiveness of compression. Modelling and / or removing this noise permits better compression. Similarly, they also conclude that if a lossy compression process achieves pixel errors lower than the image's noise floor, it will effectively provide lossless performance, because the noise introduced by the compression is not differentiable from the sensor noise. Furthermore, the post-processing stages also introduce degradations, for example rounding errors when resampling the pixels to compensate for attitude and orbital perturbations, or when transforming the imagery onto a standard map projection. The end-to-end signal-to-noise performance of the system must therefore be characterised to assess the real impact of compression-induced errors. The RMSE will not necessarily be the only measure of fidelity; the Hausdorff Image Distance proposed by [Barnsley & Sloan] and other criteria should also be considered. Once the error performance of the compression has been determined, the selection of algorithm can commence.

Based on the author's experience, a three-stage approach will probably prove most effective. The first stage will be to produce a radically compressed 'thumb-nail' image to provide a basic previewing facility. A second file will transmit the bulk of the imagery using a lossy technique to achieve a good, but imperfect, representation of the scene whilst delivering decent compression. Finally, a table of residual errors should be provided so that the image can be reconstructed to lossless levels (at least to within the signal-to-noise performance of the imager in line with the comments of the previous paragraph). As this level of fidelity will only actually be required for the 2 to 5 % of scenes which possess extremely fine conditions and / or features, the residual table will not be transmitted by default and must be explicitly requested by the ground. [5] The author feels that this will deliver the best overall trade-off between routine data reduction, without sacrificing the fidelity of the occasional exceptional image. This approach is a blend of conventional compression techniques merged with hierarichal coding [Knowlton][Rabbani & Jones].

By reviewing the literature, it will be possible to short-list a number of potentially suitable algorithms. In addition to the techniques briefly reviewed here, there are numerous other compression options available. The newly launched *IEEE Transactions on Image Processing* and the proceedings of the *Image and Multidimensional Signal Processing* section of the annual *IEEE International Conference on Acoustics, Speech and Signal Processing* provide numerous 'state-of-the-art' papers in this field. [6]

Some caution is required when contemplating the use of newer compression algorithms for on-board application. As the mathematical sophistication of the procedures increases, so do their computational requirements. On a commercial remote sensing microsatellite, the image turn-around and throughput will be vital parameters. Given the

---

[5] This approach requires several data files to be created. stored and transmitted to represent a single scene. An on-board file-server, like the SSTL OBC, is the most suitable mechanism for managing the flow of data between the imaging instrument and the ground. The simple tape recorders used for conventional remote sensing are unable to cope with this random-access of data. Interestingly, the store-and-forward concept developed for message transfer on microsatellites remains attractive, although the communications hardware and data handling protocols will need to be suitably revised and upgraded to support operational Earth observation.

[6] The author recommends that the results from non-refereed papers be treated with caution. Claims of substantial compression ratios are particularly dubious due to misleading terminology or the choice of favourable test imagery (e.g. working with low entropy source images, or employing the same data for training the coder as used in the final compression). The most measured comments are invariably obtained from review papers impartially comparing the performance of various algorithms under similar (and meaningful) conditions.

modest computing resources of a microsatellite compared to terrestrial work-stations, opting for an overly complex algorithm could easily make the compression stage the bottleneck point, which would be counter-productive, especially for real-time services.

Therefore, to implement a practical remote sensing system, there is a need to balance the data reduction capabilities and the computing overheads of the compression. For this reason, techniques like DCT or sub-band coding compression are attractive because there is appropriate digital signal processing hardware to support the on-board computers for these intensive but repetitive tasks. The successful history of flying transputers on SSTL microsatellites suggests that parallel processing is a viable option for implementing compression by manipulating the image as blocks (DCT, VQ, BTC).

Conversely, there may be some benefits in using a much simpler algorithm executed in software. The analysis of LANDSAT imagery by [Chen et al] suggests that the correlations found in remotely sensed imagery are higher than in other types of image data, and that simple predictive DPCM may provide better results for this particular application than the literature would suggest. [Arai] proposes a similar predictive technique using just two neighbours; [Memon et al] make similar deductions, finding especially tight correlations in the spectral dimension. While the remote sensing community is undeniably less sophisticated in matters of compression than the image processing specialists, these repeated conclusions do suggest that simpler coding schemes may be highly successful for this class of imagery. Certainly, it would be a routine exercise to evaluate simple coding techniques on the same data set employed for the tests described in 7.2.5.

7.3 USING ON-BOARD IMAGE PROCESSING TO ENHANCE DATA QUALITY.

While there is considerable emphasis in designing imaging systems that are free of radiometric and geometric errors, these defects will nevertheless always be present. When offering a complete imaging service, it is not adequate to merely present the customer with raw data; in particular, the image degradations suffered must be corrected prior to distribution. As discussed in section 3.4.1, traditional remote sensing satellites dump their raw data directly to the downlink, either to a master control station where image processing can be implemented centrally. In the case of low-Earth orbiting meteorological spacecraft, the data is sent straight to the users, leaving them to manage as best as possible.

The computing power available on microsatellites allows many routine procedures for noise removal to be implemented on-board. Applied to an Earth observation service, this will not only streamline and standardise the processing procedure, but will also provide support for small users and eliminate much of the duplication of effort of the larger clients, for example national weather bureaux. While on-board image processing does not present any particular advantage for correcting for systematic radiometric or geometric non-linearities, this autonomous operation can provide significant improvements to subsequent image compression stages by removing noise. The presence of noise increases the image's statistical variance, reducing its susceptibility to compression [Roger & Arnold]. Furthermore, the presence of impulse noise (spurious pixels) can distort the local mean of a group of pixels, resulting in appreciable error in the reconstructed image if non-reversible compression is used. Certainly, the Block Truncation Coding (see section 7.2.4.4 and 7.2.6) employed on PoSAT-1 to compress the imagery will suffer significant errors if impulse noise is allowed to skew the mean of the image tiles.

7.3.1 AUTOMATIC NOISE REMOVAL FROM UOSAT-5 CCD IMAGES.

Of the electronic cameras developed during this programme and operational in orbit, the UoSAT-5 system suffers from the largest noise problems. Nevertheless, the raw imagery from this camera is remarkably free from serious defects and is intelligible without any pre-processing. The degradations experienced fall into three categories: pixel drop-out, line drop-out and low-amplitude noise. Noise similar to this is found in the raw data from many remote sensing satellites and is removed during the pre-processing stages on the ground. Since the techniques used to remove the most noticeable of these blemishes can be performed automatically, it is a logical conclusion that these tasks should be performed on-board, especially when the spacecraft is in a low-Earth orbit. The nature of the noise witnessed on UoSAT-5 images and the approach used to remedy them is discussed in the following sections.

The noise performance of each successive generation of SSTL's cameras has a better noise performance that its predecessors. Therefore, the UoSAT-5 camera represents the worst case for this analysis. Some of the techniques are still used for the PoSAT-1 camera, although fewer pixels require processing and the amplitude of the noise is significantly reduced. It should be noted that the use of packet communications protocols between the spacecraft on the ground ensures that no additional errors can occur during the transmission of image data.

7.3.1.1 Pixel Drop-out in UoSAT-5 CCD Images.

The most distracting type of noise found in the UoSAT-5 camera data is the appearance of pixel drop-out within the image. Manifested by the presence of abnormally bright or dark pixels in regions of rapidly varying contrast, the drop-out has been traced to marginal slew-rate performance in the analogue-to-digital converter (pixel drop-out in other systems will have their own causes). Adjustments to the circuit had virtually removed these problems from the test images taken during calibration, but the higher contrasts of the scenes viewed in space result in more difficult slew-rate conditions. Fortunately, simple pre-processing eliminates these pixels to such an extent that they are virtually impossible to identify. This form of noise is also present in PoSAT-1 imagery, but to a much smaller extent.

The efficiency of a number of noise filters in removing the blemished pixels have been evaluated. Traditional convolutional filters, weighted low-pass filters, and median filters exhibit the well documented effect of excessive blurring [Pratt, p.319,330]; these filters cause the UoSAT-5 images to appear subjectively worse after processing than before, because they remove more valid image information than noise in this case. The failure to preserve edge information in this way is a common problem with noise filtering techniques, and many solutions offering improved performance have been proposed [Chin & Yeh] [Mastin][Wang & Wang][Nagao & Matsuyama]. Whilst the merits of these filters were considered, parallel work was under way to see if a variant of a simple filter could be made to perform acceptably.

Analysis has revealed that many of the filters described for smoothing noise in digital images are poorly suited to the removing the drop-out in the UoSAT-5 images where, as outlined above, most pixels are unscathed with only a few values needing attention. Almost as a rule, these filters have been developed to recover from corruption by a Gaussian noise source affecting all pixels in the image. Thus, all pixels are treated as 'noisy' and in need of smoothing, which is not the case here. Clearly, a filter ill-adapted to the type of noise it must combat will produce marginal results. Also, while these filters claim to be edge-preserving, many destroy the fine detail and texture that characterises remotely sensed images (including UoSAT-5 data). Furthermore, several stages of iteration are often necessary to remove all traces of high variance, spiky noise (such as the UoSAT-5 blemishes), during which the rest of the image is significantly altered.

In addition to such generic problems, some filters suffer further problems because of their smoothing strategies. For example, maximum homogeneity smoothing [Nagao & Matsuyama][Chin & Yeh] only intervenes if a given pixel is part of a uniform region. No action is taken, however, if the pixel lies on an edge. This is fundamentally inappropriate to the UoSAT-5 images where the noise is concentrated specifically in regions of high contrast (edges). K-average filtering [Davis & Rosenfeld][Chin & Yeh][Mastin] will produce badly weighted averages if multiple blemishes occur within the test window. Furthermore, it is very computationally intensive [Mastin]. The gradient-inverse filter [Wang et al][Chin & Yeh][Mastin] and variants [Wang & Wang] cannot differentiate between low-contrast features and noise and may therefore destroy fine detail in the image. Other filters, such as the sigma filter [Lee, 1983][Mastin] or the Wallis filter [Mastin] need to predetermine image statistics, often with the assistance of a human operator which makes them impractical for autonomous operation.

These filters have not been tested extensively against UoSAT-5 data to qualify the presupposition that their outputs would not be acceptable. For those filters tested, the results were disappointing, the smoothed images suffering from blurring, blockiness, and loss of texture, often without having had the noise pulses successfully removed. However, the one filter that performed tolerably in this instance, and is therefore worth mentioning, is the Nopel filter [Imme]. This filter differs from the others in that it modifies a pixel only if certain criteria have been met, resulting in less damage to the image. Six or seven iterations were needed to de-blemish the test images, and although there was some degradation of texture, much of the fine detail had been preserved. The effect this degradation can be liked to the texture of an oil painting (filtered image) compared to a photograph (original).

However, the emphasis of this research is to develop an operational imaging system, and not an extensive study of image processing techniques, so significant effort was not expended on this survey, especially when an alternative technique for eliminating the pixel drop-out that is both simple and highly effective was discovered. Even if the filters described in the literature could be made as effective at removing noise and preserving edge and texture information, they would be unable to rival its implementational and computational simplicity.

The successful strategy employed by [Imme] of selectively applying the filter to pixels meeting specific 'noisiness' criteria has been adopted. Given that the blemishes effect only a small percentage of the image pixels, it intuitively follows that a filter applied generally will fail to preserve detail and texture as well as one that operates only on contaminated pixels. Given that the grey-levels of the blemished pixels differ considerably from their unaffected neighbours, it is relatively simple to identify blemishes, and only take action where necessary. By being selective in applying its effects, the algorithm developed is suitable for use on KITSAT-1, PoSAT-1 and FASat-Alfa, even though these cameras suffer decreasing amounts of degradations.

The noise removal routine used is a derivative of the simple convolutional filter, but is tailored to the noise characteristics of UoSAT-5 images. The value of each pixel in the image is compared, in turn, with the mean of the eight adjacent pixels, and if the difference exceeds 10 % of the dynamic range of the image (i.e. 25 grey levels) the pixel under test is deemed a blemish. Although this technique may misinterpret the occasional very high contrast edge as a blemish, qualitative experiments with many (several dozen) images have revealed no perceptible errors. However, if the image is severely underexposed (less than a quarter of the of the possible dynamic range is actually used), the 10% threshold is too large to trap all the corrupted pixels and a modified threshold of 10% of the dynamic range of the image's histogram should be substituted.

Initially, a pixel identified as blemished was replaced with the mean of its neighbours, but it transpired that this was inadequate to completely smooth the image. Occasionally (a few times per image), the presence of a second blemish, in an adjacent pixel, would noticeably offset the value of the calculated mean, leaving residuals in the filtered image. By employing the neighbouring pixels' median, all drop-out is successfully erased without any discernible artefacts. Therefore the algorithm for removing UoSAT-5 and PoSAT-1 pixel drop-out is as follows:

```
FOR this.line = 1 TO all.image.lines DO
   FOR this.pixel = 1 TO all.image.pixels DO
      IF mod ( image[this.line,this.pixel] -
               (mean.of.8.neighbouring.pixels) ) > 25
         THEN image[this.line,this.pixel] :=
               (median.of.8.neighbouring.pixels)
         ELSE image[this.line,this.pixel] := this.pixel
```

In addition to providing highly acceptable filtering results, the thresholded median filter used to remove the blemishes from the UoSAT-5 images is very simple to code and low in processing requirements. Calculating medians has been done using a simple bubble-sort on the transputers. Because it only needs to be calculated for those few pixels that have been corrupted, the simplicity of implementation outweighs any slim benefits in efficiency that other routines may offer. Moreover, it is not possible to employ the Quicksort algorithm [Graham] because Occam does not support recursive procedure calling.

Once a simple algorithm was identified for removing the pixel drop-out noise plaguing the UoSAT-5 imagery, its autonomous implementation on board the spacecraft has simplified the ground-based processing routines. While this is not a major issue for conventional remote sensing programmes, it is of benefit to the numerous non-technical operators who are accessing the imagery using the satellite's store-and-forward communications facilities.

7.3.1.2 Line Drop-out in UoSAT-5 CCD Images.

When integration time control is used in the UoSAT-5 camera, the charge accumulated by the CCD is dumped for the first part of the field period. A few milliseconds later, the CCD reverts to normal charge collection, so that the signal read out as image data has only been integrated over a percentage of the full 20 milliseconds of the field period. By altering the duration of the charge-dumping and charge-collection phases, the image's integration time is varied, thereby implementing electronic shutter control.

However, when the camera switches from the charge-dumping mode to the charge-collecting mode, there is a current pulse drawn by one of the EEV buffer support chips which induces a spike on the +12 V supply rail. It is likely that a low impedance forms between the supply and ground during the changeover because filtering with capacitors and inductors failed to make any improvements. Since the CCD's output amplifier is biased by this rail, the video signal from the CCD is modulated by the 2 to 3V drop in supply regulation. The duration of the glitch is a few hundred microseconds, shifting the black level of several image lines, resulting in the appearance of a bright horizontal bar across the image when it is displayed.

The introduction of the horizontal bar into the image is a generic feature of the EEV control chipset for the CCD04, and although the problem is well known within the company, it is not publicised and is never mentioned in their data sheets or application notes. The engineers at EEV know of no cure for the phenomenon when the camera drives a monitor directly, but fortunately the digitised UoSAT-5 images can be corrected through computer processing prior to viewing.

A few pixels at the start of each image line contain black reference information, so that clamping circuitry in a television can restore the DC level of the image after AC coupling. The presence of these black reference pixels makes automatic detection of the bright bar simple, because they will be offset to the same degree as the image pixels. The pre-processing to remove the horizontal bar has been developed entirely through experimentation with UoSAT-5 imagery, as very little relevant documentation exists. As the lines modified still contain valid image information, the emphasis in the removal of the bright bar has been to preserve this data as far as possible. This implies that the valid image information should be extracted by adding and subtracting offsets wherever possible, avoiding line combination and substitution techniques (as used by LANDSAT for line drop-out [Lillesand & Kiefer, p.621]).

The first stage in this processing was to characterise the grey level offset which typifies the bar. Even though only four lines are seriously effected (shifted by 40 to 60 grey-levels), less significant offsets persist over approximately twenty lines. The specifics of the bar vary slightly for each image, but all resemble a pulse with a sharp attack and ripples in its decay. Adding and subtracting a constant offset from all the pixels in a line, despite improving the overall appearance of the image, revealed that differences in offset also exist within a single line. Therefore, while it is possible to remove artefacts from the bright bar acceptably by simply shifting the black level of individual lines, this must be performed manually for each image and is thus not practical for autonomous operation.

Through experimentation, it became clear that adjusting the offset for whole lines would not be adequate for eliminating all artefacts of the bright bar. Because the residuals are more noticeable in when the image is uniform, schemes that weighted the offsets to produce better results in homogeneous regions than in heterogeneous regions were attempted, but with mixed results.

Another approach has been adopted where, above and below the disrupted region, one line is selected and used as a reference. For each column, offsets were added to each pixel so that there would be a linear transition in grey-level between the two reference points. This tends to smear the image vertically, but removes all indication of the bright bar. An extension of this, where averages of line sections are linearly fitted, has yielded better results. Instead of simply using the value of the reference pixel as a target in a given column, the mean of an n x 1 window centred about this reference pixel is employed (i.e. the average of this pixel and a few of its horizontal neighbours). Then the linear matching is performed, but using the same n x 1 window for each pixel in the disturbed zone. Empirical tests have shown that a 13 x 1 window gives a good average of the bright bar's effect and conserves image texture, without requiring excessive computing effort. The offset calculated for the window is then subtracted from the pixel under test. By linearising averages, the common offset introduced by the bright bar is removed, but individual pixels are still allowed to have significant variations in intensity, preserving the detail in the original image. The following pseudo-code summarises the algorithm for detecting the bright bar, calculating the target values and filtering the effected pixels:

```
-- find line.drop.out
this.line  :=  0
REPEAT
   this.line  :=  this.line + 1
UNTIL  ( this.line.black.reference > average.black.reference + 20 )
start.of.line.drop.out  :=  this.line

-- calculate top.target
this.line    := start.of.line.drop.out  - 9
FOR  this.pixel  =  1  TO  all.image.pixels  DO
   top.target[this.pixel] := ( SUM (image[this.line,this.pixel - 6])  TO
                                          (image[this.line,this.pixel+6]) ) / 13

-- calculate bottom.target
this.line    := start.of.line.drop.out  + 16
FOR  this.pixel  =  1  TO  all.image.pixels  DO
   bottom.target[this.pixel] := ( SUM (image[this.line,this.pixel - 6])  TO
                                             (image[this.line,this.pixel+6]) ) / 13

-- filter for bright.bar
FOR  i =  1  TO  24  DO
   this.line   :=  start.of.line.drop.out  -  9  +  i
   scaling.factor   :=   i  /  25
   FOR  this.pixel  =  1  TO  all.image.pixels  DO
      local.average := ( SUM (image[this.line,this.pixel - 6])  TO
                                   (image[this.line,this.pixel+6]) )  /  13
      target  := (( bottom.target[this.pixel] - top.target[this.pixel] )  x
                         scaling.factor)  +  top.target[this.pixel]
      modifier  :=  target  -  local.average
      image[this.line,this.pixel]  :=  image[this.line,this.pixel]  +  modifier
```

This approach leaves barely noticeable residuals for almost all image textures, except for high contrast horizontal steps (e.g. cloud over sea) which are transformed into ramps due to the averaging of the sliding window. A marker is left along the edges of the image to indicate the location of bright bar to viewers, allowing them to take the processing stages into consideration when attempting to identify fine detail. Still, a step detector may be added to the algorithm in future to avoid this infrequently occurring, but distracting, effect.

7.3.1.3 Low Amplitude Noise in UoSAT-5 CCD Images.

As discussed in some detail in section 5.3.1.5, the analogue processing stages of the UoSAT-5 CCD camera are quite sensitive to any type of noise which may be present on the supply or ground rails. The beating of the DC-DC converters on the UoSAT-5 camera creates a faint herringbone pattern, which although low in amplitude (effecting no more than the two least significant bits of the 8-bit data - as shown in section 5.3.1.5) is nevertheless fairly noticeable. Thus, this noise is only really apparent in highly uniform regions or in poorly exposed images that have been contrast stretched, amplifying the noise.

Given that this type of degradation is not as distracting as the pixel and line drop-out, and that improved design of the supply conditioning has reduced the noise levels on the successive cameras, no significant effort has been expended in trying to remedy this noise. However, as this type of degradation are more typical of what is encountered in other imaging systems, and therefore more likely to be successfully removed using conventional techniques, a brief mention is appropriate. Furthermore, because it effects all pixels in the image, it imparts a small increase in entropy to the image, reducing the effectiveness of the image compression whilst conveying no extra useful information. Therefore, there may be some benefit in addressing this source of noise in more detail in future.

The approach generally adopted for the removal of periodic noise of this type does not involve simple filters applied to groups of pixels within the image. Instead, the image is converted from the normal spatial representation into the spatial-frequency domain using Fourier transforms. Once in the spatial-frequency domain, filters can be applied to remove or attenuate the periodic components responsible for striping or supply-carried noise [Lillesand & Kiefer, p.649].

However, past experience [Raptis] with the UoSAT-4 engineering model images, which suffered similar, but substantially more objectionable, noise patterning, have not met with success, suggesting that the most satisfactory results can often be obtained with no filtering at all. Similarly, despite being substantially degraded, the example in [Gonzalez & Woods, p.296] exhibits significant loss of detail following notch-filtering in the spatial frequency domain. In general, the use of spatial-frequency filtering requires that images need to be seriously deteriorated before noise removal enhances, or simply maintains, the quality of images. In many cases the filter removes more valid image information than noise, resulting in further degradation of image interpretability, rather than improvement. This point is alluded to by [Chin & Yeh] in their analysis of filtering methods versus signal-to-noise ratio. They found that for images with high signal-to-noise ratios (greater than 50 - most UoSAT-5 images have SNRs better than 100), the application of many smoothing filters resulted in greater deviations from the 'true' images than had the introduction of noise. Furthermore, their results were derived using synthetic test images with mainly featureless textures; real-world, especially remotely sensed imagery with its rich texturing, is likely to be much more degraded by inappropriate filtering. This, and corroborating experience from UoSAT-5, indicate that often the best policy regarding the presence of low amplitude noise is to take no action.

7.3.2 CONCLUSIONS ON AUTOMATIC NOISE FILTERING IN UOSAT-5 CCD IMAGES.

There are three different types of noise that degrade the UoSAT-5 imagery. Fortunately, completely automatic filtering algorithms have been developed to remove almost all the effects of the two most disturbing types: pixel drop-out (blemishing) and line drop-out (bright bar). By implementing these routines on the transputer units, it has been possible to provide users with pre-processed images at no extra cost.

A comparison of figures 7.3.2a and b reveals the impact of the pixel and line drop-out filters on the subjective quality of the UoSAT-5 images. It should be noted that this image is particularly corrupted by pixel drop-out, and was chosen to demonstrate the effectiveness of the filter at removing noise without degrading the rest of image. Most of the data from UoSAT-5 is significantly cleaner than this, and quite intelligible without filtering. KITSAT-1 and PoSAT-1 imagery also suffer from the bright bar effect due the continued use of the EEV chipset, but the pixel-drop out has been reduced to around a dozen blemishes per image.

While the designer of the imaging payload should make effort to minimise the impact of noise through sound electronic design, the ability the perform complex image processing tasks on-board can be used to overcome unexpected post-launch defects with a minimum of difficulty. This applies particularly to remote sensing satellites serving large numbers of users while in low-Earth-orbit and therefore not able to use a ground-based central processing station for support, although the principle holds valid for any remote image gathering system.

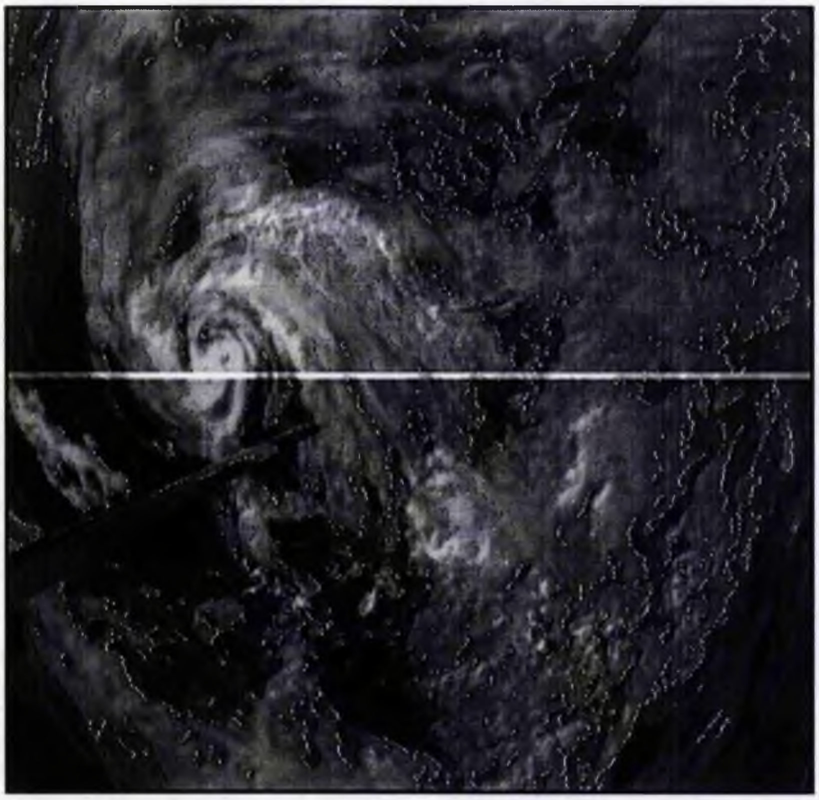

Figure 7.3.2a

Raw image from UoSAT-5.

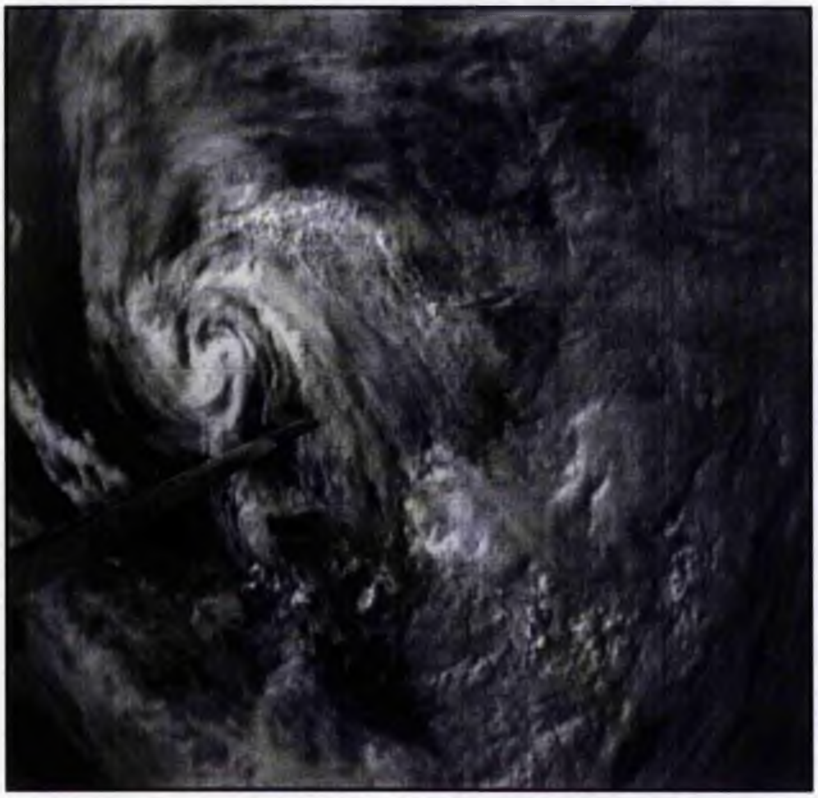

Figure 7.3.2b

Filtered image from UoSAT-5.

7.4 CONCLUSIONS.

Whereas a microsatellite's coarse attitude control dictates the characteristics of the sensor architecture, the communications system determines its productivity. In addition to various hardware measures to increase the data rates, software techniques can also be used to improve the value of the data transmitted to the ground. Although only covering a peripheral aspect of the author's research, the results of the in-orbit demonstrations in image analysis, processing and compression have generated so much interest that the author has felt compelled to discuss these issues in some depth.

Overall, the layered approach of using autonomous analysis to reject low-interest imagery, quick-look previews, and block truncation coding delivers a 400 % improvement in the daily volume of images captured by PoSAT-1. These simple techniques indicate that there are significant benefits to be had from on-board manipulation of the image data. Without doubt, more sophisticated algorithms could provide even better results.

A certain amount of image pre-processing is performed to remove various sources of noise degrading the data. While hidden from the users, this process is essential to prepare the images for the subsequent compression. If these filters were not applied, the noise would disturb the compression stage, resulting in substantial errors in the reconstructed image.

7.5 REFERENCES

Arai K: Preliminary study on information lossy and lossless coding data compression for the archiving of ADEOS data; IEEE Trans. on Geoscience and Remote Sensing, Vol.28 No.4, p.732 - 734, July 1990.

Barnsley M.F. & Sloan A.D: Fractal image compression; Proc of the Scientific Data Compression Workshop, NASA Goddard Space Flight Centre, Feb 1989, NASA-CP-3025; NASA Science & Technical Abstract Report ref N89-22346.

Begni G: SPOT image quality - Twenty months of experience; Int. J. Remote Sensing, Vol.9 No. 2, p1409-1414, 1988.

Börger J.B et al: Study on data compression systems for operational remote sensing; European Space Operations Centre contract 6141/84/D/IM(SC).

Brewer A.W: On-board image compression using adaptive MPBTC algorithm; Internal document SSAB001B, Surrey Satellite Technology Ltd, 1994.

Cappellini V: Data compression and error control techniques with applications; Academic Press, 1985; ISBN 0-12-159261-8;

Chen T.M, Staelin D.H. & Arps R.B: Information content of Landsat image data for compression; IEEE Trans. on Geoscience and Remote Sensing, Vol.25 No.4, p.499 - 501, July 1987.

Chin R.T. & Yeh C.L: Quantitative evaluation of some edge-preserving noise-smoothing techniques; Computer Vision, Graphics, and Image Processing, Vol.23 p.67-91, 1983.

Clarke R.J. & Linnett L.M: Fractals and image representation; IEE Electronics & Communications Engineering Journal, p.233 - 239, Aug 1993.

Compuserve: The Graphics Interchange Format standard; Compuserve Information Services, 1991.

Davis L.S. & Rosenfeld A: Noise cleaning by iterated local averaging; IEEE Trans. on Systems, Man and Cybernetics, Vol.8, p.705-710, 1978.

Delp E.J. & Mitchell O.R: Image compression using block truncation coding; IEEE Trans. on Communications, Vol.27 No.9, p.1135 - 1142, Sept 1979.

Dosière P. & Justice C: Spatial and radiometric resolution of the LANDSAT-3 RBV system; Int. J. Remote Sensing, Vol. 4 No. 2, p447-455, 1983.

Ersoy O.K. & Chen C.H: Transform-coding of images with reduced complexity; Computer Vision, Graphics, and Image Processing, Vol.42 p.19-31, 1988.

Fisher Y: Fractal image compression; Springer-Verlag 1995; ISBN 0-387-94211-4.

Gharavi H. & Tabatabai A: Sub-band coding of monochrome and color images; IEE Trans of Circuits and Systems, Vol.35 No.2, p.207 - 214, Feb 1988.

Gonzalez R.C. & Wintz P: Digital image processing; Addison-Wesley 1977; ISBN 0-201-02597-3.

Gonzalez R.C. & Woods RE: Digital image processing; Addison-Wesley 1992; ISBN 0-201-50803-6.

Graham N, Introduction to Pascal, p.155-172, West Publishing Co, 1980.

Gray R.M: Vector quantization; IEEE Acoustics, Speech & Signal Processing Magazine, Vol.1 No.2, p.4-29, Apr 1984.

Gray R.M: Vector quantization; Proc of the Scientific Data Compression Workshop, NASA Goddard Space Flight Centre, Feb 1989, NASA-CP-3025; NASA Science & Technical Abstract Report ref N89-22340.

Gupta S. & Gersho A: Feature predictive vector quantisation of multispectral images; IEEE Trans. on Geoscience and Remote Sensing, Vol.30 No.3, p.491 - 501, May 1992.

Halverson D.R, Griswold N.C. & Wise G.L: A generalised block truncation coding algorithm for image compression; IEEE Trans. on Acoustics, Speech & Signal Processing, Vol.32 No.3, p.664-668, Mar 1984.

Harris R.W et al: High quality image compression for rockets and satellite; Proc. of the 3rd Annual AIAA/USU Conference on Small Satellites, Utah State University, 26-28 Oct 1989.

Imme M: A noise peak elimination filter; Computer Vision, Graphics, and Image Processing, Vol.53 p.204-211, 1991.

Israelson P.D. & Harris R.W: The application of vector quantization to image compression for satellite imaging systems; Proc. of the 1st Annual AIAA/USU Conference on Small Satellites, Utah State University, 7-9 Oct 1987.

Iterated Systems; Promotional material, Iterated Systems Ltd, Wyvols Court, Swallowfield, Reading, Berks RG7 1PY.

Jacquin A: Image coding based on a theory of iterated contractive transformations; IEEE Trans on Image Processing, Vol.1 No.1, p.18 - 30, Jan 1992.

Jaggi S: Technique for compression of multispectral remotely sensed data using vector quantization; Oral presentation; SPIE Conference on Hybrid Image and Signal Processing III, SPIE Vol.1702 (if published), Orlando Florida, 21-22 April 1992.

Jain A.K: Image data compression; Proc of the IEEE, Vol.69 No.3, p.349 - 389, March 1981.

Jayant N.S. & Noll P: Digital coding of waveforms - principles and applications to speech and video; Prentice-Hall, 1984; ISBN 0-13-211913-7.

Knowlton K: Progressive transmission of grey-scale and binary picture by simple, efficient and lossless encoding schemes; Proc. IEEE, Vol.68 No.7, p.885 - 896, July 1980.

Kunt M, Ikonomopoulos A. & Kocher M: Second-generation image-coding techniques; Proc of the IEEE, Vol.73 No.4, p.549 - 574, April 1985.

Laker C: Software environment for the UoSAT-5 Earth imaging system; M.Sc. dissertation; University of Surrey, 1991.

Lee J.S: Digital image smoothing and the sigma filter; Computer Vision, Graphics, and Image Processing, Vol.24 p.255-269, 1983.

Lee J.S: Refined filtering of image noise using local statistics; Computer Graphics and Image Processing, Vol.15 p.380-389, 1981.

Lhuillier J.J. & Nguyen A.Q: Subband coding of images - comparison with DCT; Signal Processing IV - Theories and Applications, Edited by Lacoume J.L. et al, Elsevier Science Publishers, 1988.

Lillesand T.M. & Kiefer R.W, Remote sensing and image interpretation, Second edition, Wiley, 1987.

Linde Y, Buzo A. & Gray R.M: An algorithm for vector quantizer design; IEEE Trans on Communications, Vol.28 No.1, p.84 - 95, Jan 1980.

Mastin G.A: Adaptive filters for digital image noise smoothing: an evaluation; Computer Vision, Graphics, and Image Processing, Vol.31 p.103-121, 1985.

Memon N.D, Sayood K. & Magliveras S.S: Lossless compression of multispectral image data; IEEE Trans. on Geoscience and Remote Sensing, Vol.32 No.2, p.282 - 289, March 1994.

Mitchell O.R. & Delp E.J: Multilevel graphics representation using block truncation coding; Proc IEEE, Vol.68 No.7, p.868 - 873, July 1980.

Montpetit M.J, Prieur L. & Fouquet M: Compression of UoSAT-5 images; Proc. of the SPIE Conference on Small Satellite Technology and Applications III, SPIE Vol.1940, Orlando, 14-15 April 1993.

Nagao M. & Matsuyama T: Edge preserving smoothing; Computer Graphics and Image Processing, Vol.9 p.394-407, 1978.

Netravali A.N. & Limb J.O: Picture coding - a review; Proc of the IEEE, Vol.68 No.3, p.366 - 406, March 1980.

Pease C.B: Satellite imaging instruments - principles, technologies and operational systems; Ellis Horwood, 1990, ISBN 0-13-638487-0.

Pei S.O. & Jaw S.Y: Design of 2-D quadrature mirror filters for image subband coding; IEEE Trans on Circuits & Systems, Vol.34 No.4, p.438 - 441, Apr 1987.

Pratt W.K, Digital image processing, Wiley, 1978.

Rabbani M. & Jones P.W, Digital image compression techniques, SPIE Optical Engineering Press, 1991, ISBN 0-8194-0648-1.

Raptis M, Digital signal processing of image data; MSc Thesis, University of Surrey, 1990.

Reddy B.R.K. & Pai A.L: Reed-Muller transform image coding; Computer Vision, Graphics, and Image Processing, Vol.42 p.48-61, 1988.

Reichhardt T: Lewis and Clark, blazing new trails; Aerospace America, V.33 No.7, July 1995.

Roger R.E. & Arnold J.F: Reversible image compression bounded by noise, IEEE Trans. on Geoscience and Remote Sensing, Vol.32 No.1, p. 19 - 21, Jan 1994.

Udpikar V.R. & Raina J.P: BTC image coding using vector quantization; IEEE Trans. on Communications, Vol.35 No.3, p.352 - 356, March 1987.

Vaidyanathan P.P: Quadrature mirror filter banks, M-band extensions and perfect reconstruction techniques; Acoustics, Speech & Signal Processing Magazine, Vol.4 No.3, p.4-20, July 1987.

Wang D. & Wang Q: A weighted averaging method for image smoothing; Acta Electronica Sinica, Vol.14 No.6, Nov 1986.

Wang D.C.C, Vagnucci A.H. & Li C.C: Gradient inversed weighted smoothing scheme and the evaluation of its performance; Computer Graphics and Image Processing, Vol.15 p.167-181, 1981.

CHAPTER VIII

IN-ORBIT RESULTS AND PRESENTATION OF IMAGERY.

The usefulness of the imagery collected from orbit determines the success of a satellite remote sensing system. Although not of the same class as SPOT or LANDSAT data, the images collected by the author's cameras nevertheless contain a great deal of information. Chapter 8 presents some of this data to demonstrate to the reader that quality Earth observation is possible from microsatellites, and briefly considers a number of applications for this data

8. IN-ORBIT RESULTS AND PRESENTATION OF IMAGERY.

The imaging systems developed for SSTL's microsatellites during this research programme were conceived as inexpensive demonstrations of the feasibility of using microsatellites for Earth observation. As such, the CCD cameras on UoSAT-5, KITSAT-1 and PoSAT-1 have been very successful, capturing high-quality imagery containing recognisable land, sea and atmospheric features, at resolutions ranging from 4 km down to 200 metres.

However, satellite imagery has little intrinsic worth, only becoming valuable when it is used to enhance other commercial, scientific, military or humanitarian activity. This chapter presents a few of the thousands of images that have been collected by the author's cameras, and assesses the usefulness of this data for a range of applications. Despite the modest specifications of the imagery compared to that from traditional remote sensing systems, there are numerous roles for this microsatellite data.

The applications and techniques for using remotely sensed data discussed in this chapter apply to all Earth observation spacecraft, and not just microsatellites. The emphasis here is to show that inexpensive microsatellite imagers are capable of fulfilling tasks previously exclusive to much larger systems. The scenes presented have been chosen partly to show the quality of the raw data [1], and partly to demonstrate potential applications or features that can be detected by microsatellite imagery.

[1] The imagery has been subjected to the pre-processing routines described in section 7.3 to filter for 'pixel drop-out' and the 'bright bar'. Most images will have received a simple 'histogram stretch' to improve their contrast on the printed page, and will have been rotated to put north at the top. Otherwise, the data has received no processing or embellishments.

8.1 APPLICATIONS OF METEOROLOGICAL SCALE MICROSATELLITE IMAGERY.

The resolution and sensitivity of the Wide Angle Cameras on KITSAT-1 and PoSAT-1 is similar to that produced by the visible bands of the NOAA weather satellites, but at a tiny fraction of the cost. Even with their monospectral capabilities, these microsatellite cameras are appropriate for fulfilling many of the applications currently provided by much larger meteorological spacecraft (NOAA, Meteor, Feng Yun, DMSP). In the medium term, remote sensing microsatellites equipped with multispectral cameras, with mid- and thermal-IR sensitivity, and endowed with enhanced communication systems should be able to replace the existing, costly platforms.

8.1.1 METEOROLOGY.

Most of the scenes displayed in this thesis have been specifically chosen to be free of cloud, revealing features of the Earth's surface. However, much of the imagery collected from the satellites has contained clouds. This data can be used to provide information for climatology and daily weather forecasting.

The three Wide Angle Cameras have produced many examples of meteorological remote sensing including the tracking of cloud and weather systems, and hurricane and storm warnings. For most meteorological applications, a wide field of view is preferred over increased ground resolution. This makes KITSAT-1's higher orbit (1300 km) more suitable than the popular 800 km polar orbit (UoSAT-5, PoSAT-1). Figure 8.1.1 shows one such image captured of the western Mediterranean by KITSAT-1 in April 1993.

8.1.2 STORM WARNING.

An adjunct to routine weather monitoring is providing storm warning services. Although there is nothing that can be done to prevent a violent storm, hurricane or typhoon from striking land, ample warning can allow preparations to be made to ensure minimal loss of life or disruption to the economy of the effected regions. Using satellite imagery, it is possible to survey the atmosphere above the tropical oceans where these meteorological phenomena develop. When detected, these violent storms can be tracked and the appropriate warnings given to the local population to make their homes and possessions secure and to seek shelter if necessary.

Figure 8.1.1

KITSAT-1 wide angle image of western Europe.

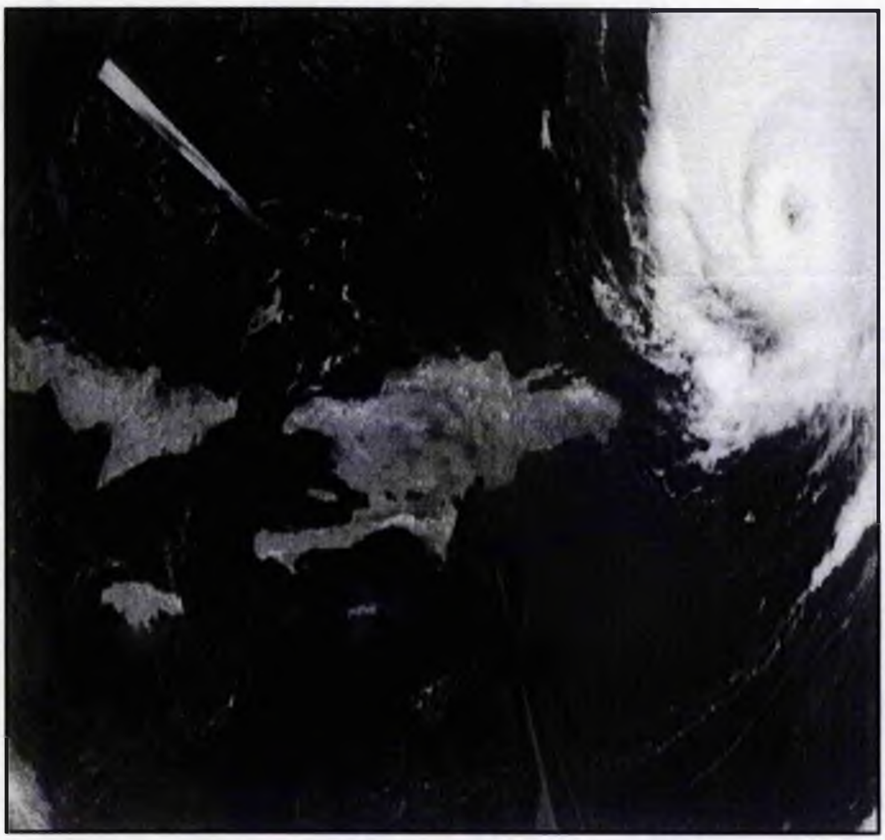

Figure 8.1.2

PoSAT-1 wide angle image of Hurricane Felix over Haiti.

The Wide Angle Cameras on the SSTL microsatellites have imaged numerous hurricanes in the Caribbean, and typhoons and cyclones in the South Pacific and the China Sea. One of the most striking examples of this type of imagery is shown in figure 8.1.2. Captured in September 1995, during a particularly violent and unseasonable spate of tropical storms. Hurricane Felix can be seen as it bypasses Haiti / the Dominican Republic, Puerto Rico and Cuba, having just ravaged several of the smaller Caribbean islands including Barbados.

The ability to make accurate and frequent updates during the last few hours before a storm of this type strikes land are particularly valuable, allowing both refugees and relief organisations to take the most appropriate actions during rapidly evolving circumstances. It is quite feasible to use inexpensive imaging microsatellites to complement the existing storm warning infrastructure, providing additional temporal resolution during these critical periods.

8.1.3 ENVIRONMENTAL MONITORING.

When looking for environmental change, it is often appropriate to use meteorological scale imagery which provides a continental perspective. The images in chapter 4 have already demonstrated the suitability of using microsatellite systems to monitor the smoke plumes from the aftermath of the Gulf War (figures 4.3.4a and b).

The environmental damage to this region did not cease with the end of the Gulf War however. Since then, the Iraqi government has been proceeding with a systematic draining of the marshes at the confluence of the Tigris and Euphrates rivers, north of the city of Basrah. Figures 8.1.3a, b and c show images from the UoSAT-5 and PoSAT-1 Wide Angle Cameras of this area, revealing the complex hydrology of the fertile Tigris and Euphrates valleys.[2] Although only the major waterways, marshes and lakes are resolvable, significant changes can be seen between the successive images. Between September 1991 (figure 8.1.3a from UoSAT-5) and October 1993 (figure 8.1.3b from PoSAT-1), the extent of the (darkish) marshland and (dark) lakes have been reduced, with a corresponding increase in (bright) soil. Overall, dozens of square kilometres of wild marsh have vanished in under two years. While some of this change could be attributable to annual variations in

[2] These images have been selected to be from late September / early October to minimise the effect of seasonal variation. The more pronounced differences apparent in figures 4.3.4b and 4.5.2a are largely attributable to natural cycles.

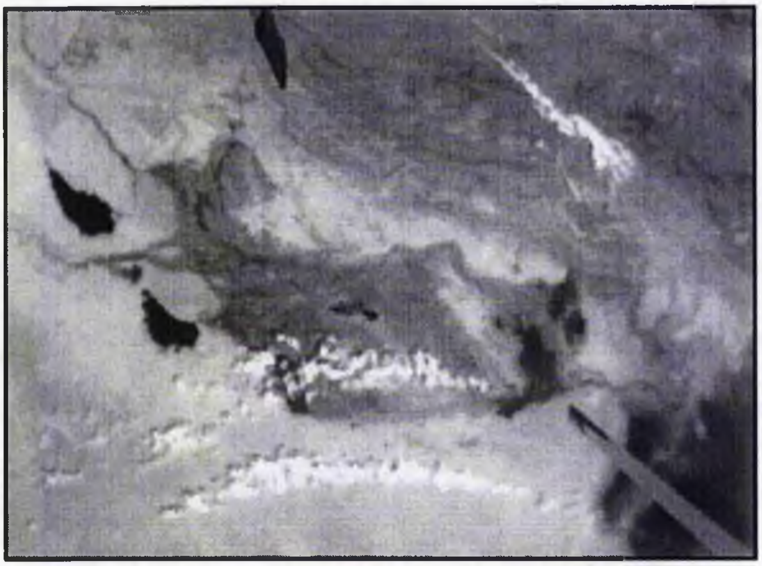

Figure 8.1.3a

(September 1991).

Figure 8.1.3b

(October 1993).

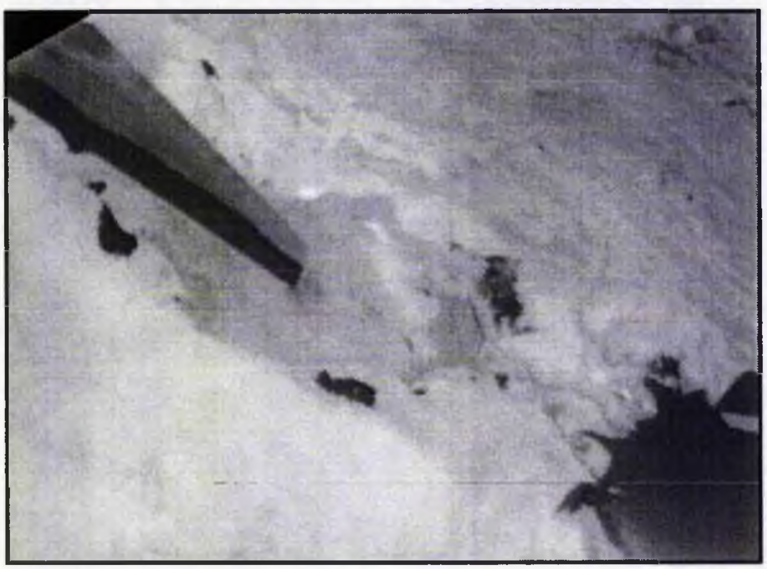

Figure 8.1.3c

(September 1995).

Enlargement of UoSAT-5 and PoSAT-1 wide angle images of southern Iraq.

rainfall, the deliberate draining of this area is irrefutable, confirmed by the man-made straight edges to the remaining marshes. Although the change from 1993 to September 1995 (figure 8.1.3c) is less dramatic, there is still a clear reduction in these delicate marshlands, and particularly a drying of the soil (visible due to its lighter shade).

The availability of satellite imagery allows impartial scientific observers access to areas that are otherwise inaccessible (geographically or politically). In addition to present-day Iraq, the Soviet Union used to present similar obstacles to international monitoring. In particular, during the Stalin regime, numerous waterways were diverted from their natural courses flowing into the land-locked Aral Sea to provide irrigation for huge state-run cotton farms. For many years, this process went unchecked, causing the level of the Aral Sea to drop significantly. As the Aral Sea shrank, fishing communities which were previously on the shore became stranded inland. The salinity of the sea water increased as the concentration of water dropped, poisoning many fish and disrupting the region's food chain. Most significantly, the Aral Sea plays a vital (and previously unappreciated) role in moderating the region's weather. As its surface area decreases, less water vapour is absorbed into the atmosphere, reducing the region's rainfall.

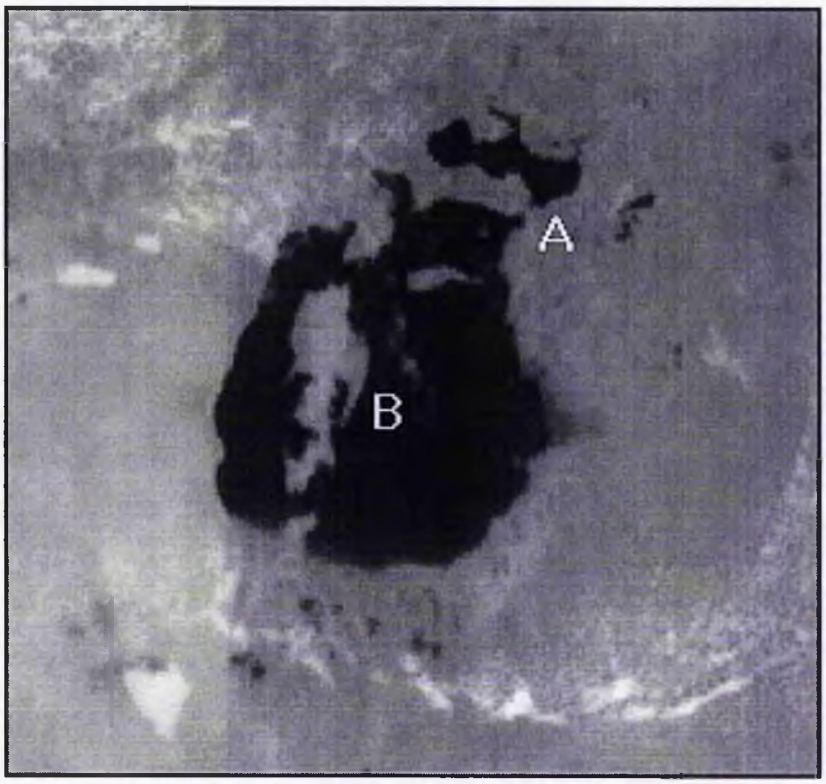

Figure 8.1.3d Enlargement of PoSAT-1 wide angle image of the Aral Sea.

Figure 8.1.3d shows an enlargement corresponding to a quarter of the scene captured by PoSAT-1 in July 1995. Comparison with any recent map will reveal just how much damage this region has suffered. The areas marked on the image show considerable differences from imagery recorded in 1985 and 1989 presented in [Ellis & Turnley]. In 1995, the northern parts of the Sea (labelled A) are connected to the main body by a thin waterway; in 1988, the channel was many times larger. The central island (labelled B) was two distinct, and much smaller, land-masses in 1985. [3]

8.1.4 SNOW COVER MONITORING.

A key advantage of orbiting satellites is their ability to collect climatic data from remote areas. High mountain ranges are amongst the most inaccessible places on Earth, yet they play a crucial role in determining weather patterns and precipitation rates. In particular, the melting of snow in these regions determines the flow rates of many of the World's major rivers. Monitoring the snowfall in these high mountain ranges can offer significant warning of forthcoming disasters, either drought or flooding. Images from PoSAT-1 clearly reveal the seasonal variations in snow cover, most notably in regions such as the Alps, the Chilean Andes and central Asia.

A sequence of images (figures 8.1.4a to f) captured by the PoSAT-1 Wide Angle Camera recorded the seasonal variations in the snow cover of the western arm of the Himalaya - Karakoram chain. Given that all the major rivers of China, south-east Asia and the Indian sub-continent originate in this region, any irregularities in the rate of precipitation has a dramatic effect on the water supplies of some 2 billion people.

The viewer can use the distinctive curve of the Indus valley to the west of the images as a reference point (labelled A in figure 8.1.4d). The three principal mountain chains of the Karakoram (most northerly), the Ladakh and the Himalayas (most southerly) are clearly visible running in parallel towards the south-east, as they stretch from Pakistan across northern India. The eastern end of these images is near the Nepalese border, beyond the distinctive twin lakes at Mapam Yumco in Tibet (labelled B). [4]

---

[3] Several dozen images of the Aral Sea have been collected by UoSAT-5 and PoSAT-1 from mid-1991 to present. No permanent change is discernable over this period, suggesting that the shrinkage has abated. However, significant seasonal variations are apparent, highlighting the need for continuous monitoring of sites of environmental concern. With inadequate samples, it is possible to misinterpret the natural cycles for dramatic and permanent change. The SSTL microsatellites will continue their imaging campaign to watch for further variations in this region.

[4] These images have been rotated and cropped to cover the same area. However, no processing has been performed to compensate for the geometric distortions caused by the spherical Earth and camera lens, resulting in slightly different perspective for the various scenes, especially for figure 8.1.4f.

The first image in the sequence (figure 8.1.4a - the wide angle image corresponding to figure 8.2.2a) was recorded in early June 1994. Although the valleys are free of snow, the mountain tops are still covered, delineating the geological structure of the area. The height of the thaw occurs in September (figure 8.1.4b), with only the highest peaks in the Karakoram and Himalayas still being covered. The lower Ladakh chain is essentially free of snow at this point. There is some high altitude cloud present in this image, which is radiometrically indistinguishable from snow in the visible bands, although the distinct fractal shapes of the mountains helps to differentiate between the two. Complementary data in the 2 μm band is essential to conclusively identify between ice, snow and cloud.

As winter approaches, snow will again start to fall at higher altitudes. By the middle of October 1994 (figure 8.1.4c), the region around the Indus is covered again although the Karakoram is essentially the same as in September. A fortnight later, on the 1st of November (figure 8.1.4d), the western Himalayas have received snow, and a week after this (figure 8.1.4e - 8th of November 1994), the summits of the Ladakh chain are again snow-locked. The progressive snow fall can be recorded as the thread-like structure of the darker valleys vanish amidst the bright white of the peaks, allowing estimates to be made of the total volume of snow fallen. By mid-winter (figure 8.1.4f - 31 January 1995), the whole region will be covered apart from the very deep valleys of the Indus and the Sutlej (less prominent, labelled C).

By compiling annual sequences of images, it is possible to build up a profile for a region. Any anomalies in terms of rates of snow fall or thaw, or in their seasonal timing can be noted and appropriate actions taken. While it remains impossible for governments to prevent natural disasters like floods or droughts from happening, any warning of these events can reduce their impact by allowing contingency plans to be drawn up in time.

8.1.5 SEA ICE MONITORING.

Using the data storage facilities of the on-board computers, SSTL's microsatellites are particularly well-suited for geographically remote applications such as iceberg and pack-ice monitoring. During a pilot scheme in March 1994, satellite imagery from a number of sources was used to compile a daily report on the risks posed to shipping by sea ice to the west of Cape Horn [Wagner]. The report [ESYS] concluded that the UoSAT-5 and PoSAT-1 imagery was of comparable usefulness to that from other systems, and a special mention was made regarding the timeliness of data delivery.

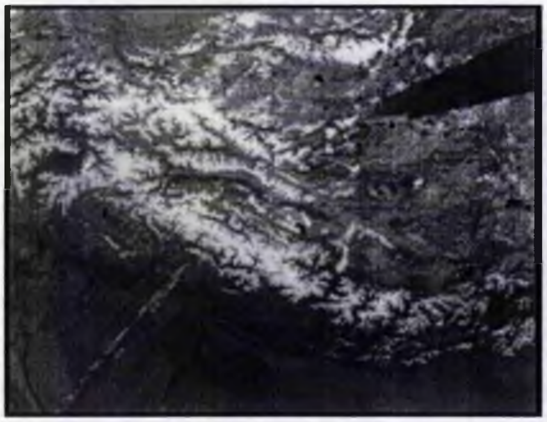

Figure 8.1.4a

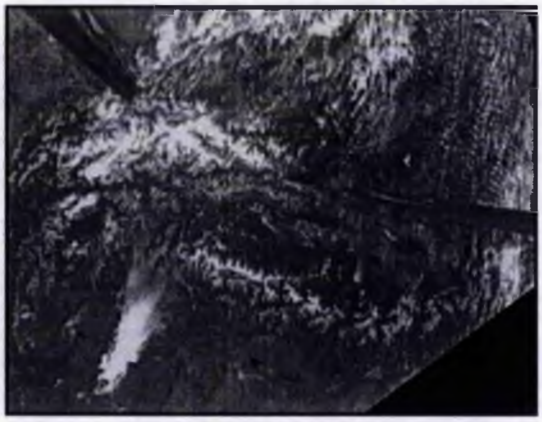

Figure 8.1.4b

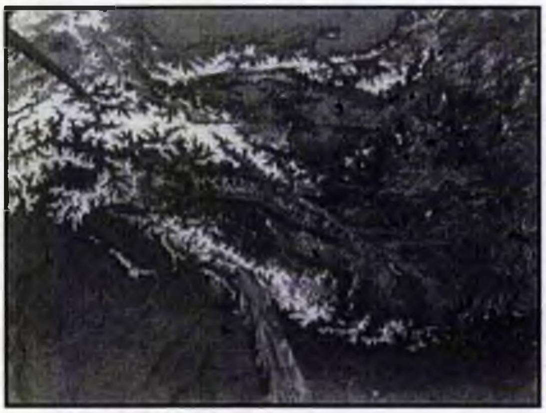

Figure 8.1.4c

Figure 8.1.4d

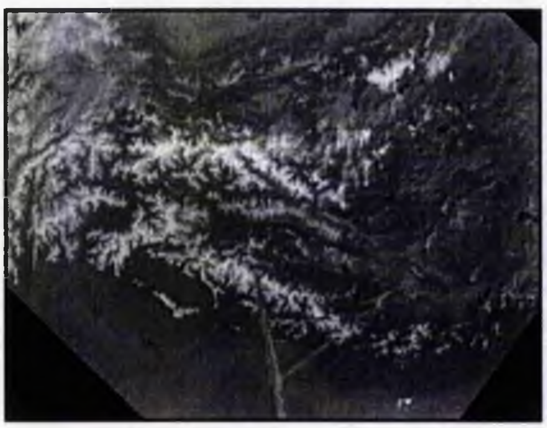

Figure 8.1.4e

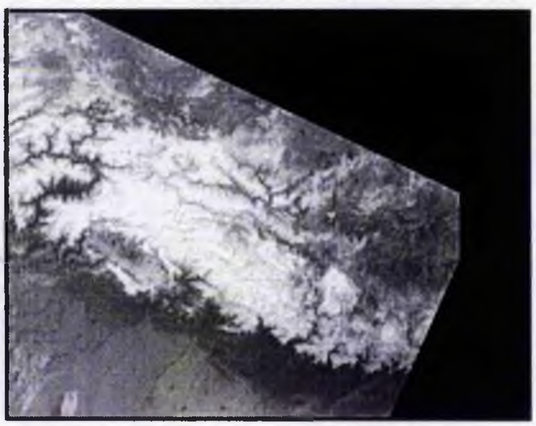

Figure 8.1.4f

PoSAT-1 wide angle images of the Himalaya - Karakoram mountains.

A more spectacular demonstration of this application was fulfilled by UoSAT-5 in November and December 1991, when a huge mass of the Larsen Ice-Shelf broke off into the Weddell Sea (figure 8.1.5). The size of this iceberg was equivalent to that of islands like Jamaica or Cyprus, with an area of 150 by 100 km visible above the surface. Given such huge dimensions, the Wide Angle Camera had little difficulty in tracking the movements of this mass of ice as it drifted away from the Antarctic continent towards the shipping lanes of the south Atlantic. Furthermore, the reflectance of the ice was often sufficiently bright to make it visible through the thick clouds prevalent in this part of the World.

8.1.6 SCENE IDENTIFICATION.

An important function of the Wide Angle Camera (WAC) on SSTL's imaging microsatellite is to act as 'spotter' camera for the Narrow Angle Camera (NAC). The relatively small coverage area of the NAC, or other high resolution imaging systems, can often make scene identification difficult. The major features (mountains, rivers, coastlines) resolved by the WAC allows the NAC image to be situated on a continental scale.

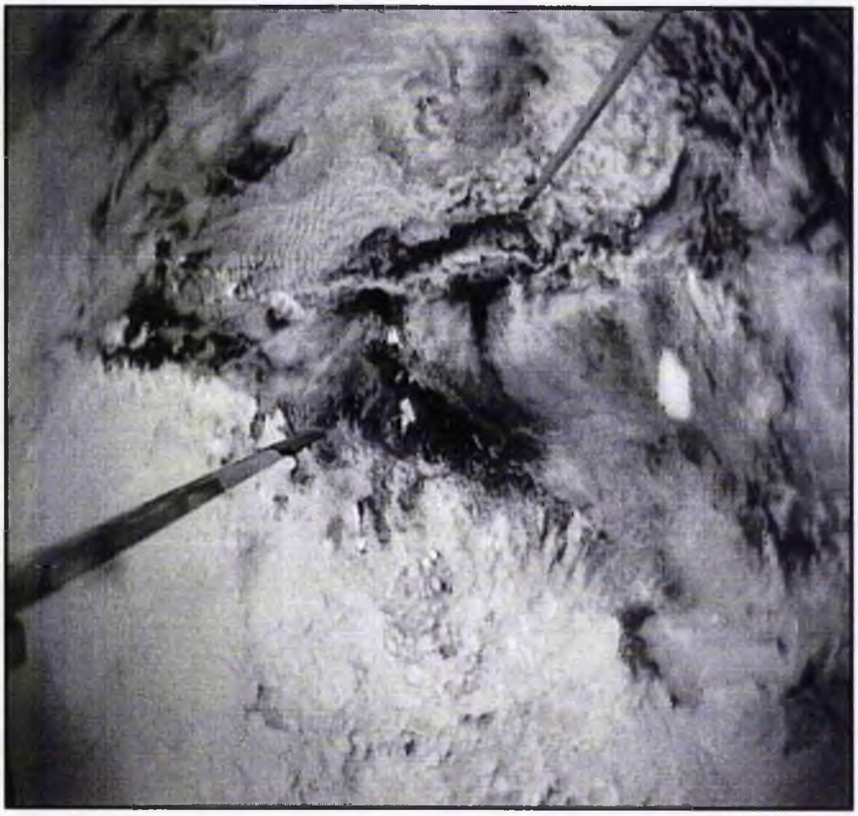

Figure 8.1.5

UoSAT-5 wide angle image of icebergs in the south Atlantic.

8.2 APPLICATIONS OF MEDIUM RESOLUTION MICROSATELLITE IMAGERY.

As already stated, the initial aim of this research programme was to demonstrate low resolution meteorology from microsatellites. It was anticipated that the principal market for microsatellite imaging technology would be the provision of low-cost weather data. The debate surrounding the continued free availability of satellite imagery (typified by ESA's stated intention to encrypt METEOSAT data) led SSTL to conclude that many nations would wish to acquire their own weather satellites.

However, it has been the success of the PoSAT-1 Narrow Angle Camera which has generated the most interest to date. Accordingly, the emphasis of this research programme has shifted slightly to encompass the study of higher resolution systems as well, in response partly to the success of the KITSAT-1 and PoSAT-1 cameras and partly to new commercial opportunities. These lie in supplying the growing demands for remote sensing systems that offer rapid, affordable and *independent* verification of events and data. This need is the cornerstone of many potential markets for small spacecraft. Principal customers are emerging nations who are unable, or unwilling, to pay the large space powers for satellite imagery. These countries view small satellites as an affordable and politically acceptable means of fulfilling their surveying needs for their large and remote territories.

The principle drivers for this expansion of remote sensing capabilities appear to be land resources, environmental monitoring and education, rather than military applications. Although the NAC's resolution is not quite sufficient for some applications (crop monitoring, urban planning, etc.), it has demonstrated that high resolution remote sensing is possible from a low-cost microsatellite, attracting considerable attention from potential customers. It is therefore appropriate to review some of the applications suited to this class of imagery. Many of the images presented here show several applications, and a certain amount of cross-referencing between the following sections is used to draw the reader's attention to these details.

Of course, these images do not posses the visual impact of the high resolution, full-colour imagery produced by LANDSAT or SPOT, but they certainly contain numerous details and evidence of human activity on the surface of the Earth. When viewing this imagery, the reader must always remember that the data was produced by the author alone, with imaging systems costing a few thousand pounds carried by two million pound microsatellites, in contrast with the programme costs of a conventional remote sensing satellite of several hundred million US dollars. Given the difference in scale of the programmes, the author is proud of the quality of the imagery from these cameras relative to existing imaging systems.

8.2.1 OBSERVING TEMPORAL VARIATION.

Given the absence of multispectral capabilities on the current SSTL microsatellites, it is difficult for this imagery to be used for the categorical classification of terrain types. Instead, the most effective role for these cameras is observing change on the Earth's surface, complementing the services of the existing large spacecraft. Traditional spacecraft, with their highly calibrated instruments, are well-suited to making instantaneous measurements with considerable accuracy. However, their usefulness is often limited by the infrequent revisit opportunities [Hannigan et al]. Inexpensive microsatellites can fulfil a valuable function by providing regular imagery to increase the temporal sampling needed for many applications.

Figures 8.2.1a and b show the differences from winter (January 1994) to summer (August 1994) in the area around Kuwait, as recorded by the NAC on board PoSAT-1. The coastline of Kuwait city and the Shatt al Arab sea way are clearly defined. [5] While the clear sea in the Persian Gulf appears very dark, the coastal waters are lighter, indicating either shallow depths (were the sea bed is visible) or turbid river water laden with sediments. The seasonal variation in the waterways of the Shatt al Arab are highlighted by these images; both the width of the estuary and the sediment carried are much greater in the winter scene. Also, in winter the vegetation on the northern terrain is lusher, reducing the scene reflectance. Conversely, there is little or no change in the more arid land around Kuwait city. Note also the plumes from the active oil wells (at the top of the scene, west of the Shatt al Arab). The wind direction is slightly different on the two occasions.

The seasonal changes experienced in Santiago, Chile are even more pronounced, as demonstrated by the scenes in figure 8.2.1c and d, captured in January (summer) and August 1994 (winter). The Maipo river is clearly discernable as a bright stripe through the centre of these scenes, as it leaves its deep valley in the Andes and flows south-west across the plains. The city of Santiago is the uniform area in the top left. The dark patch inside the city (running off the top of the scene) is a large, vegetated park atop a hill.

---

[5] A high resolution SPOT image of the Shatt al Arab is available in [Robas, p.108].

Figure 8.2.1a

PoSAT-1 narrow angle image of Kuwait in winter.

Figure 8.2.1b

PoSAT-1 narrow angle image of Kuwait in summer.

The most striking difference between the two images is the difference in snow-cover on the peaks of the Andes to the east. In figure 8.2.1c, only the highest peaks are covered in snow. As winter approaches, falling snow can adhere to lower slopes, virtually mapping the altitude contours of the mountains. In figure 8.2.1d, the peaks of the lower coastal range have received some snow-fall (bottom left of these sub-images).

In mid-winter (figure 8.2.1d), most of the agricultural lands south of Santiago are bare, creating large uniform areas within the image. This absence of surface variety highlights the area's underlying geological structure, and the shape of the city. Conversely in figure 8.2.1c, the crops are still in the fields, making the scene more heterogeneous due to the differing reflectance of the various types of vegetation. The 'busyness' of this scene makes it more difficult to identify terrain topology due to the effects of the vigorous vegetation.

Comparing these scenes to those in [Sheffield, 1981 p.46] from the mid-1970s, the city's growth is apparent. Constrained by mountains to the east and north (just off the image), the only possible direction for urban expansion has been towards the west and, more significantly, to the south-east. The 5 km agricultural 'green belt' between the city and the Maipo river visible in [Sheffield]'s images has been consumed by the urban sprawl.

8.2.2 SNOW COVER MONITORING.

In the same way that meteorological imagery can be used to provide a continental-scale view of snowfall, medium resolution data is useful for assessing local conditions. An example is the series of images from PoSAT-1 in 1994 taken to support an expedition to the area around the Shyok and Indus rivers, in the Karakoram and Ladakh mountains, in Kashmir in northern India (figure 8.2.2a, 7 June 1994 - corresponds to the WAC image in figure 8.1.4a). Given the remoteness and the on-going armed disturbances in the region, most available maps are inaccurate or out-of-date. Even though PoSAT-1's image resolution is 200 metres, it is more detailed than any commercially available maps. Note the glacier and its moraine in the top left (labelled A), and the tiny strip of darker vegetation on the banks of the Indus at Leh (labelled B).

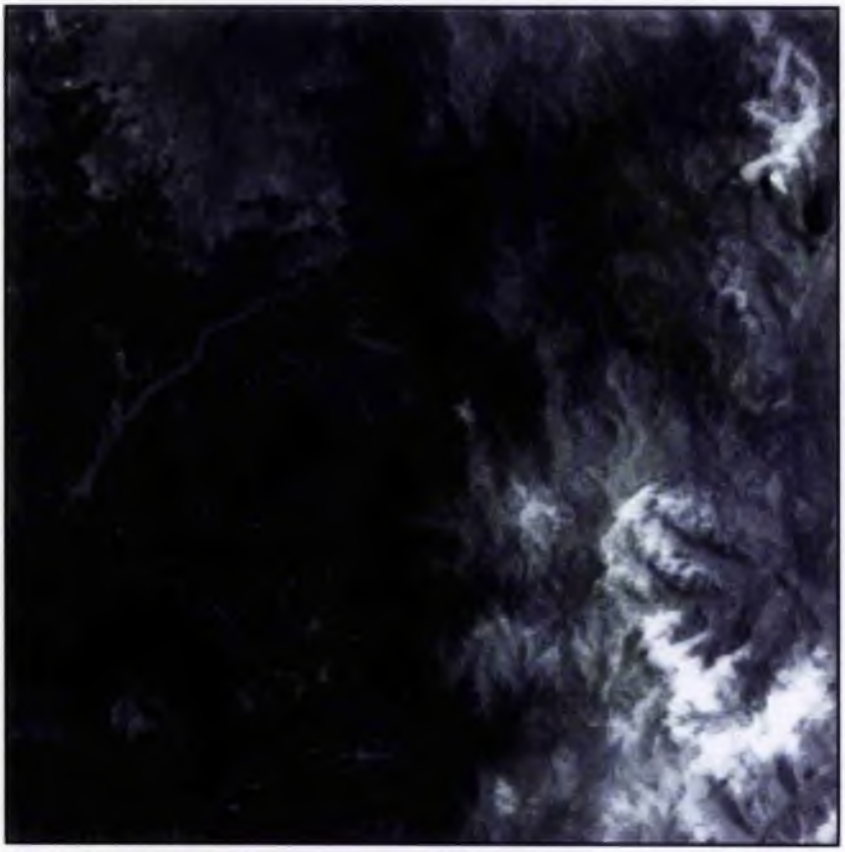

Figure 8.2.1c

PoSAT-1 narrow angle image of Santiago in summer.

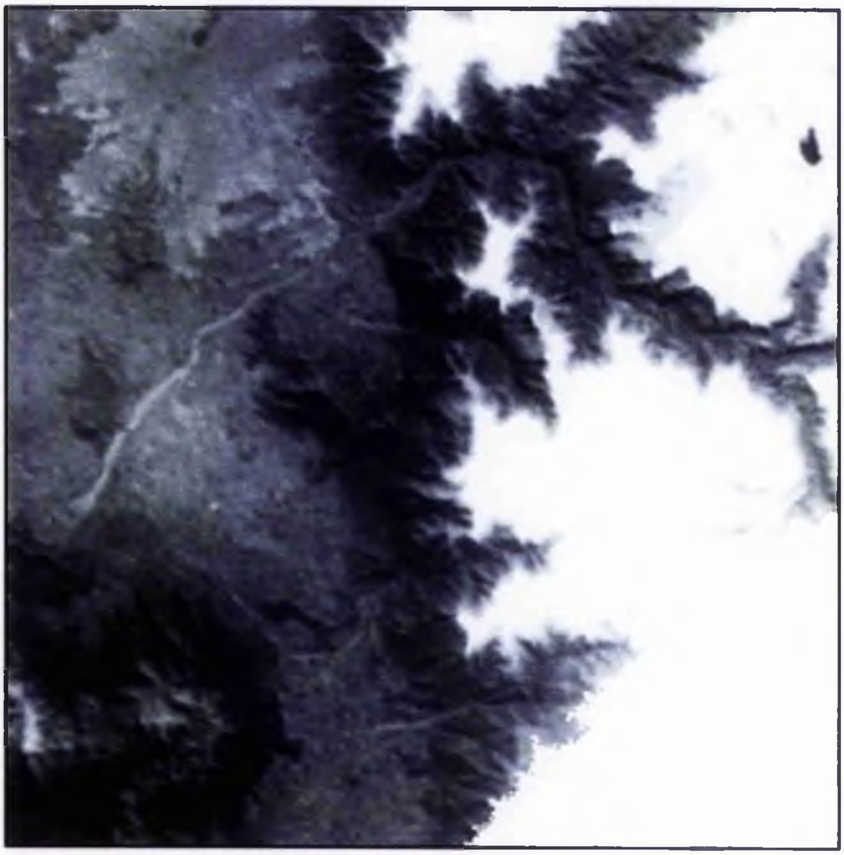

Figure 8.2.1d

PoSAT-1 narrow angle image of Santiago in winter.

Of particular interest to the party was the condition of the Khardung-La pass at Leh (labelled C). Repeated imaging of this area recorded the temporal changes in snow cover, allowing the expedition to plan it's route safely. Figures 8.2.2b, c and d show three images from June to July 1994, when the spring thaw was well under way, although many of the high peaks and passes remained impassable. The condition of this and other passes was monitored throughout the summer. The Khardung-La pass became clear in late August, in time for the planned crossing in September. (The subsequent images through the summer contain numerous small cumulus clouds which have formed along the mountain ridges, also visible in figure 8.2.2d, rendering the differentiation of snow and cloud more difficult. They have not been displayed for this reason).

Figure 8.2.2a PoSAT-1 narrow angle image of the Karakoram & Ladakh mountains.

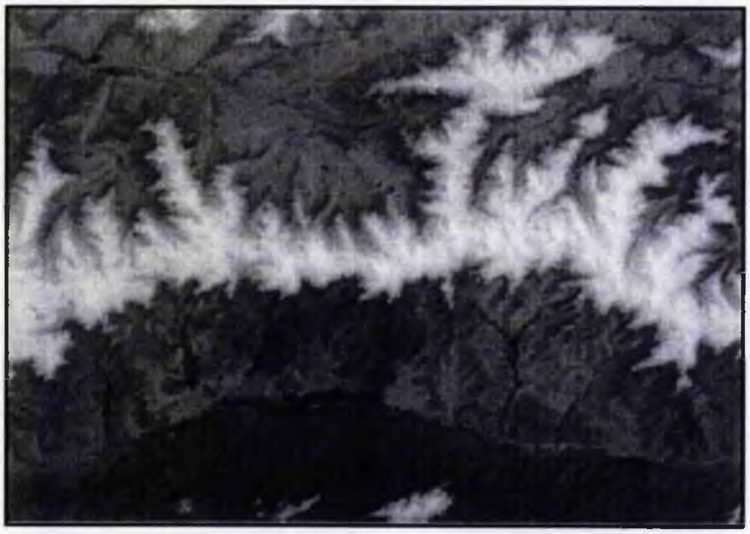

Figure 8.2.2b

(7 June 1994)

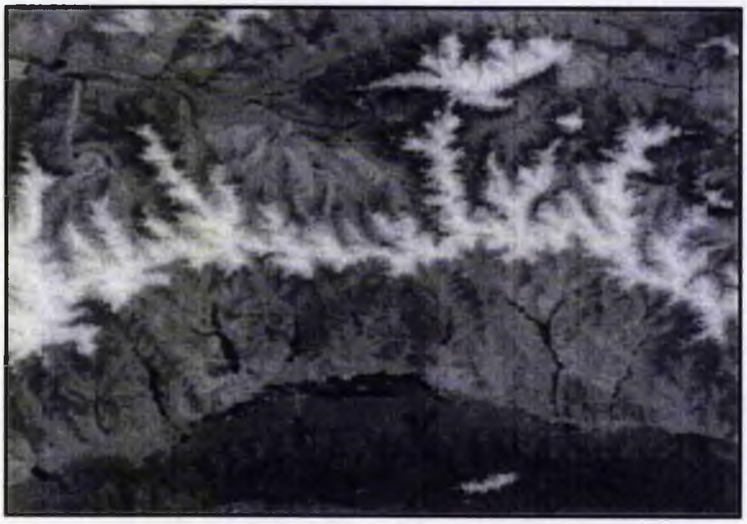

Figure 8.2.2c

(29 June 1994)

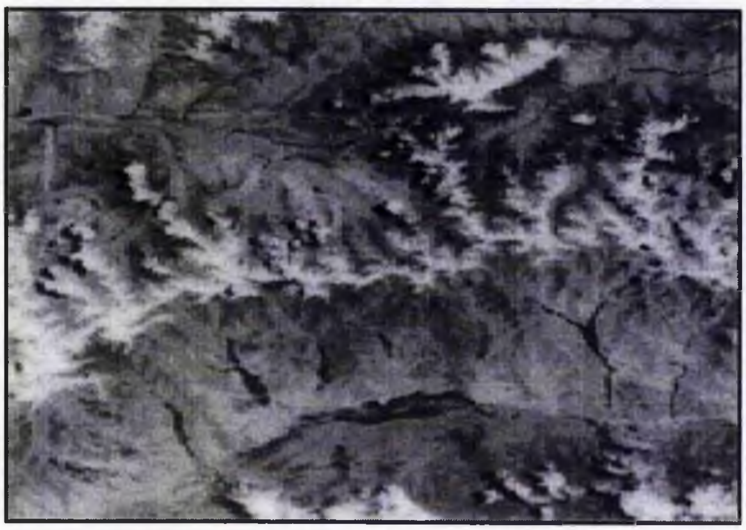

Figure 8.2.2d

(10 July 1994)

PoSAT-1 narrow angle images of the Khardung-La pass, Ladakh mountains.

8.2.3 RIVER ALLUVIUM.

Figures 8.2.3a and b show the city of Vancouver in British Columbia, Canada, two months apart (at the end of March and beginning of June 1995). As with the pair of images of Santiago (figure 8.2.1c and d), there are appreciable differences in the amount of snow-cover on the nearby Coast Mountains. These images may be compared with the LANDSAT MSS images presented in [Sheffield, 1981 p.106] and [Sheffield, 1983 p.64].

Vancouver is located on the fertile alluvial plain of the Fraser river as it flows into the Strait of Georgia and the Pacific Ocean after emerging from the mountains. Figure 8.2.3a shows the Fraser's delta to the south of the city. In this early spring image, the river's water is still clear, making its course to the sea and the nearby coastline well defined. Note the thin plume of sediment at the river mouth.

Conversely, by early June, the Fraser has swollen due to the run-off from melting snow in the Cascade and Rocky Mountains. The large amount of sediment carried by the melt-waters is visible as the river flows into the sea, muddying the clear sea water (normally dark due to its poor reflectance). By watching the patterns that form, it is possible to determine the effect of tides and currents in mixing the river water with the sea water. Some estimates of erosion up-stream may also be possible. Inland, the turbid water of the Fraser is virtually indistinguishable from the surrounding terrain.

Figure 8.2.3c shows the same area, but at the end of June in the previous year. Although, the changes in snow cover are minimal between figures 8.2.3b and c, the 1994 scene reveals that the levels of silt (and by association flow-rate) of the Fraser are further increased. Most of the harbour area is turbid (note the two 5 km long jetties), as are the deeper waters of the Burrard Inlet fjord to the north of the city. Although the total area of silted sea water is greater in figure 8.2.3c, it is interesting to note the very different mixing patterns between the two June images.

Interestingly, although the turbid Fraser remains poorly defined in figure 8.2.3c, the contrast of the various parks and open areas in the city are highlighted due to the dark reflectance of the mature, healthy vegetation. Comparing this with the LANDSAT scene from 1978 [Sheffield, 1983 p.64], the urban encroachment on the nearby forest is visible at the western end of the Burrard Inlet (labelled A). The development is particularly noticeable on the wooded hill at Burnaby Mountain Park, where the dark oval of vegetation is reduced, especially along the waterfront.

Figure 8.2.3a

Figure 8.2.3b

PoSAT-1 narrow angle images of sediment deposited by the Fraser River at Vancouver.

Figure 8.2.3c

8.2.4 TIDAL EFFECTS.

Because of the daily rise and fall of water levels, terrestrial techniques are often poorly-suited to monitoring tidal effects along coastlines. Conversely, satellite imagery can record the extent of tides with ease.

Figure 8.2.4a shows the most northerly parts of the Gulf of Khambhat in western India in February 1995. Estuaries of varying sizes can be seen flowing into the gulf. The humid soils of the tidal zones are darker than the surrounding countryside, revealing a band some 15 km wide on the northern shores of the Gulf of Khambhat. These may be mud flats, mangrove swamps or other marshy terrain, but are unlikely to be sand which would be more reflective. This interpretation is supported by the reproduction of a multispectral SPOT image in [Robas, p.104] of the Narmada estuary, further south in the Gulf of Khambhat.

Figure 8.2.4b shows an image of the same region captured eleven days later. Although the two scenes are largely similar, there are appreciable tidal variations in the coastal areas covered in the later scene (particularly in the bottom left of the image near the town of Kavi). [1] Furthermore, as the sea level rises, solid land / marshy areas previously exposed in the centre of the gulf have become covered. Even so, a few areas of the eastern-most estuary (near the town of Bhadran) exposed in the first image are submerged in the second, indicating that the tidal forces move the sedimentary deposits on a continual basis. Studying such movements is essential for any shipping activities in the region which will need to avoid these sand bars.

Whereas figures 8.2.4a and b are similar, recorded near low tide, figure 8.2.4c shows a substantially altered scene captured at high tide in October 1995. None of the tidal areas visible in the previous images are above water, making it difficult to find reference points.

---

[1] The author is not an expert on the relationship between lunar phasing and tidal phenomena. For those who are, figure 8.2.4a was captured at 06:00 UTC 15/02/95, a few hours before the full Moon. The longitude of the Moon's sub-satellite point was at 91°W. Figure 8.2.4b was captured at 06:00 UTC 26/02/95, three days before the new moon; the lunar sub-satellite point was at 51°E. Figure 8.2.4c was captured at 06:02 UTC 04/10/95, with a quarter waxing Moon; the lunar sub-satellite point was at 147°W. The longitude of the Gulf of Khambhat is 71°E.

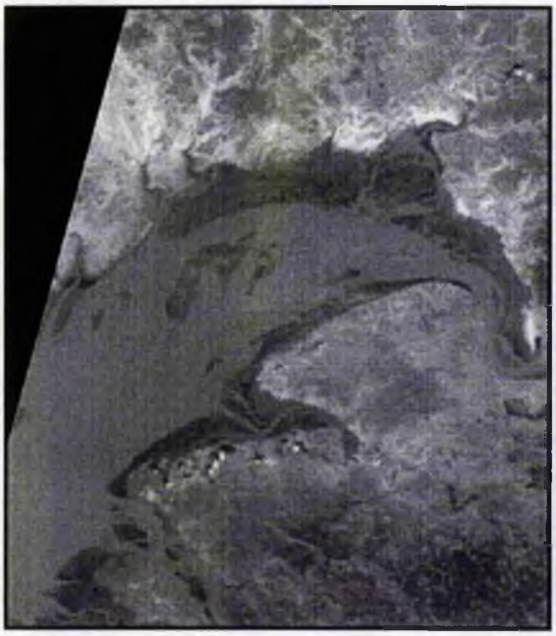

Figure 8.2.4a

Figure 8.2.4b

PoSAT-1 narrow angle images of tidal effects in the Gulf of Khambhat.

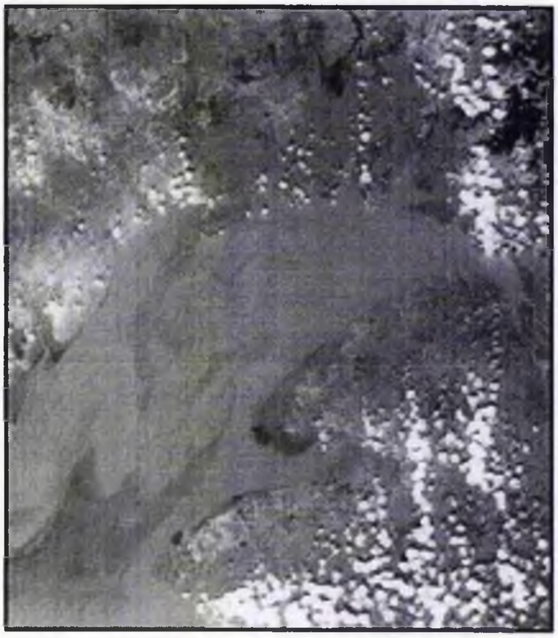

Figure 8.2.4c

8.2.5 HYDROLOGY AND LAND USE.

The complex pattern of rivers, canals and marshes in the Mississippi delta is revealed in figure 8.2.5. The image shows the meandering path taken by the Mississippi river from south of Baton Rouge (centre top of the image) through New Orleans (right) towards the Gulf of Mexico. The silt carried by the river gives it a very bright appearance. This contrasts with the relatively still waters of Lake Pontchartrin (top right corner) and the clover-shaped Lac des Allemands (centre).

Over the centuries, the Mississippi has deposited much of its sediment, creating land firm enough the build and cultivate on. The straight edges of the river banks result from man-made levees to contain periodic flooding. Elsewhere, this scene is dominated by the labyrinth of bayous and canals through the swamps. These marshes gradually give way to the sea beyond the sand bars at the bottom of the image.

This image contains many man-made features. Within New Orleans, large parks (dark rectangles), the airport (the bright patch to the west of the city) and the main thoroughfares are discernable. The causeway leaving the city across Lake Pontchartrin is very prominent, even though it is only a fraction of a pixel wide. Along the Mississippi and some of the major bayous, patchworks of small fields are discernable. The dimensions of these fields are smaller and thinner than those typically found in North America (e.g. figure 8.2.7a), showing the region's historic ties with European agricultural techniques. Finally, the large dark rectangle in the centre of the image is the Larose oil and gas field.

Throughout the area there are many bright, straight lines. These are either roads or canals, but local knowledge is necessary to determine which. In particular, the network of roads / canals to the west of New Orleans is new, not appearing in older LANDSAT images of the area [Sheffield, 1983 p.32]. A more recent PoSAT-1 image (December 1995 versus December 1993), shows a continued development of this area. The small lake has disappeared, and there are many more straight-line features. Maps indicate that this area is being drained for future real-estate development.

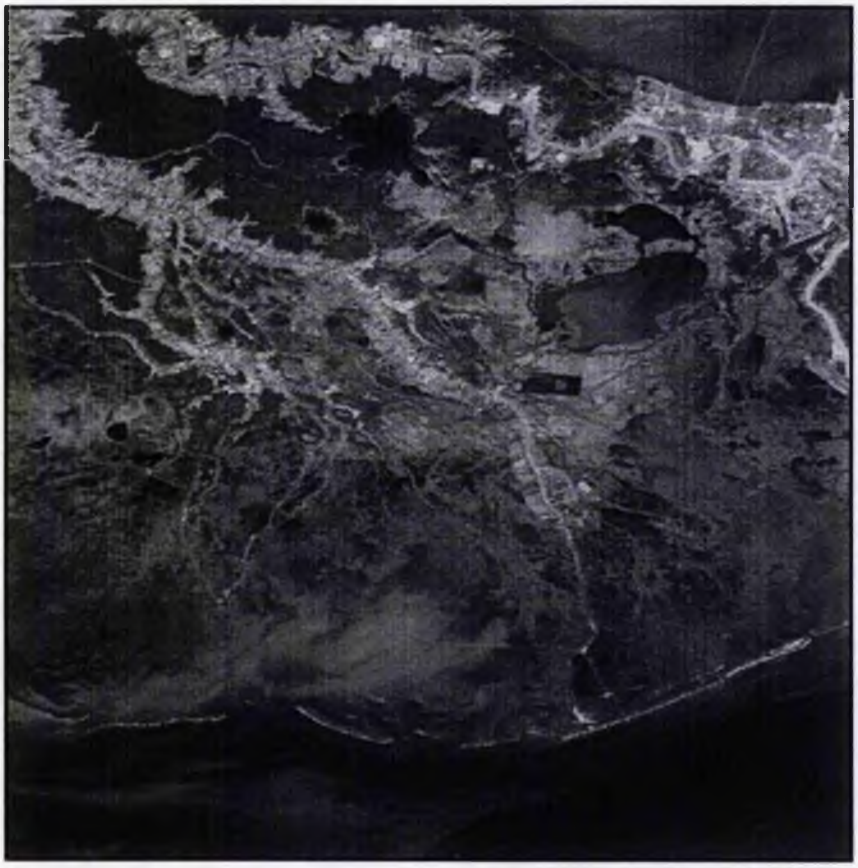

Figure 8.2.5

PoSAT-1 narrow angle image of New Orleans.

8.2.6 IRRIGATION AND AGRICULTURE.

Figure 8.2.6a shows the area around Ciudad Obregon, north-west of Navajoa, in the state of Sonora, Mexico. The region is semi-desert as characterised by the bare soils at the top of the image. Conversely, the lower part of the scene comprises a patchwork of small fields. The variation in reflectance attests to the different crops and / or plant maturity in each field. The source of such fertility in an arid region is clearly revealed in the image. A dam (the Presa Alvaro Obregon) has been built across the Yaqui river to form a large reservoir. Visible in the top left of the scene, the resultant lake possesses the characteristic shape of a flooded valley, with the dam situated at the southern end. The much narrower out-flow is visible to the south. A similar flooded valley, due to the Presa Mocuzari dam, is partially visible on the right edge of the image.

A similar scheme is shown in figure 8.2.6b from January 1994, depicting the El Gezira and Manaquil irrigation projects in the Sudanese desert. The region is located between the White Nile (wide river to the west) and the Blue Nile (narrow river to the

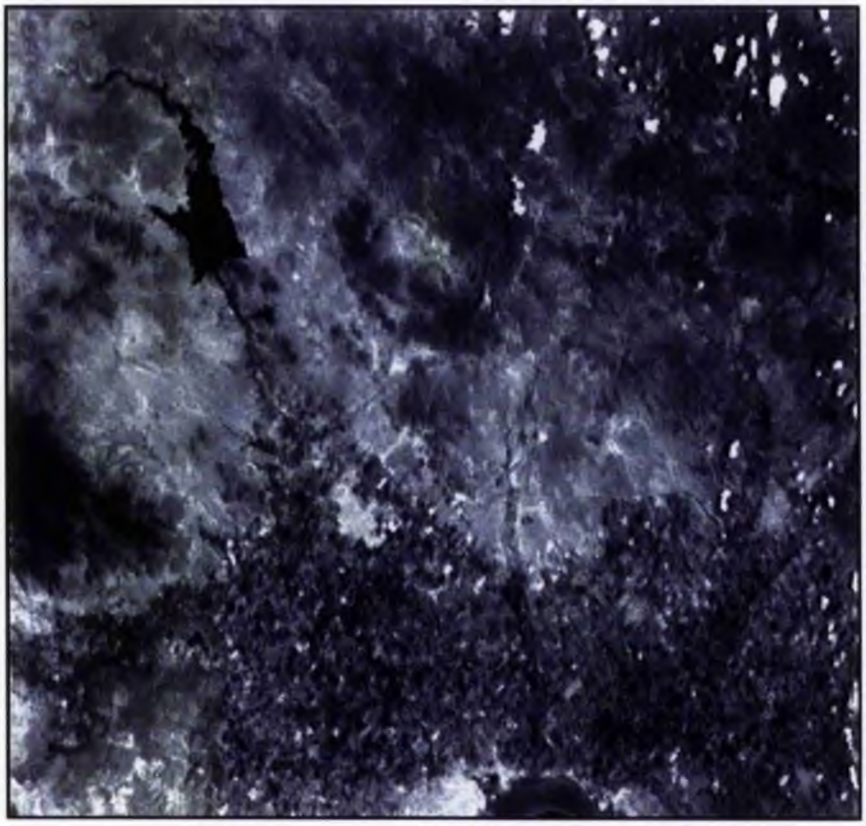

Figure 8.2.6a

PoSAT-1 narrow angle image of the reservoir at Ciudad Obregon, Mexico.

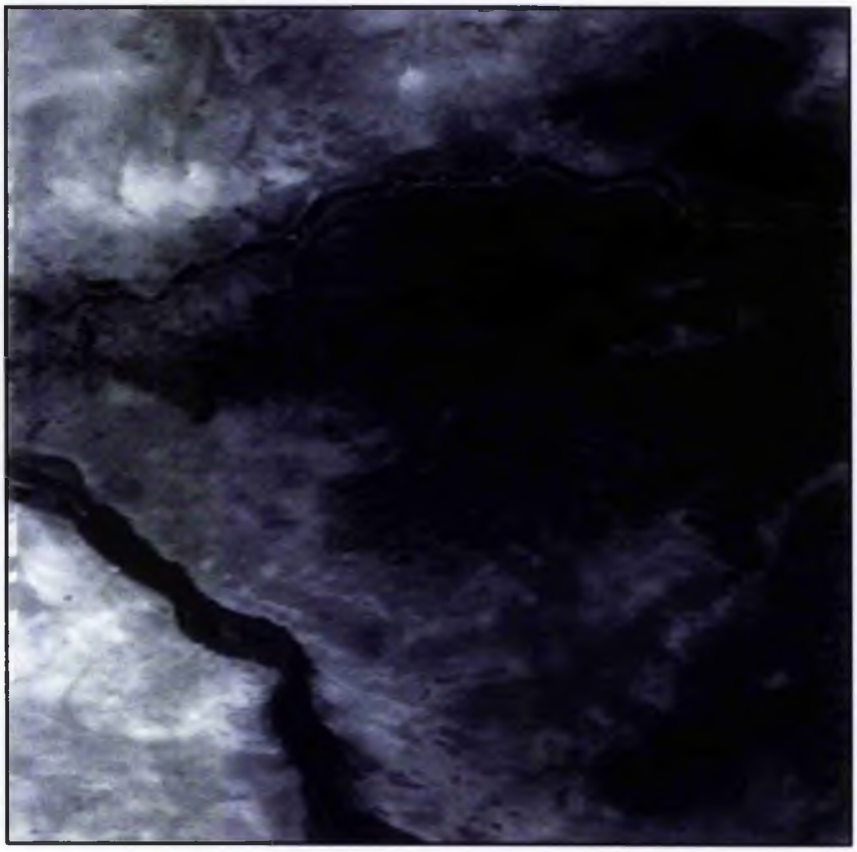

Figure 8.2.6b

PoSAT-1 narrow angle image of the irrigation programme at El Gezira, Sudan.

east), 60 km before their confluence at Khartoum. The constant flow of water needed for this extensive farming programme is provided by numerous canals fed by the dam on the Blue Nile at Sennar (off the image).

Comparing this and other PoSAT-1 image scenes to a similar LANDSAT MSS image [Sheffield, 1983 p.114] from 1979, the expansion of the programme towards the north and south-west is apparent. As with the previous image, the state of the different fields are revealed by their reflectance. Given the knowledge that planted fields are dark, fallow fields are mid-grey and harvested fields are bright (red, grey and white on the false-colour image in [Sheffield]), the monochrome imagery from PoSAT-1 is equally capable of recording the pattern of crop rotation as multispectral data. Unfortunately, the 200 metre resolution of the PoSAT-1 NAC is a little too coarse to separate the individual fields with exactitude, making this classification subject to errors.

PoSAT-1 has imaged several examples of the modern technique of centre-pivot irrigation, where a mechanical structure rotates slowly, dispensing a spray. Used primarily in desert regions where an underground source of water is available to feed the moving structures, these projects leave distinctive circles of vegetation in the middle of arid deserts. Figure 8.2.6c shows examples near the Ismailiya Canal which links Cairo and the

Figure 8.2.6c

PoSAT-1 narrow angle image of the Suez Canal.

Nile to the Suez Canal. There is no evidence of these sites in [Sheffield, 1983 p.96] recorded in 1978. (A high resolution, multispectral SPOT image of this area near Cairo is available in [Lemesle, p.54]). Similar centre-pivot irrigation has also been imaged by PoSAT-1 in southern California.

8.2.7 OBSERVING AGRICULTURAL PRACTICES.

The examples of the previous section show that much can be inferred about local agricultural conditions and techniques from remotely sensed data, particularly the range of crops planted and the size of land parcels. Although the higher resolution and multispectral imagery of the SPOT or LANDSAT instruments is generally more definitive in these studies, these images from the PoSAT-1 Narrow Angle Camera nevertheless contain a significant amount of information.

In contrast with the large and regular fields in these scenes from Mexico and the Sudan, it is not possible to resolve the individual fields in the area around Shanghai (figure 4.5.2d), although the network of irrigating canals is visible. In general, the size of fields, and therefore their ability to be resolved by satellite imagery, varies in inverse proportion to the population density. In the Far East, land parcels are so small that they cannot be resolved by the 200 metre PoSAT-1 imagery. Even though the population density of northern Europe is similar, the percentage of the workforce devoted to agriculture is lower and the average field size is correspondingly larger. Whereas images of eastern Asia are often highly uniform due to the intense rice and small vegetable mono-cultures, many European scenes possess an indistinct 'salt and pepper' texture, resulting from the wide range of crops / cover and the slightly larger field size (approaching the resolution of the PoSAT-1 NAC imagery).

The lower population density in the eastern US (e.g. New Orleans - figure 8.2.5) and Mexico (figure 8.2.6a) result in larger plots of land which can be resolved by the PoSAT-1 camera. It is therefore not surprising that the most obvious signs of agricultural activity in PoSAT-1 imagery are found in the open spaces of North America or ex-Soviet central Asia, where field sizes are correspondingly larger.

Figure 8.2.7a shows a small part of the vast agricultural region of the central plains, Canada's 'bread basket', in this case about 100 km to the south-west of Calgary, Alberta. The entire scene is a patchwork of large fields, most of which are about 500 metres a side (25 hectares). In the bottom right of this scene, are several examples of the distinctive 'strip farming', where swaths of cultivated and fallow land alternate. This assists in preserving the moisture and protects the fragile top-soil from wind erosion. The image was captured in March 1994, which accounts for the bareness of most of the fields. In the bottom left are three white objects which are frozen lakes at Namaka, south of Strathmore. Above the triangular lake, the Trans-Canada Highway is visible as it runs to the east and turns abruptly to the south. North of the bend, the Rosebud River runs to the north-east, where it eventually merges with the Red Deer River, which is flowing towards the south-east, and into the bottom right of the page. The canyon / gullies of the Red Deer River are clearly visible here. The higher ground East of Drumheller (right of image) and around Rumsey and Big Valley (top of image) are dusted with a thin coating of snow.

However, the largest evidence of human agricultural activity recorded by the PoSAT-1 NAC was in Victoria State, Australia, shown in figure 8.2.7b. In the bottom right of the image, a portion of Lake Hindmarsh is visible, along with the outlet to Lake Albacutya (off the image). Both lakes are fed by a number of rivers, principally by the Wimmera river to the south-east, but neither has an outflow to the sea. The dark area dominating the centre of figure 8.2.7b is a large marsh which is flooded regularly when the water levels in the lakes rise.

This marsh is part of a protected area (the Big Desert Wilderness National Park and the Wyperfield National Park). Around the marsh, intensive agricultural activity is clearly visible. These belts encompass a number of small towns located along the National Route 12 to the north, and National Route 8 to the south. Of particular interest are the huge fields penetrating into the southern parts of the marsh. These measure some 5 km a side, and are doubtlessly part of land reclamation projects.

This image was captured in December 1995, at the end of spring, when the water levels are ostensibly at their highest. The lighter areas within the marsh are most likely better drained, with some bare soil visible. By sensing solely in the red band, it would not be possible to determine whether this area was marshy or densely vegetated, as both types of cover have low reflectance. However, as this feature is large enough to be resolved by the WAC, which has a near-IR sensitivity, it is possible to confirm that this area is indeed water-logged. If it were a forest, the strong reflectance of the vegetation would make it as bright, or brighter, than the surrounding cultivated lands.

Figure 8.2.7a

PoSAT-1 narrow angle image of fields in Alberta, Canada.

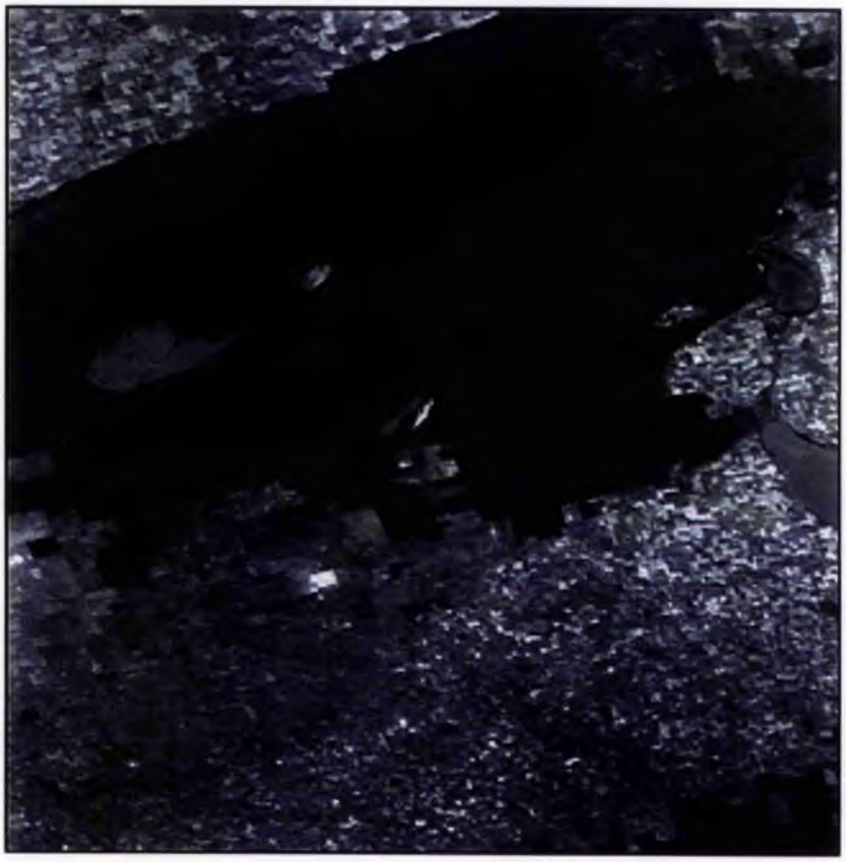

Figure 8.2.7b

PoSAT-1 narrow angle image of marshes near Lake Hindmarsh in Victoria, Australia.

8.2.8 DEFORESTATION.

One of the most critical environmental problems currently faced is the destruction of tropical rain forests. Given the remoteness and inaccessibility of these regions, satellite remote sensing is a very effective tool in detecting this deforestation, which is for the most part illegal. Although an orbiting satellite can survey rain forests, obtaining useful data can be difficult due to the prevalence of heavy clouds and haze (as alluded to in section 3.1.3). The deployment of microsatellite imaging systems would be particularly useful in improving the frequency with which data can be gathered.

A example of this type of imagery is presented in figure 8.2.8, captured over the Bolivian states of Pando and Beni in September 1995. The featureless mass of the Amazonian forest gives this image less immediate impact than others in this chapter, and requires more subtle interpretation. The left half of the image is veiled by thin cloud, further hampering analysis.

At the top of the image, the Beni river is easily recognisable due to its strong contrast with the dark forest. The river is joined from the west (from the top-left corner) by the Madre de Dios river at the town of Riberalta (labelled A). The small town of Morero is visible (labelled B). The scene also contains other smaller rivers: the Ortón (labelled C) and the Yata (labelled D). The meandering paths of the larger rivers attests to the lack of significant geological relief in the region. This is confirmed by the presence of ox-bow lakes (labelled E), which mark former water courses. A few kilometres to the west

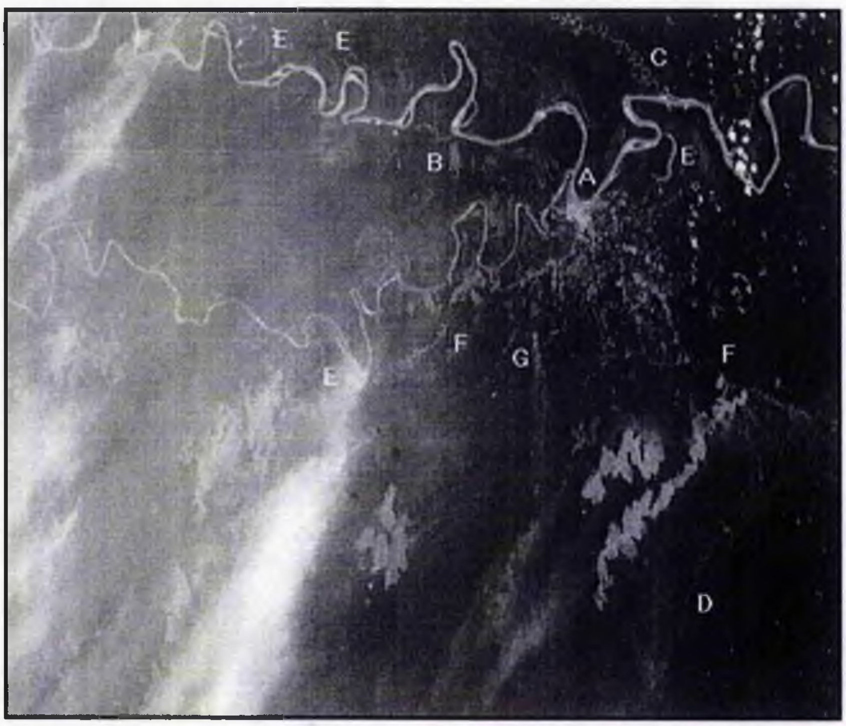

Figure 8.2.8

PoSAT-1 narrow angle image of deforestation in the Bolivian Amazon.

of this scene, the rivers flow into a tributary of the Amazon, the Mamoré, which forms the border with Brazil.

To the south of Riberalta, numerous small fields are visible, their bare soil appearing bright against the dense vegetation of the surrounding forest. A number of roads leave the town (labelled F), one running south-west, parallel to the Beni, and another towards the east. Along these roads, numerous small ingressions into the forest are discernible. These are the result of either primitive ‘slash and burn’ agricultural techniques, or of commercial logging.

A number of much larger cleared areas exist across the centre of the image. These are sufficiently large to be resolved on the WAC imagery, the near-IR sensitivity of which confirms that they are indeed bare soil. (Vegetation has low reflectance in the red band but strong reflectance in the near-IR, whereas bare soil is more consistent across these bands. Therefore, these cleared areas appear dark in the WAC image).

The most significant feature in this image is the plume of smoke emanating from the virgin forest (labelled G). The angle of the smoke (to the south) conclusively eliminates the possibility of this being a cloud (which are oriented along a south-west, north-east axis). This form of ‘proof’ is essential in the combat against illegal deforestation. Even if it is impossible to extinguish the fires before damage has been inflicted, such imagery does at least arm the authorities with evidence with which to prosecute the guilty parties.

8.2.9 GEOLOGY.

Satellite imagery is often used to provide data for geological surveys. With some prior knowledge of a region’s overall structure, experts can analyse imagery to provide a detailed profile of local characteristics. By searching for and interpreting specific features, it is possible to identify areas which are likely to yield valuable mineral resources. In many cases, access to suitable remotely sensed data can eliminate the need for expensive, lengthy, and occasionally dangerous, ground surveys when selecting sites for potential exploitation. Although satellite imagery alone will rarely be adequate to conclusively determine the presence of particular mineral deposits, it has become a valuable tool for mineral and oil exploration.

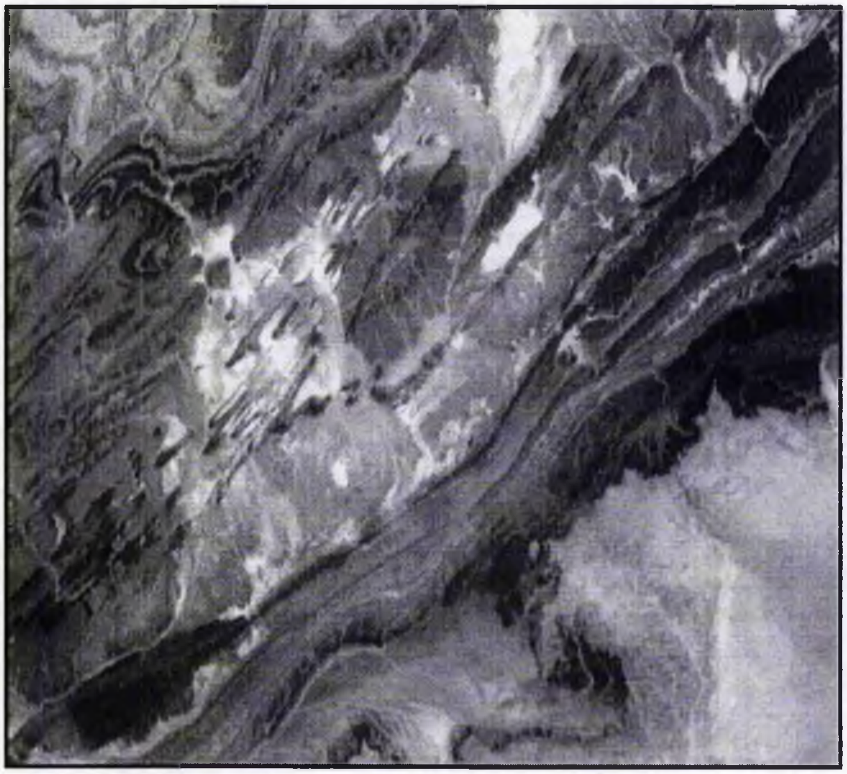

Figure 8.2.9a

PoSAT-1 narrow angle image of the Anti-Atlas mountains, Morocco.

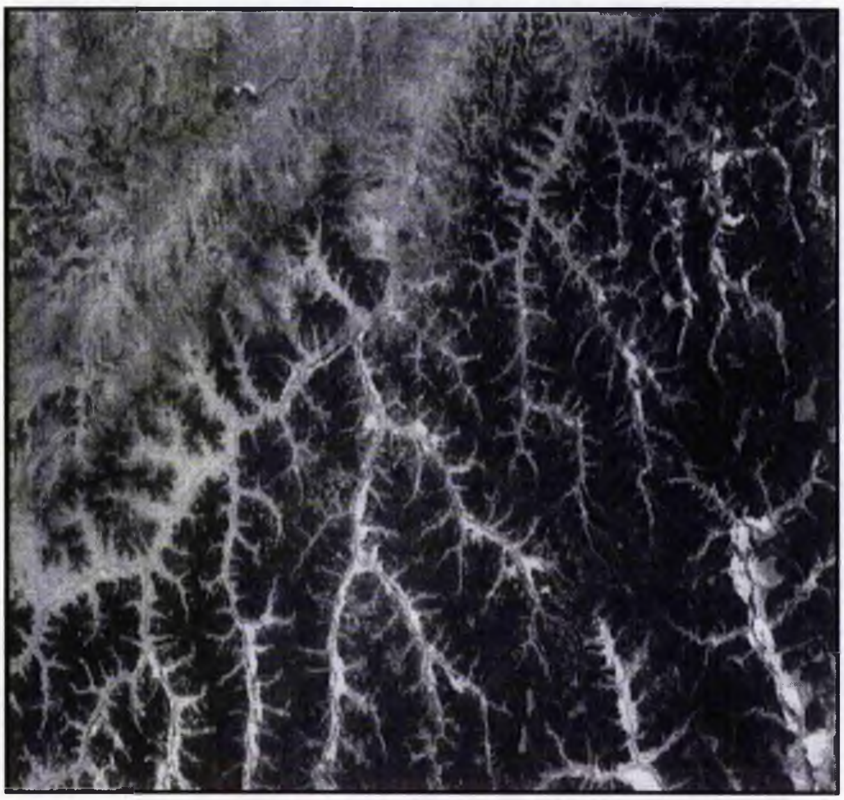

Figure 8.2.9b

PoSAT-1 narrow angle image of drainage patterns, Angola.

Figure 8.2.9a shows an image captured over the Anti-Atlas mountains in southern Morocco in July 1995. The lighter area in the bottom-right of the image are the sands of the Sahara desert over the border in Algeria. The abstract swirling patterns are caused by rock strata and the stark shadows cast by the barren landscape of buttes, mesas and canyons. The linear feature running diagonally across the image is a gorge eroded by wind and water. Although the river bed is dry in this summer image, this water course will contain a violent mountain torrent in spring. Skilled interpretation of the shadows, the drainage patterns of dry river beds and water run-off, and the accumulation of wind-blown sand would allow a terrain model to be generated from this type of two-dimensional image.

It is also possible to use satellite imagery to gain insight into the geology of more fertile regions where the bare soil is not always visible due to vegetation cover. For example, the fractal patterns of mountains and valleys 200 km east of Huambo, in Angola, is recorded in figure 8.2.9b. The dark regions are wooded hill-tops and the valleys are clear, appearing brighter. The undulations of the small rivers delineate subtle variations in relief.

8.2.10 DETECTING OIL SLICKS.

Although the possibilities for using microsatellite imagery discussed so far have concentrated primarily on terrestrial applications, a unique feature of remote sensing satellites is their ability to image the open seas. Given the poor reflectance of clear sea water to all wavelengths longer than 0.55 μm (blue-green), the red and near-IR sensitivities of the SSTL cameras is not ideal for oceanography. Nevertheless, there are some roles that these microsatellites can fulfil, most notably in the detection of oil slicks.

Oil spilled into water forms a very thin film on the surface, leaving a distinctive signature to instruments sensing visible light. The oil film changes the surface tension, reducing surface roughness, making the sea a specular, rather than diffuse, reflector [Mertikas & Giavi]. Consequently, less Sunlight is scattered back towards the satellite, making oil spills appear darker than the surrounding water. This source provides an example from Crete using SPOT imagery.

The PoSAT-1 NAC image in figure 8.2.10 shows virtually identical properties. Piraeus, the harbour of Athens (labelled A), is extremely busy, especially at the start of the summer break (July 1994). Furthermore, the sea in this region is enclosed tightly, reducing the natural dissipation of oil by wave and current action. In the sea surrounding Athens, there are two distinct areas with reduced reflectance (labelled C), both of which are along

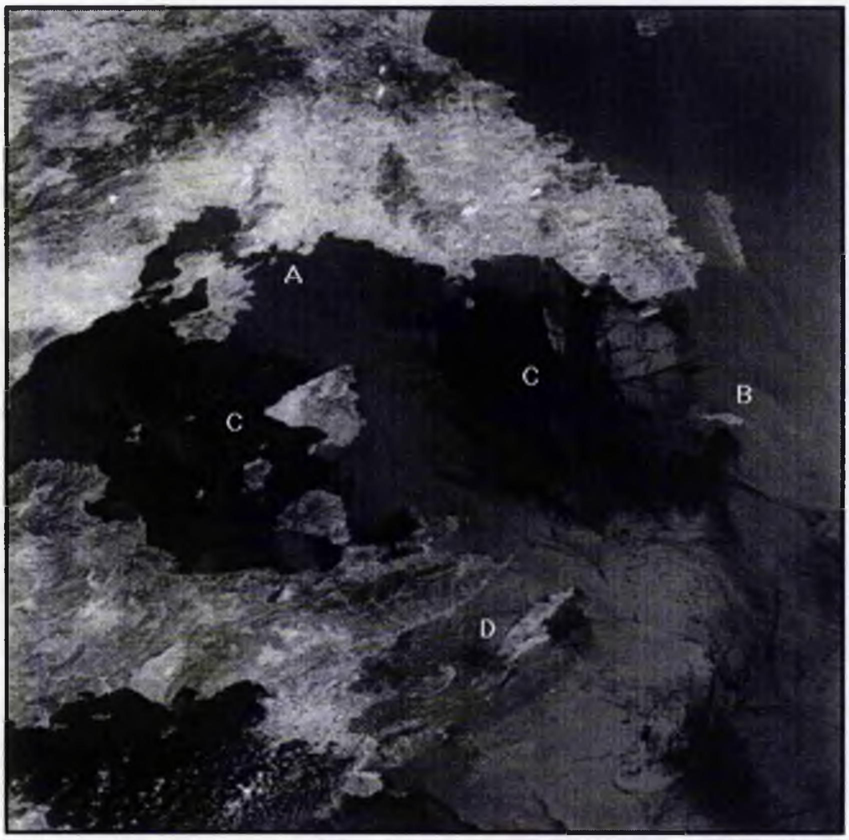

Figure 8.2.10

PoSAT-1 narrow angle image of potential oil slicks near Athens.

major shipping routes, and are therefore extremely likely to have suffered one or more oil spillages. To the west of Athens lies the Corinth Canal. To the east, the shipping routes pass west of the island of Ayios Yeoryios (labelled B), en-route to the Cycladic Islands, Crete and Cyprus. In this area, there are also numerous ship wakes that have disrupted the surface. A smaller candidate for an oil spill is at the small, but popular, holiday port on Ihdra (Hydra - labelled D).

It is necessary to supplement satellite imagery with additional data (with both UV imaging and ground-based measurements) to conclusively identify oil spillages from benign changes in sea surface reflectance. Nevertheless, microsatellite imagery appears to be as appropriate as existing data sources for detecting oil slicks. It would be feasible to use microsatellites to identify potential spillages, relying on subsequent confirmation by conventional techniques. Thereafter, established pollution zones could be monitored from remotely sensed data.

8.2.11 URBAN DEVELOPMENT.

Given the relatively coarse resolution of the PoSAT-1 NAC, it is not surprising that most of the applications identified so far emphasise fairly large scale phenomena.

Nevertheless, it is possible to use this type of imagery to monitor the development and expansion of urban areas.

Even though the individual streets of Kuwait city (figures 8.2.1a and b) are much smaller than the 200 metre pixel resolution, the structure of the town is clearly visible. Large features such as the harbour, airport, oil wells and the major roads leaving the city are discernable. The long straight lines on the Iraqi side of the Shatt al Arab are clearly man-made structures, either roads or canals.

Similarly, many aspects of US cities are large enough to be discernible. Although denser than New Orleans (figure 8.2.5), numerous features of New York can be identified by studying figure 8.2.11a. For example, the Verrezano-Narrows Bridge across the Hudson river between Staten Island and Long Island is visible (labelled A). Central Park in Manhattan (labelled B) stands out as a dark, narrow rectangle, with its lake (the Central Park Reservoir) discernible as a darker patch. Many other parks, harbours and major transport arteries can also be recognised. Kennedy Airport stands out prominently as a bright area (labelled C).

Conversely, the large urban area of Tokyo and Yokohama (in figure 8.2.11b) appears as a uniform area to the west of Tokyo bay. The snow-capped Mount Fuji is the

Figure 8.2.11a

PoSAT-1 narrow angle image of New York.

prominent white feature in the mountainous south-west of the scene. Tokyo is a much denser city than Kuwait or New York, and few details of the city's structure are visible at this resolution. Nevertheless, the major features along the shoreline stand out clearly. From the north and west, the Edo, Ara, Sumida and Tama rivers flow into the bay, and Tokyo International (Haneda) Airport is the bright oval projecting into the bay (labelled A). The jetties and wharves of Yokohama and Kawasaki (labelled B) and Ichihara (labelled C) are very distinctive on the bay's shore. The water pollution of the port is revealed by a band of lighter a shade stretching into the harbour (immediately to the east of label B).

When comparing this scene to old LANDSAT imagery from 1972 [Sheffield, 1981 p.55], it is interesting to note the extensive land reclamation projects that have been undertaken. The regularly shaped islands off Yokohama and in the mouth of the Sumida river did not exist twenty years ago (north of label B), and Haneda airport was half its current size. [2]

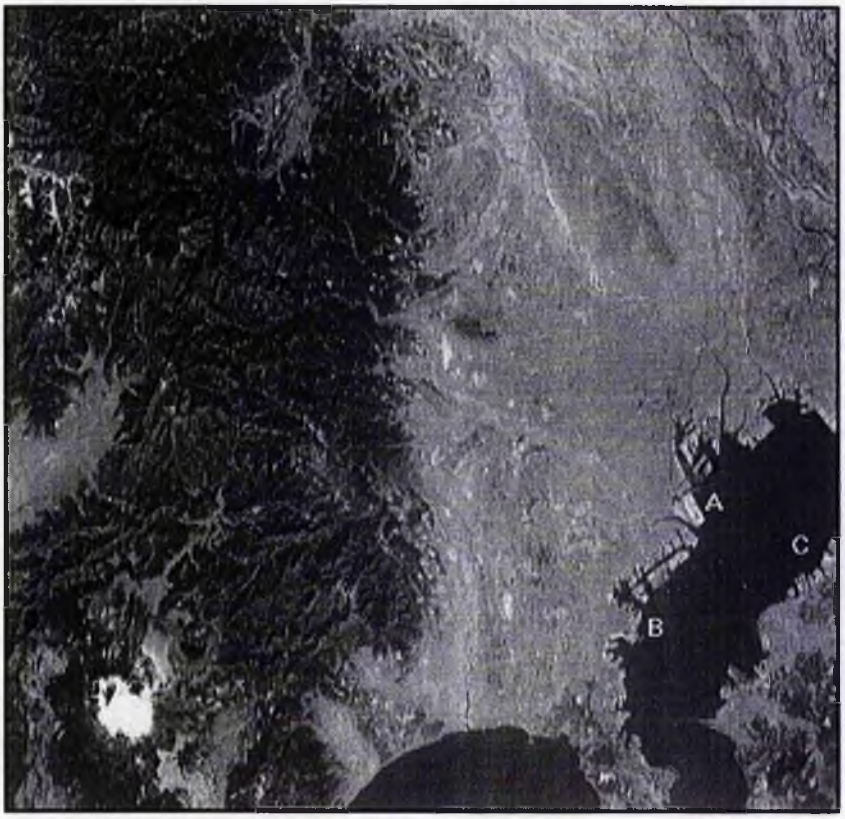

Figure 8.2.11b

PoSAT-1 narrow angle image of Tokyo.

---

[2] A contemporary high resolution, multispectral image of Tokyo harbour captured by JERS-1 is provided in [Corbley].

8.3 CONCLUSIONS.

These examples demonstrate the high quality of data obtained from the author's cameras and some of the wide range of applications that can be fulfilled by these low-cost microsatellite systems. While not offering the same pixel densities and multispectral capabilities as conventional remote sensing satellites, the discussions of this chapter demonstrate the feasibility of using microsatellite for useful scientific or commercial Earth observation. The performance of these cameras emulates that of traditional instruments, but at a tiny fraction of the cost.

A limitation of the existing remote sensing systems, based on large platforms, is the long delays between revisits over specific targets. Because of this, many transient events, such as fires, volcanic eruptions, or floods are likely to be missed. Accordingly, the author anticipates that the first commercial role for imaging microsatellites will be to augment traditional remote sensing satellites by increasing the temporal resolution of data gathering. The instruments carried by the conventional platforms will continue to be used in their current function, offering highly calibrated data for absolute classification and identification. Microsatellites will provide frequent updates which can be referenced to traditional data as needed. This two-tier approach of implementing constellations of remote sensing satellites will provide a significant enhancement to current services, at modest extra cost.

In the medium term, the platform and instrument capabilities of small spacecraft will improve to the point of rivalling the performance of traditional large satellites. Therefore, it is very feasible that small vehicles (although probably larger than 50 kg microsatellites) will soon become more attractive than the current generation of large remote sensing systems.

8.4 REFERENCES.

Corbley K.P: Remote sensing - the third great space race; Via Satellite, Vol.9 No.12, p.46-51, Dec 1994; ISSN 1041-0643.

Ellis W.S. & Turnley D.C: A Soviet sea lies dying; National Geographic, Vol.177 No.2, p.72-94, Feb 1990.

ESYS Ltd: Preliminary report of Sea Ice Demonstration, ref ESYS-LET-CB-1478-94, ESYS Ltd, Berkeley House, London Square, Cross Lanes, Guildford, United Kingdom.

Hannigan R et al: The feasibility and usefulness of Earth observation from small satellites; Conference on Small Satellites for Remote Sensing, The Space Congress, Bremen Germany, 24-25 May 1995.

Lemesle J.P: Le tour du monde en 2 heures; Le Cherche Midi, 1989; ISBN 2-86-274-1574.

Mertikas S.P. & Giavi V: Detection of oil spills using SPOT remote sensing data; Earth Space Review, Vol.4 No.2, p.19-24, Apr-June 1995; ISSN 1060-1848.

Robas: Satelliet beeldende kunst; Robas, 1991; ISBN 90-72770025-0.

Sheffield C: Earth watch; Sidgwick & Jackson, 1981; ISBN 0-283-98737-5.

Sheffield C: Man on Earth; Sidgwick & Jackson, 1983; ISBN 0-283-98956-4.

Wagner M.J: Around the world in nine months with satellite data; Earth Observation Quarterly, No.44, ESA Publication Division, June 1994.

CHAPTER IX

CONCLUSIONS AND TOPICS FOR FUTURE RESEARCH.

Chapter 9 summarises the main topics covered and the key conclusions derived in the course of the thesis. Recommendations for the choice of sensors and systems suitable for low, medium and high resolution applications are made. Finally, thoughts on the future direction and opportunities for microsatellite Earth observation are presented.

9. CONCLUSIONS AND TOPICS FOR FUTURE RESEARCH.

In this thesis, many different aspects of implementing remote sensing on board microsatellites have been reviewed. These arguments have been formulated in response to the observations made in preparing five generations of electronic cameras flown on SSTL's spacecraft.

The discussions of this thesis have shown that a 50 kg microsatellite presents a very different set of design constraints to those encountered on a conventional, large remote sensing spacecraft. This research has demonstrated that Earth imaging is possible on such small vehicles, provided a fresh approach is taken. If the author had followed the established tradition of using scanning imagers, this programme would probably have failed. Conversely, the choice of using electronic CCD cameras has met with success, demonstrating the feasibility of microsatellite remote sensing.

Before drawing the final conclusions and presenting thoughts on future development, it is appropriate to review the main points of this thesis.

9.1 REVIEW OF THE MAIN POINTS OF THIS THESIS.

9.1.1 THE CONSTRAINTS OF REMOTE SENSING WITH MICROSATELLITES.

In chapters 2 and 3, the general profile of microsatellites was defined, and the specific constraints of these small platforms for Earth imaging have been discussed. The recent advances in the development of charge-coupled device (CCD) imaging arrays has minimised the consequences of a 50 kg spacecraft's restricted mass, volume and power on the design of the imaging instrument. While it is quite possible to design solid-state imaging systems to operate within these constraints, the demands of traditional mirror-scanning (whiskbroom) instruments are too great to be accommodated by a microsatellite platform.

It is the coarse attitude control of a microsatellite, at least when compared to conventional remote sensing spacecraft, that has the greatest role in defining the type of imaging system used. Current microsatellites can only offer a limited pointing accuracy to within three to five degrees, making targeting of specific areas somewhat unpredictable. However, it is the relatively large drift rates experienced by the platform which presents the greatest difficulties. Without an exceptionally stable platform, it is impossible for scanning instruments to remain aligned with the scene, causing significant errors in the pixel-to-pixel registration of the imagery collected.

For this reason, the only viable option for implementing optical remote sensing on the current generation of microsatellites is to employ electronic cameras. Because of the two dimensional structure of an area-array CCD sensor, these instruments can capture an entire scene in a single operation, making them immune to attitude disturbances. Accordingly, solid-state cameras will remain the only suitable architecture for collecting remotely sensed data from microsatellites, until the attitude control of these small satellites can be made to achieve sub-degree pointing accuracy, coupled with very slow drift rates. Nevertheless, even when such attitude control capabilities become available, it is by no means obvious that a pushbroom scanner will be more attractive than a solid-state camera, and a suitable reappraisal of the various factors governing both the system design and image quality will be necessary.

In addition to their ability to produce registered imagery despite attitude instabilities, CCD cameras possess a number of other attributes suitable for use on microsatellites. The systems developed by the author for several SSTL missions have had modest power requirements (250 mWatts continuous, 5 Watts peak), low mass (0.6 kg without optics), and use no moving mechanics. The solid-state implementation of the sensor ensures a robustness and mechanical invariance not possessed by many other types of imaging technology. In particular, the radiometric stability (in a low radiation environment) and linearity of these silicon sensors ensures a high degree of consistency in the imagery gathered.

While the attitude stability of current microsatellites restricts the options available for implementing the imaging instrument, their small communications channels hamper the exploitation of a remote sensing payload. The designs of many existing microsatellites have been tailored for low data rate digital communications, implementing complex, multiple-access software protocols. This communications strategy is poorly suited to the requirements of remote sensing missions which need to dump large volumes of imagery to the ground. Various hardware and software techniques are needed to increase the effective data rates on the downlink from the current 9600 bps to 1 Mbps and greater.

Thus, operating Earth observation systems on microsatellites presents a number of additional difficulties and constraints not encountered on the larger platforms of traditional remote sensing spacecraft. Accordingly, alternative approaches and solutions must be employed to gathering imagery from microsatellites.

9.1.2 CHOICE OF CCD SENSOR.

There are a large number of area-array CCD sensors available for commercial and scientific applications, many of which may be suitable for remote sensing. While the general properties of most CCDs are similar, there are a number of factors which can make a particular device more attractive for satellite remote sensing. These include:

- A large number of photosites (pixels),
- The simultaneous collection of all pixels (no interlacing),
- A spectral response extending into the near-IR and / or UV,
- The presence of electronic shuttering,
- A suitable architecture giving immunity to smearing (under expected imaging conditions),
- Easily controllable integration time (exposure) and the presence of antiblooming,
- Suitable dimensions of the individual photosites and the whole array.

While these are desirable features for all imaging systems, the importance of any given parameter will reflect the specific requirements of the application, and the sensor must be selected accordingly. On the whole, higher resolution applications present more restrictions on the choice of sensor / camera to overcome the increased blurring caused by the satellite's velocity.

9.1.3 DEVELOPING THE CAMERA.

When a CCD sensor has been selected, it is necessary to develop the surrounding circuitry to support the sensor, thereby creating an electronic camera. CCD sensors are complex to operate, demanding suitable clock phasing, signal conditioning and a clean electrical environment. To assist in the development of an electronic camera, it is very beneficial to exploit as much of the manufacturer's expertise as possible. Unfortunately, it is unlikely that any off-the-shelf camera systems will meet all of the imaging and environmental criteria for remote sensing from space. A good compromise solution is to use the dedicated support chips supplied or recommended by the manufacturer wherever possible, simplifying the design task but without sacrificing too much flexibility. Although the recent developments in programmable logic and simple-to-use analogue video components are reducing the difficulty of designing the camera circuitry in-house, first-time designers are recommended to use a commercially available chipset to maximise their chances of success.

Whereas dedicated support chips are often available to drive the CCD's inputs and process the output signal, the digitisation and frame-store circuitry will need to be specifically developed for the electronic remote sensing camera. Even though these digital stages are less difficult to design than the analogue circuitry, some care is needed to ensure that the interface to the satellite's on-board data handling (OBDH) networks are sufficiently fast to service the image buffer memory within the targets imposed by the mission objectives.

Regardless of the actual design chosen for the image capture and image processing stages, a modular approach is essential. Modularity provides flexibility in configuring and operating the imaging system(s), and in fulfilling the mission objectives. Furthermore, fault tolerance is provided by isolating failures to single sub-modules, offering some redundancy through replication. Finally, modularity also simplifies an upgrade path for incorporating new functions and / or technology on future missions by creating standard, expandable interfaces. Circuit changes are confined to individual sub-modules, reducing the need for extensive re-testing and minimising the repercussions of design error.

9.2 IN-ORBIT RESULTS.

The primary objective of this research programme has been to develop electronic imaging systems, and demonstrate that they can be used successfully on tiny microsatellites. In this respect, the in-orbit performance of the various camera systems, particularly on PoSAT-1, exceeds anything that the author or his SSTL colleagues could have expected at the start of the programme.

This success is even more of an accomplishment given that it was the first demonstration that a microsatellite could collect quality imagery from around the World on a daily basis, with highly consistent and predictable results. Furthermore, the author's efforts are enhanced by the fact that no other organisation has managed to demonstrate Earth observation in this way, despite the long duration of the programme and the growing attention paid to using small satellites for remote sensing.

Based on the experience of developing the successive generations of Earth observation camera and operating them in orbit, the author has a number of recommendations to be made to aspiring designers of microsatellite imaging systems.

9.2.1 LOW RESOLUTION IMAGING.

The original ambitions of the UoSAT-4 and UoSAT-5 cameras were simply to capture recognisable images of the Earth, as a first step towards developing useful imaging systems. However, as soon as the first images returned from UoSAT-5, it was clear that the camera's sensitivity was far better than initially expected. Within a few weeks, the results from this spacecraft had shown that the concept of using microsatellite imagery for useful low resolution imaging was sound.

As discussed in chapters 4 and 8, the improved systems on KITSAT-1 and PoSAT-1 have confirmed that imagery from all-electronic cameras carried by 50 kg microsatellites can fulfil a wide range of Earth observation roles, such as meteorology (cloud and weather systems), storm warning, snow cover monitoring, iceberg monitoring for shipping forecasts, atmospheric pollution, and soil fertility / aridity (desertification). These microsatellite images stand up to comparison with those taken by the NOAA satellites, despite being captured on dramatically cheaper systems.

The existing cameras have been very low-cost demonstration systems. Equipped with high performance, multispectral CCD cameras, there can be little doubt that imaging microsatellites can fulfil many of the tasks currently performed by much more expensive spacecraft. The features required for future imaging systems to meet commercial expectations are described in section 9.3.

9.2.1.1 Recommendations for low resolution (meteorological) imaging.

The author has the following recommendations for implementing a meteorological resolution imager using area-array CCDs:

- The ground resolution / field of view trade-off should be pushed toward wide coverage, dictating the use of wide angle lenses and high orbit altitudes.
- To achieve the required angle of view without suffering excessive optical distortion, it is probably necessary to use multiple cameras fitted with individual lenses.
- The CCD sensor should use the frame transfer architecture to provide a large photosite count and good radiometric properties.
- CCDs using interlacing to build up the full resolution should be avoided if possible, although this may be tolerated if it substantially improves photosite density.
- Integration times of 20 to 40 ms should be used to provide a good trade-off between reduced noise, transfer smear, power consumption (slow speeds) and low blur (high speeds).
- In a monospectral system, the near-IR should be the principal imaging band because of good contrast between land, sea and cloud / snow / ice.
- For commercial operation, the communications channels must be capable of delivering the imagery to the ground user on the same pass in which it is captured.

9.2.2 MEDIUM RESOLUTION IMAGING.

Inspired by the clear success of the UoSAT-5 mission, the original objectives of this imaging programme were broadened to examine the possibilities of higher resolution imagery. Many of the comments made in the preceding section about low resolution imagery also apply here, and the results of the Narrow Angle Cameras on KITSAT-1 and PoSAT-1 are startling when one considers the cost and size of the imaging instruments. Indeed, the data from the PoSAT-1 Narrow Angle Camera has generated more interest than any other aspect of this research programme.

Imagery with a ground resolution of 100 to 500 metres can fulfil some of the same applications as low resolution data, but can also provide information for a range of other uses. While not possessing the same detail as SPOT or LANDSAT data, the images from the PoSAT-1 Narrow Angle Camera have recorded features of the Earth potentially of use for the study of agriculture and land use, deforestation, urban development, hydrology, and volcanism, to cite a few examples.

As with the lower resolution imagery from the Wide Angle Cameras, these instruments have demonstrated that there is scope for microsatellites to perform many classes of medium and high resolution remote sensing. Although the properties of the CCD sensor used on the SSTL missions to date are not suitable for commercial exploitation, it nevertheless appears very feasible to use similar techniques to develop cameras for microsatellite remote sensing with resolutions of 50 metres and less.

9.2.2.1 Recommendations for medium (environmental) and high resolution (land resources) imaging.

Many of the same factors already identified for low resolution remote sensing cameras also apply to high resolution systems as well. The principal changes in the design of the camera will be to cope with the increased sensitivity to blurring due to the orbital motion. Accordingly:

- The integration times need to be very short to avoid blurring.
- The CCD will need to use the interline transfer architecture to prevent excessive transfer smearing.
- Interlacing must be avoided to ensure registration between all image lines.
- The poorer radiometric and spectral properties of interline transfer devices must be accommodated. There will be no problem in supporting visible bands, but the CCD's response in the crucial near-IR band may be degraded.
- The increasing size of the optics must be catered for as medium to long telephoto lenses, with fairly low f- numbers, become necessary.
- Slower (24 hour) delivery of the imagery should be adequate for most applications.

9.2.3 IMAGE PROCESSING AND COMPRESSION.

On future microsatellites, the volume of data to be downloaded will grow due to the payloads' increasing pixel counts and multispectral capabilities. This, coupled with the need for rapid turn-around of the imagery, will place increasing pressures on the limited communications capacity of these small spacecraft. While there is a clear need to upgrade the hardware of microsatellites' communications channels, there is also considerable scope for improving the spacecraft's yield by embedding autonomous image analysis, processing and compression facilities within the payload.

To be able to exploit software techniques to reduce the volume of data passing through the satellite's communications channels, it is essential for microsatellite imaging missions to include a suitable processing unit. The hardware options are limitless, but it is crucial that this processor can be reloaded in orbit to accommodate changing mission objectives and to support progressive and continuous software development.

In a purely pragmatic fashion, a number of simple but effective software routines have been developed since the launch of UoSAT-5 to improve the volume of valuable data captured daily. Although this research has not examined image processing and compression in profound detail, the in-orbit demonstrations on the PoSAT-1 mission have highlighted the potential of this approach for all remote sensing missions, not just microsatellites.

A 400 % increase in PoSAT-1's daily capacity of imagery has been achieved (with minimal loss to image quality) by using a combination of techniques. Autonomous on-board image analysis routines assess image interest and decide whether to keep or reject images based on predefined criteria (known as 'cloud editing'). Highly compressed image previews are also used to let ground control choose which data to retrieve from the satellite, discarding scenes of low interest. Finally, image compression is applied to those images retained for transmission. Although simple, these routines have shown to be of great benefit. Undoubtedly, more sophisticated developments would lead to further enhancements.

The image compression routines need to be selected in harmony with the specific mission objectives. For example, meteorological imaging services require fast turn-around, and a balance between computational loading and bandwidth reduction must be struck. However, small errors in the reconstructed imagery will probably not have significant repercussions on its operational value. In any case, a standard format should be selected to allow easy access to the data. To meet all of these conditions, hardware solutions using dedicated image compression accelerators (presumably implementing the JPEG algorithm) are probably most suitable for these applications. Fortunately, macroscopic weather features will remain discernable despite compression-induced degradation and artefacts. JPEG coding is widely used to disseminate imagery from geostationary meteorological satellites over existing terrestrial networks.

In contrast, slower (24 hour) delivery of the imagery should be adequate for most high resolution applications. Image compression is still useful, but the driving criterion for compression should be the preservation of image detail rather than speed of delivery or the degree of compression achieved. For these applications, software solutions are generally more suitable. Complex strategies mixing various algorithms such as vector quantisation, sub-band coding and fractal transforms may be appropriate to encode images or sub-images in the fashion most appropriate for either their content or final application. However, assessing and demonstrating the suitability of various image processing and compression algorithms is outside the scope of this research, and would probably be a suitable subject for another PhD programme.

9.3 NOVEL ASPECTS OF THIS RESEARCH PROGRAMME.

Many aspects of this research programme make novel contributions to the field of small satellite engineering. Firstly, the author's methodology for studying the issue of performing remote sensing from small satellites differs from that of most of his predecessors. Most other studies use an existing (or at least conventionally defined) imaging instrument, and perform a systems-study around this payload. Because these 'paper satellites' adopt the philosophy of traditional Earth observation spacecraft, they achieve only modest reduction in size and cost. Conversely, the author has striven to implement remote sensing on a 50 kg microsatellite despite the apparent unsuitability of this type of platform. By approaching the task from an alternative, and very pragmatic, point of view, the author has not been constrained by the expectations of traditional scanning instruments.

The second novel aspect of the author's work is the use of electronic cameras for Earth observation rather than a scanning imager. Although this choice is dictated by the limited attitude control of microsatellites, the author's investigation into implementing electronic camera systems for Earth imaging addresses a gap in the repertoire of remote sensing tools.

When undertaking this research, the author was unable to draw on a reference manual telling him how to design CCD cameras to capture still imagery. Most of the knowledge encapsulated in this thesis has come from first principals, detailed practical experimentation and careful interpretation of the existing literature. Therefore, the scope of this document in providing a designer's guide for implementing electronic cameras for small satellites is also novel.

However, it is the unrivalled in-orbit demonstrations fulfilled by the author's imaging systems that most clearly fulfil the requirements for novel contributions to engineering. Despite the long duration of the research programme, no other establishment has been able to demonstrate the same level of imaging performance on a microsatellite. The principal milestones attained during this research programme are:

UoSAT-5 (1991)

- The first sub-100 kg microsatellite to demonstrate high quality, predictable and consistent Earth imaging,
- The first non-governmentally funded spacecraft to fulfil Earth observation,
- The first conclusive in-orbit demonstration of using area-array CCD sensors for Earth observation,

- The first spacecraft to implement an interactive downloading scheme ('thumb-nail' image previews) to prioritise imagery according to interest and / or usefulness,

KITSAT-1 (1992)

- The first microsatellite to demonstrate sub-500 metre resolution Earth imaging,

PoSAT-1 (1993)

- The first microsatellite to demonstrate 200 metre resolution Earth imaging,
- The first satellite to autonomously implement image analysis for selective downloading ('cloud editing'),
- The first unmanned satellite to employ software-based image compression on the downlink.

9.4 RECOMMENDATIONS FOR FUTURE DEVELOPMENT.

9.4.1 DEVELOPING SSTL'S REMOTE SENSING CAPABILITIES.

This research programme has succeeded beyond all reasonable doubt in fulfilling its primary object of demonstrating the feasibility of using low-cost 50 kg microsatellites for remote sensing. However, with equal certainty, the imagery collected by UoSAT-5, KITSAT-1 and PoSAT-1 does not possess the necessary attributes to be considered suitable for commercial remote sensing applications. The principal shortcomings of the existing system for fully operational exploitation are:

- Inadequate photosite / pixel density,
- Absence of multispectral capabilities,
- Minimal geometric calibration and absence of radiometric calibration,
- Slow recovery from an imaging event due to interface topology,
- Inadequate targeting accuracy due to coarse pointing control,
- Inadequate data rate on the downlink to support daily throughput requirements,
- Inadequate data rate on the downlink and OBDH networks to support fast turn-around requirements.

Progressing from the work of this research programme, the next phase of SSTL's programme into low-cost Earth observation is to develop new, enhanced systems which fulfil one or more commercial demands. The transition from experimental to operational systems will require significant technical effort and financial investment, but is feasible. Despite the obstacles of the attitude control and communications systems, which should be resolvable in the medium term, the principal long term limitation of microsatellites for Earth observation is the difficulty of supporting the massive optics required for high resolution imaging. Similarly, the on-board calibration and reference sources will be minimal, and alternative low-cost techniques will need to be developed (primarily based on comparison with other sources of remotely sensed data).

Given the restricted communications bandwidths, it will be difficult for the next generation of imaging microsatellites to provide the real-time delivery demanded by meteorological programmes. This is ironic because virtually all other aspects of implementing an imager are simplified at lower resolutions. Nevertheless, once the data handling aspects of microsatellites are refined to support this type of traffic continuously to small ground terminals, there may be significant opportunities for supplementing NOAA-type data with very small satellites.

Therefore, forthcoming microsatellite imaging systems should focus on medium and high resolution imaging, where the data handling and image turn-around are not so critical. Furthermore, such missions are more likely to receive funding given the general appeal of high resolution imaging. Based on the experience of this programme, the author is convinced of the feasibility of future microsatellites generating imagery very similar to that currently produced by the huge LANDSAT, SPOT and IRS spacecraft. Of course, the cost of these new platforms and imaging instruments will be appreciably higher than existing SSTL microsatellites, but will still be markedly cheaper than the traditional solutions.

These new instruments should endeavour to provide data compatible with existing systems. By making the data sets from microsatellite imagers compatible with well established remote sensing systems, this new source of imagery will be more easily acceptable to the user community. Therefore, the first objective would be to emulate the LANDSAT MSS instrument to provide imagery with 80 metre ground resolution, 185 km^2 swath, around 2000^2 pixels per scene, and with four spectral bands. However, the choice of spectral bands may be altered to those of the LANDSAT TM in the visible, which are generally accepted to be more useful. Thereafter, microsatellite designs should follow the example of the LANDSAT TM and SPOT HRV, and possibly the IRS LISS instruments, increasing in resolution and spectral sensitivity. Regardless of the exact specification, these remote sensing microsatellites will probably use full-frame electronic cameras (although pushbroom scanners are not out of the question) to deliver high resolution, multispectral imagery with large pixel counts. In any event, the electronics of these systems will be highly reminiscent of SSTL's existing cameras.

In addition to the limitations regarding calibration and supporting massive optics, microsatellite imaging systems will be confined to the visible spectra for the next half decade. By that time, the characteristics of IR sensors will hopefully have evolved to the state currently achieved by visible systems. At the time of writing, many attractive forms of IR-sensing technology are being declassified, and will soon be available on the commercial market-place (e.g. uncooled, staring bolometer arrays operating in the 8 to 12 μm band [Weiss, b]). Furthermore, the cooling mechanisms (principally Stirling-cycle coolers) will have developed to a point where it may become feasible to use them operationally on a microsatellite [Kaplan, a][Kaplan, b]. This period will give organisations like SSTL the opportunity of perfecting the electronic, mechanical and optical aspects of the imaging instrument and the attitude control and data handling of the satellite platform entirely in the visible bands before considering mid- and thermal-IR detectors seriously.

9.4.2 REQUIREMENTS FOR COMMERCIAL REMOTE SENSING.

Over the next two or three years, the electronic imaging systems deployed by SSTL's small spacecraft will need to progress from the demonstration models flown to date towards fully fledged operational remote sensing tools. Before embarking on this development programme, it is necessary to identify the requirements of an operational or commercial imaging system. In addition to the evident need for a greater data turn-around and throughput, the author believes the crucial areas to be improved upon for SSTL to deliver such a system are:

1. *Improved swath capabilities.* As mentioned at the very start of the thesis, one of the unique strengths of remote sensing satellites is their ability to provide a panoramic view. In practical terms, this implies that the pixel counts of the imagery should aim to be in the region of 4000^2 to 6000^2, and really no less than 3000^2. The larger image sizes allow users to view substantial portions of the Earth's surface at whichever scale is of interest. Irrespective of the spatial resolution, the author feels that an image footprint covering 80 to 100 km on a side is the smallest that should be considered. As higher spatial resolutions are demanded, it follows that the cost of the imaging system and the volume of data will grow as the pixel density increases to deliver both the spatial resolution and the area of coverage.

   Despite peoples' tendency to be mesmerised by it, an instrument's specification for spatial resolution is really only a secondary issue in its system and electronic design. Provided the satellite is large enough to support the increased mass of the long focal length optical system, and the detector has sufficient sensitivity to collect an image despite the short exposure times needed to contain blurring, the same electronic devices will be able to support virtually any resolution required. The ability to meet some arbitrary ground resolution, whilst sacrificing the field of view, does not constitute an operational remote sensing system.

2. *Multispectral capabilities.* The ability to sense in several spectral bands simultaneously is essential to differentiate between types of terrain and vegetation cover. Following on from the point of the previous paragraph regarding spatial resolution, most experts consider the data from LANDSAT to be of greater *general* use than SPOT imagery, due to the availability of seven spectral bands covering the visible

and thermal-IR bands. Indeed, many instruments currently under proposal stress spectral, rather than spatial, resolution offering dozens or even hundreds of simultaneous bands (known as hyperspectral imaging).

Although otherwise feasible for deployment on small satellites, the enormous volumes of data produced by hyperspectral imagers would certainly overwhelm the communications system of current, and near future, microsatellites. Accordingly, it will be necessary to sense in a handful of bands, in order to keep the data volumes manageable. The primary remote sensing bands are the red (approximately 0.6 to 0.7 μm) and near-IR (0.8 to 1.1 μm) for vegetation monitoring, often accompanied by a green or blue-green band (approximately 0.45 to 0.6 μm). Various UV spectra (shorter than 0.4 μm) may be of interest if atmospheric applications are a priority. The current development of staring CCD arrays for the short wave-IR (1.4 to 2.0 μm) will soon provide useful tools for sensing the condition of snow and ice. In the slightly longer term, mid- (3 to 5 μm for volcanology and forest fire detection) and thermal-IR (8 to 12 μm for terrestrial heat budget studies) capabilities will become available in CCD arrays.

3. *Geometric and radiometric integrity and consistency.* It is important for the users of remotely sensed data to have faith in the consistency of measurements. In geometric terms, it is important that the imagery can be registered and compared directly with other types of data to help in the search for temporal variations. The data from conventional scanning instruments must be corrected for the satellite's residual attitude perturbations before it can be used in this way. The guaranteed geometry provided by area-array CCDs is therefore very attractive to many users.

   Similarly, the radiometric information provided by the instrument will need to be stable and consistent to allow comparative analysis of time-delayed data sets. In most cases, it will not be necessary for a microsatellite imaging payload to deliver absolute radiometric accuracy, provided it maintains good linearity over time and temperature, allowing relative changes to be observed and supporting other ratio comparisons. If any specific calibration requirements exist, it will probably be most expedient to use another data source as a reference in a closed-loop system, relying only on a few rudimentary hardware systems on-board.

Based on these observations, a generic specification for the next generation of microsatellite imagers will include the following requirements:

- Area-array CCD sensors must be used to ensure geometric registration,
- The image swath should have 3000 or more pixels,
- At least three bands of multispectral imagery should be provided,
- The radiometric repeatability should be ensured by various means (improved stability of electronics, on-board calibration sources, controlled thermal environment, etc.).

9.4.3 IMAGING SYSTEMS FOR THE SSTL UOSAT-12 MINISATELLITE.

In parallel with the drafting of this thesis, the author has been devoting some attention to fulfilling these objectives for deployment on SSTL's forthcoming 200 kg minisatellite, UoSAT-12, destined for launch at the end of 1996. In terms of generating remotely sensed imagery, a minisatellite platform offers more mass and volume to the payloads, but most of the other constraints are comparable to those on a microsatellite. The increase in available payload mass will allow the SSTL design team to focus on the issues and features listed above, without the added concern of miniaturisation. However, the emphasis for these new designs is to develop systems that retain compatibility with the company's existing microsatellite platforms, albeit after some rework.

At the time of writing, the best method for transforming the author's electronic cameras into commercially viable and operational systems has not been fully determined. In many ways, following convention and selecting a pushbroom design is tempting. It is significantly easier to achieve both the increased pixel counts and (especially) the registration between spectral images with a linear sensor than it is with an area-array CCD.

Unfortunately, without a dramatic improvement in the attitude performance of SSTL's micro- and minisatellites, it will not be feasible to support this type of imager architecture. If the pointing accuracy can be improved to the region of 0.5° in all three axes, with suitably low drift rates, it will become feasible to use linear sensors for meteorological applications, although higher resolution systems will remain more elusive.

Therefore, it remains highly probable that SSTL will continue to use area-array electronic cameras, at least for the immediate future. Indeed, this is the recommendation of no less an authority than [Wertz] when reviewing the options for attitude control to allow UoSAT-12 to support remote sensing. It was estimated that the price of providing SPOT-like attitude control hardware will be around $1 million per mission, without considering the further cost of manpower to develop the hardware systems and the software control. Given SSTL's principal forte of electronic design, with correspondingly modest control and mechanical expertise, [Wertz] felt that this money would be better spent on aggressively developing imaging technology, whilst acquiring attitude control capabilities in more modest steps.

While it appears most likely that UoSAT-12 will use CCD cameras, the most suitable design strategy has not yet been decided. The various solutions available for producing multispectral imagery have been discussed in section 5.4.4.3. At the time of writing, the author feels that the use of colour wheels probably represents an advantageous and versatile solution for this mission, despite the presence of moving mechanics. Developing a suitably rated motor to drive the wheel is within SSTL's existing capabilities, whereas the opto-mechanical alignment of multiple sensors is not. If either the multiple-camera or beamsplitter configuration is chosen, the focal plane assembly will need to be developed and aligned by an external consultancy.

A similar set of trade-offs is faced when attempting to increase the imagery's pixel count. One solution is to continue to use all-electronic CCDs, mounting several side-by-side to provide adequate coverage. However, given that the largest available all-electronic CCD (the Eastman-Kodak KAI-1001) has an array of 1000^2 photosites, it will take three or four of such devices to achieve the desired swath. Time-delayed snap-shots would provide the extra pixels in the direction of the satellite's velocity, operating the system as a kind of pseudo-pushbroom. At least the pixel geometry would be constant within each swath of imagery (defined by the CCDs' structure and the physical mounting between the cameras). Some overlap could be used to help register the time-delayed data sets.

While this approach makes use of all-electronic cameras exclusively, it is unlikely to be practicable on a microsatellite, given that three or four cameras need to be supported in each spectral band. The peak power requirements for this array of sensors (three spectral bands, twelve cameras in all) would probably be in the region of 100 Watts, but the largest problem would be in providing an adequate area on the microsatellite's external surfaces on which to place the cameras. Furthermore, this is not an inexpensive solution, given the dominant cost of the CCD sensors.

Subject to an incomplete investigation, the author's favoured approach is to employ full-frame CCDs to obtain the increased coverage. Given that a 2000^2 photosite full-frame sensor and a 1000^2 all-electronic sensor cost about the same, and have similar mass, power and optical requirements, it is clear that the full-frame solution has some attractions. Furthermore, as discussed in section 5.1.2.1, the radiometric and spectral sensitivity of full-frame CCDs is significantly higher and more uniform than that of the Eastman-Kodak KAI-1001.

Of course, some form of mechanical shuttering must be provided to shield the photosensitive surface of the full-frame CCD from incoming light during read-out. Despite their longevity in terrestrial systems, a conventional camera shutter (using either a leaf or curtain design) is not very suitable for use in space due to its jerky stop-and-start action, which is likely to stick and certain to cause attitude disturbances (at precisely the instant the spacecraft needs to be at its most stable). Instead, the author envisages using a simple rotating disk to chop the optical beam. To avoid the risks associated with stopping and starting, the motor could be left on continuously, although its speed could be reduced when not imaging to reduce power consumption.

The use of a mechanical shutter would provide simpler operating conditions for the camera electronics. Varying the speed of the disk would provide the exposure control, and the read-out rate could be slowed substantially to reduce the output signal's noise bandwidth.

To fulfil the requirements of future commercial imagers, it is clear that new technology must be introduced to the imaging system. While the use of enhanced sensors is inevitable, requiring the development of new circuitry, other techniques must be also be mastered to support the new imaging payloads. While the pushbroom system would be ideal from the instrumentation view-point, selecting this option merely pushes the design difficulty into the lap of the attitude control engineers. Similarly, acquiring the additional skills needed to align multiple sensors (either spectrally or spatially) would require a significant investment. In comparison with evolving these technologies, the development of small motors to drive a colour wheel and / or a perforated disk for shuttering is the simplest option. It will also result in the most compact, low mass and low power solution.

The only unpalatable aspect of embracing full-frame cameras is the cost of the sensors. Although they are available, the very large 4000^2 (Ford Aerospace) and 5000^2 photosite arrays (Dalsa Inc.) are exceedingly expensive; figures of a quarter to half a million US dollars are typically quoted. Fortunately, at the time of writing, Eastman-Kodak and Loral-Fairchild have announced the availability of 4000^2 photosite devices; no prices have been obtained but the author hopes that such influential players in the field of electronic imaging would be able to reduce the costs to around $150,000 per device. EEV produce 3000 x 2000 arrays for around £50,000.

An attractive solution would be to use two cameras with 2000^2 elements each to provide the full swath, each fitted with its own optics, filter wheel (see section 5.4.4.3.3) and shutter mechanism. The mass and power of this system would be suitable for microsatellites, and the cost will be reasonable. The two cameras could be equipped with different moving mechanics if there was any doubt regarding the durability of one technology; if one system failed, at least the other camera would continue producing imagery.

While the author's preference for the full-frame solution over the alternatives may seem clear at the time of writing, the circumstances of the UoSAT-12 project evolve on a monthly basis. Therefore, it is very possible that the system ultimately flown will be quite different.

9.4.4 TRENDS IN THE REMOTE SENSING INDUSTRY.

Because of the particular constraints of microsatellites, it has been necessary to use all-electronic cameras using CCD area-array sensors, which contrasts with the conventional approach to implementing remote sensing using scanning instruments. Nevertheless, electronic cameras have many attributes that make them attractive for all forms of imaging, such as their low power, compactness, robustness and most importantly, guaranteed geometry independent from the platform's stability. For these reasons, CCD cameras are widely used in numerous, diverse terrestrial applications, yet have received relatively little consideration as Earth observation tools. To date, the deployment of CCD cameras in space has essentially been limited to deep-space and interplanetary probes, and star tracking / astronomical applications.

However, over the last two or three years, the improving quality of area-CCDs has been forcing a re-evaluation of this situation. NASA has used a conventional Nikon 35 mm photographic camera, but equipped with a full-frame CCD sensor (instead of the usual film-back) for imaging applications on the Space Shuttle [Holland]. Astronauts use the camera to take pictures of experiments or non-nominal systems, and the data is downloaded to a personal computer for instant viewing and transmission to ground experts.

More relevantly, the design teams of the US military Clementine and MSTI technology demonstration missions (see section 2.3.5.8) opted for CCD cameras rather than pushbroom imagers, even though all the requirements (orbital configuration, illumination conditions, and platform attitude stability) for scanning instruments were met.

This trend is continuing, with area-array CCDs being used as the primary sensors in two recently announced programmes: EarlyBird (by EarthWatch, a joint venture between WorldView Imaging Corp. and Ball Aerospace [Weiss, a]) and CRSS (Commercial Remote Sensing Satellite, by Space Imaging, a joint venture between Lockheed-Martin and E-systems Inc. [Graham]). Both systems will use an identical design, employing separate focal plane arrays (FPAs) to achieve 1 metre resolution in panchromatic mode, and 4 metre resolution in each of four spectral bands (blue, green, red, near-IR). The silicon dies of four 1024^2 photosite CCDs are mounted onto a single substrate to create a 2048^2 photosite FPA. Interestingly, these instruments use the same device, the Eastman-Kodak KAI-1001 interline transfer CCD, as the author has identified for SSTL's next generation of electronic cameras. The interline transfer architecture (needed to minimise smearing) and the large photosite count of the KAI-1001, make this device the most attractive all-electronic option for high resolution remote sensing.

On-going military research provides a stronger indication of the growing attraction of area-sensing imagers over pushbroom scanners [Lareau]. For very much the same reason that has shaped this research programme (i.e. independence from platform stability), the US and Canadian Air Forces are developing electronic cameras (principally using the Dalsa 5000 x 5000 pixel sensor) to replace the existing pushbroom arrays used on reconnaissance aircraft. To image a target area with a pushbroom scanner, an aircraft must maintain a constant, straight-line course for several seconds, during which it becomes a prime target for anti-aircraft weaponry. Conversely, if fitted with a camera, the aircraft can continue to record perfectly registered imagery, despite flying far more erratic routes. Furthermore, the turn-around in delivering imagery to the battle-front is reduced because of the camera's guaranteed geometry; data from pushbroom sensors much first be pre-processed to compensate for attitude instabilities. This directly echoes the benefits of electronic cameras advocated by the author, albeit on enormously greater budgets.

The recurring selection of cameras for such different imaging applications indicates that the technology of area-array CCDs has matured to levels of performance previously only attainable with scanning instruments. As the cost of large arrays drops, the benefits of area-arrays sensors will become increasingly attractive to users in a wide range of fields, most notably satellite remote sensing. Small and easily adaptable companies, like SSTL, will be in the best position to exploit these rapid advances in the photonics industry.

9.5 CONCLUDING REMARKS.

When the author embarked on this research programme, there was little general acceptance that microsatellites could fulfil any useful imaging tasks, let alone commercial remote sensing. According to conventional wisdom, the housekeeping systems of a 50 kg microsatellite are inadequate to support a remote sensing payload.

By carefully analysing the conditions experienced on microsatellites, and by selecting an imaging technology that is compatible with these operational constraints, the author has demonstrated that very small satellites are indeed capable of executing high quality remote sensing tasks. By adopting an alternative perspective on the design of the imaging instrument, the author arrived at the novel solution of using electronic CCD cameras for Earth observation. This approach, along with the development of autonomous on-board image analysis and compression, has resulted in the first conclusive demonstrations of remote sensing on small satellites.

The author and SSTL are very pleased with the successful demonstration of Earth imaging fulfilled by the UoSAT-5, KITSAT-1 and PoSAT-1 microsatellites during this research programme. The imagery from the cameras on these spacecraft possess a quality and sensitivity comparable to many existing, but much more expensive, remote sensing systems. Given the current advances in area-array CCD sensors, the opportunities for fulfilling operational Earth imaging from microsatellites are expanding very rapidly. SSTL is in an ideal position to be at the forefront of commercial small satellite remote sensing, blending its expertise in microsatellite and electronic camera technology.

In the eight years since this research programme commenced, the established space industry's view of small satellites in general, and for remote sensing applications in particular, has been transformed from deeply sceptical to widespread enthusiasm. Given the unprecedented and unrivalled demonstration of Earth imaging fulfilled by the author's cameras, there can be little doubt that this work summarised in this thesis is partially responsible for this significant change in attitude.

9.6 REFERENCES.

Graham J: Press release - Kodak selected to provide digital camera for Space Imaging's mission; Lockheed Martin Missiles and Space, 12 July 1995.

Holland D: The NASA electronic still camera system; Proc. of IGARSS, p.149-151, Houston Texas, IEEE CH3041, 1992.

Kaplan H: Expanding market spurs advances in Coolers; Photonics Spectra, p.46-48, Jul 1995.

Kaplan H: A new generation of Cooling devices; Photonics Spectra, p.50-51, Nov 1995.

Lareau A.G: Obtaining reconnaissance images more quickly; Photonics Spectra, p.105-108, Mar 1994.

Weiss S.A: EarlyBird to fly with Kodak sensors; Photonics Spectra, p.56, Jun 1995a.

Weiss S.A: New infrared focal plane array keeps its cool; Photonics Spectra, p.28, Nov 1995b.

Wertz J.R: Personal communication; October 1995.

APPENDICES.

APPENDIX 1. REFERENCES

Ahern F.J. et al: Radiometric correction of visible and infra-red remote sensing data at the Canada Centre of Remote Sensing; Int. J. Remote Sensing, Vol. 8 No. 9, p1349-1376, 1987.

Alex T.K. et al: Remote sensing payload for small Indian satellite; Proc of SPIE, Vol.363, p.82-87, 1983.

Alex T.K: Imaging capabilities of small satellites - Indian experience; Proc. of the SPIE Conference on Small Satellite Technology and Applications I, SPIE Vol.1495, Orlando, April 1991.

Allery M.N, Sellers J.J. & Sweeting M.N: Results of University of Surrey on-orbit microsatellite experiments; Proc. of Int. Symposium on Small Satellites Systems and Services; Biarritz, France, 27-30 June, 1994.

Allery M.N. et al: Low Earth orbit microsatellites for data communications using small terminals; 10th IEE International Conference on Digital Communications via Satellites, Proc. IEE Digital Satellite Communications 403, Vol. 2 p.457-465, Brighton UK, 15 May 1995.

Arai K: Requirements for ADEOS orbit, orbit and attitude control, and rate jitter; Proc of IGARSS Symposium, Edinburgh, Scotland, 13-16 Sept. 1988; Ref. ESA SP-284.

Arai K: Preliminary assessment of radiometric accuracies for MOS-1 sensors; Int. J. Remote Sensing, Vol. 9 No. 1, p5-21, 1988.

Arai K: Preliminary study on information lossy and lossless coding data compression for the archiving of ADEOS data; IEEE Trans. on Geoscience and Remote Sensing, Vol.28 No.4, p.732 - 734, July 1990.

Ashton J.E.U & Hopkinson G.R: High performance star trackers using direct contact peltier cooled CCDs; obtained directly from EEV Ltd, Waterhouse Lane, Chelmsford, Essex CM1 2QU.

Barrington Brown A.J, Ward A.K. & Entwistle P.M: Transputers and their use in on-board computers; Symposium on Space Electronics, British Interplanetary Society, April 1995.

Barnsley M.F. & Sloan A.D: Fractal image compression; Proc of the Scientific Data Compression Workshop, NASA Goddard Space Flight Centre, Feb 1989, NASA-CP-3025; NASA Science & Technical Abstract Report ref N89-22346.

Begni G: SPOT image quality - Twenty months of experience; Int. J. Remote Sensing, Vol.9 No. 2, p1409-1414, 1988.

Beynon J.D.E. & Lamb D.R: Charge-coupled devices and their applications; McGraw-Hill 1980; ISBN 0-07-084522-0.

Bonsall C et al: Webersat operations and experimental results; Proc. of the 4th Annual AIAA/USU Conference on Small Satellites, Utah State University, 27-30 Aug 1990.

Börger J.B et al: Study on data compression systems for operational remote sensing; European Space Operations Centre contract 6141/84/D/IM(SC).

Brewer A.W: On-board image compression using adaptive MPBTC algorithm; Internal document SSAB001B, Surrey Satellite Technology Ltd, 1994.

Brylow S.M. & Soulanille T.A: Low-cost quick-look radiation testing of electronic components for the Mars Observer Camera; Proc. of the 6th Annual AIAA/USU Conference on Small Satellites, Utah State University, 21-24 Sept 1992.

Burt D.J: MTF calculations for CCD image sensors; CCD Technical Note 19, EEV Ltd, Waterhouse Lane, Chelmsford, Essex CM1 2QU.

Cappellini V: Data compression and error control techniques with applications; Academic Press, 1985; ISBN 0-12-159261-8;

Carta R.A: Camera helps refurbish nuclear reactor; Photonics Spectra, November 1994.

Castle K.R. et al: In-flight absolute radiometric calibration of the Thematic Mapper; IEEE Trans. on Geoscience and Remote Sensing, Vol.22 No.3, p.251 - 255, May 1984.

Chen H.S: Space Remote Sensing Systems; Academic Press 1985, ISBN 0-12-170881-0.

Chen T.M, Staelin D.H. & Arps R.B: Information content of Landsat image data for compression; IEEE Trans. on Geoscience and Remote Sensing, Vol.25 No.4, p.499 - 501, July 1987.

Chin R.T. & Yeh C.L: Quantitative evaluation of some edge-preserving noise-smoothing techniques; Computer Vision, Graphics, and Image Processing, Vol.23 p.67-91, 1983.

Clarke R.J. & Linnett L.M: Fractals and image representation; IEE Electronics & Communications Engineering Journal, p.233 - 239, Aug 1993.

Clementine home page (http://www.nrl.navy.mil/clementine/clementine.html).

Compuserve: The Graphics Interchange Format standard; Compuserve Information Services, 1991.

Colwell R.N: Manual of Remote Sensing Second Edition; American Society of Photogammetry, The Sheridan Press 1983, ISBN 0-937294-41-1.

Curran P.J: Principles of Remote Sensing; Longman 1985; ISBN 0-582- 30097-5.

Das U.N. & Kasturirangan K: Development of a small satellite series - ISRO experience; Proc. of the 7th Annual AIAA/USU Conference on Small Satellites, Utah State University, 13-16 Sept 1993.

Da Silva Curiel R.A, Sun W. & Sweeting M.N: Design considerations and implementation of the VHF and UHF radio frequency systems on-board the UoSAT LEO store and forward communications network; 3rd International Symposium on Communication Theory and Applications, Lancaster University UK, 10-14 July 1995.

Da Silva Curiel R.A. & Ward J.W: Operational store and forward payload for low Earth orbit microsatellite data - collection and file transfer communications; Proc. of International Symposium on Satellite Communication and Remote Sensing, p.294-297, Xi'an China, 20-22 Sept 1995.

Davis L.S. & Rosenfeld A: Noise cleaning by iterated local averaging; IEEE Trans. on Systems, Man and Cybernetics, Vol.8, p.705-710, 1978.

Delp E.J. & Mitchell O.R: Image compression using block truncation coding; IEEE Trans. on Communications, Vol.27 No.9, p.1135 - 1142, Sept 1979.

Deshayes J.P. & Mizzi A: Earth observation payloads - user requirements; Proc of the 1st European Workshop on Flight Opportunities for Small Payloads, ESRIN, Frascati, Italy, 8 - 10 Feb 1989; ESA SP-298.

Dosière P. & Justice C: Spatial and radiometric resolution of the LANDSAT-3 RBV system; Int. J. Remote Sensing, Vol. 4 No. 2, p447-455, 1983.

DVFLR: MEOSS, an experimental CCD-camera for remote sensing; NASA Scientific and Technical Aerospace Reports (STAR) reference N83-30469 & N83-30470.

Djorgovsky S: CCDs - their cause and cure; Proc of the Workshop on Improvements to Photometry, NASA Ames Research Centre, Nov 1984, p.152-176; NASA Science & Technical Abstract Report ref N85-17905.

Dyer C.S. et al: The low-Earth orbit radiation environment and its evolution from measurements using the CREAM and CREDO experiments; IEEE Trans. on Nuclear Science, Vol.40 No.6, p.1471 - 1478, Dec 1993

Eather R.H: DMSP calibration; J. of Geophysical Research, Vol.84 No.A8, p.4134-4144, Aug 1979.

EEV Ltd: CCD Imaging III; EEV Ltd, Waterhouse Lane, Chelmsford, Essex CM1 2QU.

El-Hakim S.F, Burner A.W. & Real R.R: Video technology and real-time photogammetry; p.279 - 304 of [Karara].

Elliot C: Cost-effective environmental monitoring; Earth Space Review, Vol.1 No.2, p.7-10, Apr-June 1992; ISSN 1060-1848.

Ellis W.S. & Turnley D.C: A Soviet sea lies dying; National Geographic, Vol.177 No.2, p.72-94, Feb 1990.

EG&G Reticon: Solid State Camera Products Data Book 1993/94; EG&G Reticon, 345 Potrero Avenue, Sunnyvale, CA 94086-4197.

EOSAT Corp: A process of radiometry; EOSAT Notes, Vol.9 No.2, p.10, Summer 1994.

Erlich D. & Estes J.E: Applications of NOAA AVHRR 1 km data for environmental monitoring; Int. J. Remote Sensing, Vol.15 No.1, p145-161, 1994.

Ersoy O.K. & Chen C.H: Transform-coding of images with reduced complexity; Computer Vision, Graphics, and Image Processing, Vol.42 p.19-31, 1988.

ESA: The radiation design handbook; European Space Agency; Publication No. PSS-01-609 Draft Revision 1; ISSN 0379-4059, Jan 1987.

ESYS Ltd: Preliminary report of Sea Ice Demonstration, ref ESYS-LET-CB-1478-94, ESYS Ltd, Berkeley House, London Square, Cross Lanes, Guildford, United Kingdom.

Feig J.R, Matlock R.S. & Yeakel G.S: The Miniature Sensor Technology Integration program - an overview; Proc. of the 7th Annual AIAA/USU Conference on Small Satellites, Utah State University, 13-16 Sept 1993.

Fisher Y: Fractal image compression; Springer-Verlag 1995; ISBN 0-387-94211-4.

Forshaw M.R.B et al: Spatial resolution of remotely sensed imagery - a review paper; Int. J. Remote Sensing, Vol.4 No.3, p.497-520, Mar 1983.

Fouquet M: The UoSAT-5 Earth imaging system - in-orbit performance; Proc. of the SPIE Conference on Small Satellite Technology and Applications II, SPIE Vol.1691, Orlando Florida, 21-22 April 1992.

Fraser R.S. & Kaufman Y.J: Calibration of satellite sensors after launch; Applied Optics, Vol.25, p1177-1185, 1986.

Fryer J.G: Camera calibration in non-topographic photogammetry; p.59 - 69 of [Karara].

Garrison T.P. & Schrock S.R: QuickStar - rapid access to space for small scientific payloads; IAF Conference, 1991.

Gharavi H. & Tabatabai A: Sub-band coding of monochrome and color images; IEE Trans of Circuits and Systems, Vol.35 No.2, p.207 - 214, Feb 1988.

Ginati A. et al: Bremsat - a small scientific satellite; Proc. of the 4th Annual AIAA/USU Conference on Small Satellites, Utah State University, 27-30 Aug 1990.

Ginati A: Verbal presentation; Conference on Small Satellites for Remote Sensing, The Space Congress, Bremen Germany, 24-25 May 1995.

Gonzalez R.C. & Wintz P: Digital image processing; Addison-Wesley 1977; ISBN 0-201-02597-3.

Gonzalez R.C. & Woods RE: Digital image processing; Addison-Wesley 1992; ISBN 0-201-50803-6.

Goel P.S, Venkat Rao M. & Chandra K.S: Attitude control system specifications for a remote sensing satellite; Int. J. Remote Sensing, Vol.10 No.9, p1531-1537, 1989.

Graham N, Introduction to Pascal, p.155-172, West Publishing Co, 1980.

Gray R.M: Vector quantization; IEEE Acoustics, Speech & Signal Processing Magazine, Vol.1 No.2, p.4-29, Apr 1984.

Gray R.M: Vector quantization; Proc of the Scientific Data Compression Workshop, NASA Goddard Space Flight Centre, Feb 1989, NASA-CP-3025; NASA Science & Technical Abstract Report ref N89-22340.

Gupta S. & Gersho A: Feature predictive vector quantisation of multispectral images; IEEE Trans. on Geoscience and Remote Sensing, Vol.30 No.3, p.491 - 501, May 1992.

Halverson D.R, Griswold N.C. & Wise G.L: A generalised block truncation coding algorithm for image compression; IEEE Trans. on Acoustics, Speech & Signal Processing, Vol.32 No.3, p.664-668, Mar 1984.

Hannigan R et al: The feasibility and usefulness of Earth observation from small satellites; Conference on Small Satellites for Remote Sensing, The Space Congress, Bremen Germany, 24-25 May 1995.

Harboe-Sorensen R. et al: Observations and prediction of SEU in Hitachi SRAMs in low altitude polar orbits; IEEE Trans. on Nuclear Science, Vol.40 No.6, p.1498 - 1504, Dec 1993.

Harris R.W et al: High quality image compression for rockets and satellite; Proc. of the 3rd Annual AIAA/USU Conference on Small Satellites, Utah State University, 26-28 Oct 1989.

Harris, Satellite Remote Sensing - an introduction; Routledge & Kegan, 1987, ISBN 0-710203055.

Harris: Integrated circuits for the space environment; Space Product News, Special edition, Military & Aerospace Division, Harris Semiconductor 1993.

Hashida Y: SSTL Internal Technical Note, Document FASAD013, 2 June 1995.

Hashida Y: Personal communication, 28 Sept 1995.

Hobson G.S: Charge-transfer devices; Edward Arnold 1978; ISBN 0-7131-3396-1.

Hodgart M.S: Attitude control and dynamics of UoSAT angular motion; The IERE Journal, Vol. 52 No.8/9, Aug/Sept. 1982; ISSN 0033-7722.

Hodgart M.S. & Wright P.S: Attitude determination, control and stabilisation of UoSAT-2; The IERE Journal, Vol. 57 No.5, Sept. 1987; ISSN 0267-1689.

Hodgart M.S: Gravity gradient and magnetorquing attitude control for low-cost low Earth orbit satellites - the UoSAT experience; PhD Thesis, University of Surrey, 1989.

Hodgart M.S, Underwood C.I. & Ward J.W: Single event upset error protection for solid state data memory on microsatellites; Proc. of the 5th Annual AIAA/USU Conference on Small Satellites, Utah State University, 26-29 Aug 1991.

Hodgart M.S: Efficient coding and error monitoring for spacecraft digital memory; Int. J. Electronics, Vol.73 No.1, p.1-36, 1992.

Hodgart M.S. & Ong W.T: Gravity gradient and magnetorquing attitude control for low Earth orbit satellites; 2nd ESA Int. Conf. on Spacecraft Guidance, Navigation & Control Systems, The Netherlands, April 1994.

Hofmeister R.A: Catching the action with progressive-scan CCDs; Photonics Spectra, July 1995.

Holben B.N, Kaufmann Y.J. & Kandall J.D: NOAA-11 AVHRR visible and near-IR inflight calibration; Int. J. Remote Sensing, Vol.11 No. 8, p1511-1519, 1990.

Holland A. et al: Techniques for minimising space proton damage in scientific charge-coupled devices; IEEE Trans. on Nuclear Science, Vol.38 No.6, p.1663 - 1670, Dec 1991.

Holland D: The NASA electronic still camera system; Proc. of IGARSS, p.149-151, Houston Texas, IEEE CH3041, 1992.

Hopkinson G.R. & Chlebek C: Proton damage effects in an EEV CCD imager; IEEE Trans. on Nuclear Science, Vol.36 No.6, p.1865 - 1871, Dec 1989.

Howes M.J. & Morgan D.V: Charge-coupled devices and systems; Johm Wiley & Sons, 1979; ISBN 0-471-99665-3;

Inmos: The Military and Space Transputer Data Book, Appendix C - radiation tolerance; Inmos Ltd, 1990.

Inmos: The Transputer Data Book; Inmos Ltd, 1992.

Imme M: A noise peak elimination filter; Computer Vision, Graphics, and Image Processing, Vol.53 p.204-211, 1991.

Israelson P.D. & Harris R.W: The application of vector quantization to image compression for satellite imaging systems; Proc. of the 1st Annual AIAA/USU Conference on Small Satellites, Utah State University, 7-9 Oct 1987.

ISRO: Department of Space - Annual Report; Government of India; Published by ISRO, Bangalore, India, 1995.

Iterated Systems; Promotional material, Iterated Systems Ltd, Wyvols Court, Swallowfield, Reading, Berks RG7 1PY.

ITT Defence & Electronics technical brochure, ITT Aerospace / Communications Division.

Jackson S. & Raetzke J: The Webersat camera - an inexpensive Earth imaging system; Proc. of the 5th Annual AIAA/USU Conference on Small Satellites, Utah State University, 26-29 Aug 1991.

Jacquin A: Image coding based on a theory of iterated contractive transformations; IEEE Trans on Image Processing, Vol.1 No.1, p.18 - 30, Jan 1992.

Jaggi S: Technique for compression of multispectral remotely sensed data using vector quantization; Oral presentation; SPIE Conference on Hybrid Image and Signal Processing III, SPIE Vol.1702 (if published), Orlando Florida, 21-22 April 1992.

Jain A.K: Image data compression; Proc of the IEEE, Vol.69 No.3, p.349 - 389, March 1981.

Janesick J, Elliot T. & Pool F: Radiation damage in scientific charge-coupled devices; IEEE Trans. on Nuclear Science, Vol.36 No.1, p.572 - 578, Feb 1989.

Janesick J. & Elliot T: History and advancement of large area array scientific CCD imagers; Astronomical Society of Pacific Conference Series, Tucson Az, USA, 1991.

Jayant N.S. & Noll P: Digital coding of waveforms - principles and applications to speech and video; Prentice-Hall, 1984; ISBN 0-13-211913-7.

Jeffrey et al: Small satellites (MSTI-3) for remote sensing; Proc. of the SPIE Conference on Small Satellite Technology and Applications IV, SPIE Vol.2317, Rome, Sept 1994.

Jones G.D, Hilleary D.T. & Fridovich B: A diffuse light source for calibrating meteorological satellite television cameras; Applied Optics, Vol.4 No.3, p.307-309, March 1965.

Karara H.M: Non-topographic photogammetry; American Society for Photogammetry and Remote Sensing, 1989, ISBN 0-944426-10-7.

Kasturirangan K: The evolution of satellite-based remote sensing capabilities in India; Remote Sensing Yearbook 1986, edited by Cracknell A. & Hayes L, Taylor & Francis 1986, ISBN 0-85066-313-X.

Keller H.U. et al: Images of the nucleus of Comet Halley obtained by the Halley Multicolour Camera (HMC) on board the Giotto spacecraft; European Space Agency, ESA SP-1127, Vol.1, ISBN 92-9092-080-7.

Kim S. et al: Mission overview of engineering test satellite KITSAT-3; Proc. of the 9th Annual AIAA/USU Conference on Small Satellites, Utah State University, 18-21 Sept 1995.

King J.A. et al: The in-orbit performance of four Microsat spacecraft; Proc. of the 4th Annual AIAA/USU Conference on Small Satellites, Utah State University, 27-30 Aug 1990.

Knowlton K: Progressive transmission of grey-scale and binary picture by simple, efficient and lossless encoding schemes; Proc. IEEE, Vol.68 No.7, p.885 - 896, July 1980.

Kodak: Telephone enquiry to professional technical support, quoting the diffuse RMS granularity at a density of unity of Kodak T-MAX ISO100 film to be 8 and T-MAX ISO100 to be 10 when measured with a standard 48 μm microdensitometer; 27 July 1995.

Kumar K: Orbital and attitude prediction accuracy requirements for satellites engaged in remote sensing and scientific missions; IEEE Trans. on Aerospace and Electronic Systems, Vol.AES-18 No.2, p188-191, 1982.

Kunt M, Ikonomopoulos A. & Kocher M: Second-generation image-coding techniques; Proc of the IEEE, Vol.73 No.4, p.549 - 574, April 1985.

Lake D: Imaging sensors - why do they cost what they cost?; Advanced Imaging, June 1995; ISSN 1042-0711.

Laker C: Software environment for the UoSAT-5 Earth imaging system; M.Sc. dissertation; University of Surrey, 1991.

Lanzl G et al: The MEOSS experiment - a test case for future cartographic missions; Proc of IGARSS Symposium, Edinburgh, Scotland, 13-16 Sept. 1988; Ref. ESA SP-284.

Lareau A.G: Obtaining reconnaissance images more quickly; Photonics Spectra, p.105-108, Mar 1994.

Lee J.S: Digital image smoothing and the sigma filter; Computer Vision, Graphics, and Image Processing, Vol.24 p.255-269, 1983.

Lee J.S: Refined filtering of image noise using local statistics; Computer Graphics and Image Processing, Vol.15 p.380-389, 1981.

Leitmann M.G, Fouquet M. et al: Attitude and position determination using a star mapper on the small satellite PoSAT-1; Proc. of the SPIE Conference on Small Satellite Technology and Applications III, SPIE Vol.1940, Orlando Florida, 14-15 April 1993.

Leitmann M.G, Fouquet M. et al: PoSAT-1 star imaging system- in-orbit performance; Proc. of the SPIE Conference on Small Satellite Technology and Applications IV, SPIE Vol.2317, Rome, Sept 1994.

Lemesle J.P: Le tour du monde en 2 heures; Le Cherche Midi, 1989; ISBN 2-86-274-1574.

Lhuillier J.J. & Nguyen A.Q: Subband coding of images - comparison with DCT; Signal Processing IV - Theories and Applications, Edited by Lacoume J.L. et al, Elsevier Science Publishers, 1988.

Lillesand T.M. & Kiefer R.W: Remote Sensing and Image Interpretation; Wiley 1987; ISBN 0-471-84517-5.

Linde Y, Buzo A. & Gray R.M: An algorithm for vector quantizer design; IEEE Trans on Communications, Vol.28 No.1, p.84 - 95, Jan 1980.

LLNL (Lawrence Livermore National Laboratory): Presentation material - Clementine project review; 20 May 1992.

Lomheim T.S. et al: Imaging charge coupled device (CCD) transient response to 17 and 50 MeV proton and heavy ion irradiation; IEEE Trans. on Nuclear Science, Vol.37 No.6, p.1876 - 1885, Dec 1990.

Malin M.C. et al: Design and development of the Mars Observer camera; Int. J. of Imaging Systems and Technology, Vol.3, p.76 - 91, 1991.

Malin M.C. et al: Mars Observer camera; J. of Geophysical Research, Vol.97 No.E5, p.7699 - 7718, May 25 1992.

Mastin G.A: Adaptive filters for digital image noise smoothing: an evaluation; Computer Vision, Graphics, and Image Processing, Vol.31 p.103-121, 1985.

McGlone J.C: Analytic data-reduction schemes in non-topographic photogammetry; p.37 - 57 of [Karara].

Memon N.D, Sayood K. & Magliveras S.S: Lossless compression of multispectral image data; IEEE Trans. on Geoscience and Remote Sensing, Vol.32 No.2, p.282 - 289, March 1994.

Mertikas S.P. & Giavi V: Detection of oil spills using SPOT remote sensing data; Earth Space Review, Vol.4 No.2, p.19-24, Apr-June 1995; ISSN 1060-1848.

Meurer R.H: First class science on a coach class ticket; Proc. of the 9th Annual AIAA/USU Conference on Small Satellites, Utah State University, 18-21 Sept 1995.

Milne G.W. et al: SUNSAT, Stellenbosch University and SA-AMSAT's remote sensing and packet communications microsatellite; Proc. of the 7th Annual AIAA/USU Conference on Small Satellites, Utah State University, 13-16 Sept 1993.

Mitchell O.R. & Delp E.J: Multilevel graphics representation using block truncation coding; Proc IEEE, Vol.68 No.7, p.868 - 873, July 1980.

Montpetit M.J, Prieur L. & Fouquet M: Compression of UoSAT-5 images; Proc. of the SPIE Conference on Small Satellite Technology and Applications III, SPIE Vol.1940, Orlando, 14-15 April 1993.

Muench G: Advances in spaceborne data recorders; Space Markets, Spring 1988.

Nagao M. & Matsuyama T: Edge preserving smoothing; Computer Graphics and Image Processing, Vol.9 p.394-407, 1978.

Neeck S.P, Venator T.J. & Bolek J.T: Jitter and stability calculation for the ASTER instrument; Proc. of the SPIE Conference on Sensor Systems for Mission to Planet Earth Platforms, SPIE Vol.2317, Rome, Sept 1994.

Netravali A.N. & Limb J.O: Picture coding - a review; Proc of the IEEE, Vol.68 No.3, p.366 - 406, March 1980.

NORAD Keplerian elements sets.

Oldfield M: Personal communication, 5 Sept 1995.

Optical Transient Detector home page (http://wwwghcc.msfc.nasa.gov:5678/otd.html).

Owens J.D: Geometric corrections of UoSAT-5 CCD images; M.Sc. dissertation; University of Surrey, 1992.

Pease C.B: Satellite imaging instruments - principles, technologies and operational systems; Ellis Horwood, 1990, ISBN 0-13-638487-0.

Pei S.O. & Jaw S.Y: Design of 2-D quadrature mirror filters for image subband coding; IEEE Trans on Circuits & Systems, Vol.34 No.4, p.438 - 441, Apr 1987.

Pfeiffer: Meteosat data rates xyz.

Photometrics: New generation imager system; Photometrics Inc, Tucson Az, NASA Science & Technical Abstract Report ref N88-18398.

Pratt W.K, Digital image processing, Wiley, 1978.

Price J.C: Radiometric calibration of satellite sensors in the visible and near-IR: history and outlook; Remote Sensing of the Environment, Vol. 22, p3-9, 1987.

Price J.C: Timing of NOAA afternoon passes; Int. J. Remote Sensing, Vol.12 No.1, p193-198, 1991.

Rabbani M. & Jones P.W, Digital image compression techniques, SPIE Optical Engineering Press, 1991, ISBN 0-8194-0648-1.

Radbone J.M: The UoSAT-2 Spacecraft CCD Imaging and Digital Store/Read-out Experiments; The IERE Journal, Vol. 57 N°5, Sept. 1987; ISSN 0267-1689.

Raptis M, Digital signal processing of image data; MSc Thesis, University of Surrey, 1990.

Reddy B.R.K. & Pai A.L: Reed-Muller transform image coding; Computer Vision, Graphics, and Image Processing, Vol.42 p.48-61, 1988.

Rees W.G: Orbital sub-cycles for Earth remote sensing satellites; Int. J. Remote Sensing, Vol.13 No.5, p825-833, 1992.

Regeon P.A, Chapman R.J. & Baugh R: Clementine - the deep space program science experiment; Acta Astronautica, Vol.35 Suppl. p.307 - 321, 1995.

Reichhardt T: Lewis and Clark, blazing new trails; Aerospace America, V.33 No.7, July 1995.

Renner U, Lübke-Ossenbeck B. & Butz P: TUBSAT - low cost access to space; Proc. of the 7th Annual AIAA/USU Conference on Small Satellites, Utah State University, 13-16 Sept 1993.

Renner U, Lübke-Ossenbeck B. & Butz P: TUBSAT-A,B,C; Proc. of Int. Symposium on Small Satellites Systems and Services; Biarritz, France, 27-30 June, 1994.

Robas: Satelliet beeldende kunst; Robas, 1991; ISBN 90-72770025-0.

Roger R.E. & Arnold J.F: Reversible image compression bounded by noise, IEEE Trans. on Geoscience and Remote Sensing, Vol.32 No.1, p. 19 - 21, Jan 1994.

Roy T, Watts S.J. & Wight D: Radiation damage effects on imaging charge coupled devices; Nuclear Instrumentation Methods in Physical Research, A275 p.545 - 557, 1989.

Royer A. et al: Radiometric comparison of the LANDSAT-5 TM and MSS sensors; Int. J. Remote Sensing, Vol.9 No.2, p.187-236, 1988.

Rustan P.L: The Clementine mission; Proc. of the SPIE Conference on Small Satellite Technology and Applications IV, SPIE Vol.2317, Rome, Sept 1994.

Rustan P.L: Personal communication; 29 Sept 1994.

Rustan P.L: Clementine - mining new uses for SDI technology; Aerospace America, p.38 - 41, Jan 1994.

Rycroft M: The Cambridge Encyclopaedia of Space; Cambridge University Press, 1990; ISBN 0-521-36426-4.

Sakuma F, Ono A. Arai K: Radiometric calibration techniques for ASTER; Proc. of the SPIE Conference on Sensor Systems for Mission to Planet Earth Platforms, SPIE Vol.2317, Rome, Sept 1994.

Santana C.E: Environmental monitoring of the Amazon region with smallsats; Conference on Small Satellites for Remote Sensing, The Space Congress, 24-25 May 1995, Bremen Germany.

Schoonwinkel A, Mostert S & Milne G.W: The Sunsat microsatellite for remote sensing and packet communication; Proc. of Int. Symposium on Small Satellites Systems and Services; Biarritz, France, 27-30 June, 1994.

Shachar M. & Lapid P: The TechSAT programme; J of the British Interplanetary Society, Vol.45 No.12, p.501 - 505, Dec 1992.

Shaviv G: The Gurwin-1 Techsat project; Proc. of Int. Symposium on Small Satellites Systems and Services; Biarritz, France, 27-30 June, 1994.

Sheffield C: Earth watch; Sidgwick & Jackson, 1981; ISBN 0-283-98737-5.

Sheffield C: Man on Earth; Sidgwick & Jackson, 1983; ISBN 0-283-98956-4.

Slama C.C: Manual of Photogammetry Fourth Edition; American Society of Photogammetry, 1980, ISBN 0-937294-01-2.

Slater P.N: Remote Sensing - Optics and Optical Systems; Addison-Wesley 1980; ISBN 0-201-07250-5.

Slater P.N. et al: The in-flight radiometric calibration of ASTER by reference to well-characterised scenes; Proc. of the SPIE Conference on Sensor Systems for Mission to Planet Earth Platforms, SPIE Vol.2317, Rome, Sept 1994.

Small Satellites home page (http://www.ee.surrey.ac.uk/EE/CSER/UOSAT/SSHP/sshp.html).

Smith J.L: Restoration and enhancement of Earth images from a low cost sampled video system; Proc. of the 6th Annual AIAA/USU Conference on Small Satellites, Utah State University, 21-24 Sept 1992.

SPOT Press Pack; CNES 1985.

Stassinopoulos E.G. & Raymond J.P: The space radiation environment for electronics; Proc. of IEEE, Vol.76 No.11, p.1423 - 1442, Nov 1988.

Sudarshana R. et al: Experiments in site selection for coastal aquaculture using Indian Remote Sensing satellite: IRS-1A; Int. J. Remote Sensing, Vol. 14 No. 12, 1993.

Sun W, Sweeting M.N. & Hodgart M.S: A novel implementation of an MSK modem using digital signal processing techniques on-board a low Earth orbit microsatellite; Proc. IEEE Singapore International Conference on Communications Systems, Singapore, p.430-434, 14-18 Nov 1994.

Sun W, Sweeting M.N. & Hodgart M.S: Investigation of MSK and FSK modulation schemes for single channel communications systems using DSP techniques on-board low Earth orbit microsatellites; Proc. 10th IEE International Conference on Digital Communications via Satellites, Vol.1, p.9-16 Brighton UK, 15-19 May 1995.

Sunsat home page (http://esl.ee.sun.ac.za).

Swain P.H. & Davis S.M: Remote sensing - the quantitative approach; McGraw-Hill, 1978.

Sweeting M.N: UoSAT microsatellite missions; Electronics & Communication Engineering Journal, IEE, June 1992.

Sweeting M.N: Microsatellite & minisatellite programmes at the University of Surrey for effective technology transfer & training in satellite engineering; Proc. of Int. Symp. on Satellite Communications and Remote Sensing, 20-22 Sept 1995, Xi'an China.

UoSAT-1: special issue of the IERE Journal, Vol. 52 N°8/9, Aug. 1982.

UoSAT-2: special issue of the IERE Journal, Vol. 57 N°5, Sept. 1987.

TechSAT home page (http://www.technion.ac.il/pub/projects/techsat/).

Thomlinson J, Adams L. & Harboe-Sørensen R: The SEU and total dose response of the Inmos transputer; IEEE Trans. on Nuclear Science, Vol.NS34 No.6, p.1803-1807, Dec 1987.

Townshend J.R.G. & Justice C.O: Selecting the spatial resolution of satellite sensors required for global monitoring of land transformations; Int. J. Remote Sensing, Vol.9 No.2, p187-236, 1988.

Trayner C.P. & Jeans T.G: The Development of a Satellite-Borne Earth Imaging System for UoSAT; The IERE Journal, Vol. 52 N°8/9, Aug. 1982; ISSN 0033-7722.

Truss P: European remote sensing satellite platforms for the 1990s; Proc of IGARSS Symposium, Edinburgh, Scotland, 13-16 Sept. 1988; Ref. ESA SP-284.

Turnill R: Jane's Spaceflight Directory 2nd edition; Jane's Publishing Co. Ltd, London 1986; ISBN 0-7106-0367-3.

Udpikar V.R. & Raina J.P: BTC image coding using vector quantization; IEEE Trans. on Communications, Vol.35 No.3, p.352 - 356, March 1987.

Underwood C.I et al: Observations of single-event upsets in non-hardened high-density SRAMs in Sun-synchronous orbit; IEEE Trans. on Nuclear Science, Vol.39 No.6, Dec 1992.

Underwood C.I et al: Observations of single-event upset and multiple-event upset in non-hardened high-density SRAMs in the TOPEX/Poseidon orbit; IEEE Trans. on Nuclear Science, Vol.40 No.6, Dec 1993.

Unwin M.J: The PoSAT microsatellite GPS experiment; ION GPS-93 Conference, Salt Lake City, USA; Vol.1, p.811-817, Sept 1993.

Unwin M.J: A practical demonstration of low-cost autonomous orbit determination using GPS; ION GPS-95 Conference, Palm Springs, USA; 13-15 Sept 1995.

Vaidyanathan P.P: Quadrature mirror filter banks, M-band extensions and perfect reconstruction techniques; Acoustics, Speech & Signal Processing Magazine, Vol.4 No.3, p.4-20, July 1987.

Wagner M.J: Around the world in nine months with satellite data; Earth Observation Quarterly, No.44, ESA Publication Division, June 1994.

Wallach J: The Launch of NOAA-H Weather Satellite: A Mission Profile; The Proceedings of the AMSAT-NA 6th Space Symposium and Annual Meeting; Nov. 11-13 1988; Published by American Radio Relay League.

Wang D. & Wang Q: A weighted averaging method for image smoothing; Acta Electronica Sinica, Vol.14 No.6, Nov 1986.

Wang D.C.C, Vagnucci A.H. & Li C.C: Gradient inversed weighted smoothing scheme and the evaluation of its performance; Computer Graphics and Image Processing, Vol.15 p.167-181, 1981.Ward J.W: Personal communication, 24 Aug 1995.

Ward J.W: Microsatellites for global electronic mail networks; Electronics & Communication Engineering Journal, Vol.3 No.6, p.267-272, Dec 1991.

Ward J.W: Design, implementation and in-orbit demonstration of a store-and-forward digital communication system for low Earth orbit microsatellites; PhD thesis, University of Surrey, 1993

Ward J.W. & Price H.E: Re-usable software for microsatellite on-board computers; EUROSPACE Symposium on On-Board Data Management, Rome Italy, 25-27 Jan 1994.

Welch R: Spatial resolution for urban studies; Int. J. Remote Sensing, Vol.3 No.2, p139-141, 1982.

Wells N: The Space Technology Research Vehicles STRV-1a and -1B - one year in GTO; Proc. of the 9th Annual AIAA/USU Conference on Small Satellites, Utah State University, 18-21 Sept 1995.

Wertz J.R: Spacecraft attitude determination and control; D.Reidel Publishing, 1978; ISBN 90-277-1204-2.

Wester-Ebinghaus W: Trends in non-topographic photogammetry systems; p.377 - 387 of [Karara].

Wirth J. & Peeters M: AVCSR - an airborne radiometer as a tool for satellite data validation; Proc of IGARSS Symposium, Edinburgh, Scotland, 13-16 Sept. 1988; Ref. ESA SP-284.

Yoo S.K. et al: The KITSAT-2 Earth Imaging System Experiment; Proc. of the SPIE Conference on Small Satellite Technology and Applications IV, SPIE Vol.2317, Rome, Sept 1994.

APPENDIX 2. AUTHOR'S PUBLICATIONS DURING THIS RESEARCH PROGRAMME.

[1] Fouquet, M: The UoSAT-5 Earth Imaging System - in-orbit results; 2nd conference on Small Satellite Technologies and Applications, SPIE symposium on Aerospace Sensing, Orlando Florida, 20-22 April 1992.

[2] Leitmann M, Fouquet M, Rebordao J.M, Sepulveda T: Attitude and position determination using a star mapper on the small satellite platform PoSAT-1; 3rd conference on Small Satellite Technologies and Applications, SPIE symposium on Aerospace Sensing, Orlando Florida, 14-15 April 1993.

[3] Montpetit J-M, Prieur L, Fouquet M: Compression of UoSAT-5 EIS images; 3rd conference on Small Satellite Technologies and Applications; SPIE symposium on Aerospace & Remote Sensing, Orlando Florida, 14-15 April 1993.

[4] Leitmann M, Rebordao J.M, Gomes N.M, Fouquet M, Sweeting M.N: PoSAT-1 Star Imaging System - In-flight performance; 4th conference on Small Satellite Technologies and Applications; SPIE/Europto symposium on Satellite Remote Sensing, Rome Italy, 29-30 Sept 1994.

[5] M. Fouquet & A. Brewer: The Role of Microsatellites for Earth Observation - Eight years of orbital experience at the University of Surrey; Conference on Small Satellites for Remote Sensing, The Space Congress, 24-25 May 1995, Bremen Germany.

[6] Sweeting Prof M.N. & Fouquet M: Inexpensive remote sensing using microsatellites; Conference on Remote Sensing & GIS for Environmental Resources Management; 6-8 June 1995 Jakarta, Indonesia.

[7] Marc Fouquet & Prof. Martin N Sweeting: Remote sensing using the University of Surrey's microsatellites; Proc. of Int. Symp. on Satellite Communications and Remote Sensing, 20-22 Sept 1995, Xi'an China.

Also :

Final Report for SERC Grant GR/F29462 : Research into low cost medium resolution spacecraft imaging with advanced on-board data processing; Prof. M.N. Sweeting (Principal Investigator), M. Fouquet (RA); 1992.